



**HAL**  
open science

# Design and synthesis of multivalent glycoconjugates for anti-cancer immunotherapy

Carlo Pifferi

► **To cite this version:**

Carlo Pifferi. Design and synthesis of multivalent glycoconjugates for anti-cancer immunotherapy. Biochemistry [q-bio.BM]. Université Grenoble Alpes, 2017. English. NNT : 2017GREAV060 . tel-01735460

**HAL Id: tel-01735460**

**<https://theses.hal.science/tel-01735460>**

Submitted on 16 Mar 2018

**HAL** is a multi-disciplinary open access archive for the deposit and dissemination of scientific research documents, whether they are published or not. The documents may come from teaching and research institutions in France or abroad, or from public or private research centers.

L'archive ouverte pluridisciplinaire **HAL**, est destinée au dépôt et à la diffusion de documents scientifiques de niveau recherche, publiés ou non, émanant des établissements d'enseignement et de recherche français ou étrangers, des laboratoires publics ou privés.

## THÈSE

Pour obtenir le grade de

**DOCTEUR DE LA COMMUNAUTE UNIVERSITE  
GRENOBLE ALPES**

Spécialité : **Chimie-Biologie**

Arrêté ministériel : 25 mai 2016

Présentée par

**Carlo PIFFERI**

Thèse dirigée par **Prof. Olivier RENAUDET**, Université  
**Grenoble-Alpes**, et  
codirigée par **Dr. Nathalie BERTHET**, Université Grenoble-  
**Alpes**

préparée au sein du **Département de Chimie Moléculaire**  
dans **l'École Doctorale Chimie et Science du Vivant**

# **Design and synthesis of multivalent glycoconjugates for anti-cancer immunotherapy**

Thèse soutenue publiquement le **14 décembre 2017**

devant le jury composé de :

**Dr. Boris, VAUZEILLES**, Président  
Directeur de Recherche, Université Paris-Sud, Membre  
**Prof. Cristina, NATIVI**, Rapporteur  
Professeur, Université de Florence, Rapporteur  
**Prof. Richard, DANIELLOU**, Rapporteur  
Professeur, Université d'Orléans, Rapporteur  
**Dr. Serge, PEREZ**, Examineur  
Directeur de Recherche Émérite, Université Grenoble-Alpes, Membre  
**Dr. Nathalie, BERTHET**, Co-directeur  
Maître des conférences, Université Grenoble-Alpes, Membre  
**Prof. Olivier, RENAUDET**, Directeur  
Professeur, Université Grenoble-Alpes, Membre



# Table of contents

<b>Chapter I. Introduction</b> .....	<b>1</b>
<b>I.1. Overview of immune responses</b> .....	<b>2</b>
<b>I.1.1. Innate immunity</b> .....	<b>2</b>
<b>I.1.2. Adaptive immunity</b> .....	<b>3</b>
<b>I.1.3. Passive/active immunity</b> .....	<b>4</b>
<b>I.1.4. Humoral adaptive immune responses</b> .....	<b>5</b>
<b>I.1.5. Cellular adaptive immune responses</b> .....	<b>9</b>
<b>I.1.6. Antigen presentation</b> .....	<b>10</b>
<b>I.1.7. Interplay between innate and adaptive systems</b> .....	<b>11</b>
<b>I.1.8. T<sub>H</sub> cell activation and licensing</b> .....	<b>12</b>
<b>I.1.9. CTL activation</b> .....	<b>13</b>
<b>I.1.10. B cell activation</b> .....	<b>14</b>
<b>I.1.11. Overview of immune responses – Conclusions</b> .....	<b>15</b>
<b>I.2. Anti-cancer immunotherapy</b> .....	<b>17</b>
<b>I.2.1. Tumor-associated antigens</b> .....	<b>20</b>
<b>I.2.2. MUC1 and tumor-associated carbohydrate antigens (TACAs)</b> .....	<b>21</b>
<b>I.2.3. Key aspects related to TACA-based vaccines development</b> .....	<b>24</b>
<b>I.2.3.1. Source of epitopes</b> .....	<b>24</b>
<b>I.2.3.2. Protein-carbohydrate interactions</b> .....	<b>24</b>
<b>I.2.3.3. Enabling TACA-directed humoral adaptive responses</b> .....	<b>26</b>
<b>I.3. Syntheses and immunological properties of TACA-based anti-cancer vaccines: an overview</b> .....	<b>27</b>
<b>I.3.1. Semi-synthetic approaches</b> .....	<b>27</b>
<b>I.3.1.1. Vaccines featuring protein-carriers</b> .....	<b>27</b>
<b>I.3.1.1.1. Mono-TACA vaccines based on protein-carriers</b> .....	<b>28</b>
<b>I.3.1.1.2. Clustered mono-TACA vaccines based on protein-carriers</b> .....	<b>34</b>
<b>I.3.1.1.3. Hetero-TACA vaccines based on protein-carriers</b> .....	<b>35</b>
<b>I.3.1.1.4. Problems associated with protein carriers</b> .....	<b>40</b>
<b>I.3.1.2. Alternatives to protein-carrier delivery</b> .....	<b>42</b>
<b>I.3.1.2.1. Virus-like particles</b> .....	<b>42</b>
<b>I.3.1.2.2. Gold nanoparticles</b> .....	<b>43</b>
<b>I.3.1.2.3. Zwitterionic polysaccharides</b> .....	<b>45</b>
<b>I.3.1.3. Semi-synthetic approaches – Conclusions</b> .....	<b>46</b>
<b>I.3.2. Fully-synthetic approaches</b> .....	<b>47</b>
<b>I.3.2.1. Two-component (TACA-CD4<sup>+</sup>), fully synthetic anti-cancer vaccines</b> .....	<b>48</b>

<b>I.3.2.2.</b> Two-component (TACA-lipopeptide), fully synthetic anti-cancer vaccines.....	56
<b>I.3.2.3.</b> Multi-component, fully synthetic anti-cancer vaccines.....	60
<b>I.3.2.4.</b> Fully-synthetic approaches – Conclusions.....	66
<b>I.3.3.</b> Adjuvants.....	67
<b>I.4.</b> My project.....	69
<b>Chapter II. Synthesis of multivalent homo-glycodendrimers</b> .....	<b>73</b>
<b>II.1.</b> Introduction.....	<b>74</b>
<b>II.1.1.</b> “Core” scaffolds.....	<b>76</b>
<b>II.1.2.</b> Chemoselective “click” chemistry.....	<b>77</b>
<b>II.2.</b> Mannosylated multivalent glycodendrimer assembly based on divergent iterative oxime strategy.....	<b>81</b>
<b>II.2.1.</b> General strategy.....	<b>81</b>
<b>II.2.2.</b> Synthesis of tetravalent cyclopeptide “core” scaffold 89.....	<b>82</b>
<b>II.2.3.</b> Synthesis of cyclopeptide 64 and compound 88 as dendrimer’s “arms”.....	<b>85</b>
<b>II.2.4.</b> Hexadecavalent scaffold assembly through oxime ligation.....	<b>86</b>
<b>II.2.5.</b> Synthesis of aminoxy-mannose building block 90 and functionalization of aldehyde-bearing scaffolds via a second oxime ligation.....	<b>88</b>
<b>II.3.</b> (OX)Tn-functionalized multivalent glycodendrimer assembly based on divergent iterative oxime strategy.....	<b>92</b>
<b>II.4.</b> (TRZ)Tn-functionalized multivalent glycodendrimer assembly based on convergent oxime/CuAAC strategy.....	<b>94</b>
<b>II.4.1.</b> General strategy.....	<b>94</b>
<b>II.4.2.</b> Synthesis of propargyl-Tn building blocks 112 and 113.....	<b>96</b>
<b>II.4.3.</b> Synthesis of azido-bearing cyclopeptides 120 and 121.....	<b>97</b>
<b>II.4.4.</b> Divergent and convergent assembly of Tn-bearing hexadecavalent glycodendrimers 126 and 127.....	<b>99</b>
<b>II.4.5.</b> Evaluation of the binding activity of glycodendrimers 122, 123, 126 and 127 on SBA lectin <i>via</i> ELLA.....	<b>104</b>
<b>II.5.</b> Synthesis of a new set of mannosylated tetracosavalent glycodendrimers.....	<b>107</b>
<b>II.5.1.</b> Introducing a small library of multivalent mannosylated glycoconjugates.....	<b>107</b>
<b>II.5.2.</b> Synthesis of RAFT-, dendron-, and cyclophosphazene-based scaffolds.....	<b>108</b>
<b>II.5.3.</b> Synthesis of mannosylated tetra- and hexa-valent glycodendrimers 128-131.....	<b>112</b>
<b>II.5.4.</b> Assembly of mannosylated tetracosavalent glycodendrimers 132 and 133 by OL.....	<b>113</b>

<b>II.5.5.</b> Assembly of mannosylated tetracosavalent glycodendrimers 134 and 135 by CuAAC.....	<b>115</b>
<b>II.5.6.</b> Evaluation of the binding activity of glycodendrimers 128-135 on BCL2-A lectin <i>via</i> ITC.....	<b>118</b>
<b>Chapter III. Synthesis of multivalent hetero-glycodendrimers</b> .....	<b>124</b>
<b>III.1.</b> Introduction.....	<b>125</b>
<b>III.2.</b> Dual (OX)Tn-(TRZ)TF-based multivalent glycodendrimers assembly based on divergent OL/CuAAC strategy.....	<b>126</b>
<b>III.3.</b> General strategy.....	<b>127</b>
<b>III.4.</b> Synthesis of modified propargyl-TF antigen 155.....	<b>128</b>
<b>III.5.</b> Synthesis of cyclopeptide “cores” and “arms” building blocks 152-154.....	<b>129</b>
<b>III.6.</b> Assembly of multivalent scaffolds 171-172 bearing azide and aldehyde residues.....	<b>132</b>
<b>III.7.</b> Synthesis of multivalent hetero-glycoclusters 150-151 by sequential one-pot OL-CuAAC protocol.....	<b>135</b>
<b>Chapter IV. Interaction assays with monoclonal antibodies and synthesis of         complete vaccine prototype structures</b> .....	<b>138</b>
<b>IV.1.</b> Direct interaction assays of hetero-glycodendrimers with anti-Tn and anti-TF mAbs by ELISA.....	<b>139</b>
<b>IV.1.1.</b> ELISA direct interaction assays with anti-Tn mAb 9A7.....	<b>139</b>
<b>IV.1.2.</b> ELISA direct interaction assay with anti-TF mAb JAA-F11.....	<b>141</b>
<b>IV.1.3.</b> Synthesis of a TF-based glycocluster 186 containing a PEG linker and evaluation with anti-TF mAb JAA-F11.....	<b>143</b>
<b>IV.2.</b> Comparison between (OX)Tn-based glycodendrimers and (Ser)Tn-based glycodendrimers towards their interaction with mAb 9A7.....	<b>148</b>
<b>IV.2.1.</b> Synthesis of tetravalent glycocluster 190 containing the (Ser)Tn epitope.....	<b>148</b>
<b>IV.2.2.</b> Synthesis of hexadecavalent glycodendrimer 193 containing the (Ser)Tn epitope.....	<b>150</b>
<b>IV.2.3.</b> Comparison of binding efficacy between (OX)Tn- and (Ser)Tn-based glycoconjugates <i>via</i> ELISA direct interaction assays using anti-Tn mAb 9A7.....	<b>152</b>
<b>IV.3.</b> Synthesis of complete, fully synthetic, vaccine prototypes containing (OX)Tn and (Ser)Tn epitopes.....	<b>155</b>
<b>IV.3.1.</b> Synthesis of peptide 195 containing in-line CD4 <sup>+</sup> and CD8 <sup>+</sup> epitopes from ovalbumin.....	<b>155</b>

<b>IV.3.2.</b> Synthesis of fully synthetic anti-cancer vaccine prototypes incorporating the (OX)Tn motif.....	<b>157</b>
<b>IV.3.2.1.</b> Synthesis of tetravalent, (OX)Tn-bearing, fully synthetic anti-cancer vaccine prototype 199.....	<b>158</b>
<b>IV.3.2.2.</b> Synthesis of hexadecavalent, (OX)Tn-bearing, fully synthetic anticancer vaccine prototype 201.....	<b>160</b>
<b>IV.3.3.</b> Synthesis of fully synthetic anti-cancer vaccine prototypes incorporating the (Ser)Tn motif.....	<b>163</b>
<b>IV.3.3.1.</b> Synthesis of tetravalent, (Ser)Tn-bearing, fully synthetic anti-cancer vaccine prototype 205.....	<b>163</b>
<b>IV.3.3.2.</b> Towards the synthesis of hexadecavalent, (Ser)Tn-bearing, fully synthetic anti-cancer vaccine prototype 210.....	<b>168</b>
<b>IV.3.3.3.</b> Alternative synthesis of hexadecavalent (Ser)Tn-bearing, fully synthetic anti-cancer vaccine prototype.....	<b>172</b>
<b>IV.3.3.3.1.</b> Synthetic strategy.....	<b>172</b>
<b>IV.3.3.3.2.</b> Convergent assembly of hexadecavalent, (Ser)Tn-bearing, fully synthetic anti-cancer vaccine prototype 211.....	<b>174</b>
 <b>V. Conclusions and outlook</b> .....	 <b>180</b>
 <b>VI. Materials and methods</b> .....	 <b>184</b>
<b>VI.1.</b> Equipment.....	<b>185</b>
<b>VI.1.1.</b> High performance liquid chromatography (HPLC).....	<b>185</b>
<b>VI.1.2.</b> Mass spectrometry (MS).....	<b>185</b>
<b>VI.1.3.</b> Nuclear magnetic resonance (NMR).....	<b>185</b>
<b>VI.1.4.</b> Circular dichroism (CD).....	<b>186</b>
<b>VI.1.5.</b> Molecular models.....	<b>186</b>
<b>VI.2.</b> Interaction assays.....	<b>186</b>
<b>VI.2.1.</b> Enzyme-linked lectin assay (ELLA).....	<b>186</b>
<b>VI.2.2.</b> Isothermal titration microcalorimetry (ITC).....	<b>187</b>
<b>VI.2.3.</b> Enzyme-linked immunosorbent assay (ELISA).....	<b>187</b>
<b>VI.3.</b> General synthesis methods and procedures.....	<b>187</b>
<b>VI.3.1.</b> General procedures for solid-phase peptide synthesis (SPPS).....	<b>188</b>
<b>VI.3.2.</b> General procedures for peptide cleavage.....	<b>189</b>
<b>VI.3.3.</b> General procedure for peptide cyclization.....	<b>189</b>
<b>VI.3.4.</b> General procedure for oxidative cleavage.....	<b>189</b>
<b>VI.3.5.</b> General procedure for oxime ligation (OL).....	<b>189</b>
<b>VI.3.6.</b> General procedure for copper(I)-catalyzed alkyne-azide cycloaddition (CuAAC).....	<b>190</b>

<b>VI.3.7.</b> General procedure for disulfide bridging.....	<b>190</b>
<b>VI.4.</b> Syntheses and characterizations.....	<b>191</b>
<b>VII. Annexes</b> .....	<b>234</b>
List of publications.....	<b>235</b>
Posters and oral communications.....	<b>236</b>
<b>VIII. Bibliographic data</b> .....	<b>237</b>

## Abbreviations

<b>AA</b>	amino acid	<b>GLP</b>	glyco-lipo-peptide
<b>ACVA</b>	4,4'-azobis(4-cyanovaleric acid)	<b>GNP</b>	gold nanoparticle
<b>AcOEt</b>	ethyl acetate	<b>HATU</b>	1-[bis(dimethylamino)methylene]-1H-1,2,3-triazolo[4,5-b]pyridinium 3-oxid hexafluorophosphate
<b>APC</b>	antigen presenting cell	<b>HBTU</b>	2-(1H-benzotriazol-1-yl)-1,1,3,3-tetramethyluronium hexafluorophosphate
<b>Acm</b>	acetamidomethyl	<b>HEMAm</b>	<i>N</i> -(2-hydroxyethyl)-2-methacrylamide
<b>ACT</b>	adoptive cell transfer	<b>hGC</b>	hetero-glycocluster
<b>Alloc</b>	allyloxycarbonyl	<b>hGD</b>	hetero-glycodendrimer
<b>BCR</b>	B cell receptor	<b>HOAt</b>	1-hydroxy-7-azabenzotriazole
<b>Boc</b>	<i>tert</i> -butyloxycarbonyl	<b>HOBt</b>	<i>N</i> -hydroxybenzotriazole
<b>CAN</b>	ceric ammonium nitrate	<b>HONPhth</b>	<i>N</i> -hydroxyphthalimide
<b>CD</b>	cluster of differentiation	<b>HPAEC</b>	high-pH anion-exchange chromatography
<b>CPADB</b>	(4-cyanopentanoic acid)-4-dithiobenzoate	<b>HAS</b>	human serum albumine
<b>CPMV</b>	cowpea mosaic virus	<b>IFN-<math>\alpha</math></b>	interferon- $\alpha$
<b>CSA</b>	camphor-10-sulfonic acid ( $\beta$ )	<b>Ig</b>	immunoglobulin
<b>CuAAC</b>	copper(I)-catalyzed alkyne-azide cycloaddition	<b>IL-2</b>	interlukin-2
<b>DAST</b>	diethylaminosulfur trifluoride	<b>ITC</b>	isothermal titration microcalorimetry
<b>DC</b>	dendritic cell	<b>LC-MS</b>	liquid chromatography – mass spectrometry
<b>DCC</b>	<i>N,N'</i> -dicyclohexylcarbodiimide	<b>(m)Ab</b>	(monoclonal) antibody
<b>Dde</b>	1-(4,4-dimethyl-2,6-dioxocyclohex-1-ylidene)ethyl	<b>MAG</b>	multiple antigen glycopeptide
<b>DIPEA</b>	<i>N,N</i> -diisopropylethylamine	<b>MAGE3</b>	melanoma-associated antigen 3
<b>DMAP</b>	4-dimethylaminopyridine	<b>MALDI-TOF</b>	matrix assisted laser desorption ionization – time of flight
<b>DMF</b>	<i>N,N</i> -dimethylformamide	<b>MALT</b>	mucosa-associated lymphoid tissue
<b>DMSO</b>	dimethyl sulfoxide	<b>MAP</b>	multiple antigen peptide
<b>DPC</b>	<i>n</i> -dodecylphosphocholine	<b>MBL</b>	mannose-binding lectin
<b>DPPE</b>	1,2-bis(diphenylphosphino)-ethane	<b>MBS</b>	<i>m</i> -maleimidobenzoyl- <i>N</i> -hydroxysuccinimide ester
<b>DSC</b>	diethyl squarate coupling	<b>MESNA</b>	sodium 2-mercaptoethane sulfonate
<b>DTT</b>	1,4-dithiothreitol		
<b>EDC</b>	1-ethyl-3-(3-dimethylaminopropyl)carbodiimide		
<b>EDTA</b>	ethylenediaminetetraacetic acid		
<b>ELISA</b>	enzyme-linked immunosorbent assay		
<b>FACS</b>	fluorescent assisted cell sorting		
<b>Fmoc</b>	9-fluorenylmethyloxycarbonyl		



<b>MHC-I (-II)</b>	major histocompatibility complex class I (class II)	<b>SBA</b>	soyabean agglutinin
<b>MMCCCH</b>	4-(4- <i>N</i> -maleimidomethyl)-cyclohexane-1-carbonyl hydrazide	<b>SEA</b>	sea urchin sperm protein enterokinase and agrin
<b>MUC1</b>	mucin 1	<b>SPPS</b>	solid phase peptide synthesis
<b>NCL</b>	native chemical ligation	<b>Sulfo-MBS</b>	<i>m</i> -maleimidobenzoyl- <i>N</i> -hydroxysulfosuccinimide ester
<b>NHS</b>	<i>N</i> -hydroxysuccinimide	<b>SUV</b>	small unilamellar vesicle
<b>NK</b>	natural killer cell	<b>TAA</b>	tumor associate antigen
<b>NKT</b>	natural killer T cell	<b>TACA</b>	tumor-associated carbohydrate antigen
<b>NMM</b>	<i>N</i> -methylmorpholine	<b>TASP</b>	template-assembled synthetic protein
<b>NMP</b>	<i>N</i> -methyl-2-pyrrolidone	<b>TCEP</b>	tris(2-carboxyethyl)phosphine
<b>NMR</b>	nuclear magnetic resonance	<b>TCR</b>	T cell receptor
<b>NOESY</b>	nuclear overhauser effect spectroscopy	<b>TCC</b>	thiol-ene coupling
<b>NPys</b>	3-nitro-2-pyridinesulfonyl	<b>TEC</b>	thiol-chloroacetyl coupling
<b>OL</b>	oxime ligation	<b>TEM</b>	transmission electron microscopy
<b>OSM</b>	desialylated ovine submaxillary mucin	<b>TFA</b>	trifluoroacetic acid
<b>OV</b>	oncolytic virus	<b>T<sub>H</sub></b>	helper T cells
<b>PAD</b>	pulsed amperometric detection	<b>THF</b>	tetrahydrofuran
<b>Pam<sub>3</sub>CS</b>	tripalmitoyl- <i>S</i> -glycerylcysteinylserine	<b>TIS</b>	triisopropylsilane
<b>PAMP</b>	pathogen-associated molecular pattern	<b>TMG</b>	1,1,3,3-tetramethylguanidine
<b>PBS</b>	phosphate buffer solution	<b>TMG<sup>®</sup></b>	TiterMAX <sup>®</sup> gold adjuvant
<b>PSA</b>	prostate-specific antigen	<b>TMSOTf</b>	trimethylsilyl trifluoromethanesulfonate
<b>PSM</b>	porcine submaxillary mucin	<b>TOCSY</b>	total correlation spectroscopy
<b>Pfb</b>	2,2,4,6,7-pentamethyldihydrobenzofuran-5-sulfonyl	<b>t<sub>R</sub></b>	retention time (minutes)
<b>Pmc</b>	2,2,5,7,8-pentamethylchroman-6-sulfonyl	<b>T<sub>REG</sub></b>	regulatory T cells
<b>PV</b>	polio virus	<b>Trt</b>	trityl
<b>PD-1</b>	programmed cell death protein 1	<b>TSE</b>	trimethylsilylethyl
<b>RAFT</b>	regioselectively addressable functionalized template	<b>TTox</b>	tetanus toxoid
<b>ROESY</b>	rotating frame overhauser effect spectroscopy	<b>UPLC</b>	ultra performance liquid chromatography (Waters Corp.)
<b>SAS</b>	Sigma adjuvant system	<b>VLP</b>	virus-like particle
		<b>VNTR</b>	variable number tandem repeat
		<b>ZPS</b>	zwitterionic polysaccharide

# **Chapter I.**

## **Introduction**

## I.1. Overview of immune responses

Before presenting my research project, I will start with some fundamental reminders concerning general aspects of the immune system and its responses.

The immune system is commonly conceived as the set of cells and molecules which participate to a concerted and tuned response against foreign substances, through a process called the immune response. These foreign substances encompass microbes as well as macromolecules (*e.g.* proteins, polysaccharides) and small chemicals, which are perceived through molecular recognition events as “non-self”.

The entities which are subject to recognition processes by the immune system’s cell repertoire are called *antigens* (Ags), while the antigen’s domain which is recognized by immune-system’s surface receptors and molecules is referred as *epitope* (or *antigenic determinant*). Antigen recognition events constitutively occur in the context of the immune system, whose constant surveillance ensures a proficient discrimination between “self” and “non-self” entities. Antigens that succeed in stimulating an immune response are indicated as *immunogens*. Under certain circumstances also “self” antigens can act as immunogens, leading to so-called *autoimmune responses*.<sup>1</sup>

Immunology studies the events triggered by the encounter of self- and non-self-antigens with cells and proteins of the immuno-repertoire, investigating their physiological and pathological consequences. More than 200 years after the first Jenner’s successful vaccination, immunology achieved outstanding results against common infectious diseases, and strongly improved the understanding of the human immune system thanks to techniques involving cell culture, immunochemistry, x-ray crystallography, recombinant DNA and genetically altered animals.<sup>2-5</sup> Immunity mechanisms and its principal “actors” will be next described.

### I.1.1. Innate immunity

Innate (also referred as *natural* or *native*) immunity operates in the early stage of immune response by means of already existing mechanisms, which are reproduced every time the same kind of immunogen comes into play. As a consequence of pathogen pressures during evolution, innate responses are directed against antigen motifs that are shared across groups of pathogens, and may fail to result specific. For example, lipopolysaccharides (LPS), lipoproteins, peptidoglycan and lipoteichoic acids (LTAs) are molecules produced by bacteria but not by eukaryotic cells. They represent molecular

signatures of microbial invaders which recognition can signal the presence of infection. Because of the conservation of these recognition elements in the innate immunity, they are referred as pathogen-associated molecular patterns (PAMPs), and their recognition is entrusted to a variegated class of “primitive” receptors, called pattern recognition receptors (PRRs). Epithelial barriers, phagocytic cells (neutrophils, macrophages), dendritic cells (DCs), natural killer cells (NK), innate lymphoid cells and blood proteins (natural antibodies, complement system members ...) can be ascribed among the components of innate immunity, which represent the first barrier against microbes and play the fundamental role of antigen presenting cells (APCs, *e.g.* DCs, macrophages) (Figure 1).

### **I.1.2. Adaptive immunity**

Alongside this type of immunity, which had its origins in early eukaryotes, vertebrates developed other immune responses with increasing magnitude and defensive abilities upon repeated exposures to immunogens. The so-called adaptive (also referred as *specific* or *acquired*) immunity allows the recognition and reaction towards a large variety of microbial and non-microbial substances (*diversity*), with an improved ability to discriminate between different substance (*specificity*) and a *memory* effect, which enables a strengthened response upon subsequent encounters with the same microbe. The cellular components of adaptive immunity are B- and T- lymphocytes. Cytokines are referred to a large group of secreted proteins with different structures and functions, they also regulate and coordinate the crosstalk between innate and adaptive immunity. Indeed, the host defense system integrates innate and adaptive responses in a cooperative fashion, in which mechanisms of innate immunity can trigger and influence adaptive responses (Figure 1).<sup>6</sup>

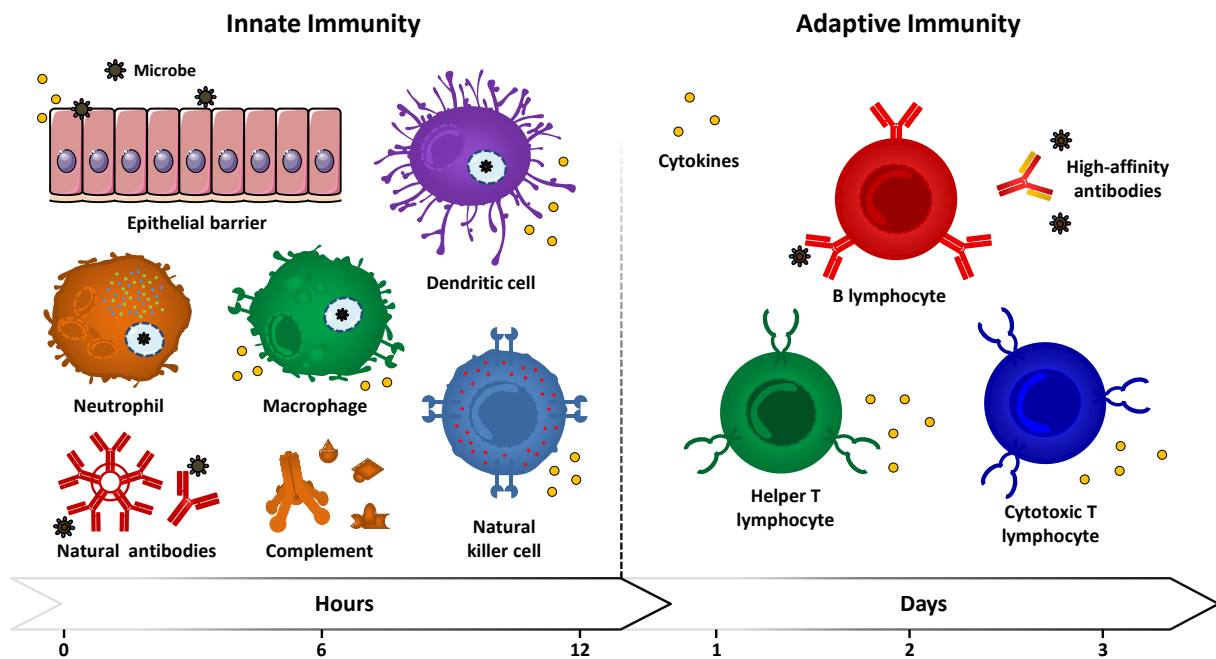


**Figure 1.** Components of innate and adaptive immunity. Innate immunity mechanisms represent the first barrier against infection; development of adaptive responses requires cross-talking events between these two types of immunity (*vide infra*).

### I.1.3. Passive/active immunity

The process whereby an individual mounts a protective immune response, as a consequence of the exposure to a microbe, is referred to as *active immunity*. Individuals and lymphocytes evolve from a *naïve* state, as they never encountered an antigen (they are immunologically inexperienced), to build an appropriate immuno-mediated response that, if successful, brings the individual to be *immune* towards the microbe threat. The activation of lymphocytes produces long-lived memory cells, which can survive for years after their generation. Those cells are more effective than *naïve* cells when the same “threat” is presented again, hence individuals are said to be *immune*.

However, through a process called *adoptive transfer*, immunity can be temporarily conferred to a subject by transferring serum or lymphocytes from a specifically immunized individual: in this case the immunity is referred to as *passive*. This event occurs physiologically, for example by the transfer of maternal antibodies to the fetus. Nevertheless, passive immunity lacks the possibility to generate immunologic memory, and therefore does not prepare the immune system for a second encounter with the same pathogen. In a clinical context, passive immunization against toxins by administration of Abs from immunized animals represented a lifesaving treatment; the adoptive transfer technique

also improved the understanding of the set of cells and molecules responsible for mediating adaptive immunity.<sup>7,8</sup>

### I.1.4. Humoral adaptive immune responses

Humoral and cellular (or *cell-mediated*) adaptive responses are described by the different components involved in the immuno-mediated clearance of pathogens such as, microbes, toxins, infected cells or cancer cells. Humoral immunity exercises its functions by means of molecules found in the bloodstream and mucosal secretions, called *antibodies* (Abs) or *immunoglobulins* (Igs).

**Antibodies** bind to antigens, and the resulting complex is able to prevent their interaction with

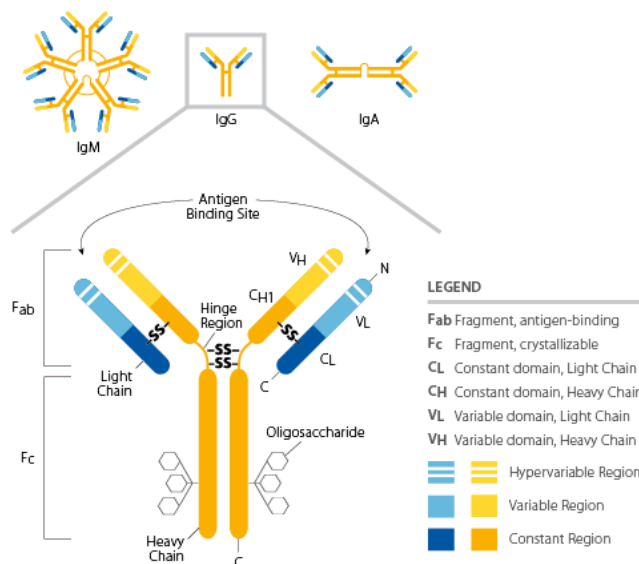


**Figure 2.** Structure of secreted antibodies

host receptors or trigger subsequent effector mechanisms. These glycoproteins are secreted by cells of the B lymphocyte lineage (plasma cells), or they can be found as membrane-bound receptors on B cells. All antibody molecules have common structural features, but display significant variability in the regions that bind antigens ( $F_{ab}$ ). Their structure is symmetrical, composed of two identical light chains and heavy chains. Heavy and light chains possess amino-terminal variable domains that are involved in the antigen recognition, and carboxy-terminal constant domains ( $F_c$  region) which mediate effector functions (Figure 2). Heavy and light chains, as well as the two heavy chains are covalently linked together by disulfide bonds in the constant regions; non-covalent interactions may also contribute to the heavy chain pairing. The presence of glycosylation patterns, especially in the  $F_c$  domain, play roles in structural conformation and during the interaction between  $F_c$  and their receptors.<sup>9-11</sup>

The antibody-mediated neutralization of microbes and toxins can be carried out by preventing their binding to cell surface receptors, thus avoiding infection processes or toxin-mediated pathologic effects (Figure 3a).

The complement system, composed by serum and cell surface proteins, whose highly regulated interaction lead to microbe elimination, can be activated through the interaction of C1 protein with two or more F<sub>c</sub> regions of antibodies bound to surface antigens (Figure 3b). The complement cascade activation culminates with the formation of several membrane attack complexes (MAC), which allow the free movement of water and ions across the membrane, causing osmotic swelling and cell rupture: this mechanism is referred to *complement-dependent cytotoxicity* (CDC).

Antibodies coating a microbe can interact through their F<sub>c</sub> portion with surface receptors (F<sub>c</sub>γRI) which belong to phagocytic cells, such as macrophages (Figure 3c). The signal transduction following the F<sub>c</sub> interaction promotes phagocytosis and killing of the microbes, through a process called *antibody-dependent cellular phagocytosis* (ADCP).

Antibodies coating surface antigen-expressing cells can also interact with F<sub>c</sub> receptors of natural killer (NK) cells (F<sub>c</sub>γRIII), provoking the liberation of cytolytic granules; this process is referred as *antibody-dependent cellular cytotoxicity* (ADCC) (Figure 3d).

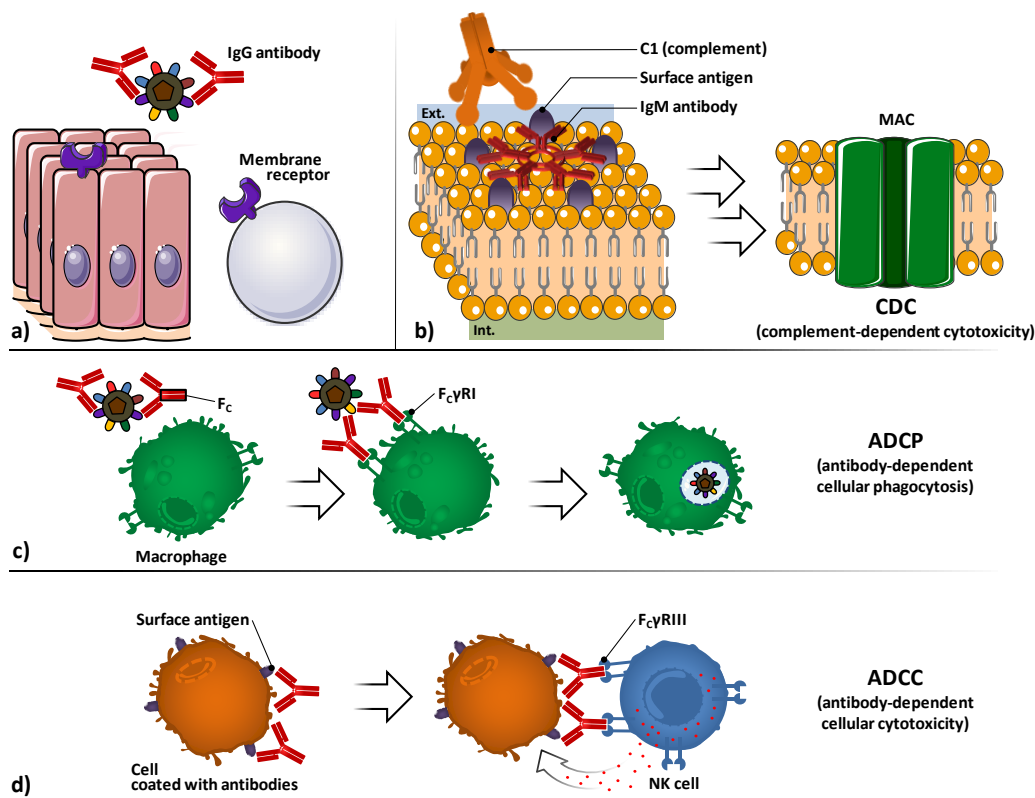



**Figure 3.** Principal effector mechanisms mediated by antibodies. a) Antibody-mediated neutralization of micro-organisms and toxins. b) Complement-dependent cytotoxicity. c) Antibody-dependent cellular phagocytosis. d) Antibody-dependent cellular cytotoxicity.

Secreted antibodies represent the principal defense against extracellular microbes and their toxins (Table 1). In addition to Ag-specific antibodies that are produced during the adaptive response, a pool of spontaneously occurring Abs is present in healthy individuals.<sup>12</sup> The antibody production of a

healthy, adult human is around 2-3 g per day, of which, almost two thirds is composed of the IgA class, found primarily in glandular secretions. IgM is the first class secreted after the antigen encounter, their concentration declines as IgG production accelerates. IgE are involved in immediate hypersensitivity reactions and defense against helminthic parasites. IgD are found as surface receptor in naïve B cells. IgG antibodies are the most effective in mediating phagocytic and cytotoxic effector mechanisms; moreover their serum half-life is remarkably higher than other classes (Table 1).

Each Ig class member is associated to different effector function, depending on its F<sub>c</sub> portion.<sup>13</sup> For example, in the early phase of the humoral response the majority of antibodies is represented by IgM isotype, lacking the support of ADCC and ADCP. A key aspect of B cells relies on their ability to tune their isotype secretion and produce mainly IgG antibodies, following a process known as *isotype switching (vide infra)*.<sup>14,15</sup>

Variations in the F<sub>ab</sub> region are related to the affinity of the interaction with the antigen. The Ab-Ag recognition process involves a non-covalent, reversible binding. The strength of the binding between the antibody and the antigen's epitope is referred as *affinity*, commonly represented by a dissociation constant ( $K_d$ , expressed in mol·L<sup>-1</sup> = M). Following the process known as *affinity maturation (vide infra)*, antibodies can undergo somatic mutations in their F<sub>ab</sub> portions, and raise their affinity towards the epitope from an initial value of  $k_d = 10^{-7} - 10^{-9}$  M to  $K_d$  values even smaller than  $10^{-11}$  M.<sup>16</sup>



Class	IgG <sub>1</sub>	IgG <sub>2</sub>	IgG <sub>3</sub>	IgG <sub>4</sub>	IgM	IgA	IgD	IgE
CDC	++	+	+++	-	+	+	-	-
ADCP	++	±	++	+	-	+	-	-
ADCC	++	-	++	-	-	-	-	-
Serum conc. (mg/mL)	13.5				1.5	3.5	traces	0.05
Half-life (days)	23				5	6	3	2
Secreted form	Monomer				Pentamer	Dimer	-	Monomer
Binding sites	2				10	4	2	2
M.W. (Da)	150000				900000	385000	180000	200000
% in plasma	75-85%				5-10%	10-15%	0.001%	0.001%

**Table 1.** Human antibody isotypes.



Lymphocytes are the set of cells able to specifically recognize and respond to foreign antigens, and are involved both in humoral and cellular immunity. They develop from bone marrow stem cells, mature in the generative lymphoid organs (bone marrow for B cells and thymus for T cells), and then circulate through the secondary lymphoid organs (lymph nodes, tonsils, spleen, Peyer's patches and mucosa-associated lymphoid tissue: MALT). Naïve lymphocytes are functionally quiescent, but if activated by antigens they proliferate and undergo through dramatic changes in phenotype and functional activity. They can be divided in different populations depending on their functions and receptors.

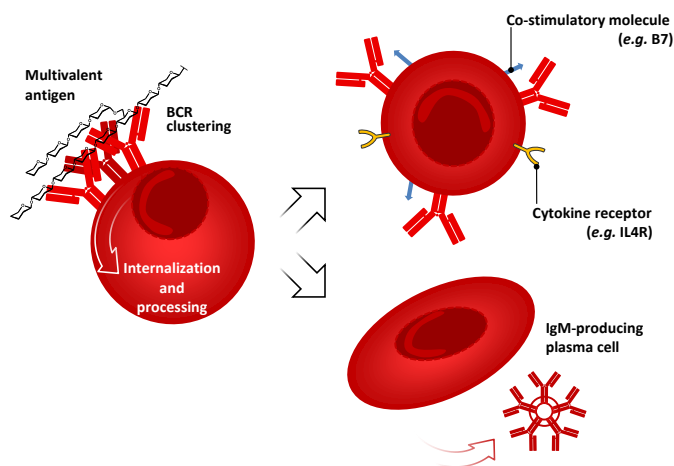


**Figure 4.** Functional activation of B cells by BCR clustering.

As well as on inputs from cytokines (*i.e.* BAFF: B-cell activating factor of the TNF family). As we anticipated earlier, antibodies found on the surface of B cells (*i.e.* IgD, IgM) serve as receptor for the internalization of antigens (BCRs). The consequences of signaling by the BCR complex for the following responses of B cells vary with the nature of the antigen and co-stimulatory events (*e.g.* complement activation, PRRs triggering).<sup>17,18</sup> *Antibodies and BCRs can recognize as antigens almost every kind of biologic molecule*, including simple intermediary metabolites, sugars, lipids and hormones, as well as macromolecules such as complex polysaccharides, phospholipids, nucleic acids and proteins. Antigens bearing multiple copies of a particular determinant interact with an overall strength that is greater than the sum of the single interactions; this phenomenon is broadly referred as *avidity* or *multivalency effect*. Multivalent antigens like polysaccharides can effectively cross-link many BCRs, causing their internalization and processing, and activating a series of mechanisms which culminates in B cell proliferation, expression of co-stimulatory membrane molecules and cytokine's receptors (Figure 4).

This kind of response, so-called "T-independent" (*vide infra*), does not lead to *affinity maturation* and generally results in the production of IgM antibodies and short-living plasma cells (Figure 4). In contrast, many globular protein antigens possess only one copy of each epitope per

### **B lymphocytes** (naïve B cells)

leave the bone marrow and complete their maturation in secondary lymphoid organs, where they may encounter foreign antigens or return to blood and recirculate. The main functions of B cells are production of antibodies, and they also act as APCs through recognition, internalization and processing of antigens. Survival of B cells is dictated by signals from B cell receptors (BCRs) as

molecule, therefore limiting their ability of BCR cross-linking. Intriguingly, the humoral response of B-cells can be tuned by another subset of lymphocytes (T-helper cells, *vide infra*).

### I.1.5. Cellular adaptive immune responses

Cellular immunity is mediated by T lymphocytes (T cells). Intracellular microbes (*eg.* viruses) which are able to survive and proliferate inside phagocytes, are not accessible to circulating antibodies; the evolutionary function of this type of adaptive response is meant to eradicate reservoirs of infection. Some T-cells also contribute to the clearance of extracellular microbes by recruiting effector leukocytes and by helping B cells to produce more effective antibodies. They can also respond by promoting phagocytosis or directly killing targeted cells.

A fundamental difference from B lymphocytes is that *T cells aren't able to recognize antigens in their native form*: they recognize peptides derived from processed proteins, which are presented upon host proteins called major histocompatibility complex (MHC). T cells are divided in four distinct populations: helper T-cells ( $T_H$ ), cytotoxic T lymphocytes (CTLs), regulatory T cells ( $T_{REG}$ ) and a small population called natural killer T cells (NKT).

$T_H$  cells are involved in several innate and adaptive cellular responses: following interaction with antigen presenting cells (APCs), they are able to induce proliferation and differentiation of themselves, B cells, macrophages and other leukocytes through secretion of stimulatory cytokines (*e.g.* IL-2). They are also indicated as  $CD4^+$ , as their coreceptor for the interaction between T cell receptor (TCR) and the complex antigen-MHC class II protein (Figure 5).

**CTLs** destroy cells exposing peptide antigens in association with MHC class I

proteins; because of the coreceptor associated to their TCR they are also called  $CD8^+$  (Figure 5).<sup>19</sup>

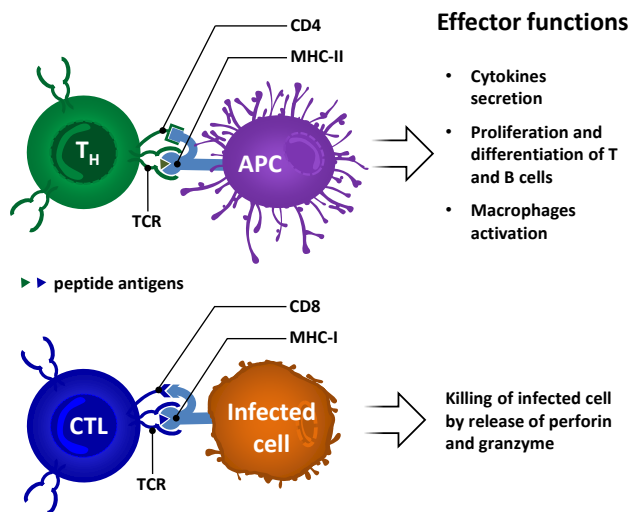


**Figure 5.** Effector functions of  $T_H$  (T helper) cells and CTLs (cytotoxic T cells) require the interaction with peptide antigens associated to MHC class I or II (major histocompatibility complex) molecules and involve coreceptors such CD8 or CD4, respectively.

$T_{REG}$  cells modify their down-regulating activity towards effector T cells to maintain tolerance towards self-antigens and avoid over-reaction situations.

**NKT cells** express invariant TCRs and other markers related to NK cells; unlike classical T cells they do not interact with MHC complexes, and show the ability to recognize lipids and glycolipids (*e.g.*  $\alpha$ -galactosylceramide). This still not well-known subpopulation is thought to modulate immunity in a broad spectrum of diseases, although NKT cells numbers vary substantially across individuals.<sup>20,21</sup>

### I.1.6. Antigen presentation

Although innate immunity reactions involve effective mechanisms able to control and even eradicate threats such as infections (not discussed in the present manuscript), many pathogens and transformed cells resist to innate immunity. We therefore focused our attention towards those factors which allow triggering more competent adaptive immune responses.

As discussed earlier, the three main mechanisms of adaptive immune response enclose: (i) secretion of Abs with increased affinity and efficacy towards the antigen of interest; (ii) enhancement of phagocytes activity; (iii) direct destruction of compromised cells.

*The first step to stimulate adaptive responses requires the proper capture, processing and display of antigens to lymphocytes by antigen-presenting cells (APCs).* Dendritic cells (DCs) represent the most specialized cell type in this regard: they capture antigens from external environment to present them, in the secondary lymphoid organs, to naïve T cells. Other cells type can act as APCs at

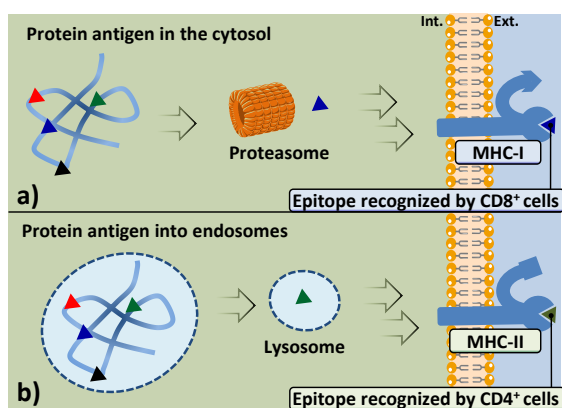


**Figure 6.** Pathways of protein antigens processing and presentation. a) MHC-I pathway. b) MHC-II pathway. It is noteworthy to observe that if the same protein undergoes through different pathways, the resulting MHC-associated peptide epitope may be different in terms of peptide sequence.

different stages of immune response (*e.g.* macrophages and B cells). The capture of microbes and subsequent digestion of their proteins is followed by the surface expression of microbial peptides ( $\approx 10$  amino acid residues) in association with MHC molecules. The antigen processing mechanisms are arranged to generate peptide fragments which are suitable for their co-expression with MHC molecules at the cell surface.

Protein antigens present in the cytosol, usually synthesized in the cell, give rise to class-I associated peptides (Figure 6a). Peptide epitopes

are obtained through proteasome-mediated degradation, in the cytosol. The abovementioned pathway occurs in all nucleated cells, indeed, protein molecules belonging to host phenotype (also those derived from viral transfection or mutations) are continually synthesized and degraded. The MHC-presentation of both self- and non-self-antigens allows the immune system to prevent the targeting of its own cells, and the recognition of infected or mutated cells. The epitopes obtained from the MHC-I pathway will interact with CD8-expressing lymphocytes.

Antigens which undergo internalization from extracellular environment through vesicles of APCs are generally processed in endo-lysosomes; this pathway leads to the expression of peptide epitopes on MHC-II molecules, which are recognized by CD4<sup>+</sup> cells (Figure 6b). Antigen-presenting cells such as macrophages, but especially DCs, express several surface receptors (PRRs) that are able to recognize structures shared by many pathogens (PAMPs); these receptors can efficiently bind and internalize a large variety of antigens, thus promoting their class-II MHC presentation. B cell receptors (BCRs) also represent an example of surface receptor able to bind a broad array of antigens with high affinity, causing their internalization, processing and expression through MHC-II complexes; therefore B cells can also be ascribed among APCs.

DCs carry the antigenic cargo to draining lymph nodes, where naïve T cells recirculate, increasing the probability of their interaction. According to the clonal selection hypothesis,<sup>22</sup> even before exposure to antigens, there is a large number of lymphocytes with different specificities for a panel of antigens in secondary lymphoid organs; each lymphocyte (and its progeny) with a common specificity is referred as a clone. Upon maturation, the expansion of the clones that better interact with the antigen is observed, increasing the magnitude of action and the effectiveness of the response.

### **I.1.7. Interplay between innate and adaptive systems**

As mentioned above, T-cell's functions are dependent on their physical interaction with other cells: they need to recognize antigens associated with MHC molecules upon the cell surface. However, the modulation of the signal is dictated by secondary interactions involving molecules induced in APCs as the consequence of a previous antigen encounter (*co-stimulators*), and by the signalling of secreted cytokines. These features ensure the adaptability and the amplification of the adaptive immune response. The expression profile of co-stimulatory molecules in resting APCs is limited, thus they cannot efficiently stimulate naïve T lymphocytes. During the innate immune response, following antigens internalization and cytokines release, APCs produce co-stimulatory molecules such as B7: this

represents a valuable example of how innate immunity can boost adaptive responses. In addition, T lymphocytes interaction with DCs, can amplify responses through a positive feedback mechanism which involves co-stimulatory protein expression.

### I.1.8. T<sub>H</sub> cell activation and licensing

The first event in helper T-cell activation involves DC-mediated antigen recognition (with or without B7), which causes the expression of co-stimulatory CD40L on T<sub>H</sub> cells (Figure 7a). The binding of CD40L to CD40 increases the expression of B7 in DCs and stimulates cytokine secretion (*e.g.* IL-12). This causes the activation of T<sub>H</sub> proliferation and differentiation, and increases the expression profile of co-stimulatory B7, improving DC's antigen presentation (Figure 7b-c). The phenomenon whereby activated T lymphocytes make APCs more powerful stimulators of immune responses is referred as *licensing*.

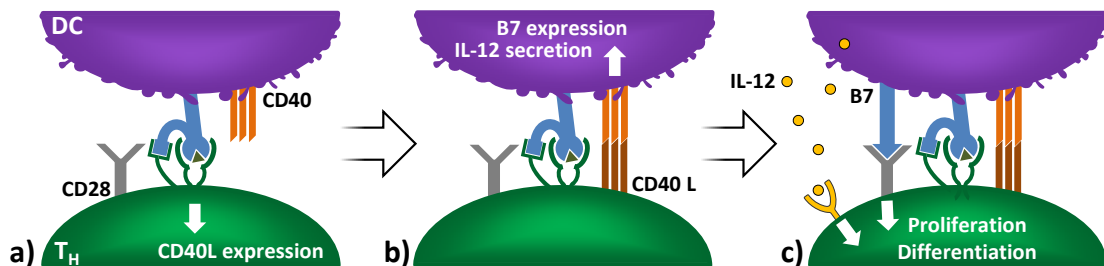


**Figure 7.** T<sub>H</sub> cell activation mechanism involves co-stimulatory molecules and second signals. Various receptors homologous to CD28 and their ligands homologous of B7 have been identified; these proteins regulate T cell response both positively and negatively and the outcome will depend on the balance between activating and inhibitory signals.

### I.1.9. CTL activation

Class I MHC pathway involves the processing of proteic antigens found in the cytosol (Figure 6a). Dendritic cells are able to capture and digest cells infected by virus or even tumor cells, and present their antigens in association with MHC-I molecules to CD8<sup>+</sup> cells. This process is referred as *cross-presentation*, while the deletion of autoreactive CTLs is termed *cross-tolerance*. Although it seems to breach the rule that ingested antigens are presented bound to MHC-II molecules, in this case, the ingested

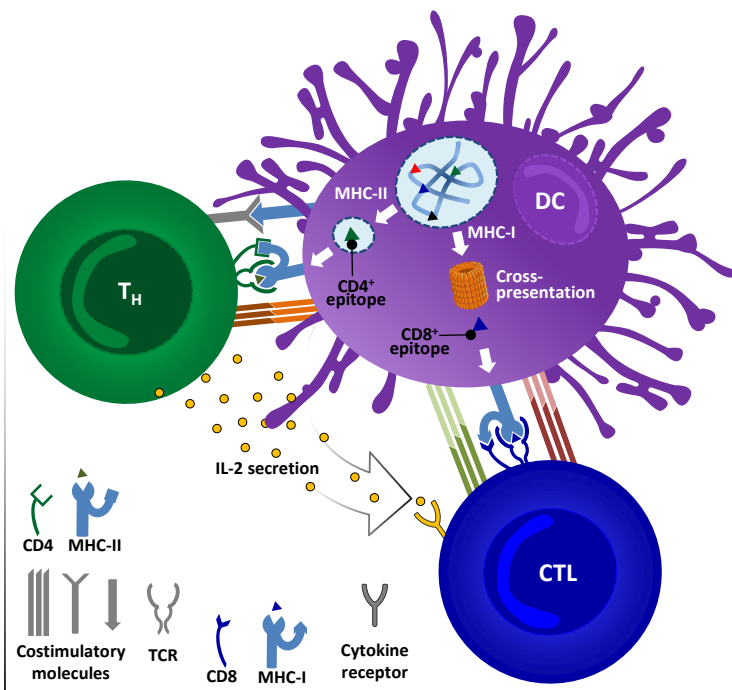


**Figure 8.** DCs take up antigens by distinct endocytosis mechanisms (not shown). Antigens are presented to CD4<sup>+</sup> cells through MHC-II complex and cross-presented to CD8<sup>+</sup> cells by MHC-I.

antigens are degraded in proteasomes and follow the class I pathway (Figure 8). The complete activation of naïve CD8<sup>+</sup> lymphocytes and their differentiation to functional CTLs and memory cells may require the participation of T<sub>H</sub> cells, which provide second signals such as co-stimulatory proteins expression and cytokine production. In the context of an acute innate response to a microbe, or if APCs are directly infected, the involvement of T<sub>H</sub> may not be necessary. The intervention of CD4<sup>+</sup> helper T cells may be required for CD8<sup>+</sup> CTLs in the setting of latent viral infections, organ transplants, and tumors, all of which have the tendency to elicit weak innate immune reactions. T<sub>H</sub> cells may indirectly promote CD8<sup>+</sup> T cell activation by licensing dendritic cells, increasing their co-stimulatory protein expression and enhancing their capacity to stimulate CTL differentiation (*vide supra*). Through a direct interaction involving CD4<sup>+</sup> T<sub>H</sub> cells, DCs and CD8<sup>+</sup> CTLs, the production of interleukin-2 (IL-2) by helper T cells stimulates the differentiation of CTLs and the production of memory CD8<sup>+</sup> T cells (Figure 8). The direct participation of T<sub>H</sub> cells can also be beneficial in enhancing the cross-presentation process.<sup>23</sup> For example, tumours contain thousands of potentially immunogenic neo-antigens caused by mutations.<sup>24</sup> Although, the occurrence of cross-tolerance have been reported on some tumor models, while in others, CTL responses resulted weak and localized in the lymph nodes.<sup>25,26</sup>

### I.1.10. B-cell activation

Antigens are presented generally in its intact form to naïve B cells through BCRs, as mentioned before this represents a fundamental distinction between B and T cells. Antigen-mediated crosslinking of BCRs by T-cell independent antigens like polysaccharides and glycolipids, which normally display multiple identical epitopes, induces events such as proliferation, increased expression of costimulatory molecules and cytokine receptors (Figure 4). Proteic antigens, once internalized through BCRs, are processed inside the B cell and presented upon MHC II molecules. In the lymph nodes, DC-activated CD4<sup>+</sup> T<sub>H</sub> cells that express CD40L (Figure 7) can recognize the same antigen on MHC II of B cells and strongly activate their proliferation and differentiation in the germinal center, producing long-living Ab-secreting plasma cells and resting memory cells (Figure 9). B cell activation by T<sub>H</sub> cells also triggers *isotype switching*, by which IgM antibodies are replaced by the more effective IgG isotype, and *affinity maturation*, leading to a more specific population of antibodies.

Therefore, *T-dependent B-cells responses exploit at least two kinds of epitopes*: (i) a surface epitope of variable nature, which is recognized and internalized through BCRs; (ii) an internal linear peptide which undergoes the MHC II pathway and is recognized by effector CD4<sup>+</sup> cells. *The antibodies that are produced are specific for the surface epitopes recognized by BCRs, leading to a fine humoral response which is independent of the fact that T<sub>H</sub> cells recognize restricted epitopes* (linear epitopes of processed peptides). This principle is known as *hapten-carrier effect* and represents the basis for the development of *conjugate vaccines*: carbohydrate epitopes conjugated to proteins are recognized by BCRs, internalized and peptide epitopes resulting from the carrier protein are exposed through MHC II complexes, thus enabling T<sub>H</sub> cells to activate B cells, and to stimulate the production of high-affinity IgG Abs against the carbohydrate epitope itself. To stimulate an effective response, the hapten (*e.g.* saccharide epitope) and the carrier portion must be covalently linked rather than administered separately. The B-T<sub>H</sub> cells interaction is class II MHC restricted, so activated T<sub>H</sub> cells can only cooperate with B cells that present the same restricted antigen which was involved in the activation of naïve T cells. These last aspects will be further discussed along the manuscript.

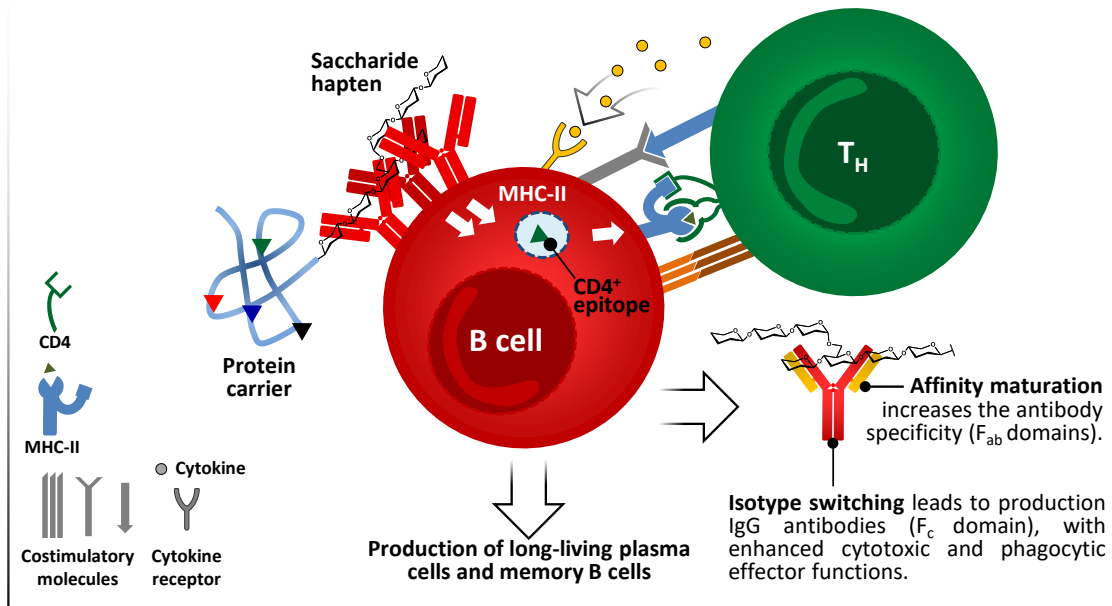


**Figure 9.**  $T_H$ -mediated B-cell activation following the administration of a conjugate vaccine composed of a saccharide hapten, linked to a carrier protein containing  $CD4^+$  epitopes.

### I.1.11. Overview of immune responses - Conclusions

In this section we outlined the main aspects of the immune response, to provide conceptual tools that are necessary to understand the rational basis of this work. A particular emphasis has been dedicated to the cardinal features of adaptive immune responses, which could be summarized as follows: (i) *Specificity* ensures the immune response to be directed against the targeted microbe/antigen; (ii) *Diversity* enables the spreading of the immune response towards a large variety of antigens; (iii) *Memory* increase the ability to fight relapses associated to the same antigen; (iv) *Clonal expansion* provides a larger number of antigen-specific lymphocytes; (v) *Specialization* generates clones with a more defined specificity for their antigen.

Stimulating an effective adaptive immune response requires the cross-talking of several cells and molecules of the immune system repertoire. The antigen capture, processing and presentation are the first important events, which can be ascribed in the innate setting; these mechanisms both trigger and maintain adaptive responses. The complete activation of lymphocytes is associated to increased specificity and effector mechanism efficacy, thanks to the production of specific cytotoxic T cells and IgG antibodies.

Mounting a proper adaptive immune response requires the orchestrated cooperation of several mechanisms; even though a comprehensive paradigm, which takes account of the multitude



of these mechanisms is far from being elucidated, progresses in immunology has improved and saved countless lives all over the world, and are of primary importance for their clinical value. One of the last challenges in immunology relies on the exploitation of the immune system mechanisms for the treatment of cancer disease.

## I.2. Anti-cancer immunotherapy

The essential cornerstones of cancer therapy have historically been surgery, radiotherapy, and chemotherapy. When disease is identified early, and tumor is small-sized and confined to a limited area, surgical resection of solid tumors still represents one of the most frequent local therapeutic choices. Nevertheless, large invasive tumors, most metastatic diseases and haematological malignancies are substantially unresectable. Radiotherapy represents another fundamental local therapy, mostly exploited to prevent tumor recurrence after surgery, and often synergistically employed with chemotherapy. Although these two last strategies demonstrated their validity and saved number of lives, the long list of adverse effect to which they associate and the need of an enhanced selectivity towards the cancer threat, justify researcher's involvement to find new tools for fighting against cancer. Moreover, it is now widely accepted that the better clinical results are obtained in multi-therapy settings.

Over the last years, the immunotherapy approach has been rising in popularity due to its promising capabilities.<sup>27</sup> In the broad sense of the term, cancer immunotherapy relies upon approaches that exploit the patient's immune system to promote the selective eradication of tumor cells. The first documentation in this field occurred in 1893, when William Coley demonstrated that bacterial products (Coley toxins) and other crude immunostimulants could be beneficial in some solid tumor.<sup>28,29</sup> From then on, it was necessary to wait until the 1970s for the spreading of this field, outlined by many approaches, involving tumor-specific monoclonal antibodies (mAbs),<sup>30</sup> antibody-drug conjugates,<sup>31</sup> cytokines (e.g. IFN- $\alpha$ , IL-2),<sup>32</sup> adoptive cell transfer (ACT),<sup>8</sup> oncolytic viruses (OVs),<sup>33</sup> cell-based vaccines (e.g. Provenge<sup>®</sup>),<sup>34</sup> and more.

Immunotherapy against cancer involves three principal strategies: (i) *Active immunotherapy* educates the patient's immune system to recognize tumor-associated antigens (TAAs) and rise an immune response in order to eliminate malignant cells; (ii) *Passive immunotherapy* uses exogenously produced components, such as lymphocytes or antibodies (Abs); (iii) *Immunomodulatory agents* enhance the immune responsiveness without targeting specific antigens.<sup>35-38</sup> The abovementioned categorization represents a useful conceptual draft, however, some overlapping in these categories can be found. In this research work, we sought to pursue the active immunotherapy strategy for the design of anticancer vaccines, a topic that has posed many challenges but have been driven by constant progress in the understanding of cancer immunology and tumor's microenvironment constitution.

Anti-cancer vaccines have been first conceived in a *therapeutic* setting, where they are meant to reverse a tumoral cell invasion which has already taken hold. In this regard, they differ from the general concept of *prophylactic* treatment, where vaccines are employed as a *prophylactic* treatment

to prevent, for example, an infectious disease. Anticancer vaccines have been proposed as innovative components in multi-therapy settings, to elicit or boost antitumor immunity in patients that formerly underwent surgical resection of a primary solid tumor, when classic treatments demonstrated ineffective or unsuitable for the patient. This approach can be beneficial in preventing and prolonging the time of recurrence at the metastatic sites, with a minimal toxicity compared to other cytotoxic treatments, such as chemo- or radio-therapy.<sup>39</sup> In this scenario, the first hurdle that therapeutic anticancer vaccines must face involves triggering an already embattled immune system, due to the immuno-compromised state of cancer patients, often worsened in case of elder people.

Malignant cells are always associated to a certain degree of mutations, giving rise to a panel of *cancer-related epitopes*. The immunosurveillance theory assumes that those mutations should trigger the immune system to promote the destruction of the cancer cells. Evidences that malignant tumor cells acquire the potency to evade on-going immune responses can be assessed by tumor-induced mechanisms involving: (i) reduced immune recognition, (ii) increased resistance towards immuno-mediated clearance, and (iii) creation of a immunosuppressive tumor microenvironment, thus delineating a perspective in which several aspects need to be taken in consideration to adequately address cancer disease in immunotherapy contextes.<sup>40,41</sup>

The current understanding of the immune response allowed to delineate some key aspects required to generate an effective immune response against TAAs (Figure 10). First, immunization with an anticancer vaccine can provide a powerful presentation of TAAs, which must be properly captured and processed by dendritic cells (DCs) (Figure 10a). Secondly, activation and/or maturation signals are required to allow DCs differentiation and migration to the lymph nodes, where they can present TAAs to naïve T cells through MHC-I or MHC-II molecules. In the absence of immunogenic maturation stimuli, DCs will instead induce tolerance, resulting in T-cell depletion, anergy or the production of regulatory T cells (T<sub>REG</sub>). Small-molecule inhibitors of immunosuppressive factors released by tumors can be used to promote DC maturation and enhance the antitumor activity (Figure 10b).<sup>42-44</sup> At the lymph node site, T cell expansion can be enhanced either by ACT (adoptive transfer of T cells specific for the TAA of interest)<sup>45</sup> or administration of immunomodulators, such as mAbs (acting as agonists of co-stimulatory proteins, *e.g.* CD40)<sup>46</sup> and cytokines (Figure 10c).<sup>47</sup> Finally, recent studies highlighted the clinical potential of checkpoint modifiers, able to prolong the cytotoxic T cell (CTL) activity by interfering with key immunosuppressive processes (Figure 10d).<sup>48</sup>

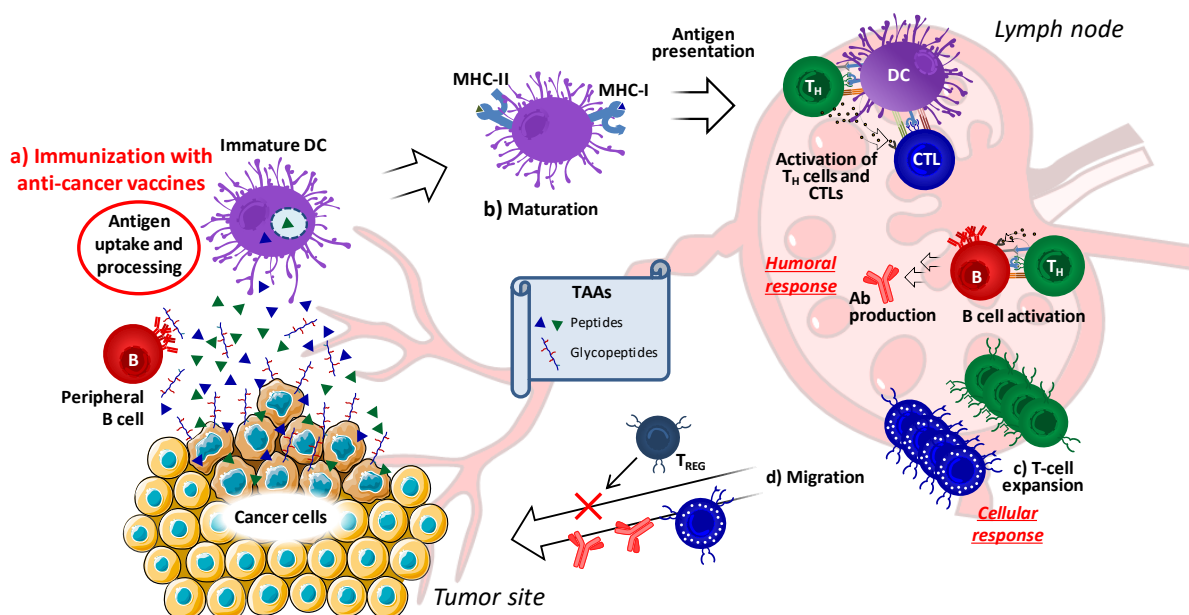


**Figure 10.** Principals steps for generating an effective cellular response against TAAs. Adapted from Melero *et. Al.* TAAs (tumor associated antigens); DC (dendritic cell); MHC-I/-II (major histocompatibility complex class-I / -II); TH (helper T cell); CTL (cytotoxic T lymphocytes); B (B lymphocytes); TREG (regulatory T cell).<sup>38</sup>

Clinical studies have experienced a better responsiveness among patients who have received less prior chemotherapy, suggesting that a lower tumor burden may imply an improved outcome.<sup>49,50</sup> Indeed, most phase I and II trials have been conducted so far in the late stage disease, and in the presence of a significant tumor burden after the failure of standard therapies. Intriguingly, it has also been suggested that many fundamental problems associated to the *therapeutic* effects of cancer vaccines, including the progressive development of heterogeneity in tumor related epitopes and the suppression or evasion to the immune response, could be overcome in the context of prevention, by priming the immune system to “anticipate” tumor antigens (in line with the common principle of *prophylactic* vaccination).<sup>51-53</sup>

Recent studies, whereby tumor grow rates and overall survival of patients were investigated, indicated that classical response criteria adopted for cytotoxic chemotherapies may not be adequate to assess clinical responses to vaccine therapy, highlighting the importance of adapting current diagnostic methodologies to better understand the impact of anticancer immunotherapies.<sup>54-56</sup> Even in the best-case scenario, the success of therapeutic and prophylactic anticancer vaccines will rely on researcher’s proficiency to face various challenges, which are not confined to the clinical context. Our approach to tackle anticancer immunotherapy belongs to an immunological chemistry context, where the design of anticancer vaccines requires a proper cross-talking between chemistry and biology.

### I.2.1. Tumor-associated antigens

The importance of choosing the right antigen to develop anticancer vaccines represents a first, important challenge, which also prompted the understanding towards other key aspects.

Following the achievements obtained by employing live attenuated pathogens vaccines, and because of the initial absence of defined *tumor-associated antigens* (TAAs), the first anticancer vaccines were constituted by whole tumor cells, previously inactivated.<sup>57</sup> As this approach was tested in models able to better mimic human tumors, its resulting weak or absent immunogenicity led immunologists to decipher additional co-stimulatory signals required to activate T cells.<sup>58,59</sup> In the case of whole tumor cell, TAAs are expected to be captured and processed along with auto-antigens. If activated DCs succeed in eliciting strong immune responses against the entire collection of epitopes, autoimmunity reactions will imply unwanted, detrimental and life-threatening consequences.<sup>60,61</sup> Moreover, the use of whole tumor cells, or complex mixtures of tumor-derived material, neutralizes the specificity of the vaccination approach.

A desirable immune response should promote the destruction of cancer cells, without harming normal tissue. Therefore, many efforts have been made to identify tumor-specific antigens, which have been used for the realization of cancer vaccines which demonstrated its ability to generate tumor-specific immunity and a memory effect, without giving rise to autoimmunity.<sup>62-64</sup> *Antigen-specific active immunization* represents a more adequate approach not only in terms of safety, but also regarding reproducibility and scale-up production. A variety of epitopes derived from mucin 1 (MUC1),<sup>65</sup> HER/NEU,<sup>66</sup> melanoma-associated antigen 3 (MAGE3),<sup>67</sup> and many others, have been already subjected to extensive studies. In principle, antigen-specific immunotherapies which exploit narrow epitope specificity might lead to a less effective immune response; on the other hand, many of these antigens fall within the category of *shared antigens*, enclosing molecules that are *expressed by many tumors and not normal tissues, or expressed also by normal tissues but in a different quantitative and qualitative manner (vide infra)*. Therefore, vaccines that include shared antigens can be envisaged for use in a large number of patients. Intriguingly, it has been shown in animal models and clinical trials that a vaccination against a single shared antigen is able to elicit an immune response which spreads towards other antigens on that tumor, a process known as *epitope spreading*.<sup>68-70</sup>

## I.2.2. MUC1 and tumor-associated carbohydrate antigens (TACAs)

Among the abundance of shared tumor associated antigens, many research groups focused their interest on carbohydrate antigens related to the glycoprotein MUC1.<sup>71</sup> This heavily glycosylated transmembrane protein is composed by two fragments: (i) a longer extracellular *N*-terminal subunit (*i.e.* MUC1-N, 250-500 kDa), featuring a tandem repeat region (VNTR: variable number tandem repeat) of multiple sequences of 20-21 amino acids, where serine and threonine (representing  $\approx$  40% of residues) constitute the anchorage sites for *O*-glycosylation; and (ii) a shorter transmembrane *C*-terminal subunit (17-25 kDa). The two domains associate through stable hydrogen bonds, at the extracellular portion of MUC1 *C*-terminal domain, which also represents its *N*-glycosylation region (Figure 11a). In healthy tissues, MUC1 is expressed in a large variety of glandular or luminal epithelial cells, its negatively charged sugar branches form a physical barrier with anti-adhesive and protective properties towards pathogens, changes in pH, desiccation and microbes.<sup>72-74</sup> The aberrantly glycosylated version of MUC1 can be found overexpressed in most human epithelial cancer;<sup>75</sup> it also represents a clinical marker for the detection of several types of cancer.<sup>76-78</sup> The deregulation of the glycosyl transferase (*e.g.*  $\beta$ 6-GlcNAc-transferase) machinery leads to hypoglycosylated, less polar structures which impact stability and localization of MUC1. One direct consequence of the cell polarity loss implies the redistribution of cell surface growth factors receptors (*e.g.* EGFR)<sup>79</sup>, normally located in the basolateral surface of epithelial cells, altering signal transduction and their local microenvironment (Figure 11b). Morphological and signaling modification of tumor-related MUC1, together with altered transcription of regulation genes, delineate the functional role in malignancy of this well-studied glycoprotein, which plays fundamental roles in phenomena such as tumor invasion, metastasis, angiogenesis, proliferation, apoptosis, drug resistance, inflammation and immune regulation.<sup>80-87</sup>

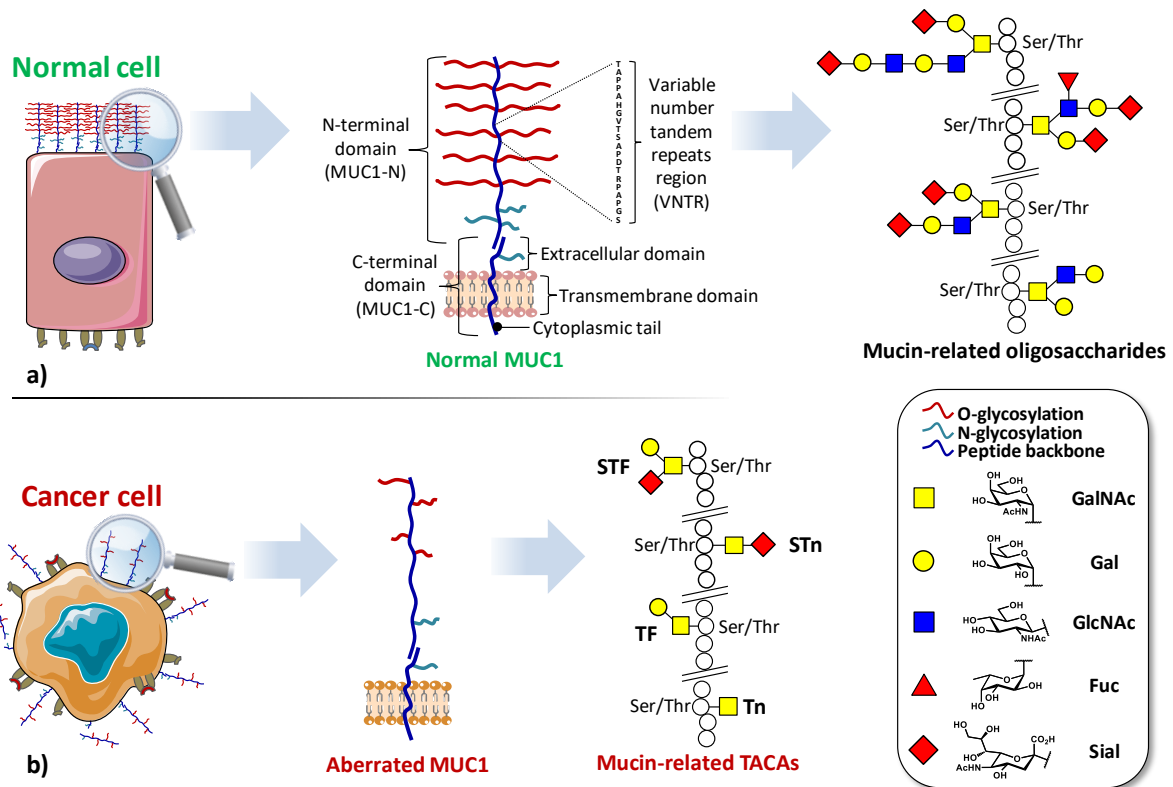


**Figure 11.** Normal (a), and aberrant (b) MUC1.

Aberrant MUC1 tandem repeats (Figure 11b) display truncated sequences at *O*-glycosylation sites, exposing saccharide epitopes that are normally hidden in “healthy” mucins. These mono- and oligosaccharides attached through  $\alpha$ -*O*-Ser/Thr linkages belong to a broader group, the so-called *tumor-associated carbohydrate antigens* (TACAs) (Figure 12).

TACAs are among the most widespread antigens detected on cancer cell surfaces, they are commonly overexpressed as glycolipids (*e.g.* gangliosides) or glycoproteins (*e.g.* mucins) across different tumor types (Table 2).<sup>88–90</sup> A natural, TACA-directed antibody response has been observed in some cancer patients.<sup>91</sup> The improvement in survival rate of these patients has been correlated with the presence of anti-TACA antibodies, reinforcing the persuading possibility that a correct TACA presentation to the human immune system could lead to an adaptive immune response, enabling the selective eradication of TACA-displaying tumor cells.<sup>12,92–95</sup>

Although TACAs are self-antigens, their inaccessibility and low expression on normal tissues represent the rationale for their utilization in anticancer vaccines design. Undertaking this route implies addressing chemical design strategies towards the conception of innovative vaccines. Before discussing in details the features that guided our research work, some fundamentals aspects related to the development of TACA-based anticancer vaccines will be examined.

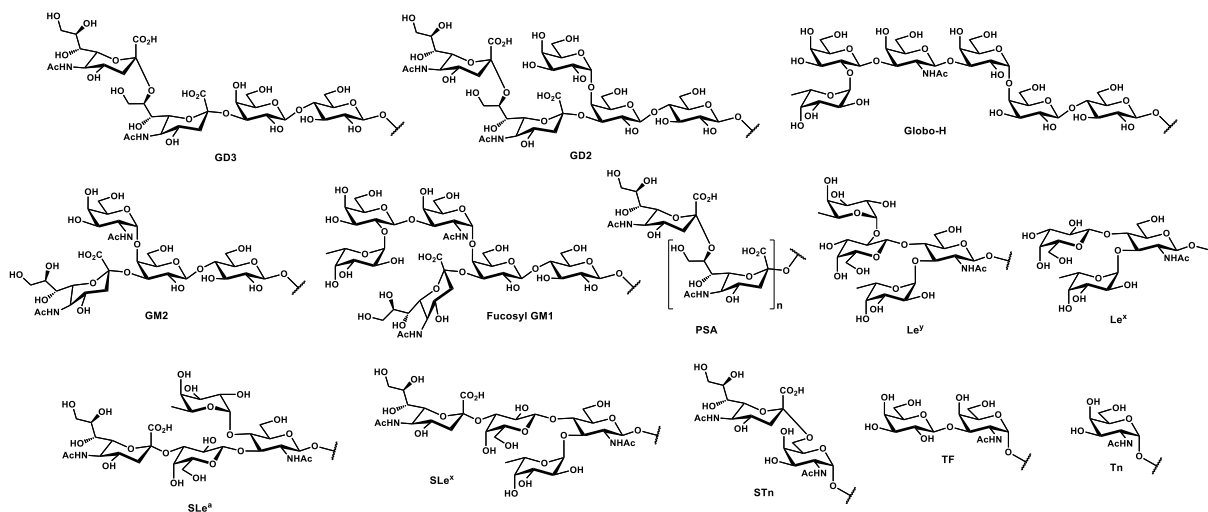


**Figure 12.** Common TACAs structures.

TACAs	Le <sup>x</sup>	SLe <sup>x</sup>	Le <sup>y</sup>	SLe <sup>a</sup>	Tn	TF	STn	Globo-H	PSA	Fucosyl GM1	GD2	GD3	GM2
B-cell lymphoma	-	-	-	-	-	-	-	-	-	-	✓	-	✓
Breast	-	-	✓	✓	✓	✓	✓	✓	-	-	-	-	✓
Colon	-	-	✓	✓	-	✓	✓	-	-	-	-	-	✓
Lung	-	✓	✓	-	-	-	✓	✓	-	-	-	-	✓
Melanoma	-	-	-	-	-	-	-	-	-	-	✓	✓	✓
Neuroblastoma	-	-	-	-	-	-	-	-	✓	-	✓	✓	✓
Ovary	-	-	✓	-	-	✓	✓	✓	-	-	-	-	✓
Prostate	-	-	✓	-	✓	✓	✓	-	-	-	-	-	✓
Sarcoma	-	-	-	-	-	-	-	-	-	-	✓	✓	✓
Small cell lung	-	-	-	✓	-	-	-	✓	✓	✓	-	-	✓
Stomach	✓	-	✓	✓	✓	✓	✓	✓	-	-	-	-	✓

**Table 2.** Expression profiles of TACAs on malignant tissues.



## **I.2.3. Key aspects related to TACA-based vaccines development**

### **I.2.3.1. Source of epitopes**

The isolation of TACAs from natural material represents an extremely arduous task; the first approaches in this field involved tedious and time-consuming operations to obtain the antigens of interest from highly heterogenic mixtures of sugar chains.<sup>96</sup> The recent advances in glycobiology and synthetic organic chemistry allowed overcoming this primary aspect, and enabled the production of structurally intact TACAs in sufficient quantities and high purities. Strategies such as automated solid-phase synthesis,<sup>97,98</sup> iterative one-pot synthesis,<sup>99,100</sup> glycal assembly,<sup>101</sup> and chemo-enzymatic synthesis<sup>102</sup> led scientist to reach complex arrays of glycans of biological interest with far less effort. These aspects will not be discussed in the present manuscript.

### **I.2.3.2. Protein-carbohydrate interactions**

Carbohydrates represent the most widespread class of biomolecules, they are ubiquitous in Nature: all cells, from prokaryotes to eukaryotes, are coated by a multifaceted array of glycans, called glycocalyx.<sup>103–105</sup> Carbohydrates can be found as components of both surface and secreted glycoproteins and glycolipids, which are involved in a large panel of key biological processes such as fertilization, implantation, pathogen invasion, immune system activation, cell proliferation, and so on.<sup>106–109</sup> Indeed, beyond their energetic (glycolysis) and structural (cell wall polysaccharides, nucleic acids backbone) functions, carbohydrates have been selected in nature to transmit biological information, which represent an essential activity for the cellular “social life”.

A distinctive feature of carbohydrate – protein receptor interactions rely on the *multivalency effect* associated to polyvalent saccharide epitopes; where *valence* (or *valency*) is referred as the number of distinct subunits which can interact with other systems. Most carbohydrate-binding proteins can associate to give *oligomeric* complexes able to interact either with multiple carbohydrate residues within a glycan or with multiple glycans on the cell surface (Figure 13). At the cellular surface, different mechanisms of interaction between carbohydrate-binding proteins and glycans can be described. Oligomeric proteins can interact with cell-surface glycans, even simultaneously with

different saccharide entities (Figure 13a,b). Soluble glycans or soluble proteins can interact with cell-surface proteins or glycans, respectively (Figure 13c,d). Signal transduction events can be triggered by clustering events induced by interactions between soluble proteins or soluble glycans with cell-surface glycans or proteins, respectively (Figure 13e,f).

In thermodynamic terms, multivalency provides an affinity enhancement that is greater than the sum of single contributions; this enhancement is also referred as *avidity*. Although it is widely accepted that multivalency allows functional activity enhancement of cell-surface carbohydrate-protein interactions, it is noteworthy mentioning the importance of polyvalent interactions in the context of signal modulation (nonlinear dependence of the signal strength) and specificity.<sup>110,111</sup> Non-covalent, reversible, multivalent interactions allow the immune repertoire to sense a vast panel of “glyco-signatures” with an efficiency that would be lost in a scenario dominated by individual, high-affinity interaction. In the last case, upon encounter between receptor and binding partner, multiple high affinity interactions would render binding irreversible; conversely, multivalent, low-affinity interactions allow the interaction to be reversible, thus for example, the same cell can interact through its receptors with a multitude of structures and even modulate the eventual signal transduction events.

As we mentioned earlier (Figure 4), antigen-dependent signaling requires the clustering of B cell receptors (BCRs). Recent studies, performed by Kiessling and co-workers, suggested a model whereby the clustering of ligand-bound BCRs and unbound BCRs provides the means of sensitivity through which B cells transmit antigen signals into outcomes that range from immune response to tolerance.<sup>112</sup> Accordingly, since protein-carbohydrate interactions are subjected to avidity effect, it is possible to mimic the so-called *cluster glycoside effect* by the chemical synthesis of multivalent structures grafted with carbohydrate units. These synthetic multivalent glycoconjugates are able to reproduce natural occurring interaction modalities, and offer the possibility to be tailored in terms of design, often giving rise to biologically relevant constructions.<sup>113–115</sup>

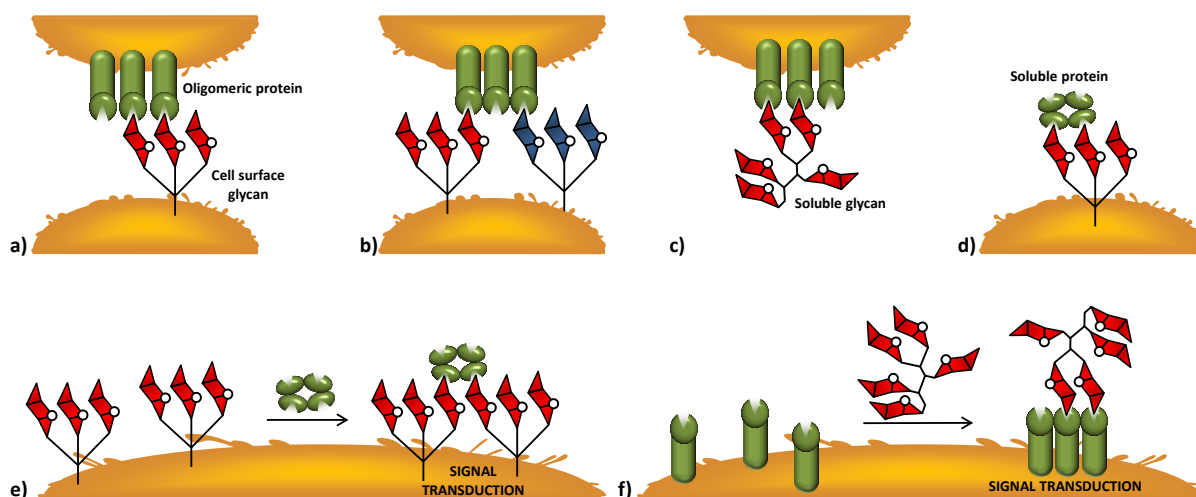


**Figure 13.** Different mechanisms of interaction between carbohydrate-binding proteins and glycans. a) Oligomeric protein interacting with individual cell-surface glycan. b) Simultaneous interactions with different cell-surface glycans. c) Oligomeric proteins interacting with soluble glycans. d) Cell-surface glycans interacting with soluble oligomeric protein. Signal transduction mediated by clustering of e) cell-surface glycans by soluble proteins, or d) cell-surface proteins by soluble glycans. Adapted from Kiessling and co-workers, *ACS Chem. Biol.* 2007.<sup>112</sup>

### I.2.3.3. Enabling TACA-directed humoral adaptive responses

In contrast to peptides and proteins, carbohydrate antigens alone fail to induce T-cell-mediated immunity because they are unable to associate with MHC molecules. Therefore, the administration of TACAs alone can only weakly activate B cells, resulting in production of low-affinity IgM and short-living plasma cells (Figure 4).<sup>116</sup> In order to induce B cells to produce specific IgG antibodies, the BCR clustering event must be followed by cytokine signaling (*i.e.* IL-4 and, to a lesser extent IL-13 and IL-10) from activated helper T cells.<sup>117</sup> In carbohydrate-based vaccine design, a valid and well established method to achieve the full activation of B cells and trigger adaptive responses such as isotype switching, affinity maturation and production of long-living plasma cells and memory B cells, consists in associating the saccharide moiety with a protein carrier (*hapten-carrier effect*), which operates as source of CD4<sup>+</sup> epitopes (Figure 9).

As introduced in section I.1.2. (*Adaptive immunity*), the benefit of obtaining memory B lymphocytes relies on their rapid production of IgG antibodies following a second encounter with the antigen, highlighting the fundamental role of T<sub>H</sub> cells for the achievement of a long-lasting humoral adaptive response.<sup>118</sup>

The inherent low immunogenicity of carbohydrate antigens is even more important in TACAs as they are self-antigens; therefore immunotolerance and immunosuppression are more easily

inducted. Indeed, a fundamental hurdle for the development of effective TACA-based vaccines involves breaking the immunotolerance to achieve the production of isotype-switched, IgG anti-TACA antibodies. Extraordinary efforts have been made to overcome these obstacles; extensive literature reports have given evidences that is possible to break immunotolerance by an accurate design, rising the interest of the scientific community towards anticancer vaccines.<sup>93,119–126</sup>

The following sections are focused on some representative, key examples in the domain of anticancer vaccines; with the aim to introduce the main design categories and the different strategies adopted for improving TACA-based anticancer vaccines.

### **I.3. Syntheses and immunological properties of TACA-based anticancer vaccines: an overview**

#### **I.3.1. Semi-synthetic approaches**

##### **I.3.1.1. Vaccines featuring protein-carriers**

Conjugating TACAs with protein carriers containing T cell epitopes represents an extensively used method for the construction of anticancer vaccines. Throughout the years, several kinds of proteins have been used, such as bovine serum albumin (BSA), human serum albumin (HSA), ovalbumin (OVA), tetanus toxoid (TTox), and keyhole limpet hemocyanin (KLH). TACA-based vaccines which use the protein-carrier approach can be classified in three main categories: (i) mono-TACA vaccines, containing one type of carbohydrate antigen, (ii) clustered mono-TACA vaccines, presenting one kind of TACA displayed in a clustered fashion, and (iii) hetero-TACA vaccines, displaying several types of saccharide antigens (Figure 14).

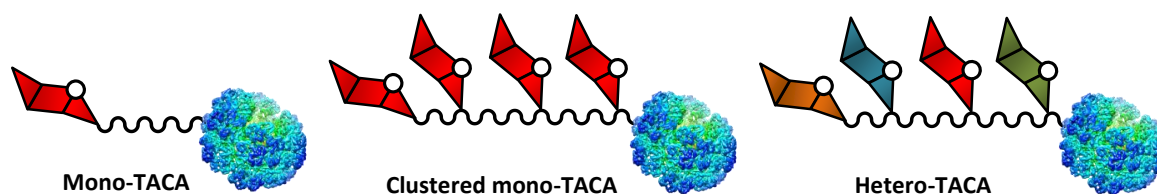
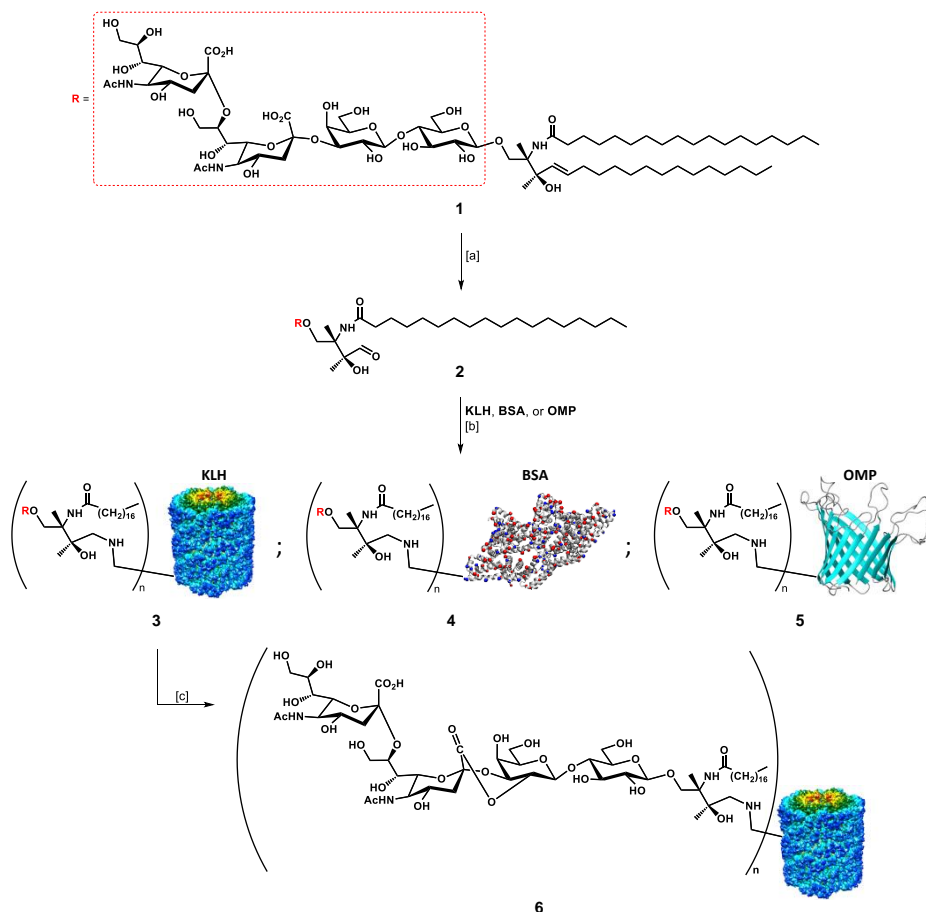


**Figure 14.** Different design strategies for semi-synthetic vaccines.

### **I.3.1.1.1. Mono-TACA vaccines based on protein-carriers**

As mentioned earlier, the first approaches for TACA-based vaccines relied on the utilization of extracted TACAs, in particular GD2, GD3, and GM2 (Figure 12).<sup>127</sup> Helling and co-workers first established that it was possible to stimulate an improved immune response in mice models by administration of a GD3 antigen covalently linked to a carrier protein, in the presence of an adjuvant.<sup>96</sup> Glycolipid GD3 **1**, extracted from bovine buttermilk, was selectively cleaved with ozone at C4-C5 double bond in the ceramide portion, in the presence of methylsulfide as reducing agent (Scheme 1). After RP-HPLC purification, GD3 **2** was incubated for 48 h at 37°C to react with amino groups of different carrier proteins (*i.e.* KLH, BSA, OMP: outer membrane protein complex of *Neisseria meningitidis*), in the presence of sodium cyanoborohydride to reduce the formed Schiff bases. The average yield of GD3 conjugate vaccines **3-5** was estimated with a colorimetric resorcinol-hydrochloric acid method at 30% for each protein.<sup>128</sup> The authors found that the utilization of keyhole limpet hemocyanin (KLH) as carrier protein, and QS-21 as adjuvant resulted in the best response, highlighting the importance of the “components” choice. Although this protocol allowed the production of anti-GD3 IgM and IgG antibodies in mice models, and these antibodies proved able to react *in vitro* with human melanoma GD3-expressing cells, it failed to induce antibody production in humans.<sup>129</sup> In an effort to increase the immunogenicity of the GD3 epitope, the same group chemically intervened on the GD3-KLH conjugate **3** to obtain the lactone form (GD3-L-KLH) (Scheme 1), which led to the production of specific anti-GD3-L antibodies. These Abs were able to cross-react with purified melanoma GD3, and melanoma cell surface GD3.<sup>130</sup> The authors suggested that the increased immunogenicity was due to low-level expression of GD3-L in normal tissues, which favoured its recognition by the immune system, or because of conformational features induced by the lactone moiety.<sup>131</sup> These findings revealed that modified TACAs were able to stimulate the production of antibodies capable to react with native TACAs.

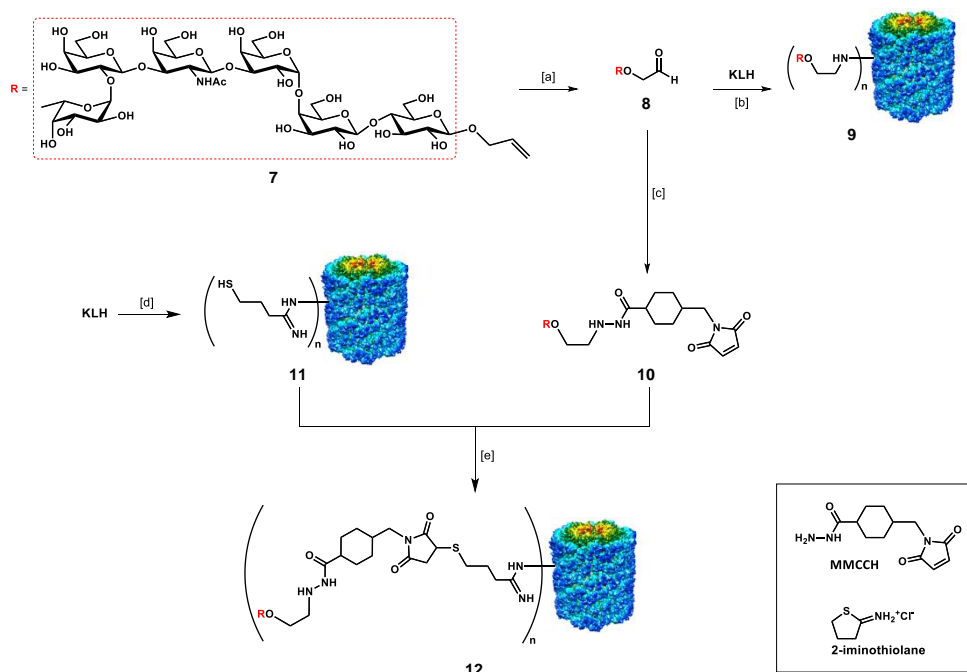


**Scheme 1.** Synthesis of GD3-protein conjugates. Conditions: [a] O<sub>3</sub>, MeOH, -78°C, 30 min., then CH<sub>3</sub>SH, -78°C for 30 min., then r.t. for 90 min. ; [b] PBS (pH 7.2), NaCNBH<sub>3</sub>, 37°C for 48 h. ; [c] CH<sub>3</sub>COOH, 37°C, 4 h, 80% conversion to lactone form. GD3:protein weight ratio is 0.69, 0.77 and 0.93 for **3**, **4** and **5**, respectively.

Danishefsky's research group represent one of the leading team in the field of semi-synthetic anticancer vaccines; over the years, the group have synthesized several TACA structures, including globo-H, Le<sup>x</sup>, Le<sup>y</sup>, MUC-1, Tn, TF, and more.<sup>132–139</sup> Advances in organic synthesis methodologies not only allowed the preparation of complex TACAs,<sup>96–101</sup> but also prompted the research towards new and more efficient bioconjugation chemistries, paving the way for the *semi-synthetic approach* towards anticancer vaccine design.<sup>140</sup>

The synthesis and evaluation of a globo-H-KLH conjugate vaccine by Danishefsky and co-workers represent an illustrative example in the context of semi-synthetic monomeric vaccines.<sup>141</sup> The modified globo H antigen **7** was prepared by total synthesis through the glycal assembly approach (Scheme 2).<sup>132</sup> The semi-synthetic construct with KLH was obtained by two different methods. The first method involved the reductive linkage of the aldehyde **8**, resulting from ozonolysis of the allyl moiety of **7**, to the amino groups of KLH. The conjugation ratio obtained for the resulting mono-TACA vaccine **9** was estimated around 373:1, in 7% yield. The second method involved the utilization of a 4-(4-*N*-maleimidomethyl)cyclohexane-1-carbonyl hydrazide bifunctional linker (MMCCH), which was reacted

with aldehyde **8** through reductive amination to give maleimidated globo-H **10**. KLH was treated with 2-iminothiolane, which converts amino groups to sulfhydryl groups, to afford thiolated KLH **11**. **10** and **11** were incubated for 2 h at room temperature to afford mono-TACA vaccine **12** through thiol-maleimide coupling, in 29% yield.<sup>142</sup> The authors reported an estimated conjugation ratio (*n*) of 732:1 for vaccine **12**. Vaccines **9** and **12** were administered to human patients with metastatic breast cancer, along with 100  $\mu\text{g}$  of QS-21. The generated IgM response was strong, independently of the conjugation strategy. Although, low IgG titers were observed. Nevertheless, vaccines **9** and **12** were well tolerated, and IgM antibodies able to react towards globo-H-positive tumor cells *via* CDC and ADCC.



**Scheme 2.** Synthesis of globo-H-protein conjugates. Conditions: [a] O<sub>3</sub>, MeOH, -78°C, 30 min., then CH<sub>3</sub>SH, -78°C for 10 min., r.t. for 120 min.; [b] PBS (pH 7.2), NaCNBH<sub>3</sub>, 37°C for 48 h; [c] AB (pH 5.5), MMCCH, NaCNBH<sub>3</sub>, r.t., 2 h; [d] 2-iminothiolane, thiolation buffer (50 mM triethanolamine, 0.15 M NaCl, 5 mM EDTA, pH 8.0), r.t., 2 h; [e] PBS (pH 7.2), r.t., 2 h.

Kunz and co-workers also greatly contributed to the protein-carrier approach for the conception of anticancer vaccines displaying mucin-related TACAs.<sup>143</sup> The aberrated glycosylation of MUC1 (Figure 11b) also expose the peptide backbone from the extracellular tandem repeat region, suggesting its influence in altering the glycopeptide epitope conformation.<sup>144,145</sup> In one of his works, Kunz's research group reported synthesis and immunological evaluations of a semisynthetic vaccine candidate composed of the tumor-associated MUC1 tandem repeat sequence Pro<sup>1</sup>-Ala<sup>2</sup>-His<sup>3</sup>-Gly<sup>4</sup>-Val<sup>5</sup>-Thr<sup>6</sup>-Ser<sup>7</sup>-Ala<sup>8</sup>-Pro<sup>9</sup>-Asp<sup>10</sup>-Thr<sup>11</sup>-Arg<sup>12</sup>-Pro<sup>13</sup>-Ala<sup>14</sup>-Pro<sup>15</sup>-Gly<sup>16</sup>-Ser<sup>17</sup>-Thr<sup>18</sup>-Ala<sup>19</sup>-Pro<sup>20</sup>, including one copy of the STn disaccharide antigen at Thr<sup>6</sup>, conjugated to the tetanus toxoid (TTox) carrier protein (**13**) (Figure 15).<sup>146</sup>

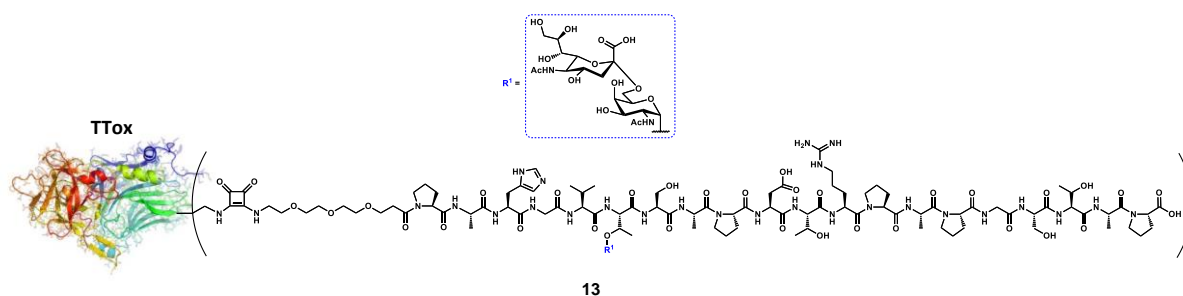
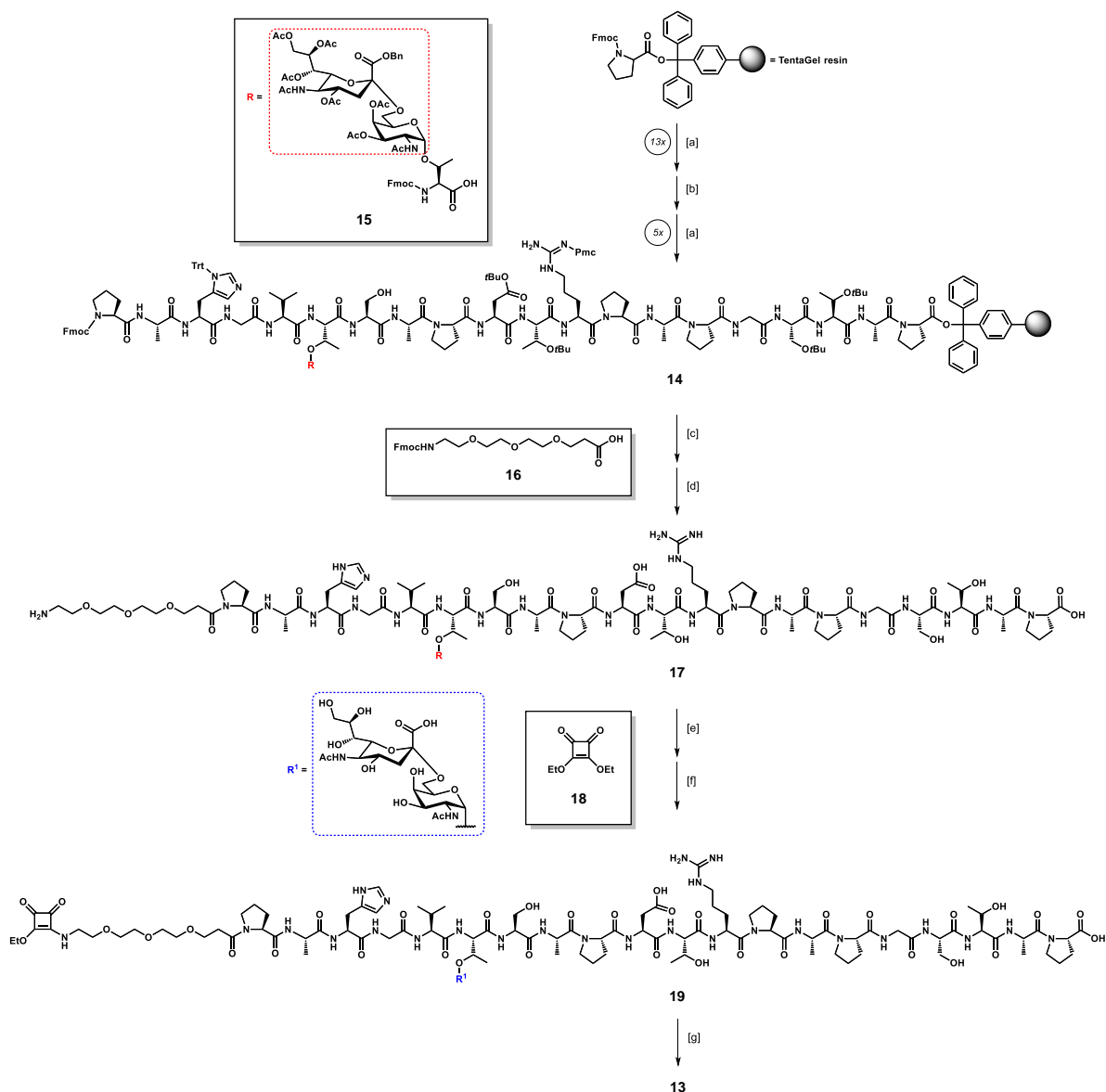


**Figure 15.** MUC1(STn)-TTox conjugate vaccine by Kunz and co-workers.

The fully protected glycopeptide sequence **14** was synthesized by solid phase peptide synthesis (SPPS) using the TentaGel<sup>®</sup> resin, pre-functionalized with a trityl-anchored Fmoc-protected proline (Scheme 3). Fmoc-protected amino acids were coupled using HBTU/HOBt as activating agents,<sup>147</sup> while for the introduction of the glycopeptide building block **15**<sup>148</sup> a procedure involving a HATU/HOAt system was chosen.<sup>149</sup> The resulting sequence **14** was further functionalized with the Fmoc-protected triethylene glycol linker **16**, following the acid-mediated cleavage from the resin with concomitant deprotection of acid-labile amino acid protecting groups, to afford partially protected glycopeptide **17** in 61% overall yield after RP-HPLC purification. Hydrogenolysis of the benzyl ester and base-catalyzed deacetylation resulted in fully deprotection of the STn moiety, with a 40% yield over two steps. The terminal amino group in the linker moiety was then reacted with diethyl squarate **18** in a water/ethanol mixture, in the presence of sodium carbonate (pH 8) to efficiently afford the mono-amido ester **19**. During diethyl squarate coupling (DSC), the mono-substitution reaction can be easily controlled by using one equivalent of primary or secondary amine under mild conditions, as those reported.<sup>150</sup> The generated mono-squaramide results less reactive probably because of its increased aromatic stabilization, compared to dialkoxysquarate **18**. The conjugation of **19** with TTox was thus performed through unsymmetrical DSC, by reaction in aqueous sodium hydrogen phosphate buffer at pH 9.5 for three days; ultrafiltration allowed the removal of unreacted ester **19** and few milligrams of conjugate vaccine **13** were obtained.





The conjugation ratio (*n*, figure 15) of the glycopeptide over the TTox protein could not be precisely determined by MALDI-TOF spectroscopy because of the high molecular weight of the protein ( $\approx 150000 \text{ g mol}^{-1}$ ). Through a comparative ELISA assay (using the serum of a mice previously immunized with a STn-containing vaccine) between **13** and a well characterized glycopeptide-BSA conjugate obtained from **19** (with  $n = 7$ ),<sup>151</sup> the authors estimated that at least 20 copies of glycopeptide were conjugated onto TTox. Immunization of 10 Balb/c-mice with 20  $\mu\text{g}$  of **13** with complete Freund's adjuvant induced a strong immune response in all mice, with high antibody titers. To investigate the specificity of the immune response, the serum extracted from one of the immunized

mice underwent neutralization experiments. The aforementioned STn-MUC1-BSA conjugate ( $n = 7$ ) was coated onto a 96-well plate and the serum was incubated for 1 h at 37°C with glycopeptides **20-27** (Figure 16).

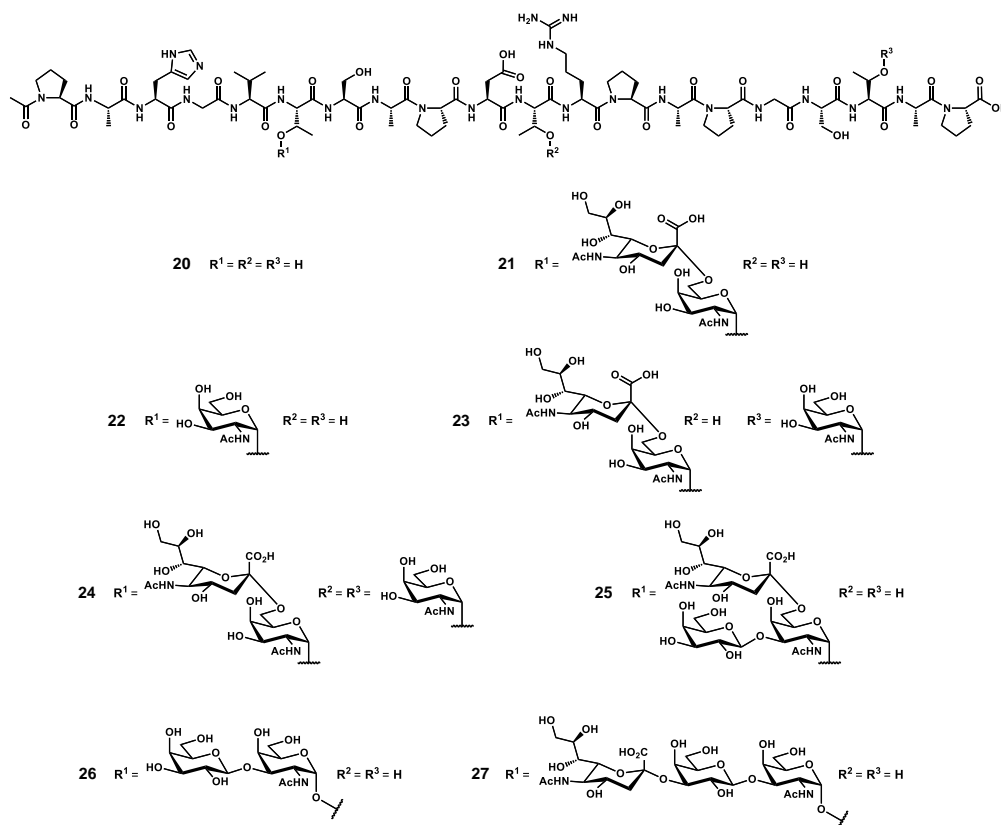


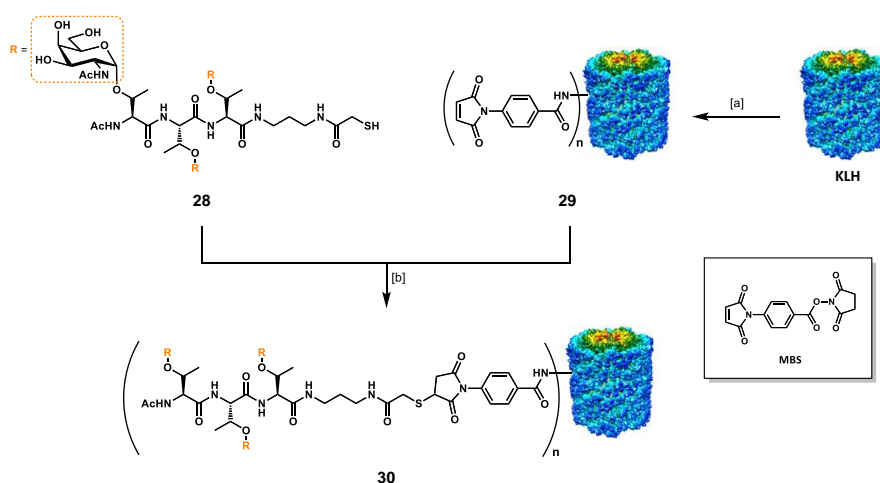
**Figure 16.** MUC1 glycopeptide antigens synthesized with a similar procedure according to **14**.

The binding of untreated mice serum was completely neutralized after incubation with glycopeptide **21**, which is the antigen contained in vaccine **13**. Interestingly, also glycopeptides **22-25**, containing the same MUC1 peptide sequence and crucial parts of the STn disaccharide, inhibited the induced antibodies to a considerable extent. Conversely, compounds **20**, **26** and **27**, featuring unglycosylated MUC1, TF antigen and 2,3-sialyl-TF, respectively, showed a weak binding even despite including identical peptide sequences. This study enabled a possible application of vaccine **13** for immunization in humans.

It is noteworthy to mention that Theratope<sup>®</sup> vaccine, composed of a STn-KLH conjugate plus QS-21 as adjuvant, was tested in phase III in more than 1000 women with breast cancer and has proven to be safe, nevertheless no improvement in survival rate was observed. Kunz and co-workers provided a valid design strategy which enabled the production of high titers of tumor-specific antibodies by employing MUC1(STn) glycopeptide (**21**) as B-cell epitope, grafted of TTox carrier protein and administered with the Freund's adjuvant.

### I.3.1.1.2. Clustered mono-TACA vaccines based on protein-carriers

In the frame of clustered monomeric vaccines, Danishefsky's research group reported synthesis and immunological evaluations of a clustered Tn-based conjugate vaccine (**30**), where a cluster of three threonine-linked Tn antigens (**28**) was conjugated to the KLH carrier protein (Scheme 4).<sup>152</sup>



**Scheme 4.** Synthesis of clustered Tn-KLH conjugate vaccine **30** by Danishefsky and co-workers. Conditions: [a] MBS, DMF, r.t., 30 min.; [b] DMF, r.t., 3 h.

The clustered B-cell epitope **28**, containing a terminal sulfhydryl group was obtained by chemical synthesis. KLH protein was treated with *m*-maleimidobenzoyl-*N*-hydroxysuccinimide ester (MBS) to obtain maleiminated KLH **29**, which subsequently underwent thiol-maleimide coupling to give vaccine **30**. The epitope ratio (*n*) was determined by high-pH anion-exchange chromatography with pulsed amperometric detection (HPAEC-PAD) assay for carbohydrate after acid hydrolysis;<sup>153</sup> two batches of **30** were obtained, with an epitope ratio of 201:1 and 648:1, respectively. The clustered vaccine **30** was tested in comparison with its monomeric version; C57BL/6 female mice were immunized three times with 3  $\mu\text{g}$  of Tn-based vaccine plus 10  $\mu\text{g}$  of QS-21. Previous reports by Kurosaka *et al.* (A monoclonal antibody that recognizes a cluster of a disaccharide, NeuAc $\alpha$ 2 $\rightarrow$ 6GalNAc, in mucin-type glycoproteins) and Nakada *et al.* (Epitopic structure of Tn glycoprotein A for an anti-Tn antibody) suggested that a clustered display of STn and Tn antigens allows an improved recognition by mAbs MLS 102 and MLS 128, respectively.<sup>154,155</sup> Danishefsky and co-workers demonstrated that clustered Tn-KLH conjugate **30** (Scheme 4) is consistently a better form of Tn for inducing high titers of antigen-specific IgG and IgM, which are able to bind two sources of naturally expressed Tn (*i.e.* dOSM: desialylated ovine submaxillary mucin, and LSC: a human colon cancer cell line that express Tn but not MUC1).

Following the same design approach, the Danishefsky group carried out a clinical trial on 20 patients with biochemically relapsed prostate cancer by administering clustered TF-KLH conjugate vaccine **31** (Figure 17).<sup>156</sup>

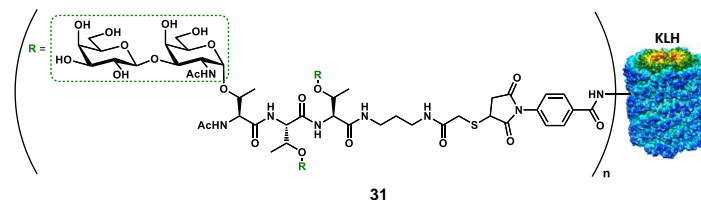


**Figure 17.** Clustered TF-KLH conjugate vaccine by Danishefsky's research group.

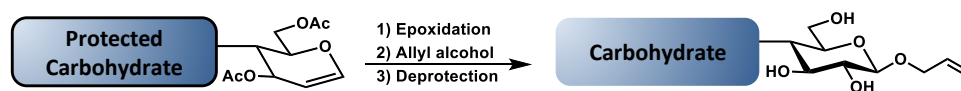
Two batches of **31** were obtained: with an estimated epitope ratio (n) of 466:1 (batch A) and 579:1 (batch B). Four cohorts, each composed of five patients, were vaccinated with different doses of **31** along with 100  $\mu\text{g}$  of QS-21: 1  $\mu\text{g}$  (batch B), 3  $\mu\text{g}$ , 10  $\mu\text{g}$  and 30  $\mu\text{g}$  (batch A). The toxicity of this vaccine formulation was comparable to that observed in previous trials, where other TACA-KLH conjugates plus QS-21 were administered. All patients developed TF-specific IgM and IgG (mainly IgG<sub>1</sub> and IgG<sub>3</sub>, determined by ELISA). Overall, the IgM and IgG titers at the 1  $\mu\text{g}$  and 3  $\mu\text{g}$  doses were at least as high as at the higher doses. Once again, clustering appears to be a valid way to mimic the way "simple" antigens, expressed on epithelial but not normal tissues.<sup>157</sup>

### I.3.1.1.3. Hetero-TACA vaccines based on protein-carriers

Mono-TACA vaccines have shown promising results in early clinical trials, nevertheless this approach does not take account of the inherent heterogeneity of TACAs expressed on transformed cell surface.<sup>88</sup> Danishefsky, Livingston and co-workers hypothesize that the combination of different carbohydrate antigens, associated with a particular cancer type, could be beneficial for the induction of a more potent immune response, reducing the ratio of tumor cells that can undergo immunoevasion. The initially envisaged strategy consisted in the administration of pooled mono-TACA KLH-based conjugate vaccines, containing up to seven different TACAs.<sup>158,159</sup> Although this approach enabled the production of antibody titers against each individual antigen (to a similar extent, compared to Abs obtained through immunization with single TACAs), several fundamental limitations discouraged this route. Firstly, the pooled mono-TACA vaccine approach requires the use of increased levels of carrier protein, which could be detrimental and may contribute to variable clinical

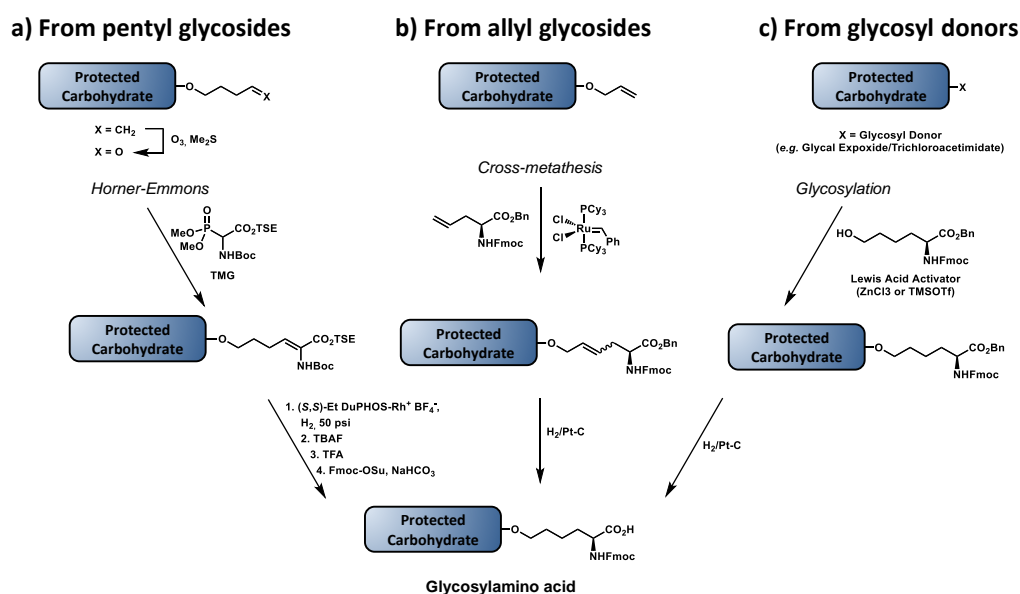
responses.<sup>160</sup> Consequently, the vaccine mixture would require the validation of each monomeric component for its clinical application. Finally, due to the low-yielding antigen-protein conjugation step, this route results not so efficient from a synthetic point of view.

The intriguing idea of developing hetero-TACA-based anticancer vaccines required strong efforts for the chemical synthesis of key building blocks, namely glycosylamino acids, which have been exploited in the cassette assembly, described by Danishefsky and co-workers.<sup>161,162</sup> As described in Scheme 2, the first generation of semi-synthetic mono-TACA conjugated vaccines were obtained by reductive amination between the aldehyde group on the carbohydrate moiety, obtained through ozonolysis of the terminal allyl group, and lysine amino group of KLH. The allyl glycoside was achieved through epoxidation of the glycal moiety, as depicted in scheme 5.



**Scheme 5.** Synthesis of allyl glycosides from protected glycals.

This strategy presents some disadvantages due to the instability of the allyl moiety towards the conditions required for the global deprotection, which require its introduction at the late per-acetate stage of the carbohydrate synthesis. Moreover, the glycal epoxidation step shows moderate stereoselectivity, causing a loss of material at a late stage of the synthetic pathway.<sup>132</sup> Nevertheless, this protocol has constituted the basis for the development of three methods which has served for reaching TACA-based glycosylamino acids (Scheme 6).



**Scheme 6.** Methods for preparation of glycosylamino acids by Danishefsky and co-workers.

The first method (Scheme 6a) involves the utilization of the more stable pentenyl glycoside, which allows for the glycal functionalization at a much earlier stage compared to the allyl ether protocol, thus reducing the impact of the chemical loss associated to the glycal epoxidation step. After ozonolysis of the terminal olefin, the resulting aldehyde is reacted under Horner-Emmons conditions, by using a Boc- and TSE-protected phosphonate, in the presence of 1,1,3,3-tetramethylguanidine (TMG) as base to give a dehydroamino acid, as shown. Subsequent enantioselective reduction of the double bond by means of an enantiopure phospholane, namely 1,2-bis((2*S*,5*S*)-2,5-diethylphospholano)ethane(cyclooctadiene)rhodium(I) tetrafluoroborate, followed by protecting group manipulation, leads to the desired glycosylamino acid.<sup>163</sup> The second method (Scheme 6b) starts with the olefin cross-metathesis between protected allyl glycoside and allyl glycine in the presence of ruthenium catalyst. Reduction of the resulting olefin, with concomitant benzyl ester deprotection provides the glycosylamino acid building block. Despite the drawbacks related to the allyl glycoside synthesis (*vide supra*), this route exploits the commercially available enantiopure form of allyl glycine, with no need to introduce a stereocenter.<sup>164</sup> In the third method (Scheme 6c) the amino acid functionality is directly introduced by coupling the glycal epoxide, or the trichloroacetimidate donor with hydroxynorleucine in the presence of a Lewis acid. Although this method allows for the direct introduction of the amino acid moiety, its efficiency is still limited by the need to synthesize hydroxynorleucine and the moderate stereoselectivity of the glycal epoxidation.<sup>165</sup> Despite their limitations, each of these three methods has been used to obtain TACA-based glycosylamino acid, where the carbohydrate moiety is separated from the amino acid stereocenter by a four- or six-carbon linker. In earlier reports a trivalent-hetero-TACA vaccine, incorporating globo-H, Le<sup>y</sup> and Tn antigens gave a proof of concept by allowing the production of antibodies against the three antigens, which strongly reacted with the MCF-7 breast cancer cell line (**32**, Figure 18).<sup>166</sup> A first generation of pentavalent-hetero-TACA vaccine, comprising globo-H, Le<sup>y</sup>, STn, TF and Tn antigens has proved its effectiveness compared to its relative pooled monomeric formulation; nevertheless, only a minimal response against the Le<sup>y</sup> antigen was observed (**33**, Figure 18).<sup>167</sup> The authors suggested that the low response was due to the nature of Le<sup>y</sup>, as its high endogenous expression levels make this antigen less effective, compared to those that are naturally present only at low levels. In 2009, the Danishefsky group reported the synthesis and preclinical data of a second-generation pentavalent-hetero-TACA vaccine, where the Le<sup>y</sup> antigen was replaced with GM2 antigen (**34**, Figure 18).<sup>168</sup>

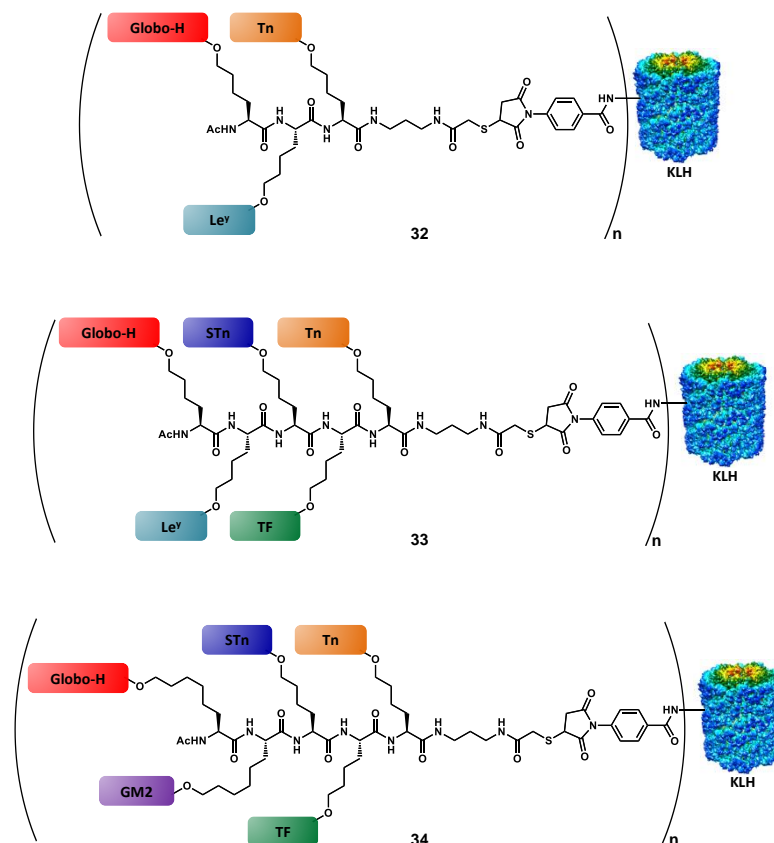


**Figure 18.** Multimeric TACA-based vaccine by Danishefsky and co-workers. **32:** “unimolecular trivalent vaccine”. **33:** first generation “unimolecular pentavalent vaccine”,  $n = 228$ . **34:** second generation “unimolecular pentavalent vaccine”,  $n = 505$ .

The choice of replacing Le<sup>y</sup> antigen with the tetra-saccharide GM2 was based not only for its presence in several cancer types (Table 2), but also taking into account previous studies, showing that (i) GM2-induced antibodies are reactive against human GM2-positive cells, and (ii) that a correlation between those antibody levels and survival rate could be traced.<sup>91,169</sup> The first step for the synthesis of the complicated “unimolecular pentavalent vaccine” involved the preparation of the glycosylamino acids **35-39** (Figure 19), by using the procedures described in scheme 6. In order to minimize steric hindrance phenomena, compounds **35** and **36** were synthesized with a six-carbon spacer. These variants were obtained through the cross-metathesis procedure (Scheme 6b) by starting from pentyl glycosides.<sup>170,171</sup> The rationale of the designed synthetic route involved the positioning of the TACAs from the smallest (*i.e.* Tn) to the largest (*i.e.* globo-H) through a sequential assembly, with the aim to reduce the loss of the more complex antigens by introducing them at a later stage of the synthesis (Scheme 7).

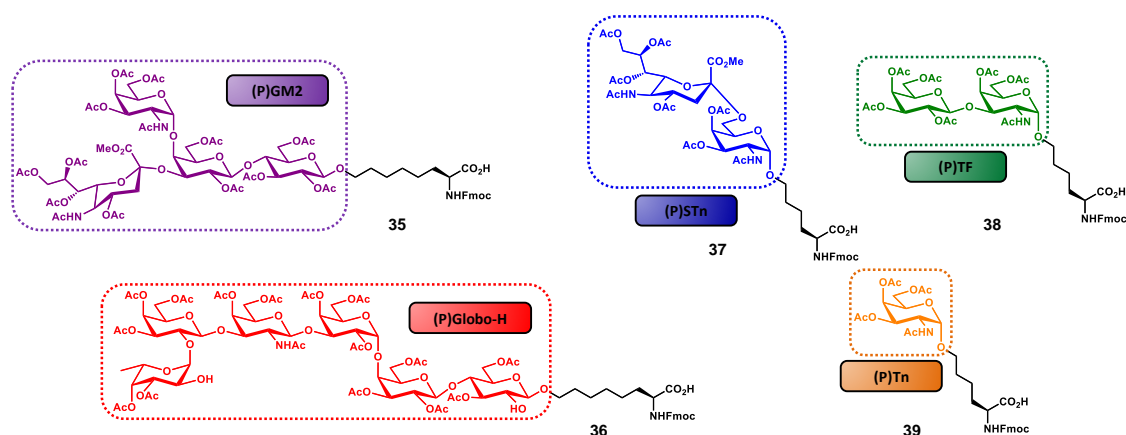
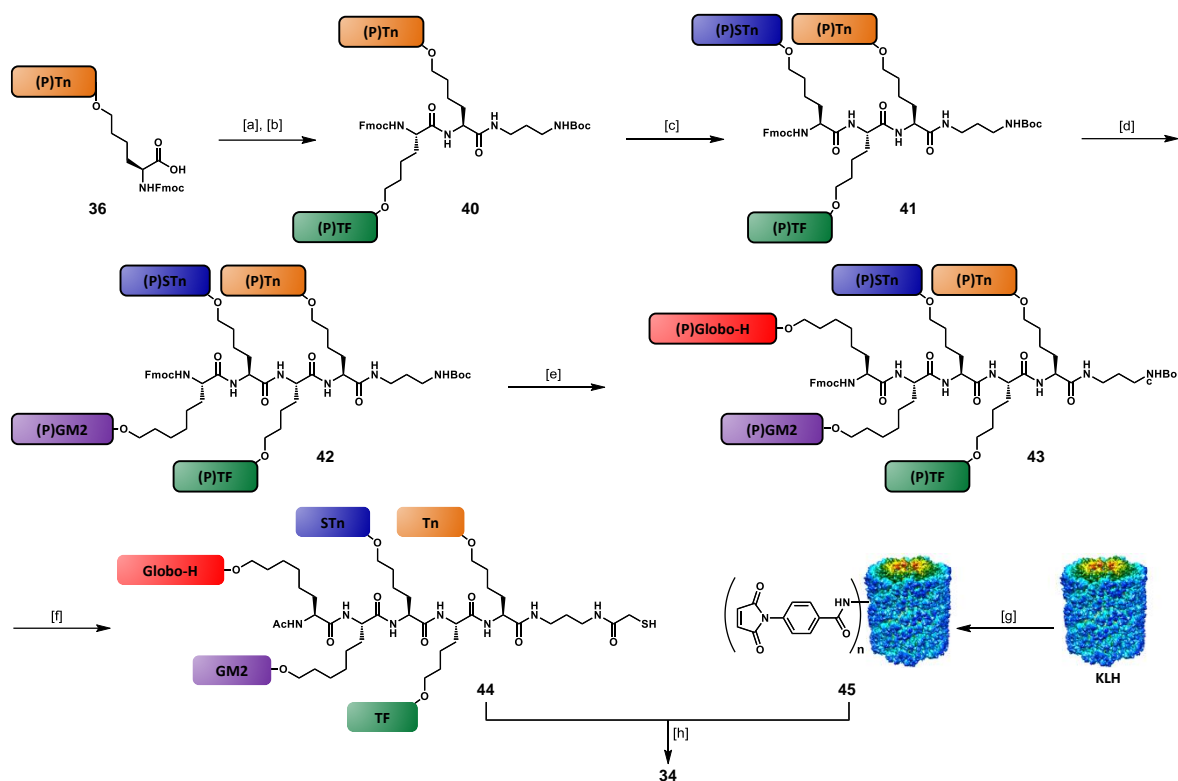


**Figure 19.** TACA-based glycosylamino acids synthesized by Danishefsky and co-workers for the preparation of the second generation “unimolecular pentavalent vaccine” *via* cassette assembly. (P) =

The synthetic route to **34** started with the coupling of the *tert*-butyl-*N*-(3-aminopropyl)carbamate linker on cassette glycosylamino acid **36**. Subsequent iterative Fmoc-removals and glycosylamino acid couplings, involving **38**, **37**, **35** and **36**, respectively, afforded fully protected intermediate **43**, with a 57% yield over nine steps. The Fmoc protecting group of **43** was cleaved and substituted with an acetate, then Boc-deprotection and functionalization of the resulting free amino group with a *S*-acetylthioglycolic activated ester, followed by global deprotection under Zemplén conditions, gave the “unimolecular pentavalent glycopeptide” **44** with a 68% yield over five steps. Another objective of the authors was to increase the protein-conjugation efficiency. Therefore, they adopted a slightly modified procedure compared to their precedents works (See scheme 4), in which KLH protein was reacted with *m*-maleimidobenzoyl-*N*-hydroxysulfosuccinimide ester (Sulfo-MBS) in pH 6.0 phosphate buffer for 1 hour, to give pure maleimidated KLH **45** after G25 Sephadex column purification. Freshly prepared glycopeptide **44** was passed through TCEP gel immediately prior to use, in order to minimize the amount of the putative disulfide oxidation by-product. Then, conjugation between **44** and **45** was carried out in PBS at pH 6.5–7.0. After 4 hours reaction and removal of unreacted **44** by a 30 000 M.W. cut-off filter, pentavalent-hetero-TACA vaccine **34** was obtained in 50% yield, and the recovery yield was approximately 98%. By using this modified procedure the authors achieved a more efficient glycopeptide:KLH conjugation ratio of 505:1, compared to the 228:1 ratio obtained for vaccine **33** (Figure 18). Five female mice (C57BL/6J) were immunized with vaccine **34** (10 µg) plus QS-21 (20 µg) and the collected sera, along with pre-immunization sera, underwent ELISA assays to assess IgM and IgG titers associated with each of the five TACAs. While none of the pre-vaccination sera showed reactivity against the five antigens, post-immunization sera contained substantial titers of antibodies, which proved to be reactive against each of the five TACAs, thus indicating that the immunological properties of the single TACAs were conserved when integrated in this complex vaccine construct.





**Scheme 7.** Synthesis of multimeric vaccine **34**. Conditions: [a] *tert*-butyl-*N*-(3-aminopropyl)carbamate (1.3 eq.), Coupling<sup>®</sup>, 93%; [b] 1. Fmoc removal<sup>‡</sup>, 2. **38** (1.02 eq.), Coupling<sup>®</sup>, 94% over two steps; [c] 1. Fmoc removal<sup>‡</sup>, 2. **37** (1.07 eq.), Coupling<sup>®</sup>, 96% over two steps; [d] 1. Fmoc removal<sup>‡</sup>, 2. **35** (1.05 eq.), Coupling<sup>®</sup>, 83% over two steps; [e] 1. Fmoc removal<sup>‡</sup>, 2. **36** (1.1 eq.), Coupling<sup>®</sup>, 82% over two steps; [f] 1. Fmoc removal<sup>‡</sup>, 2. Ac<sub>2</sub>O, pyridine, r.t., 1 h, 3. 20% TFA/CH<sub>2</sub>Cl<sub>2</sub>, r.t., 3 h, 4. pyridine, *S*-acetylthioglycolic acid pentafluorophenyl ester (8.0 eq.), r.t., 24 h, 5. 0.3M NaOH (aq.), MeOH, r.t., 72 h, TCEP 1 h, 68% over five steps; [g] Sulfo-MBS, PBS (pH 6.0), r.t. 1 h; [h] PBS (pH 6.5-7.0), N<sub>2</sub> atmosphere, r.t., 4 h, 50%. Coupling<sup>®</sup>: EDC·HCl, Et<sub>3</sub>N, HOBT, DMF/CH<sub>2</sub>Cl<sub>2</sub> (1:1), r.t., 1.5-24 h. Fmoc removal<sup>‡</sup>: 5% piperidine/DMF, r.t., 2 h.

#### I.3.1.1.4. Problems associated with protein carriers

Despite these important results obtained in the field of chemical immunology, the carrier-protein approach suffers from some limitations. The TACA-protein conjugation chemistry represents a first, problematic aspect of the semi-synthetic strategy. In early models, as seen for GD3-protein conjugates, the sugar moiety underwent ozonolysis at the ceramide portion to give an aldehyde group which allowed the conjugation to the amino groups in the KLH protein (Scheme 1).<sup>96</sup> Another classical and broadly employed method for oligosaccharide-protein conjugation involves the reductive amination between the open-chain aldehyde of the sugar reducing end and the amino groups of the protein.<sup>172</sup> The first alternative conjugation methods exploited modified carbohydrate containing linkers, such as maleimide, able to react more efficiently with thiol groups of protein's Cys residues.<sup>173</sup> As illustrated over the various examples in this section, the TACA:protein conjugation ratio (*n*, see

figure 15, 17, 18, and scheme 2, 4.) is difficult to control, giving rise to batches with different TACA densities, and therefore leading to ambiguities in composition and structure. Moreover, due to the high molecular weight of carrier proteins (e.g. KLH =  $8.6 \times 10^6$ ) the characterization of the semi-synthetic constructs remains challenging. Following the general rule that a higher loading of tumor-associated antigen is associated to a stronger immune response, it is clear how the conjugation control and the characterization of conjugate vaccines play central roles for ensuring efficient and reproducible immune responses.

The nature of the linker employed for the conjugation of the carbohydrate moiety to the carrier protein also represents an important aspect which has immunological consequences. Boons and co-workers found that the widely employed cyclohexyl maleimide linker was responsible for the reduced immune response towards a Le<sup>Y</sup>-KLH conjugate vaccine in mice (Figure 20).<sup>174</sup> It is widely known in literature that a maleimide function is susceptible to hydrolysis, even at slightly basic pH. Despite the stabilizing effect of the neighboring cyclohexane moiety, it has been demonstrated that hydrolysis occurs after only 2 hours at pH 7.0.<sup>175,176</sup> The authors reported the production of anti-linker IgG and IgM antibodies and reasoned that this epitope-suppressing immune response was directed against the hydrolyzed maleimides and not against the “internal” ones, underlining that the extent of functionalized maleimides was about 80%.

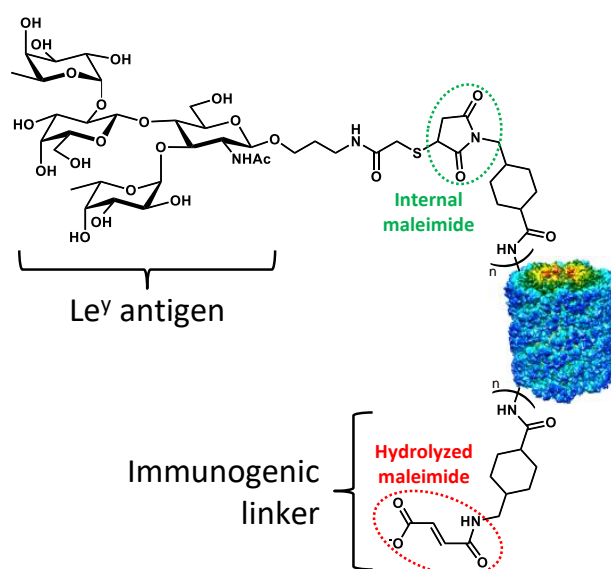


**Figure 20.** Le<sup>Y</sup>-KLH vaccine conjugate by Boons and co-workers showing the hydrolyzed maleimide function, which caused antigen suppression.

Another major drawback associated to the utilization of a protein carrier concerns their inherent high immunogenicity, which can lead to the hapten-specific immune suppression, a

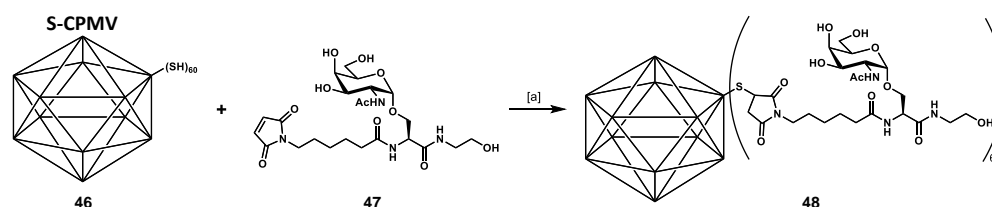
phenomenon known as *carrier-induced epitope suppression* (CIES).<sup>177,178</sup> Proteins like KLH, TTox and non-toxic bacterial toxin mutants contains several MHC-II epitopes; in CIES, interference is thought to arise from competition between haptens (peptides or saccharides) bound to carrier proteins for a limited number of carrier-specific primed helper T cells. As result, the antibody response to the carrier is increased, while the antibody production against the hapten is suppressed. This situation is exacerbated in case of repeated vaccination with the same carrier protein, and has inspired researchers to find alternative carriers and approaches.

### I.3.1.2. Alternatives to protein-carrier delivery

#### I.3.1.2.1. Virus-like particles

Virus-like particles (VLPs) are non-infectious multiprotein structures which mimic envelopes or capsids of authentic native viruses, but lacking the viral genome.<sup>179</sup> They do not need attenuation or inactivation procedures, and their potency can be enhanced if immunosuppressive native viral-proteins are excluded from the VLPs composition. Their highly repetitive surface makes them strong inducers of B-cell responses through efficient cross-linking of BCRs, even in the absence of adjuvants.<sup>180</sup> Peptide epitopes presented on the surface of viral capsids can stimulate adaptive responses by efficiently activating APCs; therefore VLPs represent interesting tools for the patterned display of TACAs and are able to increase their immunogenicity.

Huang and co-workers selected the cowpea mosaic virus (CPMV) capsid, which can be isolated in gram quantities.<sup>181,182</sup> They built a vaccine construct by loading sixty copies of Tn antigen onto a chimeric CPMV (*i.e.* S-CPMV, **46**),<sup>183,184</sup> where cysteine residues were incorporated to provide thiol groups, suitable for the antigen conjugation through thiol-maleimide coupling (Scheme 8).<sup>185</sup>



**Scheme 8.** Synthesis of Tn-S-CPMV conjugate vaccine **48** by Huang and co-workers. Conditions: [a] 0.1 M PBS (pH 7.0), 20% DMSO, 4°C, 12 h.

The Tn-derivative **47** was incubated with purified S-CPMV **46** for one night at 4°C in potassium phosphate buffer (PBS, pH 7.0) with 20% DMSO. Unreacted **47** was then removed by ultracentrifugation. The authors employed the same procedure to graft fluorescein derivatives onto the S-CPMV scaffold, confirming the assumption that  $60 \pm 10$  units were successfully conjugated on the viral capsid. To assess the presence of the Tn moiety on construct **48**, protein-binding studies with the GalNAc-specific lectin SBA (soybean agglutinin) were performed. The UV-visible spectroscopy experiments were further confirmed by TEM (transmission electron microscopy), revealing the presence of aggregates when SBA and **48** were mixed, but not with unconjugated S-CPMV. Immunization studies were carried out in C57BL/6 female mice, 500 µg of **48** in the presence of complete Freund's adjuvant were administered. The collected pre- and post-vaccination sera were analyzed for binding to the MCF-7 breast cancer cell line by FACS (fluorescent assisted cell sorting), showing reactive IgG titers production to a similar extent to those obtained from the clustered Tn-KLH conjugate **30**, described by Danishefsky, Livingston and co-workers. The antibodies generated were also able to recognize the multidrug resistant breast cancer cell line NCI-ADR RES, suggesting the validity of this approach as innovative therapeutic agent in chemical immunology.

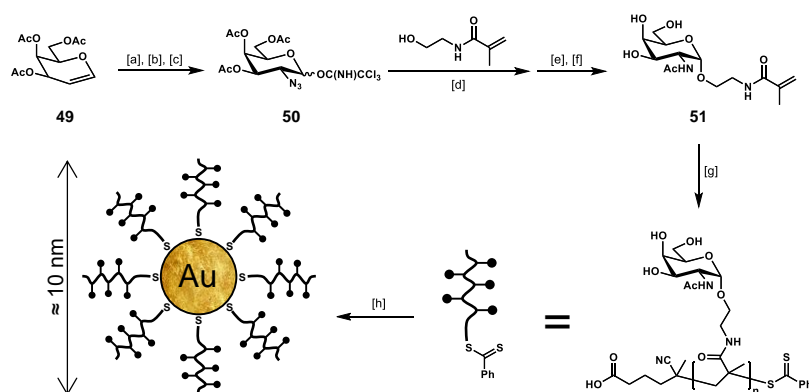
In another report, Finn, Blixt and co-workers demonstrated that a variety of carbohydrate antigens (including globo-H and sLe<sup>x</sup>) grafted on CPMV carriers, were able to generate a large amount of polyclonal IgY antibodies (the functional equivalent of mammalians IgGs) in chicken models.<sup>186</sup>

### **I.3.1.2.2. Gold nanoparticles**

Gold nanoparticles (GNPs) have recently emerged as interesting tools in the context of cancer treatment due to their ability to penetrate blood vessels and tissue barriers, and the possibility to be easily functionalized to promote their selective uptake by the cells of the immune system.<sup>187–190</sup> Along with active vectorization of GNPs, several physicochemical factors, such as size, shape, surface charge and hydrophobicity/hydrophilicity play important roles in terms of bio-distribution, cellular interactions and cellular infiltration. For example, it has been reported in literature that the optimal particle size for DCs uptake was less than 500 nm. Since the traffic to the draining lymph nodes is size-dependent, large particles (500–2000 nm) are taken up by peripheral APCs at the injection site, while small nanoparticles (20–200 nm) are internalized in lymph nodes-residing DCs and macrophages.<sup>191</sup>

In the frame of TACA-based anticancer vaccine design, Davis, Cameron and co-workers described the synthesis and immunological evaluation of glycopolymer-stabilized gold nanoparticles

based on Tn antigen (Scheme 9).<sup>192</sup> Despite the native structure of Tn antigen implies its presence on the mucin peptide backbone, the authors suggested that presenting the sugar moiety ( $\alpha$ GalNAc) in a multivalent manner might result in a nanoparticle able to mimic the cell surface of a Tn-expressing cancer cell, thus achieving an effective anticancer vaccine.



**Scheme 9.** Preparation of Tn-antigen gold nanoparticles by Davis, Cameron and co-workers. Conditions: [a]  $\text{NaN}_3$ , CAN,  $\text{CH}_3\text{CN}$ ,  $-20^\circ\text{C}$ , 30 h, 80%; [b] PhSH, DIPEA,  $\text{CH}_3\text{CN}$ , r.t., 1 h, 72%; [c]  $\text{K}_2\text{CO}_3$ ,  $\text{CCl}_3\text{CN}$ ,  $\text{CH}_2\text{Cl}_2$ , r.t., 8 h, 62%; [d] TMSOTf,  $\text{Et}_3\text{N}$ ,  $\text{Et}_2\text{O}/\text{CH}_2\text{Cl}_2$  (2:1),  $-20^\circ\text{C}$ , 30 min., 80%; [e] DPPE,  $\text{CH}_2\text{Cl}_2$ , r.t., 1 h, then  $\text{Ac}_2\text{O}$ , DMAP,  $\text{Et}_3\text{N}$ ,  $\text{H}^+$  resin, 55%  $\alpha$ -anomer; [f]  $\text{K}_2\text{CO}_3$ , MeOH, 65%; [g] CPADB, ACVA,  $70^\circ\text{C}$ , 48 h, 51-75%; [h]  $\text{HAuCl}_4$ ,  $\text{NaBH}_4$ , r.t., 2.5 h.

Starting from glycal donor **49**, the azido-galactopyranosyl trichloroacetimidate **50** was achieved in three steps with a 36% yield. Glycosylation of *N*-(2-hydroxyethyl)-2-methacrylamide (HEMAm), following one-pot Staudinger reduction of the azido-moiety and acetylation of the resulting amino group gave a anomeric mixture of protected precursor of **51**, which after separation and methanolysis afforded the key building block **51** in gram scale, ready to undergo reversible addition-fragmentation chain transfer polymerization. In scheme 9, an example of Tn-antigen glycan monocomponent homopolymer is reported. The authors also produced statistical copolymers of **51** and PEGMA (poly(ethylene glycol) methyl ether methacrylate) to vary the degree of antigen density. To obtain GNPs coated with Tn-antigen polymers, solutions of  $\text{HAuCl}_4$  (0.5 mM), glycopolymers (5.0 mM) and sodium borohydride (50 mM) were combined, stirred for 2.5 hours and purified by centrifugal filtration. Immunization of New Zealand White rabbits with Tn-based GNPs or free Tn-based polymer revealed a high IgG production for the Tn-GNP constructs and low or negligible response for the polymer form of Tn-antigen. The resulting antibodies were reactive towards different mucin glycoproteins bearing the Tn antigen, giving the proof of concept that this peptide-free vaccine was able to produce IgG antibodies. The authors also highlighted a relationship between degree of carbohydrate density and immune response, with an optimum of 20-25 Tn units per polymer chain.

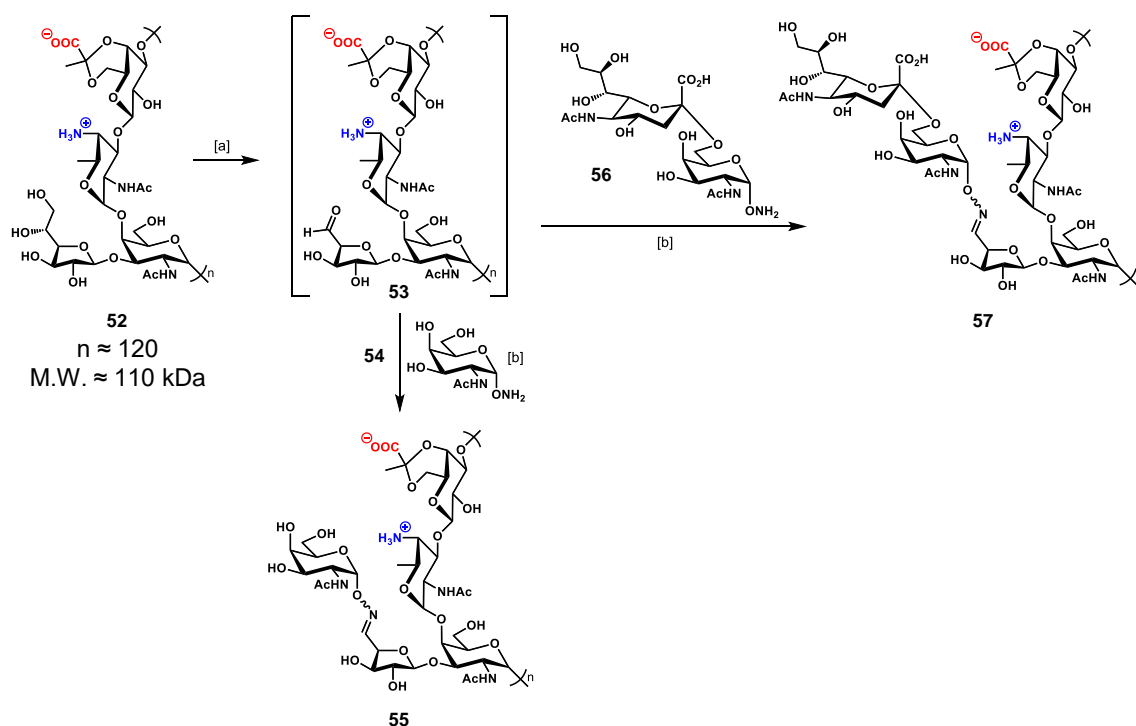
### I.3.1.2.3. Zwitterionic polysaccharides

Another promising alternative to carrier proteins for the construction of TACA-based anticancer vaccines has been exploited by Andreana and co-workers.<sup>193</sup> Zwitterionic polysaccharides (ZPSs) are carbohydrate structures isolated from the capsule of commensal anaerobic bacteria, which are able to trigger T-cell dependent immune responses.<sup>194</sup> PS A1 is the most abundant ZPS extracted from *B. fragilis*, composed of a tetrasaccharide core repeating unit, with a molecular weight of approximately 110 kDa ( $\approx 120$  repeating units). In this context, few ZPSs have been exploited in vaccinology, including: PS A2 and PS B from *B. fragilis*, Sp 1 from *Streptococcus pneumoniae*, and CP 5/8 from *Staphylococcus aureus*.

Experimental observations revealed that the processing and presentation of PS A1 result in a MHC-II – PS A1 complex, in a different but similar way compared to peptide antigens. An effective antigen presentation requires fragments of approximately 12-15 kDa, and the presence of both positive and negative charges on monosaccharide units is indispensable for maintaining the T-cell stimulation ability.<sup>195–197</sup>

Following this line, Andreana and co-workers designed anticancer vaccines based on TACAs (*i.e.* Tn, STn) by using PS A1 as carrier.<sup>198,199</sup> PS A1 fragment **52** was obtained through large-scale fermentation by using *Bacterioides fragilis* NTCT 9343 and treated with 0.5 equivalents of sodium periodate in 0.10 M acetate buffer (pH 5.0) to provide an aldehyde handle on the D-galactofuranose residue (Scheme 10).<sup>200</sup> Despite the presence of a *trans*-diol, only vicinal diol oxidation was observed because of its higher reactivity under periodate oxidation conditions.<sup>201</sup> To this solution, KCl was added in order to remove the excess of periodate as insoluble  $\text{KIO}_4$ . Addition of  $\alpha$ -aminoxy-Tn **54** afforded Tn-PS A1 vaccine construct **55** after 18 h reaction. Treatment of intermediate **53** with  $\alpha$ -aminoxy-STn **56** in similar conditions gave STn-PS A1 **57**. The tumor-associated antigen loading was determined using  $^1\text{H-NMR}$  integration (observed loading = 11%) and by means of a resorcinol-based colorimetric method (observed loading = 10%), which can be translated in an average mole ratio TACA:PS A1 of 24:1.<sup>128</sup> Immunization of C57BL/6 mice with **55** (10  $\mu\text{g}$ ) in the presence of TiterMAX<sup>®</sup> Gold (TMG<sup>®</sup>, 50  $\mu\text{L}$ ) adjuvant enabled the production of IgG antibodies (mainly IgG3) which were specifically reactive towards Tn hapten. Immunological evaluation of STn-PS A1 vaccine **57** (20  $\mu\text{g}$ ) on C57BL/6 mice gave better results in the presence of Sigma adjuvant system (SAS, 20  $\mu\text{g}$ ) than TMG. Previous reports showed that the presence of monophosphoryl lipid A (MPL), the main component of SAS, is able to conserve the immunostimulatory activity of lipid A with a decrease in toxicity; while TMG<sup>®</sup> is less toxic but also less effective in triggering antibody production than SAS.<sup>202,203</sup> Sera obtained from mice immunized with **57** + SAS contained a substantial amount of IgG antibodies which resulted reactive

towards STn-positive human breast cancer cell line MCF-7 and the ovarian cancer cell line OVCAR-5, but failed to react with normal human mammary cell line MCF-10A. Even if the dose ratio of PS A1 content was 9-fold greater than the STn moiety, ratios of anti-PSA1/anti-STn IgG and IgM antibodies were smaller than the dose ratio, indicating a relatively balanced T cell response which is unlikely to cause epitope suppression. Conversely, the IgG ratio of KLH/STn obtained from Theratope® Phase III report was about 60:1.<sup>204</sup>



**Scheme 10.** Synthesis of entire carbohydrate anticancer vaccines **55** and **57** by Andreana and co-workers. Conditions: [a] NaIO<sub>4</sub> (0.5 eq.), 0.1 M NaOAc (pH 5.0), r.t., 1.5 h, then KCl (5.0 eq.); [b] 0.1 M NaOAc (pH 5.0), r.t., 18 h.

### I.3.1.3. Semi-synthetic approaches - Conclusions

In this section, a panel of strategies to overcome the problems associated to the semisynthetic protein-carrier approach has been presented. Still today, the lack of a fine TACA-protein conjugation control and the problems associated to the characterization of the resulting vaccine construct, together with other difficulties related to the inherent immunogenicity of protein carrier themselves penalize important aspects of protein-conjugated vaccines. Uniformity in terms of TACA display should be reachable and properly detectable, since a reproducible and well characterizable vaccine construct impacts its effectiveness.

Highly immunogenic protein carriers can be replaced with different carriers (*e.g.* VLPs, GNPs, ZPSs), capable to give rise to T-cell dependent immune reactions and generate specific anti-hapten IgG antibodies with reduced toxicity and epitope suppression phenomena. A more tailored approach would allow for a better design of TACA-based anticancer vaccines by addressing both molecular and immunological aspects. For example, by introducing a multivalent TACA display, the enhancement of BCR clustering should translate in improved antigen uptake and processing. Also, the carrier, which has both the role of CD4<sup>+</sup> epitope source and scaffold for the TACA's display, can be reduced to its essential parts to provide a suitable and well-defined tool.

In the next section the fully-synthetic approach will be presented and discussed along with representative literature examples, including a brief “state of the art” of the laboratory which hosted my PhD project.

### **I.3.2. Fully-synthetic approaches**

Along with the semisynthetic approach, where synthetic glycans are conjugated to protein carriers, a fully synthetic approach has been conceived to face the limitations of the first strategy.<sup>92–94,124</sup> The main feature of this new approach, which relies entirely on chemical synthesis, involves the replacement of the protein-carrier with precise CD4<sup>+</sup> T<sub>H</sub> oligopeptide epitopes, to ensure a T-dependent TACA-directed immune response. Accordingly, the covalent linking of a TACA moiety to a short CD4<sup>+</sup> peptide epitope represents the most simple fully-synthetic TACA-based anticancer vaccine design strategy.

The utilization of non-immunogenic synthetic scaffolds allows for tuning the display of both B- and T-cell epitopes in terms of density, spatial distribution and valency.<sup>205</sup> Concerning the TACA moiety display, three types of spatial architectures have been employed: (i) glyco-dendrimers with globular tertiary structure, (ii) glyco-clusters assembled on organic templates (*e.g.* cyclopeptides) and (iii) glyco-clusters or single glycans arranged in linear or branched architectures.

Synthetic vaccines rely on a modular approach: different building blocks or units can be separately obtained and subsequently assembled. They are conceived to be devoid of any unnecessary element which could negatively influence vaccine characterization, epitope distribution and immunological outcome. The resulting fully-synthetic constructs are smaller entities compared to their semisynthetic analogues, enabling a more reliable characterization by classic techniques (*e.g.* mass spectrometry, chromatography, NMR...). The superior conjugation chemistry control allows for



monodisperse and reproducible structures, by means of a large repertoire of orthogonal, chemoselective, and “click” reactions to facilitate the assembly of the different subunits.<sup>206,207</sup>

Several research groups adopted the fully-synthetic approach. In the next sections, some of the most representative examples in this area of anticancer vaccines will be presented.

### I.3.2.1. Two-component (TACA-CD4<sup>+</sup>), fully synthetic anti-cancer vaccines

Leclerc and co-workers paved the way for the fully-synthetic approach in TACA-based anticancer vaccines. In 1997, they prepared a glyco-dendrimer, namely multiple antigen glycopeptide (MAG), displaying the Tn antigen in its  $\alpha$ -GalNAc-Ser form.<sup>208</sup> Inspired by the multiple antigen peptide (MAP) described by Tam in 1988,<sup>209</sup> the MAG construct (**58**, figure 21) is composed of a core scaffold featuring oligomeric branched lysines (in blue), which are functionalized with four peptide fragments from polio virus (PV<sub>103-115</sub>: KLF<sup>AV</sup>WKITYKDT, in green) as CD4<sup>+</sup> epitopes, and four Tn antigen copies (in orange).<sup>210</sup>

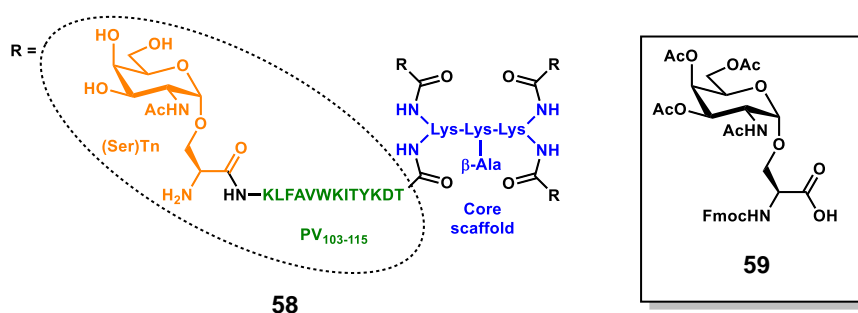


**Figure 21.** Multiple antigen glycopeptide (MAG) by Leclerc and co-workers (**58**), and protected (Ser)Tn building block (**59**).

The synthetic strategy for assembling the MAG involved a conventional solid-phase peptide methodology which started with the attachment of the  $\beta$ -alanyl spacer on the Wang resin (Synthesis not shown). The subsequent coupling with two levels of Fmoc-Lys(Fmoc)-OH residues, afforded a dendrimer-like core scaffold with four amino groups, which were further elongated with protected AAs of the PV<sub>103-115</sub> sequence. The protected building block **59**<sup>211</sup> was ultimately conjugated to the PV's amino termini in a divergent manner, following cleavage from the resin and global deprotection, to afford fully synthetic vaccine prototype **58**. It is noteworthy mentioning that the molecular weight of the entire construct corresponds to 8014 Da, allowing a precise characterization by mass spectrometry

and analytical RP-HPLC. Moreover, the TACA (*i.e.* (Ser)Tn) ratio over the entire vaccine corresponds to 0.15 in terms of molecular weight. Performing the same operation on semi-synthetic vaccine prototype **30** (Scheme 4), knowing that  $n = 648$  (conjugation ratio) and M.W. of KLH ranges between 6000-7500 kDa, the resulting ratio corresponds to 0.08, thus highlighting not only the superior precision of the MAG construct, but also its improved TACA ratio over the entire molecule.

Preliminary B-cell antigenicity studies showed the reactivity of construct **59** towards two well characterized anti-Tn mAbs: 83 D4 (IgM) and MLS 128 (IgG). Interestingly, T-cell antigenicity trials showed that the presence of the Tn antigen in construct **58** dramatically increased the presentation of the PV peptide by MHC molecules, since the same construct devoid of the Tn moiety necessitated a 10000-fold increased concentration to stimulate T-cells to the same extent.<sup>212</sup> The authors suggested that such behavior could be the consequence of a specific GalNAc-mediated receptor cross-linking, which also causes the endocytosis of the construct by APCs. Immunization studies were carried out in three different strains of mice (*i.e.* BALB/c, DBA/2 and SJL/J) with 50  $\mu\text{g}$  of **58** plus 1 mg of alum. Post-immunization sera from mice inoculated with construct **58**, but not those treated with a negative control lacking the Tn moiety, produced high titers of anti-Tn IgG antibodies (mainly IgG1) with similar reactivity towards human tumor cell lines (*i.e.* human Jurkat T-cell lymphoma cell line and LS180 adenocarcinoma cell line), compared to mAb MLS 128.<sup>213,214</sup> Moreover, immunization of DBA/1 mice, a strain which is not responsive towards PV peptide, did not develop any anti-Tn antibodies following immunization with **58**, thus confirming the occurrence of a T-cell dependent immune response in the context of this anti-Tn antibody response. Finally, the immunotherapeutic effect of construct **58** was tested in BALB/c mice grafted with TA3/Ha to investigate the survival rate and the resistance to tumor challenge, showing statistically significant differences between treated mice and mocks.

Following the good results obtained with clustered carbohydrate antigens, the same group reported the immunological evaluation of a clustered version of the MAG compound **58**.<sup>152,156,215</sup> The structure of this second generation construct integrates a tri-Tn motif at the end of each PV sequence, where the  $\alpha$ -GalNAc moiety is grafted onto a Ser-Thr-Thr (STT) sequence (**60**, figure 22).<sup>216</sup>

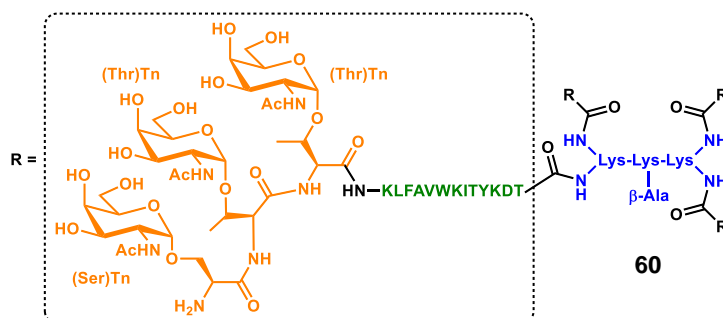


**Figure 22.** Tn-clustered multiple antigen glycopeptide (MAG) by Leclerc and co-workers (**60**).

The study highlighted that the clustered STT glycosylated sequence was the most efficient for the induction of anti-Tn antibodies able to recognize a large variety of GalNAc glycosylated MUC-1 sequences, broadening the spectrum of recognition for native forms of Tn. The ability to induce anti-Tn IgG antibodies with a mild adjuvant like alum, compared to Tn-KLH conjugates which need a stronger adjuvantation (QS-21), and also in the frame of other adjuvant settings (e.g. CpG oligonucleotides, lipopeptide adjuvants), emphasizes the validity of this fully-synthetic approach. It is important to mention that no evidence of antibodies directed against the poly-lysine core scaffold has been reported, and no adverse reaction was observed in all experimental settings.<sup>217</sup>

In 2015 compound **60** entered in a phase I clinical study, thanks to its promising pre-clinical results. This study involved patients with non-metastatic, HER2 negative, localized breast cancer at high-risk of relapse.<sup>218</sup>

In 2005, Dumy, Renaudet and co-workers, inspired by the work of Leclerc's group, gave their first contribution to the fully-synthetic approach by exploring the utilization of the cyclic RAFT template as innovative scaffold to present B- and T-cell epitopes in a multivalent and topologically separated fashion.<sup>219</sup> Conceived by Mutter and co-workers, the RAFT (regioselectively addressable functionalized template) scaffold was initially designed as tool for directing covalently attached building blocks into characteristic folding topologies (introducing the concept of template-assembled synthetic proteins: TASP).<sup>220–223</sup> RAFTs are topological templates composed by a backbone-cyclized decapeptide which contain two Pro-Gly residues as  $\beta$ -turn inducers, able to stabilize their conformation in solution and to provide a quite rigid structure, where the side chains of lysine residues point in two distinct directions, defining an upper and lower domain (Figure 23).

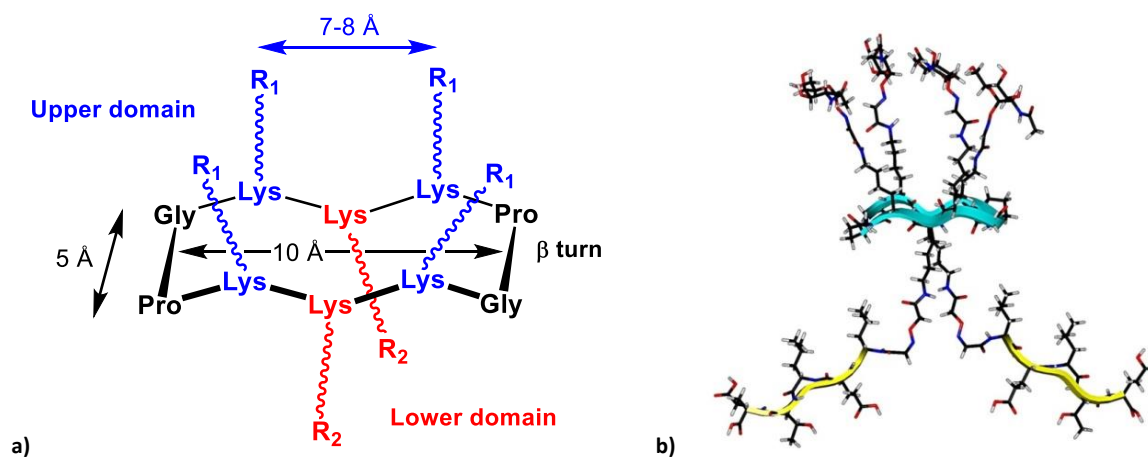


**Figure 23.** RAFT scaffold by Mutter, Dumy and co-workers. a) General structure representation. b) 3D model representation with four sugar residues in the upper domain and two peptide sequences in the lower domain.

These scaffolds have served for the construction of synthetic vaccines<sup>205</sup>, and they have also demonstrated to be useful tools as vectors in cancer therapy, and for the study of G-quadruplex folding.<sup>224–227</sup> The interesting features of RAFT scaffolds are not limited to their conformational stability and topology. Indeed, they represent attractive scaffolds for the construction of anticancer vaccines also thanks to other advantages: (i) they are easily synthesized *via* standard solid phase peptide synthesis, (ii) their *in-vivo* stability and compatibility, due to the cyclic structure and functionalized AA's side chain make them less prone to undergo protease-mediated hydrolysis; (iii) the possibility to selectively functionalize the two distinct domains (*i.e.* upper and lower domains) of the scaffold, with reduced interference phenomena between different ligands (*e.g.* B-cell epitopes in the upper domain and T-cell epitopes in the lower domain); (iv) the ease to tailor other structural and spatial parameters, by increasing the cyclopeptide core size or by introducing other multivalent elements in both convergent and divergent manners.<sup>228</sup>

The first generation of fully-synthetic anticancer vaccine prototypes conceived by Dumy, Renaudet and co-workers involved the clustered presentation of four Tn analogues, on the upper domain of the scaffold, and one (61) or two (62) PV<sub>103-115</sub> peptide sequences on the lower domain (Figure 24).<sup>219</sup>

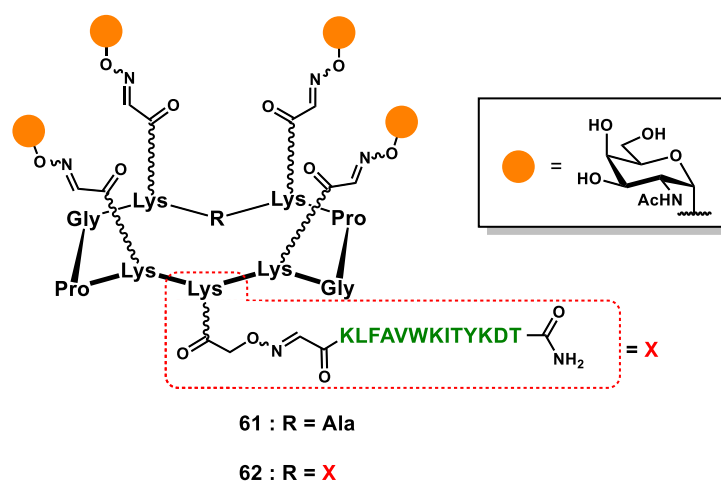
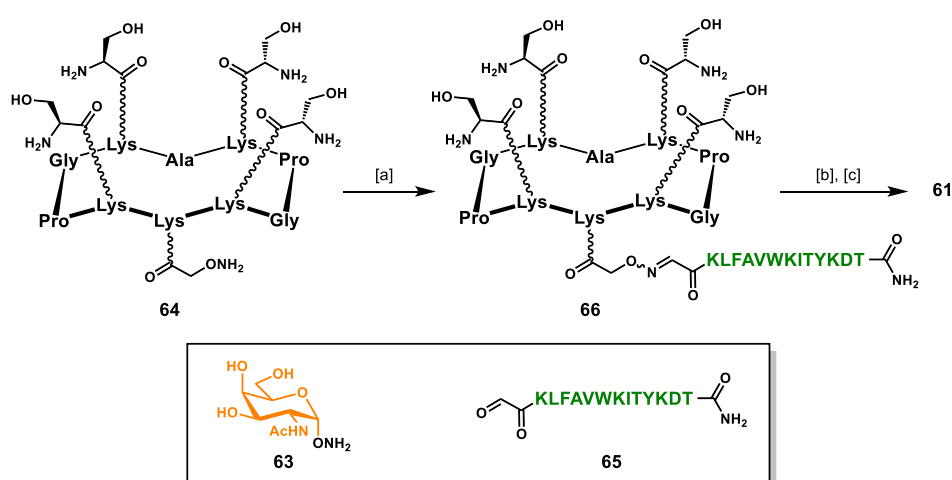


**Figure 24.** First generation of fully-synthetic Tn-based anticancer vaccine prototypes by Dumy and Renaudet.

A second aspect of this approach relies on the utilization of an iterative oxime ligation protocol, which has demonstrated to be efficient and chemoselectively compatible with a wide range of chemical functions, allowing the ligation between unprotected fragments without the need of coupling agents.<sup>229–238</sup> Such a strategy requires the preparation of the different modules (*e.g.* B-cell epitopes,

scaffold and T-cell epitopes) bearing aldehyde and aminoxy functional groups as counterparts for their condensation into the hydrolytically stable oxime bond.<sup>239</sup> The aminoxyalted  $\alpha$ GalNAc **63** (Scheme 11) has been chosen as structurally simplified carbohydrate analogue of the native Tn antigen (Ser/Thr- $\alpha$ GalNAc). This choice was supported by literature reports, where other carbohydrate-base Tn analogues showed similar antigenicity compared to the native form.<sup>240–243</sup> Similarly, the RAFT scaffold **64** and aldehyde-bearing T-cell epitope **65** represents key building blocks for the construction of such vaccine prototypes (Scheme 11). Since this chemical strategy will be discussed more in detail in the following sections, in scheme 11 we reported an essential synthetic scheme for the assembly of vaccine prototype **61**.<sup>219</sup>



**Scheme 11.** Essential synthetic pathway for the construction of synthetic vaccine prototype **61**. Conditions: [a] **65** (1.1 eq.), AcONa buffer (pH 4.0, 100 mM), r.t., 24 h, 78%; [b] NaIO<sub>4</sub>, PBS (pH 7.3, 10 mM), r.t., 5 h, 86%; [c] **63** (9.3 eq.), AcONa buffer (pH 4.0, 100 mM), r.t., 36 h, 66%.

Intermediate **64** (Scheme 11), bearing four serine residues in the upper domain and one aminoxy function in the lower domain, underwent oxime ligation with aldehyde-bearing CD4<sup>+</sup> peptide **65** in acetate buffer at pH 4.0 for 24 hours at room temperature, to afford scaffold **66**. The serine residue act as masked aldehyde function, indeed treatment of **66** with sodium periodate afforded four  $\alpha$ -oxo-aldehydes (not shown),<sup>244</sup> prone to react *via* oxime ligation with  $\alpha$ -aminoxy-GalNAc **63**. Fully-synthetic vaccine prototype **61** was obtained in good yields (44%, from intermediate **64**), excellent purity and was easily characterized by mass spectrometry and analytical RP-HPLC.

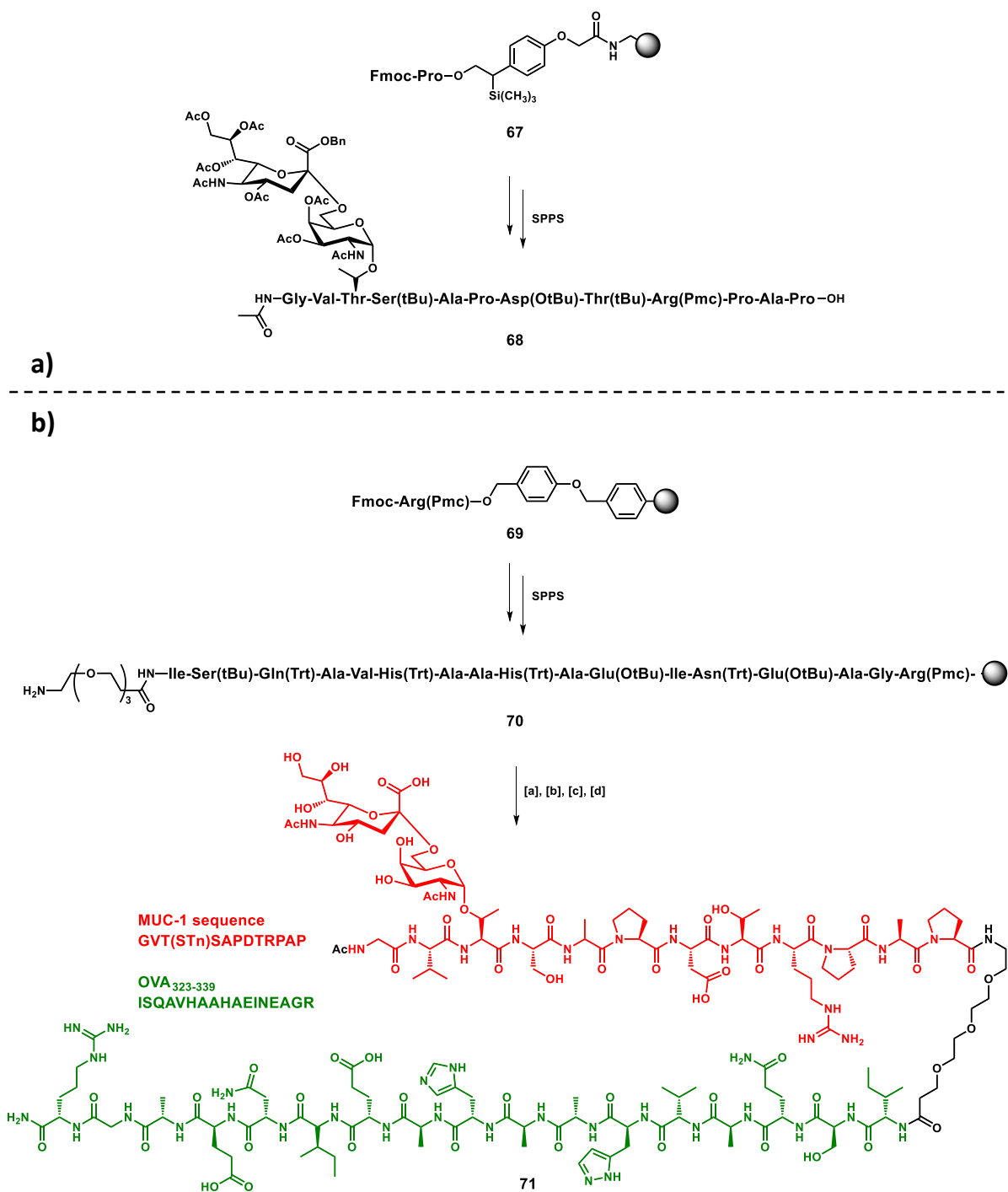
B-cell antigenicity was assessed by ELISA using two Tn-specific mAbs 6E 11 (IgG3) and an 83 D4 (IgM): compounds **61** and **62** both shown their binding abilities towards the two mAbs, but not control molecules lacking the sugar moiety or presenting a different saccharide (*i.e.* GlcNAc). The RAFT\* scaffold has proved effective for presenting the oxime-linked Tn-antigen's saccharide moiety (*i.e.*

GalNAc), in a clustered manner, to mAbs which are reactive with the natural occurring antigen. Therefore, the “unnatural” Tn derivative **63** represent a suitable model for humoral stimulation.

*In-vitro* T-cell antigenicity assays indicated an enhanced IL-2 production caused by prototypes **61** and **62**: they induced T-cell stimulation at a 10000-fold inferior concentration, compared to their unglycosylated analogues bearing the PV peptide but not the saccharide moiety. This result confirms previous observations regarding the enhanced T-cell stimulation induced by peptides bearing a GalNAc moiety, as the Tn antigen.<sup>212,241,245</sup>

Immunogenicity of compounds **61** and **62** was tested in BALB/c mice by administering 10 µg of compound in alum. Collected post-immunization sera contained IgG antibodies which were able to recognize the glycosylated RAFT (containing four Tn residues) but not the naked RAFT scaffold, assessing the non-antigenicity of the cyclodecapeptide platform. The antibody response of compound **62**, displaying two copies of the PV<sub>103-115</sub> peptide did not resulted increased compared to its homologue **61**, suggesting the relevance of the clustered B-cell epitope presentation for an effective humoral response. The obtained IgG antibodies were reactive towards the human Jurkat tumor cell line expressing the Tn antigen. These preliminary results opened interesting perspectives for the utilization of such a modular strategy for the synthesis of multicomponent vaccine constructs. Indeed, the following generations of therapeutic vaccines focalized their design on integrating new modules such as CD8<sup>+</sup> epitopes and internal adjuvants.

Following the preliminary results obtained in one of their former studies,<sup>148</sup> Kunz and co-workers reported the synthesis and immunological evaluation of a two-component fully-synthetic vaccine construct incorporating: (i) the STn antigen along with the MUC-1 sequence GVT\*SAPDTRPAP (\* = glycosylation site) as B-cell epitope, and (ii) the OVA<sub>323-339</sub> sequence (ISQAVHAAHAEINEAGR) as CD4<sup>+</sup> T<sub>H</sub> epitope (**71**, Scheme 12b).<sup>151</sup> The strategy adopted for the vaccine construct assembly started with a solid phase peptide synthesis (SPPS) protocol on resin **67**, in which glycopeptide building block **15** (Scheme 3) was integrated. Subsequent cleavage from the solid support and purification by preparative RP-HPLC afforded protected intermediate **68** in 45% overall yield (Scheme 12a). The elongation of resin **69** proceeded to give the desired OVA<sub>323-339</sub> sequence, and a triethylene glycol spacer was attached, following a similar procedure of that previously described in Scheme 3, to give **70**. The final steps involved the solid phase coupling of **68**, activated with HATU/HOAt, to the polymer bound sequence **70**, following cleavage from the resin and subsequent global deprotection, to afford pure compound **71** in 19% overall yield (from **69**) (Scheme 12b).



**Scheme 12.** a) Synthesis of protected glycopeptide **68**. b) Synthesis of vaccine construct **71**. Conditions: [a] **68** (1.05 eq.), HATU, HOAt, NMM in DMF, r.t., 16 h; [b] TFA/TIS/H<sub>2</sub>O (15:0.9:0.9), r.t., 2 h, 42% over two steps; [c] H<sub>2</sub>, Pd/C (10%), r.t., 21 h; [d] NaOMe, MeOH, r.t., 16 h, 43% over two steps. SPPS: 1) Fmoc removal: 20% piperidine in NMP; 2) AAs coupling: Fmoc-AA-OH, HBTU, HOBT, DIPEA in DMF; 3) capping: HOBT (cat.), Ac<sub>2</sub>O, DIPEA in NMP. Trt = triphenylmethyl; Pmc = pentamethylchroman-6-ylsulfonyl.

Immunization studies were carried out on transgenic mice (DO11.10), whose T cells express a specific receptor which binds to the OVA<sub>323-339</sub> epitope presented on MHC-II molecules.<sup>246</sup> Compound **71** was administered to three mice at the dose of 10 µg, in the presence of complete Freund's adjuvant (CFA). Only one out of three mice exhibited a considerable concentration of MUC1-specific antibodies,

while mocks generated only minor, unspecific reactions. The authors suggested that although DO11.10 mice are genetically identical, their individual immune response can differ, so the lower response of the other two immunized mice (comparable with mocks) was not uncommon. Nevertheless, the specificity of the produced IgG antibodies was assessed in a neutralization assay, in which neither a similar sialylated MUC-4 sequence, nor a MUC-4 peptide sequence, nor the naked GVT SAPDTRPAP sequence, were capable to interact with the antibody. Conversely, the MUC-1 sequence GVT(STn)SAPDTRPAP contained in vaccine **71** almost completely neutralized the serum. The strategy proposed by Kunz and co-workers represents another encouraging result for the development of efficient fully-synthetic anticancer vaccines based on TACAs.

### **I.3.2.2. Two-component (TACA-lipopeptide), fully synthetic anti-cancer vaccines**

Along with the abovementioned two-component synthetic constructs bearing B- and T<sub>H</sub>-cell epitopes, other research groups reported a similar design strategy involving TACAs associated with a second module which differs from the CD4<sup>+</sup> T<sub>H</sub>-cell epitope.

Singhal and co-workers reported the synthesis and immunological evaluation of a dimeric (Ser)Tn-lipopeptide conjugate (**72**, figure 25a). This represents an early report in the frame of fully synthetic immunogens, where two copies of Tn antigen displayed onto serine residues (in red), were attached through a spacer to a tripalmitoyl-S-glycerylcysteinyserine (Pam<sub>3</sub>CS) (in purple), which acts as a potent stimulator of cytokine production (*i.e.* IL-1, IL-6 and TNF- $\alpha$ ) by B-cells and macrophages.<sup>247,248</sup> The *N*-acyl-S-diacylglyceryl cysteine backbone is indeed present in all bacteria, and its role in the innate immune system activation/modulation influences the pattern of adaptive immune response. Recent reports in the frame of bacterial lipopeptides showed their involvement in the modulation of the innate immune system by interacting with APC's Toll-like receptors (TLRs).<sup>249–251</sup> In addition, lipopeptides represent an important class of self-assembling molecules. Their amphiphilic nature allows them to form supramolecular nanostructures, depending on the hydrophile/lipophile balance of the construct, as well as interactions between peptide backbones.<sup>252</sup> Recent studies investigated the self-assembly of three Pam<sub>n</sub>CSK<sub>4</sub> lipopeptides. The authors found a significant difference in morphology arising from the number of attached palmitoyl moieties.<sup>253</sup> While spherical micelles structures were observed for mono- and di- lipidated structures (PamCSK<sub>4</sub> and Pam<sub>2</sub>CSK<sub>4</sub>, respectively), the homologue containing three palmitoyl residues (Pam<sub>3</sub>CSK<sub>4</sub>) organized flexible worm-like micelles (Figure 25b)



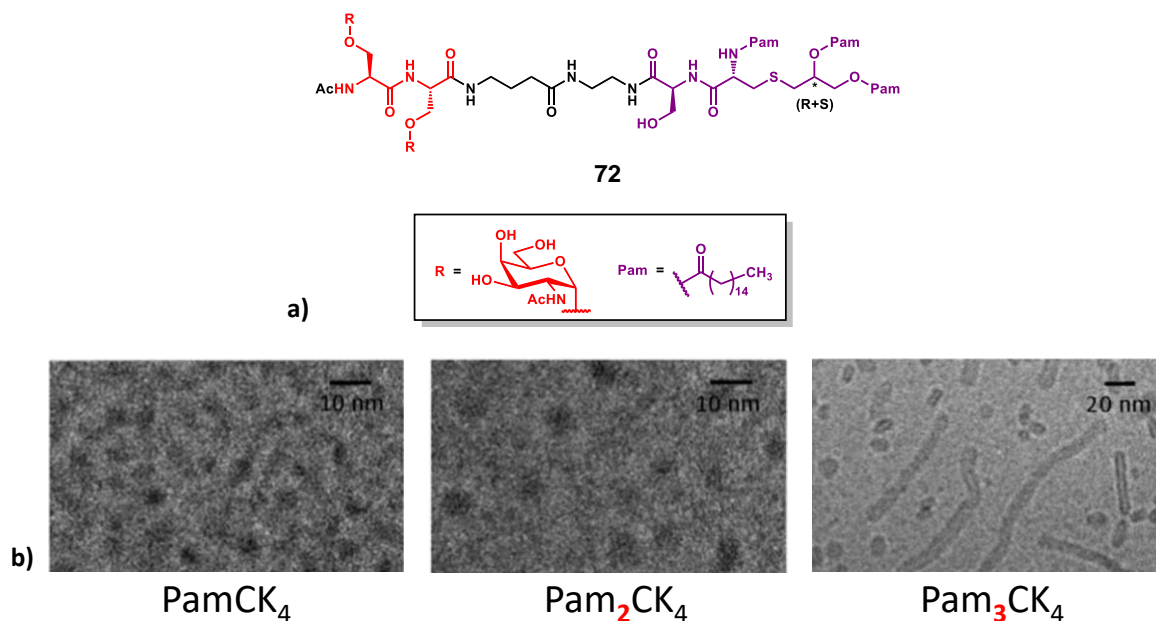


**Figure 25.** a) Fully-synthetic, two-component vaccine construct by Singhal and co-workers. b) Cryo-TEM images obtained for 2% solution of PamCSK<sub>4</sub>, Pam<sub>2</sub>CSK<sub>4</sub> and Pam<sub>3</sub>CSK<sub>4</sub>.

Immunization of CAF mice with 100 µg of vaccine construct **72** (administered as R+S enantiomer mixture) stimulated the production of high titers of anti-Tn antibodies, which were able to recognize the Tn-containing desialylated ovine submaxillary mucin (A-OSM). Surprisingly, along with high anti-Tn IgM production, also a measurable specific IgG antibodies production (normally achieved through a T-cell dependent immune response) was observed. The authors suggested that the lipopeptide moiety was responsible for the enhanced uptake of Tn antigen, resulting in an increased immune response.

Kunz and co-workers integrated the Pam<sub>3</sub>CSK<sub>4</sub> lipopeptide TLR ligand (in purple) onto a cancer-related MUC-1 sequence functionalized with a unique copy of TF antigen, to obtain compound **73** (Figure 26). Vaccination of BALB/c-J mice with compound **73** in the presence of Freund's complete adjuvant generated antibody titers in a lower extent, compared to its TTox-conjugated semisynthetic analogue.<sup>146</sup> The obtained antibodies could not be efficiently neutralized by using the same TF-MUC1 glycopeptide sequence (in red) contained in **73**. Moreover, antibodies showed binding capacity also with negative controls where the T antigen moiety was replaced with a Tn, or STn moiety, suggesting that the recognition process is dominated by the antibody-peptide interaction.

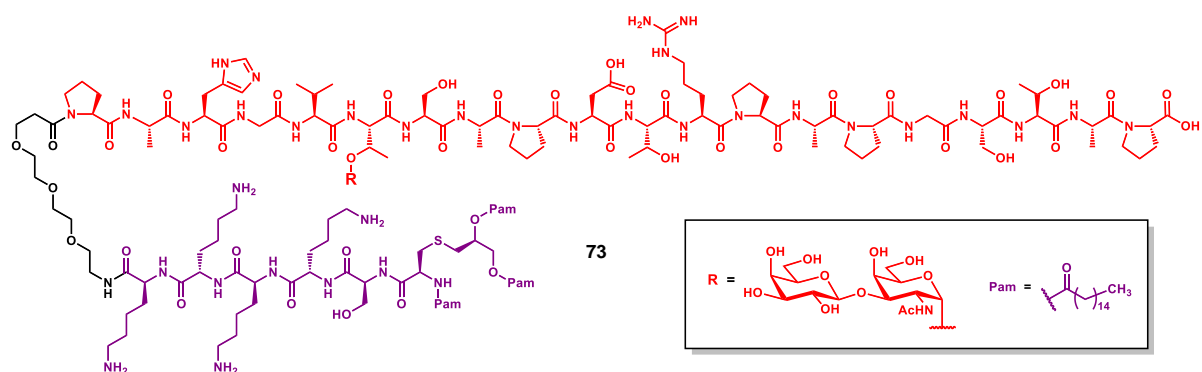


**Figure 26.** Fully-synthetic, two-component TF-based vaccine construct by Kunz and co-workers.

Inspired by precedent works focused on the development of chemically defined self-adjuncting vaccines,<sup>254–257</sup> Li and co-workers designed a small set of fully synthetic, Tn- and MUC1-containing glycopeptide vaccines, where the second element was represented by the self-assembling Q11 peptide sequence (Figure 27a).<sup>258</sup> The Q11 ability to aggregate into fibrils in mild conditions makes it a good tool for acting as both adjuvant and carrier.<sup>259</sup> The self-assembly of constructs **74–77** (Figure 27a) was assessed *via* TEM, revealing fibers over 200 nm long for all the four compounds and without a relevant influence of MUC1's glycosylation pattern (Figure 27b). The obtained supramolecular aggregates displayed the B-cell antigen on their surface, resulting in a multivalent epitope display; moreover, the equilibrium between self-assembly and disassembly can provide a slow release and long-term effect (Figure 27c).<sup>259</sup>

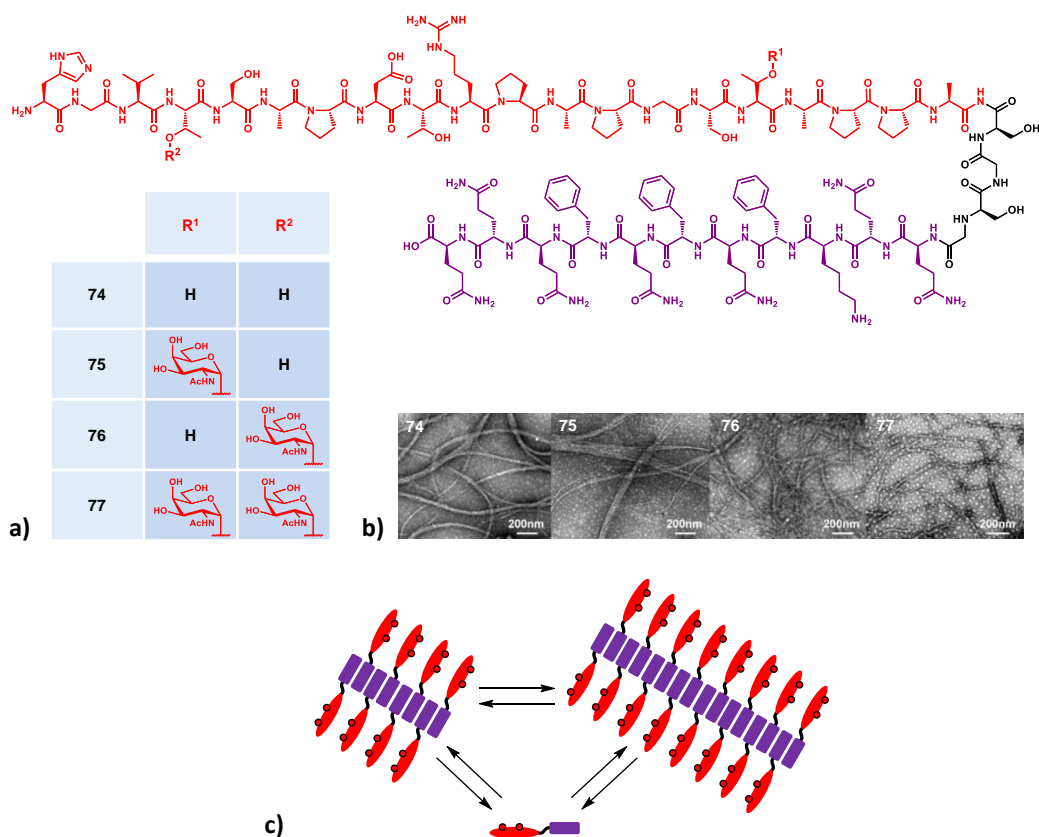


**Figure 27.** a) Fully-synthetic, self-assembling vaccine constructs by Li and co-workers. b) Fibrils aggregates of compounds **74-77**. c) Schematic self-aggregation representation of vaccine constructs.

The entirely peptide structure of Q11 subunit allows to be easily synthesized through standard SPPS procedures, and its conjugation with MUC1 backbone can be performed by elongating the nascent peptide, on the resin support.

Immunization studies were carried out on BALB/c mice by administering PBS solutions containing 100 nmol ( $\approx 400 \mu\text{g}$ ) of compounds **74-77**, alones, or in the presence of Freund's adjuvant (100  $\mu\text{L}$ ). The results showed an increased production of antibodies for mice inoculated with compounds **74** and **75**. Antibody titers were dominated by IgM isotype, although a remarkable presence of IgG was reported; these antibodies strongly reacted with human MCF-7 tumour cell line, and showed the ability to trigger CDC. In the absence of a T<sub>H</sub>-cell epitope, and because of the predominance of IgG2a and IgM antibodies production, the authors hypothesized that compounds **74-75** may activated the immune system via a T-cell independent pathway.<sup>260</sup> Interestingly, formulations including Freund's adjuvant nearly lost their ability to trigger an immune response, regardless of the glycosylation site. The authors finally confirmed the safety and biocompatibility of this strategy, indeed, no immune reaction against the Q11 domain was observed.

### I.3.2.3. Multi-component, fully synthetic anticancer vaccines

In 2007, Boons and co-workers described syntheses and immunological properties of three-component vaccine constructs **78** and **79** (Figure 28a). These multicomponent constructs incorporate a glycopeptide MUC-1 sequence as B-cell epitope (in red), the PV<sub>103-115</sub> class-II restricted T<sub>H</sub> epitope (in green), and the TLR-2/6 activator Pam<sub>2</sub>CK<sub>4</sub> (**78**, R = H), or the TLR-1/2 activator Pam<sub>3</sub>CK<sub>4</sub> (**79**, R = Pal) (in purple).<sup>261</sup>

Due to the different lipophilicity of the lipid moieties in **78** and **79**, two distinct synthetic routes were necessary to reach the desired vaccine constructs.

Compound **78** was obtained by a standard SPPS protocol, using a Rink Amide AM resin, N<sup>α</sup>-Fmoc-protected AAs, and N<sup>α</sup>-Fmoc-Thr(AcO<sub>3</sub>-α-D-GalNAc).<sup>262</sup> Glycopeptide assembly was followed by deprotection of saccharide's acetyl moieties (80% N<sub>2</sub>H<sub>2</sub>/MeOH) and manual coupling of Fmoc-Pam<sub>2</sub>C-OH.<sup>263</sup> Finally, Fmoc-removal, followed by cleavage from the resin support (TFA/phenol/H<sub>2</sub>O/TIS 88:5:5:2) afforded desired compound **78** in 30% overall yield, based on the resin loading.

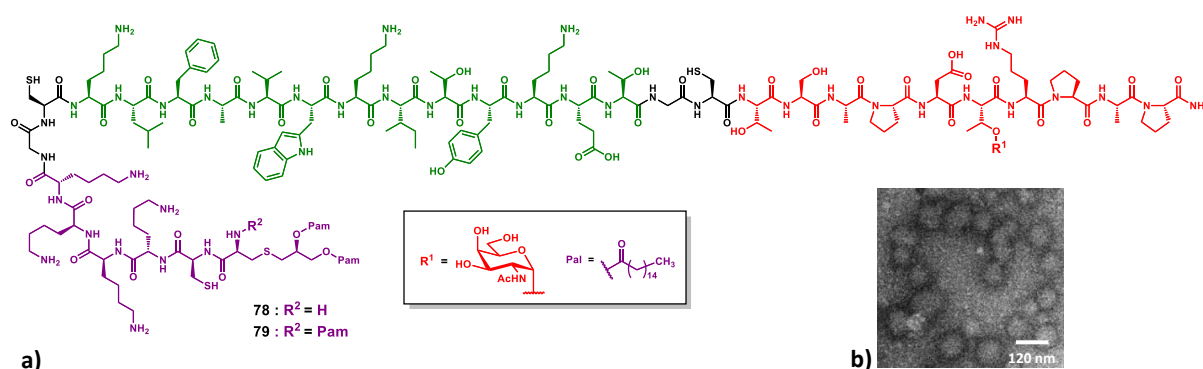
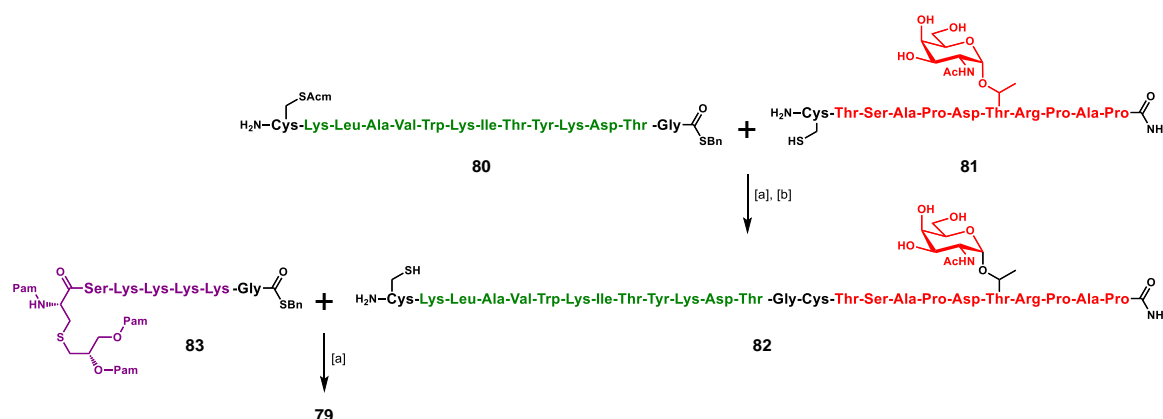


**Figure 28.** a) Fully-synthetic, three-component vaccine constructs by Boons and co-workers. b) Negative-stain transmission electron micrograph of the liposome preparation.

The same linear approach has not proved suitable for the construction of **79**, the obtained crude resulted difficult to purify and not homogeneous. The authors thus decided to undertake a liposome-mediated native chemical ligation (NCL) strategy.<sup>264</sup> NCL is a chemoselective reaction involving an N-terminal cysteine residue and a C-terminal peptide thioester, reacting in a reversible *trans*-thioesterification step to form a thioester intermediate which subsequently rearrange *via* an intramolecular S-to-N acyl transfer, providing the thermodynamically favoured native peptide bond at the ligation site. It is noteworthy mentioning that NCL occurs only at an N-terminal cysteine residues, regardless of the presence of internal cysteine residues. This reaction has served for a broad range of applications, especially for the synthesis of large peptide sequences and proteins, thanks to its

versatility which allows for the merger of unprotected (glyco)peptide fragments in aqueous media at physiological pH in nearly-quantitative yields.<sup>265–267</sup> The applicability of this reaction is reduced when peptide fragments are poorly soluble in aqueous buffer, therefore the incorporation of the reactants in liposomes allow NCS to occur between lipophilic peptides and lipopeptides.<sup>264</sup>

A film of dodecylphosphocholine (DPC), PV<sub>103-115</sub>-containing thioester **80** and unprotected building block **81** was hydrated in a phosphate buffer (pH 7.5) in the presence of tris(2-carboxyethyl)phosphine (TCEP) and EDTA, and then ultrasonicated. The resulting vesicles were sized to 1  $\mu\text{m}$  by passing through a polycarbonate membrane filter. The addition of sodium 2-mercaptoethane sulfonate (MESNA) initiated the reaction, which was completed after 2 hours. Removal of acetamidomethyl (Acm) moiety with Hg(II) acetate, followed by RP-HPLC purification using a C4 column afforded glycopeptide **82** in 61% yield over two steps. A second liposome-mediated NCL between glycopeptide **82** and lipopeptide **83** afforded vaccine construct **79**, in 85% yield.



**Scheme 13.** Synthesis of vaccine construct **79** via liposome-mediated native chemical ligation. Conditions: [a] 200 mM sodium phosphate buffer (pH 7.5), DPC, TCEP, EDTA, sonication (1 min.), extrusion, then MESNA 2% (final w/v), 79% yield for **82**, 85% yield for **79**; [b] Hg(OAc)<sub>2</sub>, 10% aq. HOAc, 50 mM DTT, 77%. DPC = *n*-dodecylphosphocholine; EDTA = ethylenediaminetetraacetic acid; DTT = 1,4-dithiothreitol.

Compounds **78** and **79** were next incorporated into phospholipid-based small unilamellar vesicles (SUVs) by hydration of a thin film of synthetic vaccine constructs, egg phosphatidylcholine, egg phosphatidylglycerol and cholesterol in a HEPES buffer followed by extrusion, to afford 100 nm sized liposomes (Figure 28b). The liposome formulation represents an attractive delivery method in vaccine design, owing to its low intrinsic immunogenicity and the resulting multivalent B-cell epitope display, which promotes B-cell activation by receptor clustering.<sup>268,269</sup>

Groups of female BALB/c mice were immunized with liposomes featuring compounds **78** or **79** (containing 3  $\mu\text{g}$  of saccharide), with or without saponin immunoadjuvant QS-21. Post-immunization

sera of mice inoculated with **79** contained high titers of IgG and IgM antibodies directed against MUC-1, with a preponderant IgG3 production.

Glycopeptide **78**, which contains Pam<sub>2</sub>CSK<sub>4</sub> instead of Pam<sub>3</sub>CSK<sub>4</sub> elicited lower titers of IgGs. The presence of QS-21 in the vaccine formulation did increased IgG titers. Each compound (**78** and **79**) produced low titers of anti-PV antibodies, indicating a negligible epitope suppression phenomenon. Further experiments assessed the effective recognition of the produced antibodies towards the MUC-1-expressing MCF-7 human breast cancer cell line, and the TLR-2-dependent production of cytokines such as TNF- $\alpha$ , which upregulate the expression of costimulatory proteins (*e.g.* CD80, CD83, CD86).<sup>270,271</sup>

The importance of the covalent attachment of the three subunits and the liposomal preparation was assessed by administering a liposome formulation containing the B-cell epitope, the T<sub>H</sub> epitope and the Pam<sub>3</sub>CSK<sub>4</sub> moiety, and a saline solution formulation containing the aforementioned components. Both formulations evoked none or very low IgG antibody responses compared to the original liposome delivery system containing **79**.

Finally, using cells transfected with different TLR receptors, the authors confirmed the presence of a TLR-2-mediated active uptake, which represents an additional mechanism to enhance antigen uptake by APC's, along with the abovementioned MGL-mediated internalization provided by the GalNAc moiety.<sup>272</sup>

The remarkable antigenicity of anticancer vaccine construct **79** can be attributed to its precise design: (i) the presence of a built-in adjuvant ensure the cytokine production at the site in which the vaccine construct interacts with the cells of the immuno-repertoire; (ii) the lipid moiety represents not only a TLR-2 ligand, but also improves the retention into liposomes and ensures a clustered display of B-cell epitopes. Again, Boons and co-workers demonstrated the advantages relative to a multicomponent fully synthetic approach, which allows for a precise optimization of the different vaccine subunits.

Following a similar route, the second generation of fully synthetic vaccine prototypes designed by Dumy and Renaudet, in collaboration with BenMohamed, associated four essential components on the RAFT platform: (i) a cluster of four Tn antigen analogues (in orange); (ii) a CD4<sup>+</sup> T<sub>H</sub> peptide epitope (in green); (iii) a CD8<sup>+</sup> CTL peptide epitope (in blue); and (iv) a palmitic acid (Pam) moiety as internal adjuvant (in purple, figure 29).<sup>273-275</sup> For the construction of compounds **84-86**, a convergent ligation strategy involving both oxime ligation and disulfide bond formation was employed (not shown). Four copies of aminoxy-Tn analogues were introduced on a RAFT scaffold bearing the complementary  $\alpha$ -oxo-aldehyde functions; subsequently, the lower domain of the scaffold was functionalized with a cysteine residue in order to merge the lipopeptide moiety through disulfide bond formation.

Disulfide moieties represent widely employed chemically cleavable linkers which have been used to build a large panel of drug conjugates.<sup>276–279</sup> Once the molecular construct crosses the cell membrane, the reversible nature of disulfide bond allows for the glutathione-mediated thiol-disulfide exchange, thus determining the liberation of the lipopeptide moiety in the intracellular domain. Indeed, inside a cell the concentration of glutathione is approximately 1000-fold higher than in the extracellular environment. Thus, this strategy is supposed to promote vaccine's intracellular delivery, which in the present case should improve the processing of CD4<sup>+</sup> and CD8<sup>+</sup> peptide epitopes.<sup>280,281</sup>

Compound **84** (Figure 29) shows the OVA<sub>257-264</sub> peptide sequence (SIINFEKL)<sup>282</sup> as a target CD8<sup>+</sup> epitope for the induction of a cellular immune response, which was synthesized in line with the Pan-DR universal CD4<sup>+</sup> T<sub>H</sub> peptide (PADRE : {dA}K{Cha}VAAWTLKAA{dA}{Ahx}),<sup>283</sup> the resulting peptide sequence was further extended with a palmitic acid moiety at the N-terminus, to confer a self-adjuvanting character to this four-components vaccine construct.

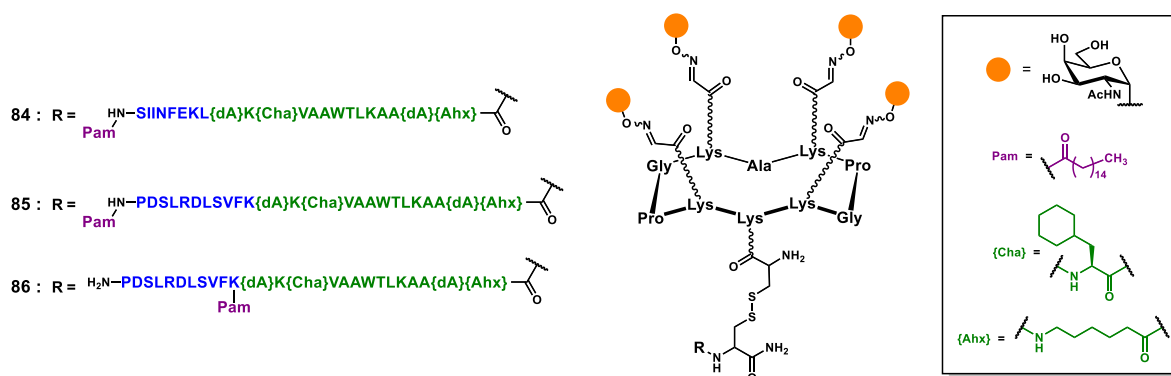


**Figure 29.** Fully-synthetic, four-component vaccine constructs by Dumy, Renaudet and co-workers.

Indeed, recent attempts have been devoted to avoid toxic adjuvants effects by introducing built-in adjuvanting moieties. Palmitic acid is a low molecular weight lipid moiety, capable of stimulating APCs such as B-cell, DCs and macrophages, by acting as TLR-2 ligand.<sup>284,285</sup> It is derived from the immunologically active N-terminal sequence of an *Escherichia coli* lipoprotein,<sup>286</sup> and has been widely used for the enhancement of carbohydrate B cell epitopes as well as for peptide T-cell epitopes; however, its efficacy in a multicomponent vaccine such **84** was never been assessed before.<sup>287</sup>

B-cell immunogenicity of **84** (OVA-GLP, 50 μM/mice in 100 μL of PBS) or its non-lipidated version (OVA-GP, devoid of the palmitoyl moiety, 50 μM/mice in 100 μL of PBS) were investigated on two groups of H2<sup>b</sup> mice in adjuvant-free PBS solutions, while a third group of mice was treated with OVA-GP along with CpG<sub>1826</sub><sup>288</sup> adjuvant (25 μg). In the first two groups (CpG-free) no adverse reaction was observed, but the OVA-GP alone did not induced specific IgG or IgM antibodies in an adjuvant-free context. Collected sera induced by both OVA-GLP (**84**) and OVA-GP + CpG<sub>1826</sub> contained high titers of

specific IgG and IgM antibodies, which were reactive towards MCF-7 cancer cell line and, to a lesser extent, T-47D cancer cell line (expressing a lower level of Tn antigen, compared to MCF-7). Immunization of MO5, OVA-transfected B16 mice with **84** allowed the *in vitro* and *ex vivo* assessment of a OVA<sub>257-264</sub>-directed T-cell response, based on the detection of IFN- $\gamma$  producing CD8<sup>+</sup> T-cells.

The authors further investigated the protective effect of adjuvant-free OVA-GLP **84** and OVA-GP + CpG<sub>1826</sub> on B6 mice. Ten days after the third immunization, mice were challenged with OVA-expressing mouse melanoma cells (B16) and then monitored for tumor growth and survival rate. Only one mouse out of ten developed a detectable tumor in the group treated with **84**, and none of the mice in the OVA-GP + CpG<sub>1826</sub> group developed detectable tumors. In terms of survival rate, 90% of mice (9 out of 10) immunized with **84** survived for 90 days, while all mice treated with OVA-GP + CpG<sub>1826</sub> survived (Figure 30a). The specificity of the protective effect was assessed by challenging other groups of mice with tumor cells which does not express the OVA antigen, and all mice developed tumors following the tumor grafts. The therapeutic effect of compound **84** was investigated by a tumor growth inhibition assay, where three groups of B6 mice challenged with MO5 cells were inoculated with vaccine preparations (*i.e.* **84** alone in PBS, or OVA-GP + CpG<sub>1826</sub>) when the tumor diameter reached 3-4 mm. Of ten mice inoculated with **84**, all were still alive eight weeks after tumor inoculation, while seven of ten mice immunized with OVA-GP + CpG<sub>1826</sub> survived (Figure 30b).

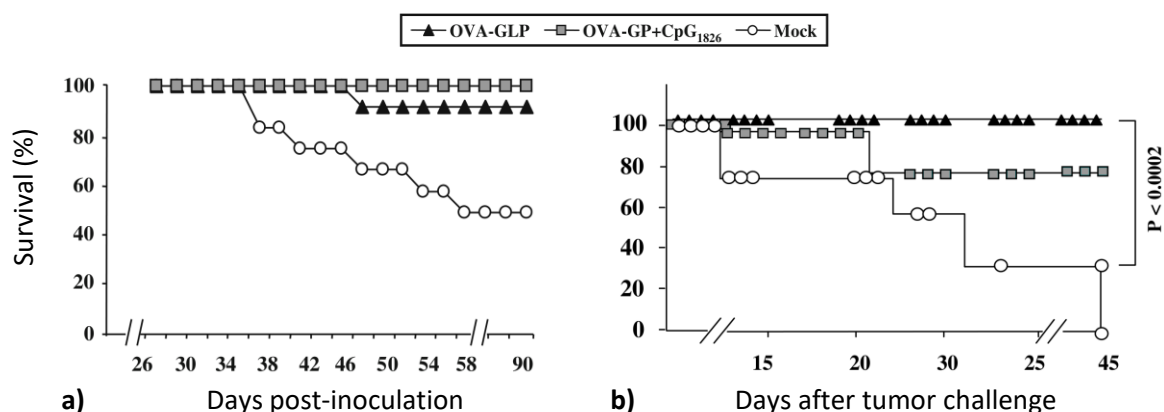


**Figure 30.** a) Protective effect. Survival represents the percentage of mice survived in OVA-GLP (**84**), OVA-GP + CpG<sub>1826</sub> immunized and control set as a function of days after MO5 challenge. b) Therapeutic effect. MO5 cells were injected in female B6 mice and eight days later OVA-GLP and OVA-GP + CpG<sub>1826</sub> were administered. Mock: PBS solution.

This study highlighted the advantages of the fully synthetic glyco-lipo-peptide (GLP) vaccine prototype **84**, where a convergent modular approach based on the mutually compatible oxime ligation



and disulfide bond formation allowed for the construction of a precise and fully characterized construct, able to trigger a self-adjuvanting specific immune response in mice models. The produced antibodies recognized the Tn-positive human cells lines MCF-7 and T-47D, but not the Tn-negative cell lines (*i.e.* T2 and RS). Moreover, protective and therapeutic immunological effects have been observed, also in the absence of an external adjuvant, improving the efficacy of the vaccine construct.

In another study, vaccine constructs **85** and **86** were investigated; they differ from **84** for the presence of the CD8<sup>+</sup> HER<sub>420-429</sub> sequence (PDSLRDLSVFK) from HER-2/neu glycoprotein, which is overexpressed by breast carcinomas (Figure 29).<sup>289</sup> The palmitoyl moiety was integrated onto the two GLPs constructs either at the N-terminus end (**85**, linear GLP), or in between the CD4<sup>+</sup> and CD8<sup>+</sup> sequences, on the HER's lysine side chain (**86**, branched GLP). The uptake, processing and cross-presentation pathway of **85** and **86** (50 µg/mice) were investigated to study whether the position of the lipid moiety would affect the B- and T-cell immunogenicity and the protective efficacy of these vaccine constructs. While more potent HER<sub>420-429</sub>-specific IFN-γ CD8<sup>+</sup> T cell responses was induced by the linear GLP **85**, the branched analogue **86** generated stronger tumor-specific IgG responses. Furthermore, although both constructs showed a TLR-2-mediated uptake mechanism to enter dendritic cells and succeeded in inducing their maturation, each construct appeared to be processed and presented to T cells differently. Thus, the position of the lipid moiety within synthetic GLP constructs profoundly affects the phenotypic and functional maturation process of DCs, the processing of the glyco-peptide molecules and their cross-presentation in DCs, as well as the magnitude of IgG and CD8<sup>+</sup> T-cell responses. Although cellular and molecular mechanisms underlying the immunogenicity of **85** and **86** remain to be fully elucidated, data suggests that the position of the lipid moiety strongly influences the immunogenicity of these constructs and is superior compared to non-lipidated analogues in the absence of an adjuvant setting. The different position of the palmitoyl moiety not only affected the uptake and cross-presentation pathways in DCs, but modulated the magnitude of antitumor antibody and CD8<sup>+</sup> T-cell protective immunity. It can be hypothesized that the presence of the lipid tail may promote the self-organisation of the vaccine candidate in solution, which may impact the resulting immunogenicity. However, this aspect has not been discussed by the authors.

A third generation of vaccine construct was elaborated by our research group, in collaboration with BenMohamed and Nativi. This vaccine prototype includes four clustered Tn-antigen mimetics as B-cell epitopes (in red) and the PADRE sequence in line with the OVA<sub>257-264</sub> peptide, as CD4<sup>+</sup> T<sub>H</sub> cell (in green) and CD8<sup>+</sup> CTL (in blue) epitopes, respectively, conjugated on the cyclopeptide carrier (**87**, Figure 31a).<sup>290</sup>

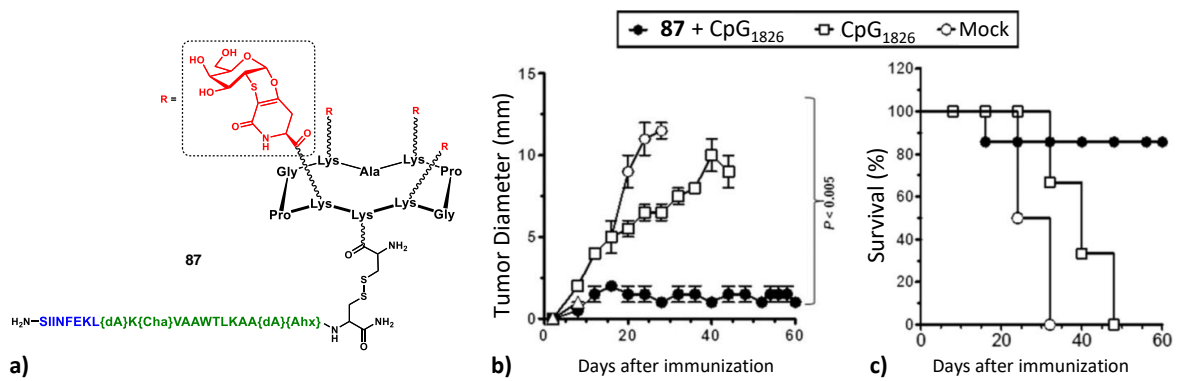


**Figure 31.** a) Fully synthetic, Tn-mimic displaying vaccine construct by Renaudet, Dumy and co-workers. b) Tumor diameter increase. c) Survival rate of mice groups.

It has been hypothesized that TACA-based vaccines displaying these mimetics instead of native Tn antigens could be more stable towards enzymatic degradation by endogenous glycosidases, thus extending its biological half-life. The bioactive Tn-antigen mimetic, developed by Nativi and co-workers, is a 2-deoxy-2-thio- $\alpha$ -D-galactoside that retains the  $^4C_1$  chair conformation of the native antigen.<sup>291</sup> It was conjugated through amidic linkage to the four lysine's side chain on the scaffold upper domain, while the immunostimulant peptide was linked on the lower domain *via* disulfide bridging.

The safety and immunogenicity were evaluated in B10.D1 mice inoculated with **87** (100  $\mu$ g/mice in 100  $\mu$ L PBS) in presence of CpG<sub>1826</sub> adjuvant (20  $\mu$ g). High levels of mucin-specific IgG/IgM antibody ratio were induced (IgG/IgM titers >8000), and approximately half of the titer was still present in the serum 240 days after the last immunization. Moreover, antibodies were found to bind to human MCF-7 cancer cell lines expressing the native carbohydrate antigens. Tumor growth and survival rate monitoring in female B10.D1 mice implanted with NT2 cells showed that out of ten mice vaccinated, seven were still alive eight weeks after tumor inoculation. Only one or none survived in negative control groups, where adjuvant alone (20  $\mu$ g) and PBS were administered, respectively (Figure 31b and 31c). Finally, *in vivo* depletion of B cells, CD4<sup>+</sup> cells, or CD8<sup>+</sup> T cells in immunized mice by using specific mAbs showed that only the lack of B cells abrogated the protection induced by **87** against tumor progression and death, suggesting that the protection is mainly due to B cells.

### **I.3.2.4. Fully-synthetic approaches – Conclusions**

In conclusion, the fully-synthetic approach demonstrated that chemically defined vaccine constructs containing precise oligopeptide T<sub>H</sub> epitopes, chemically associated with TACAs as B-cell epitopes, could efficiently give rise to high titers of TACA-specific IgG antibodies, with similar efficacy than semi-synthetic vaccines.

In several studies, the produced antibodies demonstrated to be reactive towards human tumor cell lines, and the promising results reported in this section have inspired several other research groups to explore new possibilities in terms of multicomponent vaccine design.

The reliability of solid phase (glyco)peptide syntheses, and the advances in the field of chemoselective ligations provided a panel of options for the assembly of different sub-units, facilitating the introduction of convenient antigenic elements;<sup>206</sup> such as the human universal PADRE epitope, reported to generate carrier-specific antibody response in less lower extent compared to a protein carrier.<sup>283,292</sup>

Chemical design also allowed the replacement of natural TACA structures with analogues or mimics, able to generate IgG antibodies reactive with native TACAs.<sup>121,238,274,290</sup>

The use of a non-immunogenic scaffold, which supports the versatile introduction of several elements in a convergent manner, represents a useful tool for optimizing the vaccine design in terms of sub-unit composition and multivalency.<sup>205</sup> Examples of multivalent B-cell epitope display have also been reached through dendrimer-like scaffolds, liposome formulations and self-assembling structures.<sup>212,257,276,293,294</sup>

### I.3.3. Adjuvants

To complete this overview on vaccine design, it is noteworthy at least mentioning the wide role of adjuvants: immune-enhancing additives employed since the earliest attempts to raise significant immune responses. All adjuvant systems are basically focused on two mechanisms: (i) specific immune activation, and/or (ii) delivery-depot effect. Despite the abundance of adjuvant systems employed in preclinical models, only few resulted compatible for human vaccines, being the primary limitation for this diversified class of immunomodulators their safety issues.<sup>295</sup>

Aluminium salts adjuvants, generally referred as *alums*, represent early, successful examples employed in anti-diphtheria vaccines. They are composed of a co-precipitate of aluminium hydroxide and diphtheria toxoid in carbonate buffer. Only occasional and moderate toxicities were reported with these vaccine settings.<sup>296</sup> The next step in adjuvant research was made by Freund, whose water-in-oil emulsion, formed by the mixture of one volume 10% Arlcel A and 90% mineral oil with one volume of antigen (heat-killed *Mycobacterium tuberculosis*, cf. Complete Freund's Adjuvant: CFA) in solution represented the standard for adjuvant activity from the 1930s to the 1970s.<sup>297</sup> Mechanistic studies on oil-based adjuvants revealed a correlation between maintenance of antibody titers and presence of adjuvant depot for a period of months after injection.<sup>298</sup> Nevertheless, documentations of intense inflammations, evidences that the emulsion was not entirely retained at the injection site, and the suspected role of the poorly metabolized mineral oils as carcinogens made Freund's adjuvant acceptance controversial.

Advances in immunology allowed the characterization of APC's receptors and cytokine expression profiles, posing the basis for next generations of adjuvants based on a receptor-driven rational. The families of pattern recognition receptors (PRRs) implicated in bridging innate-adaptive responses, such as TLRs and NOD (nucleotide-binding oligomerization domain), are continuously growing and offering new possibilities in adjuvant's design. Lipid A-related adjuvants, CpG oligonucleotides, alone or in combination with liposome- or particulate-based delivery systems represent just few examples of the contemporary state-of-art in adjuvant settings.

The fate and functions of activated T<sub>H</sub> cells depends in large part on the microenvironment present at the time of the initial antigen encounter. The cytokine milieu composition bias the development of naïve CD4<sup>+</sup> cells towards one or several differentiation pathways, leading to effector T<sub>H</sub> cell subsets with different functional profiles.<sup>299</sup> Likewise, the nature of the antigen acquired by APCs will affect the expression of different sets of costimulatory molecules (*e.g.* CD80, CD86), which will also influence the developmental path of antigen-stimulated T<sub>H</sub> cells.<sup>300</sup>

In the vaccine set, (i) dendritic cells maturation, (ii) migration to the lymph nodes, and (iii) their cytokine expression can be stimulated, for example by the co-administration of delivery-depot adjuvants and ligands for DC's toll-like receptors (TLRs).<sup>301,302</sup>

## I.4. My project

Fully-synthetic anticancer vaccines represent an emerging topic in chemical immunology, supported by the possibility to be obtained in an efficient, reproducible and well-defined manner. Their high potential in terms of design allows tailoring the macromolecular assembly of sub-units of choice to give rise to unprecedented vaccine constructs. They demonstrated effective as their semi-synthetic precursors based on protein-carriers, and the absence of immunogenic elements which could interfere with the targeted immune response make them more tolerable.

**Our aim is to design TACA-based anticancer vaccine prototypes with improved immunological properties.** The basis of our strategy for the synthesis of TACA-based anticancer vaccine prototypes relies upon the versatile, easily addressable and non-immunogenic RAFT platform, which represents an ideal tool for the conception of multi-modal, macromolecular constructs for biological applications. Indeed, RAFT-based synthetic vaccine prototypes, functionalized with TACAs along with CD4<sup>+</sup> and CD8<sup>+</sup> epitopes, demonstrated effective in producing high titers of specific IgG antibodies and CTL-mediated cytotoxicity in animal models. The rigid backbone of RAFT cyclopeptides allows displaying clustered B-cell epitopes, promoting a TACA-directed *humoral response*, and T-cell peptide epitopes, to sustain *adaptive immunity* (CD4<sup>+</sup>) and trigger a *cellular response* (CD8<sup>+</sup>). These elements can be easily introduced on the scaffold by means of orthogonal, chemoselective and high yielding reactions over its two distinct spatial domains.

The results obtained by our research group in the field of chemical immunology led to three generations of fully synthetic anticancer vaccine prototypes (Figure 32): (i) a *1<sup>st</sup> generation of two-components* constructs, involving four clustered copies of saccharide Tn antigen, linked *via* oxime bond, and a CD4<sup>+</sup> epitope (Figure 24); (ii) a *2<sup>nd</sup> generation of four-components* prototypes, where a CD8<sup>+</sup> epitope and a palmitoyl moiety have been introduced to provide a cellular response and a self-adjuncting effect (Figure 29); (iii) a *3<sup>rd</sup> generation*, including a rigid Tn mimic, along with CD4<sup>+</sup> and CD8<sup>+</sup> epitopes (Figure 31a).

The use of saccharide analogues (or *mimics*) of native TACAs (*e.g.* compound **63**, scheme 11), which are modified at the anomeric position to be efficiently conjugated to the “core” scaffold *via* click chemistry, allowed the production of antibodies reactive towards the native form of the antigen.

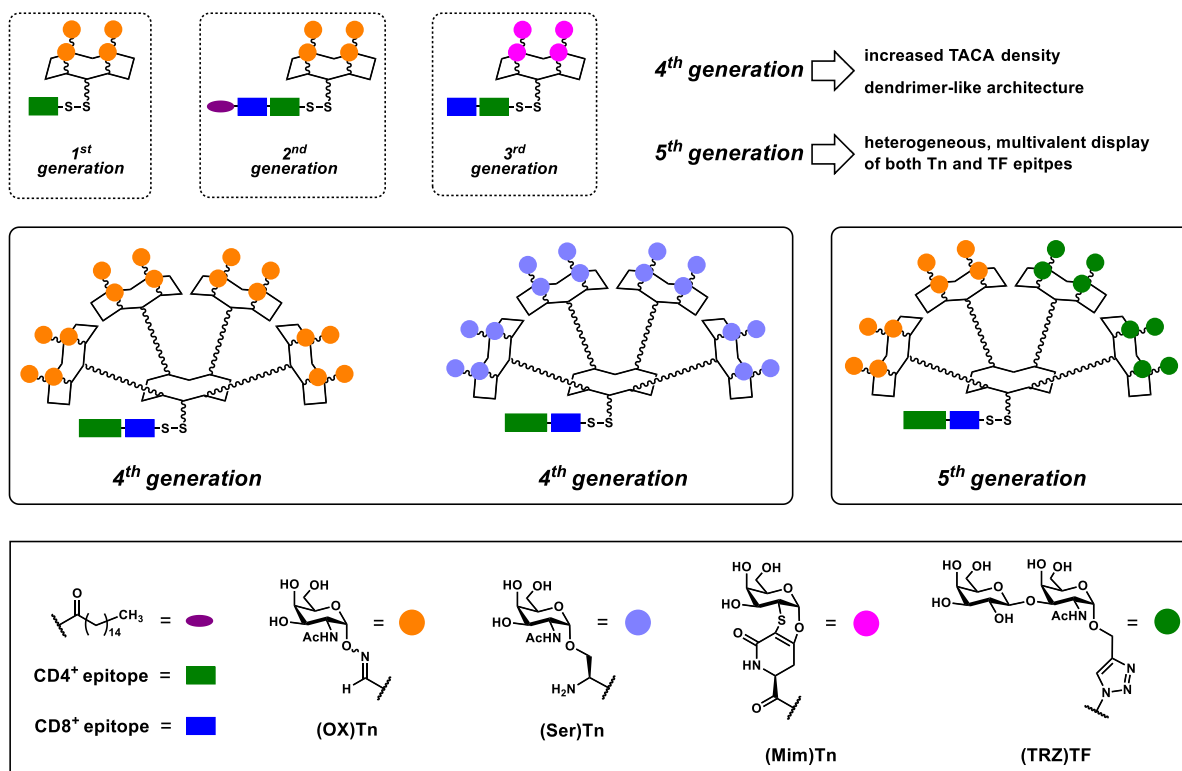


**Figure 32.** Schematic representation of the three generations of anticancer vaccines obtained by our research group and the two new generations explored in this work.

On the basis of these works, **in my PhD project we aimed to design and synthesiz two new generations of TACA-based fully synthetic vaccines** (Figure 32).

- The **4<sup>th</sup> generation** involve a *three-component* construct displaying and enhanced density of both (OX)Tn\* and (Ser)Tn epitopes (sixteen copies) on a multivalent dendrimer-like scaffold, plus CD4<sup>+</sup> and CD8<sup>+</sup> epitopes from ovalbumin (OVA). This would increase the B-cell epitope ratio over the entire molecule, and promote BCR clustering by a multivalent TACA presentation.
- The **5<sup>th</sup> generation** include a heterogenic TACA display, with both Tn and TF saccharide epitopes displayed in a multivalent manner. According to the progressive evolution of the array of TACAs expressed during the course of the disease, an heterogenic display would better mimic the cancer-associated glycocalyx, conferring a multifaceted humoral response. We thus designed an heterovalent glycodendrimer scaffold which can be readily functionalized to display eight copies of oxime-linked Tn epitopes and eight copies of triazole-linked TF epitopes, (OX)Tn and (TRZ)TF, respectively. Following functionalization with OVA CD4<sup>+</sup> and CD8<sup>+</sup>

\* For sake of clarity, from now on, when aminoxy-containing Tn-saccharide analogue **63** is conjugated to its aldehyde counterpart we will refer to it as (OX)Tn, indicating the presence of an oxime linkage. Accordingly, the Tn epitope displayed on a serine residue will be referred as (Ser)Tn. Finally, the TF epitope conjugated to the scaffold *via* a 1,4-triazole linker will be indicated as (TRZ)TF.

epitopes, this generation would represent the first example in literature of fully synthetic, hetero-TACA, *three-component* vaccines.

**The synthesis of the abovementioned generations of vaccine prototypes required efforts in designing efficient multi-step syntheses and conjugation protocols to achieve a controlled assembly of the different modules (e.g. scaffold, B-cell epitopes, T-cell epitopes). Consequently, in my PhD work the majority of efforts have been devoted to developing synthetic strategies to reach such unprecedented complex structures, for which no general methodology can be applied.**

**Chapter I** served as general introduction to provide a better understanding of the project; essential notions of immunology and the state-of-art of antitumor vaccines in the context of cancer immunotherapy have been outlined.

**Chapter II** is dedicated to the synthesis of multivalent homogeneous glycodendrimers. We first worked on mannosylated model structures, by employing a divergent oxime-based protocol already exploited in our research group (**II.2.**). In the next section, by means of this strategy, we readily obtained an hexadecavalent (OX)Tn-based glycodendrimer, essential B-cell epitope module for our 4<sup>th</sup> generation vaccines (**II.3.**). We then explored a combined protocol (CuAAC/OL) involving two click reactions: copper(I)-catalyzed alkyne-azide cycloaddition and oxime ligation (**II.4.**). This route allowed us to reach (TRZ)Tn-based glycodendrimer in a more controlled and efficient manner, also *via* a more reliable convergent assembly. (TRZ)Tn-based glycodendrimers in both anomeric configurations have been tested for their binding activity towards the SBA lectin, through an indirect binding biochemical assay (ELLA). In the last section of chapter II, a new small family of mannosylated multivalent dendrimers have been designed and efficiently assembled thanks to a convergent CuAAC-based protocol (**II.5.**). The resulting glycodendrimers demonstrated a remarkable binding avidity towards the BC2LA lectin, assessed *via* isothermal titration calorimetry experiments.

**Chapter III** is devoted to the synthesis of the hetero-TACA multivalent glycodendrimer, key module for the conception of our 5<sup>th</sup> generation of *three-component* fully synthetic vaccines. The synthetic procedures explored in the former chapter demonstrated convenient for the assembly of such a multimodal synthesis.

**Chapter IV** reports the preliminary assays on (OX)Tn/(TRZ)TF-based glycodendrimers from the 4<sup>th</sup> and 5<sup>th</sup> generations, with specific anti-Tn and anti-TF monoclonal antibodies (**IV.1.**). Before undertake *in vivo* trials we evaluated interference phenomena which could arise from the concomitant presence of Tn and TF antigens on the same macromolecular construct. We next employed the anti-Tn mAb to compare the binding efficacy of glycodendrimers functionalized either with (OX)Tn or with (Ser)Tn epitopes (**IV.2.**). The last part of the manuscript describes the final conjugation steps, including



the disulfide bridge formation between the B-cell epitope module and the CD4<sup>+</sup>-CD8<sup>+</sup> modules, to give a new generation of fully-synthetic vaccine prototypes (**IV.3**).

## **Chapter II.**

# **Synthesis of multivalent homo- glycodendrimers**

## II.1. Introduction

As described in section I.1.4. (*Humoral adaptive immune responses*) the first, key event required for B-cells activation involve the antigen-mediated crosslinking of BCRs on B lymphocytes. Given the importance of a multivalent B-cell antigen presentation for a more effective BCR clustering, we investigated the validity of the synthetic approaches developed in our laboratories to reach precise and well characterizable multivalent homo-glycodendrimer structures.<sup>303,304</sup>

In order to design a new anticancer vaccine generation with increased multivalency (compared to the tetravalent B-cell antigen display of the formers generations), in a first step we dedicated our efforts towards the synthesis of homogeneous multivalent glycodendrimers, focussing on the design of new architectures and synthetic strategies. Indeed, it is widely recognized that protein-carbohydrate interactions depend on structural criteria such as ligand's valency and topology. We thus decided to explore new macromolecular structures, which will be decorated with model carbohydrates, simpler and easily accessible compared to TACAs. This will allow us to exploit the newly synthesized multivalent structures with biological relevant targets available in our laboratories.

Dendrimers are defined as repetitively branched macromolecules, with a tree-like architecture, from the Greek term “*δέντρο*” which means “tree”.<sup>305</sup> Like polymers, dendrimers are constituted of repeating units but a clear line can be drawn to divide these two classes of compounds. First, dendrimers are never synthesized by polymerization reactions but rather step-by-step, affording reproducible, well-defined and monodisperse structures. Second, a dendrimer is typically symmetric around its multivalent “core” scaffold; the grafting of branched “arms” onto the “core” often gives rise to spherical three-dimensional morphologies.

Over the last twenty years, an extensive body of literature has been devoted to describe the role of dendrimers in several research areas such as catalysis, material science and in bio-medicine.<sup>306–310</sup> In the context of our work, we found these structures particularly interesting for their advantageous characteristic, which include the possibility to tailor and “grow” the epitope valency in a controlled fashion. We think that displaying TACAs onto multivalent glycodendrimers would provide enhanced immunostimulating properties for our fully-synthetic vaccine constructs. From now on, the term *glycodendrimer* will refer to monodisperse, dendrimer-like, branched structures decorated with a peripheral carbohydrate moiety. The term *homo-glycodendrimer* indicates that the carbohydrate moiety is homogeneous, that is to say that homo-glycodendrimers are decorated with several copies of the same carbohydrate entity, in contrast with hetero-glycodendrimers, which are grafted with different carbohydrate moieties.<sup>311</sup> In addition, the term *glycocluster* will be employed to describe glycoconjugates in which the sugar moiety is directly attached to the scaffold backbone.

There are two main approaches for the assembly of glycodendrimers (Figure 33).<sup>312</sup> Through a *divergent* approach, peripheral “naked” scaffolds are grafted onto a “core” scaffold to provide an additional layer (referred as “generation”), equipped with suitable anchorage points, which is finally functionalized with the sugar moiety. By a *convergent* assembly, peripheral scaffolds are previously functionalized with the sugar moiety, and then grafted on the “core” scaffold, to give the target glycodendrimer. While early approaches were based on the divergent approach, the convergent method allows for an easier removal of impurities and partially reacted intermediates, providing a more reliable strategy for reaching monodisperse glycodendrimers. On the other hand, the achievable size of final structures obtained *via* convergent assembly may be limited due to steric effects along the “core” scaffold.

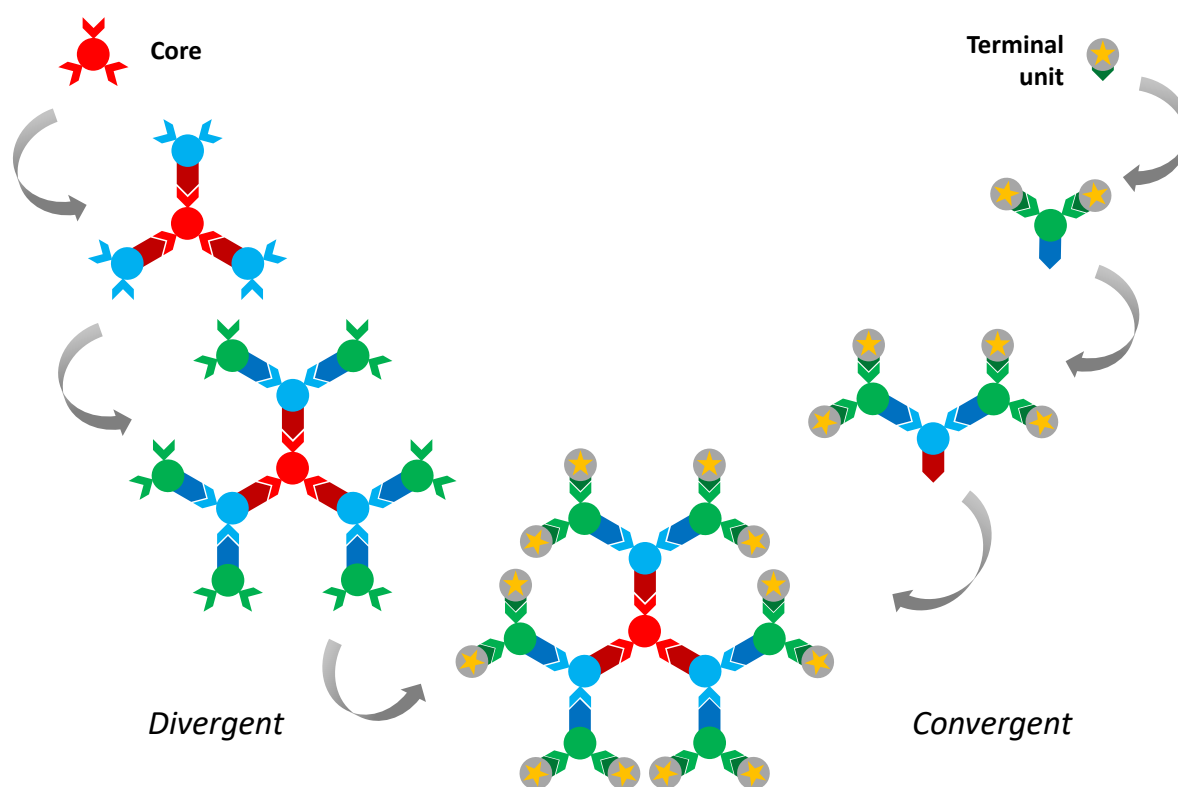


**Figure 33.** Divergent and convergent approaches for the assembly of multivalent glycodendrimers.

In addition to the divergent and convergent approaches, there are two other aspects of primary importance for achieving an efficient and rapid glycodendrimer assembly. The first relies on the utilization of multivalent scaffolds as appropriate building blocks, which can be integrated as “core” and/or peripheral “arms”, allowing for an inherent higher valency, which can be rapidly increased by installing a “second-generation” layer. The second implies the utilization of accelerated coupling

methodologies, such as those provided by the use of chemoselective, orthogonal reactions (often referred as “click-chemistry”).

### II.1.1. “Core” scaffolds

The most simple multivalent scaffolds employed for the construction of glycodendrimers are tetravalent structures (Figure 34, **A-F**).<sup>313,314</sup> Tetra-substituted benzenes (**A**), pyrenes (**B**), and tetraphenylethylenes (**C**) contain aromatic cores which have been exploited for their photochemical properties. Pentaerythritol (**D**), adamantane (**E**) and tetraazacyclododecane (**F**) represent non-aromatic tetravalent structures; they also represented valuable choices in the context of glycodendrimer chemistry and supramolecular assemblies.<sup>315</sup> Although commercially available and achievable in kilogram-scale synthesis, pentavalent corannulene (**G**)<sup>316</sup> and pentaazacyclopentadecane (**H**)<sup>315</sup> represent less employed platforms compared to the other reported structures.<sup>317</sup> Nevertheless, hexavalent cyclotriphosphazenes (**I**)<sup>318</sup> and calix[4]arenes (**J**)<sup>319,320</sup> have been widely employed and extensively described in literature by the research groups of Majoral and Ungaro, respectively. It is important to mention that “core” scaffolds can also be asymmetrically modified (red sphere in **I** and **J**), giving rise to useful building blocks for achieving high-order dendrimers.<sup>318</sup> Among higher-valency scaffolds, comprising aromatic (**K-M**, **P** and **R**), non-aromatic (**N**), cyclodextrin (**S**) and octasilsesquioxane (**Q**) “cores”, the RAFT cyclic template (**O**) pioneered by Mutter, Dumy and co-workers represents a particularly appealing structure not only for its versatility in terms of orthogonal functionalization but also because has proven to be well tolerated in vivo and non-immunogenic, therefore representing our tool of choice for the construction of anticancer vaccines.<sup>205</sup> Finally, dodecavalent C<sub>60</sub> fullerene derivatives (**T**) described by Nierengarten and co-workers, have revealed interesting tools in glycobiology, also due to their inherent photochemical properties.

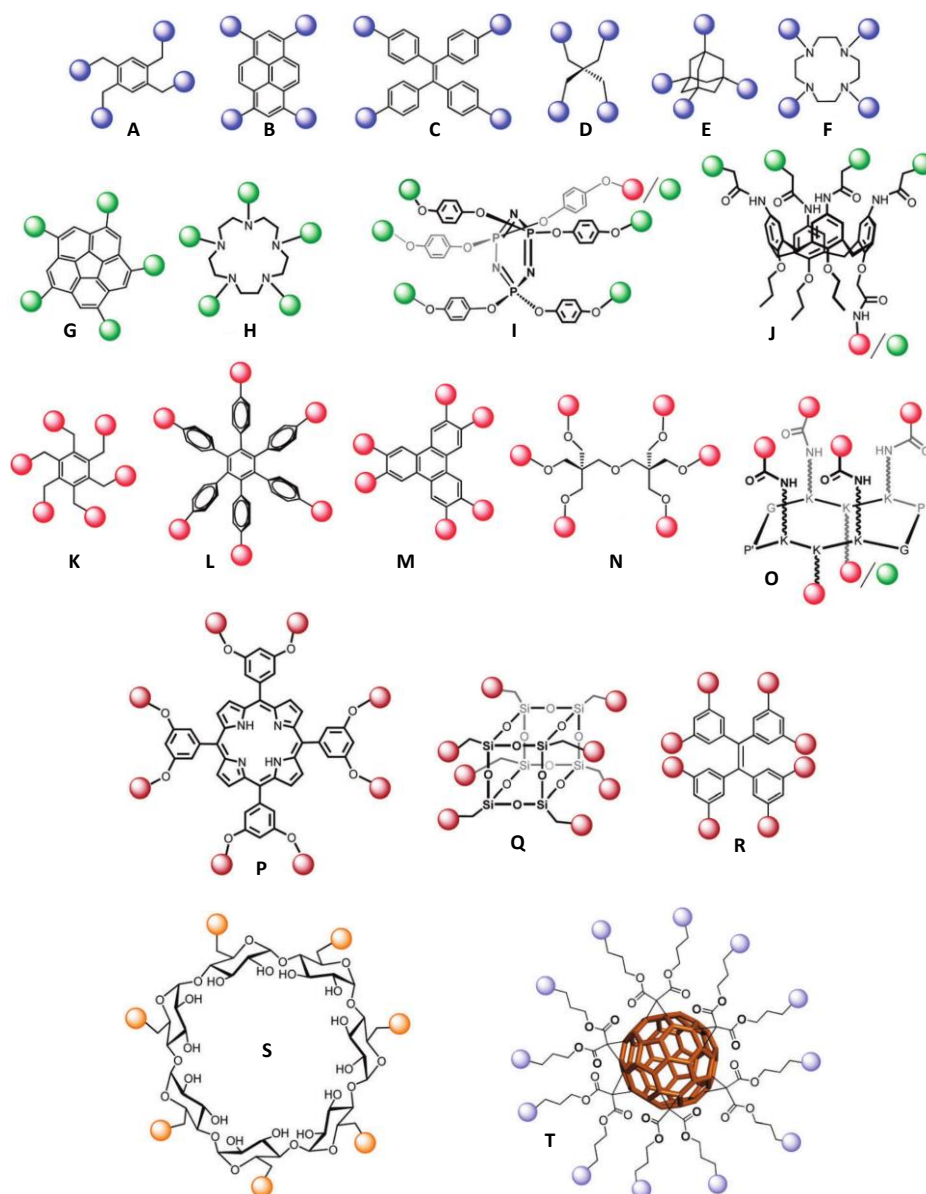


**Figure 34.** Overview of the main multivalent scaffolds employed for designing dendritic architectures. Adapted from Roy *et al.*, *RSC Chem. Soc. Rev.* 2015.

## II.1.2. Chemoselective “click” chemistry

The rise in popularity of the so-called click-chemistry over the past few years has been driven by its extraordinary achievements in the field of bioconjugation chemistry.<sup>207</sup> Click-chemistry refers to a class of chemoselective, biocompatible reactions which can be carried out in mild conditions (ideally in water or physiological buffer) to give the desired conjugation products from unprotected building blocks, with high yields and reproducibility.<sup>321</sup> According to the definition of Prof. Sharpless (2001),

who coined the term click-chemistry, the development of an expanding set of powerful, selective, and modular “blocks” that work efficiently in both small- and large-scale application, represents the foundation of this chemical approach. Other desirable features that click-chemistry reactions should have can be listed as follows: (i) only inoffensive and easily-removable by-products should be generated; (ii) reactions should be stereospecific (not necessary enantioselective), and (iii) have a high thermodynamic driving force ( $>20 \text{ kcal mol}^{-1}$ ). Ever since Cu(I)-catalyzed alkyne-azide cycloaddition (CuAAC) was widely accepted as “click” reaction, strong efforts have been made to widen the panel of chemoselective “click” reaction (Table 3).

REACTION TYPE	REAGENT 1	REAGENT 2	CATALYST & BYPRODUCT	PRODUCT
<b>R-N<sub>3</sub> involved click reactions</b>				
CuAAC	R <sub>1</sub> -N <sub>3</sub>	≡-R <sub>2</sub>	Cu(I)	
SPAAC	R <sub>1</sub> -N <sub>3</sub>			
Non-traceless Staudinger Ligation	R <sub>1</sub> -N <sub>3</sub>		N <sub>2</sub>	
Traceless Staudinger Ligation	R <sub>1</sub> -N <sub>3</sub>		N <sub>2</sub> HS-CH <sub>2</sub> -P(=O)(Ph) <sub>2</sub>	
<b>R-SH involved click reactions</b>				
Thiol-ene	R <sub>1</sub> -SH		hν	
Thiol-yne	R <sub>1</sub> -SH	≡-R <sub>2</sub>	hν	
Thiol-Michael Addition	R <sub>1</sub> -SH			
Thiol-Pyridyl Disulfide	R <sub>1</sub> -SH			
Thiol-halogen Ligation	R <sub>1</sub> -SH		HX	
		X = Br, I.		

REACTION TYPE	REAGENT 1	REAGENT 2	CATALYST & BYPRODUCT	PRODUCT
N-terminal <b>cysteine</b> involved click reactions				
Native Chemical Ligation			RSH	
Thiazolidine Ligation			H2O	
R-CHO involved click reactions				
Oxime Ligation			H2O	
Thiazolidine Ligation			H2O	
Diels-Alder Reaction				
	diene:			dienophile:
Inverse Electron Demand Diels-Alder Reaction				

**Table 3.** Examples of “click” reactions commonly employed for bioconjugation. Adapted from Tang et. Al., RSC Chem. Soc. Rev. 2014.

The vast implications that “click” chemistry has led in fields such as medicinal chemistry, chemical biology and bio-medicine cover pro-drug assembly,<sup>322</sup> chemical synthesis of modified and native (glyco)proteins,<sup>323</sup> efficient and precise introduction of labelling agents for *in vivo* imaging and synthesis of theranostic agents,<sup>324</sup> culminating in the more recent concept of *in vivo* chemistry, where the “click” reaction occurs in the context of a living organism or a cell.<sup>325</sup>

An extensive overview on “click” reactions and their utilization would be far from the scope of this manuscript, therefore we will not detail all reactions indicated in scheme 3, but we will focus on



those which have been employed in this research work. The abovementioned compelling properties of this chemical approach resulted more than appropriate for the efficient and controlled assembly of our multivalent glycodendrimer structures. The possibility to easily carry out a modular approach by the straightforward assembly of appropriately functionalized peptide and carbohydrate building blocks, made chemoselective “click” reactions a tool of choice for the development of our synthetic strategy. In this first chapter we explored two chemoselective “click” reactions: copper(I)-catalyzed alkyne-azide cycloaddition (CuAAC) and oxime ligation (OL).

CuAAC was developed by Meldal and co-workers from the previous works of Michael and Huisgen.<sup>326</sup> This [2+3] cycloaddition leads to the selective synthesis of hydrolytically stable 1,4-triazoles with high reaction rates, allowing reactions to be performed at room temperature.<sup>327</sup> The azide and terminal alkyne partners are inert to biological environments, and tolerate a wide range of solvents and reaction conditions.<sup>328</sup> A large variety of Cu(I) sources has been employed without affecting the reaction yield. Among the different sources of copper, CuSO<sub>4</sub> remains one of the most favourite options due to its ease of handling. However, Cu(I) halides are sometimes preferred for their improved solubility in organic solvents and because of the reported increase in reaction rate under these conditions. CuAAC reaction is usually highly efficient and predictable, although alkyne homocoupling side-reaction can occur in case of high alkyne density or sluggish triazole formation.<sup>329</sup> Pioneered by Bertozzi and Boons, a strain-promoted version of the dipolar alkyne-azide cycloaddition (SPAAC) has recently raised in popularity due to its high reactivity in the absence of metal catalyst.<sup>330</sup> Nevertheless, its high reactivity also correlates with a minor degree of chemo- and regio-selectivity compared to CuAAC, resulting in mixtures of 1,4- and 1,5-triazoles, and unspecific reactions with cysteine residues *via* thiol-yne coupling, respectively.<sup>331</sup>

Oxime ligation represents a reliable and versatile bioconjugation reaction which has been widely reported in literature to be compatible for a large panel of applications.<sup>332,333</sup> Although oximes may display some hydrolytic instability in aqueous media, their stability is superior to their corresponding imines and hydrazones. Raines and co-workers reported up to 600-fold lower hydrolysis rate constant for oximes compared to their corresponding hydrazones.<sup>334</sup> Hydrolysis of oxime conjugates is acid-catalyzed; their improved stability rely on the  $\alpha$ -effect provided by the heteroatom adjacent to the sp<sup>2</sup> nitrogen, electron-delocalization of lone pairs makes the sp<sup>2</sup> carbon less electrophilic, thus less susceptible to nucleophilic attack. Moreover, electron-withdrawing effects also reduce the basicity of the sp<sup>2</sup> nitrogen, whose protonation represents the first step for the acid-catalyzed hydrolysis mechanism. This reaction has been extensively employed in our research group

to reach a large panel of glycoconjugates, multivalent RGD-based platforms, oligonucleotide-based G-quadruplex buildings, and more.<sup>332</sup>

## **II.2. Mannosylated multivalent glycodendrimer assembly based on divergent iterative oxime strategy**

With the aim to assess the validity of our synthetic approach for the construction of multivalent dendrimer-like architectures, and to acquire familiarity with the related synthetic procedures, the first months of my PhD project have been devoted to the synthesis of a set of mannosylated multivalent structures by employing a divergent and iterative oxime-based protocol. The choice of such a carbohydrate residue ( $\alpha$ -D-mannopyranose) has been driven by its simplicity and the possibility to obtain multivalent constructs which could be valorised in a biological context. Indeed, mannose-binding proteins (*e.g.* MBL : mannose-binding lectin) are implicated in several fundamental biological processes such as viral infection,<sup>335</sup> bacterial adhesion,<sup>336</sup> cross-talking between adaptive and immune responses,<sup>337</sup> subcellular trafficking,<sup>338</sup> human fertilization,<sup>339</sup> cell-cell recognition,<sup>340</sup> and more.<sup>341–344</sup>

### **II.2.1. General strategy**

Following a divergent synthetic strategy already used in our group (PhD Baptiste Thomas, 2014), we designed the assembly of four copies of cyclopeptide “arm” **64**, or dendrimer “arm” **88** onto central cyclopeptide “core” **89** through oxime ligation. The resulting hexadecavalent scaffolds were equipped with  $\alpha$ -oxo-aldehyde groups, and were finally grafted with sixteen copies of  $\alpha$ -aminoxy-mannose **90**<sup>345</sup> *via* a second oxime ligation, to give mannosylated hexadecavalent glycoclusters **91** and **92** (Figure 35).

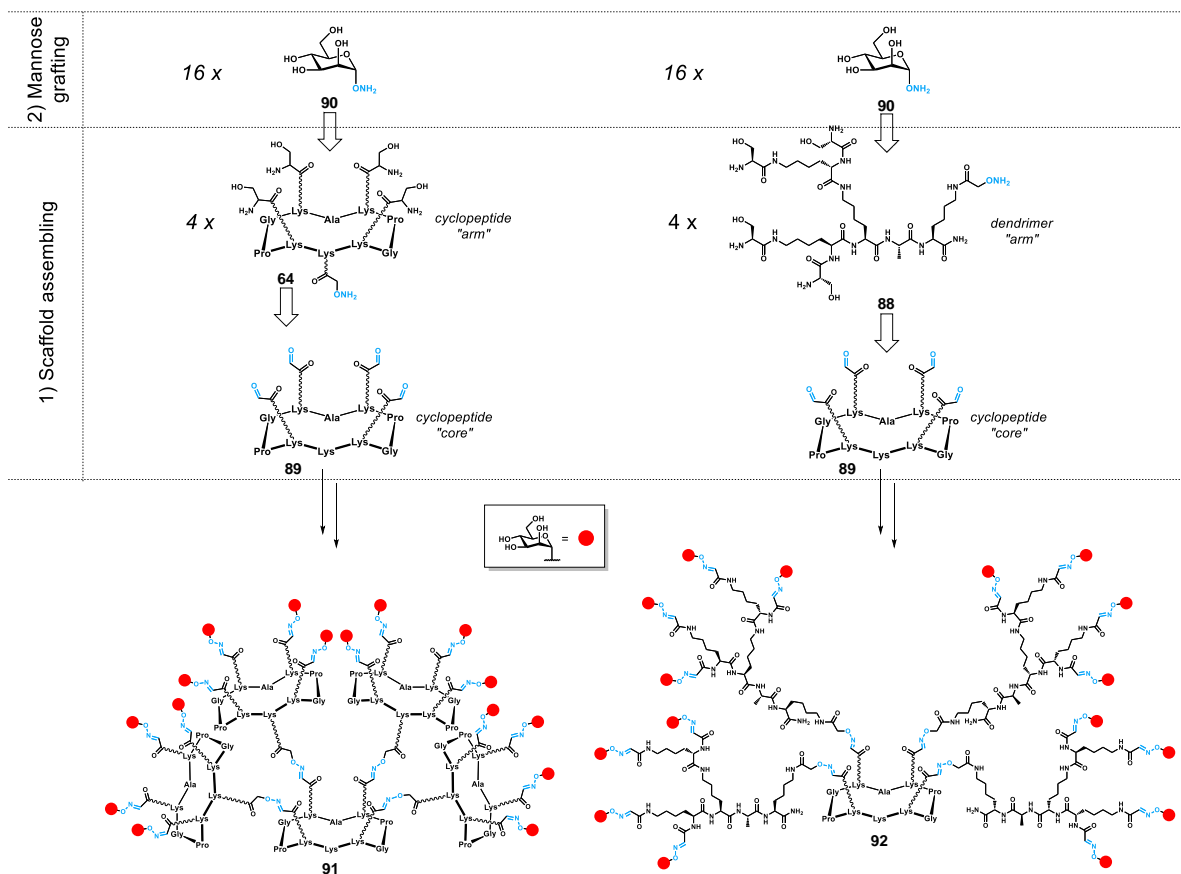


**Figure 35.** Divergent synthetic strategy for assembling mannosylated multivalent glycoclusters **91** and **92** through iterative oxime ligation.

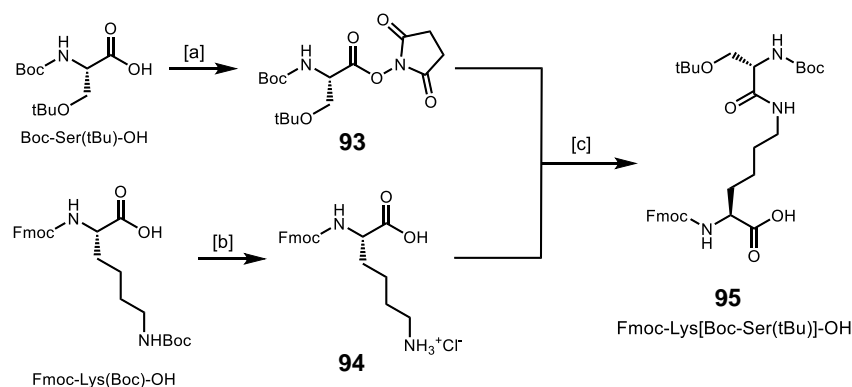
In the first instance, this modular approach required the synthesis of the different modules constituting the final macromolecule. Since the assembly was carried out in a divergent manner, the synthetic pathway will be described starting from the synthesis of cyclopeptide “core” **89**.

## II.2.2. Synthesis of tetravalent cyclopeptide “core” scaffold **89**

Scaffold **89** (Figure 35), containing four  $\alpha$ -oxo-aldehyde groups grafted on the upper domain, and one lysine’s side chain amino group in the lower domain, was synthesized by combining both solid phase and solution peptide synthesis protocols. The integration of dipeptide building blocks in the SPPS protocol simplified the synthesis by reducing the number of steps performed in solution, moreover the Fmoc-Lys[Boc-Ser(tBu)]-OH dipeptide building block (**95**, scheme 14) represents a useful intermediate for the synthesis of other constructs described in this work.

Thus, commercially available protected amino acid Boc-Ser(tBu)-OH was reacted with *N*-hydroxysuccinimide (NHS) in a AcOEt/dioxane mixture, in the presence of *N,N'*-dicyclohexyl-

carbodiimide (DCC). After 15 hours stirring at room temperature, NHS-activated serine **93** was obtained in 97% yield and used for the next reaction without further purification. Boc-removal from commercial Fmoc-Lys(Boc)-OH was carried out by stirring the amino acid in the presence of an aqueous HCl (37% v/v) solution in dioxane, at room temperature for about 20 minutes affording intermediate **94**. Coupling of activated serine moiety **93** on side chain amino group of **94** was carried out in dichloromethane (DCM, CH<sub>2</sub>Cl<sub>2</sub>) at room temperature, in the presence of DIPEA as base. Crude compound **95** was obtained and used for SPPS without any further purification (Scheme 14, Figure 36).



**Scheme 14.** Synthesis of Fmoc-Lys[Boc-Ser(tBu)]-OH building block **95**. Conditions: [a] NHS (1.1 eq.), DCC (1.1 eq.), AcOEt/dioxane, r.t., 15 h, 97%; [b] aq. HCl (37% v/v), dioxane, r.t., 20 min., 95%; [c] **93** (1.0 eq.), **94** (1.0 eq.), DIPEA, CH<sub>2</sub>Cl<sub>2</sub>, r.t., 4 h, 98%.

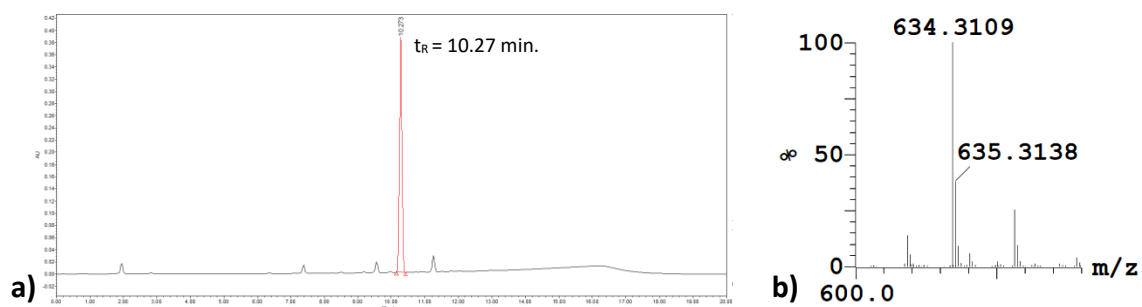
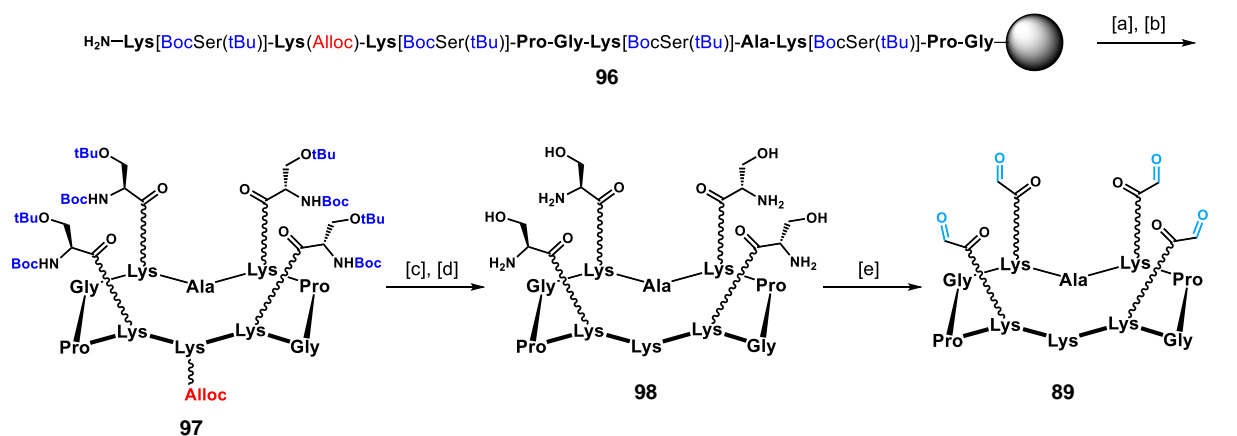


**Figure 36.** a) Analytical RP-HPLC profile ( $\lambda=214$  nm, 5-100% solv.B in 15') of **95**. b) HRMS (ESI<sup>+</sup>-TOF) of **95** (zoom).  $m/z$  calcd. for [M+Na]<sup>+</sup>: 634.3104 (monoisotopic), found: 634.3109.

The synthetic route for platform **89** started with a classic Fmoc/*t*Bu SPPS protocol with PyBOP<sup>®</sup> as activating agent and DIPEA as base (See *Material and Methods* for general procedures). Fmoc-Gly-SASRIN<sup>™</sup> resin was used as solid support for the synthesis of decapeptide sequence **96**, which incorporates four copies of the building block **95** (Scheme 15). Cleavage from the resin in mild acidic conditions, followed by cyclization in diluted DMF/CH<sub>2</sub>Cl<sub>2</sub>, and precipitation in ice-cold diethyl ether, afforded compound **97** with an overall yield of 57%. Orthogonally protected intermediate **97**

also represents a key intermediate for the synthesis of **64** (*vide infra*). It shows four serine residues cleavable in acidic conditions (in blue), while the lysine's side chain amino group is Alloc-protected, and cleaved under reductive conditions (in red). Palladium-catalyzed deprotection of Alloc group, followed by Boc and *tert*-butyl groups removal using a TFA/TIS/H<sub>2</sub>O (96:2:2) cocktail, afforded fully deprotected cyclopeptide **98** in 79% yield over two steps. Treatment of compound **98** with a large excess of sodium periodate (10 eq. per serine residue) in H<sub>2</sub>O caused oxidative cleavage of the four serine residues, to give four  $\alpha$ -oxo-aldehyde groups.<sup>244</sup> Indeed, N-terminal serine residues represent useful “masked” aldehyde functions and are easily introduced in peptide synthesis. Aldehyde-bearing “core” scaffold **89** was obtained as a white foamy powder, in 78% yield after RP-HPLC purification and lyophilization (Figure 37).



**Scheme 15.** Synthesis of cyclopeptide “core” **89**. Conditions: [a] 1% TFA, CH<sub>2</sub>Cl<sub>2</sub>; [b] PyBOP (1.2 eq.), DIPEA (2 eq.), DMF/ CH<sub>2</sub>Cl<sub>2</sub> (1:1), 0.5 mM, r.t., 30 min., 57% overall yield; [c] Pd(PPh<sub>3</sub>)<sub>4</sub> (cat.), PhSiH<sub>3</sub> (25 eq.), CH<sub>2</sub>Cl<sub>2</sub>, r.t., 30 min., then MeOH (20 mL); [d] TFA/TIS/H<sub>2</sub>O (96:2:2), r.t., 3 h, 79% over two steps; [e] NaIO<sub>4</sub> (40 eq.), r.t. 40 min, direct RP-HPLC purification, 78%.

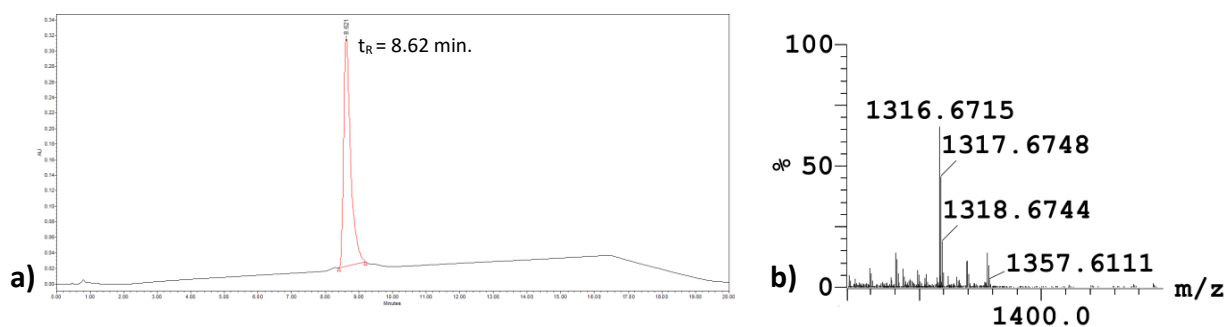
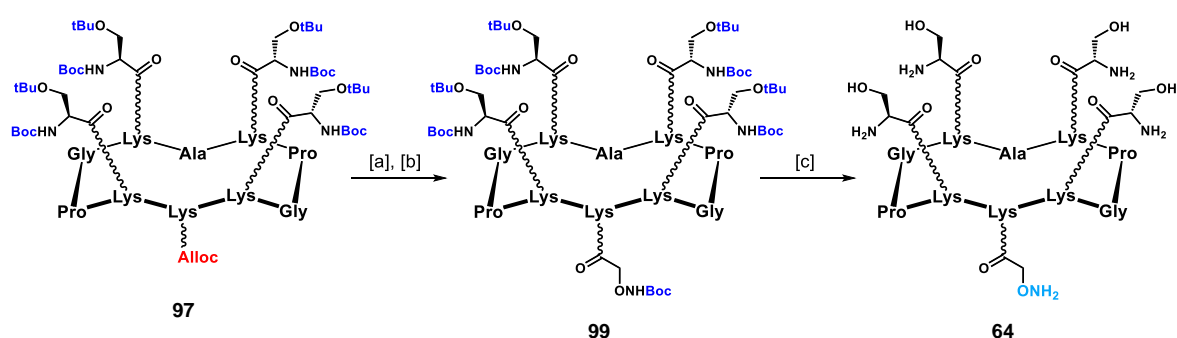


**Figure 37.** a) Analytical RP-HPLC profile ( $\lambda=214$  nm, 0-20% solv.B in 15') of **89**. b) HRMS (ESI<sup>+</sup>-TOF) of **89** (zoom).  $m/z$  calcd. for  $[M+H_2O+H]^+$ : 1316.6698 (monoisotopic), found: 1316.6715.

## II.2.3. Synthesis of cyclopeptide **64** and compound **88** as dendrimer's "arms"

Cyclopeptide "arm" **64** was obtained starting with selective Pd-catalyzed deprotection of the Alloc group in key intermediate **97**, followed by reaction between the resulting free amino group and Boc-aminoxyacetic acid *N*-hydroxysuccinimide ester.<sup>346</sup> This allowed the introduction of a Boc-protected aminoxy function in the lower domain of the scaffold (Scheme 16). Cleavage of acid-labile protecting groups of **99** was performed in the presence of appropriate scavengers (*i.e.* TIS, NH<sub>2</sub>OH and H<sub>2</sub>O) to avoid alkylation of the aminoxy group. The desired aminoxy-bearing compound **64** was obtained in 84% yield after preparative RP-HPLC (Figure 38).



**Scheme 16.** Synthesis of cyclopeptide "arm" **64**. Conditions: [a] Pd(PPh<sub>3</sub>)<sub>4</sub> (cat.), PhSiH<sub>3</sub> (25 eq.), CH<sub>2</sub>Cl<sub>2</sub>, r.t., 30 min., then MeOH (20 mL); [b] Boc-aminoxyacetic acid *N*-hydroxysuccinimide ester (1.2 eq.), DIPEA (1.5 eq.), DMF, r.t., 20 min., 72% over two steps; [c] TFA/NH<sub>2</sub>OH/TIS/H<sub>2</sub>O (94:2:2:2), r.t., 3 h, 84%.

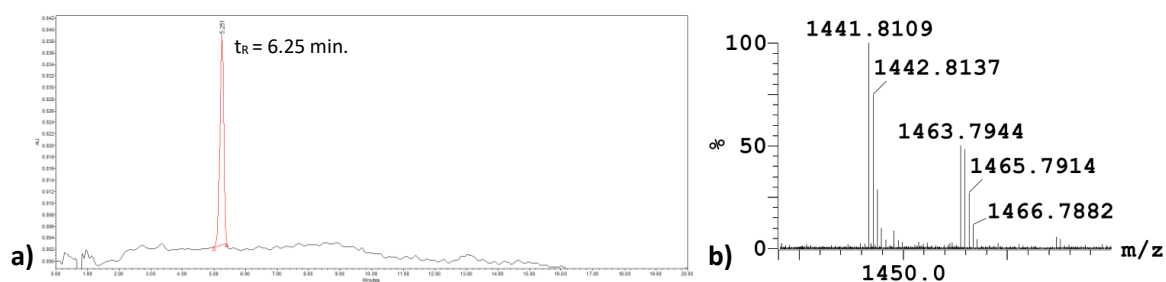
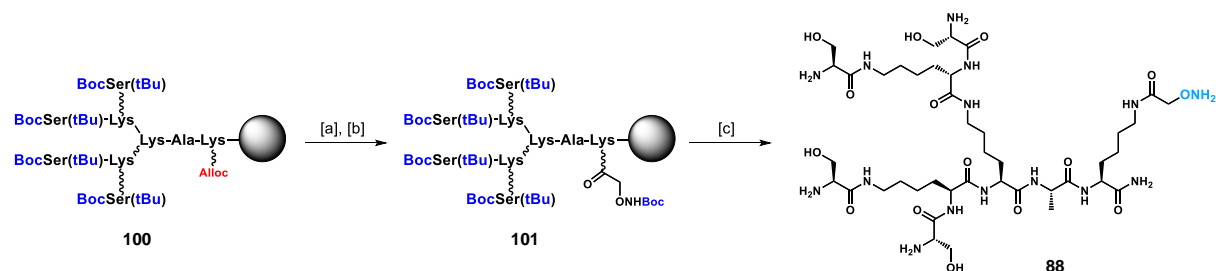


**Figure 38.** a) Analytical RP-HPLC profile ( $\lambda=214$  nm, 0-30% solv.B in 15') of **64**. b) HRMS (ESI<sup>+</sup>-TOF) of **64** (zoom).  $m/z$  calcd. for [M+ H]<sup>+</sup>: 1441.8127 (monoisotopic), found: 1441.8109; calcd. for [M+ Na]<sup>+</sup>: 1463.7946, found: 1463.7944.

Dendrimer "arm" **88** was synthesized through a SPPS protocol by using Rink amide<sup>®</sup> resin and appropriately protected commercial AAs. Once branched sequence **100** was obtained, removal of allyloxycarbonyl (Alloc) protecting group on the lysine's side chain allowed the functionalization of the resulting free amino groups with a Boc-protected aminoxy linker, as seen for intermediate **99**, to give modified sequence **101** (Scheme 17). Cleavage from the resin under strong acidic conditions, followed

by precipitation and RP-HPLC purification afforded pure compound **88** as colorless solid, in good yields and purity (Figure 39).



**Scheme 17.** Synthesis of dendrimer “arm” **88**. Conditions: [a] Pd(PPh<sub>3</sub>)<sub>4</sub> (cat.), PhSiH<sub>3</sub> (25 eq.), CH<sub>2</sub>Cl<sub>2</sub>, r.t., 30 min., then MeOH (20 mL); [b] Boc-aminoxyacetic acid N-hydroxysuccinimide ester (1.2 eq.), DIPEA (1.5 eq.), DMF, r.t., 20 min.; [c] TFA/NH<sub>2</sub>OH/TIS/H<sub>2</sub>O (94:2:2:2), r.t., 3 h, 37% overall yield.

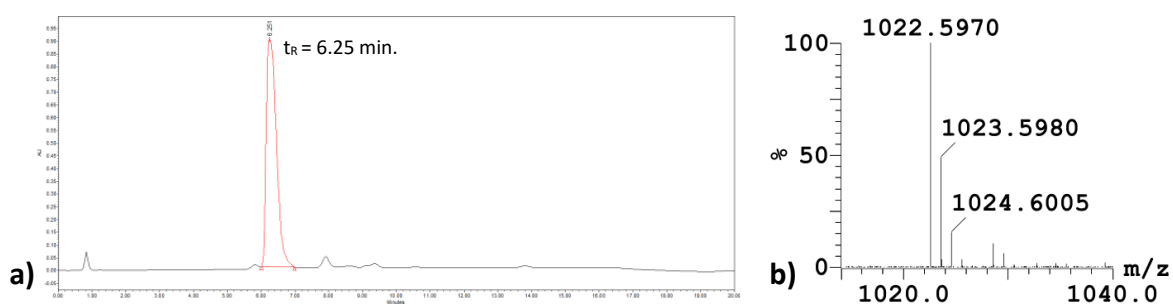


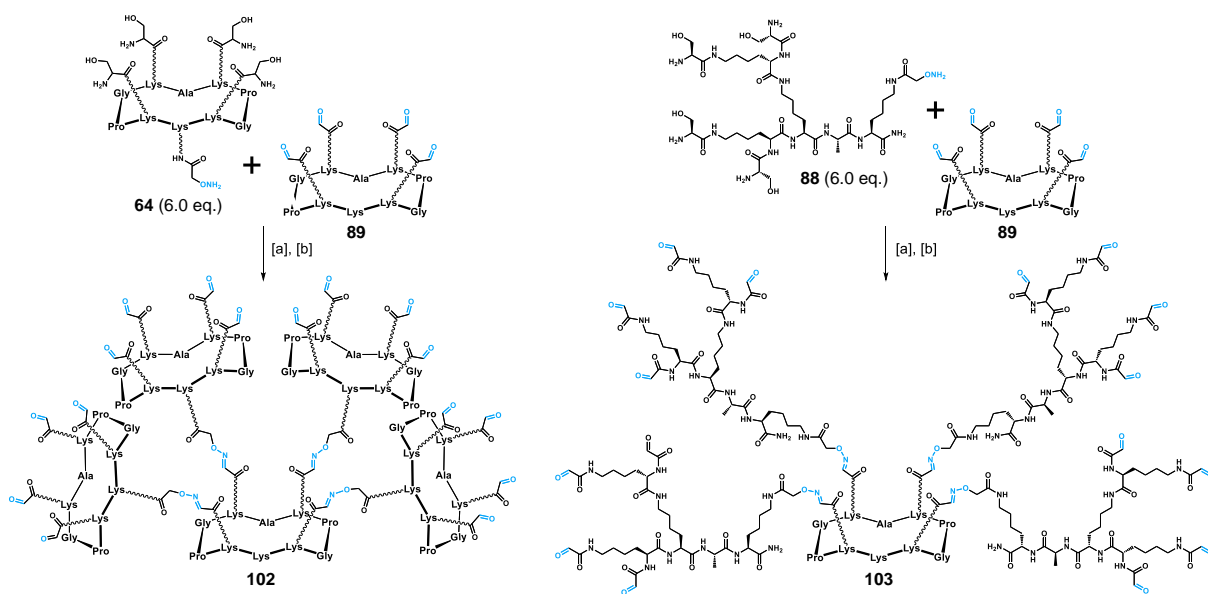
**Figure 39.** a) Analytical RP-HPLC profile ( $\lambda=214$  nm, 0-20% solv.B in 15') of **88**. b) HRMS (ESI<sup>+</sup>-TOF) of **88** (zoom).  $m/z$  calcd. for [M+ H]<sup>+</sup>: 1022.5958 (monoisotopic), found: 1022.5970.

## II.2.4. Hexadecavalent scaffold assembly through oxime ligation

With intermediates **64**, **88** and **89** in hand, we proceeded in a divergent manner by assembling the peripheral “arms” (**64**, **88**) to the central scaffold, *via* an oxime-ligation protocol developed in our laboratories (See Materials and Methods).<sup>332</sup> Subsequent oxidative cleavage of the resulting serine residues provided aldehyde-bearing hexadecavalent scaffold **102** and **103**, prone to undergo another oxime ligation with aminoxy-mannose moiety.

Four aldehyde residues on the upper domain of the “core” RAFT scaffold **89** underwent condensation with the aminoxy-bearing cyclopeptide “arm” **64** and dendrimer “arm” **88**, giving rise to hexadecavalent structures (Scheme 18). Oxime ligations were performed by dissolving aldehyde-bearing scaffold **89** (2-10 mM) with aminoxy-bearing **64**, or **88** (4.8-6.0 eq. *i.e.* 1.2-1.5 eq. per aldehyde group) in water containing 0.1% of TFA (pH  $\approx$  2.2). Solutions were incubated at 37°C without

stirring, and showed complete conversion after 45 minutes. Reaction progress was easily monitored through RP-HPLC, where hexadecavalent structures showed increased retention time and characteristic oxime absorbance at 250 nm. Moreover, the excess of **64** and **88** can be easily detected and recovered during preparative RP-HPLC. Treatment of the sixteen peripheral serine residues with a large excess of sodium periodate in water, followed by direct RP-HPLC purification, afforded compounds **102** and **103** in good yields and purity (Figure 40).



**Scheme 18.** Synthesis of aldehyde-bearing, hexadecavalent scaffold **102** and **103**. Conditions: [a] 0.1% TFA in H<sub>2</sub>O, 37°C, 45 min.; [b] NaIO<sub>4</sub> (160 eq.), r.t. 40 min, 72-78% over two steps.



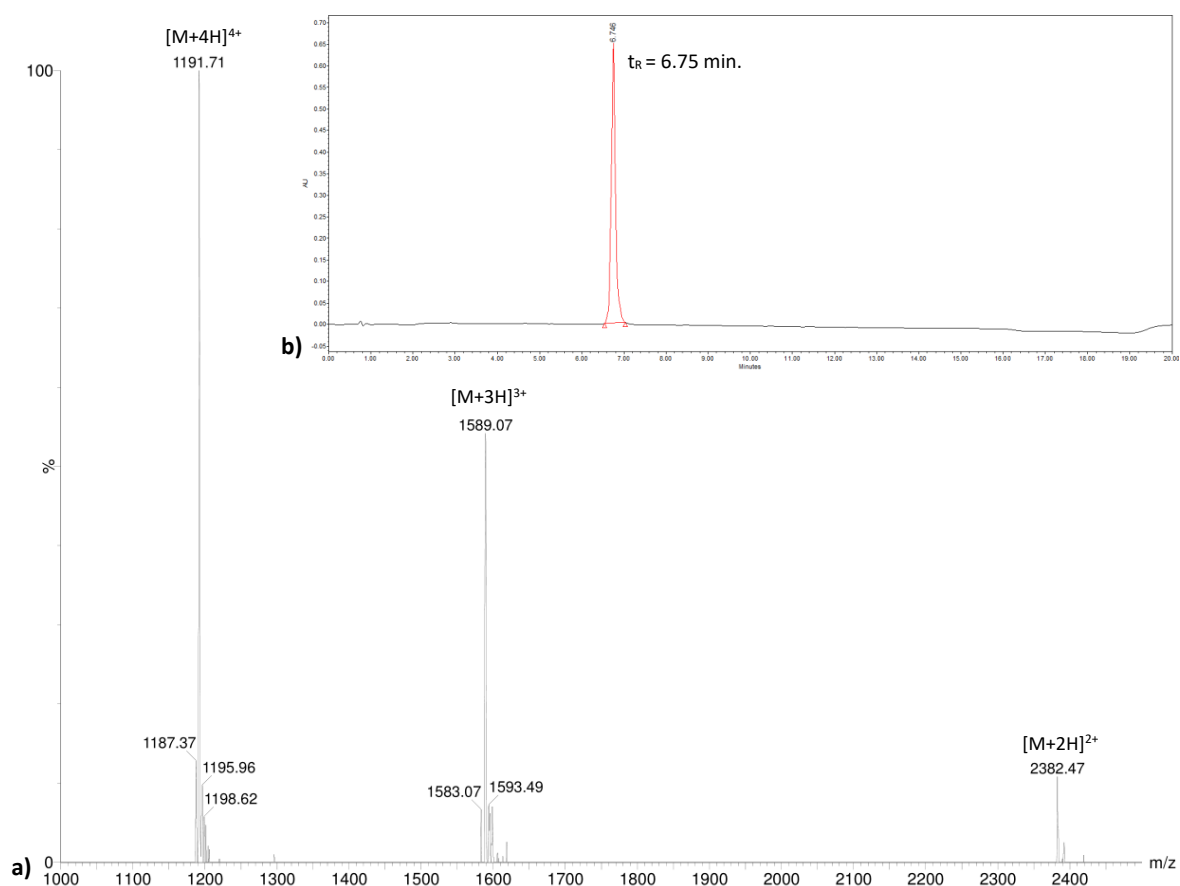
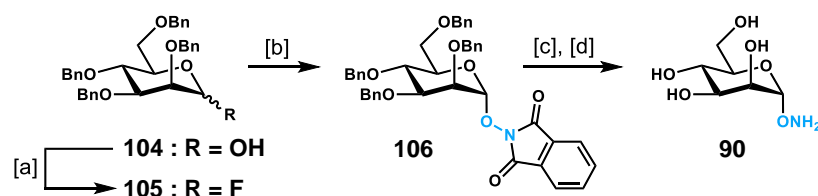


**Figure 40.** a) ESI<sup>+</sup>-MS spectrum of compound **103**. *m/z* calcd. for [M+2H]<sup>2+</sup>: 2382.6 (most intense peak of isotopic cluster), found: 2382.5; calcd. for [M+3H]<sup>3+</sup>: 1588.8, found: 1589.1; calcd. for [M+4H]<sup>4+</sup>: 1191.8, found: 1191.7. b) Analytical RP-HPLC profile ( $\lambda=214$  nm, 0-40% solv.B in 15') of **103**.

## II.2.5. Synthesis of aminoxy-mannose building block **90** and functionalization of aldehyde-bearing scaffolds via a second oxime ligation

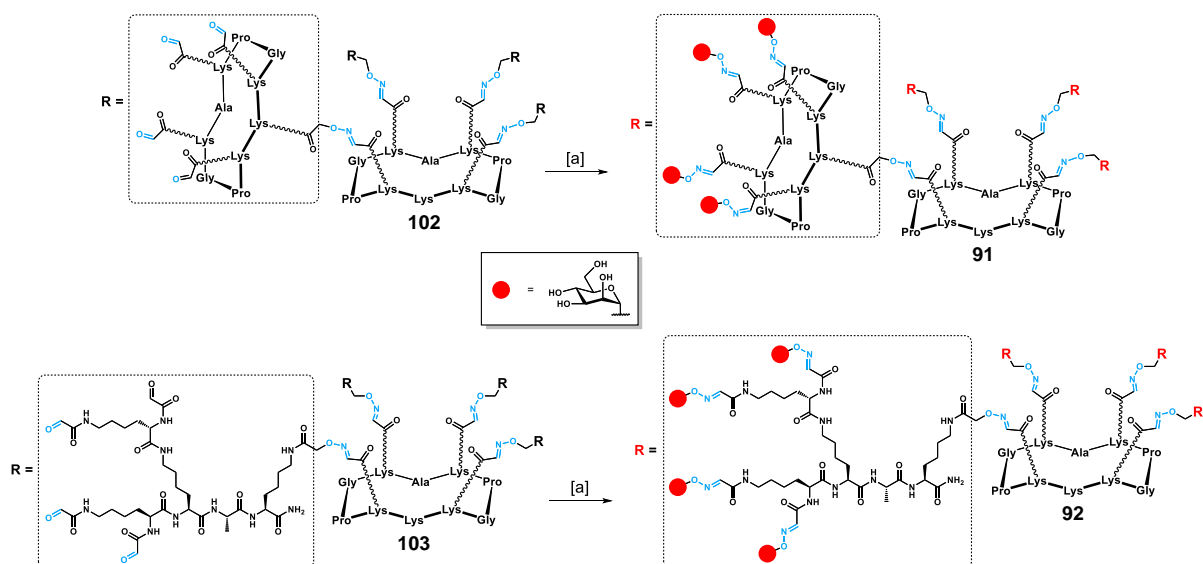
In order to obtain target compounds **91** and **92**, a mannose moiety equipped with an aminoxy function must be prepared. Aminoxyated carbohydrates have been shown to represent attractive building blocks for the preparation of natural products and for their conjugation into various entities such as oligomers, dyes, peptides, oligonucleotides and even carbon nanotubes.<sup>238,323,347</sup> Thus, using a protocol already described in literature by our group (Scheme 19), tetra-*O*-benzylated mannopyranoside **104** was activated at the anomeric position by treatment with diethylaminosulfur trifluoride (DAST) in tetrahydrofuran (THF) to obtain fluorinated compound **105**, which was used for the subsequent reaction without further purification.<sup>348</sup> Glycosylation between donor **105** and *N*-hydroxyphthalimide, in the presence of boron trifluoride-diethyl etherate (BF<sub>3</sub>·Et<sub>2</sub>O) as promoter,

afforded  $\alpha$ -anomer **106** in 75% yield. Removal of benzyl protecting groups was performed through a rapid catalytic hydrogenation, controlled by TLC in order to prevent cleavage of the N-O bond under these conditions. Methylhydrazine-mediated cleavage of phthalimido moiety, followed by silica gel chromatography afforded aminoxyolated compound **90**.



**Scheme 19.** Synthesis of  $\alpha$ -aminoxy-mannose **90**. Conditions: [a] DAST (1.2 eq.), THF,  $-30^{\circ}\text{C}$  – r.t., 30 min.; [b] HONPhth (1.0 eq.), TEA (1.0 eq.),  $\text{BF}_3 \cdot \text{Et}_2\text{O}$  (5.0 eq.),  $\text{CH}_2\text{Cl}_2$ , r.t., 1 h, 75% over two steps; [c] 10% Pd/C (0.3 eq.),  $\text{MeOH}/\text{CH}_2\text{Cl}_2$  (1:1), r.t., 2 h; [d]  $\text{EtOH}/\text{MeHNNH}_2$  (1:1), r.t., overnight, 50% over two steps.

The second oxime ligation of this iterative strategy was thus performed between aldehyde-bearing, hexadecaivalent scaffolds **102** and **103** and twenty equivalents of  $\alpha$ -aminoxy-mannose **90** (1.25 eq. per aldehyde group), in aqueous TFA at  $37^{\circ}\text{C}$  (Scheme 20). Complete conversion within 45 minutes reaction was observed. Compounds **91** and **92** were purified through preparative RP-HPLC, lyophilized and obtained as white foamy solids.



**Scheme 20.** Synthesis of. Conditions: [a] **90** (20 eq.), 0.1% TFA in  $\text{H}_2\text{O}$ ,  $37^{\circ}\text{C}$ , 45 min., 88% for **91**, 84% for **92**.

Target glycosylated multivalent structures were assembled in good yields and excellent purity (Figure 41). By way of example, analytical RP-HPLC of **92** showed a sharp, single-peak profile, suggesting compound monodispersity (Figure 41a).

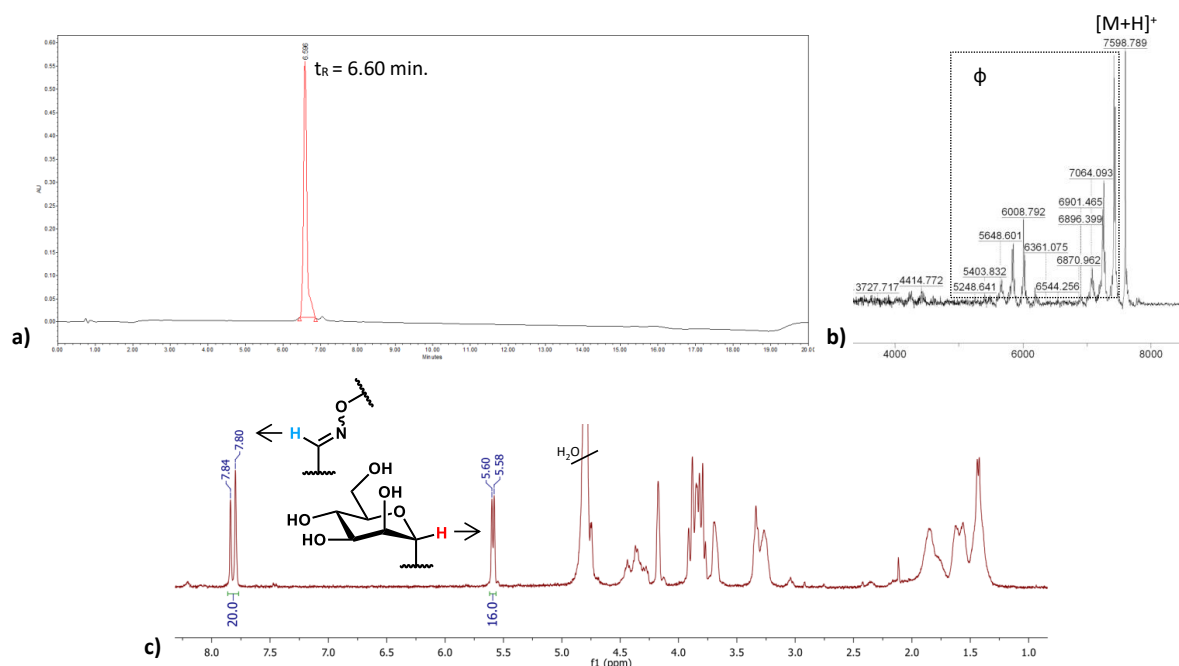


**Figure 41.** a) Analytical RP-HPLC profile ( $\lambda=214$  nm, 0–40% solv.B in 15') of **92**. b) MALDI-TOF spectrum (zoom) of compound **92**.  $m/z$  calcd. for  $[M+H]^+$ : 7599.5 (average), found: 7598.8; ( $\phi$  = fragmentation). c)  $^1\text{H-NMR}$  (400 MHz,  $\text{D}_2\text{O}$ ) zoom of compound **92**.

MALDI spectroscopy revealed the presence of entities with smaller molecular weight, which cannot be attributed to multicharged ions of compound **92**, but rather monocharged ions of target compound lacking one the four glycodendrimer “arms” (*i.e.*  $m/z \approx 6008$ , Figure 41b). To assess whether these observation were due to oxime bond fragmentation during mass spectrometry analysis or incomplete functionalization,  $^1\text{H-NMR}$  spectra of final structures in  $\text{D}_2\text{O}$  were recorded (Figure 41c). Integration ratio between characteristic oxime protons near 7.8 ppm ( $H = 20$ ), and mannose anomeric protons near 5.5 ppm ( $H = 16$ ), showed to be consistent with target molecule **92**, moreover, no characteristic hydrated-aldehyde signals near 5.3 ppm were observed. The relative asymmetry of this macromolecular glycoconjugate and the different environments of the twenty oxime bonds influence chemical shift of these characteristic protons, resulting in peak broadening and signal shifting. These factors, together with the inherent complexity of **92** (Figure 41d), make complete chemical shift assignment very hard without more powerful experiments involving high-field NMR, NOESY, TOCSY and ROESY.<sup>349</sup>

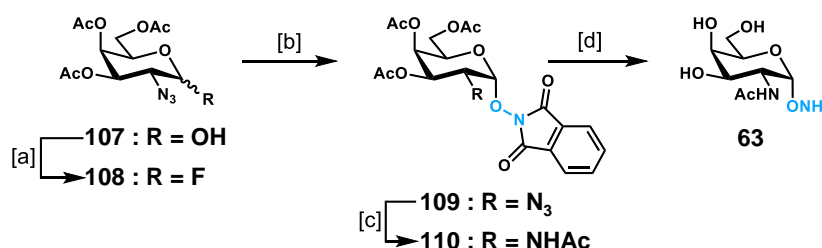
Compounds **91** and **92** represent valid models for the construction of homo-hexadecavalent TACA-based glycoclusters. This iterative, oxime-based synthetic approach has been adopted for the

construction of Tn-based multivalent glycoclusters as B-cell epitope modules, equipped with a free amino residue on the lower domain of the “core” scaffold which can be further functionalized (*vide infra*).

### II.3. (OX)Tn-functionalized multivalent glycodendrimer assembly based on divergent iterative oxime strategy

Owing to the robustness of our iterative oxime-based strategy, we exploited hexadecavalent aldehyde-bearing scaffold **102** (Scheme 18) for the construction of a multivalent glycocluster decorated with our Tn-antigen analogue **63** (Scheme 11, 21).

The synthetic route for the installation of an aminoxy residue at the anomeric position in his alpha configuration was similar to that described in scheme 19. Fluorination of per-acetylated compound **107**, bearing an azido group in C-2, afforded intermediate **108** (Scheme 21). Glycosylation with HOPhth, using  $\text{BF}_3 \cdot \text{Et}_2\text{O}$ , provided an anomeric mixture of  $\alpha$ - and  $\beta$ -anomers, which were isolated by column chromatography to give compound **109** in 88% yield. The azido moiety underwent concomitant reduction and acetylation of the resulting amino group, by catalytic hydrogenation in a methanol/acetic anhydride (9:1) mixture. Finally, methylhydrazine-mediated deprotection of acetate groups and phthalimido moiety afforded  $\alpha$ -aminoxy-Tn **63**, in 72% yield.<sup>348</sup>



**Scheme 21.** Synthesis of  $\alpha$ -aminoxy-Tn **63**. Conditions: [a] DAST (1.2 eq.), THF,  $-30^\circ\text{C}$  – r.t., 30 min.; [b] HONPhth (1.0 eq.), TEA (1.0 eq.),  $\text{BF}_3 \cdot \text{Et}_2\text{O}$  (5.0 eq.),  $\text{CH}_2\text{Cl}_2$ , r.t., 1 h, 88% over two steps; [c] 10% Pd/C (0.3 eq.), MeOH/ $\text{Ac}_2\text{O}$  (9:1), r.t., 2 h; [d] EtOH/MeHNNH<sub>2</sub> (1:1), r.t., overnight, 72% over two steps.

The final oxime conjugation step of the iterative protocol thus involved aldehyde-bearing scaffold **102** and  $\alpha$ -aminoxy-Tn **63**, and was carried out under the same conditions described above (Scheme 20). Complete functionalization was observed within 30 minutes at  $37^\circ\text{C}$ . Target compound **111** (Figure 42) was obtained in 84% yield and excellent purity. The monodispersity of the multivalent B-cell epitope carrier has been suggested by single-peak analytical RP-HPLC profile (not shown), and confirmed via mass spectrometry (Figure 42a) and  $^1\text{H-NMR}$  spectroscopy (Figure 42b).

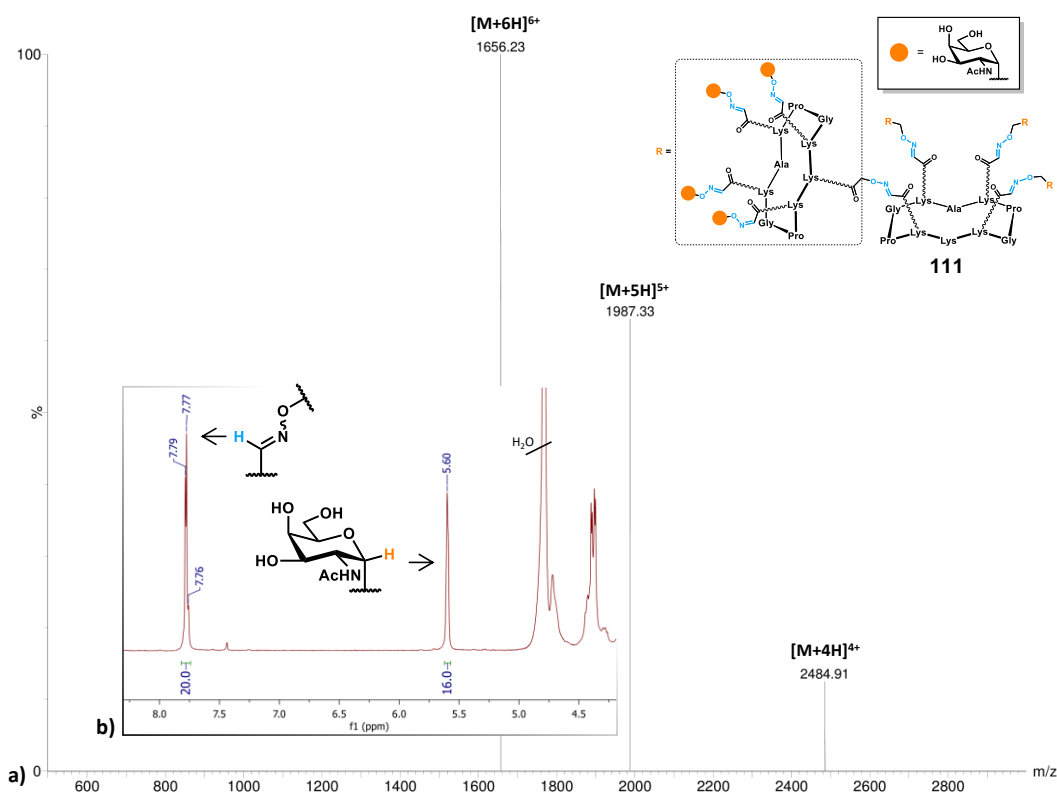


**Figure 42.** a) ESI<sup>+</sup>-MS spectrum of compound **111**.  $m/z$  calcd. for  $[M+ 6H]^{6+}$ : 1656.4 (most intense peak of isotopic cluster), found: 1656.2; calcd. for  $[M+ 5H]^{5+}$ : 1987.5, found: 1987.3; calcd. for  $[M+ 4H]^{4+}$ : 2484.2, found: 2484.9. b)  $^1H$ -NMR (400 MHz,  $D_2O$ ) zoom of compound **111**.

Tn-based glycocluster **111** represents a useful intermediate for the construction of fully synthetic anticancer vaccine prototypes, with multivalent B-cell antigen display. The subsequent steps for the construction of the final vaccine prototypes, involving the attachment of peptide CD4<sup>+</sup> and CD8<sup>+</sup> epitopes via disulfide-bond formation, along with immunological preliminary results, will be described in chapter IV.

Our modular approach, based on the iterative oxime-conjugation of appropriately functionalized building blocks, allows for an efficient multi-step synthesis of high-valency structures, which are efficiently assembled in a divergent manner.<sup>350</sup> The introduction in our synthetic strategy of another chemoselective reaction, compatible with oxime ligation, would be certainly beneficial for designing new macromolecular architectures. In the next section, a convergent synthetic approach, integrating the copper(I)-catalyzed alkyne-azide cycloaddition, will be described. Although the reported oxime-based, divergent strategy demonstrated its efficacy, a convergent assembly would provide a better control of the conjugation chemistry and, in our case, also increased the synthetic path efficiency by allowing the recovery of key intermediates.

## II.4. (TRZ)Tn-functionalized multivalent glycodendrimer assembly based on convergent oxime/CuAAC strategy

The chemistry of multivalent glycosylated systems has tremendously progressed over the past decade, enriching the panel of already described architectures by designing new structures, which represent valuable tools for both studying carbohydrate-protein interaction and for biomedical applications.<sup>94,114,313,351,352</sup> In this research field, our group has developed an iterative, oxime-based strategy for assembling glycoclusters and glycodendrimers on conformationally stable cyclopeptide RAFT scaffolds.<sup>228,353</sup> Thanks to this strategy, we have been able to reach high-orders valencies (*i.e.* up to sixty four),<sup>345,350</sup> giving rise to multivalent glycodendrimers with sub-nanomolar affinities towards vegetal and bacterial lectins.<sup>354,355</sup>

### II.4.1. General strategy

In a previous report by our research group,<sup>356</sup> the iterative oxime-based approach demonstrated to be suitable for a divergent assembly of hexadecavalent glycodendrimers (Figure 43a), but it failed when applied to a convergent assembly strategy (Figure 43b). The last step of the convergent assembly involves the conjugation of four glycosylated cyclopeptide “arms” onto a central scaffold, to give the final hexadecavalent structure (Figure 43b,d). We observed that performing this last step *via* oxime ligation was not possible when using oxime-containing cyclopeptide “arms” functionalized with aminoxy linkers. Analytical RP-HPLC chromatograms revealed crowded, multi peak profiles, presumably due to trans-oximation side-reactions.

We thus developed a synthetic approach combining oxime ligation, for linking glyco-cyclopeptide “arms” on central “core” scaffolds, and CuAAC, for the conjugation of the peripheral saccharide moiety (Figure 43c,d). This new strategy allowed the controlled assembly of cyclopeptide and carbohydrate building blocks both in a divergent and convergent fashion, with excellent yields and purity.

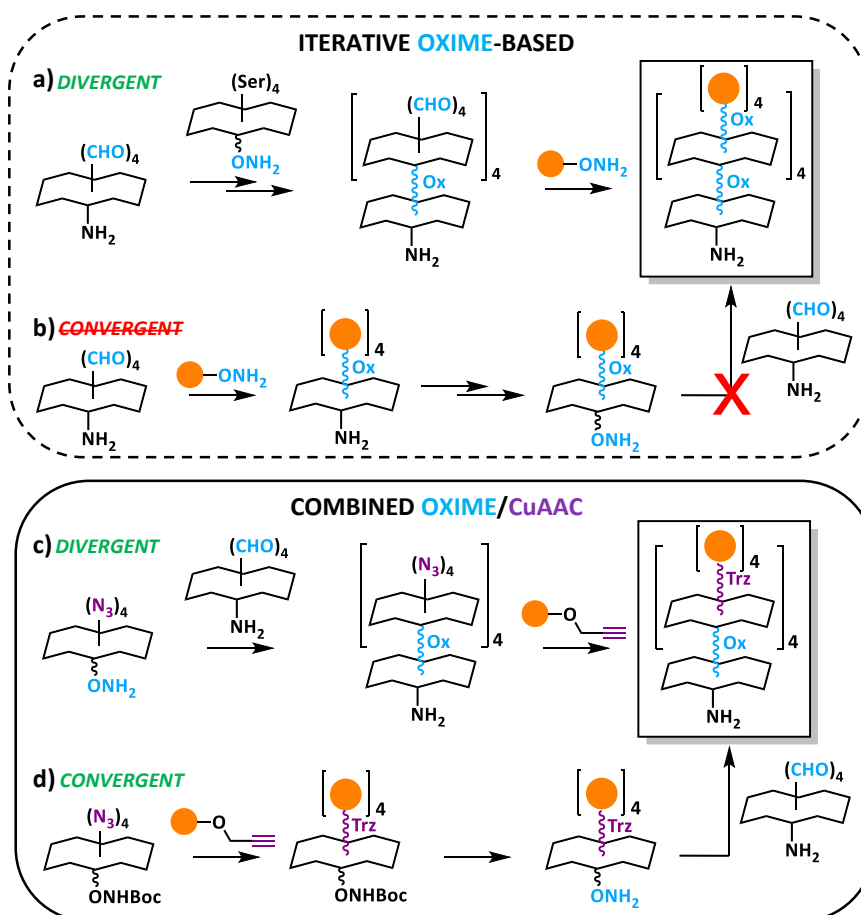


**Figure 43.** Divergent assembly of hexadecavalent glycodendrimers by: a) iterative oxime-based strategy, and c) combined oxime/CuAAC strategy. Convergent assembly of hexadecavalent glycodendrimers by: b) iterative oxime-based strategy (failed), and d) combined oxime/CuAAC strategy. Ox = oxime linker, Trz = triazole linker.

Due to the documented fragility of the peripheral oxime-linked carbohydrates during mass spectrometry analysis, we chose to use the copper(I)-catalyzed alkyne-azide cycloaddition (CuAAC) for the installation of the saccharide moiety.<sup>356</sup> This should reduce the ambiguities often observed in mass-spectrometry characterization, as reported for **92** (Figure 42b), where fragmentation phenomena could be misinterpreted as incomplete functionalization. The advantage of a convergent assembly also relies on the possibility to better assess the monodispersity of the tetravalent glycosylated “arms”, before their inclusion in the final hexadecavalent macromolecule, where deletion of peripheral saccharide units results more difficult to detect.

For the development of this new synthetic strategy we employed *N*-acetylgalactosamine (GalNAc) as carbohydrate moiety, which represents the saccharide analogue of Tn antigen, key building block for the construction of synthetic anticancer vaccines. The binding efficacy of the resulting structures has been tested *via* competitive enzyme-linked lectin assay (ELLA). To assess if the

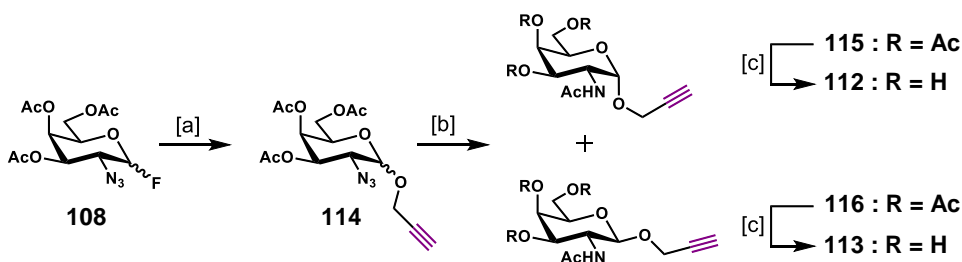


impact of sugar orientation is retained in a multivalent carbohydrate presentation, we generated two series of compounds where the GalNAc moiety is displayed in its  $\alpha$ - or  $\beta$ -configuration.

#### II.4.2. Synthesis of propargyl-Tn building blocks **112** and **113**

A few groups recently proposed different synthetic strategies for the preparation of *O*-propargyl GalNAc **112** and **113**. In 2009, Fairbanks and co-workers described the preparation of the alpha anomer **112** by a Fisher-type glycosylation.<sup>357</sup> Sulphuric acid treatment of unprotected GalNAc in the presence of silica, and equimolar amounts of propargyl alcohol, afforded the  $\alpha/\beta$  anomeric mixture (3:2) in 54% yield after recrystallization. Brimble's research group described another protocol to obtain compound **112**, involving the glycosylation of propargyl alcohol on 1,3,4,6-tetra-*O*-acetyl-2-azido-2-deoxy-D-galactose in the presence of  $\text{BF}_3 \cdot \text{Et}_2\text{O}$  as promoter.<sup>358</sup> After reduction/acetylation of the azido group, using Zn and  $\text{Ac}_2\text{O}$ /pyridine, both anomers (**115** and **116**) were separated by silica gel chromatography (26% yield,  $\alpha:\beta = 4.5:1$ ). In 2010, Sewald and co-workers also described the synthesis of **112** performing a Koenigs-Knorr reaction from the azidochloride precursor as key step.<sup>359</sup> After glycosylation, the azido group was reduced and subsequently acetylated with  $\text{AcSH}$ /pyridine, following  $\alpha/\beta$  anomers separation (20% yield,  $\alpha:\beta = 5:1$ ) and *O*-acetyl groups removal under Zemplén conditions.

Our proposed synthetic strategy relies upon fluoride donor **108**,<sup>219</sup> which underwent glycosylation with propargyl alcohol in dichloromethane, using  $\text{BF}_3 \cdot \text{Et}_2\text{O}$  as promoter (Scheme 21). An inseparable mixture of  $\alpha$  and  $\beta$  anomers **114** was obtained in 90% yield ( $\alpha:\beta = 6:4$ ). The azido group was next converted into the  $-\text{NHAc}$  group using triphenylphosphine ( $\text{PPh}_3$ ) in the presence of acetic anhydride.<sup>360</sup> Separation of  $\alpha$  and  $\beta$  anomers was performed by silica gel chromatography, affording  $\alpha$  anomer **115** (45%) and  $\beta$  anomer **116** (36%). Stereochemistry of the anomeric carbon in **115** was confirmed both by the coupling constant measured by  $^1\text{H-NMR}$  and ( $J_{\text{H1-H2}} = 4.0 \text{ Hz}$ ) and by RX diffraction analysis, which are in good agreement with literature data. Both anomers were finally deacetylated under Zemplén conditions to afford the corresponding prop-2-ynyl-2-acetamido-2-deoxy- $\alpha/\beta$ -D-galactopyranosides **112** and **113** in overall 23% and 12% yields from **108**, respectively.

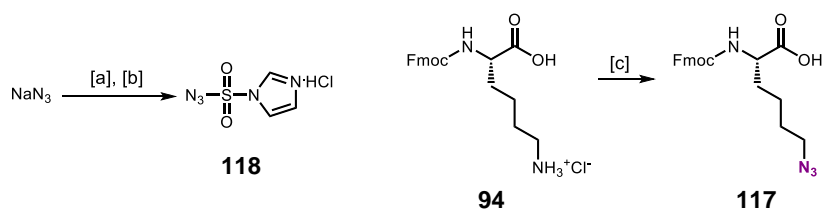


**Scheme 21.** Synthesis of  $\alpha$ -propargyl-GalNAc **112** and  $\beta$ -propargyl-GalNAc **113**. Conditions: [a] propargyl alcohol (4.0 eq.),  $\text{BF}_3 \cdot \text{Et}_2\text{O}$  (2.0 eq.),  $\text{CH}_2\text{Cl}_2$ , 0 °C, 2 h, 90%,  $\alpha:\beta = 3:2$ ; [b]  $\text{PPh}_3$  (1.25 eq.),  $\text{Ac}_2\text{O}$  (3.0 eq.),  $\text{CH}_2\text{Cl}_2$ , r.t., 16 h, 45% for **115**, 36% for **116**; [c]  $\text{NaOMe}/\text{MeOH}$ , r.t., 4 h, 95-96%.

### II.4.3. Synthesis of azido-bearing cyclopeptides **120** and **121**

In order to adapt our RAFT platform for the CuAAC-based strategy, we synthesized 6-azido-*N*-Fmoc-norleucine building block **117** (Scheme 22),<sup>361</sup> which was integrated in SPPS.

The first step involved the synthesis of the diazo-transfer agent, namely imidazole-1-sulfonyl azide hydrochloride (**118**, scheme 22).<sup>362</sup> Equimolar amounts of sulfonyl chloride were added drop-wise to an ice-cooled suspension of sodium azide in acetonitrile and the reaction was stirred overnight. Imidazole was added to the ice-cooled mixture, and the reaction was stirred again for three hours before being treated with HCl in ethanol, to obtain the more stable hydrochloride form as colorless crystalline solid. Treatment of Fmoc-lysine **94** with freshly prepared **118** in a methanol/water mixture, in the presence of two equivalents of potassium carbonate as base, afforded compound **117** *via* diazo-transfer. Concentrated crude material was taken into a water/ethyl acetate emulsion and extracted in the organic phase after acidification to pH 4. The desired building block was obtained in excellent yield and purity. Therefore it was used for SPPS without any further purification (Figure 44).



**Scheme 22.** Synthesis of 6-azido-*N*-Fmoc-norleucine building block **117**. Conditions: [a]  $\text{SO}_2\text{Cl}_2$  (1.0 eq.),  $\text{CH}_3\text{CN}$ , 0°C to r.t., overnight; [b] Imidazole (1.9 eq.), 0°C to r.t., 3 h, 78% over two steps; [c]  $\text{K}_2\text{CO}_3$  (2.1 eq.),  $\text{MeOH}/\text{H}_2\text{O}$  (2:1), r.t., 5 h, 95%.

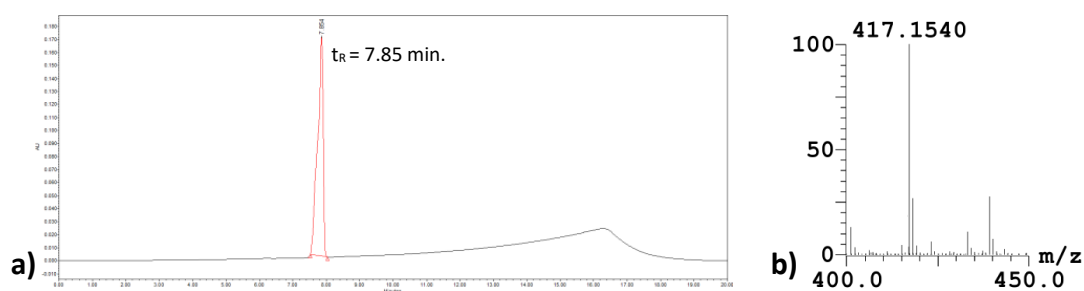
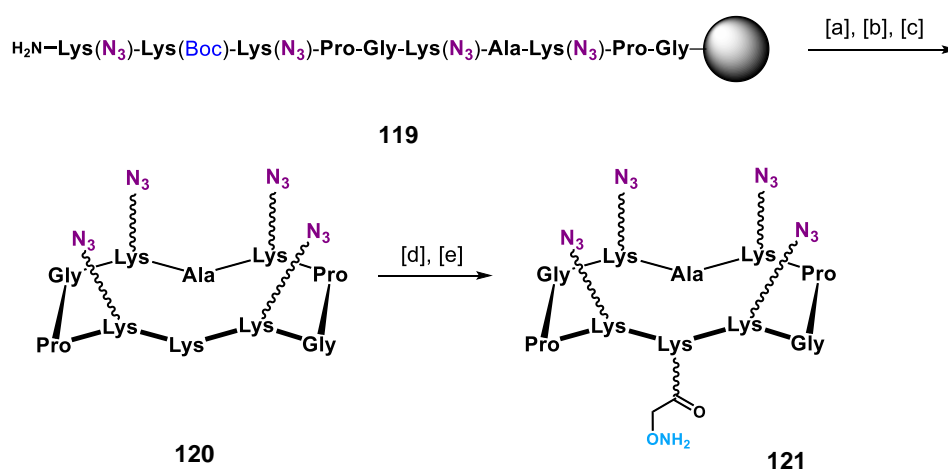


**Figure 44.** a) Analytical RP-HPLC profile ( $\lambda=214$  nm, 5-100% solv.B in 15') of **117**. b) HRMS (ESI<sup>+</sup>-TOF) of **117** (zoom).  $m/z$  calcd. for  $[M+Na]^+$ : 417.1539 (monoisotopic), found: 417.1540.

We performed our SPPS protocol on Fmoc-Gly-SASRIN™ solid support, including azido-bearing modified lysine **117** in the linear sequence, to obtain **119** (Scheme 23). The linear assembly of sequence **119** was performed manually due to the tendency of **117** to precipitate in DMF or NMP (*N*-methyl-2-pyrrolidinone) solutions at the operative concentration of automated SPPS synthesis. Cleavage from the resin in mild acidic conditions, followed by cyclization in diluted DMF/CH<sub>2</sub>Cl<sub>2</sub> mixture, in the presence of PyBOP® afforded the desired cyclopeptide scaffold. The Boc protecting group was readily removed by treatment with a 50% TFA/CH<sub>2</sub>Cl<sub>2</sub> solution. After precipitation and RP-HPLC purification, pure compound **120** was isolated in 49% overall yield. This key intermediate was used as platform for the assembly of tetravalent triazole-linked glycoclusters, and for the construction of azide-bearing cyclopeptide “arms”, which served for the divergent assembly route (Figure 45).

Functionalization of the free amino group on the lower domain of scaffold **120** with Boc-aminoxyacetic acid *N*-hydroxysuccinimide ester, followed by treatment with 50% TFA/CH<sub>2</sub>Cl<sub>2</sub> afforded the cyclopeptide “arm” **121**, in 91% yield over two steps (Scheme 23). Key intermediate **121** is equipped with four azido residues on the upper domain, and one free aminoxy function on the lower domain, prone to undergo oxime ligation with an aldehyde moiety.



**Scheme 23.** Synthesis of cyclopeptide key intermediates **120** and **121**. Conditions: [a] 1% TFA, CH<sub>2</sub>Cl<sub>2</sub>; [b] PyBOP (1.2 eq.), DIPEA (2 eq.), DMF/CH<sub>2</sub>Cl<sub>2</sub> (1:1), 0.5 mM, r.t., 30 min.; [c] TFA/CH<sub>2</sub>Cl<sub>2</sub> (1:1), r.t., 30 min., 49% overall; [d] Boc-aminoxyacetic acid *N*-hydroxysuccinimide ester (1.2 eq.), DIPEA (1.5 eq.), DMF, r.t., 20 min.; [e] TFA/NH<sub>2</sub>OH/CH<sub>2</sub>Cl<sub>2</sub> (50:2:48), r.t., 30 min., 91% over two steps.

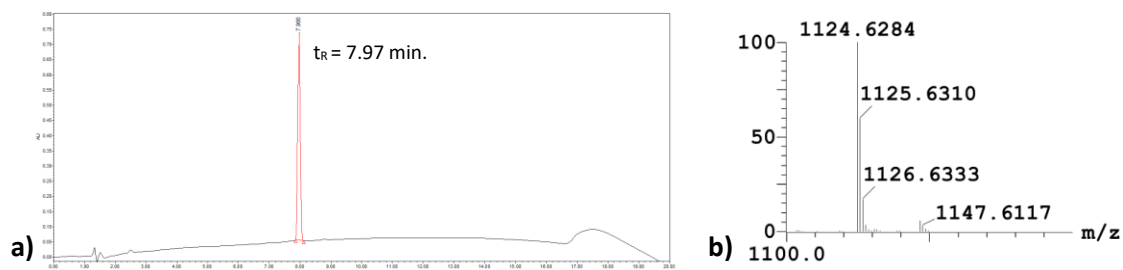
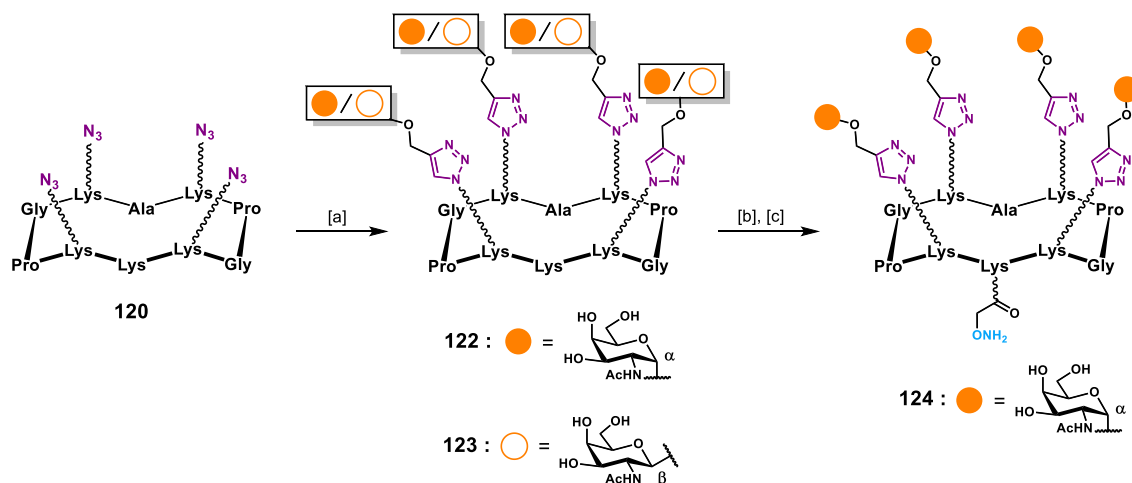


**Figure 45.** a) Analytical RP-HPLC profile ( $\lambda=214$  nm, 5-100% solv.B in 15') of **120**. b) HRMS (ESI<sup>+</sup>-TOF) of **120** (zoom).  $m/z$  calcd. for [M+H]<sup>+</sup>: 1124.6302 (monoisotopic), found: 1124.6284; calcd. for [M+ Na]<sup>+</sup>: 1147.6147 (second peak on isotopic cluster), found: 1147.6117.

#### II.4.4. Divergent and convergent assembly of (TRZ)Tn-bearing hexadecavalent glycodendrimers **126** and **127**

With compound **120** in hand, we started by synthesizing tetravalent glycoclusters **122** and **123** via CuAAC (Scheme 24). Three distinct solutions of equal volumes were prepared: (i) a first solution containing the azido-moiety **120** in DMF, plus  $\alpha$  anomer **112** or  $\beta$  anomer **113** (Scheme 21) (Solution A), (ii) a second solution containing CuSO<sub>4</sub> and tris(3-hydroxypropyltriazolylmethyl)amine (THPTA) in PBS (pH 7.4) (Solution B), (iii) a third solution of sodium ascorbate in PBS (Solution C). Blue-colored solution B, containing copper is in his oxidation state +2, also contained the THPTA ligand, a widely employed stabilizer of copper(I) during CuAAC.<sup>363</sup> Upon addition of ascorbate-containing solution C, the blue color of solution B disappeared due to the reduction of copper(II) to copper(I), which represents the active catalytic species in CuAAC. The resulting mixture, containing copper(I) and its ligand, was added to solution A, which contained azido- and alkyne-partners, and the reaction mixture was stirred at room temperature for one to two hours. All solution were previously degassed, by repeated vacuum/N<sub>2</sub> cycles, to reduce the presence of molecular oxygen which could re-oxidize copper(I) to copper(II). Indeed, when reaction mixture turned from colorless to green, suggesting the re-oxidation of copper(I), the triazole formation was incomplete, leading to partially functionalized structures. In those cases, the reaction has been able to proceed to completion upon addition of an

excess of sodium ascorbate. Nevertheless, it was possible to adjust the equivalents of CuSO<sub>4</sub>, THPTA and sodium ascorbate to limit the premature re-oxidation of copper(I), and at the same time obtain clear chromatographic profiles. Once reaction completion was confirmed by LC-MS, chelating resin Chelex® was added to the stirred mixture for 30 minutes in order to remove the excess of copper, filtration and purification *via* preparative RP-HPLC afforded tetravalent glycoclusters **122** and **123** in good yields and purity (Scheme 24).



**Scheme 24.** Synthesis of glycosylated cyclopeptide clusters **122**, **123**, and glycosylated cyclopeptide “arm” **124**. Conditions: [a] **112/113** (6.0 eq.), CuSO<sub>4</sub> (cat.), THPTA (20 eq.), Na ascorbate (32 eq.), DMF, PBS (pH 7.4, 10 mM), r.t., 2 h, 84% for **122**, 83% for **123**; [b] Boc-aminoxyacetic acid *N*-hydroxysuccinimide ester (1.2 eq.), DIPEA (1.5 eq.), DMF, r.t., 20 min., [c] TFA/NH<sub>2</sub>OH/CH<sub>2</sub>Cl<sub>2</sub> (50:2:48), r.t., 30 min., 77% over two steps.

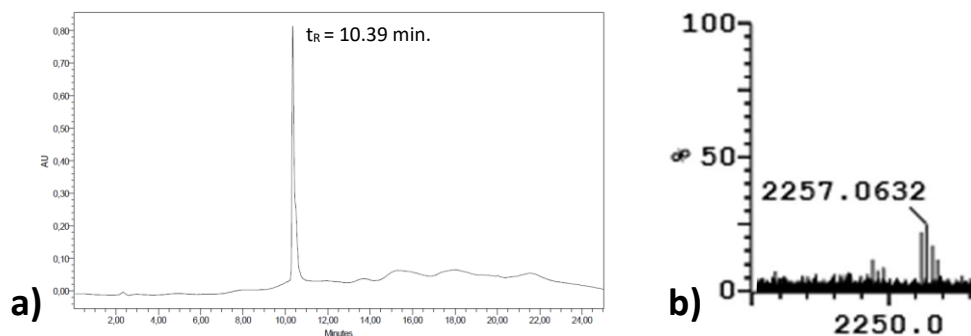
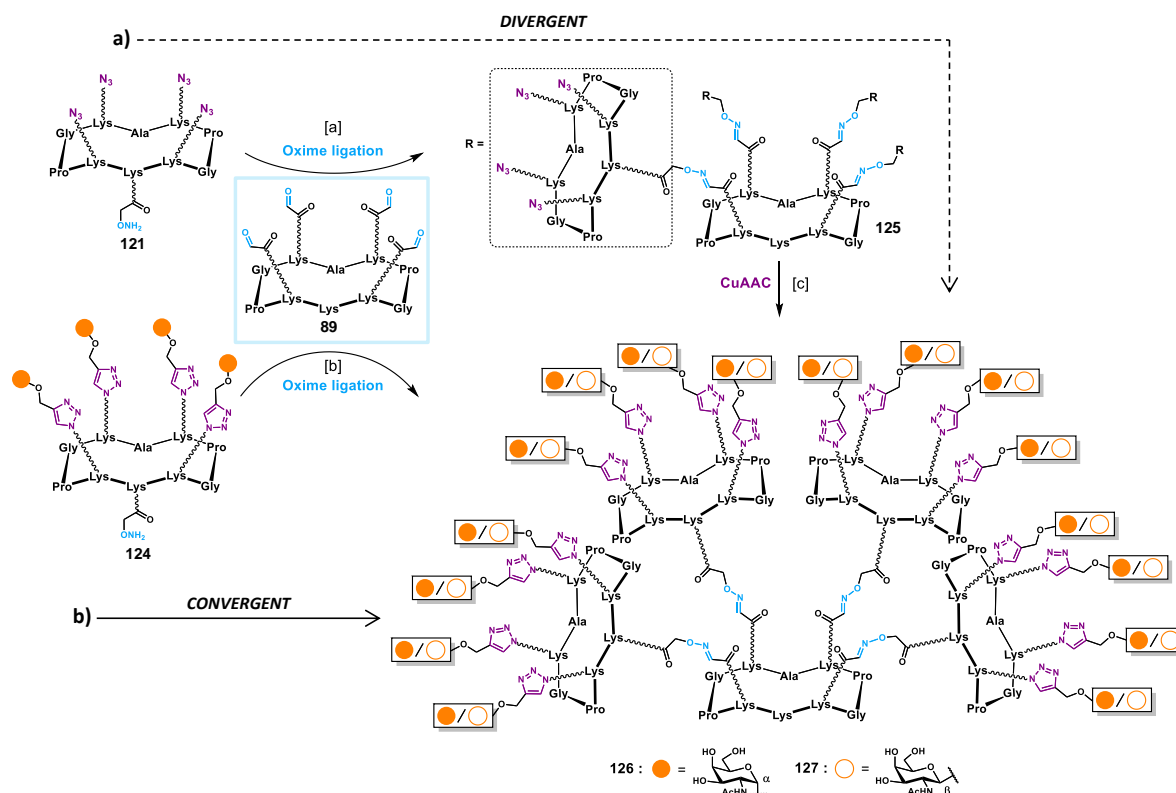


**Figure 46.** a) Analytical RP-HPLC profile ( $\lambda=214 \text{ nm}$ , 5-100% solv.B in 20') of **124**. b) HRMS (ESI<sup>+</sup>-TOF) of **124** (zoom).  $m/z$  calcd. for [M+ Na]<sup>+</sup>: 2257.0573 (most intense peak of isotopic cluster), found: 2257.0632.

Tetravalent glyco-cyclopeptide **122**, decorated with triazole-linked  $\alpha$ -GalNAc moieties, was further functionalized with an aminoxy linker on the lower domain of the platform. As seen for **121** (Scheme 23), reaction with Boc-aminoxyacetic acid *N*-hydroxysuccinimide ester,<sup>346</sup> followed by treatment with 50% TFA/CH<sub>2</sub>Cl<sub>2</sub> allowed the introduction of a reactive aminoxy function, in 77% yield over two steps. Glycosylated “arm” building block **124**, obtained in excellent purity and easily

characterized *via* mass spectrometry (Figure 46), has been used to assess the validity of the convergent assembly (*vide infra*).

With all needed intermediates in hand, we pursued our synthetic route starting from the divergent assembly of hexadecaivalent glycodendrimers **126** and **127** (Scheme 25a). Four cyclopeptide “arm” **121**, decorated with four azide residues on the upper domain and one aminoxy function on the lower domain, were grafted on aldehyde-bearing cyclopeptide “core” scaffold **89** via oxime ligation.



**Scheme 25.** a) Divergent assembly of hexadecaivalent glycodendrimers **126** and **127**. b) Convergent assembly of hexadecaivalent glycodendrimer **126**. Conditions: [a] **89**, **121** (6.0 eq.), 0.1% TFA in CH<sub>3</sub>CN/H<sub>2</sub>O (1:1), 37°C, 40 min., 85%; [b] **89**, **124** (6.0 eq.), 0.1% TFA in H<sub>2</sub>O, 37°C, 40 min., 90%; [c] **112/113** (20 eq.), CuSO<sub>4</sub> (cat.), THPTA (80 eq.), Na ascorbate (100 eq.), DMF, PBS (pH 7.4, 10 mM), r.t., 2 h, 70% for **126**, 69% for **127**.

The reaction was performed in a TFA-containing water/acetonitrile mixture (pH  $\approx$  2.2), since the presence of the azido moiety on **121** reduces its solubility in water. After 40 minutes incubation at 37°C, LC-MS revealed that the conjugation was completed (Figure 47). As reported on UPLC chromatogram in figure 47a, the more polar peak ( $t_r$ , retention time = 5.09 min.) corresponded to the excess of **121** (Scheme 25, Figure 47b) which was isolated and recovered. The single peak at  $t_R$  = 6.42 minutes contained target compound **125** (Scheme 25, Figure 47c), which was isolated in 90% yield after preparative RP-HPLC.

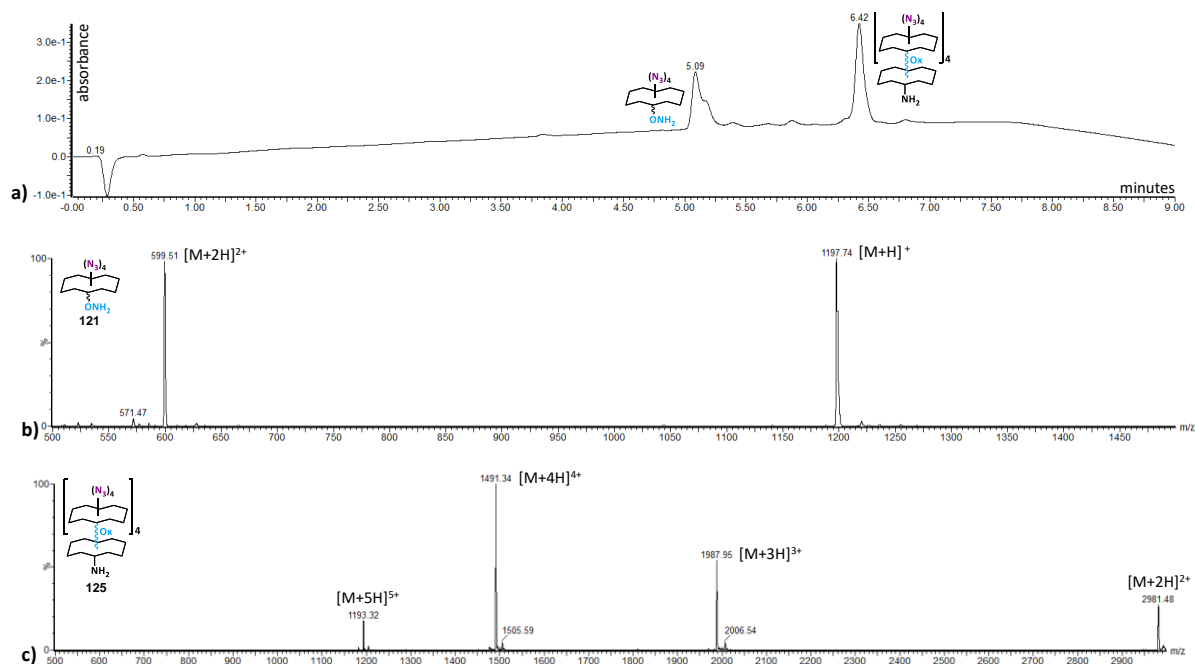


**Figure 47.** a) UPLC profile ( $\lambda=214$  nm, 5-60% solv.D in 7') of oxime ligation between **121** and **89**. b) ESI<sup>+</sup>-MS spectrum of compound **121**.  $m/z$  calcd. for [M+ H]<sup>+</sup>: 1197.7 (monoisotopic), found: 1197.7; calcd. for [M+ 2H]<sup>2+</sup>: 599.3, found: 599.5; c) ESI<sup>+</sup>-MS spectrum of compound **125**. calcd. for [M+ 2H]<sup>2+</sup>: 2981.6 (most intense peak on isotopic cluster), found: 2981.5; calcd. for [M+ 3H]<sup>3+</sup>: 1998.1, found: 1998.0; calcd. for [M+ 4H]<sup>4+</sup>: 1491.3, found: 1491.3; calcd. for [M+ 5H]<sup>5+</sup>: 1193.2, found: 1193.3.

Azide-bearing, hexadecaivalent scaffold **125** was next reacted with propargylated carbohydrate building blocks **112** and **113** via copper(I)-catalyzed alkyne-azide cycloaddition (Scheme 25a). The reaction was carried out under the same conditions to that reported for the assembly of tetravalent glycoclusters **122** and **123** (Scheme 24). Compound **126** (Figure 48) was easily isolated after preparative chromatography in 70% yield.

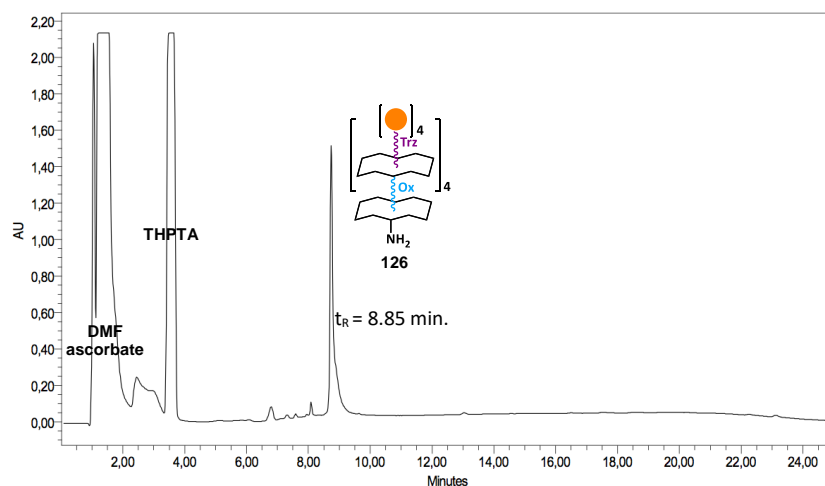


**Figure 48.** Analytical RP-HPLC profile ( $\lambda=214$  nm, 5-100% solv.B in 20') of CuAAC reaction between **125** and **112**.

Compounds **126** and **127** showed no traces of partially glycosylated structures, and their analysis *via*  $^1\text{H-NMR}$  (Figure 49) has shown characteristic signals for triazole protons ( $\approx 8.0$  ppm), oxime protons ( $\approx 7.7$  ppm) and carbohydrate anomeric protons ( $\approx 5.0$  ppm, for  $\alpha$  anomer, 4.93-4.90 for  $\beta$  anomer, not shown). Signal's integration values were in accordance with the expected ratio: four oxime protons, sixteen triazole protons and sixteen anomeric protons. In contrast with the previous iterative oxime-based synthetic approach, no peak corresponding to fragmentation of the carbohydrate moiety were observed on MALDI spectra, thus confirming the monodispersity of the glycodendrimers.<sup>356</sup>

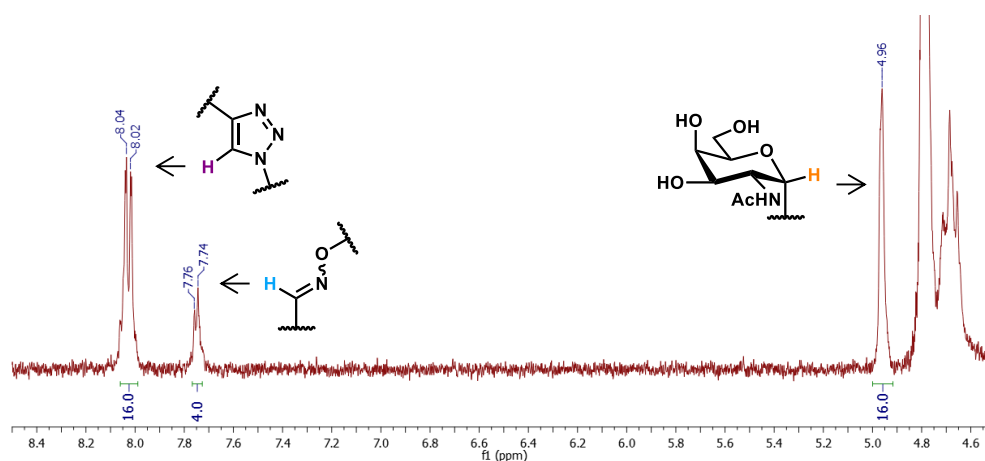


**Figure 49.**  $^1\text{H-NMR}$  (400 MHz,  $\text{D}_2\text{O}$ ) zoom of compound **126**.

We next evaluated whether the convergent approach could be used to prepare glycodendrimer **126**. For this purpose, four copies of glycocluster **124**, with an aminoxy linker on the lower domain of the scaffold, were conjugated onto aldehyde-bearing cyclopeptide “core” **89** via oxime ligation (Scheme 25b). The reaction was carried out under our general conditions, in water containing 0.1% TFA. After 40 minutes reaction at  $37^\circ\text{C}$ , compound **126** was obtained in 90% yield after RP-HPLC purification, thus confirming that the convergent approach can be successfully employed by using both oxime and CuAAC conjugations. In terms of efficiency, the synthesis of compound **126** realized *via* convergent pathway proceeded with a slightly improved yield of 58% from key precursor **120**, compared to the 54% yield obtained with the divergent assembly. Moreover our convergent strategy allowed the recovery of the excess of key building block **124**, which could be isolated during preparative RP-HPLC.



## II.4.5. Evaluation of the binding activity of glycodendrimers **122**, **123**, **126** and **127** on SBA lectin *via* ELLA

Several groups have studied the recognition of GalNAc by specific lectins. For example Bertozzi and co-workers developed microarrays systems in which glycans are presented on polymer backbones, mimicking the spatial arrangements of native mucins.<sup>364</sup> By modulating the molecular composition and surface density of these mucin mimetics, they have shown how parameters such as GalNAc valency and inter-ligand spacing affect their recognition by several GalNAc-specific lectins. In addition, if other studies have demonstrated the influence of glycan density on lectin binding, the recognition mechanism is not fully addressed.<sup>365,366</sup> Dam and co-workers reported isothermal titration microcalorimetry (ITC) measurements and hemagglutination inhibition assays for the binding of the soyabean agglutinin (SBA) lectin to modified forms of porcine submaxillary mucin (PSM), which possesses GalNAc residues (saccharide part of Tn antigen, see figure 12).<sup>367</sup> The SBA lectin is a tetramer, in which GalNAc-binding domains are located at the apexes of a quadrangle spaced by 5 and 7 nm. Its high affinity ( $K_d = 0.2$  nM) for a modified form of PSM ( $\approx 2300$  GalNAc residues) indicated that increasing the number of GalNAc epitopes leads to higher affinities (avidities). Further investigations suggested that before complete dissociation from the modified mucin, the lectin follows a “bind and jump” kinetic, interacting with one carbohydrate to another along the mucin backbone.<sup>368,369</sup>

We selected SBA lectin to evaluate how parameters such as GalNAc valency and anomeric configuration of the saccharide moiety can affect the recognition process. Thus, a competitive ELLA was carried out using a GalNAc-polymer coated to microtiter plates. Lectin binding to the polymer-coated surface was challenged with monovalent GalNAc, as positive reference, along with tetravalent compounds **122-123** (Scheme 24) and hexadecavalent glycodendrimers **126-127** (Scheme 25) (Figure 50).  $IC_{50}$  values, corresponding to the concentration of glycoconjugates required to prevent 50% of the binding, are reported in table 4.

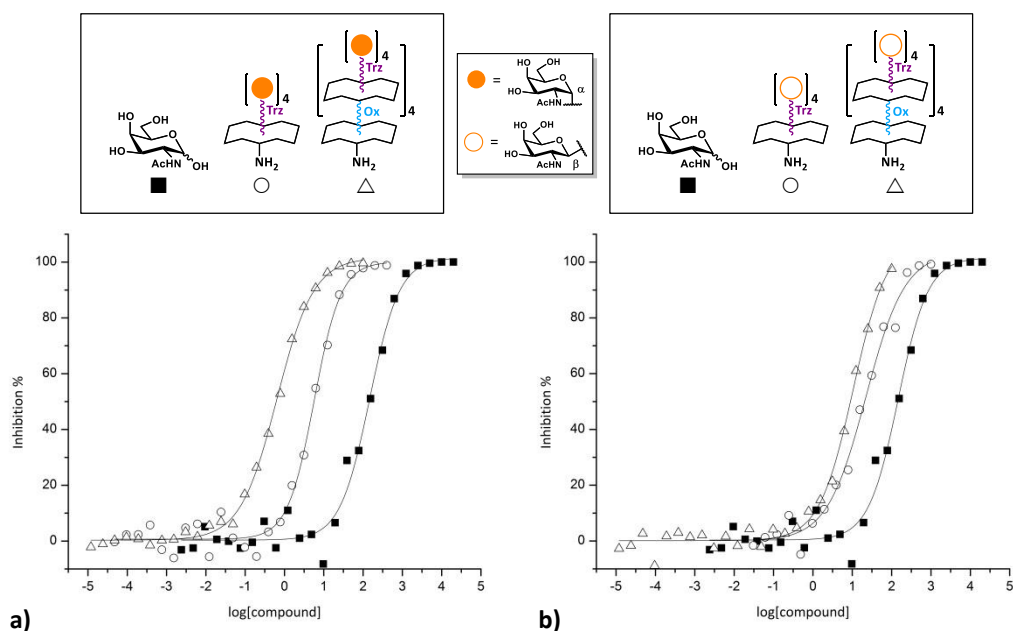


**Figure 50.** Inhibition curves for the binding of SBA-HRP to GalNAc-polymer by a) GalNAc monomer (■), compound **122** (○), or compound **126** (△); b) GalNAc monomer (■), compound **123** (○), or compound **127** (△).

Compound	n <sup>[a]</sup>	IC <sub>50</sub> <sup>[b]</sup> (μM)	rp <sup>[c]</sup>	rp/n <sup>[d]</sup>
GalNAc	-	154.8±26	1	1
<b>122</b>	4	4.9±0.6	31.6	7.9
<b>123</b>	4	27.3±2	5.6	1.4
<b>126</b>	16	0.46±0.1	330.8	20.16
<b>127</b>	16	8.6±0.3	17.9	1.1

**Table 4.** Inhibition of SBA lectin adhesion to GalNAc-coated plates determined by ELLA. [a] Number of carbohydrate residues per glycoconjugate; [b] Average of three independent experiments; [c] Relative potency “rp” = IC<sub>50</sub>(monosaccharide)/IC<sub>50</sub>(glycoconjugate); [d] Relative potency/number of carbohydrate residues “rp/n” = relative potency/n.

Results showed that all glycoclusters (**122-123**) and glycodendrimers (**126-127**), in both anomer series, are able to prevent SBA lectin adhesion at micromolar concentrations. In the beta series (Figure 50b), a binding improvement was observed when valency increased. IC<sub>50</sub> values dropped from 27.3 μM to 8.6 μM for tetraivalent glycocluster **123** and hexadecavalent glycodendrimer **127**, respectively, while for monomeric GalNAc an IC<sub>50</sub> of 154 μM was observed. Although, when relative potency (rp) values are compared to the number of saccharide copies grafted on our constructs (n), values close to 1 suggest that inhibition occurred due to a simple concentration effect instead of multivalency, which is the case of **123** and **127**. More interestingly, stronger inhibition effects were

obtained in the alpha series (Figure 50a). Firstly, a strong improvement in terms of  $IC_{50}$  was obtained when tetravalent glycocluster **122** was compared to hexadecavalent glycodendrimer **126** (from 4.9 to 0.46  $\mu$ M). Relative potency of the most potent compound (**126**) showed a 330-fold higher binding improvement compared to the GalNAc monomer (Table 4). The ratio between the obtained relative potency (*i.e.* 330.8) and number of carbohydrate copies displayed on the glycodendrimer (*i.e.* 16) gave a  $rp/n$  value of 20, meaning that each GalNAc residue grafted on the hexadecavalent scaffold has an inhibition efficacy equal to that of twenty monomeric GalNAc unities. This result suggested that glycodendrimer **126** displays  $\alpha$ -GalNAc residues in a more favorable orientation to ensure a multivalent interaction with SBA lectin binding sites. Although showing moderate binding efficacies towards SBA lectin, our trials demonstrated that the binding properties of the described glycoconjugates are strongly dependent on structural parameters represented by saccharide epitope orientation ( $\alpha/\beta$  anomeric configuration) and valency. Similar observations have been often observed for other lectins. This work has been published as a full paper in Organic & Biomolecular Chemistry (RSC).<sup>370</sup>

In conclusion, through our combined synthetic strategy we assessed the validity of a convergent approach for the controlled assembly of hexadecavalent glycodendrimers decorated with a GalNAc moiety (Figure 43). The feasibility of the convergent assembly has been assessed after performing the already described divergent method. The reported synthetic strategy involved the combination of two orthogonal chemoselective reactions: OL and CuAAC, which were carried on by using synthetic protocols developed in our laboratory. By our synthetic strategy, we exploited the oxime ligation to conjugate cyclopeptide “arms” on a central “core” scaffold, giving rise to hexadecavalent dendrimer-like architectures, while CuAAC was employed to graft the peripheral saccharide moiety. Thanks to their higher chemical stability, the introduced triazole linkers generated a minor extent of fragmentation during MALDI analyses. <sup>1</sup>H-NMR experiments confirmed the previous observation, showing characteristic signals, between 5 and 8 ppm, which have given consistent integration values.

Binding assays to SBA lectin through ELLA suggested a strong dependency on saccharide orientation and valency for the different tetravalent- and hexadecavalent compounds, enriching our understanding in the field of protein-carbohydrate interactions and allowing a multimodal assembly of large glycodendrimers with interesting biological applications.

## II.5. Synthesis of a new set of mannosylated tetracosavalent glycodendrimers

The above-described synthetic strategies allowed us to reach well-characterizable, multivalent glycosylated structures through the controlled assembly of pre-synthesized building blocks. The reliability of carbohydrate- and peptide-chemistry protocols, together with the efficacy and simplicity of click-chemistry reactions ensured the basis for the development of an efficient modular synthetic strategy. With the aim to pursue our investigations towards the design and synthesis of glycoclusters and glycodendrimers with interesting biological activity, we undertook the synthesis of a new set of multivalent constructs. Once again, we decided to decorate our structures with mannose residues, since mannose represents a simple and readily available carbohydrate unit which can be valorised with a large choice of biological targets.

### II.5.1. Introducing a small library of multivalent mannosylated glycoconjugates

The proposed mannosylated multivalent structures (**128-135**, figure 51) have different topology, carbohydrate density, and valencies of four, six and twenty-four. We generated this small library of compounds using our synthetic protocols, involving OL and CuAAC orthogonal chemoselective reactions; tetracosavalent (24-valent) structures were reached by the assembly of both clustered and dendrimer-like tetravalent glycosylated “arms” on both hexavalent RAFT and cyclophosphazene “core” scaffolds. Thus, we started by synthesizing backbone peptide structures based on: (i) rigid RAFT scaffolds displaying four or six lysine residues in the upper domain, and (ii) a flexible lysine-based tetravalent dendron. In addition, we prepared a (iii) hexavalent cyclophosphazene-based “core” inorganic platform, which has been shown by X-ray crystallography to adopt a conformation in which three substituents point toward the upper face of the planar phosphazene, and the other three point downward (*vide infra*).<sup>371,372</sup> With these platform in hand, different combinations were prepared to provide tetravalent (**128, 130**), hexavalent (**129, 131**) and tetracosavalent (**132-135**) glycodendrimers (Figure 51). The resulting glycoclusters and glycodendrimers were characterized and evaluated by isothermal titration calorimetry for their binding to BCL-2A lectin: a well-characterized, pathogen-related bacterial protein, with high affinity for  $\alpha$ -D-mannopyranoside ( $K_d = 2.7 \mu\text{M}$ ).

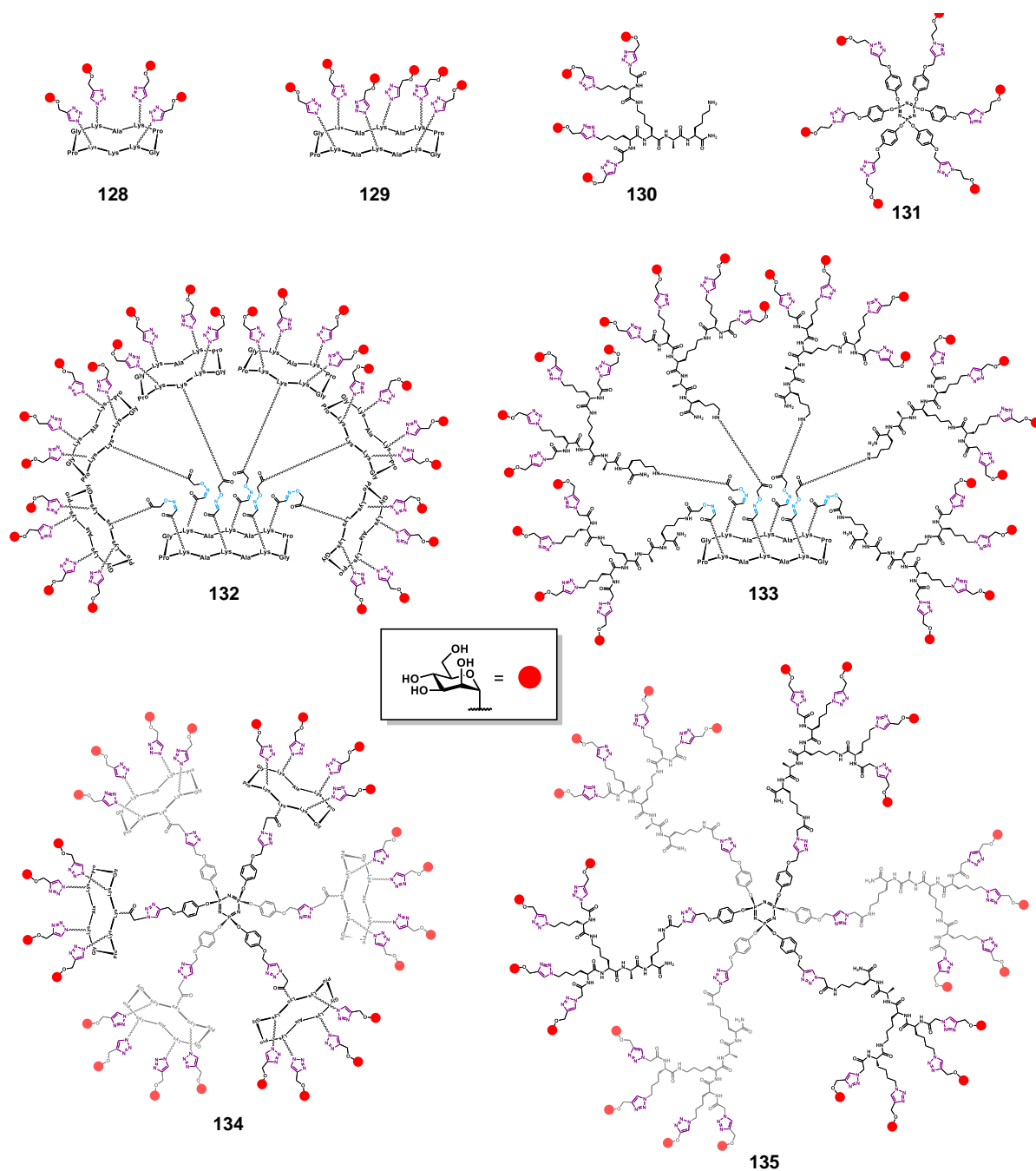


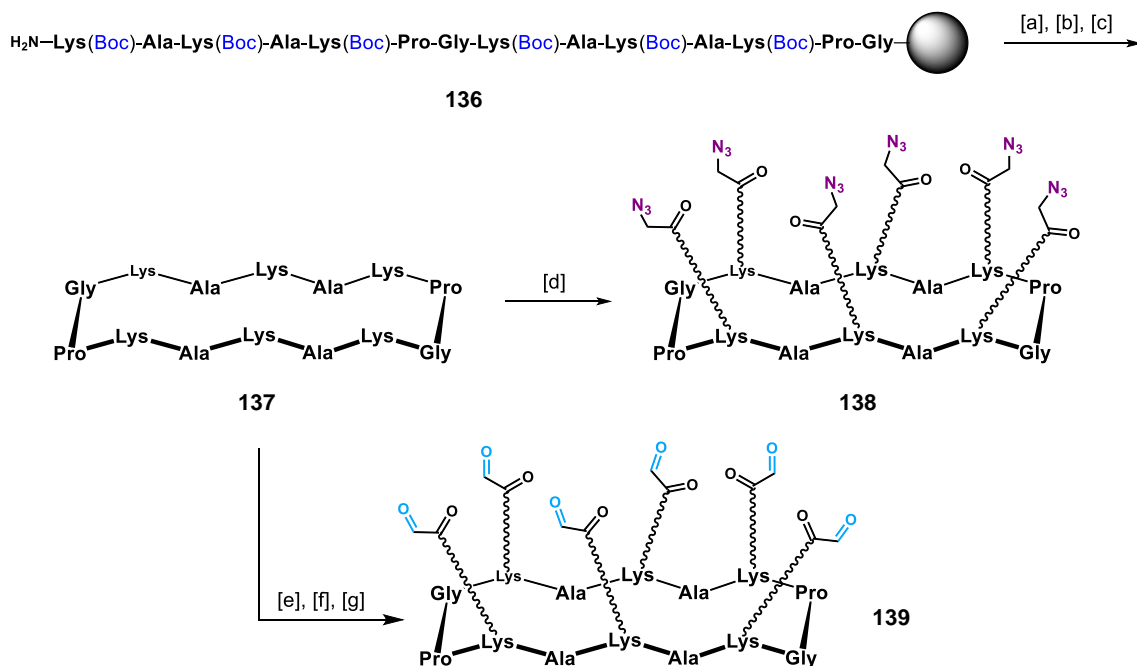
**Figure 51.** Structures of tetra-, hexa- and tetracosavalent glycodendrimers **128-135**.

## II.5.2. Synthesis of RAFT-, dendron-, and cyclophosphazene-based scaffolds

The first step of syntheses involved the preparation of appropriately functionalized scaffolds. We adapted our previously reported procedures to synthesize RAFT cyclopeptide **137**, with six lysine residues pointing their side chains in the upper domain of the scaffold (Scheme 25). This platform

would allow for an extended multivalency, owing to its two additional conjugation sites, in a rigid and well oriented backbone, on condition that antiparallel  $\beta$ -sheet conformation is retained. Resin-bound sequence **136** was thus obtained *via* a classic Fmoc/*t*Bu SPPS protocol (Resin = Fmoc-Gly-SASRIN™) using commercially available amino acids. Cleavage from the resin in mild acidic conditions, followed by cyclization in diluted conditions and Boc-groups deprotection (Scheme 25) afforded RAFT **137** in 49% overall yield. We were glad to observe that cyclization proceeded smoothly, using the same conditions as for 10-mer oligopeptides **96** (Scheme 15) and **119** (Scheme 23). After purification, cyclopeptide **137** was characterized by analytical RP-HPLC and mass spectrometry (Figure 52a, b). With intermediate **137** in hand, we next performed circular dichroism (CD) experiments to assess its antiparallel  $\beta$ -sheet conformation. Results were in agreement with literature, showing a positive band at  $\approx$  200 nm and negative band around 220 nm. Moreover CD profiles of **137** and **120** (Scheme 23) were consistently comparable (Figure 52c). This observations confirm that the addition of four amino acids in the cyclopeptide does not seem to affect the conformational stability of the scaffold.<sup>373</sup>

Having confirmed the chemical and conformational identity of intermediate **137**, we next functionalized its six free amino-residues with either azido- or aldehyde -functions, to provide appropriate anchorage points for CuAAC and oxime-ligation, respectively (Scheme 26). 2,5-dioxopyrrolidin-1-yl-2-azidoacetate<sup>374</sup> was coupled to RAFT **137** in the presence of DIPEA as base, to give azido-bearing scaffold **138**. In-solution coupling between **137** and Boc-Ser(*t*Bu)-OH was carried on in DMF, in the presence of DIPEA and PyBOP® as activating agent. Following acid-mediated Boc/*t*Bu deprotection, and oxidative cleavage of the six serine residues,  $\alpha$ -oxo-aldehyde functionalized “core” scaffold **139** was obtained in 56% yield over three steps.



**Scheme 26.** Synthesis of hexavalent cyclopeptides **137-139**. Conditions: [a] 1% TFA,  $\text{CH}_2\text{Cl}_2$ ; [b] PyBOP (1.2 eq.), DIPEA (2.0 eq.), DMF/ $\text{CH}_2\text{Cl}_2$  (1:1), 0.5 mM, r.t., 30 min.; [c] 50% TFA/ $\text{CH}_2\text{Cl}_2$ , r.t., 30 min, 49% overall yield; [d] **137**, 2,5-dioxopyrrolidin-1-yl-2-azidoacetate (10 eq.), DIPEA (7.1 eq.), DMF, r.t., 30 min., 85%. [e] **137**, Boc-Ser(*t*Bu)-OH (7.8 eq.), DIPEA (11.2 eq.), DMF, r.t., 1 h; [f] TFA/TIS/ $\text{H}_2\text{O}$  (96:2:2), r.t., 3 h; [g]  $\text{NaIO}_4$  (60 eq.),  $\text{H}_2\text{O}$ , r.t., 40 min., direct RP-HPLC purification, 56% over three steps.

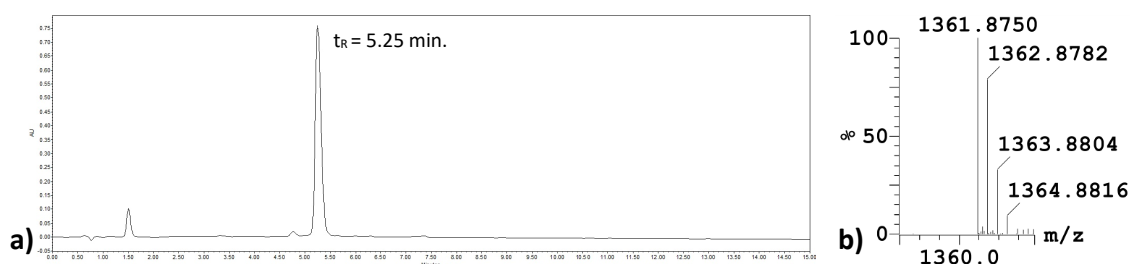
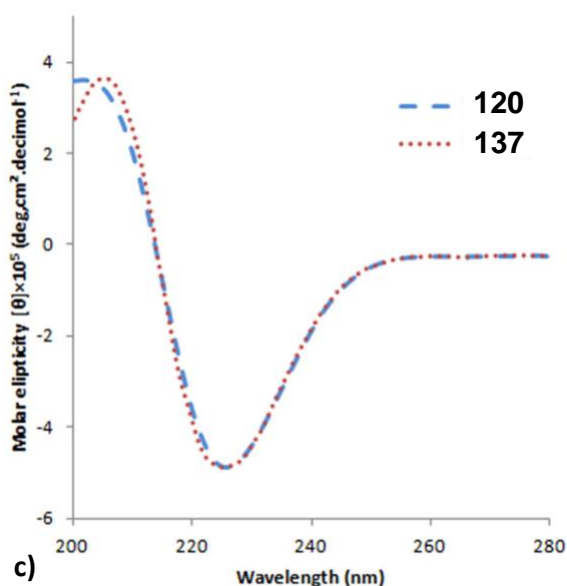
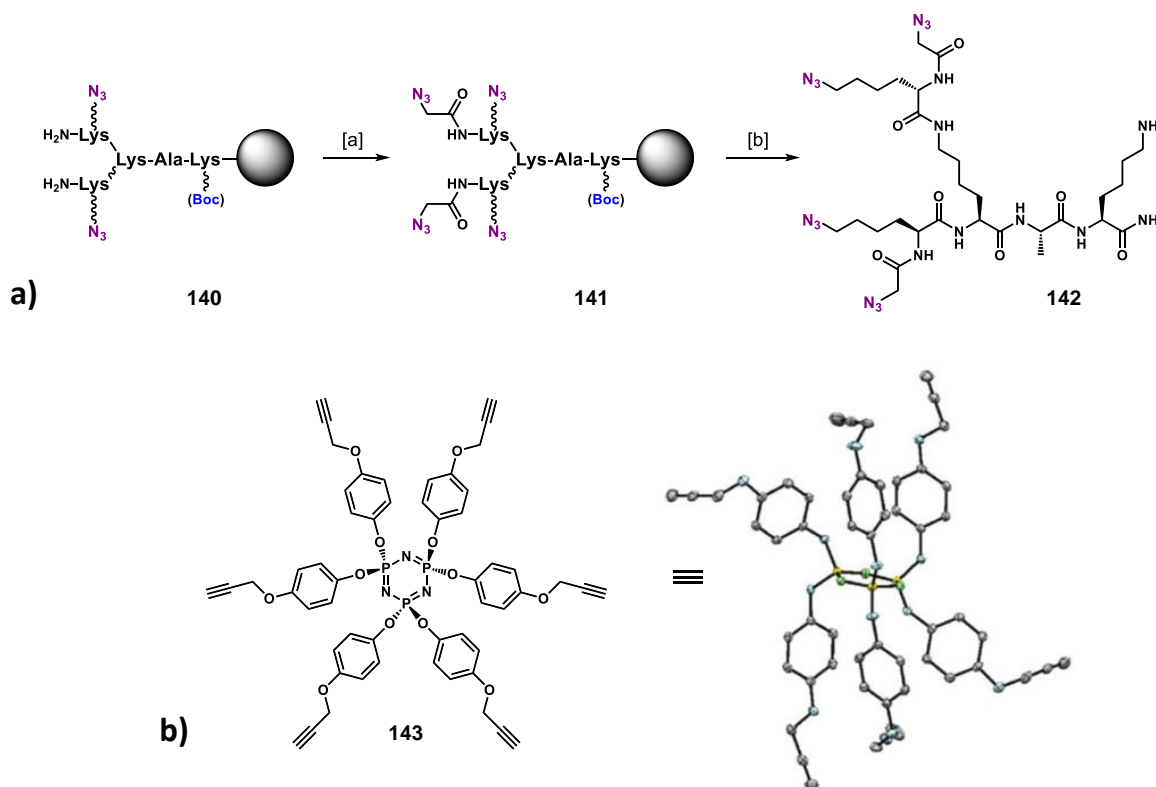


**Figure 52.** a) Analytical RP-HPLC profile ( $\lambda=214$  nm, 0-30% solv.B in 15') of **137**. b) HRMS (ESI<sup>+</sup>-TOF) of **137** (zoom).  $m/z$  calcd. for  $[\text{M}+\text{H}]^+$ : 1361.8745 (monoisotopic), found: 1361.8750. c) Superposed circular dichroism spectra of compounds **120** and **138**.



Branched penta-peptide sequence **140** was synthesized on Rink amide resin by employing 6-azido-*N*-Fmoc-norleucine building block **117** (Scheme 22). The two free amino groups were then reacted with 2,5-dioxopyrrolidin-1-yl-2-azidoacetate<sup>374</sup> to install two additional azido moieties (**141**, scheme 27a). Subsequent cleavage from the resin under strong acidic conditions afforded tetravalent azido-bearing dendrimer **142** in 65% overall yield (Scheme 27a).

Hexavalent propargylated scaffold **143** was synthesized by Dr. David Goyard (post-doctoral researcher) *via* nucleophilic substitution between hexachlorocyclophosphazene and 4-(prop-2-yn-1-yloxy)phenol, using an already described procedure by Roy and co-workers.<sup>372</sup> X-ray diffraction studies performed on compound **143** led to the expected double tripododal pattern, with three branches located above the central ring and the other three below (Scheme 27b).



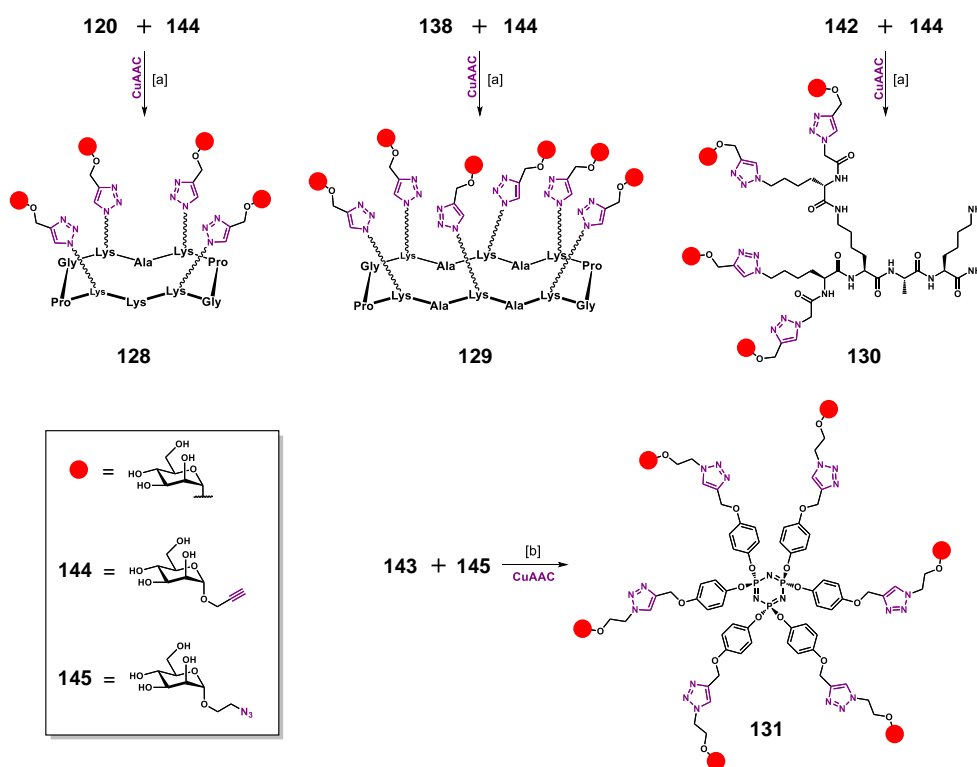
**Scheme 27.** a) Synthesis of tetravalent dendrimer **142**. Conditions: [a] 2,5-dioxopyrrolidin-1-yl-2-azidoacetate (5.5 eq.), DIPEA (3.1 eq.), DMF, r.t., 1 h.; [b] TFA/TIS/H<sub>2</sub>O (96:2:2), r.t., 3 h, 65% overall yield. b) Structure and ORTEP representation of hexapropargylated cyclophosphazene **143**. Hydrogen atoms were omitted for clarity. From Roy and co-workers (Polym. Chem., 2015).<sup>372</sup>



## II.5.3. Synthesis of mannosylated tetra- and hexa-valent glycodendrimers 128-131

Decoration of scaffolds **120** (Scheme 23), **138** (Scheme 26), **142** and **143** (Scheme 27) was performed through CuAAC, using either propargylated or azido-modified mannose residues **144**<sup>375</sup> and **145**<sup>376</sup>, respectively (Scheme 28). Reaction conditions were similar to those employed for the construction of GalNAc-based dendrimers **122**, **123**, **126** and **127** (See section 4.4, Scheme 24-25).

All compounds were obtained in good yields (71-85%) as white foamy solids after RP-HPLC purification and lyophilization. Analytical RP-HPLC, mass spectrometry and <sup>1</sup>H-NMR experiments confirmed product's identity and monodispersity (Figure 53a-c). As an example, phosphazene-based compound **143** (P<sub>6</sub>) showed a clean <sup>1</sup>H-NMR spectrum, where integration of triazole and mannose H-4 protons gave a consistent ratio of six (Figure 53a). Moreover, <sup>31</sup>P-NMR represents a useful tool to assess the equivalence of the three phosphorus atoms, suggesting a symmetrical functionalization of the core scaffold (Figure 53a).



**Scheme 28.** Synthesis of tetra- and hexavalent mannosylated structures **128-131** via CuAAC. Conditions: [a] Azide-containing scaffold (**120/138/142**) (1-5 mM), **144** (1.5 eq. per azide), CuSO<sub>4</sub> (cat.), THPTA (5.0 eq. per azide), Na ascorbate (7.0 eq. per azide), DMF, PBS (pH 7.4, 10 mM), r.t., 2 h, yields: 85% (**128**), 85% (**129**), 71% (**130**); [b] **143**, **145** (1.5 eq. per alkyne), CuSO<sub>4</sub> (cat.), THPTA (5.0 eq. per alkyne), Na ascorbate (7.0 eq. per alkyne), DMF, PBS (pH 7.4, 10 mM), r.t., 2 h, 76%.

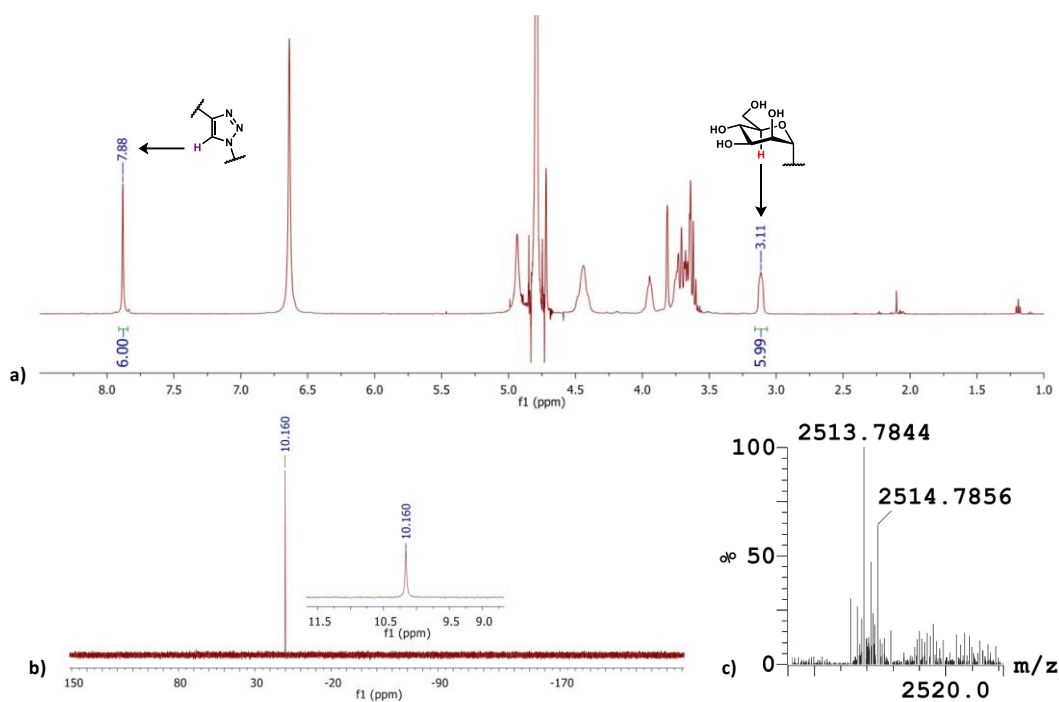
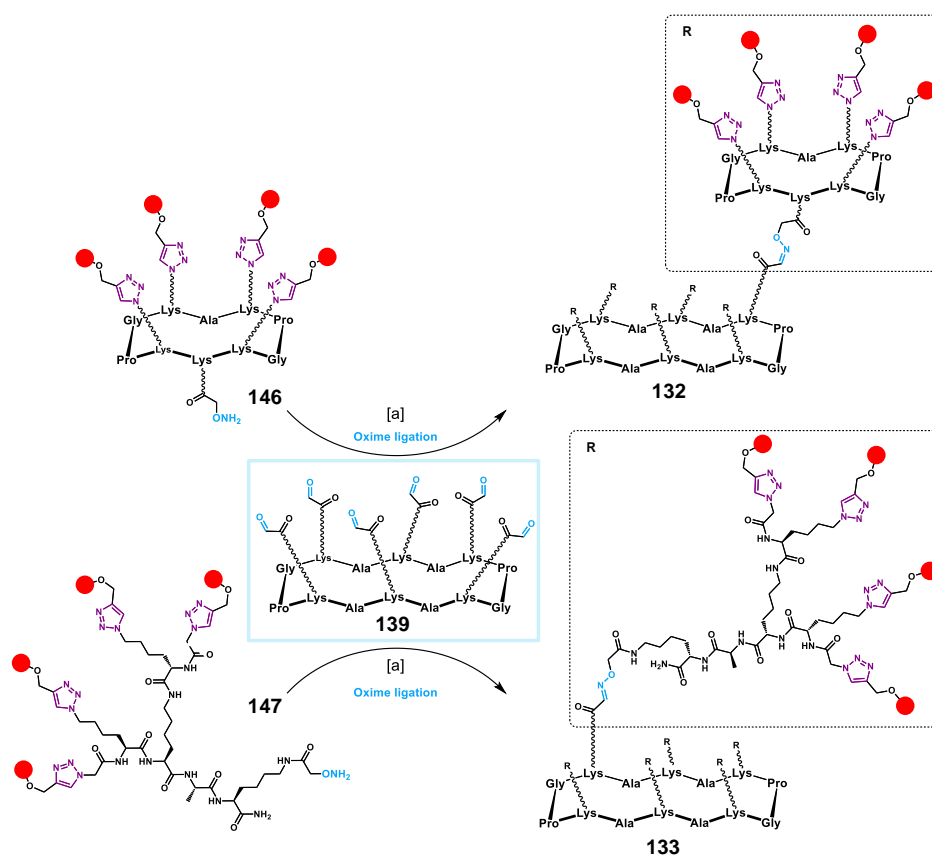


**Figure 53.** a)  $^1\text{H}$ -NMR (400 MHz,  $\text{D}_2\text{O}$ ) spectrum of compound **131**. b)  $^{31}\text{P}$ -NMR (162 MHz,  $\text{D}_2\text{O}$ ) spectrum of compound **131**. c) HRMS (ESI $^+$ -TOF) of **131** (zoom).  $m/z$  calcd. for  $[\text{M}+\text{Na}]^+$ : 2513.7903 (monoisotopic), found: 2513.7844.

## II.5.4. Assembly of mannosylated tetracosavalent glycodendrimers **132** and **133** by OL

Capitalizing on our previously introduced convergent assembly approach based on orthogonal OL/CuAAC ligation (See section 4.4, scheme 25), we undertook the synthesis of glycodendrimers **132** and **133** through the condensation of aminoxy-bearing mannosylated “arms” **146** and **147** on aldehyde-bearing “core” scaffold **139** (Scheme 28). Conjugations were completed within 45 minutes reaction at  $37^\circ\text{C}$ , allowing to retrieve the excess of **146** and **147**, to afford final structures in good yields (77-84%) after purification.



**Scheme 29.** Convergent assembly of tetracosavalent glycodendrimers **132** and **133** by oxime ligation. Conditions: [a] **139**, **146/147** (9.0 eq.), 0.1% TFA in H<sub>2</sub>O, 37°C, 45 min., 84% (**132**), 77% (**133**).

Along the signals corresponding to the desired products, MALDI mass spectrometry analysis (as example we reported the data relative to compound **132**) showed the presence of several signals which could suggest an incomplete functionalization of the “core” structure (Figure 54a). Conversely, analytical RP-HPLC (not shown) and <sup>1</sup>H-NMR (Figure 54b) showed a sharp single-peak profile and a consistent integration ratio between triazole, oxime and mannose anomeric protons, respectively. According to literature reports,<sup>377</sup> we interpreted these additional peaks as the result of oxime bond fragmentation during the MALDI-TOF analysis, as observed for compound **92** (Figure 41b).

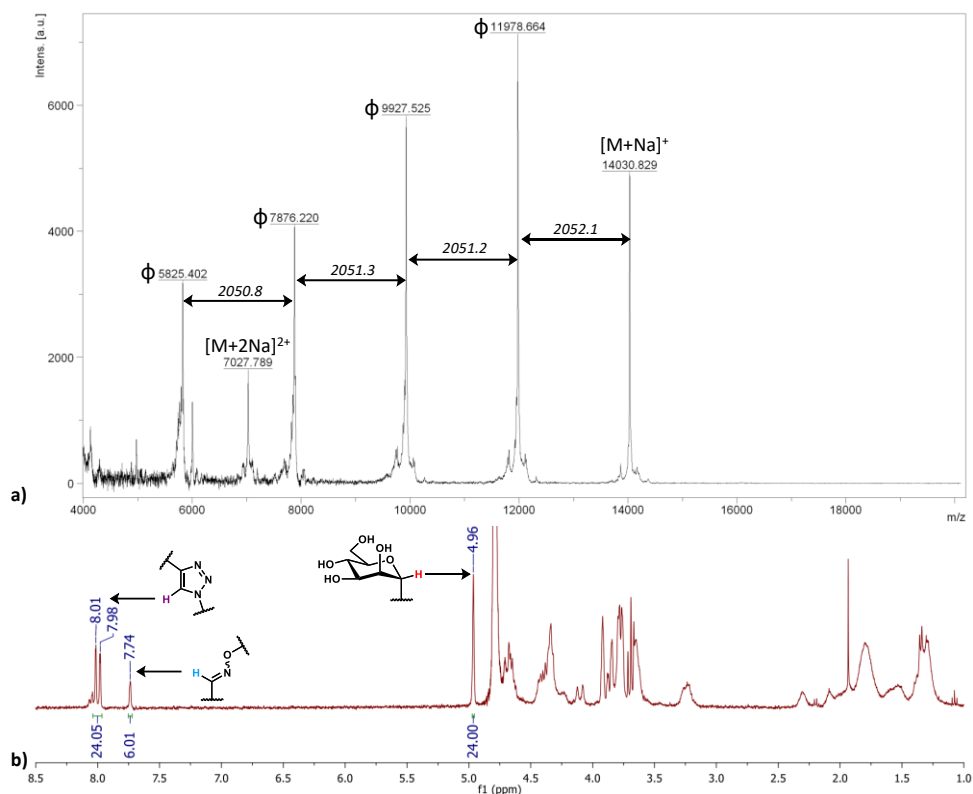
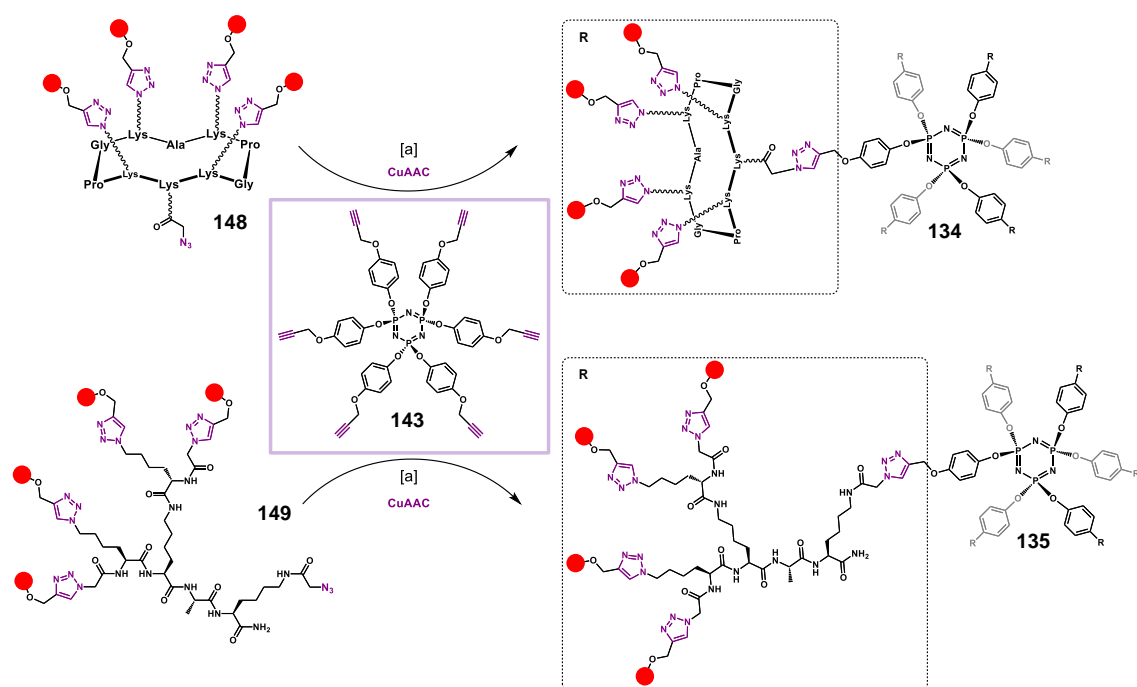


**Figure 54.** a) MALDI-TOF spectrum of **132**.  $m/z$  calcd. for  $[M+H]^+$ : 7599.5 (average), found: 7598.8. Observed fragmentation peaks ( $\phi$ ;  $\Delta m/z \approx 2051.3$ ) correspond to the loss of oxime-linked “arm” **146**. b)  $^1\text{H-NMR}$  (400 MHz,  $\text{D}_2\text{O}$ ) spectrum of compound **132**.

## II.5.5. Assembly of mannosylated tetracosavalent glycodendrimers **134** and **135** by CuAAC

The convergent assembly of mannosylated glycodendrimers **134** and **135** was next performed using phosphazene-based propargylated “core” scaffold **143** (Scheme 27b). Thus, azido-functionalized glycosylated “arms” **148** and **149** were reacted under CuAAC conditions with **143** to afford the desired compounds in 71-72% yields, and allowing the recovery of key building blocks **148** and **149** (Scheme 30).



**Scheme 30.** Convergent assembly of tetracosavalent glycodendrimers **134** and **135** by CuAAC. Conditions: [a] **143**, **148/149** (9.0 eq.), THPTA (5.0 eq. per azide), Na ascorbate (7.0 eq. per azide), DMF, PBS (pH 7.4, 100 mM), r.t., 2 h, yields: 72% (**134**), 71% (**135**).

Analysis of compounds **134** and **135** by  $^1\text{H-NMR}$  spectrometry showed a consistent integration ratio between triazole, mannose's anomeric and aromatic protons of 30:24:30 (Figure 55a). Moreover,  $^{31}\text{P-NMR}$  experiments showed the presence of a single phosphorus-related peak, confirming the exhaustive functionalization of the "core" scaffold with six glycosylated "arms" (Figure 55b). As expected, MALDI spectra showed the occurrence of fragmentation to a lower extent (Figure 55c), compared to oxime-bearing glycodendrimers **92** (Figure 41b) and **132** (Figure 54a).

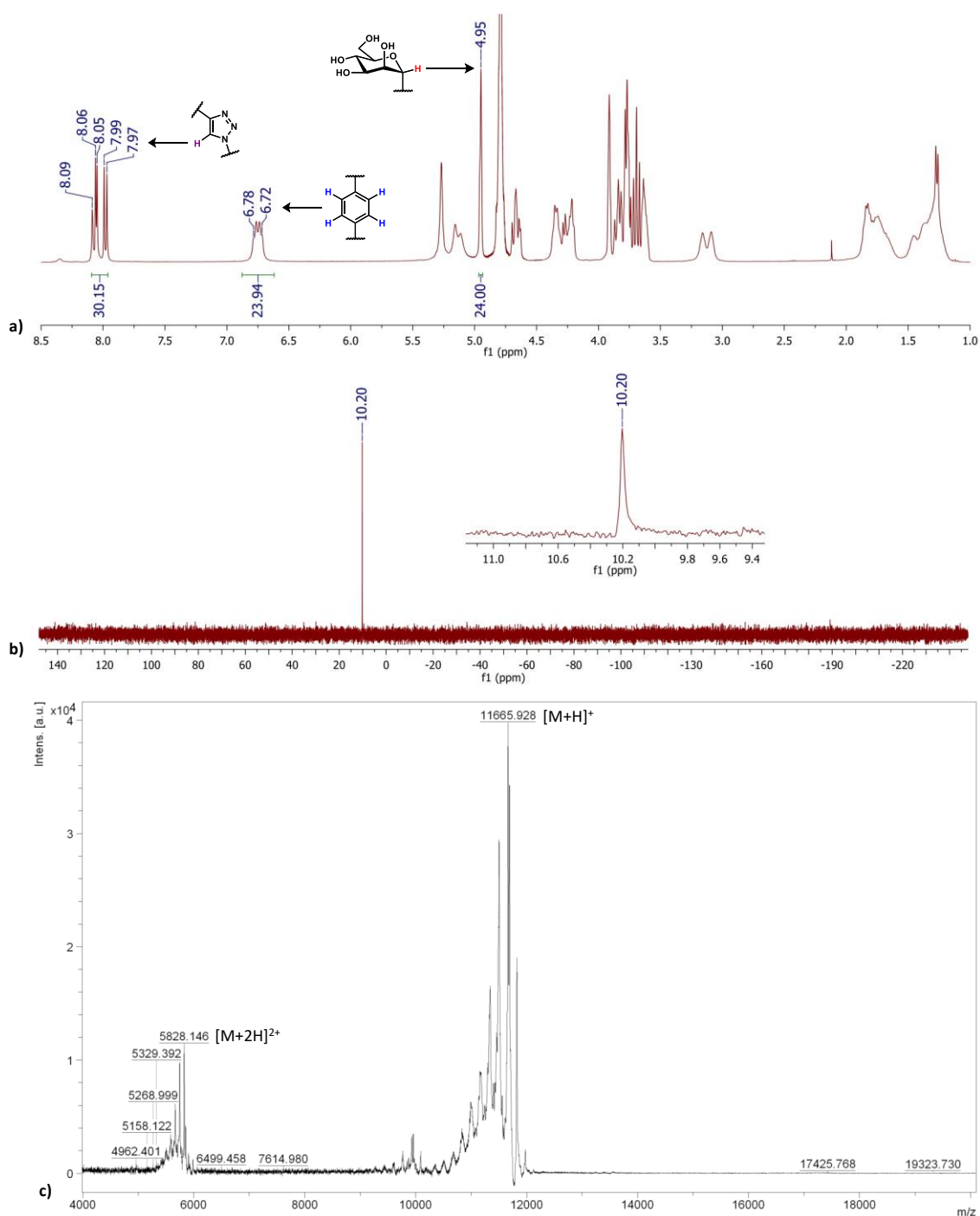


**Figure 55.** a)  $^1\text{H}$ -NMR (400 MHz,  $\text{D}_2\text{O}$ ) spectrum of compound **135**. b)  $^{31}\text{P}$ -NMR (162 MHz,  $\text{D}_2\text{O}$ ) spectrum of compound **135**. c) MALDI-TOF spectrum of **135**.  $m/z$  calcd. for  $[\text{M}+\text{H}]^+$ : 11667.4 (average), found: 11665.9; calcd. for  $[\text{M}+2\text{H}]^{2+}$ : 5834.2 (average), found: 5828.1.

Unlike the initially employed iterative oxime-based strategy (**II.2.**), the iterative CuAAC-based synthetic protocol employed for the construction of glycodendrimers **134** and **135** can be used both in a convergent and divergent manner. In addition, glycopeptide “arms” **148** and **149** are more stable compared to their analogues **146** and **147** (Scheme 30), because of the higher reactivity of the free aminoxy group compared to the azido moiety. Nevertheless, despite the iterative CuAAC-based

strategy allows for a more efficient recovery of key intermediates, the inherent higher simplicity of oxime reaction set-up (*i.e.* aminoxy- and aldehyde-bearing partners need just to be solubilized in aqueous mild acidic media and incubated at 37°C) make both reactions very useful for our purposes.

## II.5.6. Evaluation of the binding activity of glycodendrimers 128-135 on BCL2-A lectin via ITC

The biologic relevance of our small library of mannosylated glycodendrimers was investigated in the context of inhibition of lectin-mediated cell adhesion and biofilm formation. The opportunistic bacterium *Burkholderia cenocepacia* is responsible for numerous nosocomial infections affecting mainly cystic fibrosis and immunocompromised patients.<sup>378</sup> Treatment of *B. cenocepacia* infections remains difficult owing to widespread multidrug resistance and its ability to form biofilms.<sup>379</sup> New strategies for inhibiting the formation of *P. aeruginosa* biofilms have been developed recently; these target the binding sites of LecA and LecB lectins.<sup>380–384</sup> LecB-like genes have been identified in several Gram-negative bacteria, including *B. cenocepacia*, which produces three related proteins: BC2L-A (BCAM0186), BC2L-B (BCMA0184) and BC2L-C (BCMA0185). We have focused our attention on BC2L-A, which has been structurally characterized in detail.<sup>385–387</sup> BC2L-A assembles as a dimer of 13.8 kDa monomers with a  $\beta$ -sheet core structure and a dependence on two  $\text{Ca}^{2+}$  ions for binding to carbohydrate targets. Whereas LecB is tetrameric and shows a high affinity for L-fucose, BC2L-A is a dimer and binds poorly to this ligand ( $K_d = 2.3$  mM) but has a high affinity toward methyl  $\alpha$ -D-mannopyranoside ( $K_d = 2.7$   $\mu\text{M}$ ). BC2L-A also binds also to L-glycero-D-mannoheptose,<sup>386</sup> a major constituent of bacterial lipopolysaccharide, with a strict diastereoselectivity for (6S)-mannoheptose.<sup>388</sup> Only a few studies have been conducted to evaluate the affinity of multivalent structures toward BC2L-A. For example, Lameignere et al. have tested a tri-mannoside as well as two di-mannoside analogues separated by either a flexible or rigid spacer. They have measured a  $K_d$  value of 220 nM for their best-binding compound.<sup>387</sup> More recently, Faure et al. have prepared tetravalent thiomannoside clusters, the most potent of which having a  $K_d$  value of 204 nM.<sup>389</sup> Higher valency architectures were obtained with mannosylated GNPs and a  $K_d$  value of 19 nM was measured for a construct with an average valency of 46.<sup>390</sup>

Mannosylated glycodendrimers **128-135** (Figure 51) were used in titration microcalorimetry experiments to determine the stoichiometry and thermodynamic parameters of their binding to BC2L-A in solution. Monovalent methyl  $\alpha$ -D-mannoside was used as a reference to calculate the relative

potency of each multivalent compound. Titrations were performed in the direct injection mode (*i.e.*, ligand in syringe and protein in cell). When aggregation was observed, it happened after the titration stage, therefore not affecting the quality of the results (Figure 56 and Table 4).

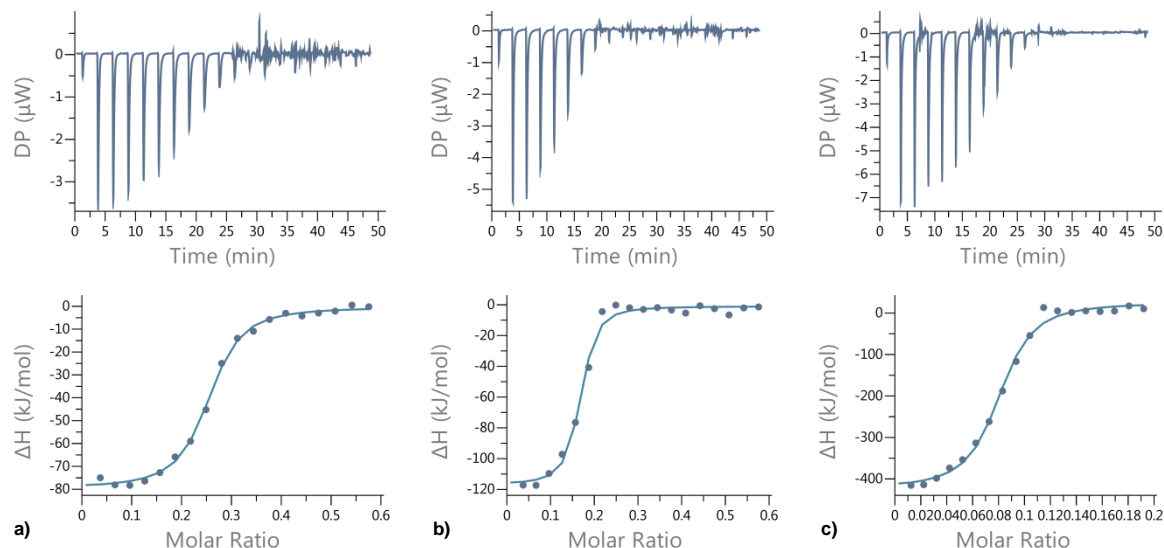


**Figure 56.** Isothermal titration calorimetry data: thermograms (top) and corresponding integrated titration curves (bottom) obtained by injections of a) **128** (300  $\mu\text{M}$ ); b) **129** (300  $\mu\text{M}$ ); d) **135** (100  $\mu\text{M}$ ) into a solution of BC2L-A (100  $\mu\text{M}$ ). Molar ratio is defined as the number of mannosylated molecules per lectin monomer.

Compound	Valency	$K_d$ [nM]	n	$-\Delta H$ [kJ mol <sup>-1</sup> ]	$-\Delta G$ [kJ mol <sup>-1</sup> ]	$-\Delta S$ [kJ mol <sup>-1</sup> ]	$rp^{[a]}$	$rp/n^{[b]}$
$\alpha$ -Me-Man	1	3570	0.90	24.1	31.1	- 7.1	1	1
<b>128</b>	4	481 $\pm$ 9	0.27	81.1 $\pm$ 0.4	36.1	45.0	7.4	1.9
<b>130</b>	4	449 $\pm$ 32	0.26	99.0 $\pm$ 2	36.3	62.8	7.9	2.0
<b>129</b>	6	199 $\pm$ 3	0.16	119.0 $\pm$ 2	38.2	80.6	17.9	3.0
<b>131</b>	6	368 $\pm$ 6	0.20	130.5 $\pm$ 2.5	36.75	93.7	9.7	1.6
<b>132</b>	24	256 $\pm$ 16	0.09	335.0 $\pm$ 1	37.7	297	13.9	0.6
<b>133</b>	24	195 $\pm$ 2	0.061	335.0 $\pm$ 2	38.4	296.5	18.3	0.8
<b>134</b>	24	215 $\pm$ 6	0.10	273.5 $\pm$ 10.5	38.3	235.5	16.6	0.7
<b>135</b>	24	52 $\pm$ 3	0.077	335.0 $\pm$ 1	41.7	293	70	2.9

**Table 4.** ITC data for glycoconjugated **128-135** binding to BC2L-A. Thermodynamic data refers to moles of glycoconjugates and stoichiometry is expressed as the number of molecules per lectin monomer. Standard deviations are indicated on experimentally derived values (at least two experiments). [a] relative potency compared to the monovalent compound, [b] relative potency per mannose residue.



The analysis of the thermodynamic contributions showed that for all the compounds the binding is driven by enthalpy but is counterbalanced by a strong entropy barrier resulting from the loss of flexibility induced upon lectin binding. Interestingly, tetravalent compounds **128** and **130** that are built on different scaffolds exhibited a significant difference in binding entropy contribution ( $16.2 \text{ kJ mol}^{-1}$ ) in favor of the cyclopeptide-based cluster. This difference is also noticeable between hexavalent compounds **129** and **131** ( $12.9 \text{ kJ mol}^{-1}$ ), also in favor of the cyclopeptide-based cluster. The well-known rigidity of cyclopeptide scaffolds seems to provide a more favorable geometry for the binding with BC2L-A. Of these four glycoclusters, compound **129** has the highest affinity ( $K_d = 199 \text{ nM}$ ), albeit with a modest relative potency factor ( $rp = 17.9$ ). These data suggest that the interaction is due to an aggregative effect, implying one binding site per lectin rather than a real chelate complex in which both binding sites are occupied by the same glycocluster molecule. More interestingly, thermodynamic data obtained with the tetracosavalent glycodendrimers **132-135** revealed that compound **134** ( $\text{PR}_{24}$ ) has a significantly less favorable binding enthalpy ( $-\Delta H = -273.5 \text{ kJ mol}^{-1}$ ) than the three other compounds ( $-\Delta H = -335 \text{ kJ mol}^{-1}$  for each). This observation suggests that despite a lower entropy barrier ( $-T\Delta S = 235.5 \text{ kJ mol}^{-1}$  versus  $\approx 295 \text{ kJ mol}^{-1}$ ) the sugar presentation does not favor binding with BC2L-A, as confirmed by its dissociation constant ( $K_d = 215 \text{ nM}$ ). In comparing the  $K_d$  values of dendrimers constructed around the same core structure but with different peripheral scaffolds (**132** versus **133** and **134** versus **135**), we observed that the sugar presentation through the lysine-based dendron leads to stronger binding in each series. This effect can be explained by the flexibility of the dendron, which might facilitate the positioning of the sugars in the lectin binding site. Among the glycodendrimers, the highest affinity ligand is compound **135** ( $K_d = 51 \text{ nM}$ ), which contains a hexachlorocyclotriphosphazatriene “core” functionalized with six lysine-based dendrons. The binding of this molecule is between three and five times stronger than the others, each sugar being almost three times more potent than monovalent methyl  $\alpha$ -D-mannoside.

The stoichiometry data for tetravalent compounds **128** and **130** indicated that all of the four mannose residues can bind to a monomer of lectin. The same accessibility is observed with hexavalent clusters **129** and **131** in which each lectin monomer binds one of the mannose residue, that is, one cluster binds five or six lectins. In the case of the tetracosavalent dendrimers, the stoichiometry was different between compounds **132** and **134**, which can bind approximately 10 lectin monomers, and compounds **133** and **135**, which interact with approximately 15 lectin monomers. This indicates a higher accessibility for mannose residues presented on dendrimer-like “arms”, than for the RAFT-presented ones.

In order to rationalize this analysis, models of compounds **134** and **135** were built using Sybyl molecular graphics editor (Certara, Munich, Germany). Starting from the crystal structure of the N<sub>3</sub>P<sub>3</sub>-based scaffold,<sup>372</sup> the linkers were built and terminal mannose residues added either onto a model of branched peptide or onto the structure of a cyclic peptide taken from an NMR model.<sup>355</sup> The models were constructed in order to alleviate any steric contact and to orientate all torsional angles in reasonable conformations, but no energy calculations were performed (Figure 57). The differences in global size is not significant, with compound **134** extending to approximately 65 Å, whereas compound **135** spans at a maximum distance of 80 Å. Nevertheless, variations occur at the local level, with mannose residues being clearly closer to each other in model **134** than in model **135**. Fitting of mannose-bound BC2L-A to the accessible mannose residues in model **135** allowed for positioning of eleven BC2L-A dimers with no significant steric clashes, illustrating that this compound represent a valuable model for displaying glycans in a multivalent and accessible manner. This work have been published as full paper in ChemPlusChem (Wiley).<sup>391</sup>

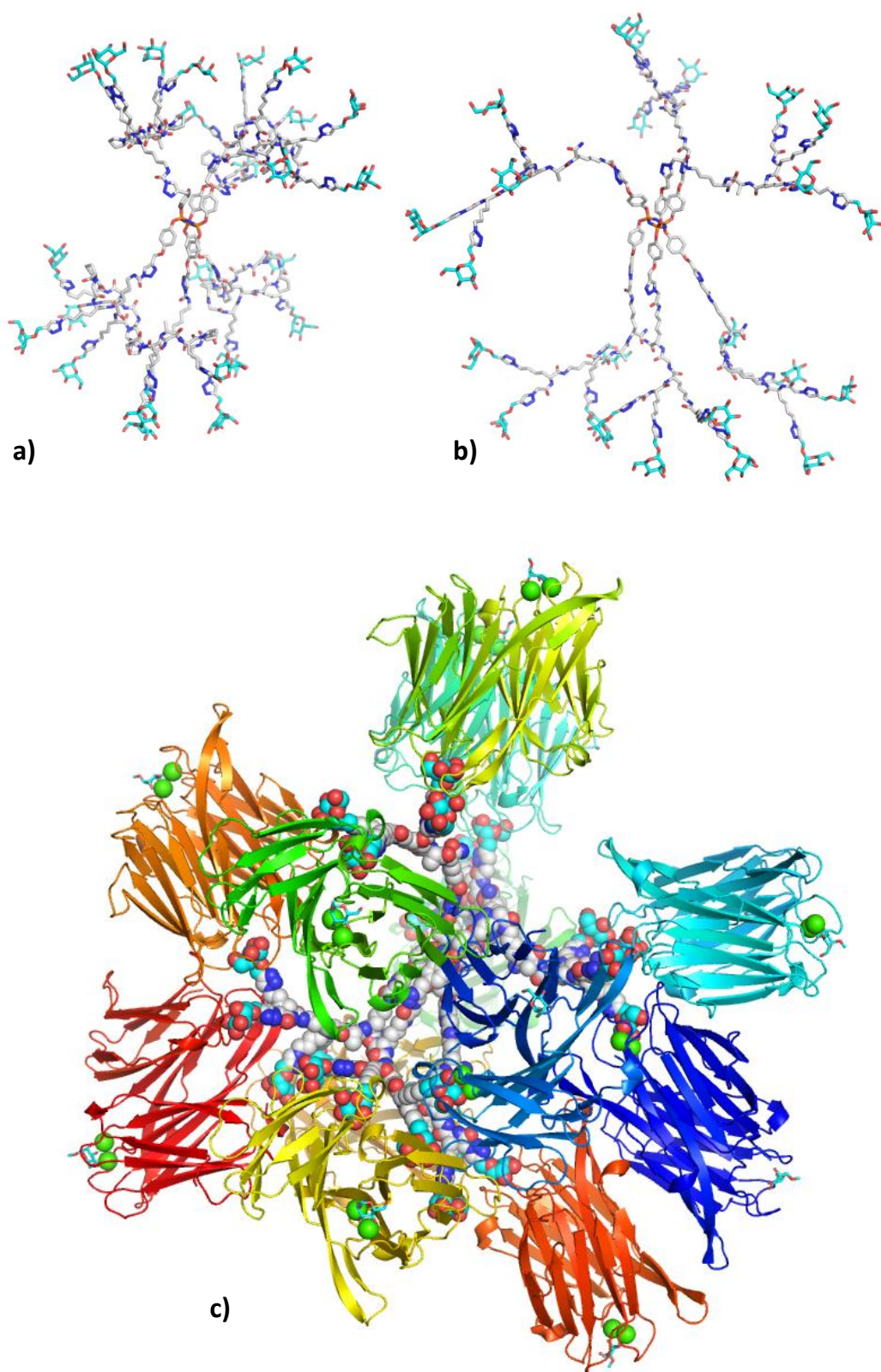


**Figure 57.** Possible conformations of a) **134** and b) **135** represented as sticks with mannose residues colored in blue. c) Same conformation of **135** with eleven BCL2-A dimers positioned on accessible mannose residues by superposition with mannose in binding sites. Compound **135** and  $\text{Ca}^{2+}$  ions are represented as spheres and lectins are represented as ribbons. Hydrogen atoms have been omitted for clarity in all panels.

In conclusion, cyclodecapeptide- and tetradecapeptide-based as well as cyclotriphosphazene- and lysine-based glycoclusters were prepared, affording a new series of tetra- and hexavalent mannosylated ligands. Both hexavalent scaffolds were then combined with tetravalent dendrons to afford a set of four tetracosavalent glycodendrimers. These eight compounds, displaying various flexibilities and architectures were then tested for their binding affinity with BC2L-A lectin using isothermal titration microcalorimetry. We first demonstrated that both hexa- and tetravalent architectures allowed a good presentation of the sugar residues to the binding site of the lectin, forming complexes in which all mannosides are involved in the binding, albeit with modest enhancements of affinity compared to the monovalent interaction. Within this set of glycoclusters, cyclopeptide-based hexavalent compound **129** exhibited the best binding properties ( $K_d = 199$  nM) where each sugar residue is three times more potent than the monovalent methyl  $\alpha$ -D-mannoside. The evaluation of the tetracosavalent glycodendrimers showed that the core architecture does not have a significant effect on the binding affinity. On the contrary, the scaffold used to present the sugars at the periphery seems to have a significant influence. The binding is stronger if mannose residues are exposed through the more flexible lysine-based dendron. The combination of this architecture with the cyclotriphosphazene core afforded compound **135** with the lowest binding constant in this study ( $K_d = 51$  nM), which also represents the highest affinity known to date for a fully synthetic multivalent glycodendrimer binding to BC2L-A (compared to  $K_d = 204$  nM).<sup>389</sup> Analysis of thermodynamic contributions to the binding tend to show that the affinity arises from an aggregative binding mode rather than a chelate complex, which typically leads to stronger affinities. This is not surprising considering that BC2L-A is a dimer in which the two sugar-binding pockets are located on opposite sides of the protein, therefore preventing the ligand to reach both sites at the same time. Nevertheless, high affinities can be achieved if the sugar residues are presented with enough flexibility to accommodate several protein monomers, as it is the case for compound **135**. This compound represents an excellent candidate for structural optimization to achieve higher affinity and to expect anti-adhesive properties against *B. cenocepacia*. It may be also interesting to evaluate the same scaffolds for the presentation of carbohydrate antigens.

## **Chapter III.**

# **Synthesis of multivalent hetero- glycodendrimers**

## III.1. Introduction

In the former chapter we designed and explored synthetic strategies to reach precise multivalent homo-glycodendrimers with interesting biological activities. In general terms, by increasing ligand valency on multivalent constructs, enhanced binding avidities towards protein receptors are observed.<sup>110</sup> Following this concept, many efforts have been made in chemical design for the generation of a large panel of multivalent glycosylated architectures. These constructions have been proven to be inhibitors for pathogen-related processes involving interactions between proteins (*e.g.* bacterial lectins and toxins, DC-SIGN, *etc.*) and glycans.<sup>351</sup> In those cases, the rationale behind the design of such multivalent inhibitors can be guided by the knowledge of discrete carbohydrate-binding domains (CRDs), by means of crystal structures of isolated proteins, together with molecular modelling and NMR methodologies.<sup>392–394</sup>

For our purposes, as discussed in section **I.2.3.**, the reaching of densely glycosylated multivalent structures is devoted to two main aspects: (i) to promote BCR clustering and signalling, and facilitate receptor-mediated internalization of antigens,<sup>395</sup> and (ii) to enhance the carbohydrate epitope ratio over the entire construct, in order to promote a specific TACA-directed humoral immune response.<sup>208</sup> In this scenario immunization trials would provide more reliable answers regarding the validity of our fully synthetic anticancer vaccine prototypes.

In a first part of my PhD work we focussed our attention towards synthetic methodologies which could be translated for the synthesis of a new generation of anticancer vaccines with increased density of tumor-associated carbohydrate epitopes. A second, important point that we wanted to investigate was the generation of a broader immune response by introducing a dual TACA presentation (*i.e.* Tn and TF antigens), following the evidence that TACA-expression patterns are heterogeneous among cancer types, individuals and evolve during the course of the disease.<sup>88,89</sup>

In this chapter we report the synthesis of hetero-glycodendrimers, grafted with Tn- and TF-antigen analogues [*i.e.* (OX)Tn and (TRZ)TF, see **I.4.**], which can be further functionalized with appropriate CD4<sup>+</sup> and CD8<sup>+</sup> epitopes, as key B-cell antigens carriers for the construction of a generation of fully synthetic hetero-multivalent anticancer vaccine prototypes.

### III.2. Dual (OX)Tn-(TRZ)TF-based multivalent glycodendrimers assembly based on divergent OL/CuAAC strategy

The large majority of vaccines target only one carbohydrate antigen expressed on tumors, which is likely to lead to the incomplete destruction of cancer cells by neglecting a compelling population of transformed cells. Therefore, the stimulation of a multifaceted response which takes account of the inherent tumor heterogeneity appeared to us an essential point to be considered. Following this idea, the first semi-synthetic vaccine candidates combining multiple TACAs have been pioneered by Danishefsky and co-workers (**32-34**, figure 18).<sup>125,166-168</sup> Promising preclinical results were obtained with semi-synthetic vaccine construct **34**, which proved able to elicit, in mice models, high titers of IgG and IgM against each of all the five displayed antigens (*i.e.* Tn, TF, STn, GM2, globo-H). This vaccine candidate is currently under phase I clinical trial against ovarian cancer.

While this approach opens promising perspectives in cancer immunotherapy and was used only in semi-synthetic approaches, no fully synthetic vaccine prototype displaying different associations of TACAs has been described to date, presumably due to synthetic difficulties to achieve well-defined molecules. We thus directed our efforts towards the synthesis of heterogeneously glycosylated constructs displaying multiple copies of Tn- and TF-antigens, with a free-amino functionality constituting the anchorage point for the conjugation of CD4<sup>+</sup> and CD8<sup>+</sup> epitopes (Figure 58).

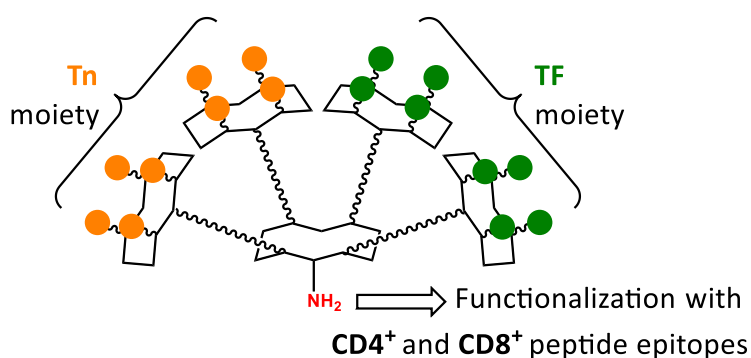


**Figure 58.** General structure of heterovalent glycodendrimer as TACA carrier for fully synthetic anticancer vaccines.

### III.3. General strategy

Recently, a few reports highlighted the interest of heterogeneously glycosylated multivalent structures as attractive tools to deepen the understanding in molecular recognition phenomena between carbohydrates and proteins.<sup>396–400</sup> Indeed, homogeneously glycosylated structures (glycodendrimers, glycoclusters, glyco-nanoparticles, *etc.*) barely reflect the heterogeneity of glycocalyx, limiting their utility towards the design of novel glycomimetics and the deciphering of more complex recognition processes, relying on cooperative effects.<sup>401,402</sup> Nevertheless, despite few synthetic procedures have been described,<sup>403–409</sup> the assembly of such heterogeneous structures remains challenging. Our group has previously described the synthesis of tetravalent heteroglycoclusters (hGCs) based on clickable RAFT scaffolds decorated with two different carbohydrate residues, either in 2:2 or 3:1 relative proportions, which were obtained in a stepwise protocol combining OL and CuAAC.<sup>410</sup> Subsequently we have demonstrated the orthogonality of both thiol-ene and thiol-chloroacetyl couplings (TEC and TCC, respectively) for the synthesis of hexavalent hGCs displaying two different sugars, in a 4:2 relative proportion and in two possible orientations on the scaffold.<sup>411</sup> More recently, we have reported an unprecedented multi-click approach involving four different conjugation methods: OL, TEC, CuAAC and TCC.<sup>412</sup> By using a proper reaction order, this approach gave access to tetravalent hGCs displaying four different sugar units, through a sequential one-pot assembly, in excellent yields and with a single purification step. Finally, we recently explored the assembly of octavalent, two-faced, hGCs decorated with different combination of three monosaccharide units, involving TEC, CuAAC and diethyl squarate coupling (DSC).<sup>413</sup>

The synthesis of Tn-TF-based hetero-glycodendrimers (hGDs) with enhanced valencies represents a more complicated objective. Owing to the solid methodologies developed in our research group, and in the framework of my PhD project, we envisioned to build hGDs with carbohydrate epitopes in a separate (**150**) and shuffled (**151**) fashion (Figure 59), by using orthogonal OL and CuAAC chemoselective “click” reactions.



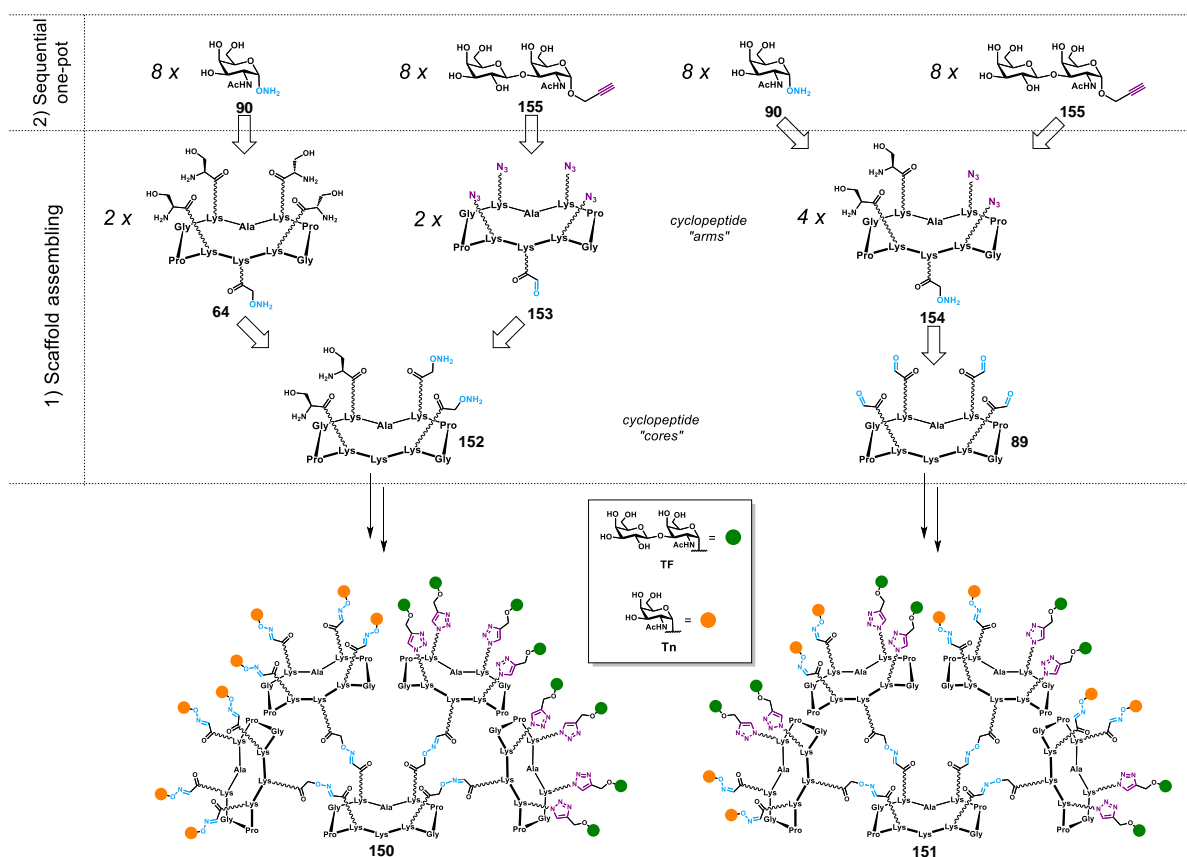


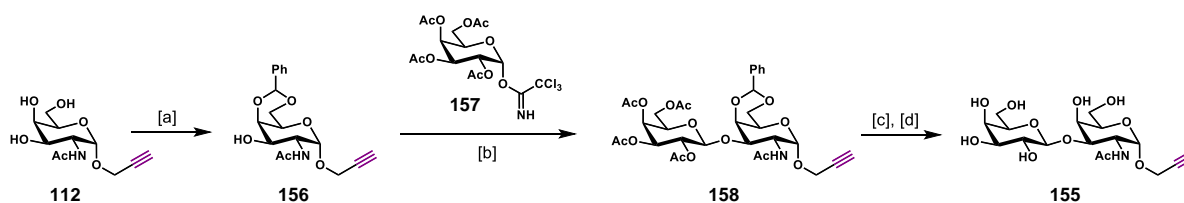
**Figure 59.** Divergent synthetic strategy for assembling Tn-TF-based hetero-glycodendrimers **150** and **151** through dual OL/CuAAC approach.

We thus designed a divergent strategy that requires the synthesis of functionalized building blocks: (i) two cyclopeptide “cores” containing two aminoxy groups and two serine residues (**152**) in the upper domain of the scaffold, or four aldehyde groups (**89**); (ii) three additional cyclopeptide “arms” bearing one aminoxy group on the lower domain and four serine residues on the upper domain (**64**), one aldehyde and four azido groups (**153**), or one aminoxy, two serine residues and two azido groups (**154**); (iii) aminoxy-Tn (**90**) and propargyl-TF (**155**) modified TACAs (Figure 59).

### III.4. Synthesis of modified propargyl-TF antigen **155**

The propargylated TF antigen **155** was synthesized as shown in scheme 31, starting from the already described intermediate **112** (Scheme 21).<sup>370</sup> Compound **112** was selectively protected on positions 4 and 6 to give the glycosyl acceptor **156** in 90% yield. Trimethylsilyl trifluoromethanesulfonate-promoted glycosylation with trichloroacetimidate **157**<sup>414</sup> yielded

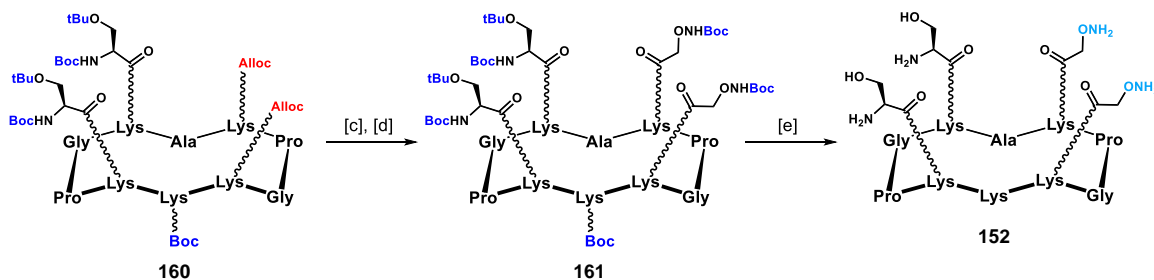
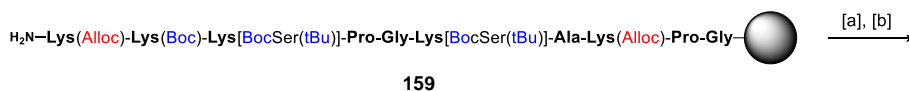
disaccharide **158**, which was fully deprotected by treatment with aqueous acetic acid, followed by Zemplén deacetylation to afford desired propargyl-TF **155** (Scheme 31).



**Scheme 31.** Synthesis of propargylated TF antigen **155**. Conditions: [a]  $\text{PhC(OMe)}_2$  (1.5 eq.), CSA (0.1 eq.),  $\text{CH}_3\text{CN}$ , r.t., 48 h, 90%; [b] **157** (1.5 eq.), TMSOTf (0.2 eq.),  $\text{CH}_2\text{Cl}_2$ ,  $-15^\circ\text{C}$ , 30 min., 60%; [c] 70%  $\text{AcOH}/\text{H}_2\text{O}$ ,  $60^\circ\text{C}$ , 4 h, 85%; [d]  $\text{MeONa}/\text{MeOH}$  (pH 10), r.t., 2 h, 95%.

### III.5. Synthesis of cyclopeptide “cores” and “arms” building blocks

The synthesis of hGDs **150** and **151** is based on a divergent modular approach in which a central RAFT scaffold (“core”) has first to be functionalized with four “arms”, and the obtained multivalent scaffold successively decorated with TACAs. The first step of our multi-step synthetic route involved the solid phase peptide synthesis of sequence **159** (Scheme 32) on the Fmoc-Gly-SASRIN™ resin, in which we introduced the dipeptide building block **95** (Scheme 14) to reduce the number of steps in solution. After cleavage from the resin support under mild acidic conditions and cyclization in diluted  $\text{DMF}/\text{CH}_2\text{Cl}_2$ , compound **160** was obtained with an overall yield of 54%. Compound **160** underwent palladium-catalyzed deprotection of Alloc groups. The two resulting free amino groups in the upper domain were reacted with Boc-aminoxyacetic acid *N*-hydroxysuccinimide ester<sup>346</sup> to afford fully protected intermediate **161**. The “core” scaffold was obtained after treatment of **161** with TFA in the presence of a mixture of TIS, water and hydroxylamine as scavengers (Scheme 32, figure 60). Key Intermediate **152** shows: (i) two aminoxy groups, prone to react under OL conditions; (ii) two serine residues as masked  $\alpha$ -oxo aldehyde residues, and (iii) a free amino group on lysine’s side chain, on the lower domain.



**Scheme 32.** Synthesis of cyclopeptide “core” scaffold **152**. Conditions: [a] 1% TFA,  $\text{CH}_2\text{Cl}_2$ ; [b] PyBOP (1.2 eq.), DIPEA (2.0 eq.), DMF/ $\text{CH}_2\text{Cl}_2$  (1:1), 0.5 mM, r.t., 30 min., 54% overall yield; [c]  $\text{Pd}(\text{PPh}_3)_4$  (cat.),  $\text{PhSiH}_3$  (25 eq.), DMF/ $\text{CH}_2\text{Cl}_2$  (1:1), r.t., 30 min., then MeOH; [d] Boc-aminoxyacetic acid *N*-hydroxysuccinimide ester (2.4 eq.), DIPEA (3.0 eq.), DMF, r.t., 20 min., 67% over two steps; [e] TFA/TIS/ $\text{NH}_2\text{OH}/\text{H}_2\text{O}$  (94:2:2:2), r.t., 3 h, 93%.

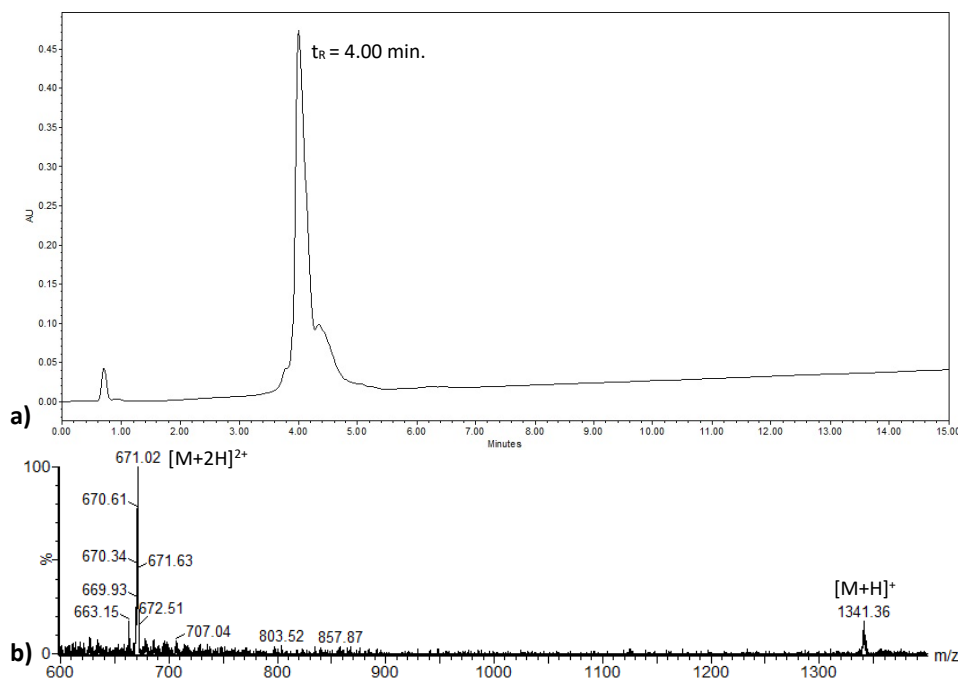
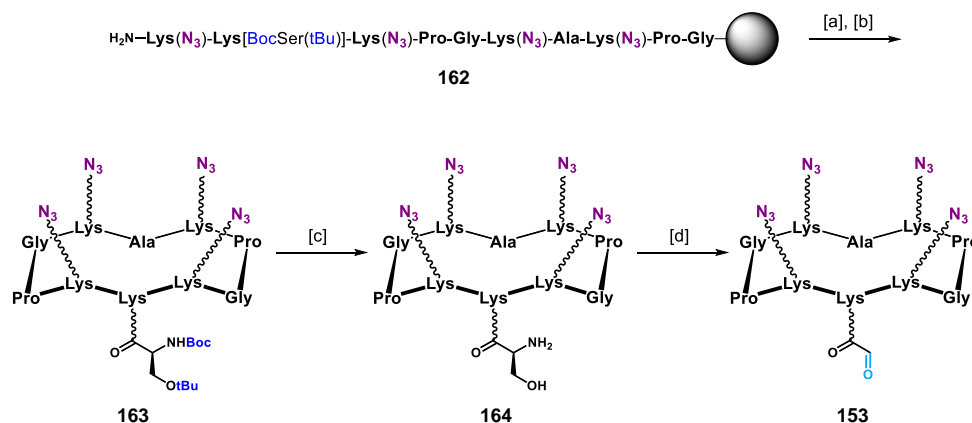


**Figure 60.** a) Analytical RP-HPLC profile ( $\lambda=214$  nm, 0-30% solv.B in 15') of **152**. b) ESI<sup>+</sup>-MS of **152** (zoom).  $m/z$  calcd. for  $[\text{M}+\text{H}]^+$ : 1341.5 (average), found: 1341.4; calcd. for  $[\text{M}+2\text{H}]^{2+}$ : 671.3, found: 671.0.

Synthesis of “right arm” **153** (Scheme 32) was performed starting from sequence **162**, where four copies of 6-azido-*N*-Fmoc-norleucine building block **117** (Scheme 22) have been included. Cleavage from the solid support, and subsequent cyclization gave compound **163** with a 48% overall yield. Removal of acid-labile protecting groups of compound **163** in strong acidic conditions afforded intermediate **164**, presenting four azido functionalities on the upper domain and a serine residue in

the lower domain. This last residue was treated with a large excess of sodium periodate to give  $\alpha$ -oxo aldehyde-containing intermediate **153** in 71% yield (Scheme 32, figure 61).



**Scheme 33.** Synthesis of cyclopeptide “right arm” scaffold **153**. Conditions: [a] 1% TFA, CH<sub>2</sub>Cl<sub>2</sub>; [b] PyBOP (1.2 eq.), DIPEA (2 eq.), DMF/CH<sub>2</sub>Cl<sub>2</sub> (1:1), 0.5 mM, r.t., 30 min., 48% overall yield; [c] TFA/TIS/H<sub>2</sub>O (96:2:2), r.t., 3 h, 96%; [d] NaIO<sub>4</sub> (10 eq.), H<sub>2</sub>O, r.t., 40 min., 71%.

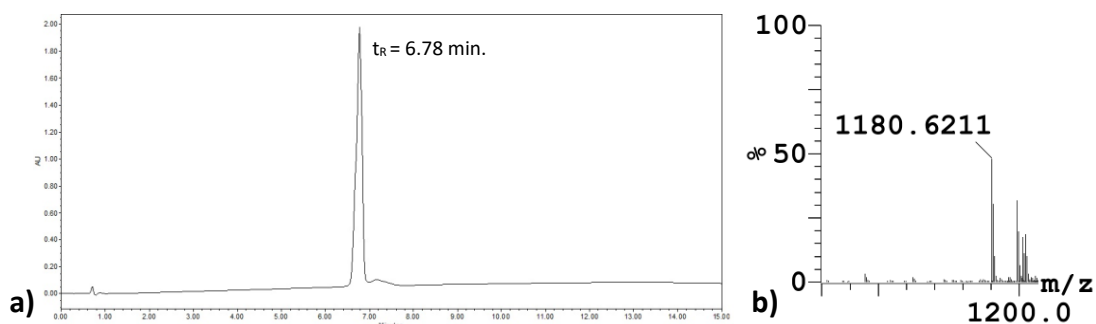
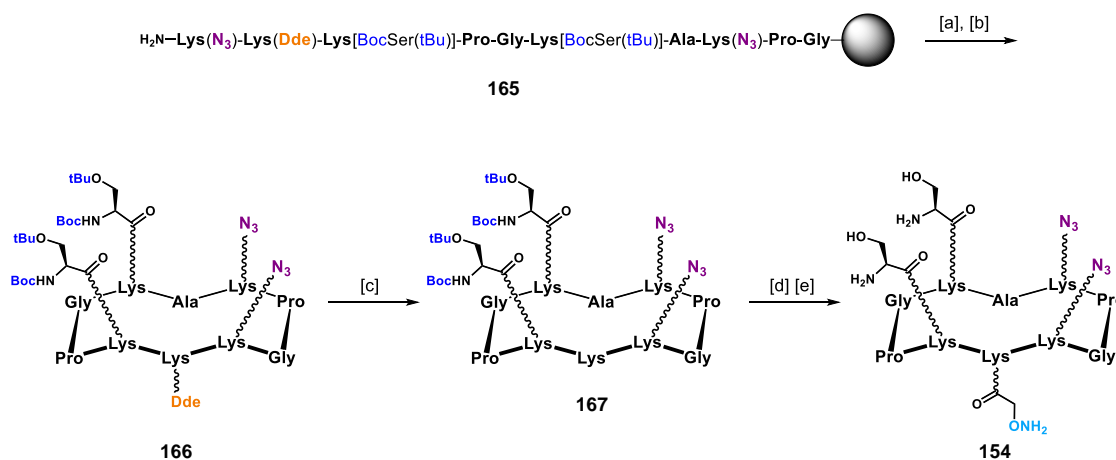


**Figure 61.** a) Analytical RP-HPLC profile ( $\lambda=214$  nm, 5-100% solv.B in 15') of **153**. b) HRMS (ESI<sup>+</sup>-TOF) of **153** (zoom).  $m/z$  calcd. for [M+H]<sup>+</sup>: 1180.6200 (monoisotopic), found: 1180.6211.

Synthesis of cyclopeptide scaffold **154** started with resin-bound peptide sequence **165** (Scheme 34), where a lysine residue protected with 1-(4,4-dimethyl-2,6-dioxocyclohex-1-ylidene)ethyl (Dde) group was integrated, along with serine- and azido-containing amino acid building blocks. Cleavage from the support and cyclization under our standard conditions gave cyclopeptide **166**, exposing the Dde-protected lysine's side chain in the lower domain of the RAFT, with a 55% overall yield. Deprotection of Dde by means of a 2% solution of hydrazine monohydrate in DMF afforded compound **167**. The resulting free amino group was further functionalized with Boc-aminoxyacetic acid *N*-hydroxysuccinimide ester.<sup>346</sup> After precipitation in ice-cold Et<sub>2</sub>O, the crude reaction was treated

with a strong acidic deprotection cocktail to simultaneously cleave Boc and *tert*-butyl groups, affording the desired functionalized scaffold **154** (Scheme 34, figure 62).



**Scheme 34.** Synthesis of cyclopeptide “arm” scaffold **154**. Conditions: [a] 1% TFA,  $\text{CH}_2\text{Cl}_2$ ; [b] PyBOP (1.2 eq.), DIPEA (2 eq.), DMF/ $\text{CH}_2\text{Cl}_2$  (1:1), 0.5 mM, r.t., 30 min., 55% overall yield; [c] 2%  $\text{N}_2\text{H}_4$ /DMF, r.t., 20 min., 94%; [d] Boc-aminoxyacetic acid *N*-hydroxysuccinimide ester (1.2 eq.), DIPEA (1.5 eq.), DMF, r.t., 20 min; [e] TFA/TIS/ $\text{NH}_2\text{OH}/\text{H}_2\text{O}$  (94:2:2:2), r.t., 3 h, 86% over two steps.

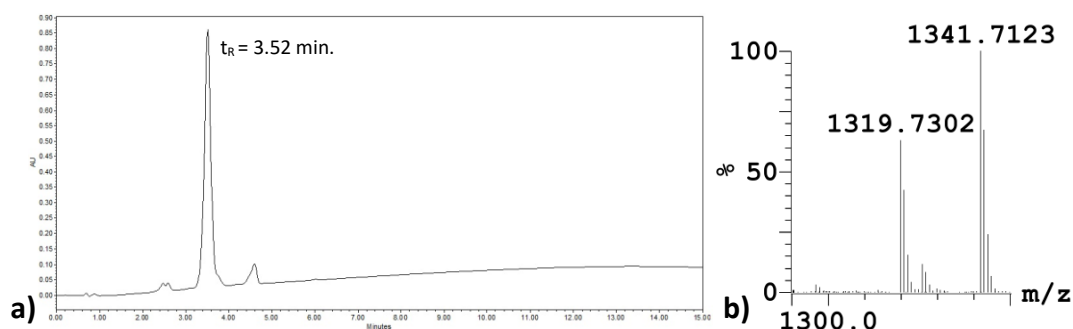


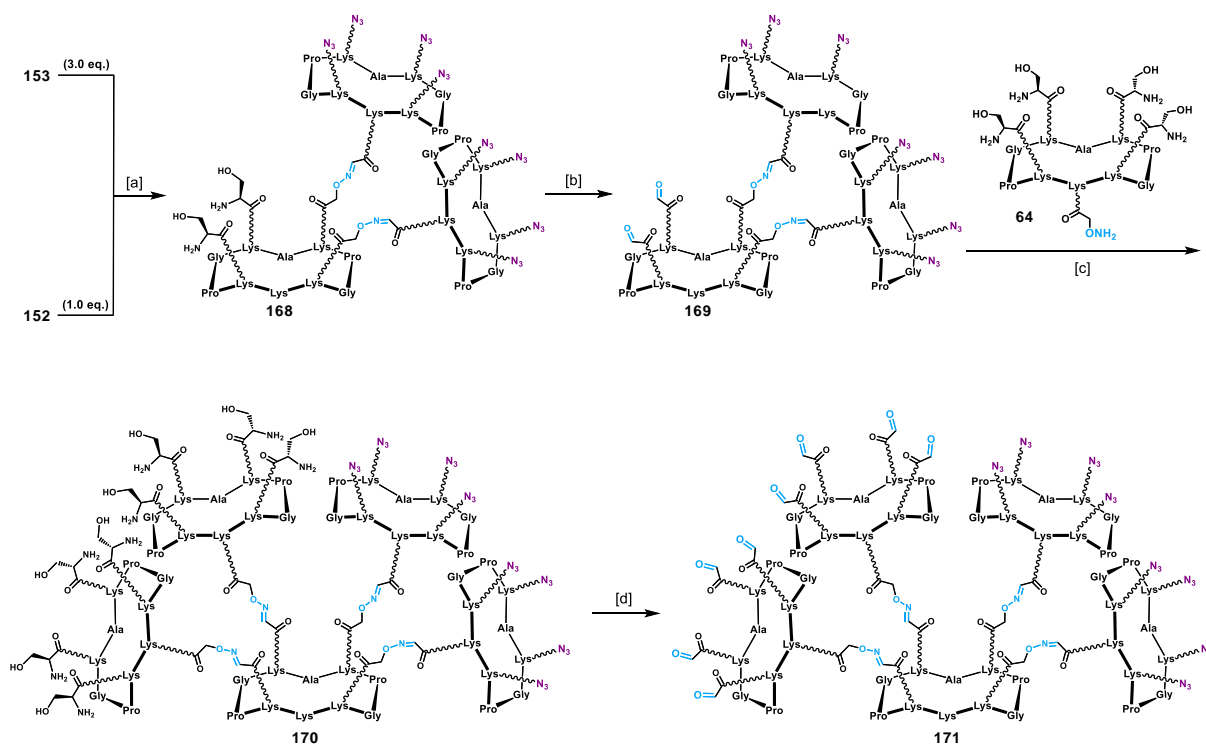
**Figure 62.** a) Analytical RP-HPLC profile ( $\lambda=214$  nm, 5-100% solv.B in 15') of **154**. b) HRMS (ESI<sup>+</sup>-TOF) of **154** (zoom).  $m/z$  calcd. for  $[\text{M}+\text{H}]^+$ : 1319.7296 (monoisotopic), found: 1319.7302; calcd. for  $[\text{M}+\text{Na}]^+$ : 1341.7116, found: 1341.7123.

### III.6. Assembly of multivalent scaffolds **171** and **172** bearing azide and aldehyde residues

With all properly functionalized cyclopeptide building blocks in hand, the next step of our divergent synthetic route involved the grafting of peripheral RAFT “arms” onto cyclopeptide “cores”.

This allowed us reaching two dendrimer-like structures displaying eight azido groups and eight aldehyde groups, displayed in a separated or shuffled fashion.

Conjugation between “core” scaffold **152** (Scheme 32) and “right arm” **153** (Scheme 33) was carried out *via* oxime ligation, in a H<sub>2</sub>O/CH<sub>3</sub>CN (1:1) mixture containing 0.1% of TFA (Scheme 35). Bis-functionalized compound **168** was obtained in good yields (75%) and purity, after RP-HPLC purification. Oxidative cleavage of serine residues on **168** by treatment with sodium periodate afforded two  $\alpha$ -oxo aldehyde groups on intermediate **169**, prone to react with “left arm” **64** through OL to give compound **170** in good yields (60% over two steps). Finally, compound **171** was obtained upon treatment of **170** with a large excess of sodium periodate and subsequent direct purification by RP-HPLC (Scheme 35, figure 63). The resulting multivalent scaffold **171**, featuring eight  $\alpha$ -oxo aldehyde and eight azido functionalities displayed in separates “arms”, was thus ready for the final conjugation step, with saccharide epitopes **90** (Scheme 19) and **155** (Scheme 31), through OL and CuAAC, respectively (*vide infra*).



**Scheme 35.** Synthesis of multivalent scaffold **171**. Conditions: [a] **152**, **153** (3.0 eq.), 0.1% TFA in H<sub>2</sub>O/CH<sub>3</sub>CN (1:1), 37°C, 30 min., 75%; [b] NaIO<sub>4</sub> (20 eq.), H<sub>2</sub>O, r.t., 40 min., 75%. [c] **64** (3.0 eq.) 0.1% TFA in H<sub>2</sub>O/CH<sub>3</sub>CN (1:1), 37°C, 30 min., 85%; [d] NaIO<sub>4</sub> (80 eq.), H<sub>2</sub>O/CH<sub>3</sub>CN (1:1), r.t., 40 min., 78%.

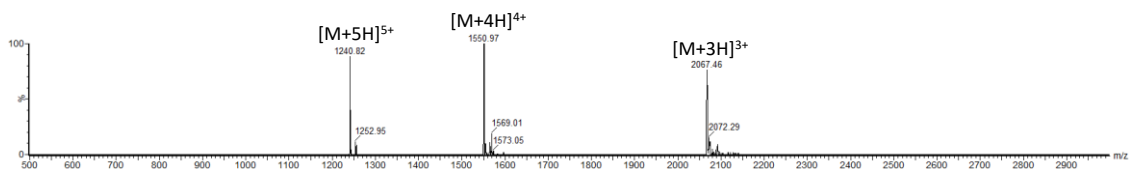
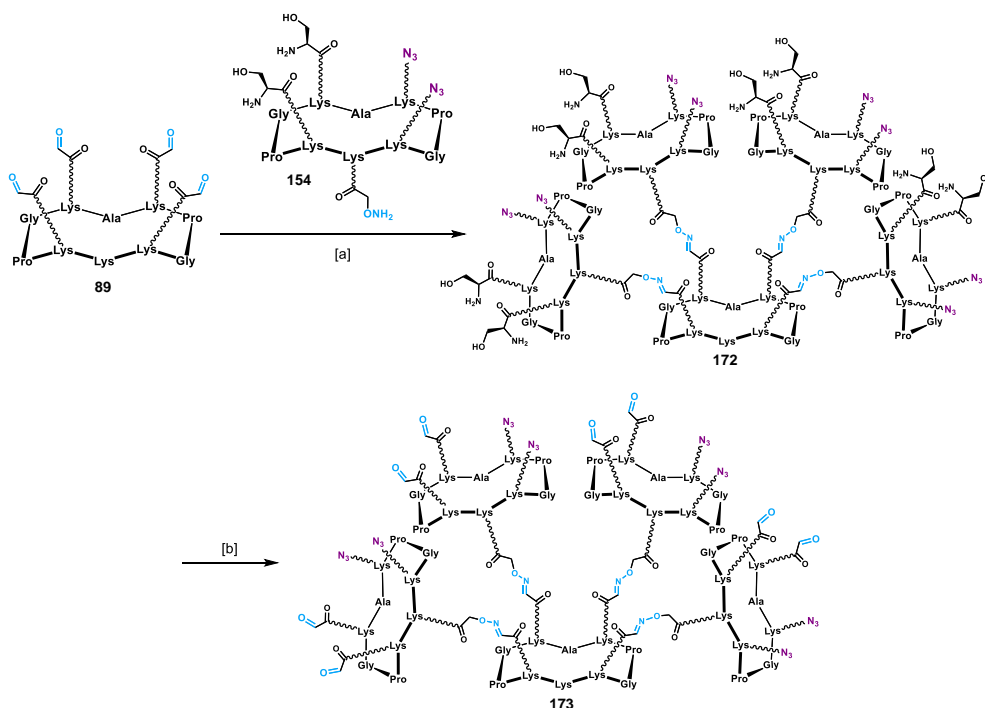


**Figure 62.** ESI<sup>+</sup>-MS of **171**.  $m/z$  calcd. for  $[M+3H]^{3+}$ : 2067.1 (monoisotopic), found: 2067.5; calcd. for  $[M+4H]^{4+}$ : 1550.3, found: 1551.0; calcd. for  $[M+5H]^{5+}$ : 1240.6, found: 1240.8.

For the synthesis of “shuffled” hetero-glycodendrimer **151**, we envisioned a divergent synthetic protocol based on “core” scaffold **89** displaying four aldehyde groups (Figure 59). This central unit was reacted with six equivalents of aminoxy-containing “cyclopeptide arm” **154** (Scheme 34) under classic OL conditions, to give intermediate **172** (Scheme 36). Subsequent oxidative cleavage of serine residues afforded the desired compound **173** in good yields (64% over two steps).

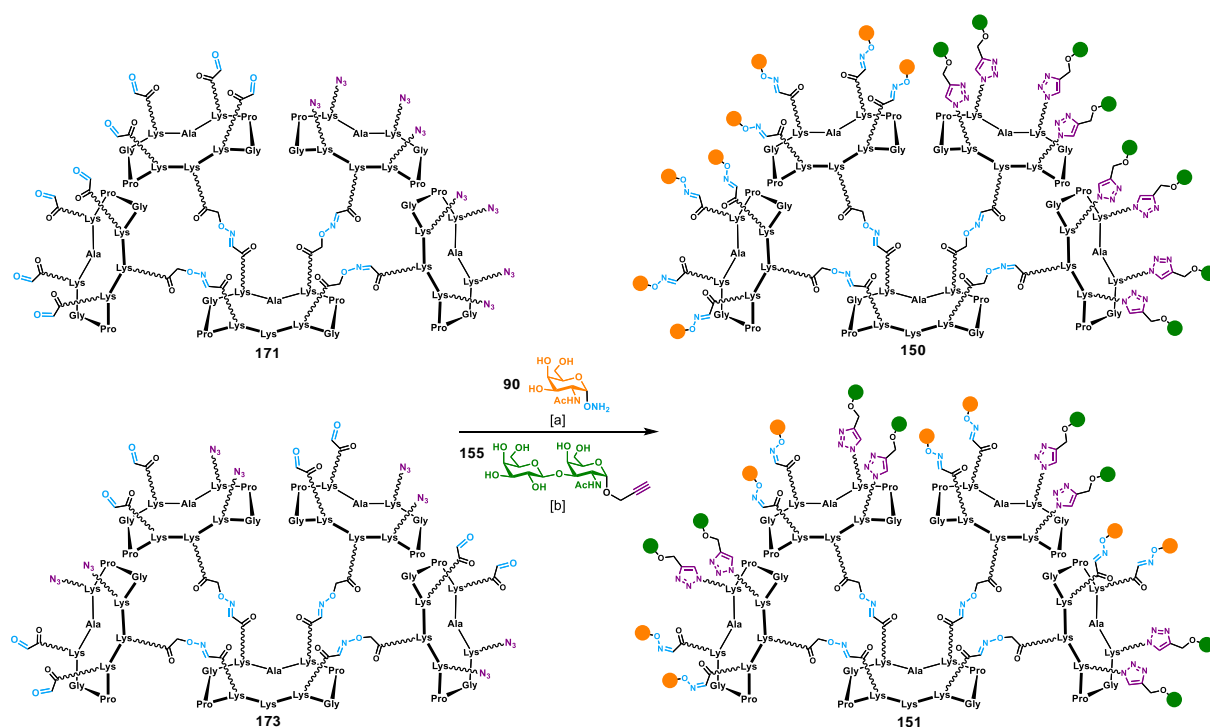


**Scheme 36.** Synthesis of multivalent scaffold **173**. Conditions: [a] **89**, **154** (6.0 eq.), 0.1% TFA in H<sub>2</sub>O, 37°C, 30 min., 87%; [b] NaIO<sub>4</sub> (80 eq.), H<sub>2</sub>O/CH<sub>3</sub>CN (1:1), r.t., 40 min., 73%.

### III.7. Synthesis of multivalent hetero-glycoclusters **150-151** by sequential one-pot OL-CuAAC protocol

The final conjugation step to achieve target molecules **150** and **151** (Figure 59) was performed by reacting scaffolds **171** and **173** (Scheme 35 and 36, respectively), both equipped with eight aldehyde and eight azido functionalities, with aminoxy Tn **90** (Scheme 19) and propargyl-TF **155** (Scheme 31). In order to perform only one purification step and reduce the loss of material, we carried out the reaction by means of a sequential one-pot protocol, where the established reaction order involved first OL, and then CuAAC. Due to the sensitivity of the  $\alpha$ -oxo aldehyde groups over the other functionalities, we decided to perform oxime ligation first.<sup>412</sup>

As described in scheme 37, reaction conditions involved 1.5 equivalents of aminoxy-saccharide per aldehyde, in a water/acetonitrile mixture containing 0.1 % of TFA. After 30 minutes incubation at 37°C, UPLC-MS analysis showed complete conversion in the expected octa-Tn intermediate (Figure 64a). A previously degassed phosphate buffer solution (pH 7.4, 100 mM), containing CuSO<sub>4</sub>, THPTA, sodium ascorbate and propargyl-TF **155** were then added to the crude mixture (Scheme 37). After 1.5 hours at room temperature, UPLC-MS showed complete conversion (Figure 64b).



**Scheme 37.** Synthesis of hetero-glycodendrimers **150** and **151**. Conditions: [a] **171** or **173**, **90** (12 eq.), 0.1% TFA in H<sub>2</sub>O, 37°C, 30 min.; [b] CuSO<sub>4</sub> (1.5 eq.), Na ascorbate (15 eq.), THPTA (8 eq.), PBS (pH 7.4, 100 mM), r.t., 90 min., 55% overall for **150**, 60% overall for **151**.



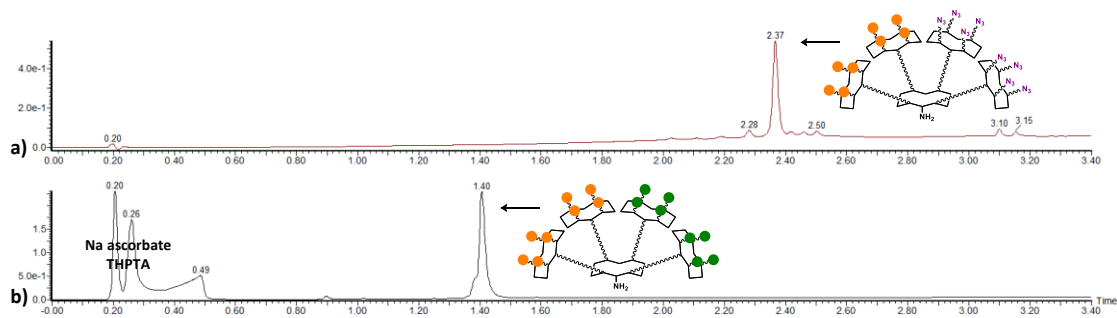


**Figure 64.** Follow-up of sequential one-pot reaction on substrate **171** by UPLC ( $\lambda=214$  nm, 5-60% solv.D in 3'). a) Profile of oxime ligation. b) Profile of copper(I)-catalyzed alkyne-azide cycloaddition.

Despite the structural complexity of these compounds, in addition to classic mass spectrometry and analytical HPLC, we have confirmed the correct functionalization of heteroglycodendrimers **150** and **151** by  $^1\text{H-NMR}$  (Figure 65a and 65b, respectively). Characteristic signals for anomeric protons of Tn ( $\approx 5.6$  ppm) and TF ( $\approx 5.0$  ppm), oxime protons ( $\approx 7.8$  ppm) and 1,4-triazole ( $\approx 8.0$  ppm) have been detected and integrated showing the expected ratio.<sup>415</sup>

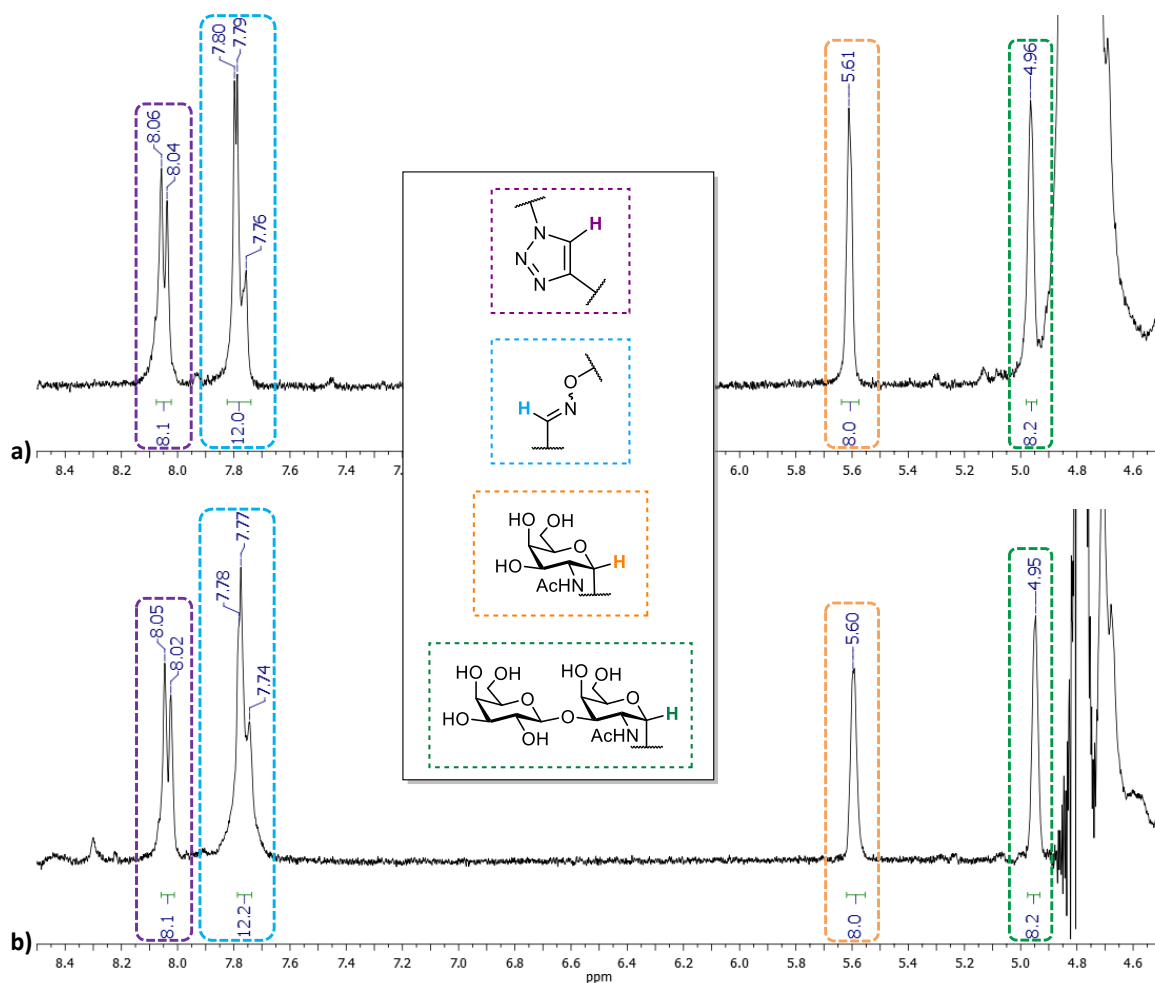


**Figure 65.**  $^1\text{H-NMR}$  ( $\text{D}_2\text{O}$ , 400 MHz) zoom of a) compound **150**, and b) compound **151**.

In conclusion, by using a divergent modular approach, based on oxime ligation (OL) and copper(I)-catalyzed alkyne-azide cycloaddition (CuAAC), we successfully obtained two unprecedented multivalent hetero-glycodendrimers displaying both Tn and TF saccharide antigens (Figure 59). These two constructs represent key components, which can be further functionalized to graft CD4<sup>+</sup> and CD8<sup>+</sup> peptide epitopes, to obtain the complete vaccine prototype structure. Indeed, as seen for other vaccine prototypes developed by our research group,<sup>219,273–275,290</sup> the free amino residue on the lower domain of the “core” scaffold represent an ideal anchorage point for grafting the immunostimulant peptide moiety, in a spatially-separated fashion compared to the carbohydrate moiety (Figure 58).

Before performing the final conjugation steps towards the complete synthetic vaccine structure and perform immunological assays in mice, we decided to first evaluate the ability of our multivalent glycosylated scaffolds to interact with anti-Tn and anti-TF monoclonal antibodies, kindly provided by our collaborators. This represents an essential step to assess (i) if our B-cell epitope display modality is compatible for an effective interaction with antibodies, and (ii) if the presence of a second antigen (*e.g.* TF) could interfere with the specific recognition between the first antigen (*i.e.* Tn) with his specific mAb. This work have been published as full paper in Chemistry, A European Journal.<sup>415</sup>

## **Chapter IV.**

# **Interaction assays with monoclonal antibodies and synthesis of complete vaccine prototype structures**

## IV.1. Direct interaction assays of hetero-glycodendrimers with anti-Tn and anti-TF mAbs by ELISA

The synthesis of hetero-glycodendrimers reported in the former chapter allowed us to achieve two multivalent architectures which display both Tn and TF antigens in two different modalities, that we called “separated” and “shuffled” (**150** and **151**, respectively. Figure 59). According to our fully synthetic approach in anticancer vaccine design, these constructs represent two modules dedicated to the presentation of B-cell carbohydrate antigens to the immune system. Compounds **150** and **151** are equipped with a free amino group, and are therefore suitable for being further functionalized in order to achieve the envisaged complete vaccine prototype structures, featuring: (i) a multivalent, heterogeneous TACA display (*i.e.* Tn and TF), (ii) a CD4<sup>+</sup> T<sub>H</sub>-cell epitope (*i.e.* OVA<sub>323-339</sub>),<sup>416</sup> and (iii) a CD8<sup>+</sup> CTL epitope (*i.e.* OVA<sub>257-264</sub>).<sup>417</sup>

Before undertaking product-consuming syntheses and assays in mice, which are subjected to strict ethical rules, using vaccine prototypes with poor efficacy, we decided to first evaluate the viability of our multivalent hetero-glycodendrimers through ELISA assays. These experiments have been performed between compounds **150** and **151**, along with positive and negative controls, and anti-Tn or anti-TF monoclonal antibodies which proved able to interact with human cancer cell lines (Figure 65). These trials would provide clearer insights regarding the capacity of our synthetic multivalent constructs to mimic the native display of TACAs upon the tumor surface, and to interact with specific mAbs against a given TACA in the presence of a second saccharide epitope, without generating detrimental interference phenomena.

### IV.1.1. ELISA direct interaction assays with anti-Tn mAb 9A7

In order to test our compounds, we have selected the monoclonal antibody 9A7 which has been shown to have good to excellent ability to recognize Tn-positive human cancer cells such as MCF-7, LS174T and Jurkat.<sup>418</sup> To perform ELISA binding studies with hetero-glycodendrimers **150** and **151**, we prepared a set of positive and negative controls, including: homo-glycodendrimer **111** (Figure 42), featuring sixteen copies of Tn antigen (positive control), the tetravalent homoclusters **174** and **175**, decorated with *N*-acetyl glucosamine (negative controls), and tetravalent heterocluster **176**, displaying two copies of Tn and two copies of TF antigens, as inferior homologue of compounds **150** and **151** (Figure 66).

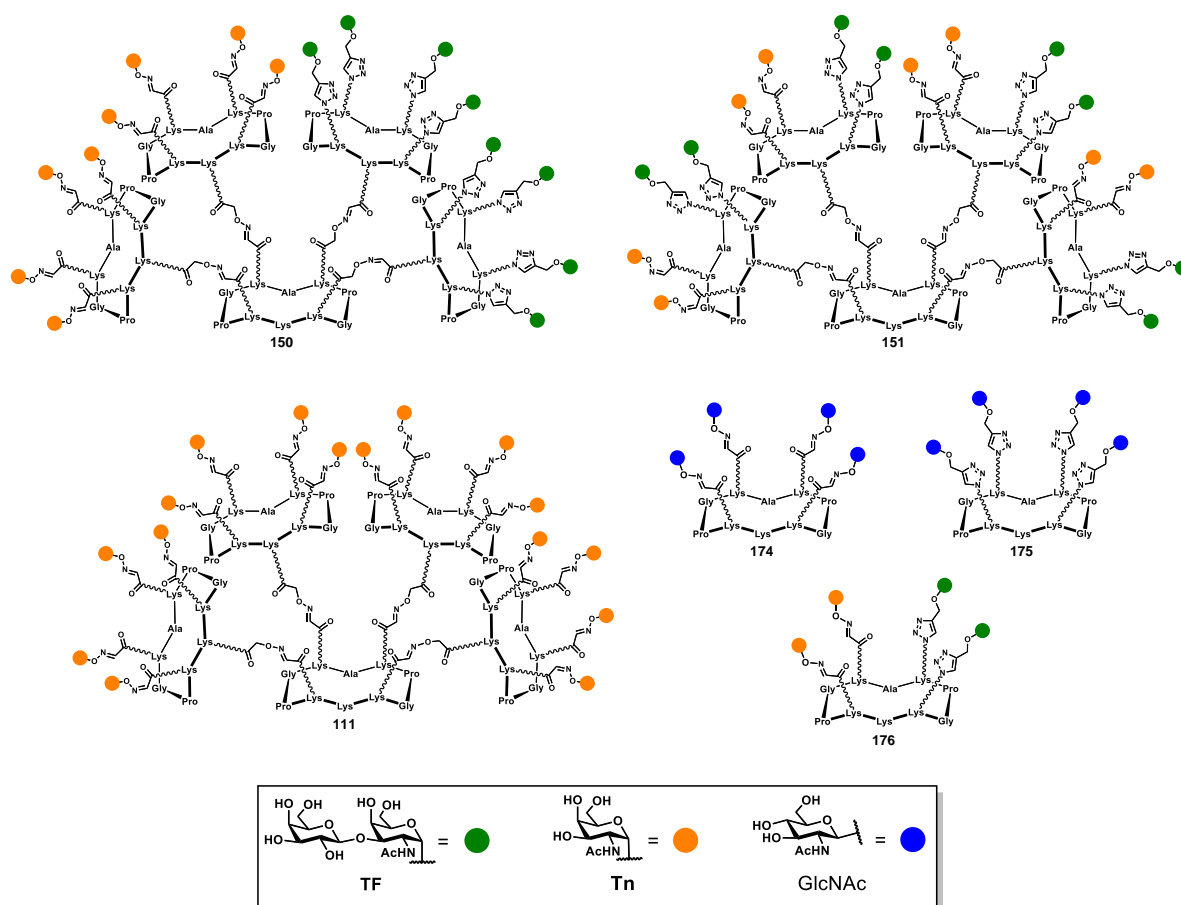


**Figure 66.** Set of compounds tested in direct interaction ELISA assay with anti-Tn mAb 9A7.

Each molecule has been coated at decreasing concentrations, starting from 100  $\mu$ M, into microtiter wells and compound's ability to recognize mAb 9A7 was studied. The extent of antibody binding towards each compound was reported as absorbance values at 490 nm, therefore this method allowed a qualitative, but not quantitative affinity measurement (Figure 67).

Although the best interaction was observed for compound **111**, hetero-glycodendrimers **150** and **151** were both recognized by the anti-Tn mAb. Keeping in mind that **111** displays a 2-fold increased Tn ratio compared to **150-151** (*i.e.* 16 vs 8), compound **150** resulted less efficient than **111**. More interestingly, 9A7 mAb showed a certain degree of sensitivity regarding the epitope display of **150** and **151**. Indeed, compound **151**, equipped with the same epitope density than **150**, resulted less efficient for the interaction with 9A7. These results suggested that TF epitope did not influenced the Tn-antigen recognition by 9A7 only in compound **150**. These results could also be alternatively interpreted as a consequence of the differences in the spatial distribution and interspace distances between Tn-antigen residues in compounds **150** and **151**. Although, tetraivalent hetero-glycocluster **176** failed to show a significant interaction with 9A7, suggesting that only two copies of Tn are not sufficient for an efficient recognition. As expected, tetraivalent homoclusters **174-175**, used as negative controls, did not

exhibited any signal, thus confirming the absence of unspecific interactions between 9A7 and similar carbohydrate residues, and/or the peptide scaffold itself.

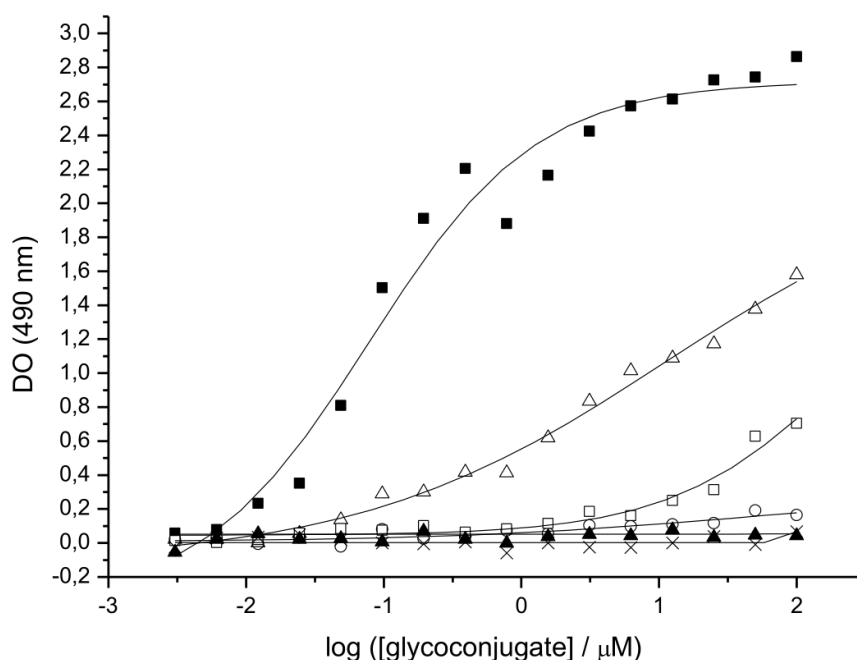


**Figure 67.** Interaction curves of the anti-Tn monoclonal antibody 9A7 with glycoconjugates **111** (■), **150** (△), **151** (□), **176** (○), **174** (▲) and **175** (×).

In summary, this direct interaction assay showed that either the presence of the second TF epitope or the epitope distribution itself interfere with the recognition of Tn in compound **151**, while no significant decrease of binding has been observed for compound **150**. It should also be mentioned that our “unnatural” presentation of the saccharide moiety of Tn antigen, relying on  $\alpha$ -N-acetyl galactosamine residues linked to the multivalent scaffold through oxime linkages [*i.e.* (OX)Tn], represented a valid model to build synthetic vaccine prototypes, since compound **111** showed detectable interaction even at concentrations near to 10 nM (Figure 67).

#### IV.1.2. ELISA direct interaction assay with anti-TF mAb JAA-F11

In order to validate constructs **150** and **151** as valid models for the heterogenic display of Tn and TF epitopes, we pursued our interaction studies by using the anti-TF mAb JAA-F11.<sup>419,420</sup> For this purpose, along with compounds **150** and **151**, a set of positive and negative controls were tested (Figure 68).

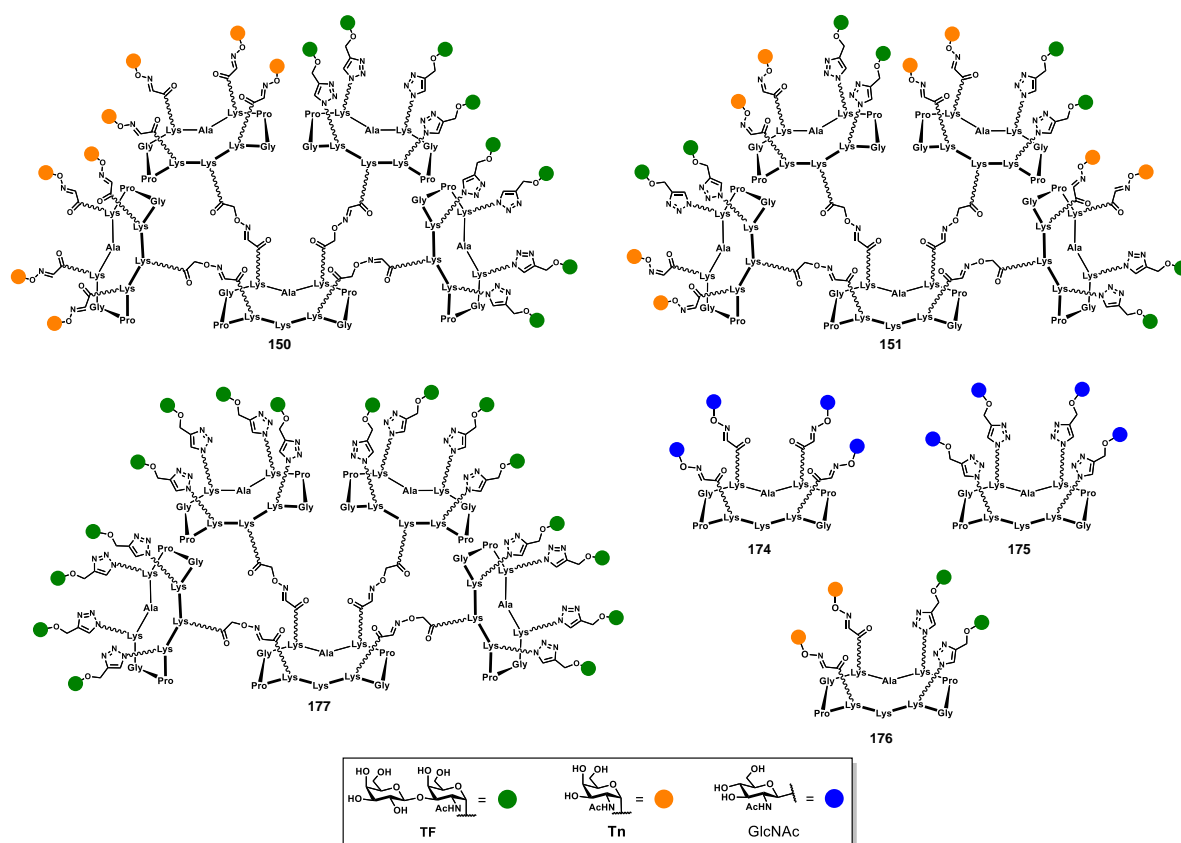


**Figure 68.** Set of compounds tested in direct interaction ELISA assay with anti-TF mAb JAA-F11.

According to the set of molecules employed in the former experiment, we included, along with our hetero-glycodendrimers **150** and **151**, GlcNAc-containing negative controls **174-175**, tetra-valent hetero-glycocluster **176**, and hexadeca-valent TF-based homo-glycodendrimer **177** (Figure 68). This last was synthesised by reacting hexadeca-valent azido-bearing scaffold **125** (Scheme 25) with propargylated TF **155** (Scheme 31) through our established CuAAC procedure (**VI.3.6**).

ELISA direct interaction assays with mAb JAA-F11 were carried out in the same conditions reported for those involving anti-Tn mAb 9A7: we coated our compounds into microtiter wells by performing cascade dilutions, at a starting concentration of 100  $\mu$ M. Unfortunately, no interaction curves have been obtained, since neither negative controls (*i.e.* **174-175**), nor TF-functionalized compounds (*i.e.* **150**, **151**, **176** and **177**) showed detectable binding.

The only compound that showed a consistent binding with JAA-F11 was the commercial TF-based polymer (**178**, figure 69a, Lectinity, Cat. #0048-PA) employed for the antibody calibration. This poly[*N*-(2-hydroxyethyl)acrylamide]-based polymer, of approximately 30 kDa has a 20% carbohydrate content, and displays the TF moiety through flexible chains, irradiating from its backbone structure.

In addition, Roy and co-workers reported the synthesis and binding evaluation of TF-containing di- and tetra-valent glycodendrimers containing long “arm” spacers. Among the small family of TF-

based glycodendrimers synthesized, tetravalent compound **179** (Figure 69b) showed the strongest binding activity towards mAb JAA-F11 ( $IC_{50} = 19 \text{ nM}$ ).<sup>419</sup>

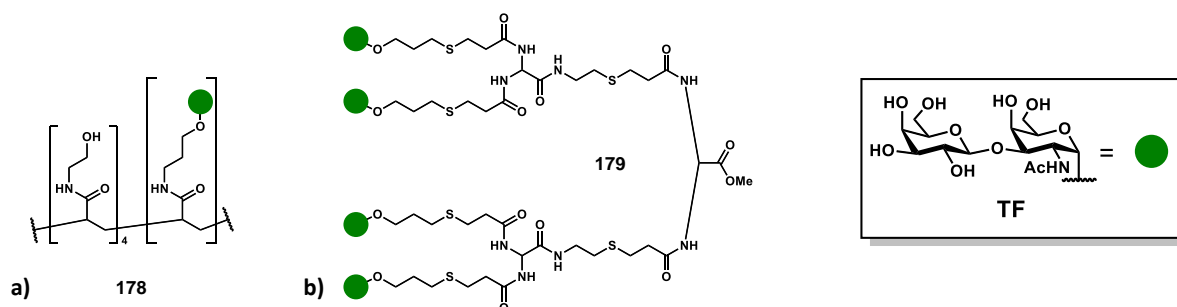


**Figure 69.** a) Commercially available TF-functionalized polymer used for the calibration of JAA-F11 mAb. b) TF-base tetravalent dendrimer by Roy and co-workers.

We hypothesized that the unsuccessful binding of our TF-functionalized compounds to JAA-F11 mAb could arise from the need of longer arm spacers for a correct disaccharide presentation. This could reduce steric hindrance phenomena between disaccharide units, enabling a higher degree of liberty for TF epitopes.

Therefore, we designed a synthetic pathway to reach a TF-based glycocluster equipped with longer spacers between the cyclopeptide “core” and the disaccharide moiety.

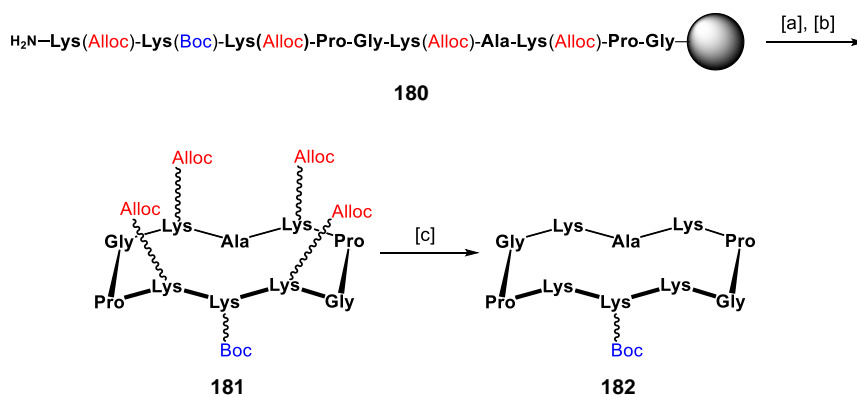
### IV.1.3. Synthesis of a TF-based glycocluster **186** containing a PEG linker and evaluation with anti-TF mAb JAA-F11

In order to investigate the possibility of obtaining an efficient binding between our TF-based modules and anti-TF mAb JAA-F11, we undertook the synthesis of a tetravalent glycocluster displaying the TF-antigen where the carbohydrate residues are linked to the cyclopeptide “core” through a PEG (polyethylene glycol) spacer. To this purpose, we first needed to synthesize a properly functionalized RAFT scaffold.

Resin-bound sequence **180** was thus cleaved under mild acidic conditions, followed by cyclization in solution, to afford orthogonally protected cyclopeptide scaffold **181** in 59% overall yield (Scheme 38). Palladium-catalyzed cleavage of the four Alloc protecting groups afforded partially deprotected scaffold **182**, displaying four amino residues on the upper domain, in excellent purity after RP-HPLC purification and lyophilization (Scheme 38, figure 70). The moderate yield of this last reaction



was caused by the large amount of phenylsilane in the reaction media. The routine protocol for the cleavage of Alloc groups involves the utilization of 25 equivalents of PhSiH<sub>3</sub> per Alloc group as scavenger; the large amount employed for this tetra-deprotection (100 eq.) has made necessary a pre-treatment of the crude reaction mixture before RP-HPLC purification, involving repeated extractions in water. We think that this caused a substantial loss of product, thus lowering the final yield.



**Scheme 38.** Synthesis of cyclopeptide scaffold **182**. Conditions: [a] 1% TFA, CH<sub>2</sub>Cl<sub>2</sub>; [b] PyBOP (1.2 eq.), DIPEA (2.0 eq.), DMF/CH<sub>2</sub>Cl<sub>2</sub> (1:1), 0.5 mM, r.t., 30 min., 58% overall yield; [c] Pd(PPh<sub>3</sub>)<sub>4</sub> (cat.), PhSiH<sub>3</sub> (100 eq.), CH<sub>2</sub>Cl<sub>2</sub>, r.t., 30 min., then MeOH, 42% yield.

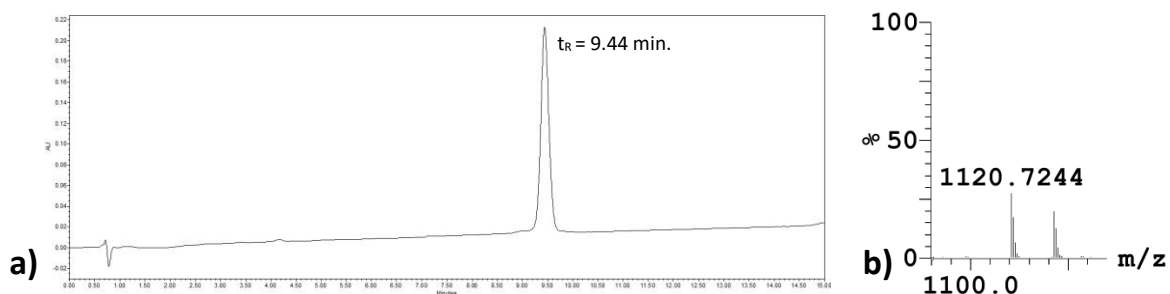
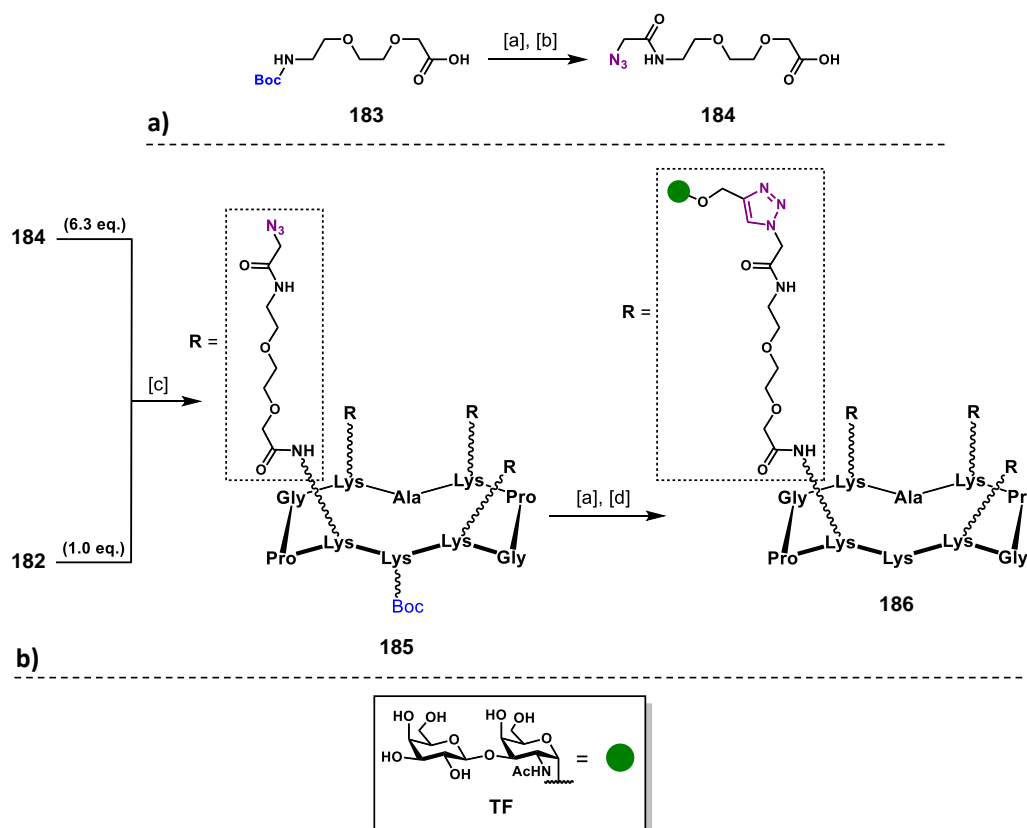


**Figure 70.** a) Analytical RP-HPLC profile ( $\lambda=214$  nm, 0-30% solv.B in 15') of **182**. b) HRMS (ESI<sup>+</sup>-TOF) of **182** (zoom).  $m/z$  calcd. for [M+H]<sup>+</sup>: 1120.7206 (monoisotopic), found: 1120.7244.

With scaffold **182** in hand, we proceeded by the appropriate functionalization of the PEG spacer (Scheme 39a). Commercially available 2,2-dimethyl-4-oxo-3,8,11-trioxa-5-azatridecan-13-oic acid **183**, was first treated with 50% TFA in CH<sub>2</sub>Cl<sub>2</sub> to remove the Boc protecting group, then solvent mixture was precipitated in Et<sub>2</sub>O and the resulting solid crude was used for the next reaction without any further purification. The resulting free amino group was reacted with a slight excess of the activated ester of 2-azidoacetic acid (2,5-dioxopyrrolidin-1-yl 2-azidoacetate) in the presence of DIPEA as base, in a CH<sub>3</sub>CN/DMF (1:1) mixture. Compound **184**, featuring a terminal azido- and carboxylic-

groups separated by a di-PEG linker, was obtained in 78% yield over two steps after RP-HPLC purification.



**Scheme 39.** a) Synthesis of azido-bearing di-PEG spacer **184**. Conditions: [a] 50% TFA in  $\text{CH}_2\text{Cl}_2$ , r.t., 30 min.; [b] 2,5-dioxopyrrolidin-1-yl 2-azidoacetate (1.2 eq.), DIPEA (1.5 eq.),  $\text{CH}_3\text{CN}/\text{DMF}$  (1:1), r.t., 20 min., 82% over two steps. b) Synthesis of TF-bearing glycocluster **186**. Conditions: [c] **182**, **184** (6.3 eq.), PyBOP® (6.3 eq.), DIPEA (8.0 eq.),  $\text{CH}_3\text{CN}/\text{DMF}$  (1:1), r.t., 30 min., 88% yield; [d] **155** (6.0 eq.),  $\text{CuSO}_4$  (cat.), THPTA (10 eq.), Na ascorbate (28 eq.), 67% yield over two steps.

The final steps for obtaining our target molecule involved the coupling of four copies of azido-PEG spacer **184** on tetravalent RAFT scaffold **182** by a classic amidation in solution, in the presence of PyBOP® as activating agent, and DIPEA as base (Scheme 39b). Scaffold **185**, featuring four azido residues connected through PEG spacers to the cyclopeptide backbone, and one Boc-protected amino group on the lower domain, was treated with a 50% TFA solution in  $\text{CH}_2\text{Cl}_2$ , then ice-cold ether was added to induce precipitation. The resulting crude mixture was reacted with propargyl-TF **155** (Scheme 31) through CuAAC ligation, under our standard protocol, to give target compound **186** in 67% yield over two steps (Figure 71).

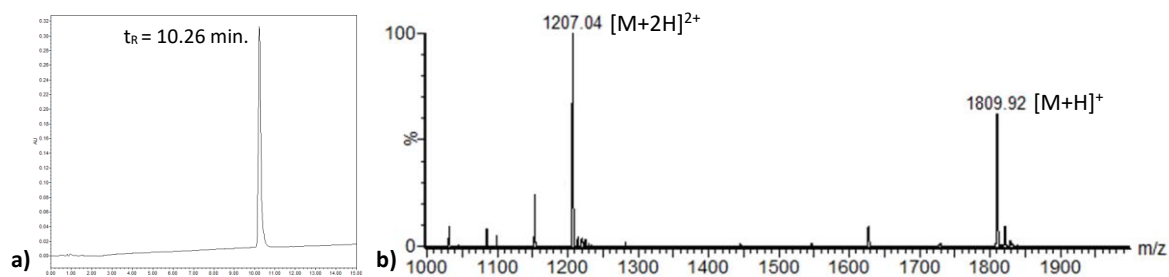


**Figure 71.** a) Analytical RP-HPLC profile ( $\lambda=214$  nm, 0-30% solv.B in 15') of **186**. b) ESI<sup>+</sup>-MS spectrum of **186** (zoom).  $m/z$  calcd. for  $[M+2H]^{2+}$ : 1809.8 (most intense peak of isotopic cluster), found: 1809.9; calcd. for  $[M+3H]^{3+}$ : 1206.9, found: 1207.0.

Compound **186** was thus tested for a direct ELISA interaction assay with anti-TF mAb JAA-F11, along with its tetravalent analogue with reduced spacers (**187**), and a negative control (**175**) (Figure 72). The effectiveness of all the species involved in the assay, including (i) the JAA-F11 mAb, (ii) the secondary antibody which binds to JAA-F11, (iii) the SIGMAFAST™ OPD (*O*-phenylenediamine dihydrochloride) tablets used for the revelation, and (iv) the BSA employed for the blocking procedure, was confirmed. Nevertheless, even raising the initial concentration of glycoconjugates up to 600  $\mu$ M (corresponding to a 6-fold increase, compared to the previous assays), neither compound **186**, nor **187** demonstrated able to bind JAA-F11; again, only the TF-based polymer **179** (Figure 69) showed binding activity towards JAA-F11.

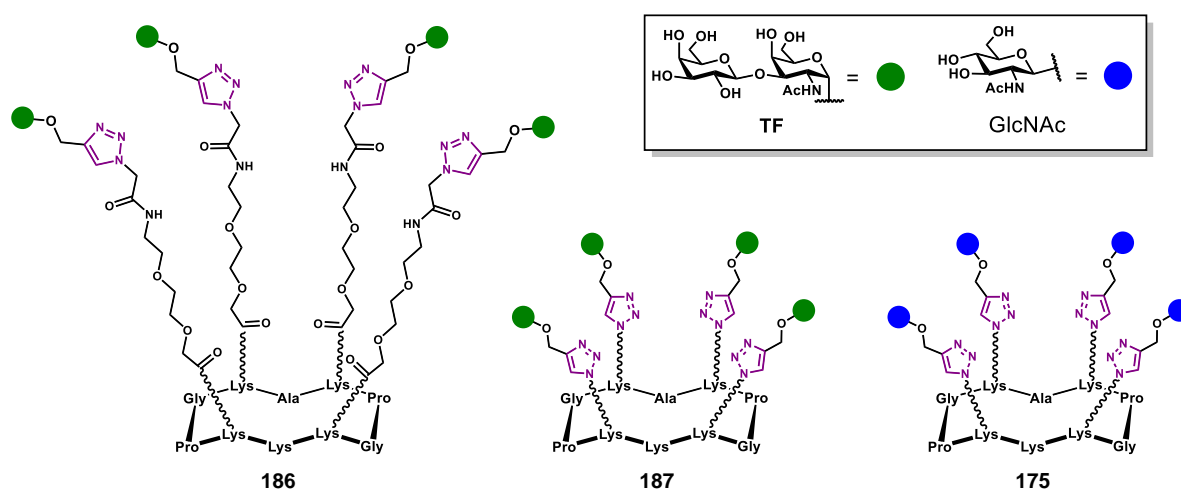


**Figure 72.** Set of compounds employed for the direct ELISA interaction test with mAb JAA-F11.

The negative outcomes obtained by our TF-functionalized compounds raised doubts about the presence of the triazole moiety close to the disaccharide units, which may cause interference phenomena towards the antibody recognition. Indeed, even if the spacer arms between the carbohydrate moiety and the cyclopeptide scaffold are longer in molecule **186** (Figure 71), compared

to those present in molecules **177** (Figure 68) and **187** (Figure 71), the position of the 1,2,3-triazole ring remains the same in all the abovementioned compounds.

These results were obtained in the last months of my PhD fellowship, with a limited amount of JAA-F11 antibody, and time constraints which kept us to further investigate the reasons of these findings. Nevertheless, multivalent hetero-glycodendrimers **150** and **151** (Figure 59) still represent innovative and unprecedented structures for the conception of anticancer vaccines, and further studies will be addressed to overcome the reported negative outcomes. A possible avenue which can be explored concerns the replacement of the triazole moiety with a different linker unit (*e.g.* thioether, as for compound **179**, figure 69), this would require a rethinking of the synthetic strategy and the synthesis of different building blocks, a task that we evaluated unfeasible for the abovementioned reasons of time.

Consequently, we decided to focus our efforts towards the finalization of the vaccine prototypes structures based on the hexadecavalent display of Tn-antigen residues. The achievement of Tn-based fully synthetic vaccines, displaying an enhanced density of B-cell epitopes (*i.e.* compound **111**, figure 42, displaying a 4-fold increased Tn-antigen density compared to the previous vaccine generations designed by our research group) could be valorised in the context of immunization trials in mice models.

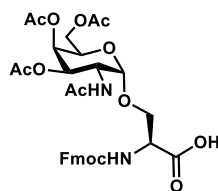
## IV.2. Comparison between (OX)Tn-based glycodendrimers and (Ser)Tn-based glycodendrimers towards their interaction with mAb 9A7

Another aspect that we sought to investigate concerned the validity of our modality to display the Tn-antigen. As explained in section I.2.2., TACAs like Tn and TF are naturally displayed upon serine or threonine residues, while our vaccine design relies on the utilization of the saccharide moieties alone, linked to multivalent scaffolds through “unnatural” linkages [*i.e.* (OX)Tn]. Although our compounds proved able to interact with 9A7 mAb, which previously demonstrated its ability to recognize Tn-positive human cancer cell lines, a direct comparison between our multivalent scaffolds decorated with oxime-linked and serine-linked Tn-antigens would provide a better understanding regarding the viability of our approach.

We thus envisaged to synthesize tetravalent and hexadecavalent glycoconjugates decorated with the serine-Tn antigen to test them in comparison with our oxime-linked analogues through a direct ELISA interaction assay.

### IV.2.1. Synthesis of tetravalent glycocluster 190 containing the (Ser)Tn epitope

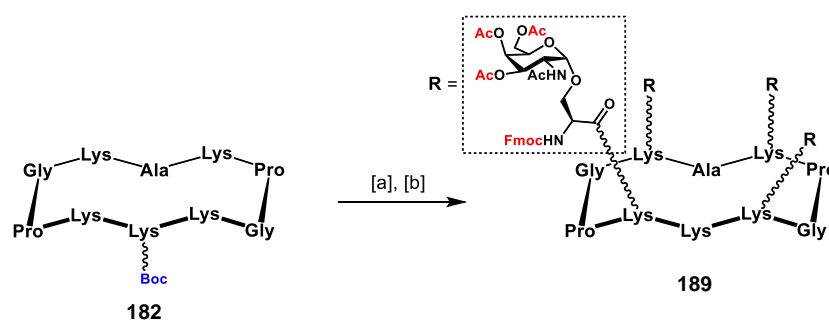
In order to synthesize serine-Tn-containing glycoconjugates, we first needed to obtain the *N*- $\alpha$ -Fmoc-O- $\beta$ -(2-acetamido-2-deoxy-3,4,6-tri-*O*-acetyl- $\alpha$ -D-galactopyranosyl)-L-serine building block **188** (Figure 73). The synthesis was performed by Dr. David Goyard, post-doctoral researcher of our group, according to the procedure described in literature.<sup>421</sup>



**188**

**Figure 73.** *N*- $\alpha$ -Fmoc-O- $\beta$ -(2-acetamido-2-deoxy-3,4,6-tri-*O*-acetyl- $\alpha$ -D-galactopyranosyl)-L-serine building block.

Key intermediate **189** (Scheme 40), displaying four Fmoc- and acetate- protected serine-Tn residues, was obtained through a two-step procedure from cyclopeptide **182** (Scheme 38). In solution amidation of the four amino residues on lysine's side chains was performed under standard coupling conditions, by reacting **182** with **188** in DMF, in the presence of PyBOP<sup>®</sup> as activating agent and DIPEA as base. Due to the low polarity of the fully-protected conjugation product, whose identity was assessed *via* MALDI-MS, we preferred not to perform the RP-HPLC purification at this stage, but rather remove the solvent mixture under high vacuum and cleave the Boc-protecting group on the lower domain of the RAFT scaffold. Compound **189** was obtained after preparative RP-HPLC in 67% yield over two steps (Figure 74).



**Scheme 40.** Synthesis of key intermediate **189**. Conditions: [a] **188** (4.8 eq.), DIPEA (6.0 eq.), PyBOP (5.0 eq.), DMF, r.t., 30 min.; [b] 50% TFA in CH<sub>2</sub>Cl<sub>2</sub>, r.t., 30 min., 67% over two steps.

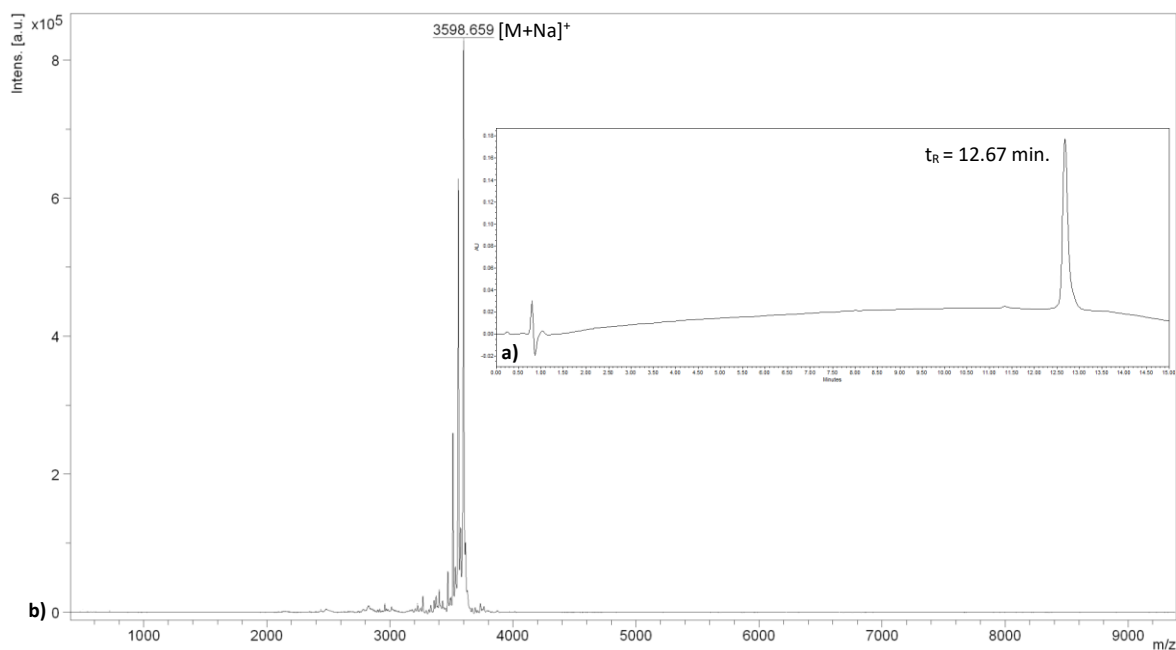
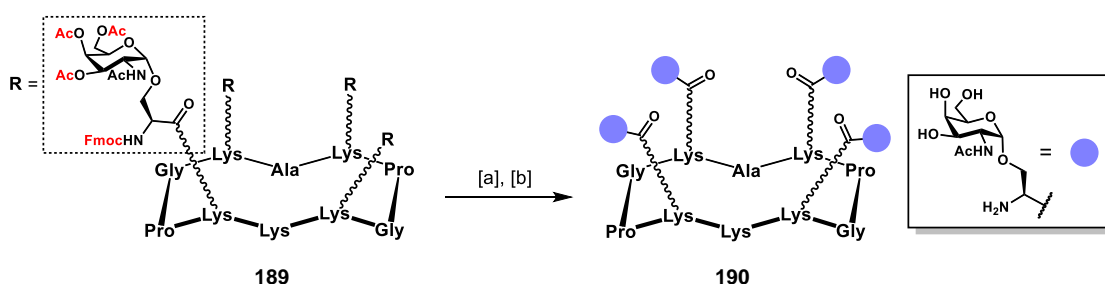


**Figure 74.** a) Analytical RP-HPLC profile ( $\lambda=214$  nm, 5-100% solv.B in 15') of **189**. b) MALDI-TOF spectrum of **189**.  $m/z$  calcd. for [M+Na]<sup>+</sup>: 3597.7 (average), found: 3598.7.

From key intermediate **189**, the tetravalent serine-Tn-containing glycocluster **190** was readily obtained by the sequential cleavage of Fmoc and acetate protecting groups (Scheme 41). Compound **189** was thus dissolved in a 5% piperidine in CH<sub>3</sub>CN solution, and stirred in the presence of a large excess of piperidine, after 15 minutes stirring at room temperature, the reaction was monitored via UPLC-MS, showing the complete conversion to the partially deprotected intermediate. The crude solvent mixture was concentrated to dryness under high vacuum, and the acetate groups were deprotected under Zemplén conditions. After 20 minutes stirring at room temperature, UPLC-MS confirmed the presence of target glycocluster **190** (Scheme 41, figure 75).



**Scheme 41.** Synthesis of tetravalent glycocluster **190**. Conditions: [a] 5% piperidine in CH<sub>3</sub>CN, r.t., 15 min.; [b] MeONa/MeOH (pH≈10), r.t., 20 min., 82% over two steps.

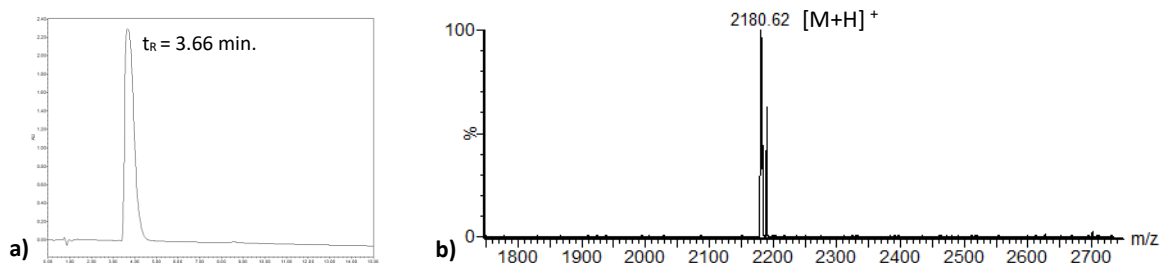
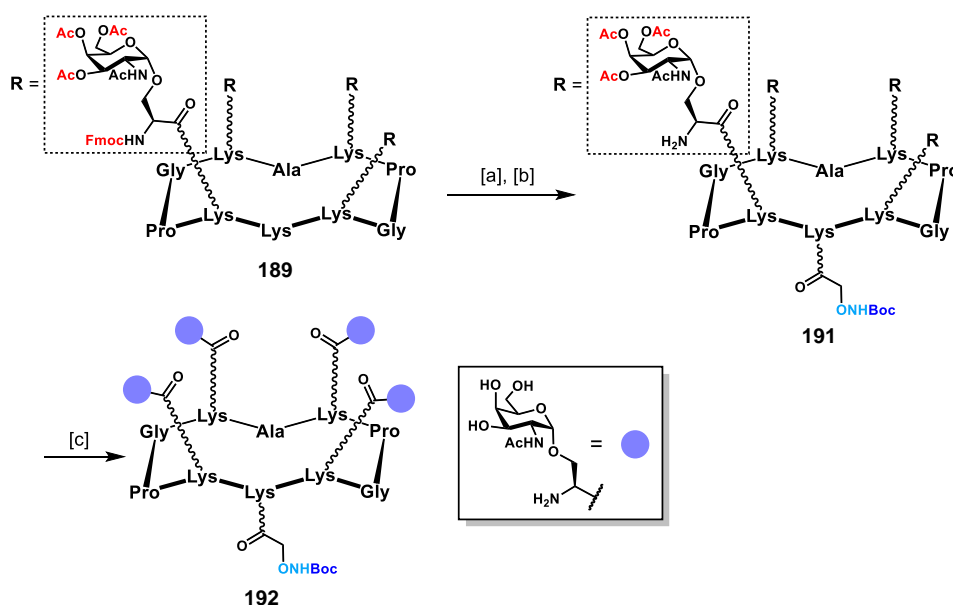


**Figure 75.** a) Analytical RP-HPLC profile ( $\lambda=214$  nm, 0-20% solv.B in 15') of **190**. b) ESI<sup>+</sup>-MS spectrum of **190** (zoom).  $m/z$  calcd. for [M+H]<sup>+</sup>: 2181.1 (monoisotopic), found: 2180.6.

#### IV.2.2. Synthesis of hexadecavalent glycodendrimer **193** containing the (Ser)Tn epitope

The synthetic route towards the hexadecavalent glycoconjugate displaying serine-Tn epitopes has been designed in a convergent manner, by employing OL to decorate a tetravalent “core” scaffold with four glycosylated “arms”. Treatment of key intermediate **189** (Scheme 41) with Boc-

aminoxyacetic acid *N*-hydroxysuccinimide ester,<sup>346</sup> in the presence of DIPEA provided a suitable anchorage point in the lower domain of the RAFT scaffold (Scheme 42). To avoid RP-HPLC purification of the very apolar resulting intermediate, the crude was treated with an excess of piperidine in order to cleave the Fmoc moiety, thus affording compound **191** in 73% yield over two steps. Deacetylation of compound **191** under Zemplén conditions afforded glycosylated “arm” scaffold **192** (Scheme 42, figure 76), equipped with a Boc-protected aminoxy group in the lower domain of the scaffold.



**Scheme 42.** Synthesis of compound **191**. Conditions: [a] Boc-aminoxyacetic acid *N*-hydroxysuccinimide ester (1.2 eq.), DIPEA (2.0 eq.), CH<sub>3</sub>CN/DMF (1:1), 20 min.; [b] 5% piperidine in CH<sub>3</sub>CN, r.t., 15 min., 73% over two steps; [c] MeONa/MeOH (pH 10), r.t., 20 min., 89%.

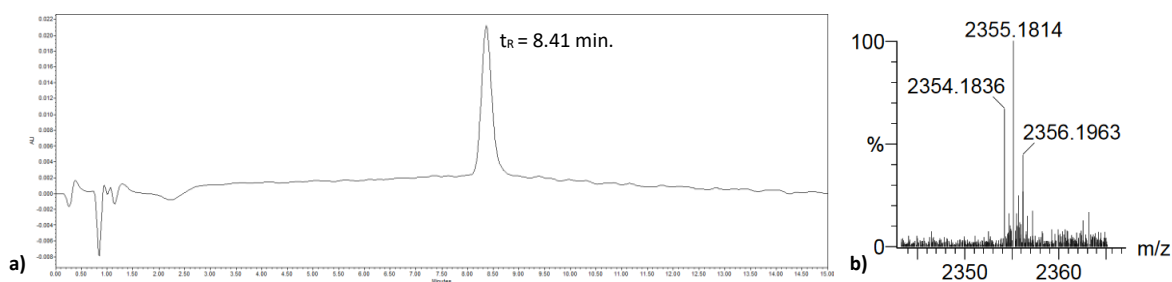
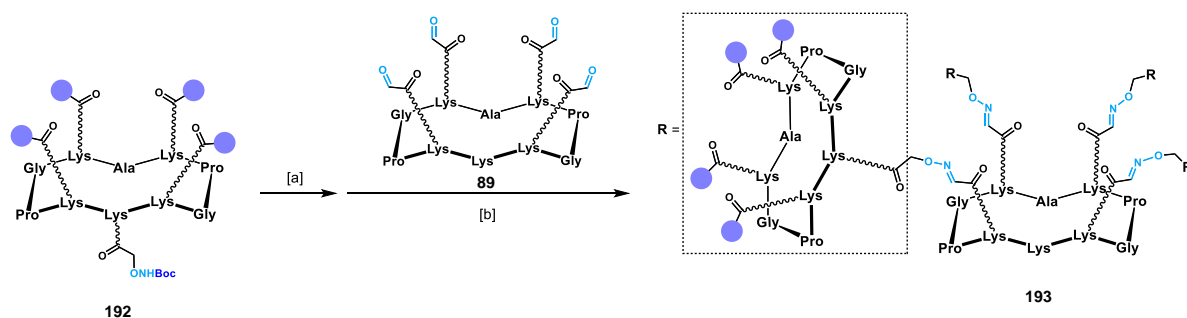


**Figure 76.** a) Analytical RP-HPLC profile ( $\lambda=214$  nm, 0-40% solv.B in 15') of **192**. b) HRMS (ESI<sup>+</sup>-TOF) of **192** (zoom).  $m/z$  calcd. for  $[M+H]^+$ : 2354.1826 (monoisotopic), found: 2354.1836.

Tetravalent “arm” glycocluster **192** was then treated with a 50% TFA solution to remove Boc-protecting group (Scheme 43). After 30 minutes stirring at room temperature, the crude reaction mixture was added to ice-cold diethyl ether to induce precipitation of the free-aminoxy product. The resulting crude was obtained as a white solid, and reacted with aldehyde-bearing “core” scaffold **89** (Scheme 15) through oxime ligation to afford final compound **193** (Scheme 43, figure 77).





**Scheme 43.** Synthesis of hexadecavalent serine-Tn-based glycodendrimer **193**. Conditions: [a] 50% TFA in  $\text{CH}_2\text{Cl}_2$ , r.t., 30 min.; [b] **89** (0.17 eq.), 0.1% TFA in  $\text{H}_2\text{O}$ , 37°C, 45 min., 82% over two steps.

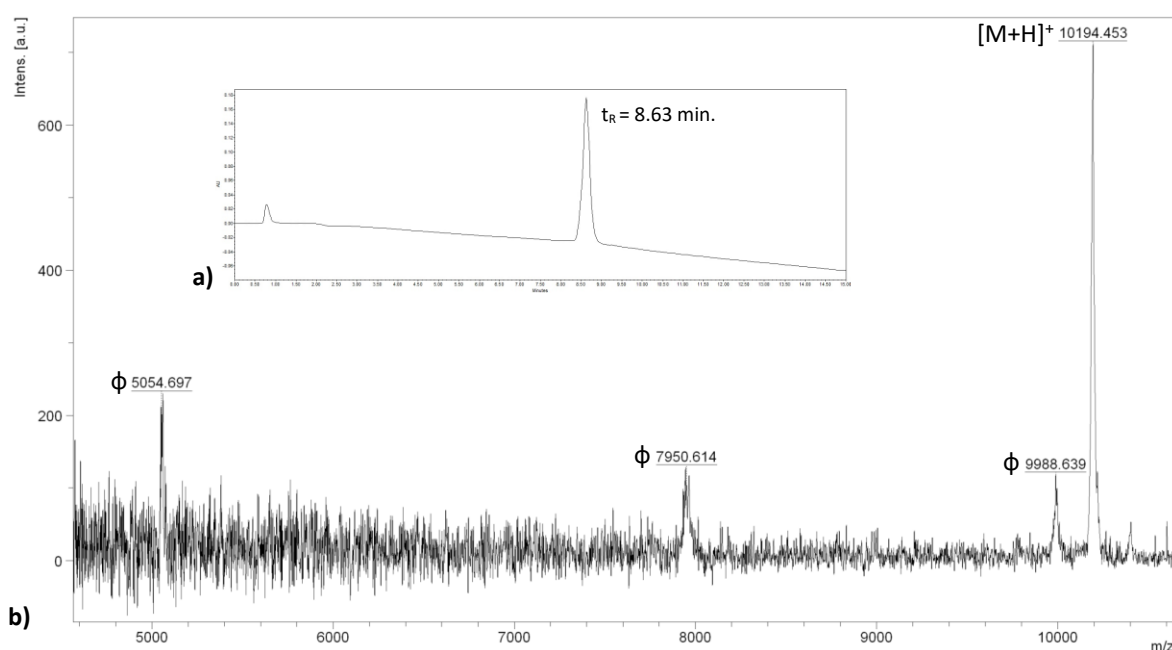


**Figure 77.** a) Analytical RP-HPLC profile ( $\lambda=214$  nm, 0-40% solv.B in 15') of **193**. b) MALDI-TOF spectrum of **193**.  $m/z$  calcd. for  $[\text{M}+\text{H}]^+$ : 10190.9 (average), found: 10194.5. ( $\phi$  = fragmentation)

### IV.2.3. Comparison of binding efficacy between (OX)Tn- and (Ser)Tn-based glycoconjugates *via* ELISA direct interaction assays using anti-Tn mAb 9A7

With compounds **190** and **193** in hand we performed an ELISA direct interaction assay with mAb 9A7, involving hexadecavalent (OX)Tn-based glycodendrimer **111**, tetravalent (OX)Tn-based glycocluster **194**, and GlcNAc-containing glycocluster **174** as negative control (Figure 78). The

experiments were carried out in the same conditions as those reported in section IV.1.1., by coating our compounds into microtiter wells by cascade dilutions, starting from a concentration of 100  $\mu$ M.

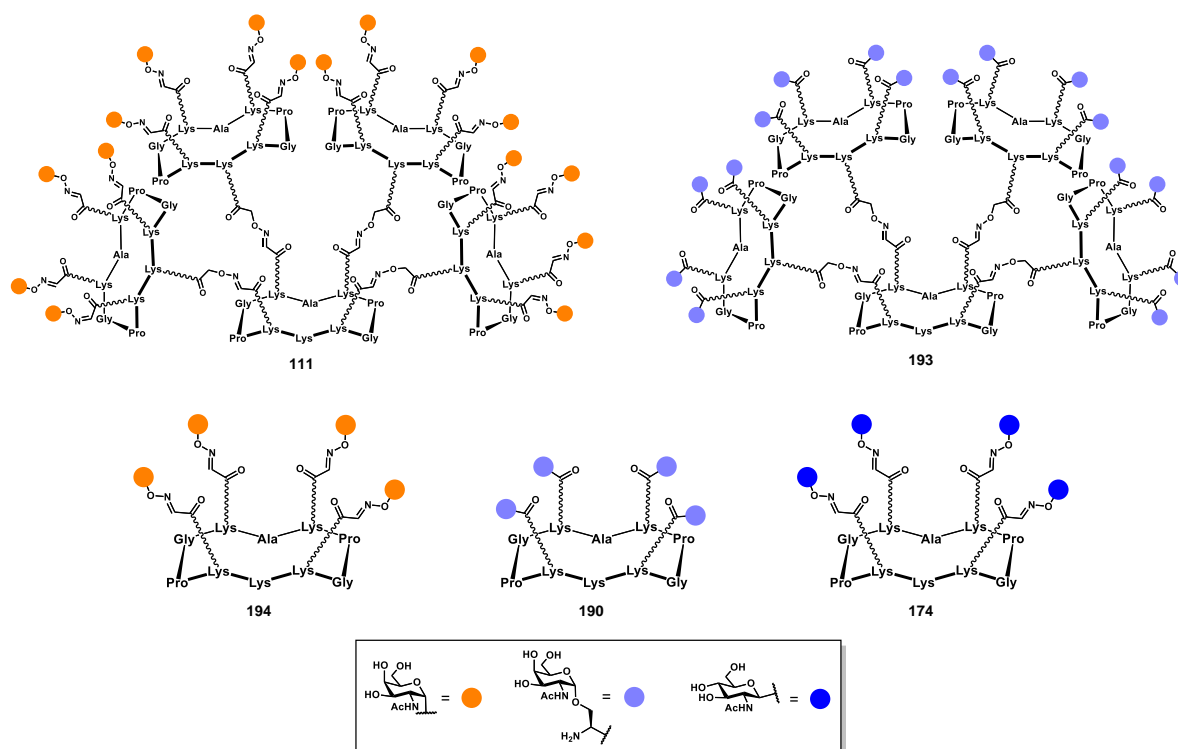


**Figure 78.** Set of compounds tested in direct interaction ELISA assay with anti-Tn mAb 9A7 to compare oxime-based Tn glycoconjugates and serine-based Tn glycoconjugates.

Results of binding assays are reported in figure 79, expressed as absorbance values at 490 nm. Although hexadeca-valent, (Ser)Tn-based compound **193** exhibited the strongest binding efficacy, the binding extent to 9A7 mAb of our (OX)Tn-based glycodendrimer **111** demonstrated to be suitable for its incorporation in anticancer vaccine prototypes. Tetra-valent, Tn-containing compounds **190** and **194** have not shown the same trend. Their absorbance values did not remarkably emerged from baseline values, suggesting that a tetra-valent epitope display does not allow for an effective binding.

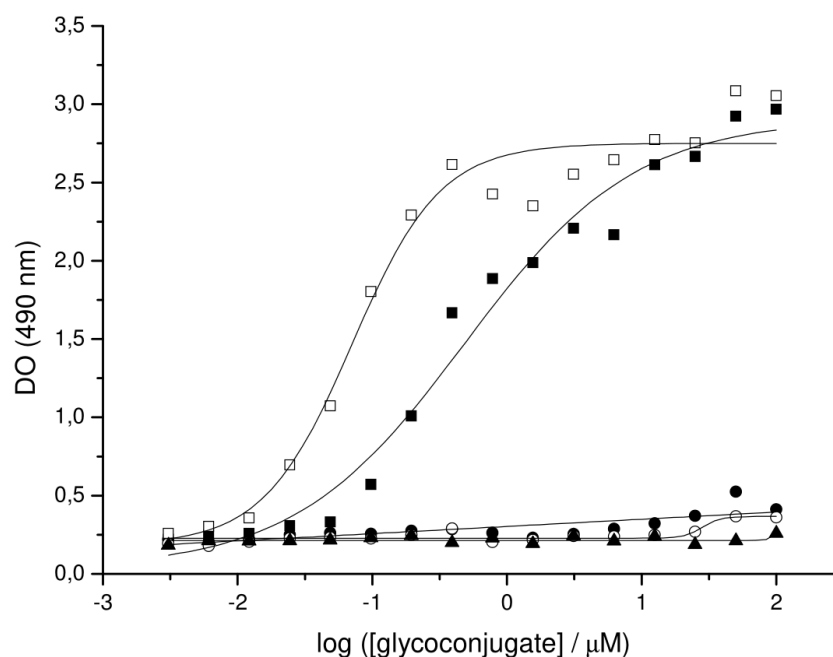


**Figure 79.** Interaction curves of the anti-Tn monoclonal antibody 9A7 with glycoconjugates **193** (□), **111** (■), **190** (○), **194** (●) and **174** (▲).

Taken together, these results prompted us to pursue the synthesis of a set of new fully synthetic vaccine structures displaying the Tn antigen both in the oxime-based and serine-based fashion. Along with hexadecavalent vaccine prototypes, tetravalent analogues will be tested too, in order to confirm the impact of a higher B-cell epitope density towards the generation of a more effective humoral immune response. In the subsequent sections the syntheses of complete, fully synthetic vaccine structures will be described; while synthetic routes for obtaining (OX)Tn-based vaccine prototypes revealed to be relatively straightforward and accessible, the generation of (Ser)Tn-based vaccine prototypes necessitated more complex manipulations (*vide infra*).

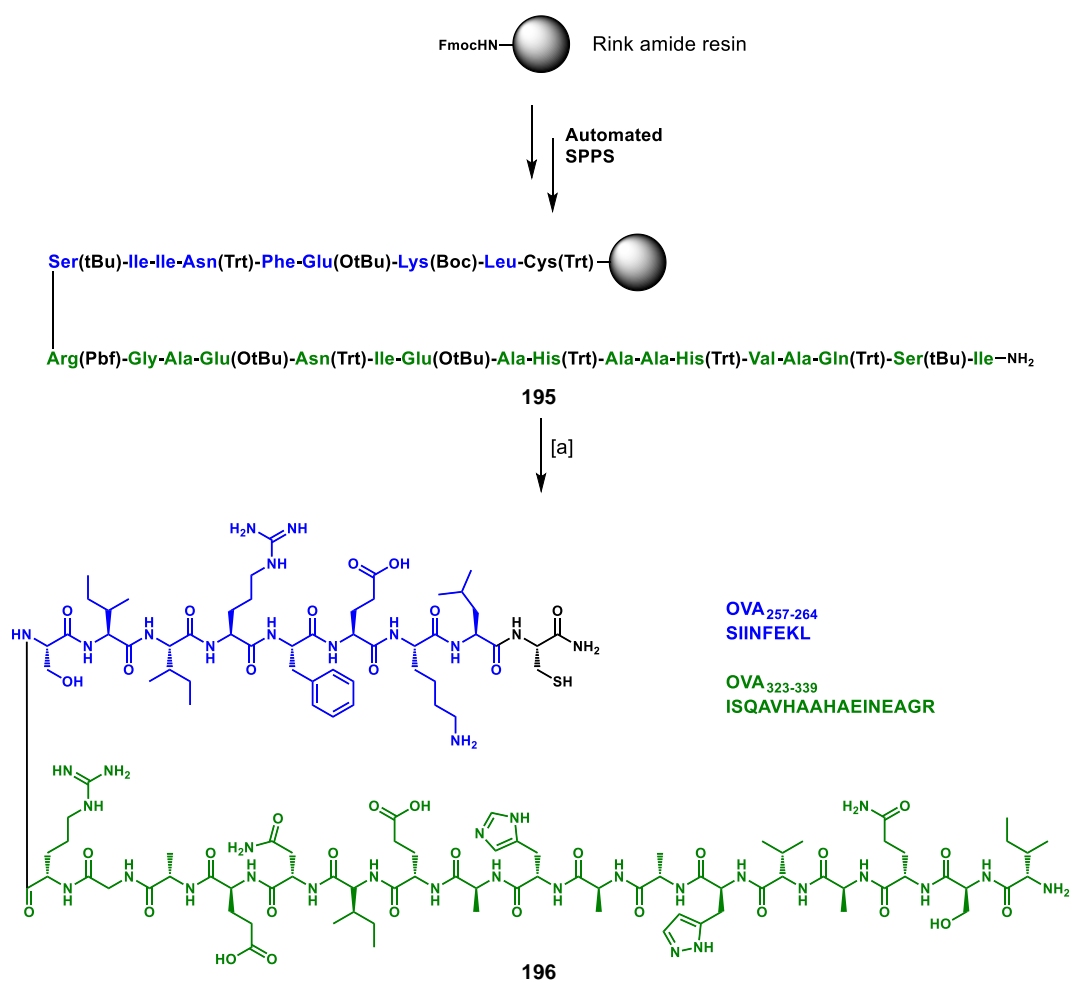
The achievement of fully synthetic, (OX)Tn- or (Ser)Tn-based vaccine prototypes would allow performing immunization trials in mice models and assessing the viability of our synthetic strategy involving the rapid and efficient construction of multivalent TACA-based glycodendrimers *via* click-chemistry. It could be also interesting to introduce in our scaffolds minimal MUC1 sequences displayed in a multivalent fashion.

### **IV.3. Synthesis of complete, fully synthetic, vaccine prototypes containing (OX)Tn and (Ser)Tn epitopes**

#### **IV.3.1. Synthesis of peptide 196 containing in-line CD4<sup>+</sup> and CD8<sup>+</sup> epitopes from ovalbumin**

According to our fully synthetic strategy, we selected CD4<sup>+</sup> T<sub>H</sub> cell, and CD8<sup>+</sup> CTL oligopeptide epitopes from chicken ovalbumin (OVA) to build our vaccine prototypes.<sup>151,282,290,416,417</sup> The choice of these epitopes was due to their widespread utilization in immunological studies. Indeed OVA is among the best characterized antigens, and many different OVA-expressing transgenic mouse models are available for research studies. Moreover, OVA-transfected tumor cell lines represent useful resources for the study of cancer immunology.<sup>422</sup>

Peptide sequence **195** (Scheme 44), containing amino acids with acid-labile protecting groups (*i.e.* Trt, Boc, *t*Bu, Pfb) was obtained through automated SPPS by robot synthesizer, on a Rink amide resin support. Cleavage from the resin by treatment with a TFA/TIS/H<sub>2</sub>O (96:2:2) cocktail afforded peptide **196**, containing CD4<sup>+</sup> (*i.e.* OVA<sub>323-339</sub>, in green) and CD8<sup>+</sup> (*i.e.* OVA<sub>257-264</sub>, in blue) epitopes (Scheme 44).



**Scheme 44.** Synthesis of immunostimulant peptide **196** containing in-line CD4<sup>+</sup> and CD8<sup>+</sup> epitopes. Conditions: [a] TFA/TIS/H<sub>2</sub>O (96:2:2), r.t., 3 h (x 3), 41% overall yield.

Following the design strategy of compounds **84-87** (Figure 30 and 32a), CD4<sup>+</sup> and CD8<sup>+</sup> epitopes have been synthesized “in-line”, equipped with a cysteine residue at the C-terminus, which represents the anchorage point for the attachment of **196** to multivalent TACA-bearing glycoconjugates **111**, **190**, **193** and **194** (Figure 78). Indeed, the aforementioned constructs display a free amino residue in the lower domain of the “core” RAFT scaffold, which can be readily functionalized with a cysteine residue. The latter, can subsequently undergoes disulfide bridging to give rise to the target, three-components, fully synthetic vaccine prototypes (Figure 80a-d), whose syntheses are the object of the following sections.

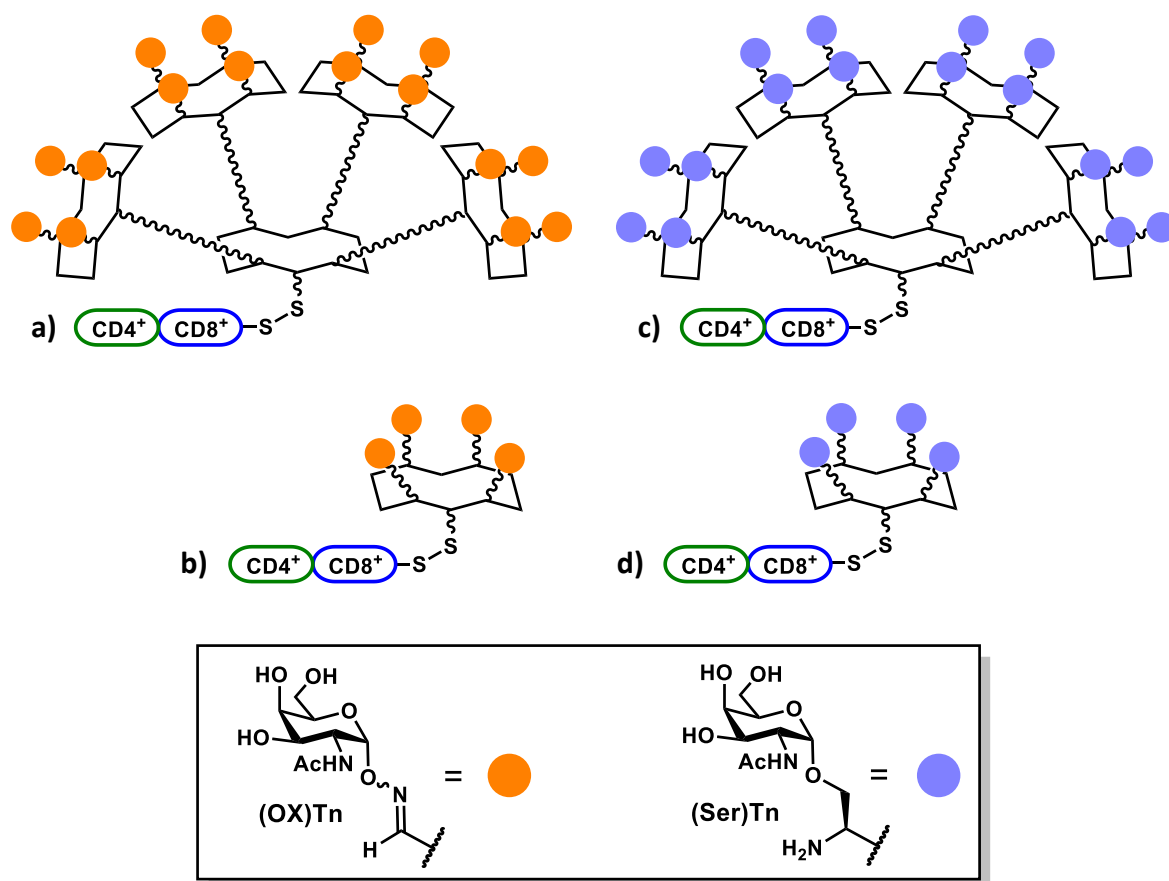


**Figure 80.** Schematic representation of target, three-components, fully synthetic vaccines constructs. They include a multivalent a) hexadecaivalent, or b) tetraivalent display of oxime-linked (orange) saccharide Tn antigen; and c) hexadecaivalent, or d) tetraivalent serine-linked (azure) Tn antigens as B-cell epitopes. All final compounds are equipped with  $\text{CD4}^+$  (green) and  $\text{CD8}^+$  (blue) peptides as  $T_H$  cell and CTL epitopes, respectively.

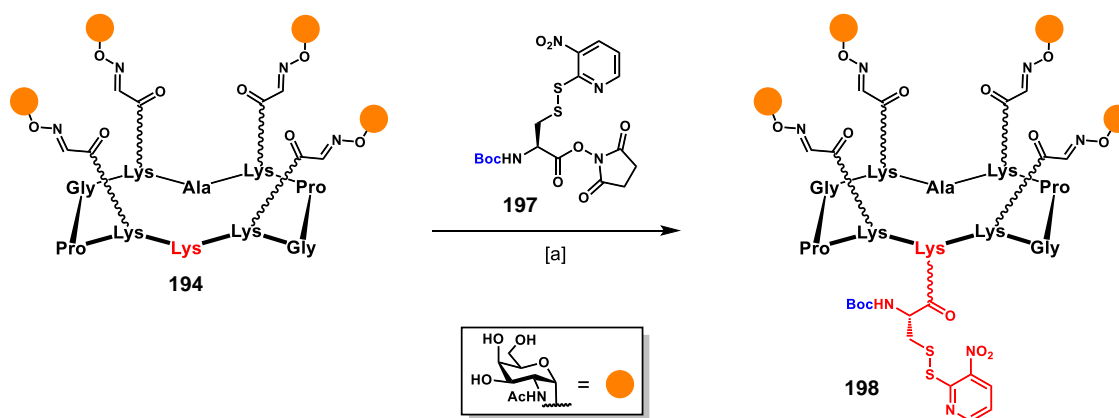
### IV.3.2. Synthesis of fully synthetic anti-cancer vaccine prototypes incorporating the (OX)Tn motif

The fully synthetic structure represented in figure 80b, contains the tetraivalent glycocluster **194** (Figure 78) as B-cell epitope carrier. It does not represent an innovative compound to our group, since similar structures have already been described (*e.g.* compound **84-86**, figure 29). In the frame of my PhD work, where one main objective was to test the effect of an enhanced saccharide B-cell epitope density over the entire construct, this tetraivalent compound represent a useful control to be tested *in vivo*, along with the target hexadecaivalent Tn-bearing compounds.

### IV.3.2.1. Synthesis of tetravalent, (OX)Tn-bearing, fully synthetic anti-cancer vaccine prototype 199

The synthetic procedure for the construction of tetravalent, (oxime)Tn bearing, OVA-conjugated vaccine prototype involved as first step the functionalization of the free amino residue on the lower domain of the scaffold with compound **197** (Scheme 45), the *N*-hydroxysuccinimide ester of Boc-[S-(3-nitro-2-pyridinesulfonyl)]-cysteine, also referred as Boc-Cys(NPys)-OSu.<sup>423,424</sup> Among various options for the protection of thiol function of cysteine, the NPys (3-nitro-2-pyridinesulfonyl) group represented a valuable and versatile choice. Thanks to its stability towards most of common solvents, and under classical synthetic conditions (including strong acids and tertiary amines), it can be integrated in both solid-phase and in-solution peptide synthesis protocols relying on Boc/benzyl strategies. Nevertheless, it is not compatible with Fmoc-based strategies. The most intriguing feature of NPys relies on his double character of S-protecting and S-activating group, which under acidic conditions (pH 4.5-7.0) enables rapid and efficient conjugations with free thiol groups, in the presence of other nucleophiles.

We thus proceeded by coupling tetravalent glycocluster **194** with a slight excess of Boc-Cys(NPys)-OSu (**197**) in DMF, in the presence of DIPEA as base (Scheme 45). Compound **198** was obtained as a light-yellow, foamy solid after RP-HPLC purification and lyophilization (Figure 81).



**Scheme 45.** Synthesis of Cys(NPys)-containing compound **198**. Conditions: [a] **197** (1.5 eq.), DIPEA (1.5 eq.), DMF, r.t., 30 min., 74% yield.

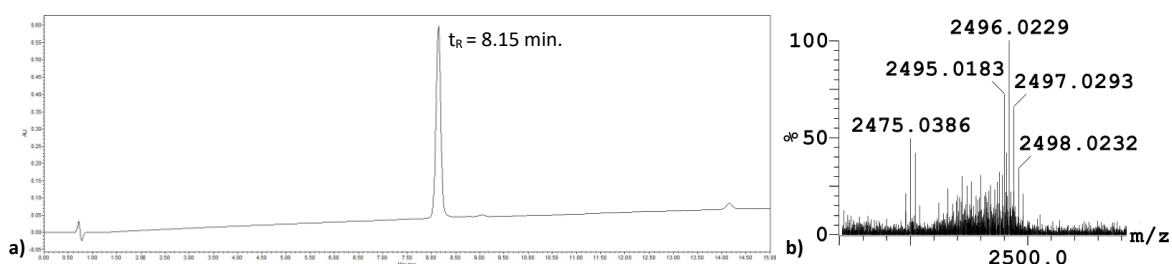
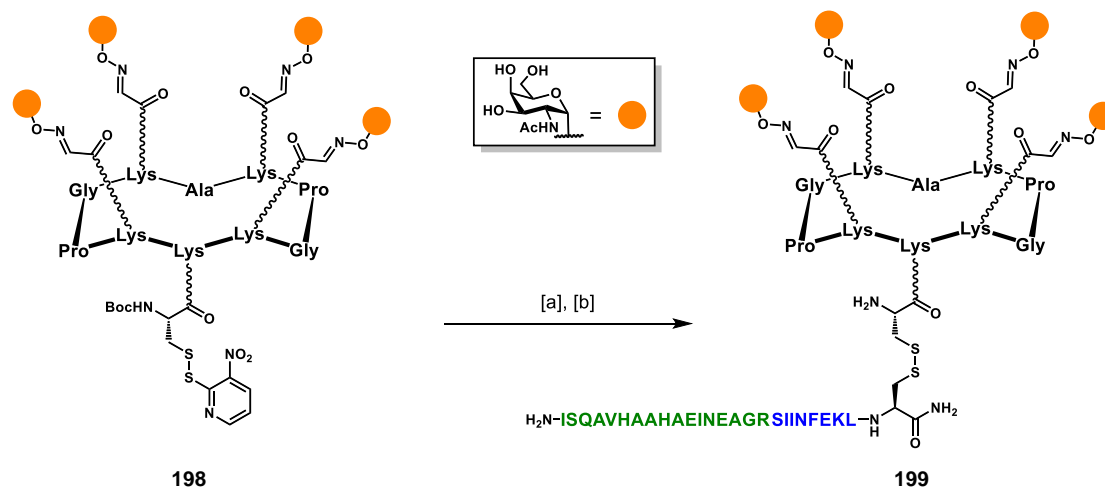


**Figure 81.** a) Analytical RP-HPLC profile ( $\lambda=214$  nm, 5-60% solv.B in 15') of **198**. b) HRMS (ESI<sup>+</sup>-TOF) of **198** (zoom).  $m/z$  calcd. for [M+H]<sup>+</sup>: 2475.0368 (most intense peak on isotopic cluster), found: 2475.0386, calcd. for [M+Na]<sup>+</sup>: 2496.0159 (monoisotopic), found: 2496.0229.

Compound **198** was then subjected to Boc-deprotection by treatment with a 50% TFA solution in CH<sub>2</sub>Cl<sub>2</sub> for 30 minutes at room temperature (Scheme 46). Ice-cold diethyl ether was added to induce precipitation, and the crude deprotected intermediate was obtained as a white solid after centrifugation and drying under high vacuum. HRMS and analytical RP-HPLC experiments confirmed the identity of the desired deprotected product, thus the crude was employed without any further purification for the final conjugation step. To a degassed solution of Boc-deprotected compound **198** in sodium acetate buffer (pH 4.5, 40 mM), a solution of cysteine-containing peptide **196** (Scheme 44) in DMF was added, and the reaction progression monitored *via* RP-HPLC. Upon addition of the peptide solution, the reaction mixture color progressively turned into intense yellow, indicating the displacement of the NPys group. Accordingly, after 20 minutes stirring at room temperature the conversion was complete, showing no trace of the starting materials. Pure vaccine prototype **199** was obtained in 72% yield over two steps after RP-HPLC purification and lyophilization (Figure 82).



**Scheme 46.** Synthesis of tetravalent vaccine prototype **199**. Conditions: [a] 50% TFA/CH<sub>2</sub>Cl<sub>2</sub>, r.t., 30 min.; [b] **196** (1.1 eq.), NaOAc buffer (pH 4.5, 40 mM), DMF, r.t., 20 min, 72% yield over two steps.



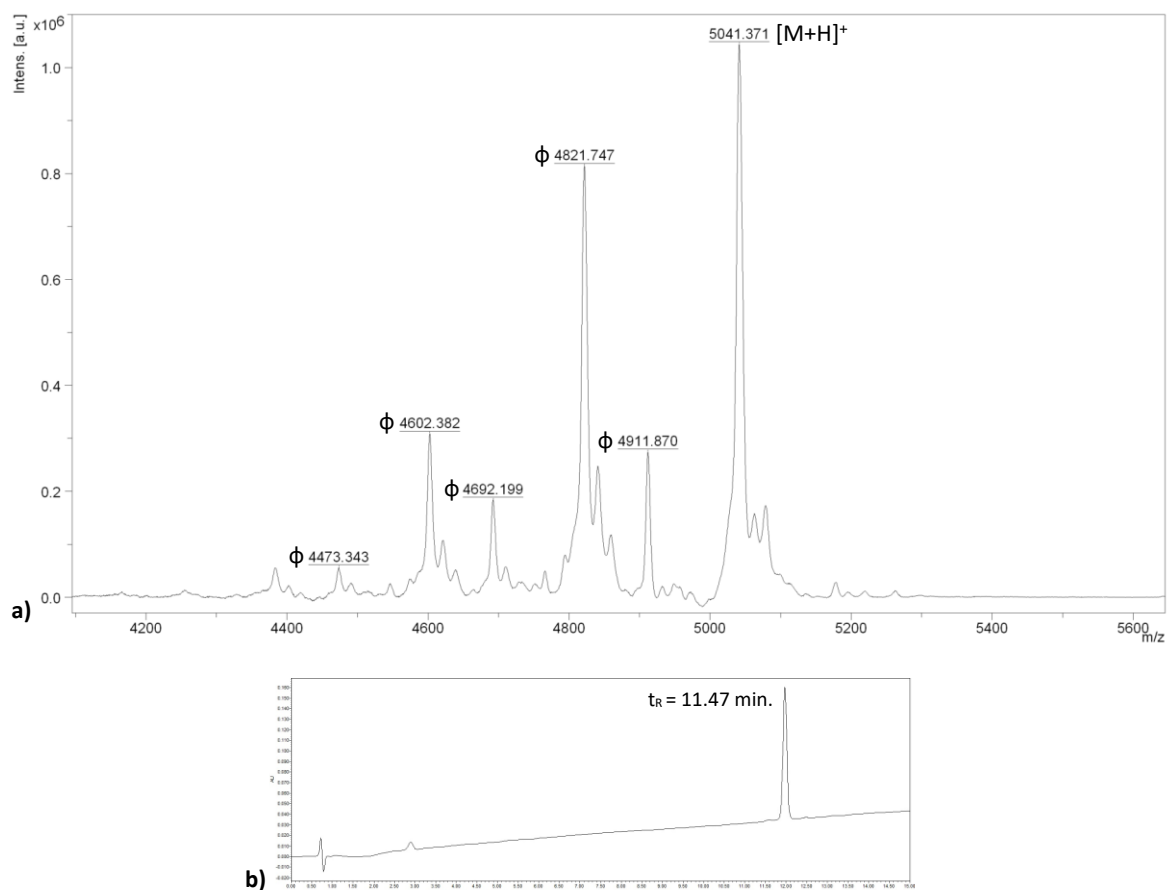
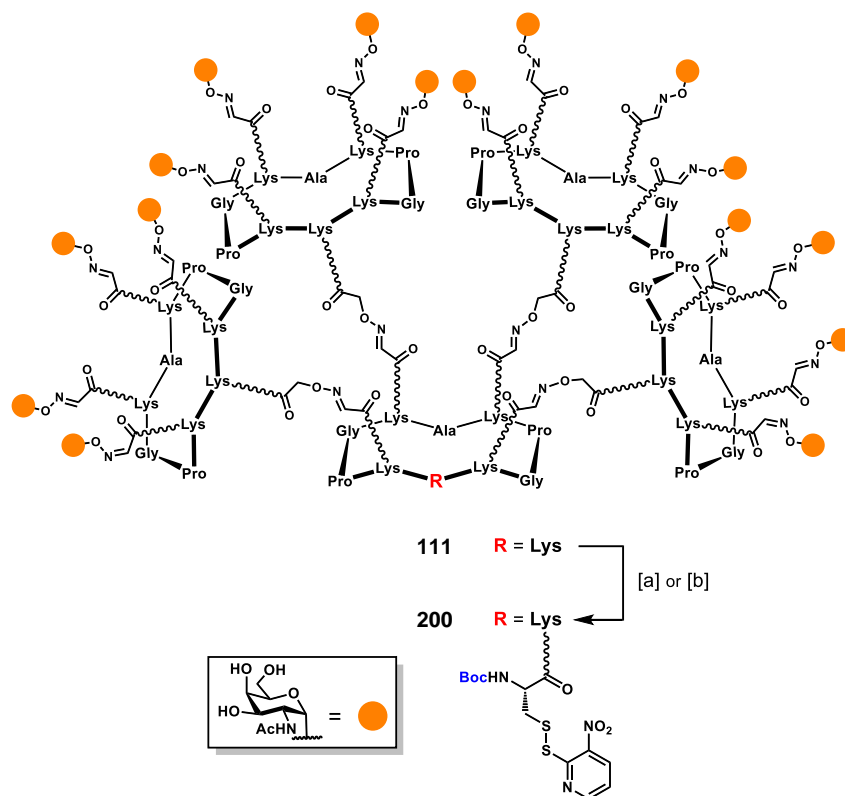


**Figure 82.** a) MALDI-TOF spectrum of **199**.  $m/z$  calcd. for  $[M+H]^+$ : 5040.5 (average), found: 5041.4. ( $\phi$  = fragmentation) b) Analytical RP-HPLC profile ( $\lambda=214$  nm, 0-40 solv.B in 15') of **199**.

### IV.3.2.2. Synthesis of hexadecaivalent, (OX)Tn-bearing, fully synthetic anti-cancer vaccine prototype 201

The synthetic strategy described above was next employed for the synthesis of the vaccine prototype incorporating hexadecaivalent oxime-Tn glycodendrimer **111** (Figure 78). The first problem that we encountered was related to the solubility of our glycosylated compound. Surprisingly, the addition of DMF to **111** caused the formation of a gel, whose dissolution could not be induced neither by adding more solvent, nor gently warming the mixture under vigorous agitation or sonication. Most of the material was sticking to the reaction flask's walls. In a first attempt to at least obtain a homogeneous dispersion of the product, addition of equal volumes of DMSO allowed the reaction to occur, using slightly modified reaction conditions compared to those described in scheme 45. It has been possible to isolate pure intermediate **200** (Figure 83), with a poor 30% yield after RP-HPLC

purification and lyophilization (Scheme 47). Compound **111** is completely soluble in water, conversely, Boc-Cys(NPys)-OSu **197** is highly apolar and soluble in organic solvents such as CH<sub>2</sub>Cl<sub>2</sub>, AcOEt or DMF. We managed to raise the yield up to 41% by performing the reaction in a mixture containing PBS buffer (pH 7.4, 10 mM) and DMF in 1:1 proportions. Nevertheless, given the loss of material at this late stage of the synthetic route, improving the yield of this step remains an important task to be addressed in the future.



**Scheme 47.** Synthesis of Cys(NPys)-containing compound **200**. Conditions: [a] **197** (1.5 eq.), DIPEA (1.4 eq.), DMF/DMSO (1:1), r.t., 60 min., 30% yield; [b] **197** (1.5 eq.), PBS (pH 7.4, 10 mM)/DMF (1:1), r.t., 60 min., 41% yield.

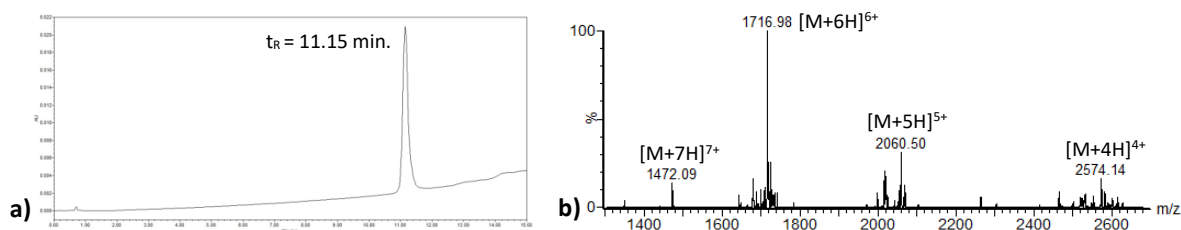
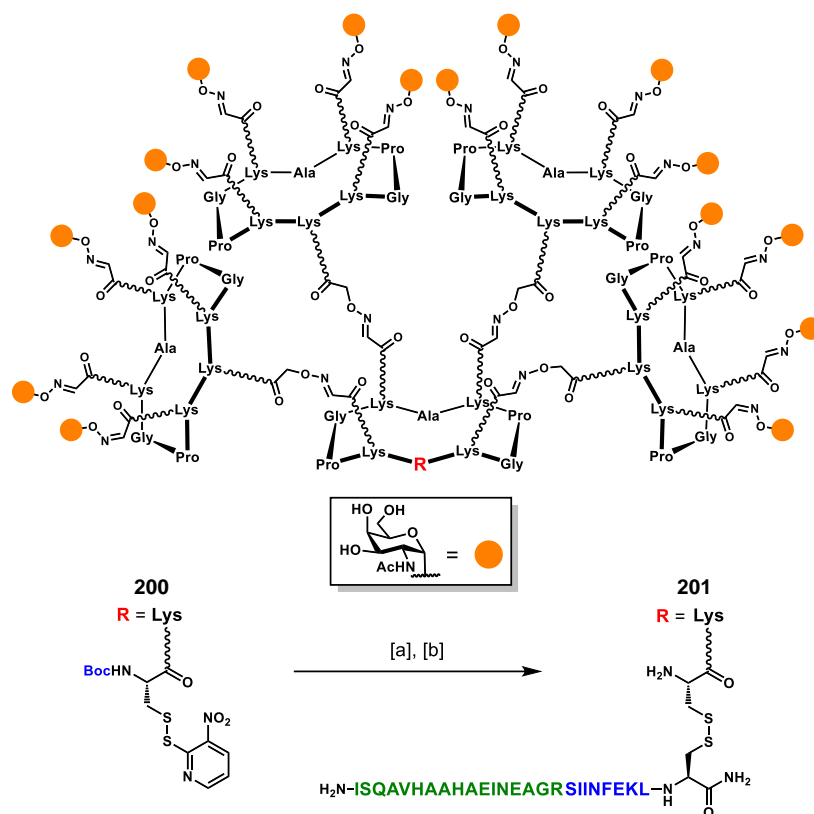


**Figure 83.** a) Analytical RP-HPLC profile ( $\lambda=214$  nm, 0-40 solv.B in 15') of **200**. b) ESI<sup>+</sup>-MS spectrum of **200** (zoom).  $m/z$  calcd. for [M+4H]<sup>4+</sup>: 2573.7 (average), found: 2574.1; calcd. for [M+5H]<sup>5+</sup>: 2059.1, found: 2060.5; calcd. for [M+6H]<sup>6+</sup>: 1716.1, found: 1717.0; calcd. for [M+7H]<sup>7+</sup>: 1471.1, found: 1472.1.

The final conjugation step was carried out under the same conditions described for vaccine prototype **199** in scheme 46. Hexadecavalent vaccine prototype **201** (Scheme 48, Figure 84), was

obtained in 61% yield over two steps, after RP-HPLC purification and lyophilization, as white foamy solid.



**Scheme 48.** Synthesis of hexadecaivalent vaccine prototype **201**. Conditions: [a] 50% TFA/CH<sub>2</sub>Cl<sub>2</sub>, r.t., 30 min.; [b] **196** (1.1 eq.), NaOAc buffer (pH 4.5, 40 mM), DMF, r.t., 20 min, 61% yield over two steps.

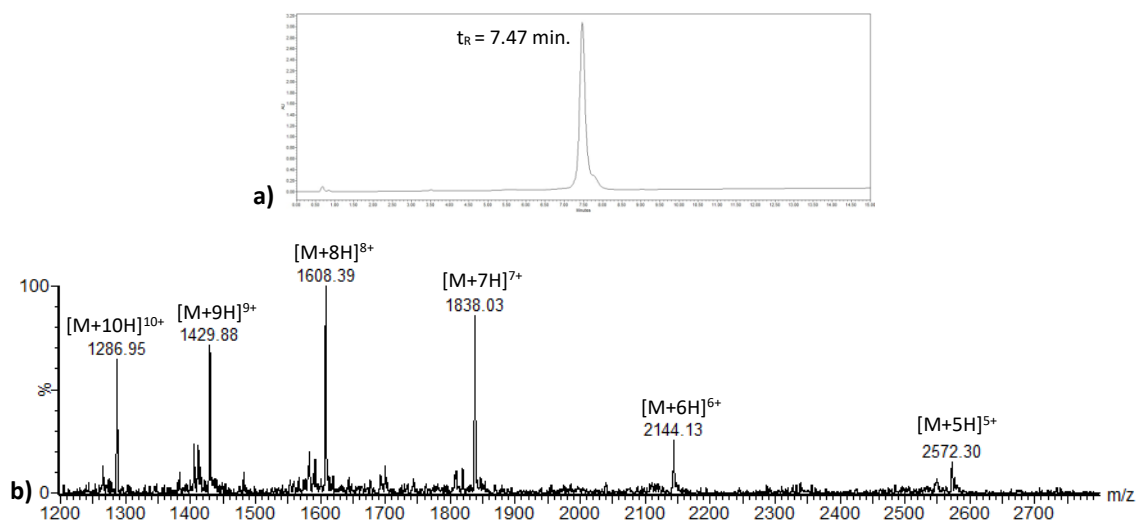


**Figure 84.** a) Analytical RP-HPLC profile ( $\lambda=214 \text{ nm}$ , 5-60 solv.B in 15') of **201**. b) ESI<sup>+</sup>-MS spectrum of **201** (zoom).  $m/z$  calcd. for [M+5H]<sup>5+</sup>: 2572.1 (average), found: 2572.3; calcd. for [M+6H]<sup>6+</sup>: 2143.6, found: 2144.1; calcd. for [M+7H]<sup>7+</sup>: 1837.5, found: 1838.0; calcd. for [M+8H]<sup>8+</sup>: 1607.9, found: 1608.4; calcd. for [M+9H]<sup>9+</sup>: 1429.4, found: 1429.9; calcd. for [M+10H]<sup>10+</sup>: 1286.6, found: 1287.0.

In the next sections the synthesis of tetravalent and hexadecaivalent serine-Tn containing vaccine prototypes (Figure 80d and 80c, respectively) will be described. The completion of this small

set of fully synthetic vaccine prototypes will be valorised by immunization trials, performed by our immunologist collaborators.

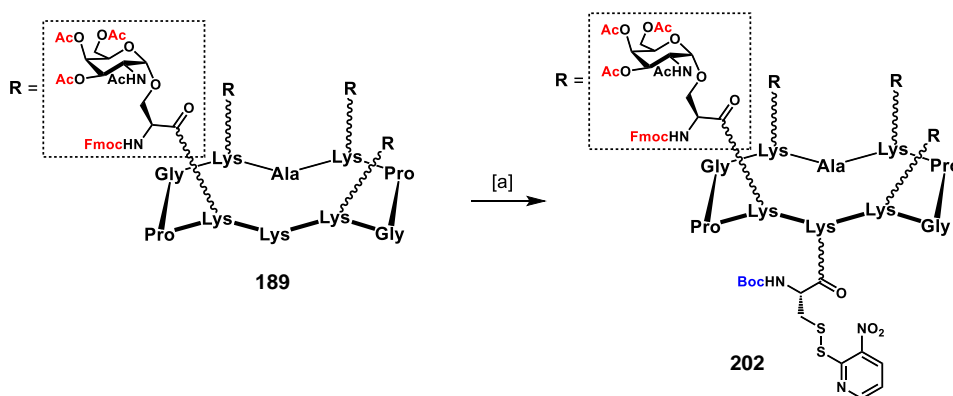
### **IV.3.3. Synthesis of fully synthetic anti-cancer vaccine prototypes incorporating the (Ser)Tn motif**

In the former section we described a synthetic strategy to obtain tetravalent and hexadecaivalent vaccine constructs (**199** and **201**, respectively) starting from oxime-Tn glycoconjugates **111** and **194** (Figure 78), which have been formerly employed for ELISA direct binding assays with anti-Tn mAb 9A7 (**IV.2.2.**). In order to produce fully synthetic vaccine prototypes displaying (Ser)Tn B-cell epitopes, as those designed in figures 80c and 80d, we could not apply the above described straightforward methodology by starting from compounds **190** and **193** (Figure 78) due to the presence of several, chemically equivalent free amino groups.

That inconvenience forced us to undertake alternative pathways and think differently in terms of design, with considerable synthetic efforts. It also represented an opportunity to explore new chemical strategies that revealed useful for extending the toolbox for the design and synthesis of such multi-modal macromolecules.

#### **IV.3.3.1. Synthesis of tetravalent, (Ser)Tn-bearing, fully synthetic anti-cancer vaccine prototype 205**

The synthetic route for (Ser)Tn-based tetravalent vaccine prototype started from key intermediate **189** (Scheme 40). Functionalization of the free amino residue in the lower domain of the scaffold with Boc-Cys(NPys)-OSu (**197**) afforded compound **202** in 77% yield after RP-HPLC purification and lyophilization (Scheme 49, figure 85).



**Scheme 49.** Synthesis of Cys(NPys)-containing compound **202**. Conditions: [a] **197** (1.5 eq.), DIPEA (1.5 eq.), DMF, r.t., 30 min., 77% yield.

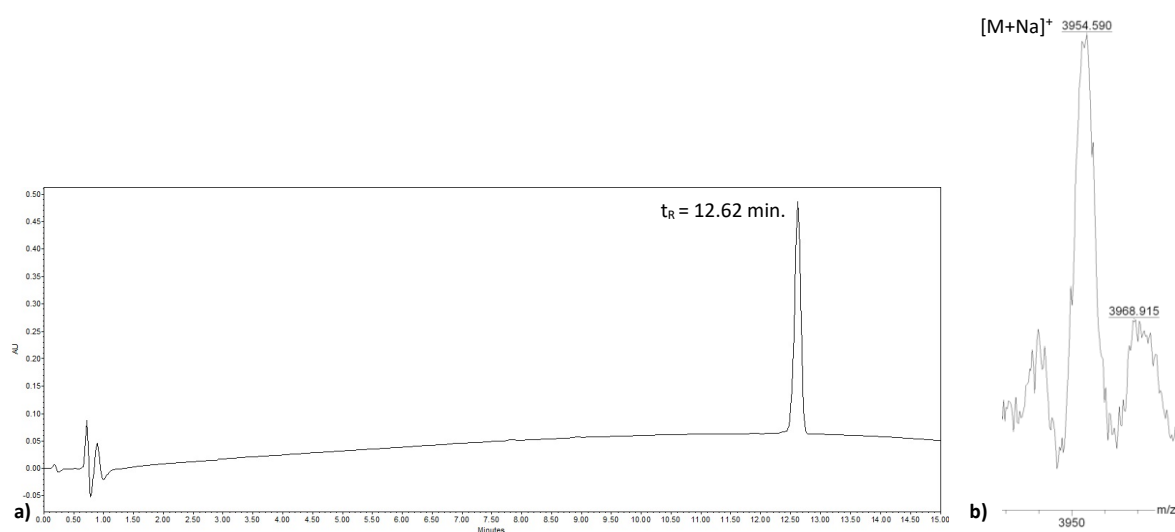
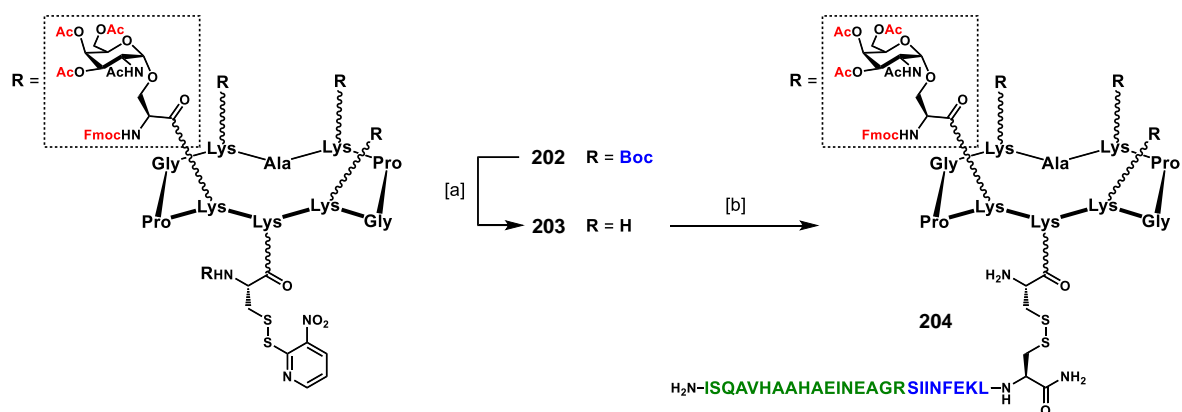


**Figure 85.** a) Analytical RP-HPLC profile ( $\lambda=214$  nm, 5-100 solv.B in 15') of **202**. b) MALDI-TOF spectrum (zoom) of **202**.  $m/z$  calcd. for  $[\text{M}+\text{Na}]^+$ : 3955.1 (average), found: 3954.6.

Due to the low polarity of the starting material, the reaction did not show solubility problems in DMF, accordingly, yields were higher than those reported for compound **200** (Scheme 47).

Compound **202** was next treated with a 50% TFA in  $\text{CH}_2\text{Cl}_2$  solution to remove the Boc protecting group (Scheme 50). The crude product **203** was obtained as a white solid after precipitation in ice-cold diethyl ether, centrifugation and drying under high vacuum, and used without further purification for the next step. The disulfide bridge formation between **203** and cysteine-containing peptide **196** (Scheme 44) was carried out under slightly modified conditions, compared to those reported for the synthesis of **199** and **201** (Scheme 46 and 48, respectively). Due to the low polarity of **203**, a DMF/NaOAc buffer (pH 4.5, 40 mM) mixture (2:1) was necessary to provide a proper solubilisation (Scheme 50). Compound **204** was thus obtained in 69% yield over two steps, after RP-HPLC purification and lyophilization.



**Scheme 50.** Synthesis of compound **204**. Conditions: [a] 50% TFA/CH<sub>2</sub>Cl<sub>2</sub>, r.t., 30 min.; [b] **196** (1.1 eq.), DMF/NaOAc buffer (pH 4.5, 40 mM) (2:1), r.t., 30 min, 69% yield over two steps.

Along with the signal corresponding to compound **204**, MALDI analysis also showed the presence of its reduced cysteine-containing partners: **196** and M-**196** (Corresponding to **203** without the NPys moiety, figure 86a). Since during preparative RP-HPLC purification a single peak was collected, and assuming that no co-elution phenomena happened (according to the observed retention times, see figures 86b and 86c), this could be either due to the reduction of disulfide bridge in the sample containing **204** before or during the MALDI analysis, or the experimental conditions by which MALDI measurements were carried on converted single compound **204** into a mixture.<sup>425</sup>

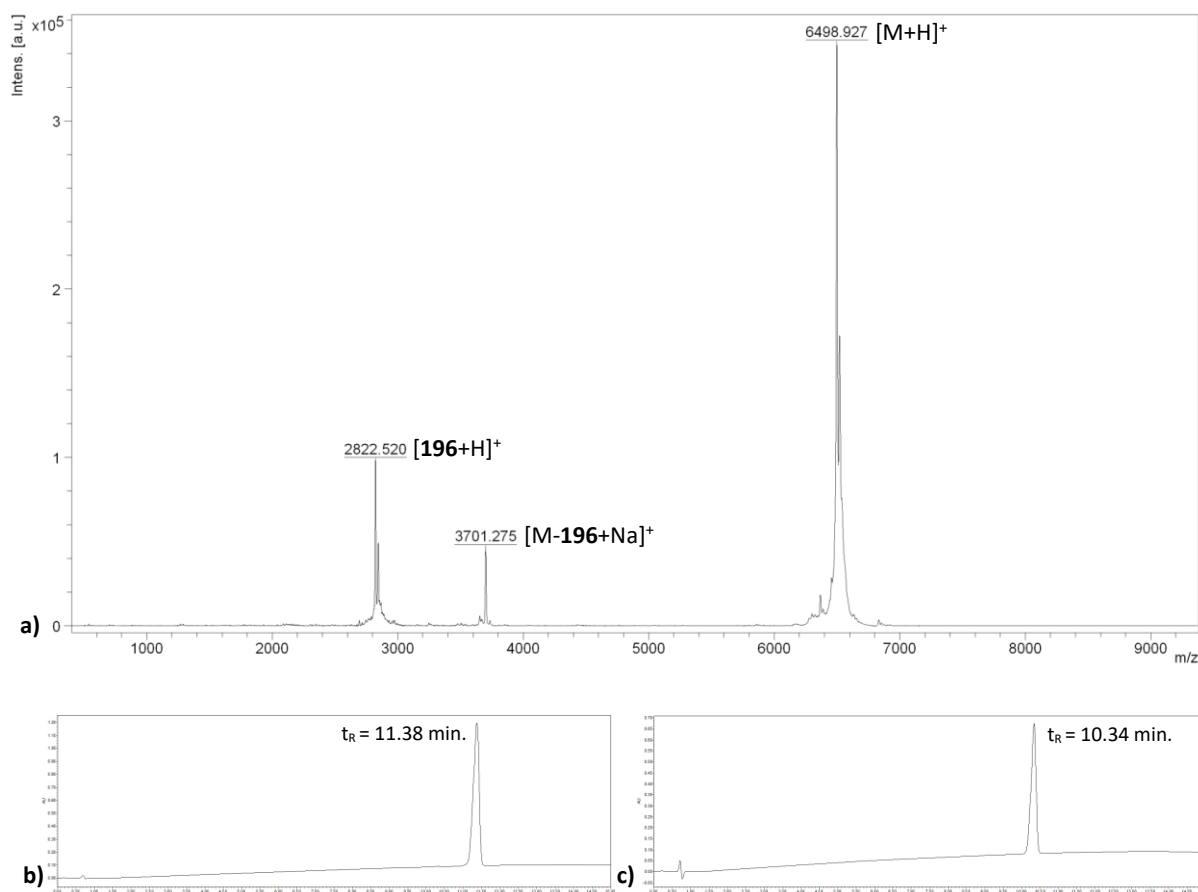
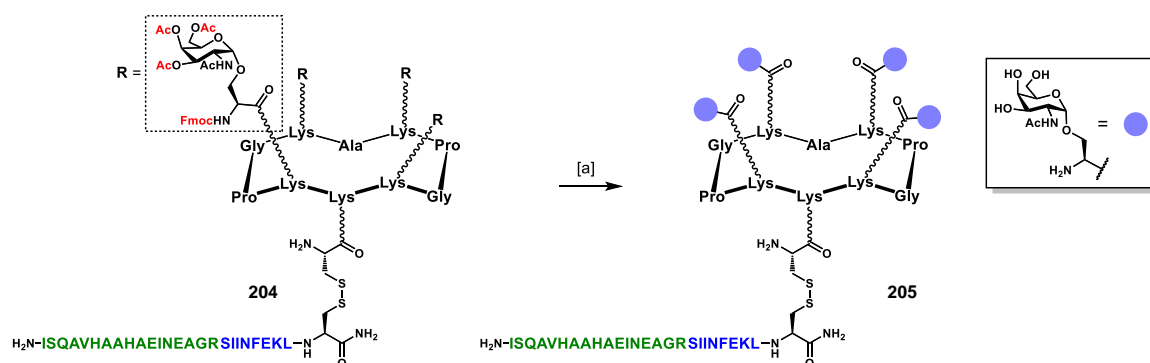


**Figure 86.** a) MALDI-TOF spectrum of **204**.  $m/z$  calcd. for  $[M+H]^+$ : 6498.1 (average), found: 6498.9.  $m/z$  calcd. for  $[M-196+Na]^+$ : 3700.9 (average), found: 3701.3.  $m/z$  calcd. for  $[196+H]^+$ : 2822.2 (average), found: 2822.5. b) Analytical RP-HPLC profile ( $\lambda=214$  nm, 5-100 solv.B in 15') of **203**. c) Analytical RP-HPLC profile ( $\lambda=214$  nm, 5-100 solv.B in 15') of **204**.

In an attempt to reduce the number of manipulations for the final deprotection of Fmoc and *O*-acetyl protecting groups, we treated compound **204** under Zemplén conditions overnight to induce its complete deprotection (Scheme 51). Nevertheless, this protocol did not result sufficiently efficient, indeed UPLC-MS analysis showed the presence of partially deprotected intermediates where Fmoc groups were still present, affording final compound **205** in 43% yield. Fmoc-protected intermediates were collected during preparative RP-HPLC and treated with a 5% piperidine in DMF solution for 20 minutes, allowing the recovery of a second batch of compound **205** (62% overall yield, including the former deprotection).



**Scheme 51.** Synthesis of compound **205**. Conditions: [a] MeONa/MeOH (pH $\approx$ 10), r.t., overnight, 43% yield.

As observed for compound **204** (Figure 86), despite the collection of a single peak during RP-HPLC purification (Figure 87a), MALDI spectrum of **205** also exhibited signals relative to its reduced cysteine-containing partners (Figure 87b).

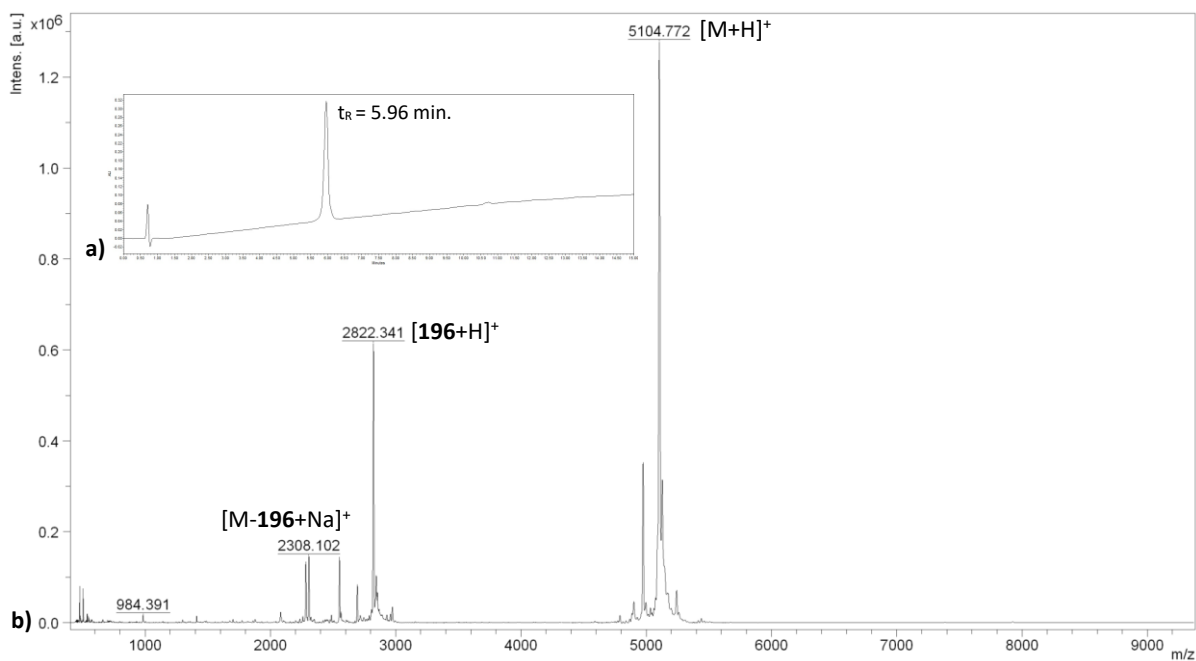
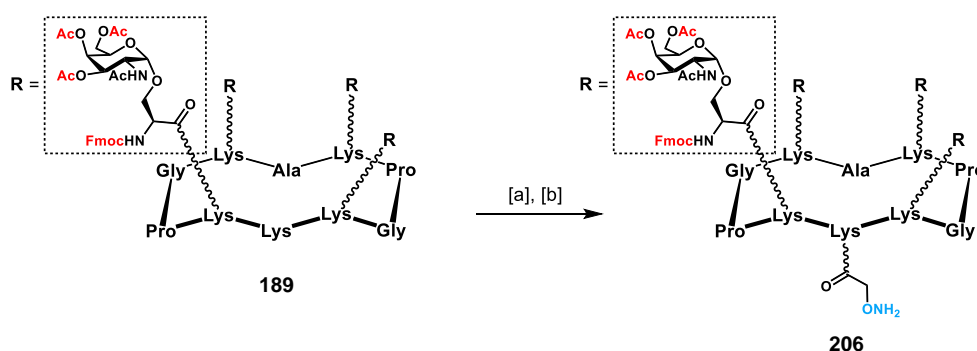


**Figure 87.** a) Analytical RP-HPLC profile ( $\lambda=214$  nm, 5-80 solv.B in 15') of **205**. b) MALDI-TOF spectrum of **205**.  $m/z$  calcd. for  $[\text{M}+\text{H}]^+$ : 5104.7 (average), found: 5104.8.  $m/z$  calcd. for  $[\text{196}+\text{H}]^+$ : 2822.2 (average), found: 2822.3.  $m/z$  calcd. for  $[\text{M}-\text{196}+\text{Na}]^+$ : 2307.5 (average), found: 2308.1.



### IV.3.3.2. Towards the synthesis of hexadecaivalent, (Ser)Tn-bearing, fully synthetic anti-cancer vaccine prototype 210

As for the above described synthesis of tetravalent (Ser)Tn-displaying vaccine prototype **205**, the designed synthetic route for our last three-component vaccine construct started from key intermediate **189** (Scheme 40). The latter was reacted with Boc-aminoxyacetic acid *N*-hydroxysuccinimide ester<sup>346</sup> in DMF, in the presence of DIPEA, to install a Boc-protected aminoxy function in the lower domain of the scaffold (Scheme 52). The reaction mixture was concentrated to dryness under high vacuum, and the resulting crude compound treated with a TFA/NH<sub>2</sub>OH/CH<sub>2</sub>Cl<sub>2</sub> (50:2:48) cocktail for Boc removal from the aminoxy moiety. Aminoxy-bearing compound **206** was obtained as a white powder in 78% yield over two steps, after RP-HPLC purification and lyophilization (Figure 88).



**Scheme 52.** Synthesis of compound **206**. Conditions: [a] Boc-aminoxyacetic acid *N*-hydroxysuccinimide ester (1.2 eq.), DIPEA (1.5 eq.), DMF, r.t., 30 min., [b] TFA/NH<sub>2</sub>OH/CH<sub>2</sub>Cl<sub>2</sub> (50:2:48), r.t., 30 min., 78% over two steps.

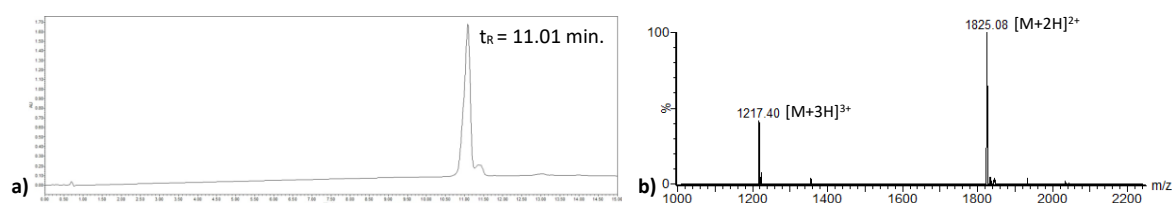
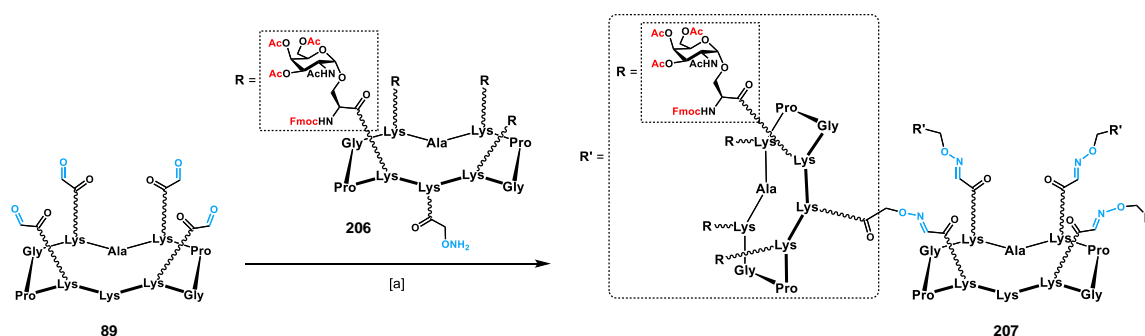


**Figure 88.** a) Analytical RP-HPLC profile ( $\lambda=214$  nm, 5-100 solv.B in 15') of **206**. b) ESI<sup>+</sup>-MS spectrum of **206**.  $m/z$  calcd. for [M+2H]<sup>2+</sup>: 1824.9 (average), found: 1825.1; calcd. for [M+3H]<sup>3+</sup>: 1216.9, found: 1217.4.

Aldehyde-bearing, tetravalent “core” scaffold **89** was reacted with freshly prepared compound **206** under oxime ligation conditions (Scheme 53). Due to the low polarity of intermediate **206**, the H<sub>2</sub>O/CH<sub>3</sub>CN ratio of the 0.1% TFA solvent mixture was adjusted to 1:9; under these conditions, and

upon heating at 37°C, the expected product **207** was readily formed in 69% yield after preparative RP-HPLC and lyophilization.



**Scheme 53.** Synthesis of compound **207** through oxime ligation. Conditions: [a] **89**, **206** (6.0 eq.), 0.1% TFA in H<sub>2</sub>O/CH<sub>3</sub>CN (1:9), 37°C, 60 min., 69% yield.

MALDI analysis of oxime-containing compound **207** showed the presence of the expected monocharged ion, along with fragmentation signals relative to the breaking of one or more oxime bonds (Figure 89).

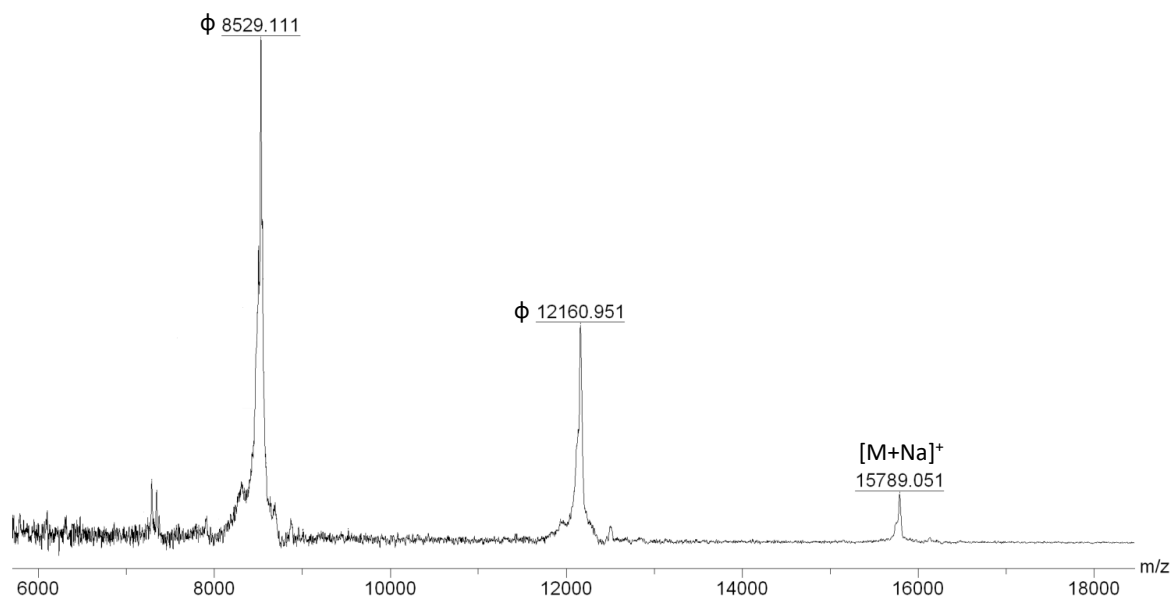
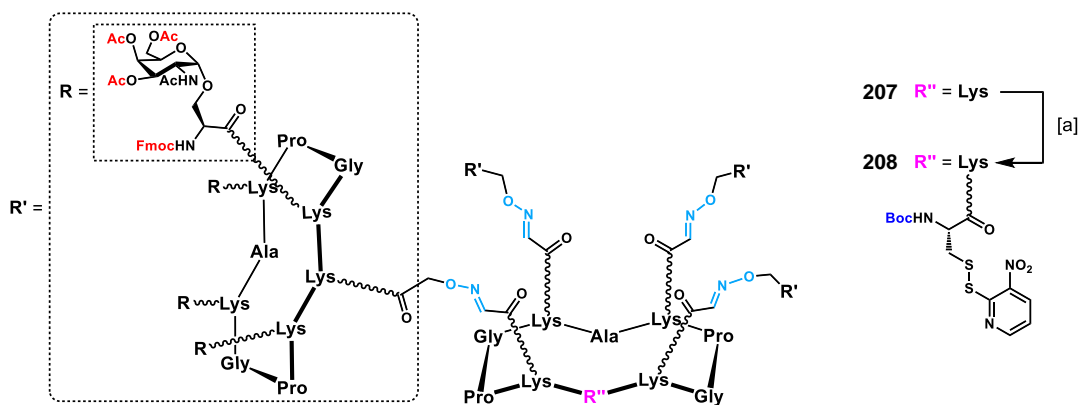


**Figure 89.** a) MALDI-TOF spectrum of **207**.  $m/z$  calcd. for  $[M+Na]^+$ : 15786.5 (average), found: 15789.1. ( $\phi$  = fragmentation)

The subsequent attachment of the Boc-Cys(NPys) moiety to the lower domain of scaffold **207** proceeded under classic conditions, by using DMF as solvent and DIPEA as base (Scheme 54). Compound **208** was obtained in 62% yield after RP-HPLC purification and lyophilization (Figure 90).



**Scheme 54.** Synthesis of Cys(NPys)-containing compound **208**. Conditions: [a] **197** (1.5 eq.), DIPEA (2.15 eq.), DMF, r.t., 30 min., 62% yield.

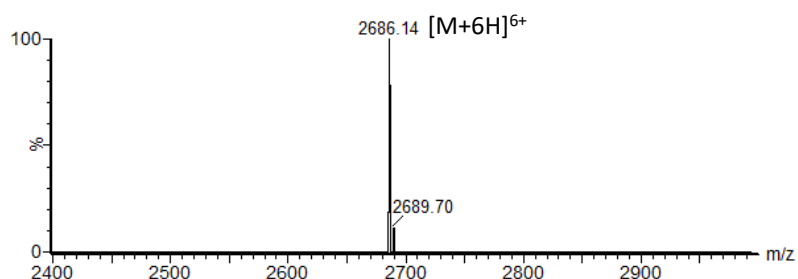
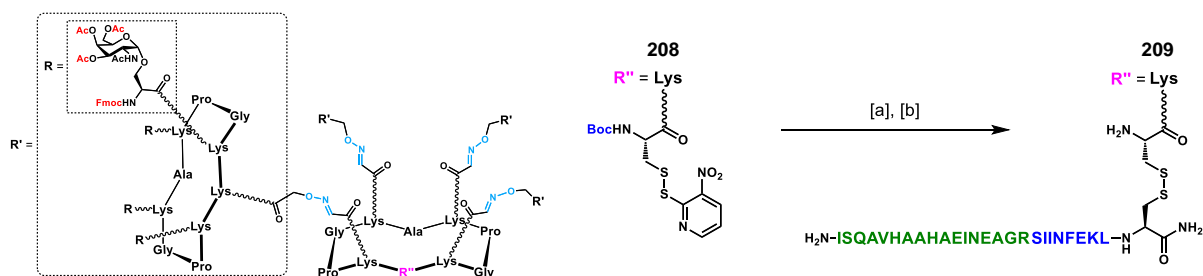


**Figure 90.** ESI<sup>+</sup>-MS of **208** (zoom).  $m/z$  calcd. for  $[M+6H]^{6+}$ : 2686.1 (monoisotopic), found: 2686.1.

Even in this case, we were obliged to keep Fmoc and *O*-acetyl protecting groups to selectively introduce one copy of Cys(NPys) at the selected position. The following steps involved the disulfide bridging between intermediate **208** and cysteine-containing peptide **196** (Scheme 44), under similar conditions to those reported for the synthesis of compound **204** (Scheme 50). Compound **209** was obtained as white foamy solid after RP-HPLC purification and lyophilization (Scheme 55, figure 91).



**Scheme 55.** Synthesis of compound **209** via disulfide bridging. Conditions: [a] 50% TFA/CH<sub>2</sub>Cl<sub>2</sub>, r.t., 30 min.; [b] **196** (1.1 eq.), DMF/NaOAc buffer (pH 4.5, 40 mM) (2:1), r.t., 30 min, 62% yield over two steps.

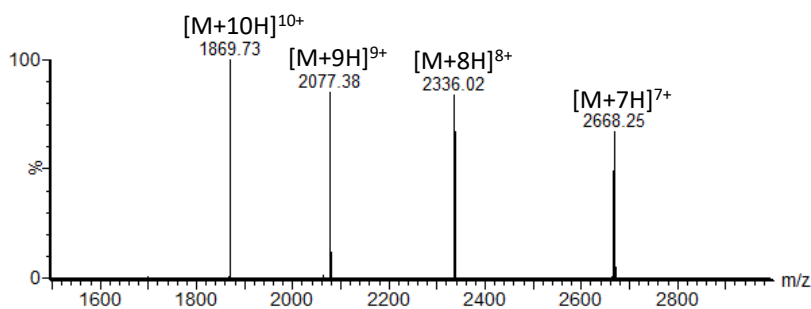
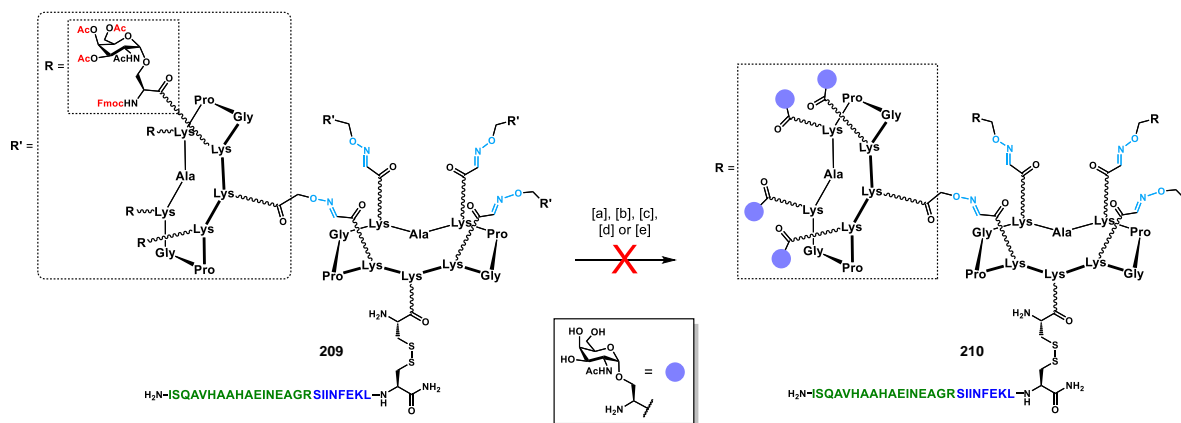


**Figure 91.** ESI<sup>+</sup>-MS of **209** (zoom). *m/z* calcd. for [M+7H]<sup>7+</sup>: 2670.8 (average), found: 2668.3; calcd. for [M+8H]<sup>8+</sup>: 2336.6, found: 2336.0; calcd. for [M+9H]<sup>9+</sup>: 2077.1, found: 2077.4; calcd. for [M+10H]<sup>10+</sup>: 1869.5, found: 1869.7.

With compound **209** in hand, we proceeded towards the Fmoc and *O*-acetyl protecting groups removal in order to obtain the target hexadecaivalent vaccine prototype **210** containing the serine-displayed Tn epitope (Scheme 56).

In a first attempt, owing to the incomplete deprotection observed for compound **205** (Scheme 51), we decided to perform the piperidine-mediated Fmoc deprotection as first step, and subsequently cleave *O*-acetyl groups under Zemplén conditions. Compound **209** was thus dissolved in MeOH and, after 10 minutes stirring in the presence of piperidine (2 equivalents per Fmoc group), UPLC-MS analysis showed an irregular, multi-peaks chromatographic profile and incoherent mass signals, suggesting product decomposition. We thus reconsidered the aforementioned protocol based on Zemplén conditions (Scheme 51), unfortunately the deprotection was sluggish, and UPLC-MS analyses showed again unclear profiles, progressively leading to decomposition of compound **209** rather than deprotection. Treatment with potassium carbonate (20 mM in MeOH) showed similar results to those reported for the Zemplén protocol. Aqueous hydrochloric acid treatment resulted in a sluggish and incomplete *O*-acetyl deprotection, showing a crowded, multi-peak chromatographic profile. The last procedure that we tested, involved the utilization of a 50% solution of methylhydrazine in methanol. After 30 minutes reaction at room temperature, UPLC-MS analysis showed a cleaner chromatogram, and ESI<sup>+</sup>-MS analysis suggested the presence of multicharged ions that could be attributed to compound **210**. Nevertheless it was not possible to isolate the target compound since it rapidly decomposed.



**Scheme 56.** Attempt of deprotection of compound **209**. Conditions: [a] Piperidine (32 eq.), [b] NaOMe (pH 10), [c]  $K_2CO_3$  (20 mM), [d] 37% aq. HCl (50% v/v), [e] MeHN $NH_2$  (50% v/v). Reactions were carried out in MeOH at 0.1-1 mM concentrations of **209**, at room temperature. Their evolutions were monitored *via* UPLC-MS at t = 10, 30, 60, 120 min., to overnight.

Given the difficulties encountered in obtaining final compound **210** we decided to design a different synthetic pathway to reach hexadeca-valent, (Ser)Tn-displaying, three-components synthetic vaccine prototype (Figure 80c).

### IV.3.3.3. Alternative synthesis of hexadeca-valent (Ser)Tn-bearing, fully synthetic anti-cancer vaccine prototype

#### IV.3.3.3.1. Synthetic strategy

The weak points of the synthetic route described in the former section mainly involve two related aspects. The first relies on the need to manipulate the (Ser)Tn glycocluster in its fully protected form until the late steps of the synthetic pathway, whose low polarity implies long and solvent-consuming purifications with inherent loss of product, impacting the ease of manipulation. The second aspect concerns the presence of oxime bonds, employed for the conjugation of peripheral glycosylated arm on the “core” scaffold, which are likely to be incompatible with the common basic conditions employed for the deprotection of Fmoc and *O*-acetyl moieties.

Therefore we designed an alternative fully synthetic vaccine prototype, by replacing oxime linkers with the more stable 1,4-triazole function (**211**, Figure 92).

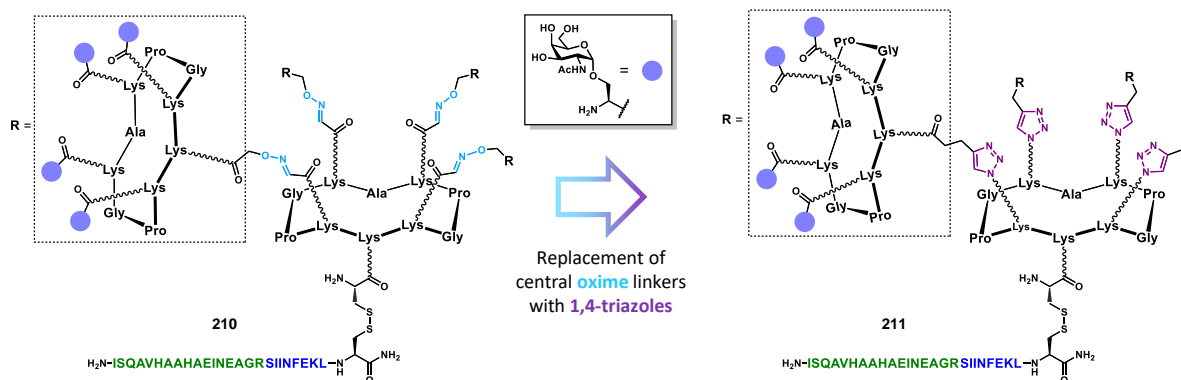


**Figure 92.** We designed a synthetic strategy for obtaining vaccine prototype **211**, having 1,4-triazole functions *in lieu* of oxime bonds.

Since this modification involves an “internal” part of the final glycodendrimer structure, the binding capacity of the B-cell epitope moiety should not be affected. Thus, compound **211** represents to us a good candidate as vaccine prototype, with similar structural features to oxime-containing compound **193** (Figure 78).

Moreover, in contrast to **210**, the alternative structure **211**, featuring internal triazole linkers, allows to be assembled in a convergent manner, making the synthesis more elegant and enabling the deprotection of Fmoc and *O*-acetyl groups at an earlier stage of the synthetic pathway (Figure 93).

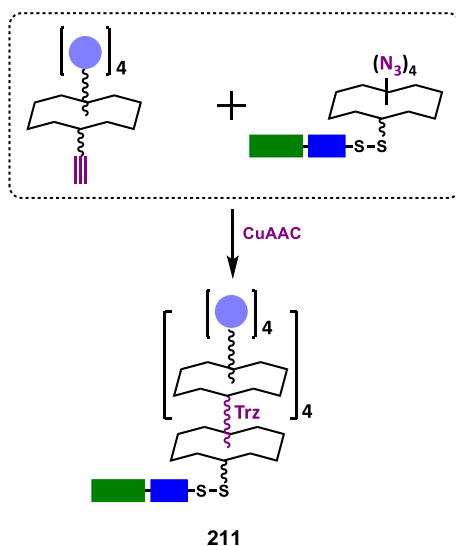
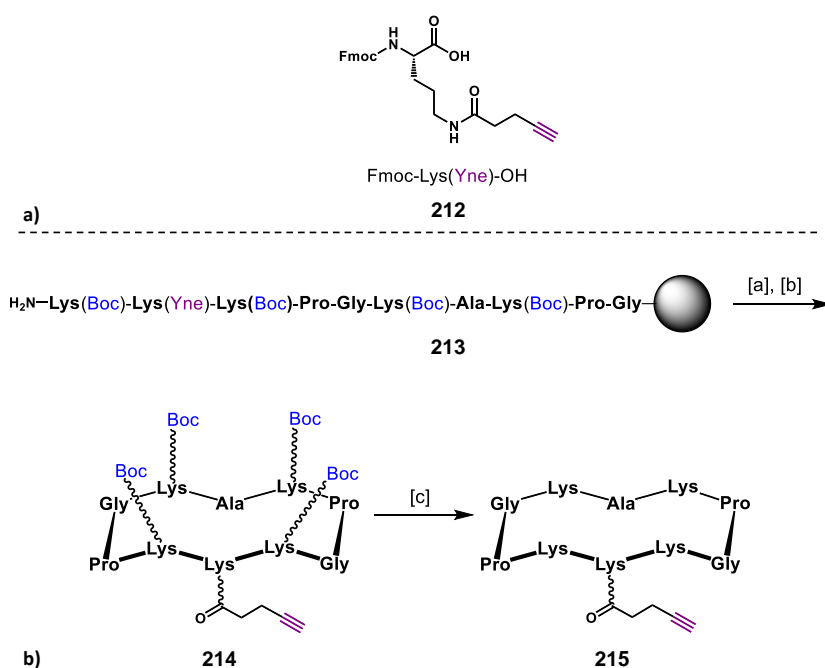


**Figure 93.** Convergent pathway for the synthesis of vaccine prototype **211**.

### IV.3.3.3.2. Convergent assembly of hexadecaivalent, (Ser)Tn-bearing, fully synthetic anti-cancer vaccine prototype **211**

Peptide sequence **213** (Scheme 57b) was obtained by including the alkyne-containing building block **212** (referred as Fmoc-Lys(Yne)-OH, scheme 57a).<sup>426</sup> Cleavage from the resin under mild acidic conditions followed by cyclization in solution, afforded cyclopeptide **214** in 51% overall yield. Subsequent deprotection of the Boc moiety by treatment with 50% TFA in CH<sub>2</sub>Cl<sub>2</sub> solution, afforded RAFT **215**, bearing four amino residues on the upper domain of the scaffold, and a terminal alkyne residue in the lower domain (Scheme 57b, figure 94).



**Scheme 57.** a) Alkyne-containing lysine building block **122**. b) Synthesis of scaffold **215**. Conditions: [a] 1% TFA, CH<sub>2</sub>Cl<sub>2</sub>; [b] PyBOP (1.2 eq.), DIPEA (2.0 eq.), DMF/ CH<sub>2</sub>Cl<sub>2</sub> (1:1), 0.5 mM, r.t., 30 min., 51% overall yield; [c] 50% TFA in CH<sub>2</sub>Cl<sub>2</sub>, r.t., 30 min., 92%.

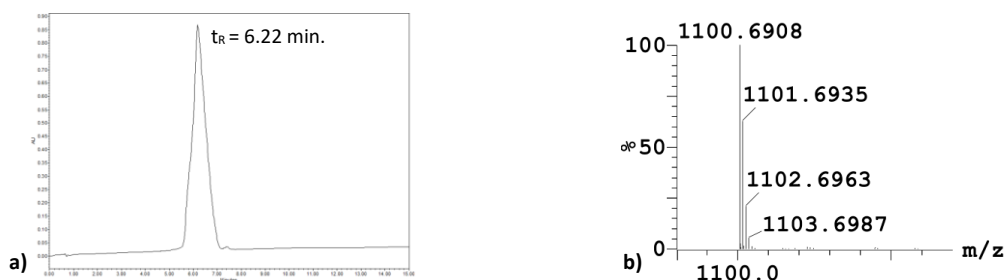
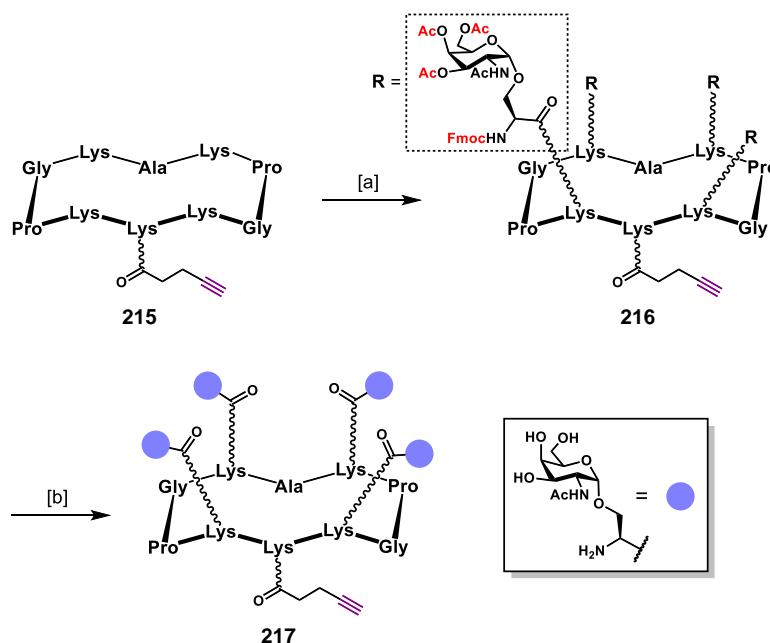


**Figure 94.** a) Analytical RP-HPLC profile ( $\lambda=214 \text{ nm}$ , 0-20 solv.B in 15') of **215**. b) HRMS (ESI<sup>+</sup>-TOF) of **215** (zoom).  $m/z$  calcd. for  $[\text{M}+\text{H}]^+$ : 1100.6944 (monoisotopic), found: 1100.6908.

Scaffold **215** was then reacted with building block **188** (Figure 73) in DMF, in the presence of PyBOP® as activating agent and DIPEA as base (Scheme 58). Compound **216** was obtained in 82% yield after preparative RP-HPLC and lyophilization. The deprotection of Fmoc and *O*-acetyl groups was performed by dissolving **216** in MeOH, in the presence of 32 equivalents of methylhydrazine. After stirring overnight at room temperature, desired fully deprotected glycoconjugate **217** was isolated in 72% yield (Scheme 58, figure 95).



**Scheme 58.** Synthesis of alkyne-bearing glycocluster **217**. Conditions: [a] **188** (4.8 eq.), DIPEA (6.0 eq.), PyBOP (5.0 eq.) DMF, r.t., 30 min., 82%; [b] MeHNNH<sub>2</sub> (32 eq.), dry MeOH, r.t., overnight, 72%.

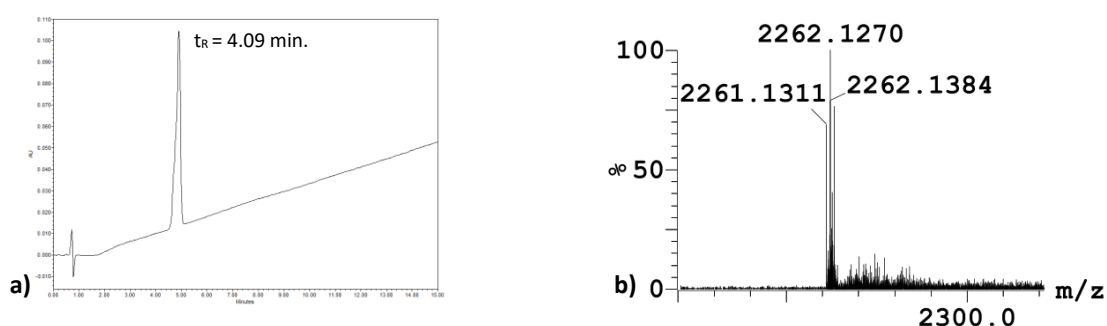
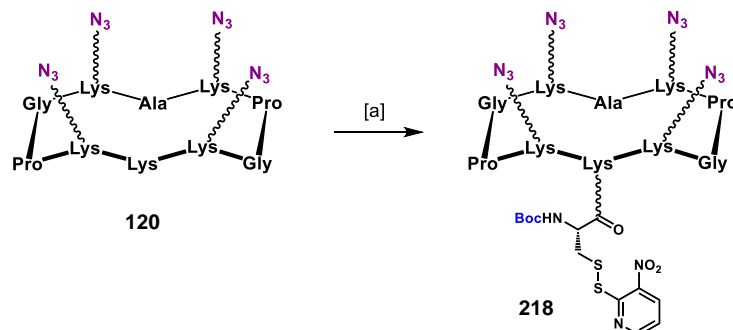


**Figure 95.** a) Analytical RP-HPLC profile ( $\lambda=214$  nm, 0-40 solv.B in 15') of **217**. b) HRMS (ESI<sup>+</sup>-TOF) of **217** (zoom).  $m/z$  calcd. for [M+H]<sup>+</sup>: 2261.1400 (monoisotopic), found: 2261.1311.

According to our convergent strategy (Figure 93), once obtained compound **217**, which serves as peripheral glycosylated “arm”, we undertook the synthesis of a central “core” scaffold, previously functionalized with the immunostimulant peptide sequence **196** (Scheme 44).



Compound **120** (Scheme 23) was functionalised with Boc-Cys(NPys)-OSu (**197**) in DMF, in the presence of DIPEA as base, to give compound **218** in 71% yield after RP-HPLC purification and lyophilization (Scheme 59, Figure 96).



**Scheme 59.** Synthesis of Cys(NPys)-containing compound **218**. Conditions: [a] **197** (1.5 eq.), DIPEA (1.5 eq.), DMF, r.t., 30 min., 71% yield.

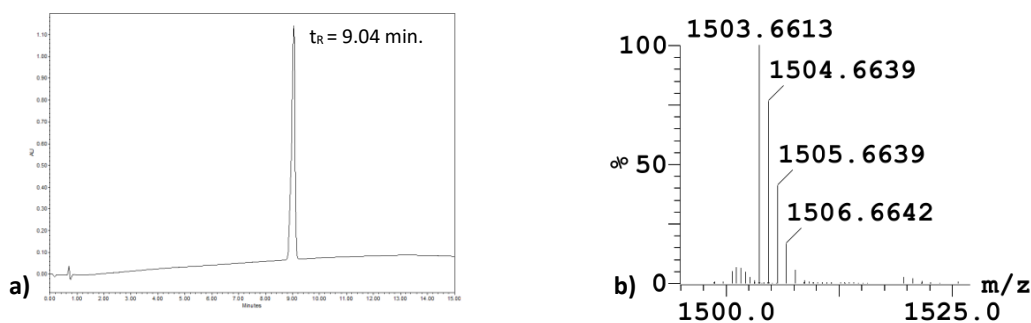
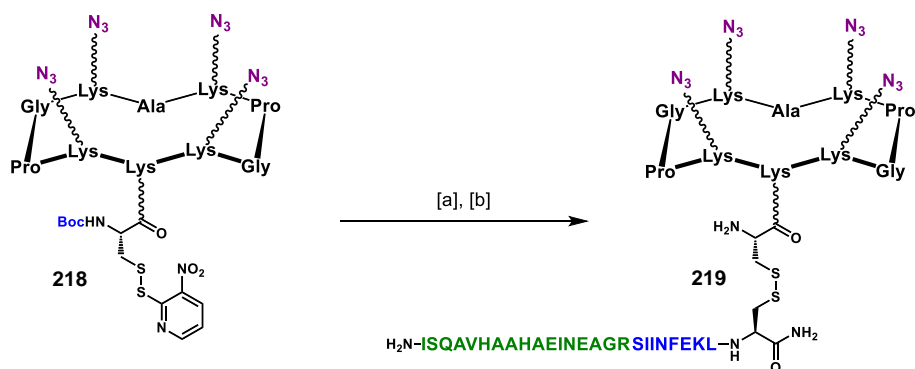


**Figure 96.** a) Analytical RP-HPLC profile ( $\lambda=214 \text{ nm}$ , 0-20 solv.B in 15') of **218**. b) HRMS (ESI<sup>+</sup>-TOF) of **218** (zoom).  $m/z$  calcd. for  $[M+Na]^+$ : 1503.6575 (monoisotopic), found: 1503.6613.

Disulfide bridging between freshly prepared scaffold **218** and cysteine-containing OVA sequence **196** (Scheme 44) was performed under classic conditions. First, treatment with a 50% TFA in  $\text{CH}_2\text{Cl}_2$  solution caused the Boc protecting group removal, confirmed by HRMS data (Scheme 60). The second step was performed dissolving **218** in a previously degassed DMF/AcONa buffer (pH 4.5, 40 mM) (2:1). Addition of a DMF solution containing peptide **196**, caused the instantaneous yellow coloration of the reaction mixture, and UPLC-MS analysis revealed complete conversion after 30 minutes stirring at room temperature. OVA-containing “core” scaffold **219** was isolated in 85% yield over two steps, after preparative RP-HPLC and lyophilization (Scheme 60, figure 97).



**Scheme 60.** Synthesis of OVA-containing “core” scaffold **219**. Conditions: [a] 50% TFA/CH<sub>2</sub>Cl<sub>2</sub>, r.t., 30 min.; [b] **196** (1.1 eq.), DMF/NaOAc buffer (pH 4.5, 40 mM) (2:1), r.t., 30 min, 85% yield over two steps.

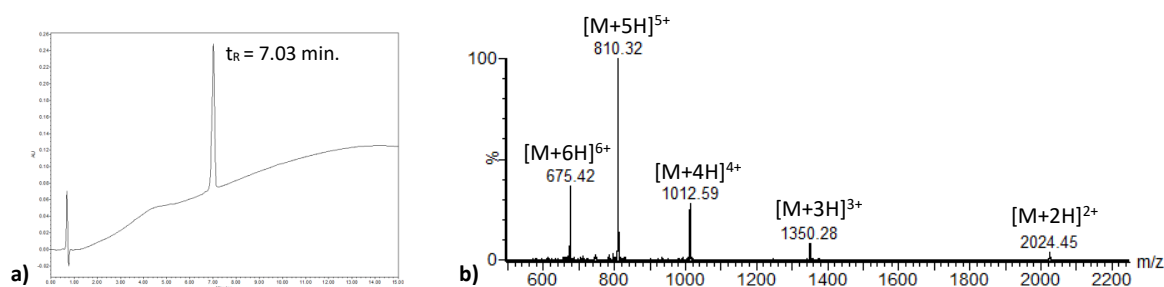
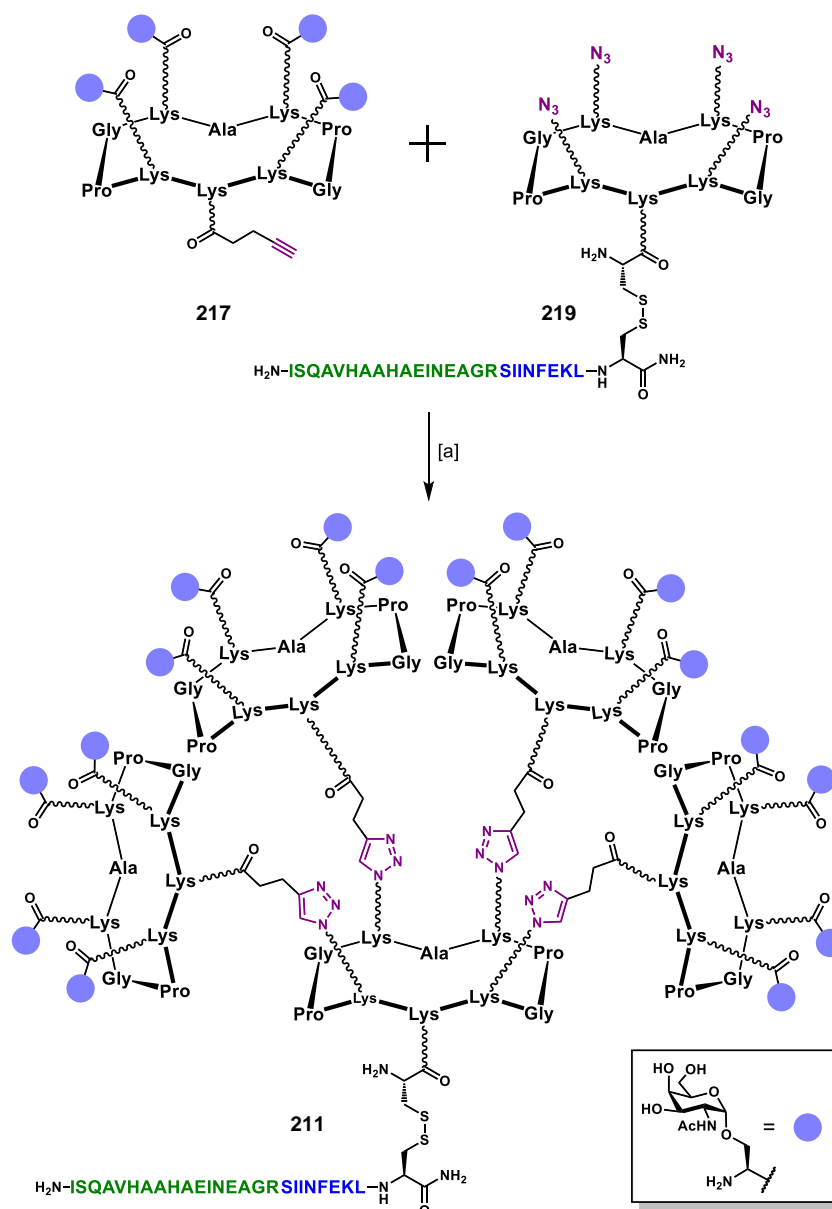


**Figure 97.** a) Analytical RP-HPLC profile ( $\lambda=214$  nm, 5-100 solv.B in 15') of **219**. b) ESI<sup>+</sup>-MS spectrum of **219**.  $m/z$  calcd. for [M+2H]<sup>2+</sup>: 2024.3 (average), found: 2024.5; calcd. for [M+3H]<sup>3+</sup>: 1349.9, found: 1350.3; calcd. for [M+4H]<sup>4+</sup>: 1012.6, found: 1012.6; calcd. for [M+5H]<sup>5+</sup>: 810.3, found: 810.3; calcd. for [M+6H]<sup>6+</sup>: 675.4, found: 675.4.

With compounds **217** and **219** in hand, representing our glycosylated “arms” and OVA-bearing “core” scaffolds, respectively, we were ready to perform the final copper(i)-catalyzed alkyne-azide cycloaddition to reach target vaccine prototype **211** (Figure 93).

Even though performing CuAAC in the presence of sodium ascorbate could also lead to disulfide bridge reduction,<sup>427</sup> we decided to perform the reaction under our standard conditions to assess its feasibility (Scheme 61). Thus, compounds **217** and **219** were dissolved in a previously degassed DMF/PBS (pH 7.4, 10 mM) mixture, in the presence of copper sulphate, THPTA and sodium ascorbate. Even though UPLC-MS analyses, performed at  $t = 1$  h and  $t = 2$  h showed an increased formation of by-products, target compound **211** was isolated, after RP-HPLC purification and lyophilization, in a good 75% yield (Figure 98-99).



**Scheme 61.** Convergent assembly of fully synthetic vaccine prototype **211** by CuAAC. Conditions: [a] **219**, **217** (5.0 eq.), THPTA (10 eq.), CuSO<sub>4</sub> (cat.), Na ascorbate (30 eq.), DMF, PBS (pH 7.4, 10 mM), r.t., 2 h, 75%.

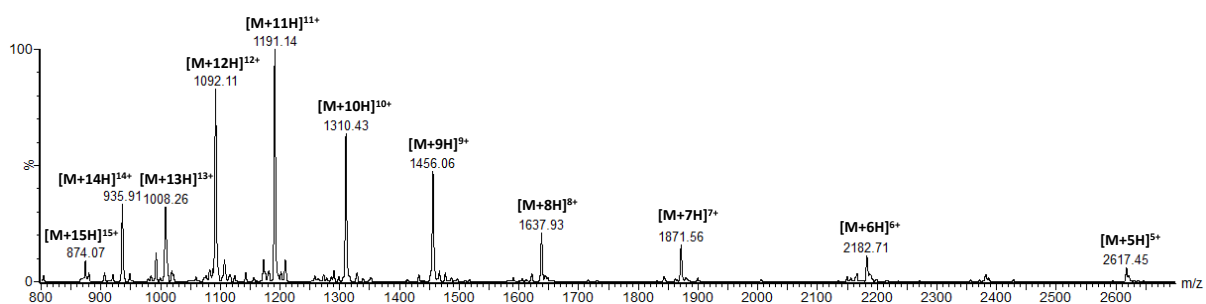


**Figure 98.** ESI<sup>+</sup>-MS spectrum of **211**. *m/z* calcd. for [M+5H]<sup>5+</sup>: 2619.5 (average), found: 2617.5; calcd. for [M+6H]<sup>6+</sup>: 2183.0, found: 2182.7; calcd. for [M+7H]<sup>7+</sup>: 1871.3, found: 1871.6; calcd. for [M+8H]<sup>8+</sup>: 1637.5, found: 1638.0; calcd. for [M+9H]<sup>9+</sup>: 1455.7, found: 1456.1; calcd. for [M+10H]<sup>10+</sup>: 1310.2, found: 1310.4; calcd. for [M+11H]<sup>11+</sup>: 1191.2, found: 1191.1; calcd. for [M+12H]<sup>12+</sup>: 1092.0, found: 1092.1; calcd. for [M+13H]<sup>13+</sup>: 1008.1, found: 1008.3; calcd. for [M+14H]<sup>14+</sup>: 936.2, found: 935.9; calcd. for [M+15H]<sup>15+</sup>: 873.8, found: 874.1.

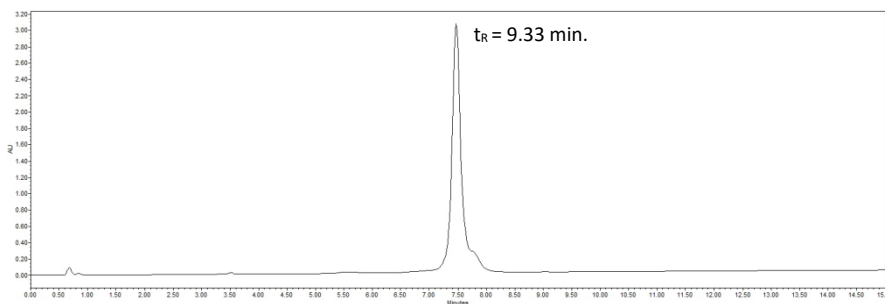


**Figure 99.** Analytical RP-HPLC profile ( $\lambda=214$  nm, 5-60% solv.B in 15') of **211**.

In conclusion, hexadecavalent (OX)Tn- and (Ser)Tn-bearing synthetic vaccines **201** (Scheme 48) and **211** (Scheme 61), respectively, have been successfully synthesized along with their tetravalent homologues (**199**, scheme 46, and **205**, scheme 51). The immunological properties of these compounds will be evaluated in OVA-transfected mice models, in collaboration with Dr. Fernández-Tejada's research group.

**V.**

## **Conclusions and Outlook**

The objective of this work was to design and synthesize fully synthetic anticancer vaccine prototypes with improved immunological properties. On the basis of the previous results obtained by our research group we directed our efforts for the construction of new generations of prototypes focussing on two aspects: (i) the enhanced density of saccharide epitopes and (ii) their heterogeneous display.

In the first part of this manuscript (**Chapter II**) we focused our attention on the synthesis of multivalent homo-glycodendrimers, which represent our module of choice for the presentation of saccharide B-cell epitopes. To prevent the misuse of TACAs, which are harder to functionalize compared to simple monosaccharides, all our syntheses have been developed by using mannose, which is also relevant for other biological processes. We firstly reported the synthesis of mannose-based hexadecavalent glycodendrimers following an iterative, oxime-based approach. The resulting mannosylated compounds have been tested in parallel with several targets to emphasize our synthetic efforts. We did not report these results for reasons of brevity, but briefly, these mannose-based glycodendrimers showed interesting binding activities towards DC-SIGN receptors, in the context of a collaboration with Prof. Fieschi, and served for the construction of a synthetic anti-HIV vaccine, in collaboration with Dr. Chebloune. The above-mentioned synthetic strategy allowed the straightforward construction of (OX)Tn-based glycodendrimers, which can be further functionalized to reach fully synthetic vaccine structures. We next reported a chemoselective strategy combining oxime ligation and CuAAC for the synthesis of (TRZ)Tn-based glycodendrimers, allowing a controlled assembly of hexadecavalent structures in both divergent and convergent fashion, which was not possible with the previous methods employed in our laboratory. The biological properties of the abovementioned glycodendrimers (containing the GalNAc moiety, *i.e.* saccharide part of Tn antigen) were evaluated through their binding activity towards the SBA lectin, showing the influence of saccharide orientation and valency. We then explored the synthesis and the biological properties of a new small family of mannose-based glycodendrimers with valencies ranging from four to twenty-four. One of these structures showed the highest binding potency for a monodisperse entity towards the bacterial lectin BC2L-A, reaching dissociation constants in the nanomolar range.

The second part of this manuscript (**Chapter III**) has been devoted to the synthesis of multivalent hetero-glycodendrimers grafted with (OX)Tn and (TRZ)TF epitopes. This route was represented by considerable synthetic efforts, involving multi-step procedures which required the preparation and characterization of several key building blocks, equipped with appropriate orthogonal functionalities. Through a multi-modal divergent protocol, we achieved the controlled assembly of multivalent di-topic scaffolds, with aldehyde and azide groups displayed in both separated and shuffled manners. The sequential one-pot decoration of these scaffolds with (OX)Tn and (TRZ)TF moieties, *via*

OL and CuAAC, led to unprecedented macromolecules which can be readily modified to obtain hetero-multivalent fully synthetic vaccines.

In the third part of the manuscript (**Chapter IV**) we first disclosed preliminary results involving the interaction of the presented (OX)Tn/(TRZ)TF homo- and hetero-glycoclusters towards specific anti-Tn and anti-TF mAbs. Results suggested the absence of interference phenomena for the recognition of the (OX)Tn epitope by the anti-Tn mAb 9A7 in the presence of the (TRZ)TF epitope; although the negative outcomes obtained by performing the same assays with anti-TF mAb JAA-F11 needed insights which cannot be undertaken due to time constraints. We next exploited the anti-Tn mAb 9A7 to compare the binding activities of (OX)Tn- and (Ser)Tn-based hexadecavalent glycodendrimers and tetravalent glycoclusters. The similar extent of interaction of these two multivalent structures suggested the validity of our (OX)Tn analogue to mimic the native (Ser)Tn antigen presentation modality, and highlighted the impact of an enhanced valency when tetravalent compounds were compared to their hexadecavalent analogues.

Finally, we reported the synthesis of both tetravalent and hexadecavalent fully synthetic, three-component, vaccine prototypes based on (OX)Tn or (Ser)Tn epitopes, associated to OVA-derived CD4<sup>+</sup> and CD8<sup>+</sup> peptide epitopes. Hexadecavalent (Ser)Tn-based vaccine prototypes resulted much more difficult to obtain, compared to their (OX)Tn analogues. This prompted us to design an alternative synthetic strategy which demonstrated effective, and extended the panel of methodologies for the construction of complex biomolecular systems.

The new generation of anticancer vaccine prototypes, with enhanced density of saccharide epitopes, will be evaluated in mice models, in collaboration with Dr. Fernández-Tejada.

As emphasized in the introduction (**Chapter I**), there are many aspects which should be considered in designing fully synthetic anticancer vaccines. The modular approaches for their construction allow tailoring design aspects on each subunit, giving access to a large variety of parameters. In the present work we focused our attention on the B-cell epitope presentation, by enhancing the saccharide antigens density and providing a heterogenic epitope display. In this scenario the future perspectives that can be envisaged involve the introduction of more complex TACAs as B-cell epitopes (*e.g.* STn, globo-H, GM2...), as well as minimal glycosylated MUC-1 sequences, since several studies demonstrated the importance of the oligopeptide sequence on which the carbohydrate epitope is displayed. The current improved understanding in specific immune activation provided by adjuvants allows for a better sustain of vaccine-induced immune responses. This may provide new alternatives in adjuvant settings, overcoming the safety issues which made the use of alum so controversial. Finally, the identification of new tumor-associated markers can be of great impact not only in a diagnostic context, but also for the conception of new generations of vaccines.

Despite interesting preclinical results, and the large variety of possibilities in term of design, one main problem associated to therapeutic anticancer vaccines remains the immunocompromised condition of cancer patients. An innovative approach in the field of anticancer immunotherapy, which could represents a more straightforward way to promote the immuno-mediated clearance of cancer cells has been paved by the group of Dr. Spiegel. This approach involves the use of so-called antibody-recruiting molecules: bi-functional entities whereby the first module recognizes and binds to cancer cells and the second interacts with naturally occurring IgG antibodies, redirecting the humoral immune response against targeted transformed cells. This represents a more straightforward strategy than an immunization protocol, since it does not require the immune system to mount an *ex novo* immune response, but exploits antibodies which are constitutively present in our bloodstream. The synthetic methodologies developed in the course of my PhD project can be exploited for reaching such bi-functional constructs, contributing for this new avenue in chemical immunology.



## **VI.**

# **Materials and methods**

## VI.1. Equipment

### VI.1.1. High performance liquid chromatography (HPLC)

- Analytical RP-HPLC was performed on a Waters Alliance 2695 separation module, equipped with a Waters 2489 UV/visible detector. Analyses were carried out at  $1.23 \text{ mL}\cdot\text{min}^{-1}$  (Interchim UPTISPHERE X-SERIE,  $\text{C}_{18}$ ,  $5 \mu\text{m}$ ,  $125\times 3.0 \text{ mm}$ ) with UV monitoring at 214 nm and 250 nm, using a linear A–B gradient (A: 0.1%  $\text{CF}_3\text{CO}_2\text{H}$  in water; B: 0.1%  $\text{CF}_3\text{CO}_2\text{H}$  in 90% aq. acetonitrile).
- Preparative RP-HPLC was performed on Gilson GX 281 equipped with a fraction collector, or on Waters equipment composed by a Waters 600 controller and a Waters 2487 Dual Absorbance Detector. Purifications were carried out at  $22.0 \text{ mL}\cdot\text{min}^{-1}$  (Macherey-Nagel VP,  $\text{C}_{18}$ ,  $7 \mu\text{m}$ ,  $300 \text{ \AA}$ ,  $250\times 21 \text{ mm}$ ) with UV monitoring at 214 nm and 250 nm, using a linear A–B gradient.
- Analytical RP-UPLC (coupled with ESI-MS) was performed on a Waters Acquity UPLC system. Analyses were carried out at  $0.6 \text{ mL}/\text{min}$  (Phenomenex WIDEPORÉ XB,  $\text{C}_{18}$ ,  $3.6 \mu\text{m}$ ,  $300 \text{ \AA}$ ,  $50\times 2.1 \text{ mm}$ ) with UV monitoring at 214 nm, using a linear C–D gradient (C: 0.1%  $\text{CH}_2\text{O}_2$  in water; D: 0.1%  $\text{CH}_2\text{O}_2$  in acetonitrile).

### VI.1.2. Mass spectrometry (MS)

- ESI-MS spectra were recorded on Waters Acquity UPLC-MS equipped with a SQ Detector 2.
- HRMS spectra were recorded by ICMG's mass platform service, on a Waters Xevo G2-S QToF.
- MALDI-TOF spectra were recorded by ICMG's mass platform service, on a AutoFlex I Bruker after sample pre-treatment in an OligoR3 microcolumn (Applied Biosystems, USA) using a 2,5-dihydroxybenzoic acid matrix.

### VI.1.3. Nuclear magnetic resonance (NMR)

$^1\text{H}$  and  $^{13}\text{C}$  NMR spectra were recorded on BrukerAvance 400 MHz or BrukerAvance III 500 MHz spectrometers and chemical shifts ( $\delta$ ) were reported in parts per million (ppm). Spectra were referenced to the residual proton solvent peaks relative to the signal of  $\text{CDCl}_3$  ( $\delta$  7.27 and 77.23 ppm for  $^1\text{H}$  and  $^{13}\text{C}$ ),  $\text{D}_2\text{O}$  ( $\delta$  4.79 ppm for  $^1\text{H}$ ),  $\text{CD}_3\text{OD}$  ( $\delta$  3.31 and 49.00 ppm for  $^1\text{H}$  and  $^{13}\text{C}$ ),  $\text{DMSO-d}_6$  ( $\delta$  2.50 and 39.55 ppm for  $^1\text{H}$  and  $^{13}\text{C}$ ), acetone- $\text{d}_6$  ( $\delta$  2.05 and 29.84 ppm for  $^1\text{H}$  and  $^{13}\text{C}$ ) assignments were done by GCOSY and GHMQC experiments. Standard abbreviations s, d, t, dd, br s, m, app refer to singlet, doublet, triplet, doublet of doublets, broad singlet, multiplet and apparent, respectively.

#### **VI.1.4. Circular dichroism (CD)**

CD spectra were acquired with signal averaging on a Jasco J-810 spectropolarimeter equipped with a Jasco Peltier PTC-423S temperature controller, and a baseline was recorded separately and subtracted. Far-UV spectra were recorded from 340 to 200 nm at 25 °C, in a quartz cell with 1 mm path-length. Spectra are reported as the averages of four scans and ellipticities are reported as molar ellipticity. To reduce noise, the data were smoothed with a Savitzky–Golay smoothing algorithm using a convolution window of seven data points. Spectra were acquired using solutions of glycoclusters in Milli-Q H<sub>2</sub>O at a concentration of 200 μM.

#### **VI.1.5. Molecular models**

Models in figure 57 were built using Sybyl molecular graphics editor (Certara, Munich, Germany). Starting from the crystal structure of the N<sub>3</sub>P<sub>3</sub> scaffold,<sup>372</sup> linkers were built and terminal mannose residues added either onto a model of branched peptide or onto the structure of a cyclic peptide taken from an NMR model.<sup>355</sup>

### **VI.2. Interaction assays**

#### **VI.2.1. Enzyme-linked lectin assay (ELLA)**

ELLA experiments were conducted using 96-well microtiter Nunc-Immuno plates (Maxi-Sorp) coated with 100 μL of polymeric sugar (PAA-α-N-acetyl-D-galactosamine, 5 μg·mL<sup>-1</sup>; Lectinity Holding, Inc., Moscow) diluted in carbonate buffer, pH 9.6 for 1 h at 37 °C. Excess of PAA-sugar was removed, and then wells were blocked with BSA in PBS (3% w/v, 100 μL per well) at 37 °C for 1 h. The soybean agglutinin (SBA) lectin conjugated HRP (0.1 μg·mL<sup>-1</sup>) was mixed with various concentrations of inhibitors for 1 h at 37 °C. Then the mixture was added to the PAA-sugar-coated microwells and incubated for 1 h at 37 °C. The wells were washed with T-PBS (3 × 100 μL per well) and then the colour was developed using 100 μL per well of 0.05 M phosphate/citrate buffer containing O-phenylenediamine dihydrochloride (OPD, 0.4 mg·mL<sup>-1</sup>) and urea hydrogen peroxide (0.4 mg·mL<sup>-1</sup>, Sigma-Aldrich). The reaction was quenched after 10 minutes by adding H<sub>2</sub>SO<sub>4</sub> (30% v/v, 50 μL per well). Absorbance was read at 490 nm using a microtiter plate reader (SPECTRAMax, model PLUS384, Molecular Devices). Percentage inhibition was calculated as follows: inhibition (%) = [(A<sub>max</sub> - A)/A<sub>max</sub>] × 100, where A<sub>max</sub> is the absorbance of the SBA lectin without inhibitor and A is the absorbance of the SBA lectin with inhibitor. The percentage of inhibition was plotted against log [inhibitor].

## VI.2.2. Isothermal titration microcalorimetry (ITC)

ITC experiments were performed with a PEAQ-ITC isothermal titration microcalorimeter (Malvern Instruments, Malvern, UK). The experiments were performed at 25°C. Lyophilized glycoconjugates and BC2L-A were dissolved in the same buffer composed of Tris-HCl (20 mM) containing NaCl (100 mM) and CaCl<sub>2</sub> (100 μM) at pH 7.5. BC2L-A (100–300 μM) was placed in the 200 μL sample cell operating at 25°C. Titrations were performed with 19 injections of sugar derivatives (65 μM to 3 mM, 2 μL) spaced by 150 seconds. The experimental data were fit to a theoretical titration curve using the supplied MicorCal PEAQ-ITC analysis software, with  $\Delta H$  (enthalpy change),  $K_d$  (dissociation constant) and  $n$  (number of binding sites per monomer) as adjustable parameters. Free energy change ( $\Delta G$ ) and entropy contributions ( $T\Delta S$ ) were derived from the equation  $\Delta G = \Delta H - T\Delta S = -R \cdot T \cdot \ln K_a$  (where  $T$  is the absolute temperature and  $R=8.314 \text{ J}\cdot\text{mol}^{-1}\cdot\text{K}^{-1}$  and  $K_a = 1/K_d$ ). Two or three independent titrations were performed for each tested ligand.

## VI.2.3. Enzyme-linked immunosorbent assay (ELISA)

96-well microtiter Nunc-Immuno plates (Maxi-Sorp) were coated with serial two-fold dilutions of each glycoclusters in PBS buffer pH 7.4 (from 100 μM to 3 nM, 100 μL per well,) for 1 h at 37°C. The wells were then washed with T-PBS (3 x 100 μL per well, PBS pH 7.4 containing 0.05% (v/v) Tween 20). This washing procedure was repeated after each incubation step. The coated microtiter plates were then blocked with BSA in PBS (3% w/v, 1 h at 37°C, 100 μL per well). Primary mouse anti-Tn monoclonal antibody (9A7 or JAA-F11) was then added (100 μL per well) and plates were incubated for 1 h at 37°C. Anti-Tn/TF antibody interaction with coated glycoclusters was revealed by using goat anti-mouse IgG peroxidase conjugate 1:1000 (100 μL per well, incubation 1 h at 37°C) and o-phenyldiamine/H<sub>2</sub>O<sub>2</sub> substrate (OPD, 100 μL per well). The reaction was quenched after 10 minutes by adding H<sub>2</sub>SO<sub>4</sub> (30% v/v, 50 μL per well) and the absorbance was measured at 490 nm. The optical density (OD at 490 nm) was plotted against the logarithm of the concentration for each glycocluster. Sigmoidal curves were fitted using Origin v6.1 software.

## VI.3. General synthesis methods and procedures

All chemical reagents were purchased from Sigma–Aldrich (Saint Quentin Fallavier, France) or Acros (Noisy-Le-Grand, France) and were used without further purification. All protected amino acids, Fmoc-Gly-Sasrin, and Rink amide resins were obtained from Advanced ChemTech Europe (Brussels, Belgium), Bachem Biochimie SARL (Voisins-Les-Bretonneux, France) and France Biochem S.A. (Meudon, France). For carbohydrates, progress of reactions was monitored by thin layer chromatography using silica gel 60 F254 pre-coated plates (Merck). Spots were visualised by charring

with 10% H<sub>2</sub>SO<sub>4</sub> in EtOH. Silica gel 60 (0.063–0.2 mm or 70–230 mesh, Merck) was used for column chromatography.

### VI.3.1. General procedures for solid-phase peptide synthesis (SPPS)

Assembly of all linear protected peptides was performed manually or automatically by solid-phase peptide synthesis (SPPS) using the standard 9-fluorenylmethoxycarbonyl/*tert*-butyl (Fmoc/*t*Bu) protection strategy. In manual SPPS, the device consisted in a polypropylene syringe-shaped reactor (150 mL volume) (#5147808 Grace SA, USA), equipped with a filter and a valve in the lower end. The resin was weighed and added to the reactor, then gently stirred with an orbital laboratory agitator (IKA Vibrax VXR basic, USA) in the presence of CH<sub>2</sub>Cl<sub>2</sub> for 10 minutes to promote its swelling. The employed reaction volumes were equal to 10 mL of solvent per gram of resin, reactors could be charged up to 4 g of resin. After the swelling phase, CH<sub>2</sub>Cl<sub>2</sub> was removed through filtration assisted by compressed air and the resin was stirred again for 10 minutes in the presence of DMF. After DMF removal, the resin was treated with a 20% piperidine solution in DMF, three times for ten minutes. The collected deprotection cocktail was transferred in a volumetric flask and made up to the mark. Using a fraction of this solution, the effective loading of the resin was indirectly calculated by measuring the absorption at 299 nm, corresponding to the deprotection by-product (dibenzofulvene-piperidine adduct), which indicates the moles of free amino groups per gram of resin according to the following formula:

$$n = \frac{A \cdot V \cdot d \cdot 1000}{l \cdot m \cdot \epsilon_{299}}$$

with: **n** = free amino groups (mmol·g<sup>-1</sup>); **A** = absorbance value at 299 nm; **V** = volumetric flask volume (L); **d** = dilution factor; 1000 = factor conversion of mol to mmol; **l** = optical path length of the cell (cm); **m** = sample weight of resin (g); **ε<sub>299</sub>** = molar attenuation coefficient of dibenzofulvene at 299 nm (7800 L·mol<sup>-1</sup>·cm<sup>-1</sup>).<sup>428</sup>

The resin was then washed several times with DMF (5 x 10 min.) before proceed with the coupling phase. Couplings were performed using 1.5 – 2.0 eq. of N-Fmoc-protected amino acids activated *in situ* with 1.5 – 2.0 eq. of PyBOP<sup>®</sup> and 3.0 – 4.0 eq. of DIPEA in DMF (10 mL per gram of resin) for 30 minutes at room temperature. The resin was washed again (5 x 10 min.), and the completeness of amino acid coupling was assessed *via* TNBS test.<sup>429</sup> A small portion of resin beads were treated with a solution containing 2,4,6-trinitrobenzene-sulphonic acid (1% w/v in DMF), which reacts with free primary amino groups to form an orange-red trinitrophenylated derivative. After completion of the coupling cycle, the procedure for the peptide elongation was repeated from the Fmoc-deprotection step. Automated syntheses of peptides were performed on a 348 Ω Synthesizer (Louisville, KY), using similar conditions to that reported above.

### VI.3.2. General procedures for peptide cleavage

- Peptides linked to SASRIN™ resin were treated with a TFA/CH<sub>2</sub>Cl<sub>2</sub> (1:99) cocktail (10 x 10 min.). The collected solutions were neutralized with DIPEA and concentrated under reduced pressure. Ice-cold diethyl ether was added to induce precipitation. After filtration and dessiccation, the resulting white solid was triturated to give a powder, and analysed by mass spectrometry.
- Peptides linked to Rink amide® resin were treated with a TFA/TIS/H<sub>2</sub>O (96:2:2) cocktail (2 x 3 h.). The collected solutions were concentrated under reduced pressure, and ice-cold diethyl ether was added to induce precipitation. After filtration and dessiccation, the resulting white solid was triturated to give a powder, and analysed by mass spectrometry.

### VI.3.3. General procedure for peptide cyclization

Linear peptides were dissolved in CH<sub>2</sub>Cl<sub>2</sub>/DMF (1:1) at ≈ 0.5 mM (based on the calcd. loading) in the presence of 1.5 eq. of DIPEA and 1.2 eq. of PyBOP®. After 30 minutes stirring the solvent mixture was removed under vacuum and the crude residue dissolved in the minimum amount of CH<sub>2</sub>Cl<sub>2</sub>. To this solution, ice-cold diethyl ether was added, and the crude cyclic peptide was obtained as a white powder after filtration and drying. The crude was then purified through preparative RP-HPLC and lyophilized.

### VI.3.4. General procedure for oxidative cleavage

To a solution of serine-containing substrate in H<sub>2</sub>O (plus CH<sub>3</sub>CN, where necessary), 10 eq. per serine group of sodium periodate (M.W. 213.89) were added. After stirring at room temperature for 40 minutes the reaction mixture was directly purified through RP-HPLC and the collected fractions lyophilized, to give desired α-oxo-aldehyde-containing products as white foamy solids.

### VI.3.5. General procedure for oxime ligation (OL)

A solution containing the aldehyde-bearing substrate, the aminoxy-functionalized compound (1.2 – 1.5 eq. per aldehyde) in 0.1% TFA in H<sub>2</sub>O (plus CH<sub>3</sub>CN, where necessary), was heated at 37°C for 30-60 min. The reaction completion was controlled *via* analytical RP-HPLC or UPLC-MS, then the crude was purified through preparative HPLC and the collected fractions lyophilized to give the oxime-containing product as white foamy solid.

### **VI.3.6. General procedure for copper(I)-catalyzed alkyne-azide cycloaddition (CuAAC)**

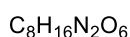
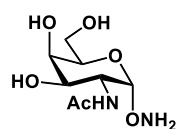
Three solutions were prepared. Solution A contained the azido-bearing substrate and the alkyne-functionalized compound in DMF. Solution B contained CuSO<sub>4</sub>·5H<sub>2</sub>O (M.W. 249.69, cat.) and THPTA (M.W. 434.50, 1–8 eq. per azido group) in PBS buffer (pH 7.4, 10 – 100 mM). Solution C contained sodium ascorbate (M.W. 198.11, 5–10 eq. per azido group) in PBS buffer. All solutions were degassed by performing vacuum/N<sub>2</sub> cycles (x3), then Solution C was added to Solution B, causing the reduction of Cu(II) to Cu(I) and turning the solution color from blue to colorless. The resulting mixture was added to Solution A, and the reaction was stirred at room temperature for 2 hours. After reaction completion check *via* HPLC or UPLC, a small amount of Chelex® resin (50-100 mesh, Sigma Aldrich) was added to the reaction mixture to chelate copper ions. After 30 minutes stirring at room temperature the reaction mixture was filtered and purified through preparative HPLC, to give the triazole-containing product as a white foamy solid after lyophilization.

### **VI.3.7. General procedure for disulfide bridging**

To a solution of Cys(NPys)-containing substrate in a previously degassed NaOAc buffer (pH 4.5, 40 mM) (plus DMF, when required), a solution in DMF containing 1.1 eq. of cysteine-functionalized peptide were added. Reaction progress can be suggested by an intense yellow coloration of the reaction mixture, indicating the cleavage of the NPys moiety. After 20-30 minutes stirring at room temperature, reaction completion was controlled *via* analytical HPLC or UPLC-MS and the crude reaction was directly purified and lyophilized to give a white foamy solid.

## VI.4. Syntheses and characterizations

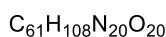
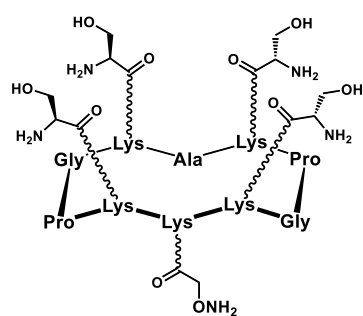
### Compound 63



Compound **63** was synthesized according to the published procedure: Renaudet, O., and Dumy, P. (2006) On-bead synthesis and binding assay of chemoselectively template-assembled multivalent neoglycopeptides. *Org. Biomol. Chem.* 4, 2628–2636.

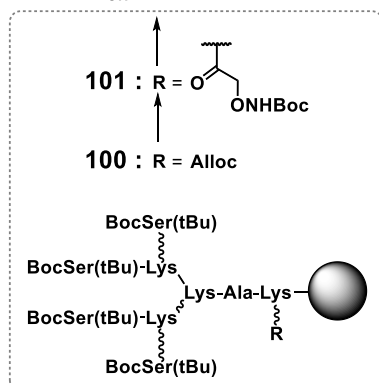
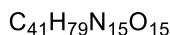
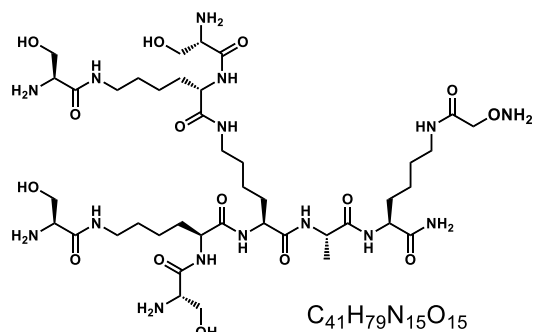
Characterization data were in accordance with the previous report.

### Compound 64



A solution of **99** (158.0 mg, 72.9  $\mu\text{mol}$ ) in a TFA/ $\text{NH}_2\text{OH}$ /TIS/ $\text{H}_2\text{O}$  cocktail (94:2:2:2) was stirred at room temperature for 3 hours. The reaction mixture was concentrated under reduced pressure and the resulting solution was added to ice-cold diethyl ether to induce precipitation. The solid was filtered and purified through RP-HPLC. After lyophilization, compound **64** (88.3 mg) was obtained in 84% yield. HRMS (ESI<sup>+</sup>-TOF):  $m/z$  calcd. for  $[\text{M}+\text{H}]^+$ : 1441.8127 (monoisotopic), found: 1441.8109; calcd. for  $[\text{M}+\text{Na}]^+$ : 1463.7946, found: 1463.7944.  $t_R = 6.25$  min. ( $\lambda = 214$  nm, 0-30% solv.B in 15').

### Compound 88



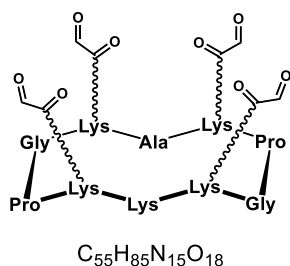
Peptide sequence **100** was synthesized manually, in a polypropylene reactor, following the general procedure for SPPS (**VI.3.1.**) on 1.215 g of Rink amide<sup>®</sup> support (measured loading = 0.490  $\text{mmol}\cdot\text{g}^{-1}$ ). The Alloc group was cleaved by treating the resin with a suspension of  $\text{Pd}(\text{PPh}_3)_4$  (13.6 mg, 11.8  $\mu\text{mol}$ , 2% mol) and  $\text{PhSiH}_3$  (1850  $\mu\text{L}$ , 15.994 mmol, 27 eq.) in dry  $\text{CH}_2\text{Cl}_2$  (12 mL). After 30 minutes stirring at room temperature MeOH (20 mL) was added, and the reactor stirred until the  $\text{CO}_2$  bubbling ceased. The resin was then washed with  $\text{CH}_2\text{Cl}_2$  (3 x 30 mL) and suspended in DMF. Boc-aminoxyacetic acid *N*-hydroxysuccinimide ester<sup>346</sup> (203.4 mg, 0.706 mmol, 1.2 eq.) and DIPEA (154  $\mu\text{L}$ , 0.884 mmol, 1.5 eq) were added, and the reactor stirred at room temperature for 30 minutes to give modified sequence **101** (not isolated). Finally, for the cleavage step the resin support was transferred in a round bottom flask

(500 mL) and treated with a TFA/ $\text{NH}_2\text{OH}$ /TIS/ $\text{H}_2\text{O}$  (94:2:2:2) cocktail, following the general procedure for Rink amide<sup>®</sup> cleavage (**VI.3.2.**). After RP-HPLC purification and lyophilization, compound **88** (225.1



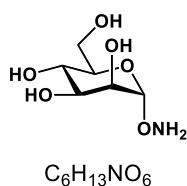
mg) was obtained in 37% overall yield. HRMS (ESI<sup>+</sup>-TOF):  $m/z$  calcd. for  $[M+H]^+$ : 1022.5958 (monoisotopic), found: 1022.5970.  $t_R$  = 6.25 min. ( $\lambda$ =214 nm, 0-20% solv.B in 15').

### Compound 89



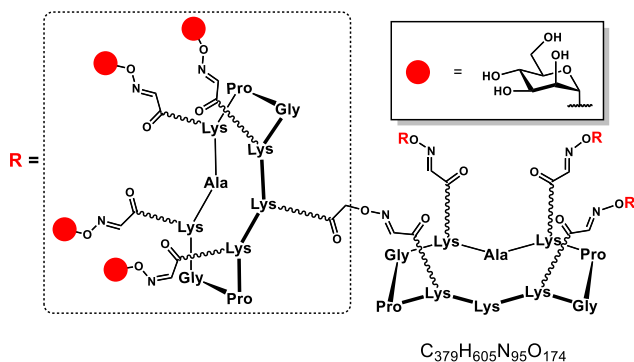
Compound **98** (88.2 mg, 64.4  $\mu$ mol) was treated with a solution of  $NaIO_4$  (551.4 mg, 2.578 mmol) in  $H_2O$  (4.5 mL) following the general procedure for oxidative cleavage (VI.3.4.). Compound **89** was obtained in 78% yield (62.5 mg). HRMS (ESI<sup>+</sup>-TOF):  $m/z$  calcd. for  $[M+H_2O+H]^+$ : 1316.6698 (monoisotopic), found: 1316.6715.  $t_R$  = 8.62 min. ( $\lambda$ =214 nm, 0-20% solv.B in 15').

### Compound 90



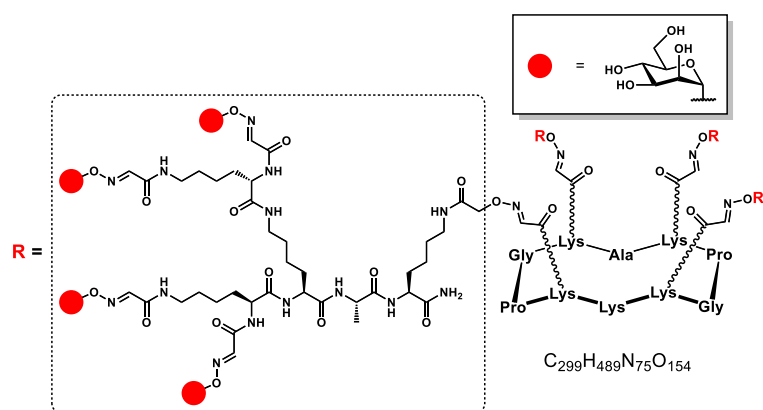
Compound **90** was synthesized according to the published procedure: Renaudet, O., and Dumy, P. (2006) On-bead synthesis and binding assay of chemoselectively template-assembled multivalent neoglycopeptides. *Org. Biomol. Chem.* 4, 2628–2636. Characterization data were in accordance with the previous report.

### Compound 91



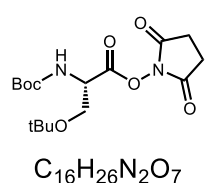
Compound **91** (11.4 mg) was obtained in 88% yield by reacting **102** (9.1 mg, 1.4  $\mu$ mol) and **90** (5.5 mg, 28.2  $\mu$ mol) following the general procedure for oxime ligation (VI.3.5.). ESI<sup>+</sup>-MS:  $m/z$  calcd. for  $[M+5H]^{5+}$ : 1856.3 (average), found: 1855.8; calcd. for  $[M+6H]^{6+}$ : 1547.1, found: 1546.8.  $t_R$  = 6.75 min. ( $\lambda$ =214 nm, 0-40% solv.B in 15').

### Compound 92



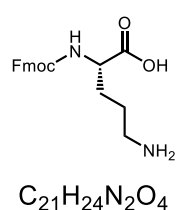
Compound **92** (11.5 mg) was obtained in 84% yield by reacting **103** (8.5 mg, 1.8  $\mu$ mol) and **90** (7.0 mg, 35.9  $\mu$ mol) following the general procedure for oxime ligation (**VI.3.5.**). MALDI-TOF:  $m/z$  calcd. for  $[M+H]^+$ : 7599.5 (average), found: 7598.8.  $t_R$  = 6.60 min. ( $\lambda=214$  nm, 0-40% solv.B in 15').

### Compound 93



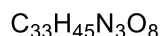
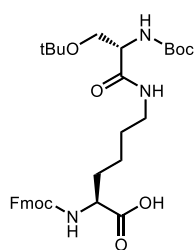
A stirred solution of commercial Boc-Ser(tBu)-OH (6.082 g, 23.274 mmol) and *N*-hydroxysuccinimide (2.860 g, 25.290 mmol) in a AcOEt/dioxane (1:1) mixture (230 mL) was cooled to 0°C. Solid DCC (5.168 g, 25.047 mmol) was added portion-wise, and the resulting suspension stirred at room temperature overnight. Reaction mixture was then filtrated through a Celite pad to remove insoluble dicyclohexylurea, the pad was washed with AcOEt (2 x 30 mL) and the collected filtrated was concentrated under reduced pressure. The obtained oily residue was taken into 300 mL AcOEt and washed with 5 % aqueous NaHCO<sub>3</sub> (2 x 150 mL), water (2 x 150 mL) and brine (2 x 150 mL). The collected organic fraction was dried over MgSO<sub>4</sub> and the solvent removed under vacuum, to give compound **93** in 92% yield (7.674 mg). <sup>1</sup>H-NMR (400 MHz, CDCl<sub>3</sub>)  $\delta$  = 5.40 (1H, d,  $J$  = 9.0 Hz), 4.75 (1H, m), 3.89 (1H, m), 3.64 (1H, m), 2.80 (4H, s), 1.43 (9H, s), 1.18 (9H, s) ppm; <sup>13</sup>C-NMR (100 MHz, CDCl<sub>3</sub>)  $\delta$  = 168.59, 166.96, 155.13, 80.43, 73.94, 61.81, 53.07, 28.34, 27.22, 25.64 ppm. ESI<sup>+</sup>-MS:  $m/z$  calcd. for  $[M+Na]^+$ : 381.2 (monoisotopic), found: 381.5.  $t_R$  = 9.82 min. ( $\lambda=214$  nm, 0-40% solv.B in 15').

### Compound 94



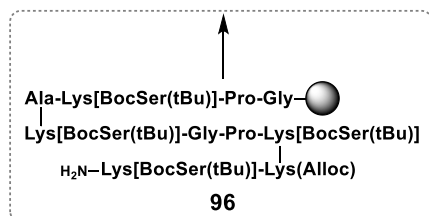
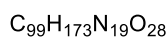
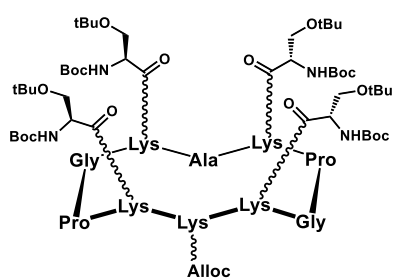
To a stirred solution of commercial Fmoc-Lys(Boc)-OH (27.453 g, 58.593 mmol) in dioxane (210 mL), aq. HCl (37%, 90 mL) was added. After 20 minutes stirring at room temperature the solvent mixture was evaporated to dryness, and the obtained crude was dissolved in a H<sub>2</sub>O/CH<sub>3</sub>CN (8:2) mixture and lyophilized to give compound **94** in 95% yield (22.538 g) as white solid, in its hydrochloride form. <sup>1</sup>H-NMR (400 MHz, DMSO-d<sub>6</sub>)  $\delta$  = 7.89 (2H, d,  $J$  = 7.2 Hz), 7.79 (1H, bs), 7.72 (1H, m), 7.63 (1H, d,  $J$  = 7.2 Hz), 7.42 (2H, t,  $J$  = 7.2 Hz), 7.33 (2H, m), 4.31 (2H, m), 4.24 (1H, m), 3.93 (1H, m), 2.75 (2H, m), 1.60 (4H, m), 1.38 (2H, m) ppm; <sup>13</sup>C-NMR (100 MHz, DMSO-d<sub>6</sub>)  $\delta$  = 173.85, 156.20, 143.81, 143.79, 140.79, 140.73, 127.65, 127.08, 127.07, 125.26, 120.14, 120.16, 65.58, 53.61, 46.66, 38.59, 30.17, 26.51, 22.57. ESI<sup>+</sup>-MS:  $m/z$  calcd. for  $[M+H]^+$ : 369.2 (monoisotopic), found: 369.0.  $t_R$  = 7.16 min. ( $\lambda=214$  nm, 0-40% solv.B in 15').

### Compound 95



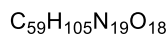
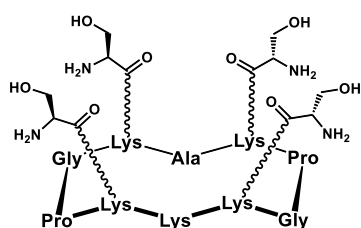
To a stirred suspension of **94** (13.421 g, 33.147 mmol) in CH<sub>2</sub>Cl<sub>2</sub> (190 mL) containing DIPEA (23.0 mL, 132.0 mmol), a solution of **93** (11.912 g, 33.238 mmol) in CH<sub>2</sub>Cl<sub>2</sub> (110 mL) was added drop-wise over 30 minutes. After 4 hours stirring at room temperature, the solvent mixture was concentrated under reduced pressure and the oily residue was taken in 500 mL AcOEt. The organic phase was washed with 10% aq. citric acid solution (100 mL), water (2 x 200 mL) and brine (2 x 200 mL). The organic fraction was dried over MgSO<sub>4</sub> and the solvent removed under vacuum, to give crude **93** as yellow syrup. The crude oil was dissolved in CH<sub>2</sub>Cl<sub>2</sub> (30 mL), then a cyclohexane/Et<sub>2</sub>O mixture (95:5, 290 mL) was added to induce precipitation. The precipitate was filtrated, washed with cyclohexane (2 x 30 mL) and dried to give compound **93** (20.033 g) as a white solid, in 99% yield. <sup>1</sup>H-NMR (400 MHz, DMSO-d<sub>6</sub>) δ = 12.55 (1H, s), 8.00 (1H, s), 7.88 (2H, d, *J* = 7.5 Hz), 7.81 (1H, t, *J* = 5.0 Hz), 7.74 (2H, d, *J* = 7.4 Hz), 7.64 (1H, d, *J* = 7.9 Hz), 7.42 (2H, t, *J* = 7.3 Hz), 7.34 (2H, t, *J* = 7.4 Hz), 6.48 (1H, d, *J* = 8.4 Hz), 4.27 (3H, m), 3.98 (1H, m), 3.91 (1H, m), 3.42 (2H, m), 3.10 (1H, m), 3.01 (1H, m), 1.69 (1H, m), 1.61 (1H, m), 1.37 (12H, m), 1.09 (9H, s) ppm; <sup>13</sup>C-NMR (100 MHz, DMSO-d<sub>6</sub>) δ = 174.03, 169.16, 156.16, 155.05, 143.80, 140.73, 127.64, 127.07, 125.30, 120.12, 78.13, 72.63, 65.60, 62.03, 54.97, 53.77, 46.66, 30.38, 28.14, 27.20, 25.23, 22.94 ppm. HRMS (ESI<sup>+</sup>-TOF): *m/z* calcd. for [M+Na]<sup>+</sup>: 634.3104 (monoisotopic), found: 634.3109. *t<sub>R</sub>* = 10.27 min. (λ=214 nm, 5-100% solv.B in 15').

### Compound 97



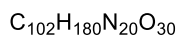
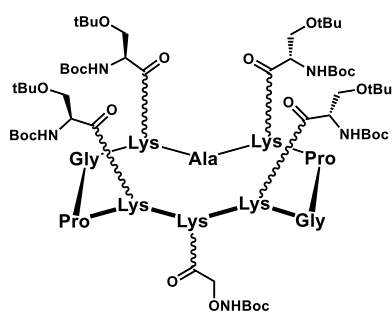
Peptide sequence **96** was synthesized manually in a polypropylene reactor, following the general procedure for SPPS (VI.3.1.) on 1.855 g of Fmoc-Gly-SASRIN™ support (measured loading = 0.572 mmol·g<sup>-1</sup>). Cleavage from the resin was performed following the reported general procedure (VI.3.2.). Mass spectrometry analysis revealed the presence of the expected mass for sequence **96**. HRMS (ESI<sup>+</sup>-TOF): *m/z* calcd. for C<sub>99</sub>H<sub>176</sub>N<sub>19</sub>O<sub>29</sub> [M(**96**)+H]<sup>+</sup>: 2095.2881 (monoisotopic), found: 2095.2932. Linear peptide **96** was dissolved in a CH<sub>2</sub>Cl<sub>2</sub>/DMF (1:1, 2.2 L) mixture, in the presence of DIPEA (280 μL, 1.607 mmol) and PyBOP® (662 mg, 1.272 mmol). Compound **97** (1.256 g) was obtained in 57% overall yield, following the general procedure for peptide cyclization (VI.3.3.). HRMS (ESI<sup>+</sup>-TOF): *m/z* calcd. for [M+Na]<sup>+</sup>: 2099.2595 (monoisotopic), found: 2099.2678. *t<sub>R</sub>* = 11.01 min. (λ=214 nm, 5-100% solv.B in 15').

### Compound 98



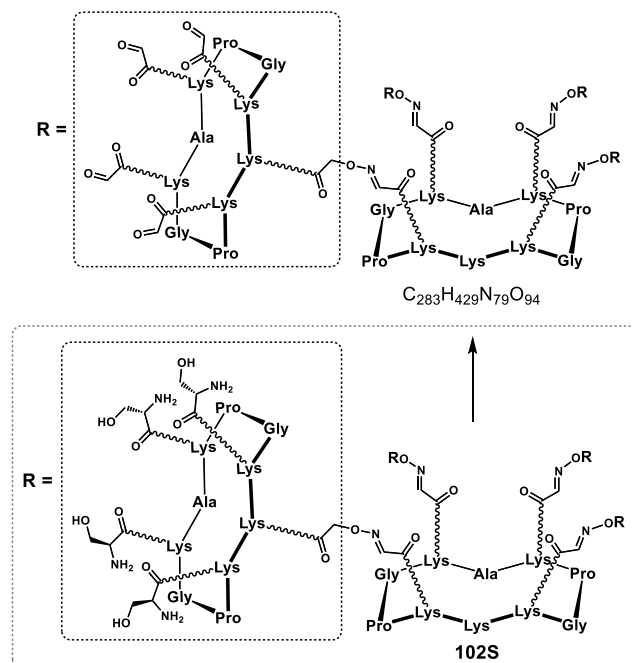
To a solution of compound **97** (373.9 mg, 180.0  $\mu$ mol) in dry  $CH_2Cl_2$  (100 mL),  $Pd(PPh_3)_4$  (4.2 mg, 3.6  $\mu$ mol, 2% mol) and  $PhSiH_3$  (560  $\mu$ L, 4.538 mmol) were added. The reaction mixture was stirred for 30 minutes at room temperature, MeOH (20 mL) was added and the mixture stirred until  $CO_2$  bubbling ceased. The solvent mixture was removed and the residue taken into  $CH_2Cl_2$  (10 mL); this solution was added drop-wise to ice-cold diethyl ether (200 mL) causing the precipitation of the Alloc-deprotected intermediate, which was filtrated and dried under vacuum. The presence of the expected intermediate was confirmed by mass spectrometry. HRMS (ESI<sup>+</sup>-TOF):  $m/z$  calcd. for  $C_{95}H_{170}N_{19}O_{26}$  [M(**97**-Alloc)+H]<sup>+</sup>: 1993.2564 (monoisotopic), found: 1993.2654. The crude intermediate was employed for the next deprotection without any further purification; it was treated with a TFA/TIS/H<sub>2</sub>O (96:2:2, 12 mL) cocktail for 3 hours at room temperature, then the solvent mixture was added drop-wise to ice-cold diethyl ether (200 mL). The resulting precipitate was filtrated and purified *via* RP-HPLC and lyophilized. Compound **97** (194.6 mg) was obtained in 79% yield over two steps. HRMS (ESI<sup>+</sup>-TOF):  $m/z$  calcd. for [M+H]<sup>+</sup>: 1368.7963 (monoisotopic), found: 1368.7964; calcd. for [M+Na]<sup>+</sup>: 1390.7783, found: 1390.7783.  $t_R$  = 4.28 min. ( $\lambda$ =214 nm, 0-20% solv.B in 15').

### Compound 99



To a solution of compound **97** (754.5 mg, 363.2  $\mu$ mol) in dry  $CH_2Cl_2$  (250 mL),  $Pd(PPh_3)_4$  (8.4 mg, 7.3  $\mu$ mol, 2% mol) and  $PhSiH_3$  (1120  $\mu$ L, 9.077 mmol) were added. The reaction mixture was stirred for 30 minutes at room temperature, MeOH (30 mL) was added and the mixture stirred until  $CO_2$  bubbling ceased. The solvent mixture was removed and the residue taken into  $CH_2Cl_2$  (15 mL); this solution was added drop-wise to ice-cold diethyl ether (300 mL) causing the precipitation of the Alloc-deprotected intermediate, which was filtrated, dried and used for the next step without any further purification. The crude intermediate was dissolved in DMF (100 mL), then DIPEA (95  $\mu$ L, 545.2  $\mu$ mol) and Boc-aminoxyacetic acid *N*-hydroxysuccinimide ester<sup>346</sup> (125.6 mg, 435.7  $\mu$ mol) were added. After 20 minutes stirring at room temperature, reaction mixture was concentrated under reduced pressure, purified *via* RP-HPLC and lyophilized. Compound **99** (566.6 mg) was obtained in 72% yield over two steps. HRMS (ESI<sup>+</sup>-TOF):  $m/z$  calcd. for [M+Na]<sup>+</sup>: 2188.3072 (monoisotopic), found: 2188.3142.  $t_R$  = 10.97 min. ( $\lambda$ =214 nm, 5-100% solv.B in 15').

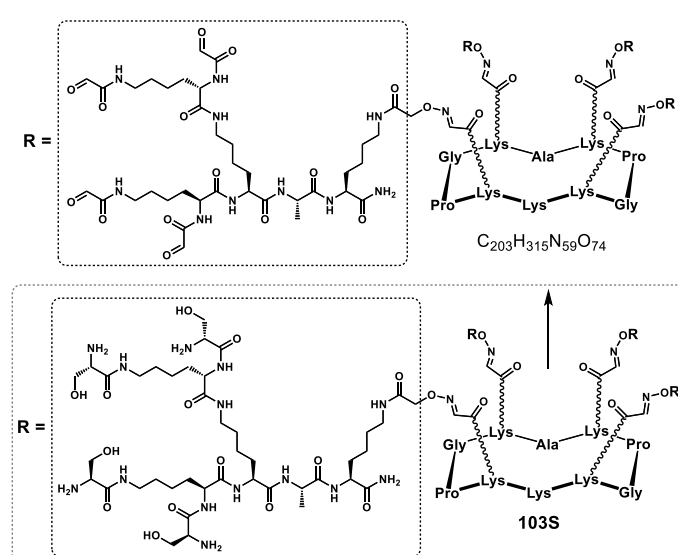
### Compound **102**



1611.5, found: 1611.9; calcd. for  $[M+5H]^{5+}$ : 1289.4, found: 1289.4.  $t_R = 8.84$  min. ( $\lambda=214$  nm, 0-40% solv.B in 15').

Compound **102S** was obtained by reacting **89** (12.2 mg, 9.8  $\mu\text{mol}$ ) with **64** (84.8 mg, 58.8  $\mu\text{mol}$ ) in 0.1% aq. TFA (5.0 mL) following the general procedure for oxime ligation (VI.3.5.). ESI<sup>+</sup>-MS:  $m/z$  calcd. for  $[M+3H]^{3+}$ : 2314.6, found: MALDI-TOF:  $m/z$  calcd. for  $C_{299}H_{511}N_{95}O_{94}$   $[M(\mathbf{102S})+H]^+$ : 6940.8 (average), found: 6939.4.  $t_R = 7.74$  min. ( $\lambda=214$  nm, 0-40% solv.B in 15'). The obtained amount of **102S** (59.8 mg, 88%) was dissolved in H<sub>2</sub>O (3.0 mL) and treated with NaIO<sub>4</sub> (295.1 mg, 160 eq.) according to the general procedure for oxidative cleavage (VI.3.4.). Compound **102** (45.5 mg) was obtained in 72% yield over two steps. ESI<sup>+</sup>-MS:  $m/z$  calcd. for  $[M+3H]^{3+}$ : 2148.3 (average), found: 2148.7; calcd. for  $[M+4H]^{4+}$ :

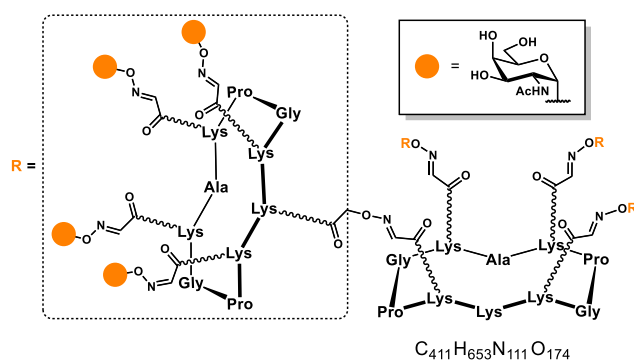
### Compound **103**



1191.8, found: 1191.7.  $t_R = 6.75$  min. ( $\lambda=214$  nm, 0-40% solv.B in 15').

Compound **103S** was obtained by reacting **89** (11.0 mg, 8.8  $\mu\text{mol}$ ) with **88** (54.0 mg, 52.8  $\mu\text{mol}$ ) in 0.1% aq. TFA (5.0 mL) following the general procedure for oxime ligation (VI.3.5.). MALDI-TOF:  $m/z$  calcd. for  $C_{219}H_{394}N_{75}O_{74}$   $[M(\mathbf{103S})+H]^+$ : 5261.9 (average), found: 5258.4.  $t_R = 6.25$  min. ( $\lambda=214$  nm, 0-40% solv.B in 15'). The obtained amount of **103S** (42.6 mg, 92%) was dissolved in H<sub>2</sub>O (3.0 mL) and treated with NaIO<sub>4</sub> (277.1 mg, 160 eq.) according to the general procedure for oxidative cleavage (VI.3.4.). Compound **103** (32.7

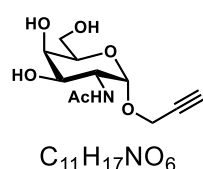
### Compound **111**



Compound **111** (18.4 mg) was obtained in 84% yield by reacting **102** (14.2 mg, 2.2  $\mu\text{mol}$ ) and **63** (10.4 mg, 44.0  $\mu\text{mol}$ , 20 eq.) following the general procedure for oxime ligation (VI.3.5.). ESI<sup>+</sup>-MS:  $m/z$  calcd. for  $[M+6H]^{6+}$ : 1656.4 (most intense peak of isotopic cluster), found: 1656.2; calcd. for  $[M+5H]^{5+}$ : 1987.5, found: 1987.3; calcd. for  $[M+4H]^{4+}$ : 2484.2, found: 2484.9.  $t_R = 8.78$  min. ( $\lambda=214$  nm, 0-40% solv.B

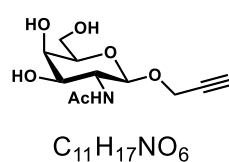
in 15').

### Compound **112**



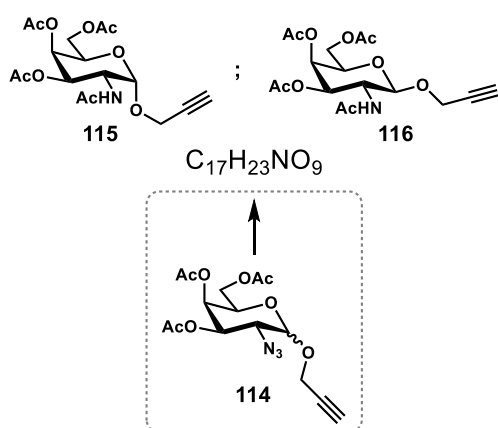
To a solution of **115** (230.7 mg, 598.6  $\mu\text{mol}$ ) in dry MeOH (10 mL), a 25% w/w solution of NaOMe in MeOH (63  $\mu\text{L}$ , 275.5  $\mu\text{mol}$ ) was added, and the reaction stirred at room temperature. After 4 hours, the reaction mixture was neutralized by adding Dowex<sup>®</sup> 50W-X8 (H<sup>+</sup>), filtered and concentrated to dryness to give **112** (149.0 mg) in 96% yield, as a white solid. <sup>1</sup>H-NMR (400 MHz, D<sub>2</sub>O)  $\delta = 5.12$  (1H, d,  $J = 4.0$  Hz, H-1), 4.38 (2H, m, -OCH<sub>2</sub>), 4.27 (1H, dd,  $J = 12.0, 3.8$  Hz, H-2), 4.04 (2H, m, H-4, H-5), 3.95 (1H, dd,  $J = 12.0, 4.0$  Hz, H-3), 3.81 (2H, m, H-6<sub>a,b</sub>), 2.94 (1H, bs, -C $\equiv$ CH), 2.10 (3H, s, NHAc) ppm; <sup>13</sup>C-NMR (100 MHz, D<sub>2</sub>O)  $\delta = 147.71$  (C=O), 96.12 (C-1), 77.05 (-C $\equiv$ CH), 75.72 (-C $\equiv$ CH), 74.12 (C-4 or C-5), 71.42 (C-4 or C-5), 68.51 (C-3), 61.17 (C-6), 55.15 (OCH<sub>2</sub>), 49.60 (C-2), 21.94 (CH<sub>3</sub>) ppm.  $R_f = 0.39$  (CH<sub>2</sub>Cl<sub>2</sub> : MeOH, 4:1).  $[\alpha]_D^{25} = -38$  (c, 1.0 in H<sub>2</sub>O). HRMS (ESI<sup>+</sup>-TOF):  $m/z$  calcd. for  $[M+Na]^+$ : 282.0954, (monoisotopic), found: 282.0956.

### Compound **113**



Compound **113** (61.1 mg) was obtained in 95% yield from **116** (95.6 mg, 248.1  $\mu\text{mol}$ ), by following the same methodology described for **112**. <sup>1</sup>H-NMR (400 MHz, D<sub>2</sub>O)  $\delta = 4.89$  (1H, d,  $J = 8.0$  Hz, H-1), 4.40 (2H, m, -OCH<sub>2</sub>), 4.27 (1H, dd,  $J = 12.0, 3.8$  Hz, H-2), 3.94 (2H, m, H-4, H-5), 3.90 (1H, dd,  $J = 12.0, 4.0$  Hz, H-3), 3.75 (2H, m, H-6<sub>a,b</sub>), 2.95 (1H, bs, -C $\equiv$ CH), 2.15 (3H, s, NHAc) ppm; <sup>13</sup>C-NMR (100 MHz, D<sub>2</sub>O)  $\delta = 148.33$  (C=O), 98.10 (C-1), 77.62 (-C $\equiv$ CH), 76.27 (-C $\equiv$ CH), 75.24 (C-4 or C-5), 70.78 (C-4 or C-5), 69.05 (C-3), 61.01 (C-6), 55.46 (OCH<sub>2</sub>), 49.88 (C-2), 22.13 (CH<sub>3</sub>) ppm.  $R_f = 0.35$  (CH<sub>2</sub>Cl<sub>2</sub> : MeOH, 4:1).  $[\alpha]_D^{25} = -98$  (c, 1.0 in H<sub>2</sub>O). HRMS (ESI<sup>+</sup>-TOF):  $m/z$  calcd. for  $[M+Na]^+$ : 282.0954, (monoisotopic), found: 282.0962.

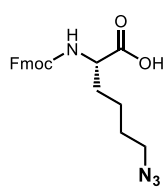
## Compounds **115** and **116**



To a stirred solution of 3,4,6-tri-*O*-acetyl-2-azido-2-deoxy-D-galactopyranosyl fluoride<sup>219</sup> (575.2 mg, 1.726 mmol) in  $CH_2Cl_2$  (10 mL) at 0°C, propargyl alcohol (402  $\mu$ L, 6.712 mmol) and  $BF_3 \cdot Et_2O$  (426  $\mu$ L, 3.452 mmol) were slowly added. After 2 hours stirring at room temperature, the reaction mixture was poured into water (25 mL) and extracted with  $CH_2Cl_2$  (3 x 25 mL). Combined organic fractions were washed with 10% aq.  $NaHCO_3$  (2 x 25 mL), dried over  $MgSO_4$  and the obtained organic solution concentrated under reduced pressure. The crude was purified by flash chromatography ( $Et_2O$  : cyclohexane, 1:1)

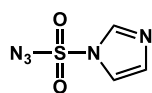
to afford **114** (537.7 mg) in 90% yield as a mixture of anomers ( $\alpha/\beta$ , 3:2). To a solution of **114** (525.8 mg, 1.424 mmol) in  $CH_2Cl_2$  (5 mL), triphenylphosphine (466.9 mg, 1.780 mmol) and acetic anhydride (407  $\mu$ L, 4.272 mmol) were added. After 16 hours stirring at room temperature reaction mixture was poured into water (25 mL) and extracted with  $CH_2Cl_2$  (4 x 25 mL). Combined organic fractions were washed with 10% aq.  $NaHCO_3$  (2 x 25 mL), dried over  $MgSO_4$  and the obtained organic solution concentrated under reduced pressure. The crude was purified by flash chromatography ( $AcOEt$  :  $CH_2Cl_2$ , 4:1) to afford **115** (246.9 mg, 45%) and **116** (192.1 mg, 36%) as white solids. **115**:  $^1H$ -NMR (100 MHz,  $CDCl_3$ )  $\delta$  = 5.60 (1H, d,  $J$  = 9.8 Hz,  $NHAc$ ), 5.38 (1H, app dd,  $J$  = 1.2, 4.0 Hz, H-4), 5.17 (1H, dd,  $J$  = 12.0, 4.0 Hz, H-3), 5.06 (1H, d,  $J$  = 4.0 Hz, H-1), 4.62 (1H, ddd,  $J$  = 12.0, 9.8, 4.0 Hz, H-2), 4.26 (2H, dd,  $J$  = 5.4, 2.4 Hz,  $OCH_2$ ), 4.19 (1H, m, H-5), 4.10 (2H, dd,  $J$  = 6.4, 1.8 Hz, H-6<sub>a,b</sub>), 2.47 (1H, t,  $J$  = 2.4 Hz,  $-C\equiv CH$ ), 2.16 (3H, s,  $OAc$ ), 2.04 (3H, s,  $OAc$ ), 1.99 (3H, s,  $OAc$ ), 1.97 (3H, s,  $OAc$ ) ppm;  $^{13}C$ -NMR (100 MHz,  $CDCl_3$ )  $\delta$  = 171.02–170.21 (C=O), 96.82 (C-1), 78.40 ( $-C\equiv CH$ ), 75.50 ( $-C\equiv CH$ ), 68.37 (C-3), 67.40 (C-4), 67.44 (C-5), 61.85 (C-6), 55.41 ( $OCH_2$ ), 47.7 (C-2), 23.41 ( $CH_3$ ), 20.94 ( $CH_3$ ), 20.83 ( $CH_3$ ) ppm.  $R_f$  = 0.39 ( $AcOEt$  :  $CH_2Cl_2$ , 4:1).  $[\alpha]_D^{25}$  = -21 (*c*, 1.0 in  $CHCl_3$ ). HRMS (ESI<sup>+</sup>-TOF):  $m/z$  calcd. for  $[M+Na]^+$ : 408.1270, (monoisotopic), found: 408.1264. **116**:  $^1H$ -NMR (400 MHz,  $CDCl_3$ )  $\delta$  = 5.58 (1H, d,  $J$  = 8.8 Hz,  $NHAc$ ), 5.36 (1H, br d,  $J$  = 3.4 Hz, H-4), 5.32 (1H, dd,  $J$  = 11.0, 3.4 Hz, H-3), 4.88 (1H, d,  $J$  = 8.0 Hz, H-1), 4.38 (2H, br d,  $J$  = 2.4 Hz,  $OCH_2$ ), 4.14 (2H, m, H-6<sub>a,b</sub>), 4.03 (1H, td,  $J$  = 11.0, 8.0 Hz, H-2), 3.94 (1H, t,  $J$  = 6.6 Hz, H-4), 2.46 (1H, t,  $J$  = 2.4 Hz,  $-C\equiv CH$ ), 2.14 (3H, s,  $OAc$ ), 2.04 (3H, s,  $OAc$ ), 1.99 (3H, s,  $OAc$ ), 1.96 (3H, s,  $OAc$ ) ppm;  $^{13}C$ -NMR (100 MHz,  $CDCl_3$ )  $\delta$  = 170.63–170.39 (C=O), 98.75 (C-1), 78.71 ( $-C\equiv CH$ ), 75.39 ( $-C\equiv CH$ ), 70.94 (C-3), 70.04 (C-4), 66.83 (C-5), 61.54 (C-6), 56.03 ( $OCH_2$ ), 52.29 (C-2), 23.61 ( $CH_3$ ), 20.85 ( $CH_3$ ), 20.83 ( $CH_3$ ) ppm.  $R_f$  = 0.36 ( $AcOEt$  :  $CH_2Cl_2$ , 4:1).  $[\alpha]_D^{25}$  = +83 (*c*, 1.0 in  $CHCl_3$ ). HRMS (ESI<sup>+</sup>-TOF):  $m/z$  calcd. for  $[M+Na]^+$ : 408.1270, (monoisotopic), found: 408.1258.

### Compound **117**



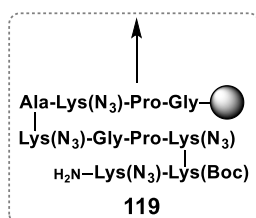
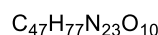
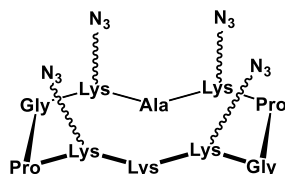
To a stirred solution of **94** (9.763 g, 20.134 mmol) in a MeOH/H<sub>2</sub>O (2:1, 300 mL), CuSO<sub>4</sub>·5H<sub>2</sub>O (50.3 mg, 201.5 μmol, 1% mol), K<sub>2</sub>CO<sub>3</sub> (5.844 g, 42.283 mmol) and **118** (5.064 g, 24.159 mmol) were added. The reaction was stirred at room temperature for 5 hours, and then the solvent mixture was concentrated under reduced pressure to remove MeOH. The resulting crude mixture was acidified with aq. HCl (2N) until pH ≈ 2 and extracted with AcOEt (3 x 200 mL). Combined organic fractions were washed with water (2 x 200 mL), brine (2 x 200 mL), dried over MgSO<sub>4</sub>, filtrated and concentrated under vacuum to give **117** (7.544 g) as yellow syrup in 95% yield. <sup>1</sup>H-NMR (400 MHz, DMSO-d<sub>6</sub>) δ = 8.95 (1H, s), 7.89 (2H, d, *J* = 7.4 Hz), 7.73 (1H, d, *J* = 7.4 Hz), 7.65 (1H, d, *J* = 7.4 Hz), 7.42 (4H, m), 4.29 (2H, m), 4.23 (1H, m), 3.95 (1H, m), 3.32 (2H, t, *J* = 6.8 Hz), 1.72 (1H, m), 1.61 (1H, m), 1.50 (2H, m), 1.37 (2H, m) ppm; <sup>13</sup>C-NMR (100 MHz, DMSO-d<sub>6</sub>) δ = 174.35, 156.63, 144.37, 144.28, 141.30, 141.28, 128.15, 127.60, 125.77, 125.74, 120.59, 120.56, 66.05, 54.13, 51.02, 47.18, 30.77, 28.29, 23.40 ppm. HRMS (ESI<sup>+</sup>-TOF): *m/z* calcd. for [M+Na]<sup>+</sup>: 1368.7963 (monoisotopic), found: 1368.7964; calcd. for [M+Na]<sup>+</sup>: 417.1539, found: 417.1540. *t*<sub>R</sub> = 7.85 min. (λ=214 nm, 5-100% solv.B in 15').

### Compound **118**



Sulfonyl chloride (97%, 16.3 mL, 0.195 mmol) was added drop-wise to an ice-cooled suspension of NaN<sub>3</sub> (12.677 g, 0.195 mmol) in CH<sub>3</sub>CN (200 mL) and the mixture was stirred overnight at room temperature. Imidazole (25.4904 g, 0.3705 mmol) was added portion-wise, and the mixture stirred at room temperature for 3 hours. The reaction mixture was diluted with AcOEt (400 mL), washed with water (2 x 200 mL), saturated aq. NaHCO<sub>3</sub> (2 x 400 mL) and the organic phase dried over MgSO<sub>4</sub> and filtered. The resulting solution was cooled to 0°C and a solution of HCl in EtOH [prepared by adding 22.65 mL of acetyl chloride (318.5 mmol) on ice-cold EtOH (75 mL)] was added drop-wise upon vigorous stirring to obtain a hydrochloride salt of **118**. The obtained solid was filtered and washed with AcOEt (3 x 100 mL) to give **118** (31.882 g) as colorless needles in 78% yield. ESI<sup>+</sup>-MS: *m/z* calcd. for [M+H]<sup>+</sup>: 174.0 (monoisotopic), found: 174.2. Characterization data were in agreement with literature.<sup>362</sup>

### Compound **120**

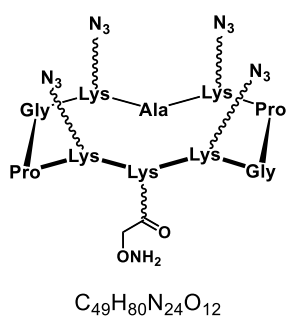


Peptide sequence **119** was synthesized manually in a polypropylene reactor, following the general procedure for SPPS (**VI.3.1.**) on 2.425 g of Fmoc-Gly-SASRIN™ support (measured loading = 0.537 mmol·g<sup>-1</sup>). Clivage from the resin was performed following the reported general procedure (**VI.3.2.**). Mass spectrometry analysis revealed the presence of the expected mass for sequence **119**. HRMS (ESI<sup>+</sup>-TOF): *m/z* calcd. for C<sub>52</sub>H<sub>88</sub>N<sub>23</sub>O<sub>13</sub> [M(**119**)+H]<sup>+</sup>: 1242.6932 (monoisotopic), found: 1242.6943. Linear peptide **119** was dissolved in a CH<sub>2</sub>Cl<sub>2</sub>/DMF (1:1, 3.0 L) mixture, in the presence of DIPEA (454 μL, 2.605 mmol) and PyBOP® (813 mg, 1.563 mmol). Cyclization was performed following the general procedure (**VI.3.3.**), the obtained solid crude was dissolved in a 50% TFA solution in CH<sub>2</sub>Cl<sub>2</sub> (25 mL) and stirred at



room temperature for 30 minutes. Solvent mixture was removed under reduced pressure and the reaction crude purified *via* RP-HPLC and lyophilized. Compound **120** (717.4 mg) was obtained in 49% overall yield. HRMS (ESI<sup>+</sup>-TOF): *m/z* calcd. for [M+H]<sup>+</sup>: 1124.6302 (monoisotopic), found: 1124.6284. *t<sub>R</sub>* = 7.97 min. ( $\lambda$ =214 nm, 5-100% solv.B in 15').

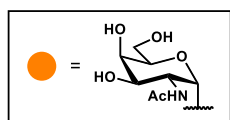
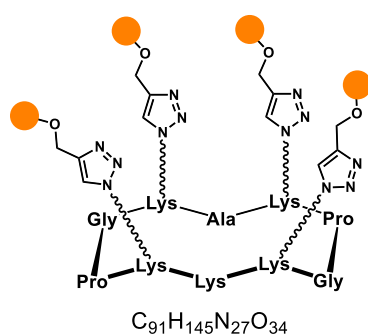
### Compound **121**



To a stirred solution of **120** (115.6 mg, 102.8  $\mu$ mol) in DMF (15 mL), DIPEA (27  $\mu$ L, 154.9  $\mu$ mol) and Boc-aminoxyacetic acid *N*-hydroxysuccinimide ester<sup>346</sup> (35.6 mg, 123.5  $\mu$ mol) were added and the reaction stirred at room temperature for 20 minutes. The reaction was neutralized by adding a 0.1% TFA/CH<sub>3</sub>CN solution and the solvent mixture concentrated under reduced pressure. The crude mixture was dissolved in a TFA/NH<sub>2</sub>OH/CH<sub>2</sub>Cl<sub>2</sub> (50:2:48, 5.0 mL) cocktail and stirred for 30 minutes at room temperature. The solvent mixture was removed under vacuum and the obtained residue purified

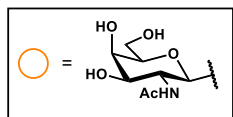
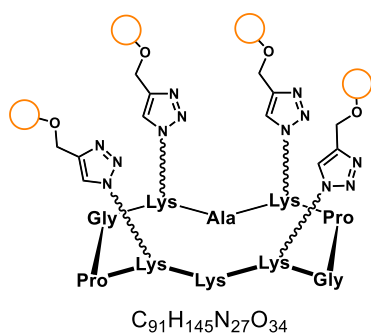
through RP-HPLC and lyophilized. Compound **121** (112.0 mg) was obtained in 91% yield over two steps. HRMS (ESI<sup>+</sup>-TOF): *m/z* calcd. for [M+Na]<sup>+</sup>: 1219.6285 (monoisotopic), found: 1219.6302. *t<sub>R</sub>* = 6.93 min. ( $\lambda$ =214 nm, 5-100% solv.B in 15').

### Compound **122**



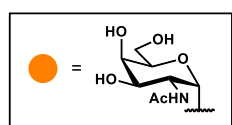
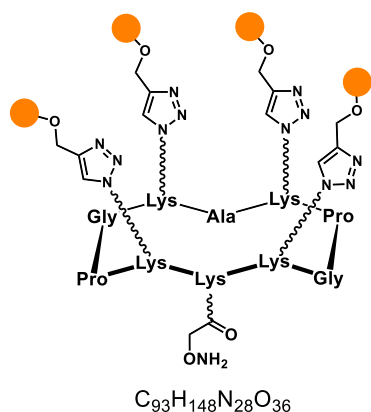
To a solution of **120** (5.6 mg, 5.0  $\mu$ mol) and **112** (7.8 mg, 30.1  $\mu$ mol) in DMF (600  $\mu$ L), a solution of THPTA (43.5 mg, 100.1  $\mu$ mol), CuSO<sub>4</sub>·5H<sub>2</sub>O (0.1 mg, 0.4  $\mu$ mol) and sodium ascorbate (31.7 mg, 160.0  $\mu$ mol) in aq. PBS (pH 7.4, 10 mM, 1200  $\mu$ L) were added. Compound **122** (9.1 mg) was obtained in 84% yield, following the general procedure for CuAAC (**VI.3.6**). HRMS (ESI<sup>+</sup>-TOF): *m/z* calcd. for [M+H]<sup>+</sup>: 2161.0525 (monoisotopic), found: 2161.0474. *t<sub>R</sub>* = 10.52 min. ( $\lambda$ =214 nm, 5-80% solv.B in 20').

### Compound **123**



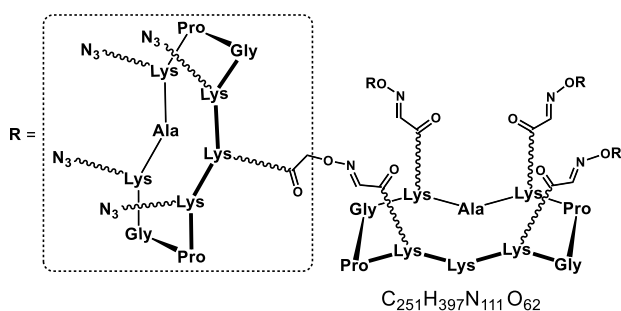
To a solution of **120** (4.7 mg, 4.2  $\mu\text{mol}$ ) and **112** (6.5 mg, 25.1  $\mu\text{mol}$ ) in DMF (600  $\mu\text{L}$ ), a solution of THPTA (36.5 mg, 84.0  $\mu\text{mol}$ ),  $\text{CuSO}_4 \cdot 5\text{H}_2\text{O}$  (0.1 mg, 0.4  $\mu\text{mol}$ ) and sodium ascorbate (26.6 mg, 134.3  $\mu\text{mol}$ ) in aq. PBS (pH 7.4, 10 mM, 1200  $\mu\text{L}$ ) were added. Compound **122** (9.1 mg) was obtained in 84% yield, following the general procedure for CuAAC (**VI.3.6.**). HRMS (ESI<sup>+</sup>-TOF):  $m/z$  calcd. for  $[\text{M}+\text{H}]^+$ : 2161.0525 (monoisotopic), found: 2161.0471.  $t_R = 10.45$  min. ( $\lambda=214$  nm, 5-80% solv.B in 20').

### Compound **124**



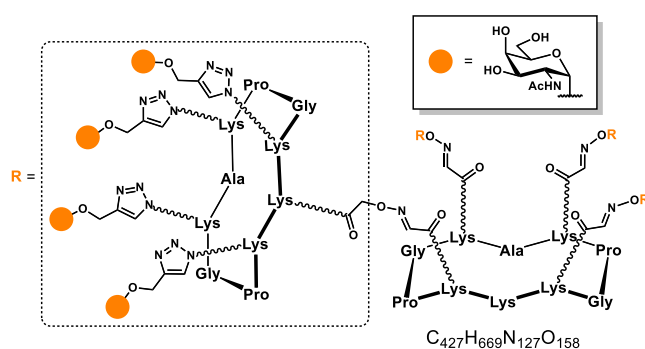
To a solution of **122** (13.4 mg, 6.2  $\mu\text{mol}$ ) in DMF (2 mL), DIPEA (1.5  $\mu\text{L}$ , 8.6  $\mu\text{mol}$ ) and Boc-aminoxyacetic acid *N*-hydroxysuccinimide ester<sup>346</sup> (2.2 mg, 7.6  $\mu\text{mol}$ ) were added and the reaction stirred at room temperature for 20 minutes. The reaction was neutralized by adding a 0.1% TFA/ $\text{CH}_3\text{CN}$  solution and the solvent mixture concentrated under reduced pressure. The crude mixture was dissolved in a TFA/ $\text{NH}_2\text{OH}/\text{CH}_2\text{Cl}_2$  (50:2:48, 2.0 mL) cocktail and stirred for 30 minutes at room temperature. The solvent mixture was removed under vacuum and the obtained residue purified through RP-HPLC and lyophilized. Compound **124** (112.0 mg) was obtained in 77% yield over two steps. HRMS (ESI<sup>+</sup>-TOF):  $m/z$  calcd. for  $[\text{M}+\text{Na}]^+$ : 2356.1033 (monoisotopic), found: 2356.0977.  $t_R = 10.39$  min. ( $\lambda=214$  nm, 5-100% solv.B in 15').

### Compound **125**



Compound **125** (35.0 mg) was obtained in 85% yield by reacting **89** (8.6 mg, 6.9  $\mu\text{mol}$ ) and **121** (49.5 mg, 41.3  $\mu\text{mol}$ ) in a  $\text{H}_2\text{O}/\text{CH}_3\text{CN}$  mixture (1:1, 2.0 mL) containing 0.1% TFA, following the general procedure for oxime ligation (**VI.3.5.**). MALDI-TOF:  $m/z$  calcd. for  $[\text{M}+\text{H}]^+$ : 5962.6 (average), found: 5962.7.  $t_R = 10.29$  min. ( $\lambda=214$  nm, 5-100% solv.B in 15').

### Compound 126

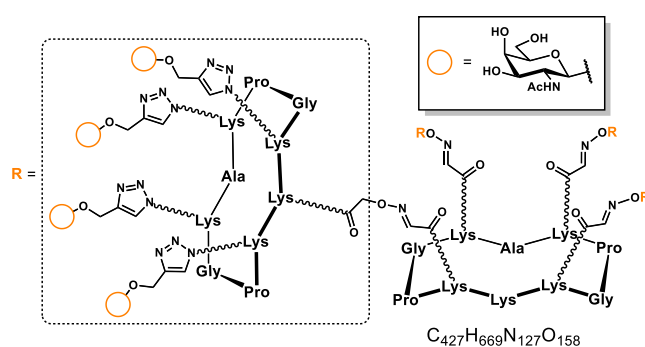


To a solution of **125** (5.2 mg, 0.9  $\mu$ mol) and **112** (4.7 mg, 18.1  $\mu$ mol) in DMF (600  $\mu$ L), a solution of THPTA (31.3 mg, 72.0  $\mu$ mol),  $CuSO_4 \cdot 5H_2O$  (0.1 mg, 0.4  $\mu$ mol) and sodium ascorbate (17.8 mg, 89.8  $\mu$ mol) in aq. PBS (pH 7.4, 10 mM, 1200  $\mu$ L) were added. Compound **126** (6.4 mg) was obtained in 70% yield, following the general procedure for CuAAC (**VI.3.6**). MALDI-TOF:  $m/z$  calcd. for  $[M+H]^+$ :

10110.6 (average), found: 10106.1.  $t_R = 11.89$  min. ( $\lambda=214$  nm, 5-100% solv.B in 25').

Alternatively, compound **126** (7.3 mg, 90%) has been synthesized through a convergent procedure by reacting **89** (1.0 mg, 0.8  $\mu$ mol) with **124** (10.7 mg, 4.8  $\mu$ mol) in a 0.1% TFA/ $H_2O$  solution (800  $\mu$ L) following the general procedure for oxime ligation (**VI.3.5**).

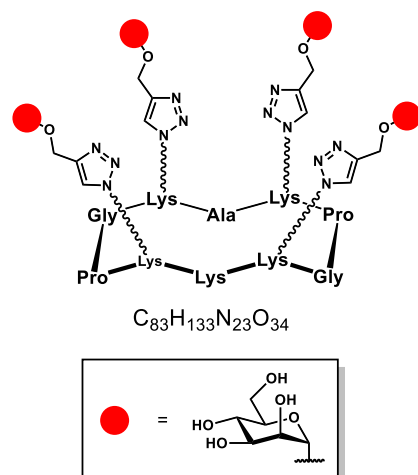
### Compound 127



To a solution of **125** (4.8 mg, 0.8  $\mu$ mol) and **113** (4.2 mg, 16.2  $\mu$ mol) in DMF (600  $\mu$ L), a solution of THPTA (27.8 mg, 64.0  $\mu$ mol),  $CuSO_4 \cdot 5H_2O$  (0.1 mg, 0.4  $\mu$ mol) and sodium ascorbate (15.8 mg, 79.8  $\mu$ mol) in aq. PBS (pH 7.4, 10 mM, 1200  $\mu$ L) were added. Compound **126** (6.4 mg) was obtained in 70% yield, following the general procedure for CuAAC (**VI.3.6**). MALDI-TOF:  $m/z$  calcd. for  $[M+H]^+$ :

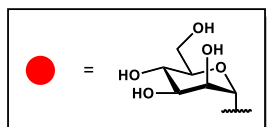
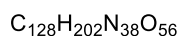
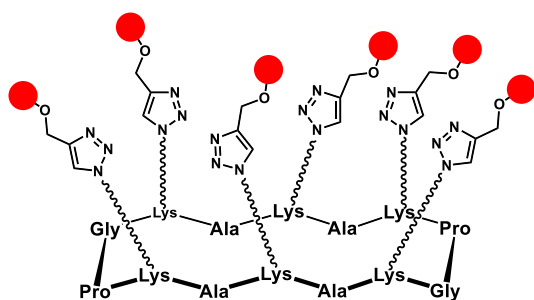
10110.6 (average), found: 10110.6.  $t_R = 11.47$  min. ( $\lambda=214$  nm, 5-100% solv.B in 25').

### Compound 128



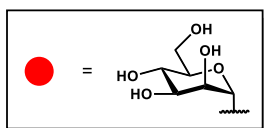
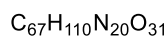
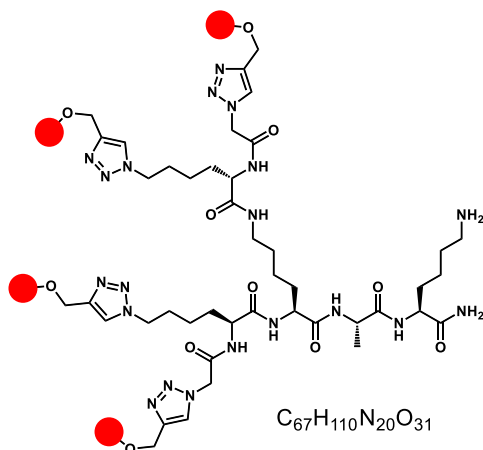
To a solution of **120** (34.4 mg, 30.6  $\mu$ mol) and **144** (40.1 mg, 183.8  $\mu$ mol) in DMF (2 mL), a solution of THPTA (266.0 mg, 612.2  $\mu$ mol),  $CuSO_4 \cdot 5H_2O$  (0.3 mg, 1.2  $\mu$ mol) and sodium ascorbate (170.2 mg, 859.1  $\mu$ mol) in aq. PBS (pH 7.4, 10 mM, 4 mL) were added. Compound **128** (51.9 mg) was obtained in 85% yield, following the general procedure for CuAAC (**VI.3.6**). HRMS (ESI<sup>+</sup>-TOF):  $m/z$  calcd. for  $[M+H]^+$ : 1996.9463 (monoisotopic), found: 1996.9457.  $t_R = 6.79$  min. ( $\lambda=214$  nm, 0-30% solv.B in 15').

### Compound **129**



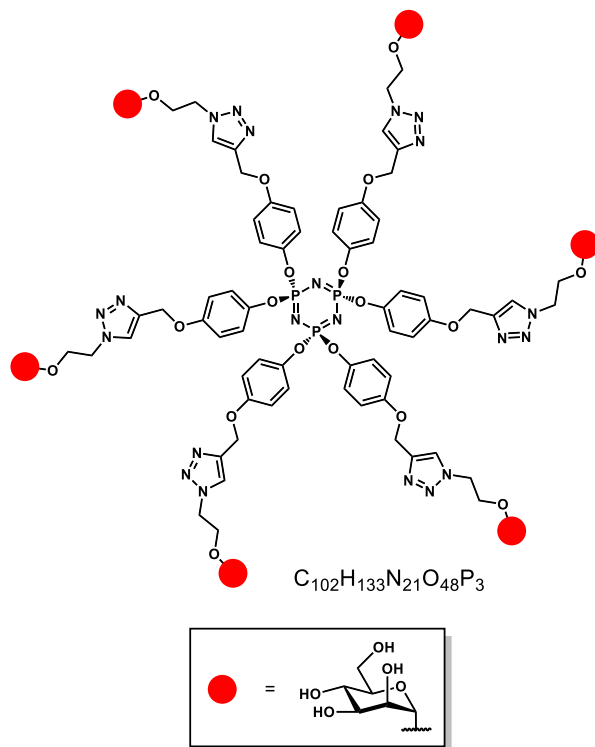
To a solution of **138** (5.8 mg, 3.8  $\mu$ mol) and **144** (7.5 mg, 34.4  $\mu$ mol) in DMF (600  $\mu$ L), a solution of THPTA (49.5 mg, 113.9  $\mu$ mol),  $CuSO_4 \cdot 5H_2O$  (0.1 mg, 0.4  $\mu$ mol) and sodium ascorbate (31.6 mg, 159.5  $\mu$ mol) in aq. PBS (pH 7.4, 10 mM, 1200  $\mu$ L) were added. Compound **129** (10.2 mg) was obtained in 85% yield, following the general procedure for CuAAC (**VI.3.6.**). MALDI-TOF:  $m/z$  calcd. for  $[M+Na]^+$ : 3191.4 (average), found: 3191.4.  $t_R = 7.37$  min. ( $\lambda=214$  nm, 0-30% solv.B in 15').

### Compound **130**



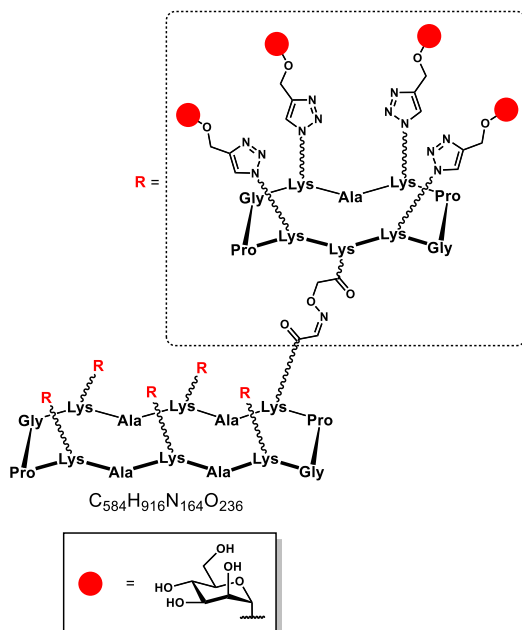
To a solution of **142** (45.1 mg, 55.1  $\mu$ mol) and **144** (72.1 mg, 330.4  $\mu$ mol) in DMF (2 mL), a solution of THPTA (478.8 mg, 1.102 mmol),  $CuSO_4 \cdot 5H_2O$  (0.3 mg, 1.2  $\mu$ mol) and sodium ascorbate (305.6 mg, 1.543 mmol) in aq. PBS (pH 7.4, 10 mM, 4 mL) were added. Compound **130** (66.2 mg) was obtained in 71% yield, following the general procedure for CuAAC (**VI.3.6.**). HRMS (ESI<sup>+</sup>-TOF):  $m/z$  calcd. for  $[M+H]^+$ : 1692.7753 (monoisotopic), found: 1692.7739.  $t_R = 5.34$  min. ( $\lambda=214$  nm, 0-30% solv.B in 15').

### Compound **131**



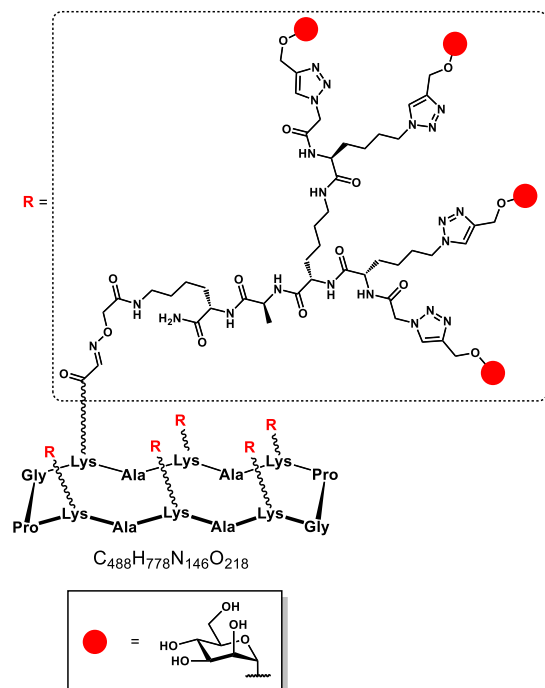
To a solution of **143** (9.0 mg, 8.8  $\mu\text{mol}$ ) and **145** (19.7 mg, 79.0  $\mu\text{mol}$ ) in DMF (600  $\mu\text{L}$ ), a solution of THPTA (114.7 mg, 264.0  $\mu\text{mol}$ ),  $\text{CuSO}_4 \cdot 5\text{H}_2\text{O}$  (0.1 mg, 0.4  $\mu\text{mol}$ ) and sodium ascorbate (73.2 mg, 369.5  $\mu\text{mol}$ ) in aq. PBS (pH 7.4, 10 mM, 1200  $\mu\text{L}$ ) were added. Compound **131** (16.8 mg) was obtained in 76% yield, following the general procedure for CuAAC (**VI.3.6**). HRMS (ESI<sup>+</sup>-TOF):  $m/z$  calcd. for  $[\text{M}+\text{H}]^+$ : 2513.7903 (monoisotopic), found: 2513.7844.  $t_R = 11.75$  min. ( $\lambda = 214$  nm, 0-40% solv.B in 15').  $^{31}\text{P}$ -NMR (162 MHz,  $\text{D}_2\text{O}$ )  $\delta = 10.16$  ppm.

### Compound **132**



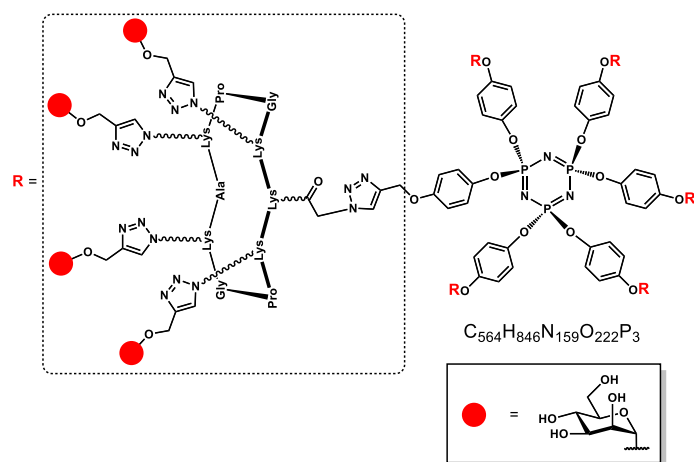
Compound **132** (13.1 mg) was obtained in 84% yield by reacting **139** (1.8 mg, 1.1  $\mu\text{mol}$ ) and **146** (20.0 mg, 9.7  $\mu\text{mol}$ ) in a 0.1% TFA/ $\text{H}_2\text{O}$  solution (1.0 mL), following the general procedure for oxime ligation (**VI.3.5**). MALDI-TOF:  $m/z$  calcd. for  $[\text{M}+\text{Na}]^+$ : 14032.5 (average), found: 14030.8.  $t_R = 8.38$  min. ( $\lambda = 214$  nm, 0-40% solv.B in 15').

### Compound **133**



Compound **133** (12.5 mg) was obtained in 77% yield by reacting **139** (2.2 mg, 1.3  $\mu\text{mol}$ ) and **147** (20.5 mg, 11.6  $\mu\text{mol}$ ) in a 0.1% TFA/ $\text{H}_2\text{O}$  solution (1.0 mL), following the general procedure for oxime ligation (VI.3.5.). MALDI-TOF:  $m/z$  calcd. for  $[\text{M}+\text{H}]^+$ : 12179.3 (average), found: 12183.0.  $t_R = 7.10$  min. ( $\lambda=214$  nm, 0-40% solv.B in 15').

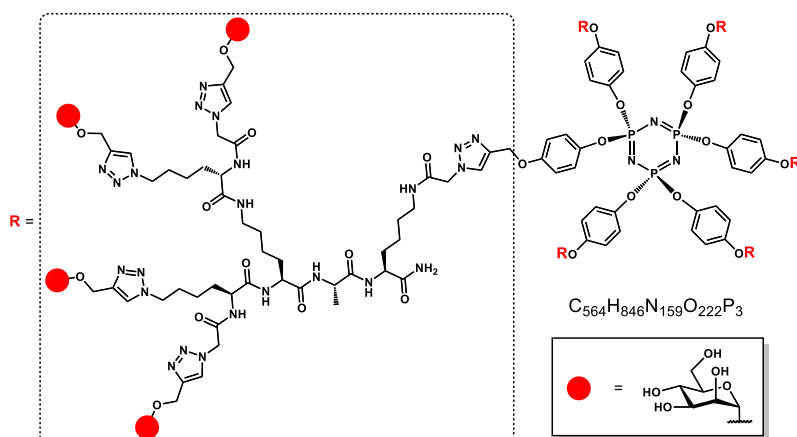
### Compound **134**



To a solution of **133** (1.3 mg, 1.3  $\mu\text{mol}$ ) and **148** (24.4 mg, 11.7  $\mu\text{mol}$ ) in DMF (600  $\mu\text{L}$ ), a solution of THPTA (16.9 mg, 38.9  $\mu\text{mol}$ ),  $\text{CuSO}_4 \cdot 5\text{H}_2\text{O}$  (0.1 mg, 0.4  $\mu\text{mol}$ ) and sodium ascorbate (10.8 mg, 54.5  $\mu\text{mol}$ ) in aq. PBS (pH 7.4, 10 mM, 1200  $\mu\text{L}$ ) were added. Compound **134** (12.6 mg) was obtained in 72% yield, following the general procedure for CuAAC (VI.3.6.). MALDI-TOF:  $m/z$  calcd. for  $[\text{M}+\text{H}]^+$ : 13498.9 (average), found: 13497.8.  $t_R =$

10.51 min. ( $\lambda=214$  nm, 0-40% solv.B in 15').  $^{31}\text{P}$ -NMR (162 MHz,  $\text{D}_2\text{O}$ )  $\delta = 10.22$  ppm.

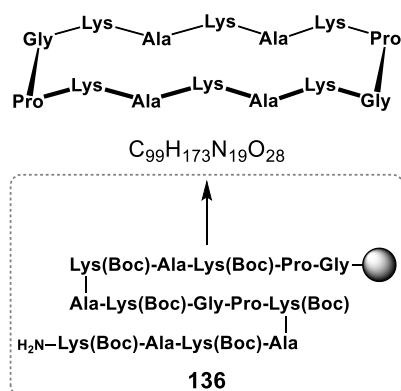
### Compound **135**



To a solution of **143** (0.7 mg, 0.7  $\mu\text{mol}$ ) and **149** (11.2 mg, 6.3  $\mu\text{mol}$ ) in DMF (500  $\mu\text{L}$ ), a solution of THPTA (9.1 mg, 20.9  $\mu\text{mol}$ ),  $\text{CuSO}_4 \cdot 5\text{H}_2\text{O}$  (0.1 mg, 0.4  $\mu\text{mol}$ ) and sodium ascorbate (5.8 mg, 29.3  $\mu\text{mol}$ ) in aq. PBS (pH 7.4, 10 mM, 1000  $\mu\text{L}$ ) were added. Compound **135** (5.8 mg) was obtained in 71% yield, following the general procedure for CuAAC

(**VI.3.6.**). MALDI-TOF:  $m/z$  calcd. for  $[\text{M}+\text{H}]^+$ : 11666.9 (average), found: 11665.9.  $t_R = 9.12$  min. ( $\lambda=214$  nm, 0-40% solv.B in 15').  $^{31}\text{P}$ -NMR (162 MHz,  $\text{D}_2\text{O}$ )  $\delta = 10.20$  ppm.

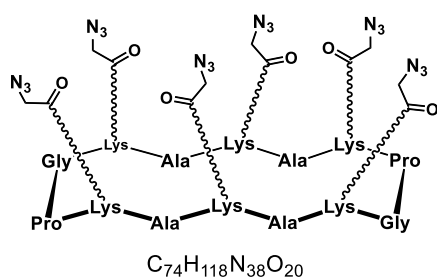
### Compound **137**



Peptide sequence **136** was synthesized manually in a polypropylene reactor, following the general procedure for SPPS (**VI.3.1.**) on 1.127 g of Fmoc-Gly-SASRIN™ support (measured loading = 0.544  $\text{mmol} \cdot \text{g}^{-1}$ ). Clivage from the resin was performed following the reported general procedure (**VI.3.2.**). Linear peptide **136** was dissolved in a  $\text{CH}_2\text{Cl}_2/\text{DMF}$  (1:1, 1.2 L) mixture, in the presence of DIPEA (214  $\mu\text{L}$ , 1.228 mmol) and PyBOP® (383 mg, 0.736 mmol). Cyclization was performed following the general procedure (**VI.3.3.**), the obtained solid crude was dissolved in a 50% TFA solution in  $\text{CH}_2\text{Cl}_2$  (25 mL) and stirred at room

temperature for 30 minutes. Solvent mixture was removed under reduced pressure and the reaction crude purified *via* RP-HPLC and lyophilized. Compound **137** (409.0 mg) was obtained in 49% overall yield. HRMS (ESI<sup>+</sup>-TOF):  $m/z$  calcd. for  $[\text{M}+\text{H}]^+$ : 1361.8745 (monoisotopic), found: 1361.8750.  $t_R = 5.25$  min. ( $\lambda=214$  nm, 0-30% solv.B in 15').

### Compound **138**

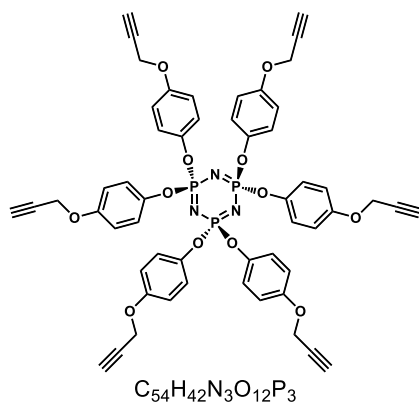


To a solution of **137** (13.6 mg, 10.0  $\mu\text{mol}$ ) in DMF (2 mL), DIPEA (12.5  $\mu\text{L}$ , 71.7  $\mu\text{L}$ ) and 2,5-dioxopyrrolidin-1-yl-2-azidoacetate<sup>374</sup> (20.0 mg, 101.0  $\mu\text{mol}$ ) were added and the solution stirred at room temperature for 30 minutes. The crude mixture was purified through RP-HPLC and lyophilized, to afford compound **138** (15.8 mg) in 85% yield. HRMS (ESI<sup>+</sup>-TOF):  $m/z$  calcd. for  $[\text{M}+\text{H}]^+$ : 1859.9463 (monoisotopic), found: 1859.9496.  $t_R = 6.79$

min. ( $\lambda=214$  nm, 5-80% solv.B in 15').

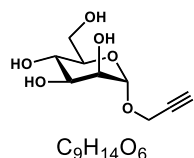






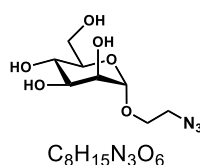
Compound **143** was synthesized according to the published procedure: Abbassi, L., Chabre, Y. M., Kottari, N., Arnold, A. A., Andre, S., Josserand, J., Gabius, H.-J., and Roy, R. (2015) Multifaceted glycodendrimers with programmable bioactivity through convergent, divergent, and accelerated approaches using polyfunctional cyclotriphosphazenes. *Polym. Chem.* *6*, 7666–7683. Characterization data were in accordance with the previous report.

#### Compound **144**



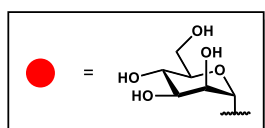
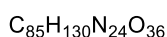
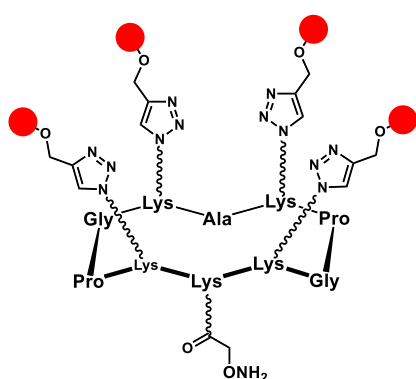
Compound **144** was synthesized according to the published procedure: Percec, V., Leowanawat, P., Sun, H.-J., Kulikov, O., Nusbaum, C. D., Tran, T. M., Bertin, A., Wilson, D. A., Peterca, M., Zhang, S., Kamat, N. P., Vargo, K., Moock, D., Johnston, E. D., Hammer, D. A., Pochan, D. J., Chen, Y., Chabre, Y. M., Shiao, T. C., Bergeron-Brlek, M., André, S., Roy, R., Gabius, H.-J., and Heiney, P. A. (2013) Modular Synthesis of Amphiphilic Janus Glycodendrimers and Their Self-Assembly into Glycodendrimersomes and Other Complex Architectures with Bioactivity to Biomedically Relevant Lectins. *J. Am. Chem. Soc.* *135*, 9055–9077. Characterization data were in accordance with the previous report.

#### Compound **145**



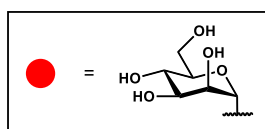
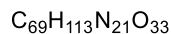
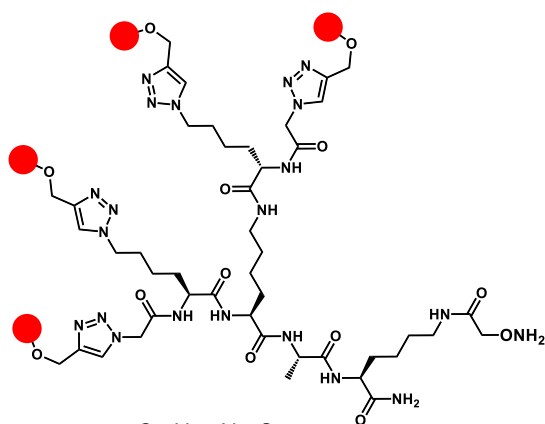
Compound **145** was synthesized according to the published procedure: Dowlut, M., Hall, D. G., and Hindsgaul, O. (2005) Investigation of Nonspecific Effects of Different Dyes in the Screening of Labeled Carbohydrates against Immobilized Proteins. *J. Org. Chem.* *70*, 9809–9813. Characterization data were in accordance with the previous report.

### Compound **146**



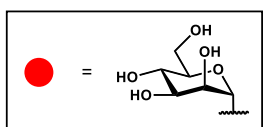
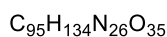
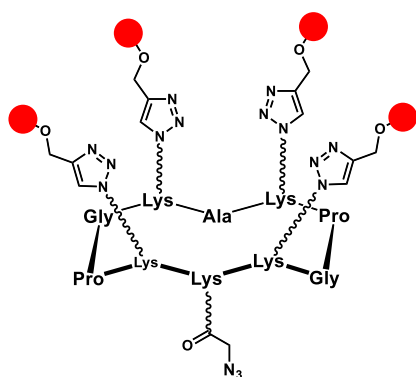
To a stirred solution of **128** (40.1 mg, 20.1  $\mu\text{mol}$ ) in DMF (3 mL), DIPEA (4.2  $\mu\text{L}$ , 24.3  $\mu\text{mol}$ ) and Boc-aminoxyacetic acid *N*-hydroxysuccinimide ester<sup>346</sup> (7.0 mg, 24.3  $\mu\text{mol}$ ) were added, and the reaction stirred at room temperature for 20 minutes. The solvent mixture was concentrated under reduced pressure and the resulting crude was treated with a TFA/ $\text{NH}_2\text{OH}$ / $\text{CH}_2\text{Cl}_2$  cocktail (50:2:48, 3.0 mL) for 30 minutes at room temperature. The mixture was concentrated and added drop-wise to ice-cold diethyl ether to induce the precipitation of the product. The obtained white solid was filtered, purified through RP-HPLC and lyophilized to give compound **146** (34.1 mg) in 82% yield over two steps. HRMS (ESI<sup>+</sup>-TOF):  $m/z$  calcd. for  $[\text{M}+\text{H}]^+$ : 2069.9627 (monoisotopic), found: 2069.9606.  $t_{\text{R}}$  = 7.10 min. ( $\lambda$ =214 nm, 0-30% solv.B in 15').

### Compound **147**



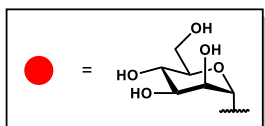
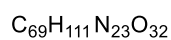
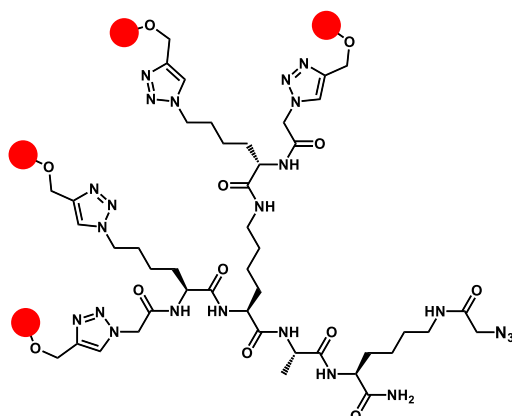
Compound **147** (31.5 mg) was obtained in 80% yield over two steps by reacting **130** (37.8 mg, 22.3  $\mu\text{mol}$ ) with Boc-aminoxyacetic acid *N*-hydroxysuccinimide ester<sup>346</sup> (7.8 mg, 27.1  $\mu\text{mol}$ ), following the same procedure described for compound **146** (*vide supra*). HRMS (ESI<sup>+</sup>-TOF):  $m/z$  calcd. for  $[\text{M}+\text{H}]^+$ : 1764.7888 (monoisotopic), found: 1764.7915; calcd. for  $[\text{M}+\text{Na}]^+$ : 1786.7707, found: 1786.7726.  $t_{\text{R}}$  = 5.65 min. ( $\lambda$ =214 nm, 0-30% solv.B in 15').

### Compound **148**



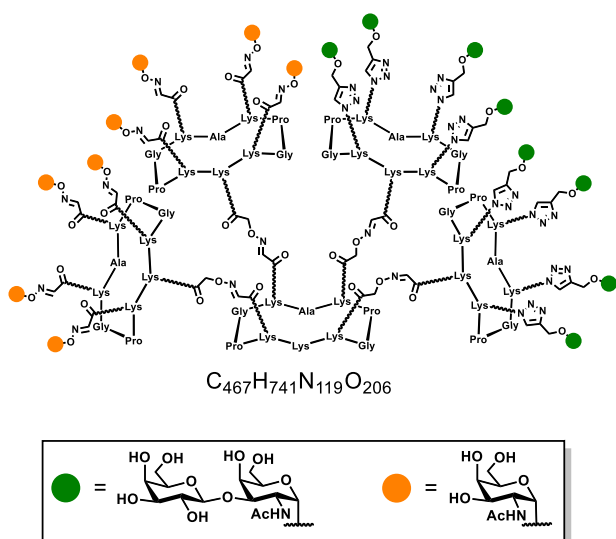
To a stirred solution of **128** (22.3 mg, 11  $\mu\text{mol}$ ) in DMF (2 mL), DIPEA (2.3  $\mu\text{L}$ , 13.2  $\mu\text{mol}$ ) and 2,5-dioxypyrrrolidin-1-yl-2-azidoacetate<sup>374</sup> (2.9 mg, 14.6  $\mu\text{mol}$ ) were added and the reaction stirred at room temperature for 30 minutes. The crude mixture was purified *via* RP-HPLC and lyophilized to give compound **148** (19.6 mg) in 84% yield.  $[\text{M}+\text{H}]^+$ : 2079.9583 (monoisotopic), found: 2079.9609.  $t_{\text{R}}$  = 8.27 min. ( $\lambda$ =214 nm, 0-30% solv.B in 15').

### Compound **149**



Compound **149** (21.8 mg) was obtained in 81% yield over two steps by reacting **130** (25.7 mg, 15.2  $\mu\text{mol}$ ) with 2,5-dioxypyrrrolidin-1-yl-2-azidoacetate<sup>374</sup> (3.9 mg, 19.7  $\mu\text{mol}$ ), following the same procedure described for compound **148** (*vide supra*). HRMS (ESI<sup>+</sup>-TOF):  $m/z$  calcd. for  $[\text{M}+\text{H}]^+$ : 1774.7844 (monoisotopic), found: 1774.7834; calcd. for  $[\text{M}+\text{Na}]^+$ : 1796.7663, found: 1796.7656.  $t_{\text{R}}$  = 6.64 min. ( $\lambda$ =214 nm, 0-30% solv.B in 15').

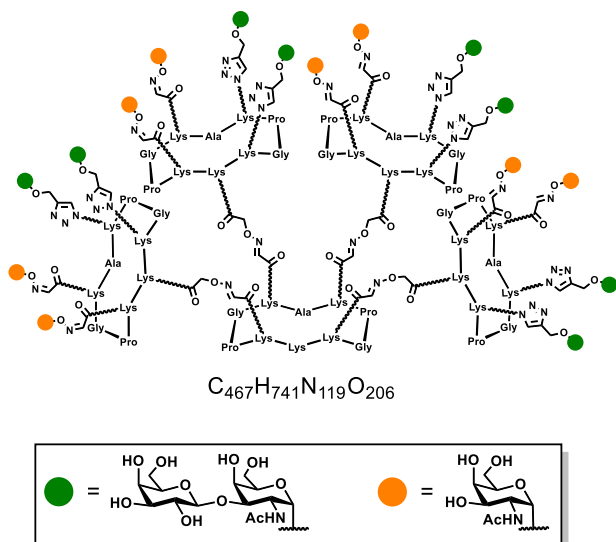
### Compound **150**



To a solution of **171** (10.2 mg, 1.6  $\mu\text{mol}$ ) in a  $\text{H}_2\text{O}/\text{CH}_3$  (1:1, 1.0 mL) mixture containing 0.1% TFA, **63** (4.6 mg, 19.5  $\mu\text{mol}$ ) was added and the reaction heated at 37°C without stirring. After 30 minutes, UPLC-MS showed complete conversion to the octa-Tn intermediate (**150i**, not isolated). ESI<sup>+</sup>-MS:  $m/z$  calcd. for  $C_{331}H_{530}N_{111}O_{118}$   $[\text{M}(\mathbf{150i})+5\text{H}]^{5+}$ : 1590.5 (average), found: 1590.5; calcd. for  $C_{331}H_{529}N_{111}O_{118}$   $[\text{M}(\mathbf{150i})+4\text{H}]^{4+}$ : 1987.9, found: 1987.7.  $t_R = 2.37$  min. ( $\lambda=214$  nm, 5-60% solv.D in 3'). To this mixture, a solution of **155** (4.6 mg, 19.5  $\mu\text{mol}$ , 12 eq.) in PBS (pH 7.4, 100 mM, 1.0

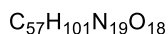
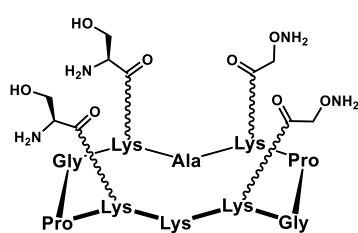
mL) was added and the reaction mixture degassed by argon bubbling for 15 minutes. A previously degassed solution of THPTA (5.7 mg, 13.1  $\mu\text{mol}$ , 8 eq.),  $\text{CuSO}_4 \cdot 5\text{H}_2\text{O}$  (0.1 mg, 0.4  $\mu\text{mol}$ ) and sodium ascorbate (10.4 mg, 23.9  $\mu\text{mol}$ , 15 eq.) in PBS (pH 7.4, 100 mM, 1.0 mL) was added to the reaction mixture. After 90 minutes stirring at room temperature, UPLC-MS analysis showed complete conversion to compound **150**. ESI<sup>+</sup>-MS:  $m/z$  calcd. for  $[\text{M}+6\text{H}]^{6+}$ : 1887.4 (average), found: 1887.4.  $t_R = 1.40$  min. ( $\lambda=214$  nm, 5-60% solv.D in 3'). Chelex<sup>®</sup> resin was added to the reaction mixture and stirred for 30 minutes at room temperature to remove copper ions. The crude was then purified by RP-HPLC and lyophilized to give pure compound **150** (10.2 mg) in 55% yield over two steps.  $t_R = 7.54$  min. ( $\lambda=214$  nm, 0-40% solv.B in 15').

### Compound **151**



Compound **151** (10.0 mg) was obtained in 60% yield over two steps by following the same procedure reported for **150** (*vide supra*). ESI<sup>+</sup>-MS:  $m/z$  calcd. for  $[\text{M}+6\text{H}]^{6+}$ : 1887.4 (average), found: 1887.5.  $t_R = 7.60$  min. ( $\lambda=214$  nm, 0-40% solv.B in 15').

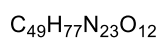
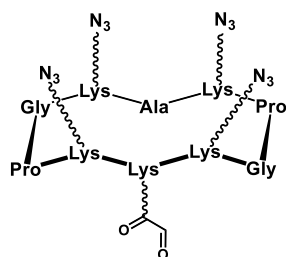
### Compound **152**



nm, 0-30% solv.B in 15').

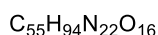
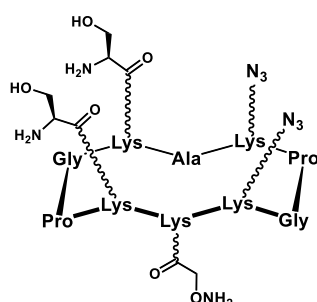
Compound **161** (22.1 mg, 11.3  $\mu$ mol) was treated with a TFA/TIS/ $NH_2OH/H_2O$  cocktail (94:2:2:2, 3.0 mL) for 3 hours at room temperature. After ice-cold diethyl-ether addition (15 mL) and filtration of the obtained precipitate, the crude product was purified by RP-HPLC and lyophilized to give pure compound **152** (14.1 mg) in 93% yield. ESI<sup>+</sup>-MS:  $m/z$  calcd. for  $[M+H]^+$ : 1341.5 (average), found: 1341.4; calcd. for  $[M+2H]^{2+}$ : 671.3, found: 671.0.  $t_R$  = 4.00 min. ( $\lambda$ =214

### Compound **153**



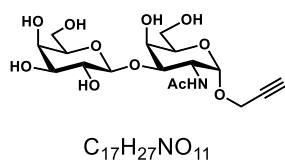
Compound **164** (50.7 mg, 41.9  $\mu$ mol) was treated with a solution of  $NaIO_4$  (89.6 mg, 419  $\mu$ mol) in  $H_2O$  (2.0 mL) following the general procedure for oxidative cleavage (VI.3.4.). Compound **153** was obtained in 71% yield (35.1 mg). HRMS (ESI<sup>+</sup>-TOF):  $m/z$  calcd. for  $[M+H]^+$ : 1180.6200 (monoisotopic), found: 1180.6211; calcd. for  $[M+H_2O+Na]^+$ : 1220.6125, found: 1220.6138.  $t_R$  = 6.78 min. ( $\lambda$ =214 nm, 5-100% solv.B in 15').

### Compound **154**



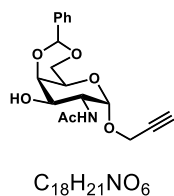
To a solution of **167** (69.4 mg, 44.5  $\mu$ mol) in DMF (5 mL), DIPEA (12  $\mu$ L, 68.9  $\mu$ mol) and Boc-aminoxyacetic acid *N*-hydroxysuccinimide ester<sup>346</sup> (15.4 mg, 53.4  $\mu$ mol) were added. After 20 minutes stirring at room temperature the reaction was neutralized by adding a 0.1% TFA/ $CH_3CN$  solution and the solvent mixture concentrated under reduced pressure. The crude product was treated with a TFA/ $NH_2OH$ /TIS/ $H_2O$  cocktail (94:2:2:2, 5.0 mL) for 3 hours at room temperature, then it was added to ice-cold diethyl ether (40 mL) to induce precipitation. The obtained solid was filtrated and purified by RP-HPLC to give, after lyophilization, pure compound **154** (50.5 mg) in 86% yield over two steps. HRMS (ESI<sup>+</sup>-TOF):  $m/z$  calcd. for  $[M+H]^+$ : 1319.7296 (monoisotopic), found: 1319.7302; calcd. for  $[M+Na]^+$ : 1341.7116, found: 1341.7123.  $t_R$  = 3.52 min. ( $\lambda$ =214 nm, 5-100% solv.B in 15').

### Compound 155



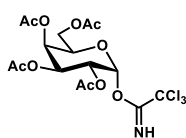
A solution of **158** (250 mg, 0.37 mmol) in 70% aq. acetic acid (2.5 mL) was stirred at 60°C for 4 hours. The mixture was concentrated under reduced pressure and co-evaporated with toluene. The residue was solubilized in dry MeOH (5.0 mL) and a solution of NaOMe in MeOH (25 wt%,  $d = 0.945 \text{ g}\cdot\text{mL}^{-1}$ ) was added to reach  $\text{pH} \approx 9$ . The reaction was stirred at room temperature overnight and neutralized with Amberlite IR-120  $\text{H}^+$ . The resin was filtered off, washed with MeOH and the filtrate was concentrated under vacuum. Compound **155** (147 mg) was obtained in 95% yield, as white amorphous solid after precipitation ( $\text{MeOH}/\text{CH}_2\text{Cl}_2$ ).  $^1\text{H-NMR}$  (400 MHz,  $\text{CD}_3\text{OD}$ )  $\delta = 5.02$  (1H, d,  $J = 3.7$  Hz, H-1), 4.48 (dd, 1H,  $J = 3.7, 11.1$  Hz, H-2), 4.40 (d, 1H,  $J = 7.6$  Hz, H-1'), 4.31 (dd, 1H,  $J = 2.4, 15.9$  Hz,  $-\text{CH}_2\text{C}\equiv\text{CH}$ ), 4.25 (dd, 1H,  $J = 2.4, 15.9$  Hz,  $\text{CH}_2\text{C}\equiv\text{CH}$ ), 4.17 (d, 1H,  $J = 2.2$  Hz, H-4'), 3.91 (dd, 1H, 3.0, 11.1 Hz, H-3), 3.85 (app t, 1H,  $J = 6.0$  Hz, H-5'), 3.81 (d, 1H,  $J = 2.9$  Hz, H-4), 3.75 (dd, 2H,  $J = 6.9, 11.3$  Hz, H-6<sub>a</sub>, H-6'<sub>a</sub>), 3.70 (dd, 2H,  $J = 5.1, 11.4$  Hz, H-6<sub>b</sub>, H-6'<sub>b</sub>), 3.50-3.56 (m, 2H, H-2', H-5'), 3.44 (dd, 1H,  $J = 3.2, 9.7$  Hz, H-3'), 2.85 (t, 1H,  $J = 2.3$  Hz,  $\text{CH}_2\text{C}\equiv\text{CH}$ ), 1.97 (s, 3H,  $\text{CH}_3$ ) ppm;  $^{13}\text{C-NMR}$  (100 MHz,  $\text{CD}_3\text{OD}$ )  $\delta = 174.68, 104.72, 96.27, 77.08, 75.83, 75.02, 72.56, 71.06, 70.65, 68.67, 68.62, 61.40, 61.01, 55.04, 48.37, 22.04$  ppm. HRMS (ESI<sup>+</sup>-TOF):  $m/z$  calcd. for  $[\text{M}+\text{H}]^+$ : 422.1662 (monoisotopic), found: 422.1674.

### Compound 156



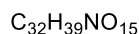
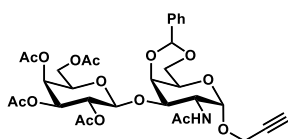
To a suspension of **112** (1.285 g, 4.956 mmol) and benzaldehyde dimethyl acetal (1.116 mL, 7.436 mmol) in dry  $\text{CH}_3\text{CN}$  (200 mL), ( $\pm$ )-camphor-10-sulfonic acid (115 mg, 0.495 mmol) was added and the mixture stirred at room temperature for 48 hours. The reaction was quenched with  $\text{Et}_3\text{N}$  (300  $\mu\text{L}$ ) and concentrated under reduced pressure. The crude mixture was purified over silica gel chromatography ( $\text{CH}_2\text{Cl}_2/\text{MeOH}$ , 98:2) to afford compound **156** (1.550 g) in 90% yield.  $^1\text{H-NMR}$  (400 MHz, acetone- $d_6$ )  $\delta = 7.55$  (m, 2H, H-Ar), 7.35 (m, 3H, H-Ar), 6.95 (d, 1H,  $J = 7.8$  Hz, NH), 5.65 (s, 1H, CHPh), 5.07 (d, 1H,  $J = 3.5$  Hz, H-1), 4.38 (app td, 1H,  $J = 8.6, 3.5$  Hz, H-2), 4.30 (app d, 1H,  $J = 3.4$  Hz, H-4), 4.29 (dd, 1H,  $J = 16.0, 2.5$  Hz,  $\text{CH}_2\text{C}\equiv\text{CH}$ ), 4.25 (dd, 1H,  $J = 16.0, 2.5$  Hz,  $\text{CH}_2\text{C}\equiv\text{CH}$ ), 4.17 (dd, 1H,  $J = 12.4, 1.6$  Hz, H-6<sub>a</sub>), 4.13 (dd, 1H,  $J = 12.5, 1.7$  Hz, H-6<sub>b</sub>), 3.88 (ddd, 1H,  $J = 11.1, 9.2, 3.4$  Hz, H-3), 3.79 (app d, 1H,  $J = 1.1$  Hz, H-5), 3.75 (d, 1H,  $J = 9.2$  Hz, OH-3), 2.97 (t, 1H,  $J = 2.4$  Hz,  $\text{CH}_2\text{C}\equiv\text{CH}$ ), 1.91 (s, 3H,  $\text{CH}_3$ ) ppm;  $^{13}\text{C-NMR}$  (100 MHz, acetone- $d_6$ )  $\delta = 170.92$  (C=O, acetyl), 139.91 (C-Ar), 129.46 (CH-Ar), 128.7 (2 $\times$ CH-Ar), 127.3 (2 $\times$ CH-Ar), 101.44 (CH-Ph), 98.3 (C-1), 80.3 ( $\text{CH}_2\text{C}\equiv\text{CH}$ ), 76.9 (C-4), 76.1 ( $\text{CH}_2\text{C}\equiv\text{CH}$ ), 69.8 (C-6), 68.2 (C-3), 64.4 (C-5), 55.4 ( $\text{CH}_2\text{C}\equiv\text{CH}$ ), 51.1 (C-2), 22.9 ( $\text{CH}_3$ ). HRMS (ESI<sup>+</sup>-TOF):  $m/z$  calcd. for  $[\text{M}+\text{H}]^+$ : 348.1447 (monoisotopic), found: 348.1445.

### Compound **157**



Compound **144** was synthesized according to the published procedure: Yu, H., and Chen, X. (2006) Aldolase-Catalyzed Synthesis of  $\beta$ -d-Galp-(1 $\rightarrow$ 9)-d-KDN: A Novel Acceptor for Sialyltransferases. *Org. Lett.* *8*, 2393–2396. Characterization data were in accordance with the previous report.

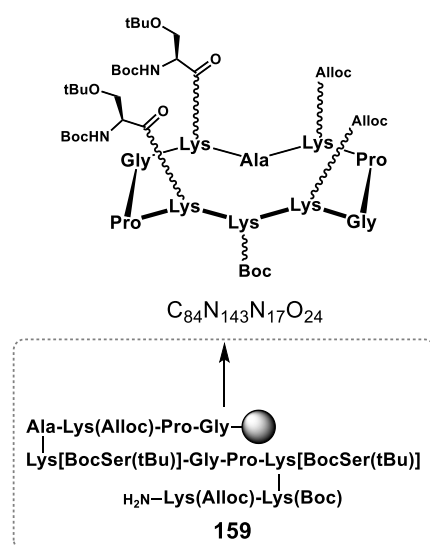
### Compound **158**



A solution of **156** (430 mg, 1.238 mmol) and **157**<sup>414</sup> (912 mg, 1.851 mmol) in dry  $\text{CH}_2\text{Cl}_2$  (10 mL) was stirred for 1 hour under argon atmosphere at room temperature, in the presence of activated 4 Å molecular sieves. The reaction was cooled to  $-15^\circ\text{C}$  and TMSOTf (45  $\mu\text{L}$ , 248  $\mu\text{mol}$ ) was added. After 30 minutes stirring at  $-15^\circ\text{C}$ , the reaction mixture was allowed to reach room temperature, quenched with  $\text{Et}_3\text{N}$  (50  $\mu\text{L}$ ), filtered on a Celite pad and the filtrate concentrated under reduced pressure. The crude mixture was next purified over silica gel chromatography ( $\text{CH}_2\text{Cl}_2/\text{MeOH}$ , 98:2) to afford compound **158** (503 mg) in 60% yield as white amorphous solid.  $^1\text{H}$  NMR (400 MHz,  $\text{CDCl}_3$ )  $\delta$  = 7.53

(m, 2H, H-Ar), 7.35 (m, 3H, H-Ar), 5.64 (d, 1H,  $J$  = 9.1 Hz, NHAc), 5.54 (s, 1H, CH-Ph), 5.37 (d, 1H,  $J$  = 3.3 Hz, H-4'), 5.18 (dd, 1H,  $J$  = 10.3, 7.9 Hz, H-2'), 5.12 (d, 1H,  $J$  = 3.5 Hz, H-1), 4.97 (dd, 1H,  $J$  = 10.3, 3.5 Hz, H-3'), 4.75 (d, 1H,  $J$  = 7.9 Hz, H-1'), 4.70 (ddd, 1H,  $J$  = 3.6, 9.1, 11.4 Hz, H-2), 4.02-4.30 (m, 7H, H-4, 2 $\times$ H-6, 2 $\times$ H-6', 2 $\times$  $\text{CH}_2\text{C}\equiv\text{CH}$ ), 3.95 (dd, 1H,  $J$  = 3.2, 11.2 Hz, H-3), 3.89 (app t, 1H,  $J$  = 5.9 Hz, H-5'), 3.69 (app t, 1H,  $J$  = 10.3 Hz, H-5), 2.46 (t, 1H,  $J$  = 2.4 Hz,  $\text{CH}_2\text{C}\equiv\text{CH}$ ), 2.14, 2.04, 2.03, 1.99, 1.96 (5s, 15H, 5 $\times$  $\text{CH}_3$ );  $^{13}\text{C}$ -NMR (125 MHz,  $\text{CDCl}_3$ )  $\delta$  = 170.71, 170.63, 170.41, 170.32, 170.22 (5 $\times$  $\text{C}=\text{O}$ ), 128.51 (C-Ar), 128.32 (CH-Ar), 126.76 (2 $\times$ CH-Ar), 126.68 (2 $\times$ CH-Ar), 100.83 (C-1'), 97.04 (C-1), 78.66 ( $\text{CH}_2\text{C}\equiv\text{CH}$ ), 75.45 ( $\text{CH}_2\text{C}\equiv\text{CH}$ ), 72.72 (C-5'), 71.06 (C-3'), 70.90 (C-5), 69.06 (C-3), 68.64 (C-2'), 68.04 (C-4), 66.99 (C-4'), 62.63 (C-6), 61.3 (C-6'), 55.3 ( $\text{CH}_2\text{C}\equiv\text{CH}$ ), 53.6 (C-2), 23.6, 20.9, 20.9, 20.8, 20.7 (5 $\times$  $\text{CH}_3$ ). HRMS (ESI<sup>+</sup>-TOF):  $m/z$  calcd. for  $[\text{M}+\text{H}]^+$ : 678.6577 (monoisotopic), found: 678.6570.

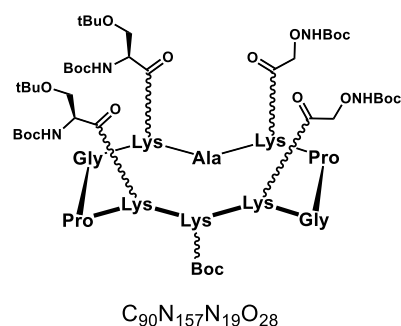
### Compound **160**



HRMS (ESI<sup>+</sup>-TOF):  $m/z$  calcd. for  $[M+Na]^+$ : 1797.0390 (monoisotopic), found: 1797.0406.  $t_R$  = 9.62 min. ( $\lambda$ =214 nm, 5-100% solv.B in 15').

Peptide sequence **159** was synthesized manually in a polypropylene reactor, following the general procedure for SPPS (VI.3.1.) on 985 mg of Fmoc-Gly-SASRIN<sup>™</sup> support (measured loading = 0.513 mmol·g<sup>-1</sup>). Cleavage from the resin was performed following the reported general procedure (VI.3.2.). Mass spectrometry analysis revealed the presence of the expected mass for sequence **159**. HRMS (ESI<sup>+</sup>-TOF):  $m/z$  calcd. for  $C_{84}H_{146}N_{17}O_{25}$   $[M(\mathbf{159})+H]^+$ : 1794.0706 (most intense peak on isotopic cluster), found: 1794.0641. Linear peptide **159** was dissolved in a CH<sub>2</sub>Cl<sub>2</sub>/DMF (1:1, 1.0 L) mixture, in the presence of DIPEA (178  $\mu$ L, 1.021 mmol) and PyBOP<sup>®</sup> (319 mg, 0.613 mmol). Compound **160** (489.8 mg) was obtained following the general procedure for cyclization (VI.3.3.) in 54% overall yield.

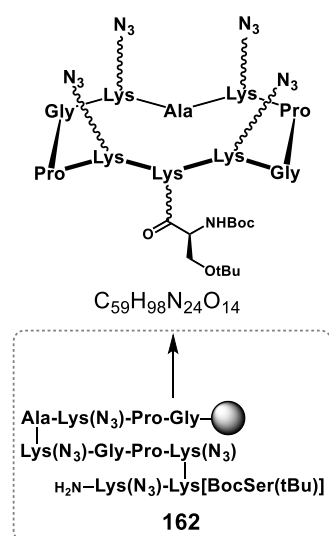
### Compound **161**



To a solution of **160** (72.3 mg, 40.7  $\mu$ mol) in a mixture of DMF/CH<sub>2</sub>Cl<sub>2</sub> (1:1, 20 mL), PhSiH<sub>3</sub> (250  $\mu$ L, 2.026 mmol) and Pd(PPh<sub>3</sub>)<sub>4</sub> (2.0 mg, 1.7  $\mu$ mol, 4% mol) were added and the reaction stirred at room temperature for 30 min. MeOH (5.0 mL) was added, and the mixture stirred until CO<sub>2</sub> bubbling ceased. The solvent mixture was evaporated to dryness, the residue taken into CH<sub>2</sub>Cl<sub>2</sub> (2.0 mL) and the resulting solution added drop-wise to ice-cold diethyl ether (100 mL) causing the precipitation of the Alloc-deprotected intermediate. The crude solid was filtrated, dried and analyzed *via* mass spectrometry, confirming its identity. HRMS (ESI<sup>+</sup>-TOF):  $m/z$  calcd. for  $C_{76}H_{136}N_{17}O_{20}$   $[M(\mathbf{160}\text{-Alloc})+H]^+$ : 1607.0148 (monoisotopic), found: 1607.0110. The crude was dissolved in DMF (5.0 mL), DIPEA (22  $\mu$ L, 126.2  $\mu$ mol) and Boc-aminoxyacetic acid *N*-hydroxysuccinimide ester<sup>346</sup> (28.2 mg, 97.8  $\mu$ mol) were added. After 20 minutes stirring at room temperature the reaction mixture was purified *via* RP-HPLC and lyophilized, to give compound **161** (54.1 mg) in 67% yield over two steps. HRMS (ESI<sup>+</sup>-TOF):  $m/z$  calcd. for  $[M+Na]^+$ : 1975.1343 (monoisotopic), found: 1975.1371.  $t_R$  = 9.72 min. ( $\lambda$ =214 nm, 5-100% solv.B in 15').



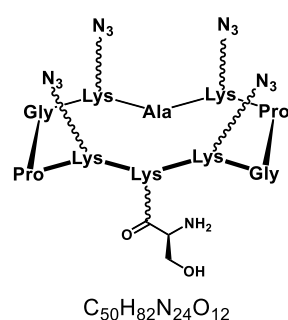
### Compound 163



min. ( $\lambda=214$  nm, 5-100% solv.B in 15').

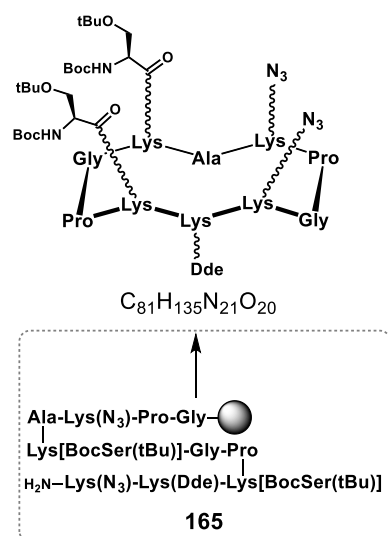
Peptide sequence **162** was synthesized manually in a polypropylene reactor, following the general procedure for SPPS (**VI.3.1.**) on 1.128 mg of Fmoc-Gly-SASRIN™ support (measured loading = 0.496 mmol·g<sup>-1</sup>). Clivage from the resin was performed following the reported general procedure (**VI.3.2.**). Mass spectrometry analysis revealed the presence of the expected mass for sequence **162**. HRMS (ESI<sup>+</sup>-TOF):  $m/z$  calcd. for C<sub>59</sub>H<sub>101</sub>N<sub>24</sub>O<sub>15</sub> [M(**162**)+H]<sup>+</sup>: 1385.7878 (monoisotopic), found: 1385.7856. Linear peptide **162** was dissolved in a CH<sub>2</sub>Cl<sub>2</sub>/DMF (1:1, 1.2 L) mixture, in the presence of DIPEA (195  $\mu$ L, 1.119 mmol) and PyBOP® (349 mg, 0.671 mmol). Compound **163** (366.9 mg) was obtained following the general procedure for cyclization (**VI.3.3.**) in 48% overall yield. HRMS (ESI<sup>+</sup>-TOF):  $m/z$  calcd. for [M+H]<sup>+</sup>: 1367.7773 (monoisotopic), found: 1367.7745; calcd. for [M+Na]<sup>+</sup>: 1389.7592, found: 1389.7561.  $t_R$  = 8.52

### Compound 164



Compound **163** (78.5 mg, 57.4  $\mu$ mol) was treated with a TFA/TIS/H<sub>2</sub>O cocktail (96:2:2, 2.0 mL) for 3 hours at room temperature. The reaction mixture was added drop-wise to ice-cold diethyl ether (50 mL) and the formed precipitate was filtrated, dried and purified through RP-HPLC. After lyophilization of the collected fractions, compound **164** (64.7 mg) was obtained in 96% yield. HRMS (ESI<sup>+</sup>-TOF):  $m/z$  calcd. for [M+H]<sup>+</sup>: 1211.6622 (monoisotopic), found: 1211.6602.  $t_R$  = 6.59 min. ( $\lambda=214$  nm, 5-100% solv.B in 15').

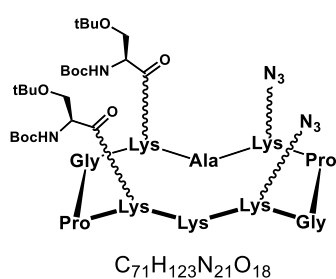
### Compound 166



1724.0282.  $t_R$  = 9.60 min. ( $\lambda=214$  nm, 5-100% solv.B in 15').

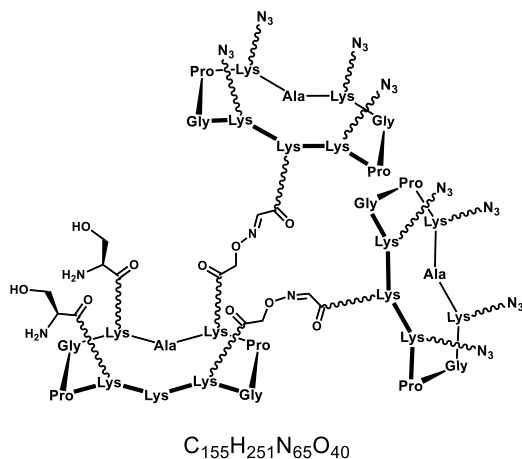
Peptide sequence **165** was synthesized manually in a polypropylene reactor, following the general procedure for SPPS (**VI.3.1.**) on 1.582 mg of Fmoc-Gly-SASRIN™ support (measured loading = 0.498 mmol·g<sup>-1</sup>). Clivage from the resin was performed following the reported general procedure (**VI.3.2.**). Mass spectrometry analysis revealed the presence of the expected mass for sequence **165**. HRMS (ESI<sup>+</sup>-TOF):  $m/z$  calcd. for C<sub>81</sub>H<sub>137</sub>N<sub>21</sub>O<sub>21</sub>Na [M(**165**)+Na]<sup>+</sup>: 1741.0376 (monoisotopic), found: 1741.0366. Linear peptide **165** was dissolved in a CH<sub>2</sub>Cl<sub>2</sub>/DMF (1:1, 1.6 L) mixture, in the presence of DIPEA (274  $\mu$ L, 1.572 mmol) and PyBOP® (492 mg, 0.946 mmol). Compound **166** (746.8 mg) was obtained following the general procedure for cyclization (**VI.3.3.**) in 55% overall yield. HRMS (ESI<sup>+</sup>-TOF):  $m/z$  calcd. for [M+H]<sup>+</sup>: 1724.0300 (monoisotopic), found:

### Compound 167



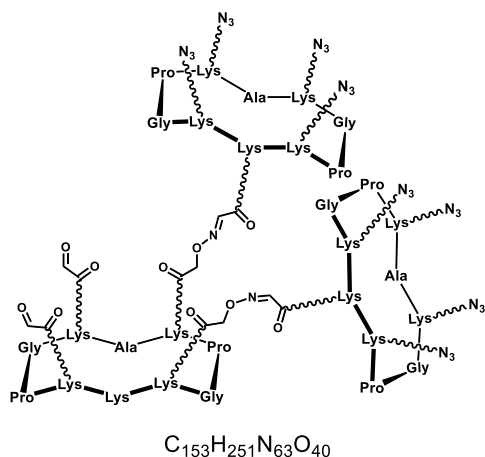
To a 2% solution of N<sub>2</sub>H<sub>4</sub>·H<sub>2</sub>O in DMF (5.0 ml), **166** (90.3 mg, 52.4 μmol) was added and the reaction stirred at room temperature for 20 minutes. The solvent mixture was concentrated under reduced pressure, purified *via* RP-HPLC and lyophilized to give compound **167** (76.8 mg) in 94% yield. HRMS (ESI<sup>+</sup>-TOF): *m/z* calcd. for [M+H]<sup>+</sup>: 1558.9433 (monoisotopic), found: 1558.9458. *t<sub>R</sub>* = 8.65 min. (λ=214 nm, 5-100% solv.B in 15').

### Compound 168



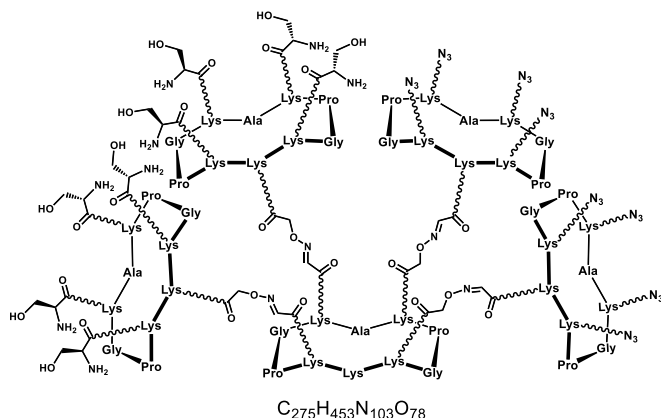
Compound **168** (24.7 mg) was obtained in 75% yield by reacting **152** (12.1 mg, 9.0 μmol) and **153** (31.9 mg, 27.0 μmol) in a H<sub>2</sub>O/CH<sub>3</sub>CN mixture (1:1, 2.0 mL) containing 0.1% TFA, following the general procedure for oxime ligation (VI.3.5.). ESI<sup>+</sup>-MS: *m/z* calcd. for [M+2H]<sup>2+</sup>: 1833.5 (average), found: 1833.5; calcd. for [M+3H]<sup>3+</sup>: 1222.7, found: 1222.6; calcd. for [M+3H+Na]<sup>4+</sup>: 922.8, found: 922.8. *t<sub>R</sub>* = 8.17 min. (λ=214 nm, 5-100% solv.B in 15').

### Compound 169



Compound **168** (22.3 mg, 6.1 μmol) was treated with a solution of sodium periodate (26.1 mg, 0.122 mmol) in a H<sub>2</sub>O/CH<sub>3</sub>CN mixture (1:1, 2.0 mL), following the general procedure for oxidative cleavage (VI.3.4.), to afford compound **169** (16.5 mg) in 75% yield. ESI<sup>+</sup>-MS: *m/z* calcd. for [M+H<sub>2</sub>O+H+Na]<sup>2+</sup>: 1831.5 (average), found: 1831.5; calcd. for [M+H<sub>2</sub>O+H+2Na]<sup>3+</sup>: 1228.7, found: 1228.6; calcd. for [M+H<sub>2</sub>O+H+3Na]<sup>4+</sup>: 927.2, found: 927.2. *t<sub>R</sub>* = 8.49 min. (λ=214 nm, 5-100% solv.B in 15').

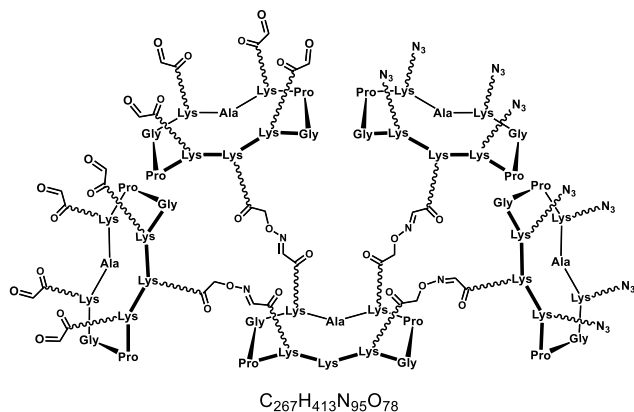
### Compound **170**



922.5.  $t_R = 7.23$  min. ( $\lambda=214$  nm, 5-100% solv.B in 15').

Compound **170** (24.1 mg) was obtained in 85% yield by reacting **169** (16.0 mg, 4.4  $\mu$ mol) and **64** (19.0 mg, 13.2  $\mu$ mol) in a  $H_2O/CH_3CN$  mixture (1:1, 1.0 mL) containing 0.1% TFA, following the general procedure for oxime ligation (VI.3.5.). ESI<sup>+</sup>-MS:  $m/z$  calcd. for  $[M+4H]^{4+}$ : 1613.6 (average), found: 1613.5; calcd. for  $[M+5H]^{5+}$ : 1291.0, found: 1291.0; calcd. for  $[M+6H]^{6+}$ : 1076.0, found: 1076.1; calcd. for  $[M+7H]^{7+}$ : 922.5, found:

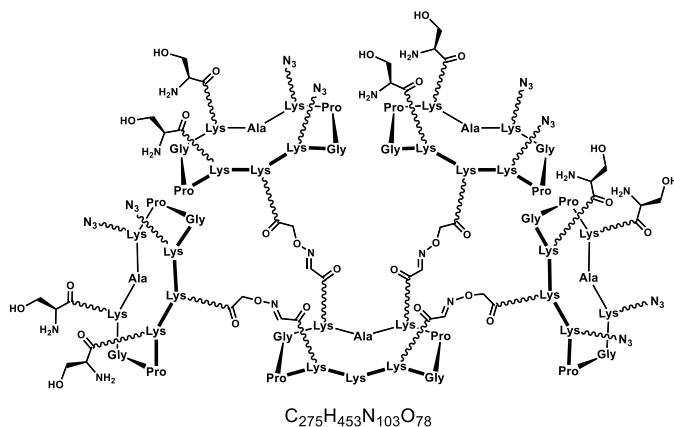
### Compound **171**



100% solv.B in 15').

Compound **170** (23.6 mg, 3.7  $\mu$ mol) was treated with a solution of sodium periodate (62.6 mg, 0.293 mmol) in a  $H_2O/CH_3CN$  mixture (1:1, 2.0 mL), following the general procedure for oxidative cleavage (VI.3.4.), to afford compound **171** (17.7 mg) in 78% yield. ESI<sup>+</sup>-MS:  $m/z$  calcd. for  $[M+3H]^{3+}$ : 2068.2 (average), found: 2067.7; calcd. for  $[M+4H]^{4+}$ : 1551.4, found: 1551.1; calcd. for  $[M+5H]^{5+}$ : 1241.4, found: 1241.1.  $t_R = 8.11$  min. ( $\lambda=214$  nm, 5-

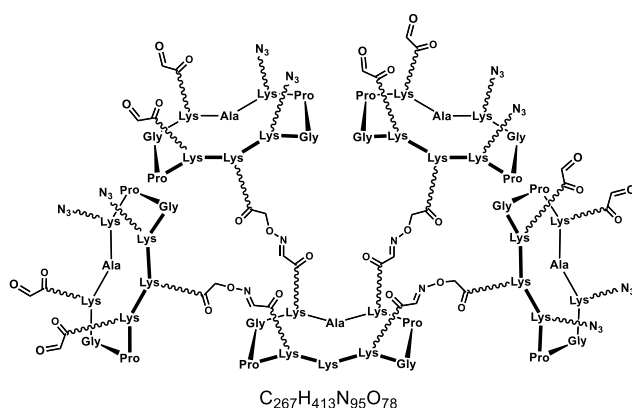
### Compound **172**



$[M+7H]^{7+}$ : 922.5, found: 922.5.  $t_R = 5.17$  min. ( $\lambda=214$  nm, 5-100% solv.B in 15').

Compound **172** (34.2 mg) was obtained in 87% yield by reacting **89** (7.6 mg, 6.1  $\mu$ mol) and **154** (48.1 mg, 36.4  $\mu$ mol) in a  $H_2O/CH_3CN$  mixture (1:1, 1.0 mL) containing 0.1% TFA, following the general procedure for oxime ligation (VI.3.5.). ESI<sup>+</sup>-MS:  $m/z$  calcd. for  $[M+4H]^{4+}$ : 1613.6 (average), found: 1613.5; calcd. for  $[M+5H]^{5+}$ : 1291.0, found: 1291.1; calcd. for  $[M+6H]^{6+}$ : 1076.0, found: 1076.2; calcd. for

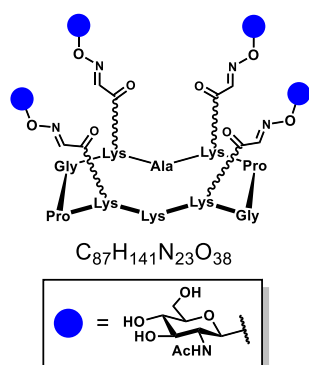
### Compound **173**



100% solv.B in 15').

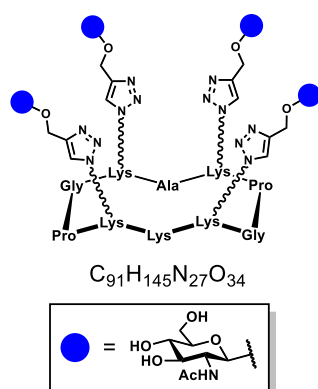
Compound **172** (21.8 mg, 3.4  $\mu\text{mol}$ ) was treated with a solution of sodium periodate (58.2 mg, 0.272 mmol) in a  $\text{H}_2\text{O}/\text{CH}_3\text{CN}$  mixture (1:1, 2.0 mL), following the general procedure for oxidative cleavage (**VI.3.4.**), to afford compound **173** (15.3 mg) in 73% yield. ESI<sup>+</sup>-MS:  $m/z$  calcd. for  $[\text{M}+3\text{H}]^{3+}$ : 2068.2 (average), found: 2068.5; calcd. for  $[\text{M}+4\text{H}]^{4+}$ : 1551.4, found: 1551.7; calcd. for  $[\text{M}+5\text{H}]^{5+}$ : 1241.4, found: 1241.6.  $t_R = 8.08$  min. ( $\lambda=214$  nm, 5-

### Compound **174**



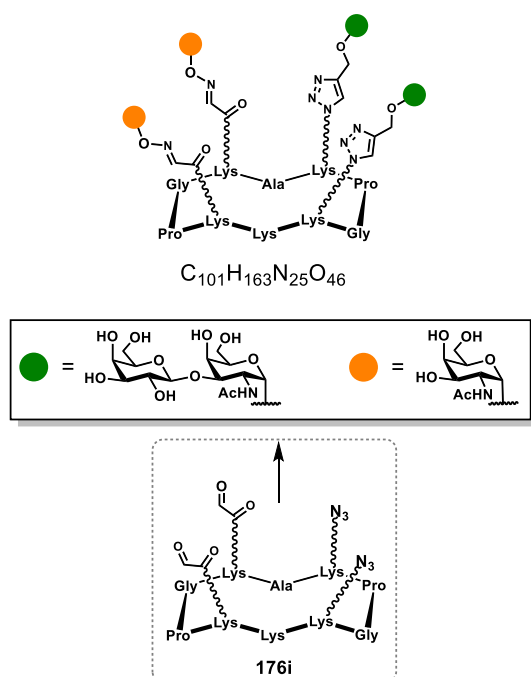
Compound **174** (7.3 mg) was obtained in 88% yield by reacting **89** (4.9 mg, 3.9  $\mu\text{mol}$ ) and 2-acetamido-2-deoxy- $\beta$ -D-glucopyranosyl hydroxylamine<sup>354</sup> (5.5 mg, 23.3  $\mu\text{mol}$ ) in 0.1% TFA/ $\text{H}_2\text{O}$  (1.0 mL), following the general procedure for oxime ligation (**VI.3.5.**). HRMS (ESI<sup>+</sup>-TOF):  $m/z$  calcd. for  $[\text{M}+\text{H}]^+$ : 2116.9886, found: 2116.9878; calcd.  $[\text{M}+\text{Na}]^+$ : 2138.9706, found: 2138.9624.  $t_R = 5.39$  min. ( $\lambda=214$  nm, 0-40% solv.B in 15 min.).

### Compound **175**



To a solution of **120** (5.4 mg, 4.8  $\mu\text{mol}$ ) and prop-2-ynyl 2-acetamido-2-deoxy- $\beta$ -D-glucopyranoside<sup>354</sup> (7.5 mg, 28.9  $\mu\text{mol}$ ) in DMF (600  $\mu\text{L}$ ), a solution of THPTA (8.3 mg, 19.1  $\mu\text{mol}$ ),  $\text{CuSO}_4 \cdot 5\text{H}_2\text{O}$  (0.1 mg, 0.4  $\mu\text{mol}$ ) and sodium ascorbate (7.6 mg, 38.4  $\mu\text{mol}$ ) in aq. PBS (pH 7.4, 10 mM, 1200  $\mu\text{L}$ ) was added. Compound **175** (8.4 mg) was obtained in 81% yield, following the general procedure for CuAAC (**VI.3.6.**). HRMS (ESI<sup>+</sup>-TOF):  $m/z$  calcd. for  $[\text{M}+\text{H}]^+$ : 2161.0526, found: 2161.0530; calcd. for  $[\text{M}+\text{Na}]^+$ : 2184.0373, found: 2184.0386.  $t_R = 5.48$  min. ( $\lambda=214$  nm, 0-40% solv.B in 15 min.).

## Compound 176

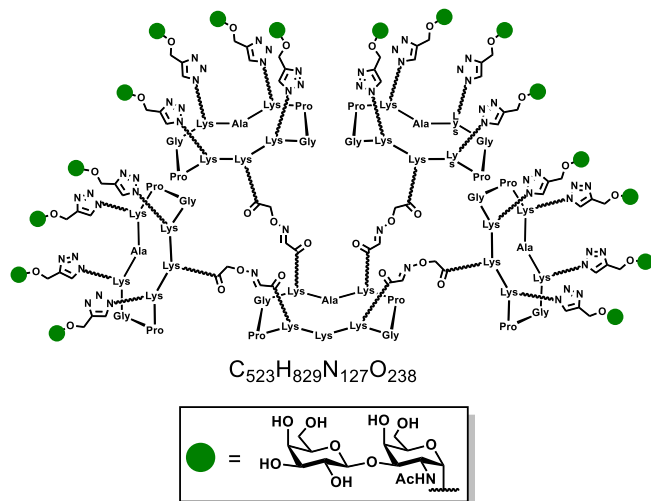


Compound **167** (6.8 mg, 4.4  $\mu\text{mol}$ ) was treated with a TFA/TIS/ $\text{H}_2\text{O}$  cocktail (96:2:2, 1.0 mL) for 3 hours at room temperature. The reaction mixture was added drop-wise to ice-cold diethyl ether (5.0 mL), the formed precipitate was filtrated and dissolved in  $\text{H}_2\text{O}/\text{CH}_3\text{CN}$  (1:1, 1.0 mL) for the next step, which involved the treatment with sodium periodate (18.8 mg, 87.9  $\mu\text{mol}$ ), according to the general procedure for oxidative cleavage (VI.3.4.). Compound **176i** (3.8 mg) was obtained in 74% yield over two steps. HRMS (ESI<sup>+</sup>-TOF):  $m/z$  calcd. for  $[\text{M}(\mathbf{176i})+\text{H}]^+$ : 1184.6289, found: 1184.6309; calcd. for  $[\text{M}(\mathbf{176i})+\text{H}_2\text{O}+\text{H}]^+$ : 1220.6500, found: 1220.6527.  $t_R = 3.78$  min. ( $\lambda = 214$  nm, 5-100% solv.B in 15 min.).

To a solution of **176i** (2.2 mg, 1.9  $\mu\text{mol}$ ) in a  $\text{H}_2\text{O}/\text{CH}_3\text{CN}$  (1:1, 500  $\mu\text{L}$ ) mixture containing 0.1% TFA, **63** (1.4 mg,

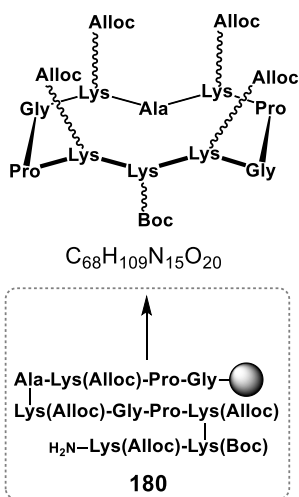
5.9  $\mu\text{mol}$ ) was added and the reaction heated at 37°C without stirring. After 30 minutes, **155** (2.4 mg, 5.7  $\mu\text{mol}$ ) was added to this mixture, then 1.0 mL of PBS buffer (pH 7.4, 100 mM) was added and the solution degassed by argon bubbling for 15 minutes. A separate solution, containing  $\text{CuSO}_4$  (0.1 mg, 0.4  $\mu\text{mol}$ ), THPTA (1.7 mg, 3.9  $\mu\text{mol}$ ) and sodium ascorbate (1.5 mg, 7.6  $\mu\text{mol}$ ) in previously degassed PBS buffer (1.0 mL, pH 7.4, 100mM) was added to the reaction mixture. After 90 minutes stirring at room temperature, Chelex<sup>®</sup> resin was added to the reaction mixture and stirred for 30 minutes at room temperature in order to remove residues of copper. The crude was then purified by preparative RP-HPLC and lyophilized to give compound **176** (3.4 mg) in 72% yield over two steps. HRMS (ESI<sup>+</sup>-TOF):  $m/z$  calcd. for  $[\text{M}+\text{H}]^+$ : 2463.1262, found: 2463.1223; calcd. for  $[\text{M}+\text{Na}]^+$ : 2485.1081, found: 2485.1047.  $t_R = 5.40$  min. ( $\lambda = 214$  nm, 0-40% solv.B in 15 min.).

## Compound 177



To a solution of **125** (5.8 mg, 1.0  $\mu\text{mol}$ ) and **155** (8.4 mg, 20.0  $\mu\text{mol}$ ) in DMF (600  $\mu\text{L}$ ), a solution of THPTA (13.9 mg, 32.0  $\mu\text{mol}$ ),  $\text{CuSO}_4 \cdot 5\text{H}_2\text{O}$  (0.1 mg, 0.4  $\mu\text{mol}$ ) and sodium ascorbate (16.3 mg, 82.3  $\mu\text{mol}$ ) in aq. PBS (pH 7.4, 10 mM, 1200  $\mu\text{L}$ ) was added. Compound **177** (9.5 mg) was obtained in 75% yield, following the general procedure for CuAAC (VI.3.6.). MALDI-TOF:  $m/z$  calcd. for  $[\text{M}+\text{H}]^+$ : 12704.9 (average), found: 12700.2.  $t_R = 8.22$  min. ( $\lambda = 214$  nm, 0-40% solv.B in 15').

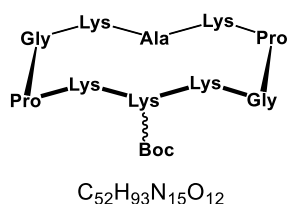
Compound 181



1478.7893.  $t_R = 7.75$  min. ( $\lambda=214$  nm, 5-100% solv.B in 15').

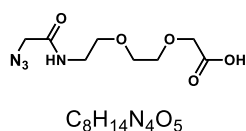
Peptide sequence **180** was synthesized manually in a polypropylene reactor, following the general procedure for SPPS (**VI.3.1.**) on 2.342 mg of Fmoc-Gly-SASRIN™ support (measured loading = 0.488 mmol·g<sup>-1</sup>). Cleavage from the resin was performed following the reported general procedure (**VI.3.2.**). Mass spectrometry analysis revealed the presence of the expected mass for sequence **165**. HRMS (ESI<sup>+</sup>-TOF):  $m/z$  calcd. for C<sub>68</sub>H<sub>111</sub>N<sub>15</sub>O<sub>21</sub>Na [M(**180**)+Na]<sup>+</sup>: 1496.7977 (monoisotopic), found: 1496.7992. Linear peptide **180** was dissolved in a CH<sub>2</sub>Cl<sub>2</sub>/DMF (1:1, 3.0 L) mixture, in the presence of DIPEA (398 μL, 2.284 mmol) and PyBOP® (715 mg, 1.374 mmol). Compound **181** (965.6 mg) was obtained following the general procedure for cyclization (**VI.3.3.**) in 58% overall yield. HRMS (ESI<sup>+</sup>-TOF):  $m/z$  calcd. for [M+Na]<sup>+</sup>: 1478.7871 (monoisotopic), found:

#### Compound **182**



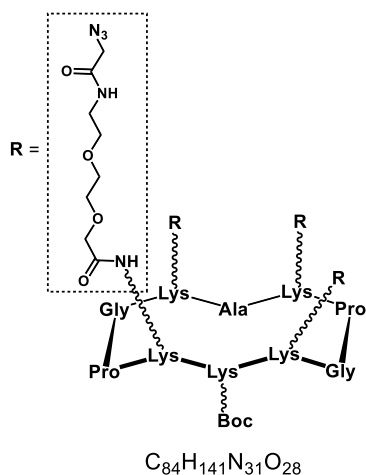
To a stirred solution of **181** (824.6 mg, 566.1 μmol) in CH<sub>2</sub>Cl<sub>2</sub> (100 mL), of Pd(PPh<sub>3</sub>)<sub>4</sub> (65.4 mg, 56.6 μmol, 10% mol) and PhSiH<sub>3</sub> (6.985 mL, 56.611 mmol) were added. After 30 minutes stirring at room temperature MeOH (30 mL) was added, and the reaction stirred until the CO<sub>2</sub> bubbling ceased. The solvent mixture was removed under reduced pressure, the residue was taken into CH<sub>2</sub>Cl<sub>2</sub> (50 mL) and the resulting fine suspension extracted with H<sub>2</sub>O (4 x 50 mL). The combined aqueous fractions were lyophilized, and the obtained solid dissolved in H<sub>2</sub>O (10 mL) and purified through RP-HPLC. Compound **182** (396.5 mg) was obtained in 42% yield as white solid after lyophilization. HRMS (ESI<sup>+</sup>-TOF):  $m/z$  calcd. for [M+H]<sup>+</sup>: 1120.7206 (monoisotopic), found: 1120.7244.  $t_R = 9.44$  min. ( $\lambda=214$  nm, 0-30% solv.B in 15').

#### Compound **184**



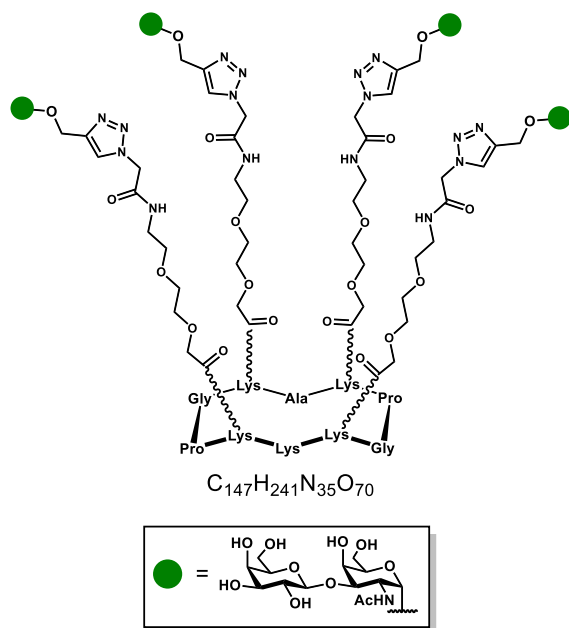
Compound **183** (54.2 mg, 206.6 μmol) was treated with a TFA/CH<sub>2</sub>Cl<sub>2</sub> (1:1, 2.0 mL) mixture for 30 minutes at room temperature. The reaction mixture was added drop-wise to ice-cold diethyl ether (20 mL), the solid was filtrated, dried and dissolved in a CH<sub>3</sub>CN/DMF mixture (2.0 mL). To this solution, DIPEA (54 μL, 309.9 μmol) and 2,5-dioxopyrrolidin-1-yl-2-azidoacetate<sup>374</sup> (49.1 mg, 247.8 μmol) were added and the reaction stirred at room temperature for 20 minutes. The reaction mixture was purified through RP-HPLC and lyophilized to give compound **184** (41.7 mg) in 82% yield over two steps. ESI<sup>+</sup>-MS:  $m/z$  calcd. for [M+H]<sup>+</sup>: 247.1 (monoisotopic), found: 247.3.  $t_R = 4.12$  min. ( $\lambda=214$  nm, 0-30% solv.B in 15').

### Compound **185**



To a solution of **182** (18.5 mg, 16.5  $\mu\text{mol}$ ) in a  $\text{CH}_3\text{CN}/\text{DMF}$  (1:1, 2.0 mL) mixture, DIPEA (23  $\mu\text{L}$ , 132.0  $\mu\text{mol}$ ), PyBOP<sup>®</sup> (53.2 mg, 102.2  $\mu\text{mol}$ ) and **184** (25.6 mg, 104.0  $\mu\text{mol}$ ) were added. After 20 minutes stirring at room temperature, the reaction mixture was purified *via* RP-HPLC and lyophilized, to give compound **185** (29.5 mg) in 88% yield. ESI<sup>+</sup>-MS:  $m/z$  calcd. for  $[\text{M}+\text{H}]^+$ : 2034.2 (average), found: 2033.9.  $t_R = 11.02$  min. ( $\lambda=214$  nm, 5-60% solv.B in 15').

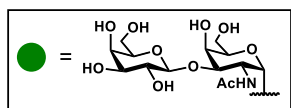
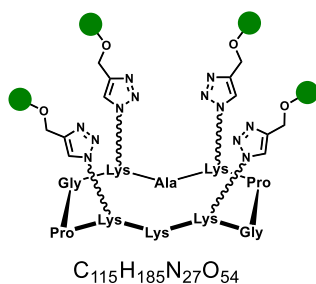
### Compound **186**



Compound **185** (15.2 mg, 7.5  $\mu\text{mol}$ ) was treated with a  $\text{TFA}/\text{CH}_2\text{Cl}_2$  mixture (1:1, 1.0 mL) for 30 minutes at room temperature. The reaction mixture was added drop-wise to ice-cold diethyl ether (20 mL), the obtained solid was filtrated, dried and used for the next step without any further purification. The crude intermediate was dissolved in a  $\text{CH}_3\text{CN}/\text{DMF}$  (1:1, 1.0 mL) mixture, in the presence of **155** (19.0 mg, 45.1  $\mu\text{mol}$ ). To this solution, a mixture containing THPTA (32.6 mg, 75.0  $\mu\text{mol}$ ),  $\text{CuSO}_4 \cdot 5\text{H}_2\text{O}$  (0.1 mg, 0.4  $\mu\text{mol}$ ) and sodium ascorbate (41.6 mg, 210.0  $\mu\text{mol}$ ) in aq. PBS (pH 7.4, 10 mM, 2.0 mL) was added. Compound **186** (18.2 mg) was obtained in 67% yield over two steps, according to the general procedure for CuAAC

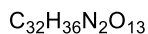
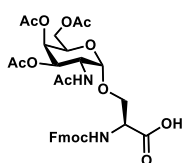
(**VI.3.6.**). ESI<sup>+</sup>-MS:  $m/z$  calcd. for  $[\text{M}+2\text{H}]^{2+}$ : 1809.8 (most intense peak of isotopic cluster), found: 1809.9; calcd. for  $[\text{M}+3\text{H}]^{3+}$ : 1206.9, found: 1207.0.  $t_R = 10.23$  min. ( $\lambda=214$  nm, 0-30% solv.B in 15').

### Compound **187**



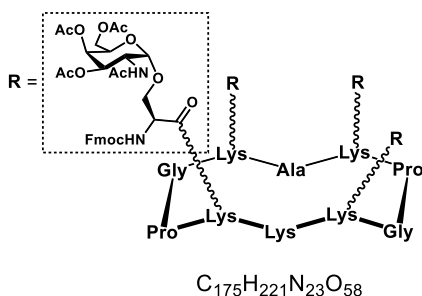
To a solution of **120** (4.2 mg, 3.7  $\mu\text{mol}$ ) and **155** (9.5 mg, 22.5  $\mu\text{mol}$ ) in DMF (600  $\mu\text{L}$ ), a solution containing THPTA (12.9 mg, 29.7  $\mu\text{mol}$ ),  $\text{CuSO}_4 \cdot 5\text{H}_2\text{O}$  (0.1 mg, 0.4  $\mu\text{mol}$ ) and sodium ascorbate (14.7 mg, 74.2  $\mu\text{mol}$ ) in aq. PBS (pH 7.4, 10 mM, 1200  $\mu\text{L}$ ) was added. Compound **187** (7.6 mg) was obtained in 73% yield, according to the general procedure for CuAAC (**VI.3.6**). HRMS (ESI<sup>+</sup>-TOF):  $m/z$  calcd. for  $[\text{M}+\text{H}]^+$ : 2809.2638 (monoisotopic), found: 2809.2549.  $t_R = 5.43$  min. ( $\lambda=214$  nm, 0-40% solv.B in 15').

### Compound **188**



Compound **188** was synthesized according to the published procedure: Wu, Z., Guo, X., and Guo, Z. (2010) Chemoenzymatic synthesis of glycosylphosphatidylinositol-anchored glycopeptides. *Chem. Commun.* 46, 5773–5774. Characterization data were in accordance with the previous report.

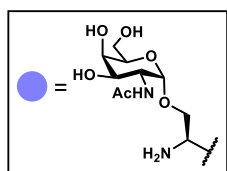
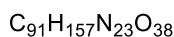
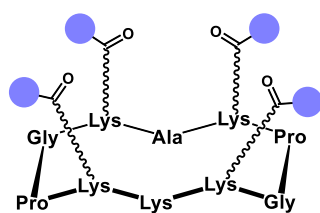
### Compound **189**



To a solution of **182** (87.8 mg, 78.4  $\mu\text{mol}$ ) in DMF (15.0 mL), DIPEA (92  $\mu\text{L}$ , 528.0  $\mu\text{mol}$ ), PyBOP<sup>®</sup> (205.2 mg, 394.4  $\mu\text{mol}$ ) and **188** (247.1 mg, 376.3  $\mu\text{mol}$ ) were added. After 20 minutes stirring at room temperature the solvent mixture was removed under high vacuum and the resulting oily residue was treated with a TFA/ $\text{CH}_2\text{Cl}_2$  (1:1, 1.0 mL) mixture for 30 minutes at room temperature. The reaction mixture was added drop-wise to ice-cold diethyl ether (100 mL), the obtained solid was filtrated, dried and purified through preparative RP-HPLC. After lyophilization, compound **189** (187.8 mg) was obtained in 67% yield over two steps. MALDI-TOF:  $m/z$  calcd. for  $[\text{M}+\text{Na}]^+$ : 3597.7 (average), found: 3598.7.  $t_R = 12.67$  min. ( $\lambda=214$  nm, 5-100% solv.B in 15').

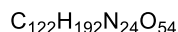
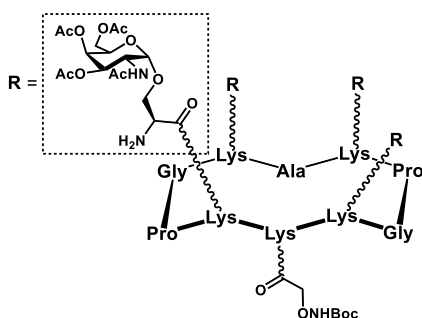


### Compound 190



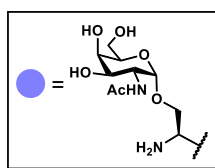
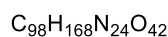
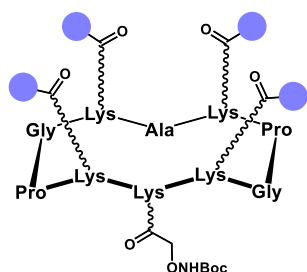
Compound **189** (9.2 mg, 2.6  $\mu\text{mol}$ ) was dissolved in a piperidine/ $\text{CH}_3\text{CN}$  (5% v/v, 1.0 ml) mixture. After 15 minutes stirring UPLC-MS showed complete Fmoc-deprotection. The solvent mixture was concentrated to dryness to give a white residue. A solution of NaOMe/MeOH (25 wt%,  $d = 0.945 \text{ g}\cdot\text{mL}^{-1}$ ) in dry MeOH ( $\text{pH}\approx 10$ ) was added to the crude. After 20 minutes stirring at room temperature UPLC-MS showed complete deprotection. The reaction was neutralized with Amberlite IR-120  $\text{H}^+$ , the resin filtered off, washed with MeOH and the filtrate purified *via* RP-HPLC. After lyophilization, compound **190** (4.6 mg) was obtained in 82% yield over two steps. ESI<sup>+</sup>-MS:  $m/z$  calcd. for  $[\text{M}+\text{H}]^+$ : 2181.1 (monoisotopic), found: 2180.6.  $t_R = 3.66 \text{ min}$ . ( $\lambda=214 \text{ nm}$ , 0-20% solv.B in 15').

### Compound 191



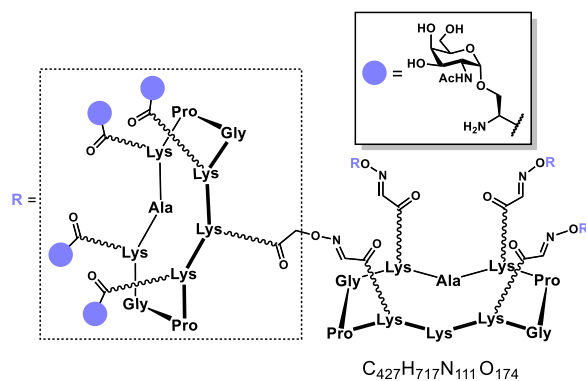
To a solution of **189** (37.3 mg, 10.4  $\mu\text{mol}$ ) in a  $\text{CH}_3\text{CN}/\text{DMF}$  (1:1, 3.5 mL) mixture, DIPEA (3.6  $\mu\text{L}$ , 20.7  $\mu\text{mol}$ ) and Boc-aminoxyacetic acid *N*-hydroxysuccinimide ester<sup>346</sup> (3.6 mg, 12.5  $\mu\text{mol}$ ) were added. After 20 minutes stirring at room temperature the solvent mixture was evaporated to dryness and the resulting residue was used for the next step without any further purification. A piperidine/ $\text{CH}_3\text{CN}$  mixture (5% v/v, 2.0 mL) was added to the crude. After 15 minutes stirring at room temperature the reaction mixture was purified through RP-HPLC and lyophilized. Compound **191** (21.7 mg) was obtained in 73% yield over two steps. ESI<sup>+</sup>-MS:  $m/z$  calcd. for  $[\text{M}+\text{H}]^+$ : 2860.0 (average), found: 2860.8; calcd. for  $[\text{M}+2\text{H}]^{2+}$ : 1430.5, found: 1429.8.  $t_R = 9.95 \text{ min}$ . ( $\lambda=214 \text{ nm}$ , 5-60% solv.B in 15').

### Compound 192



A solution of NaOMe/MeOH (25 wt%,  $d = 0.945 \text{ g}\cdot\text{mL}^{-1}$ ) in dry MeOH ( $\text{pH}\approx 10$ ) was added to **191** (35.2 mg, 12.3  $\mu\text{mol}$ ). After 20 minutes stirring at room temperature, UPLC-MS showed complete conversion. The reaction was neutralized with Amberlite IR-120  $\text{H}^+$ , the resin filtered off, washed with MeOH and the filtrate purified *via* RP-HPLC. After lyophilization, compound **192** (25.8 mg) was obtained in 89% yield. HRMS (ESI<sup>+</sup>-TOF):  $m/z$  calcd. for  $[\text{M}+\text{H}]^+$ : 2354.1826 (monoisotopic), found: 2354.1836.  $t_R = 8.41 \text{ min}$ . ( $\lambda=214 \text{ nm}$ , 0-40% solv.B in 15').

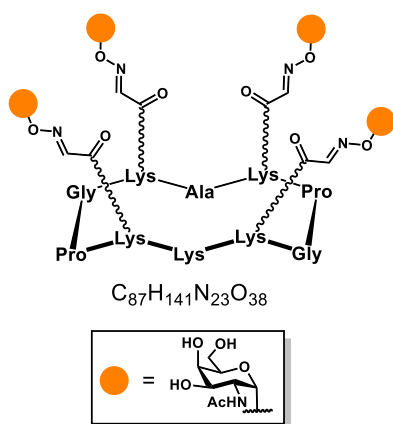
### Compound **193**



Compound **192** (19.8 mg, 8.4  $\mu\text{mol}$ ) was treated with a TFA/ $\text{CH}_2\text{Cl}_2$  (1:1, 1.0 mL) mixture for 30 minutes at room temperature. The reaction mixture was added drop-wise to ice-cold diethyl ether (20 mL), the obtained solid was filtrated, dried and used for the next step without any further purification. The crude solid was reacted with **89** (1.7 mg, 2.1  $\mu\text{mol}$ ) in  $\text{H}_2\text{O}$  containing 0.1% TFA (1.0 mL), following the general procedure for oxime ligation (VI.3.5.). Compound **193** (17.5 mg)

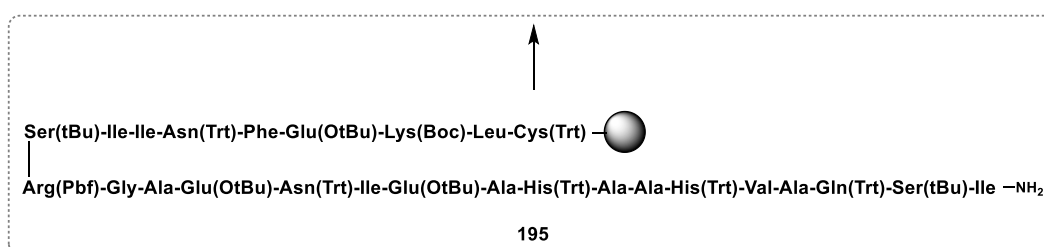
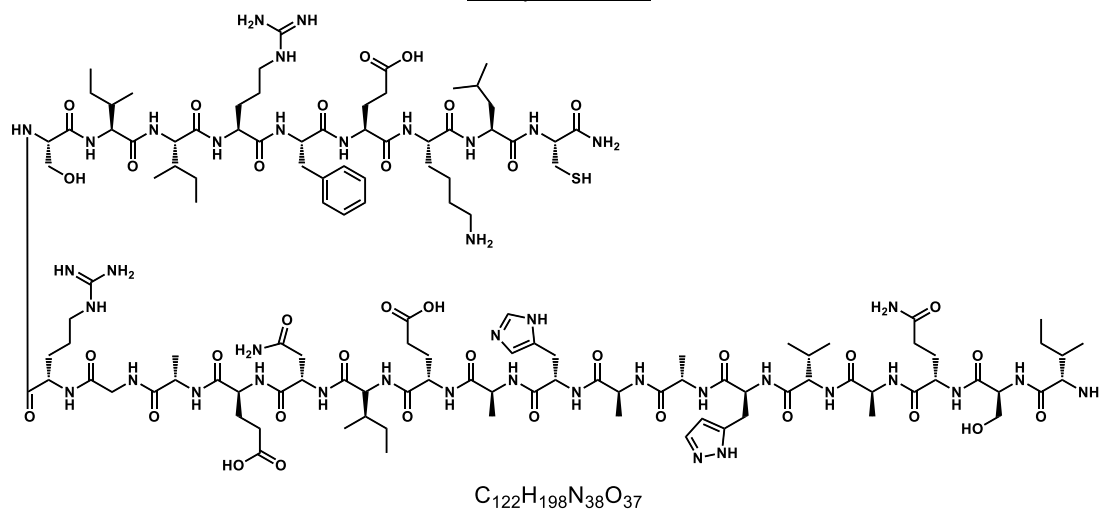
was obtained in 82% yield over two steps. MALDI-TOF:  $m/z$  calcd. for  $[\text{M}+\text{H}]^+$ : 10190.9 (average), found: 10194.5.  $t_R = 8.63$  min. ( $\lambda=214$  nm, 0-40% solv.B in 15').

### Compound **194**



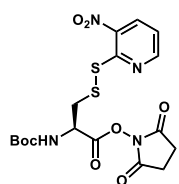
Compound **194** (17.9 mg) was obtained in 91% yield by reacting **89** (11.6 mg, 9.3  $\mu\text{mol}$ ) and **63** (13.2 mg, 55.9  $\mu\text{mol}$ ) following the general procedure for oxime ligation (VI.3.5.). HRMS (ESI<sup>+</sup>-TOF):  $m/z$  calcd. for  $[\text{M}+\text{H}]^+$ : 2116.9886 (monoisotopic), found: 2116.9854.  $t_R = 5.76$  min. ( $\lambda=214$  nm, 0-40% solv.B in 15').

### Compound **196**

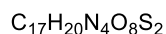


Peptide sequence **195** was synthesized automatically, following the general procedure for SPPS (VI.3.1.) on 535 mg of Rink amide<sup>®</sup> support (measured loading = 0.524 mmol·g<sup>-1</sup>). Clivage from the resin was performed following the reported general procedure (VI.3.2.). After RP-HPLC purification and lyophilization, compound **196** (324.2 mg) was isolated in 41% overall yield. HRMS (ESI<sup>+</sup>-TOF): *m/z* calcd. for [M+H]<sup>+</sup>: 2821.4607 (most intense peak of isotopic cluster), found: 2821.4568. *t<sub>R</sub>* = 7.24 min. (λ=214 nm, 0-40% solv.B in 15').

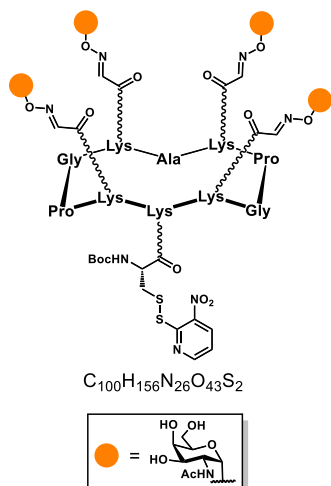
### Compound **197**



Compound **197** was synthesized according to the published procedure: Mezö, G., Mihala, N., Andreu, D., and Hudecz, F. (2000) Conjugation of epitope peptides with SH group to branched chain polymeric polypeptides via Cys(Npys). *Bioconjug. Chem.* **11**, 484–491. Characterization data were in accordance with the previous report.

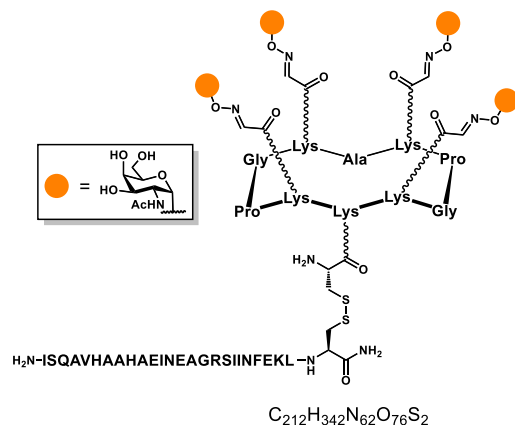


### Compound 198



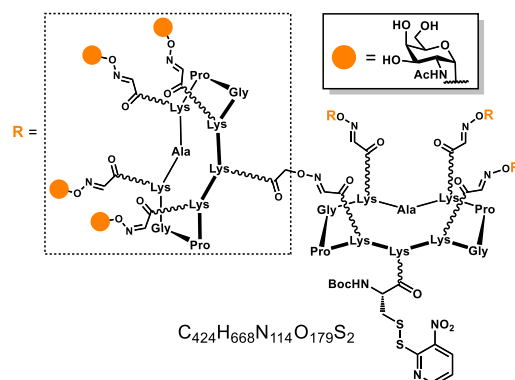
To a solution of **194** (14.0 mg, 6.6  $\mu\text{mol}$ ) in DMF (1.5 mL), DIPEA (1.7  $\mu\text{L}$ , 9.8  $\mu\text{mol}$ ) and **97** (4.7 mg, 9.9  $\mu\text{mol}$ ) were added. After 20 minutes stirring at room temperature the reaction was purified *via* RP-HPLC and lyophilized to give compound **198** (12.0 mg) in 74% yield. HRMS (ESI<sup>+</sup>-TOF):  $m/z$  calcd. for  $[M+H]^+$ : 2475.0368 (most intense peak of isotopic cluster), found: 2821.4568; calcd. for  $[M+Na]^+$ : 2496.0159 (monoisotopic), found: 2496.0229.  $t_R$  = 8.15 min. ( $\lambda$ =214 nm, 5-60% solv.B in 15').

### Compound 199



Compound **198** (8.4 mg, 3.4  $\mu\text{mol}$ ) was treated with a TFA/ $\text{CH}_2\text{Cl}_2$  (1:1, 1.0 mL) mixture for 30 minutes at room temperature. The reaction mixture was added drop-wise to ice-cold diethyl ether (10 mL), the obtained solid was filtrated, dried and used for the next step without any further purification. To a solution of the crude compound in NaOAc buffer (pH 4.5, 40 mM, 1.0 mL), a solution of **196** (10.5 mg, 3.7  $\mu\text{mol}$ ) in DMF (200  $\mu\text{L}$ ) was added, according to the general procedure for disulfide bridging (VI.3.7.). Compound **199** (12.3 mg) was obtained in 72% yield over two steps. MALDI-TOF:  $m/z$  calcd. for  $[M+H]^+$ : 5040.5 (average), found: 5041.4.  $t_R$  = 11.47 min. ( $\lambda$ =214 nm, 0-40% solv.B in 15').

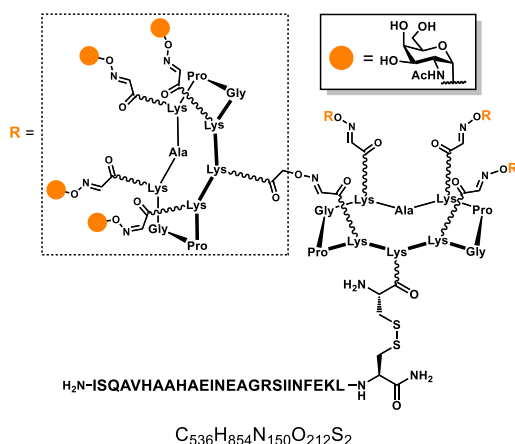
### Compound 200



Compound **111** (10.3 mg, 1.0  $\mu\text{mol}$ ) was suspended in a DMF/DMSO (1:1, 1.0 mL) mixture, DIPEA (0.25  $\mu\text{L}$ , 1.4  $\mu\text{mol}$ ) and **197** (0.7 mg, 1.5  $\mu\text{mol}$ ) were added. After 1 hour stirring at room temperature the reaction mixture was purified and lyophilized to give compound **200** (3.1 mg) in 30% yield. ESI<sup>+</sup>-MS:  $m/z$  calcd. for  $[M+4H]^{4+}$ : 2573.7 (average), found: 2574.1; calcd. for  $[M+5H]^{5+}$ : 2059.1, found: 2060.5; calcd. for  $[M+6H]^{6+}$ : 1716.1, found: 1717.0; calcd. for  $[M+7H]^{7+}$ : 1471.1, found: 1472.1.  $t_R$  = 11.15 min. ( $\lambda$ =214 nm, 0-40% solv.B in 15').

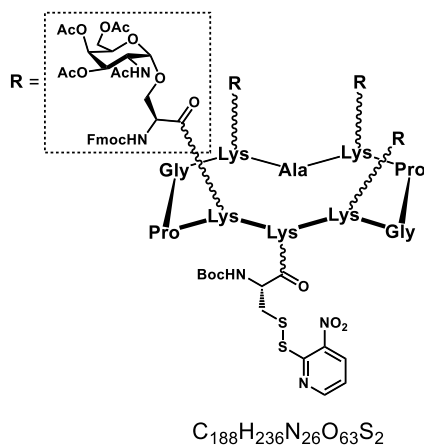
Alternatively, compound **200** (3.4 mg) was obtained in 41% yield by adding **197** (0.6 mg, 1.3  $\mu\text{mol}$ ) to a solution of **111** (7.9 mg, 0.8  $\mu\text{mol}$ ) in a PBS(pH 7.4, 10 mM)/DMF mixture (1:1, 400  $\mu\text{L}$ ) and stirring at room temperature for 1 hour.

### Compound **201**



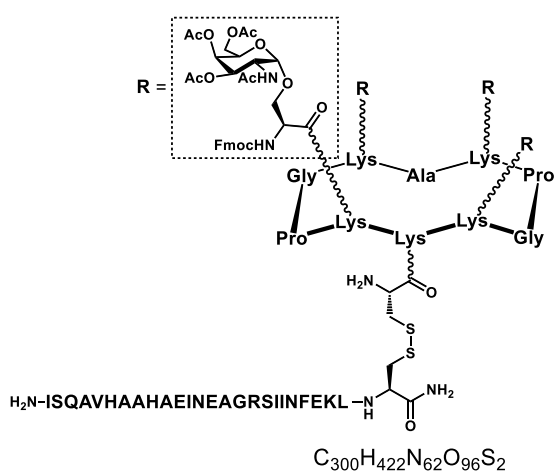
Compound **200** (5.4 mg, 0.5  $\mu\text{mol}$ ) was treated with a TFA/ $\text{CH}_2\text{Cl}_2$  (1:1, 1.0 mL) mixture for 30 minutes at room temperature. The reaction mixture was added drop-wise to ice-cold diethyl ether (10 mL), the obtained solid was filtrated, dried and used for the next step without any further purification. To a solution of the crude compound in NaOAc buffer (pH 4.5, 40 mM, 1.0 mL), a solution of **196** (1.7 mg, 0.6  $\mu\text{mol}$ ) in DMF (50  $\mu\text{L}$ ) was added, according to the general procedure for disulfide bridging (**VI.3.7**). Compound **201** (3.9 mg) was obtained in 61% yield over two steps. ) ESI<sup>+</sup>-MS:  $m/z$  calcd. for  $[\text{M}+5\text{H}]^{5+}$ : 2572.1 (average), found: 2572.3; calcd. for  $[\text{M}+6\text{H}]^{6+}$ : 2143.6, found: 2144.1; calcd. for  $[\text{M}+7\text{H}]^{7+}$ : 1837.5, found: 1838.0; calcd. for  $[\text{M}+8\text{H}]^{8+}$ : 1607.9, found: 1608.4; calcd. for  $[\text{M}+9\text{H}]^{9+}$ : 1429.4, found: 1429.9; calcd. for  $[\text{M}+10\text{H}]^{10+}$ : 1286.6, found: 1287.0.  $t_R = 7.47$  min. ( $\lambda=214$  nm, 5-60% solv.B in 15').

### Compound **202**



To a solution of **189** (13.2 mg, 3.7  $\mu\text{mol}$ ) in DMF (1.0 mL), DIPEA (0.97  $\mu\text{L}$ , 5.6  $\mu\text{mol}$ ) and **197** (2.6 mg, 5.5  $\mu\text{mol}$ ) was added and the reaction stirred at room temperature for 30 minutes. The reaction mixture was purified through RP-HPLC and lyophilized to give compound **202** (11.2 mg) in 77% yield. MALDI-TOF:  $m/z$  calcd. for  $[\text{M}+\text{Na}]^+$ : 3955.1 (average), found: 3954.6.  $t_R = 12.62$  min. ( $\lambda=214$  nm, 5-100% solv.B in 15').

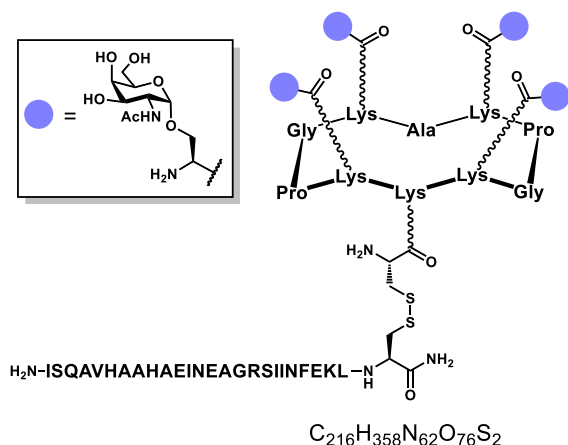
### Compound **204**



Compound **202** (9.5 mg, 2.4  $\mu\text{mol}$ ) was treated with a TFA/ $\text{CH}_2\text{Cl}_2$  (1:1, 1.2 mL) mixture for 30 minutes at room temperature. The reaction mixture was added drop-wise to ice-cold diethyl ether (15 mL), the obtained solid was filtrated, dried and used for the next step without any further purification. To a solution of the crude compound in a DMF/NaOAc buffer (pH 4.5, 40 mM) (2:1, 1.5 mL) mixture, a solution of **196** (7.4 mg, 2.6  $\mu\text{mol}$ ) in DMF (500  $\mu\text{L}$ ) was added, according to the general procedure for disulfide bridging (**VI.3.7.**). Compound **204** (10.8 mg) was obtained in 69% yield over two steps. MALDI-

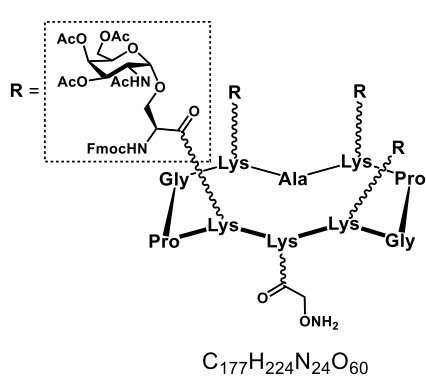
TOF:  $m/z$  calcd. for  $[\text{M}+\text{H}]^+$ : 6498.1 (average), found: 6498.9.  $t_{\text{R}} = 10.34$  min. ( $\lambda=214$  nm, 5-100% solv.B in 15').

### Compound 205



A solution of NaOMe/MeOH (25 wt%,  $d = 0.945$   $\text{g}\cdot\text{mL}^{-1}$ ) in dry MeOH (pH $\approx$ 10, 3.0 mL) was added to compound **204** (7.2 mg, 1.1  $\mu\text{mol}$ ) and the resulting mixture was stirred overnight at room temperature. The reaction was neutralized with Amberlite IR-120  $\text{H}^+$ , the resin filtered off, washed with MeOH and the filtrated purified *via* RP-HPLC. After lyophilization, compound **205** (2.4 mg) was obtained in 43% yield. MALDI-TOF:  $m/z$  calcd. for  $[\text{M}+\text{H}]^+$ : 5104.7 (average), found: 5104.8.  $t_{\text{R}} = 5.95$  min. ( $\lambda=214$  nm, 5-80% solv.B in 15').

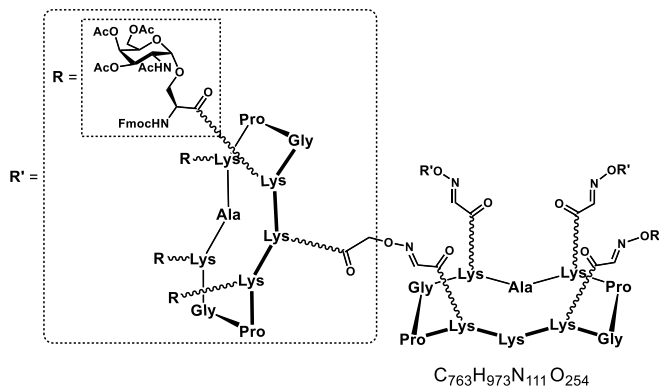
### Compound 206



To a solution of **189** (22.6 mg, 6.3  $\mu\text{mol}$ ) in DMF (3.0 mL), DIPEA (1.6  $\mu\text{L}$ , 9.2  $\mu\text{mol}$ ) and Boc-aminoxyacetic acid *N*-hydroxysuccinimide ester<sup>346</sup> (2.2 mg, 7.6  $\mu\text{mol}$ ) were added. After 30 minutes stirring at room temperature, the reaction mixture was concentrated to dryness and the crude was treated with a TFA/ $\text{NH}_2\text{OH}/\text{CH}_2\text{Cl}_2$  (50:2:48, 2.0 mL) cocktail for 30 minutes at room temperature. The reaction mixture was added drop-wise to ice-cold diethyl ether (30 mL), and the obtained solid was filtrated and purified *via* RP-HPLC. After lyophilization,

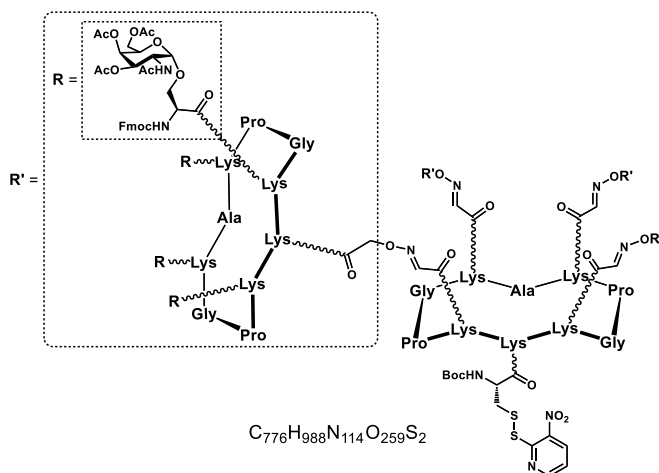
compound **206** (17.9 mg) was isolated in 78% yield over two steps. ESI<sup>+</sup>-MS:  $m/z$  calcd. for  $[\text{M}+2\text{H}]^{2+}$ : 1824.9 (average), found: 1825.1; calcd. for  $[\text{M}+3\text{H}]^{3+}$ : 1216.9, found: 1217.4.  $t_{\text{R}} = 11.01$  min. ( $\lambda=214$  nm, 5-100% solv.B in 15').

### Compound **207**



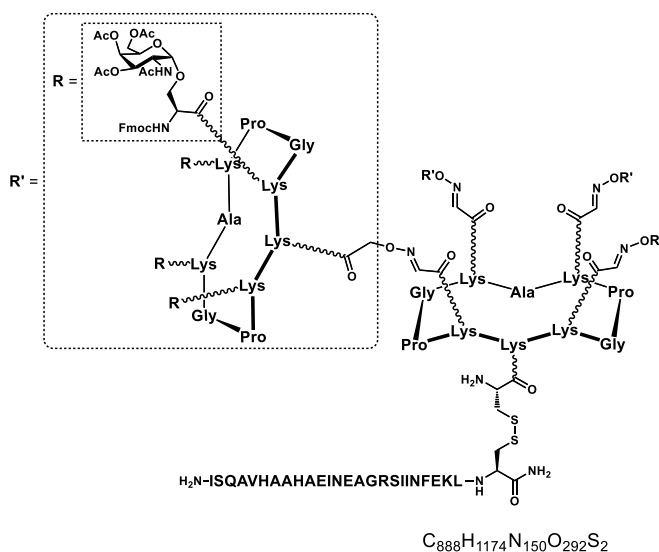
Compound **207** (7.61 mg) was obtained in 69% yield by reacting **89** (0.87 mg, 0.70  $\mu$ mol) and **206** (15.42 mg, 4.23  $\mu$ mol) in a CH<sub>3</sub>CN/H<sub>2</sub>O mixture (9:1, 1.0 mL) containing 0.1% of TFA, following the general procedure for oxime ligation (VI.3.5.). MALDI-TOF:  $m/z$  calcd. for [M+Na]<sup>+</sup>: 15786.5 (average), found: 15789.1.  $t_R$  = 12.51 min. ( $\lambda$ =214 nm, 50-100% solv.B in 15').

### Compound **208**



Compound **207** (6.24 mg, 0.40  $\mu$ mol) was dissolved in DMF (1.0 mL), DIPEA (0.15  $\mu$ L, 0.86  $\mu$ mol) and **197** (0.28 mg, 0.59  $\mu$ mol) were added and the reaction stirred at room temperature for 30 minutes. The solvent mixture was purified *via* RP-HPLC and lyophilized to give compound **208** (3.40 mg) in 62% yield. ESI<sup>+</sup>-MS:  $m/z$  calcd. for [M+6H]<sup>6+</sup>: 2686.1 (monoisotopic), found: 2686.1.  $t_R$  = 12.63 min. ( $\lambda$ =214 nm, 50-100% solv.B in 15').

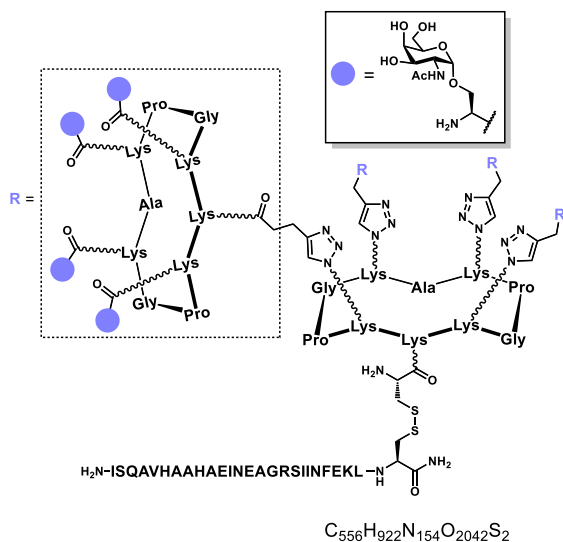
### Compound 209



Compound **208** (2.84 mg, 0.18  $\mu$ mol) was treated with a TFA/CH<sub>2</sub>Cl<sub>2</sub> (1:1, 500  $\mu$ L) mixture for 30 minutes at room temperature. The reaction mixture was added drop-wise to ice-cold diethyl ether (5.0 mL), the obtained solid was filtrated, dried and used for the next step without any further purification. To a solution of the crude compound in a DMF/NaOAc buffer (pH 4.5, 40 mM) (2:1, 800  $\mu$ L) mixture, a solution of **196** (0.56 mg, 0.20  $\mu$ mol) in DMF (50  $\mu$ L) was added, according to the general procedure for disulfide bridging (VI.3.7.). Compound **209** (2.08 mg) was obtained in

62% yield over two steps. ESI<sup>+</sup>-MS: *m/z* calcd. for [M+7H]<sup>7+</sup>: 2670.8 (average), found: 2668.3; calcd. for [M+8H]<sup>8+</sup>: 2336.6, found: 2336.0; calcd. for [M+9H]<sup>9+</sup>: 2077.1, found: 2077.4; calcd. for [M+10H]<sup>10+</sup>: 1869.5, found: 1869.7. *t<sub>R</sub>* = 11.40 min. ( $\lambda$ =214 nm, 50-100% solv.B in 15').

### Compound 211

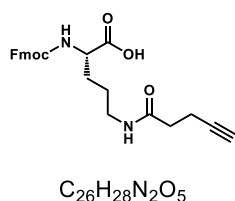


To a solution of **219** (2.1 mg, 0.52  $\mu$ mol) and **217** (6.0 mg, 2.65  $\mu$ mol) in DMF (600  $\mu$ L), a solution containing THPTA (2.3 mg, 5.3  $\mu$ mol), CuSO<sub>4</sub>·5H<sub>2</sub>O (0.1 mg, 0.4  $\mu$ mol) and sodium ascorbate (3.1 mg, 15.6  $\mu$ mol) in aq. PBS (pH 7.4, 10 mM, 1200  $\mu$ L) was added. Compound **211** (5.11 mg) was obtained in 75% yield, according to the general procedure for CuAAC (VI.3.6.). ESI<sup>+</sup>-MS spectrum of **211**. *m/z* calcd. for [M+5H]<sup>5+</sup>: 2619.5 (average), found: 2617.5; calcd. for [M+6H]<sup>6+</sup>: 2183.0, found: 2182.7; calcd. for [M+7H]<sup>7+</sup>: 1871.3, found: 1871.6; calcd. for [M+8H]<sup>8+</sup>: 1637.5, found: 1638.0; calcd. for [M+9H]<sup>9+</sup>: 1455.7, found: 1456.1; calcd. for [M+10H]<sup>10+</sup>: 1310.2, found: 1310.4; calcd. for [M+11H]<sup>11+</sup>: 1191.2, found: 1191.1; calcd.

for [M+12H]<sup>12+</sup>: 1092.0, found: 1092.1; calcd. for [M+13H]<sup>13+</sup>: 1008.1, found: 1008.3; calcd. for [M+14H]<sup>14+</sup>: 936.2, found: 935.9; calcd. for [M+15H]<sup>15+</sup>: 873.8, found: 874.1. *t<sub>R</sub>* = 9.33 min. ( $\lambda$ =214 nm, 5-40% solv.B in 15').

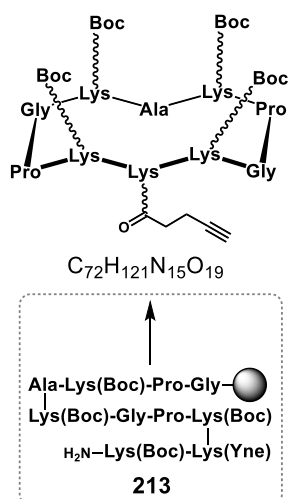


### Compound **212**



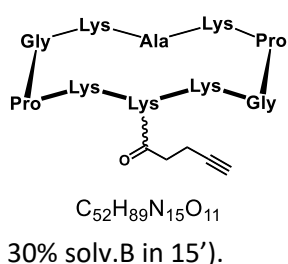
Compound **212** was synthesized according to the published procedure: Galibert, M., Dumy, P., and Boturyn, D. (2009) One-Pot Approach to Well-Defined Biomolecular Assemblies by Orthogonal Chemoselective Ligations. *Angew. Chemie Int. Ed.* 48, 2576–257. Characterization data were in accordance with the previous report.

### Compound **214**



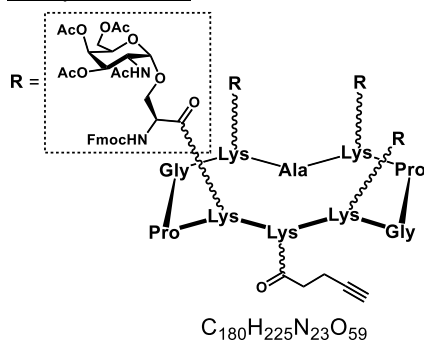
Peptide sequence **213** was synthesized manually in a polypropylene reactor, following the general procedure for SPPS (VI.3.1.) on 956 mg of Fmoc-Gly-SASRIN™ support (measured loading = 0.528 mmol·g<sup>-1</sup>). Clivage from the resin was performed following the reported general procedure (VI.3.2.). Mass spectrometry analysis revealed the presence of the expected mass for sequence **213**. HRMS (ESI<sup>+</sup>-TOF):  $m/z$  calcd. for  $C_{72}H_{124}N_{15}O_{20}$  [M(**213**)+H]<sup>+</sup>: 1518.9147 (monoisotopic), found: 1518.9182. Linear peptide **213** was dissolved in a CH<sub>2</sub>Cl<sub>2</sub>/DMF (1:1, 1.0 L) mixture, in the presence of DIPEA (176 μL, 1.010 mmol) and PyBOP® (315 mg, 0.605 mmol). Compound **181** (386.5 mg) was obtained following the general procedure for cyclization (VI.3.3.) in 51% overall yield. HRMS (ESI<sup>+</sup>-TOF):  $m/z$  calcd. for [M+Na]<sup>+</sup>: 1522.8861 (monoisotopic), found: 1522.8902.  $t_R$  = 7.92 min. ( $\lambda$ =214 nm, 5-100% solv.B in 15').

### Compound **215**



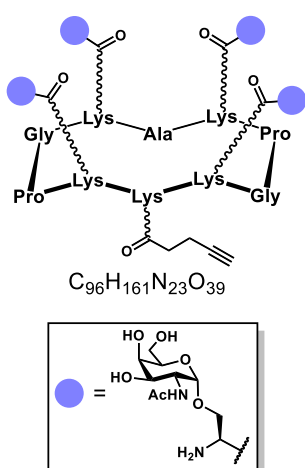
Compound **214** (56.7 mg, 37.8 μmol) was treated with a TFA/CH<sub>2</sub>Cl<sub>2</sub> (1:1, 5.0 mL) mixture for 30 minutes at room temperature. The reaction mixture was added drop-wise to ice-cold diethyl ether (100 mL), the obtained solid was filtrated and purified *via* RP-HPLC. After lyophilization, compound **215** (38.3 mg) was obtained in 92% yield. HRMS (ESI<sup>+</sup>-TOF):  $m/z$  calcd. for [M+H]<sup>+</sup>: 1100.6944 (monoisotopic), found: 1100.6908.  $t_R$  = 6.22 min. ( $\lambda$ =214 nm, 0-30% solv.B in 15').

### Compound **216**



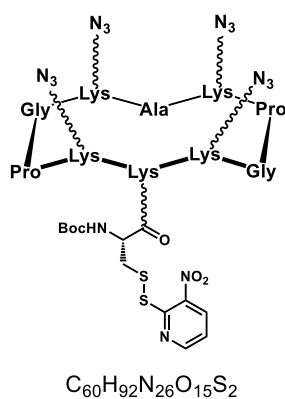
To a solution of **215** (32.4 mg, 29.4 μmol) in DMF (3.0 mL), DIPEA (30.7 μL, 176.2 μmol), PyBOP® (76.5 mg, 147.0 μmol) and **188** (92.7 mg, 141.2 μmol) were added. After 30 minutes stirring at room temperature the reaction mixture was concentrated and purified through RP-HPLC. After lyophilization, compound **216** (88.1 mg) was obtained in 82% yield. MALDI-TOF:  $m/z$  calcd. for [M+Na]<sup>+</sup>: 3677.8 (average), found: 3675.3.  $t_R$  = 10.65 min. ( $\lambda$ =214 nm, 5-100% solv.B in 15').

### Compound **217**



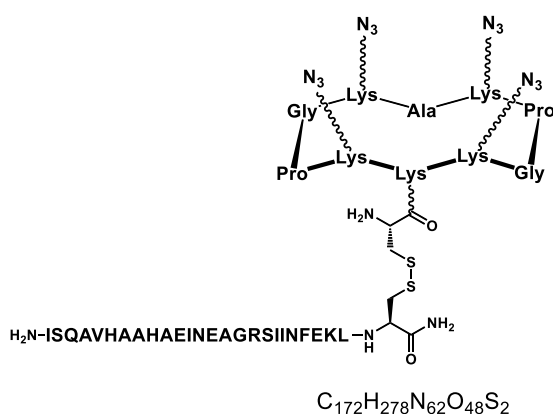
To a solution of **216** (45.6 mg, 12.5  $\mu\text{mol}$ ) in dry MeOH (2.0 mL), methylhydrazine (21.0  $\mu\text{L}$ , 398.8  $\mu\text{mol}$ ) was added and the reaction stirred overnight at room temperature. The solvent mixture was concentrated under reduced pressure and the resulting crude was purified through RP-HPLC. After lyophilization, compound **217** (20.4 mg) was obtained in 72% yield. HRMS (ESI<sup>+</sup>-TOF):  $m/z$  calcd. for  $[M+H]^+$ : 2261.1400 (monoisotopic), found: 2261.1311.  $t_R = 4.09$  min. ( $\lambda=214$  nm, 0-40% solv.B in 15').

### Compound **218**



To a solution of **120** (16.2 mg, 14.4  $\mu\text{mol}$ ) in DMF (2.0 mL), DIPEA (3.8  $\mu\text{L}$ , 21.8  $\mu\text{mol}$ ) and **197** (10.2 mg, 20.5  $\mu\text{mol}$ ) were added. After 30 minutes stirring at room temperature the reaction mixture was purified through RP-HPLC and lyophilized. Compound **218** (15.1) was obtained in 71% yield. HRMS (ESI<sup>+</sup>-TOF):  $m/z$  calcd. for  $[M+Na]^+$ : 1503.6575 (monoisotopic), found: 1503.6613.  $t_R = 9.04$  min. ( $\lambda=214$  nm, 5-100% solv.B in 15').

### Compound **219**



Compound **218** (6.2 mg, 4.2  $\mu\text{mol}$ ) was treated with a TFA/ $\text{CH}_2\text{Cl}_2$  (1:1, 1 mL) mixture for 30 minutes at room temperature. The reaction mixture was added dropwise to ice-cold diethyl ether (10 mL), the obtained solid was filtrated, dried and used for the next step without any further purification. To a solution of the crude compound in a DMF/NaOAc buffer (pH 4.5, 40 mM) (2:1, 800  $\mu\text{L}$ ) mixture, a solution of **196** (13.0 mg, 4.6  $\mu\text{mol}$ ) in DMF (200  $\mu\text{L}$ ) was added, according to the general procedure for disulfide bridging (VI.3.7.). Compound **219** (14.4 mg) was obtained in 85% yield over two steps. ESI<sup>+</sup>-MS:  $m/z$  calcd. for  $[M+2H]^{2+}$ : 2024.3 (average), found: 2024.5; calcd. for  $[M+3H]^{3+}$ : 1349.9, found: 1350.3; calcd. for  $[M+4H]^{4+}$ : 1012.6, found: 1012.6; calcd. for  $[M+5H]^{5+}$ : 810.3, found: 810.3; calcd. for  $[M+6H]^{6+}$ : 675.4, found: 675.4.  $t_R = 7.03$  min. ( $\lambda=214$  nm, 5-100% solv.B in 15').

## **VII.**

# **Annexes**

## List of publications

1. Pifferi, C., Thomas, B., Goyard, D., Berthet, N. and Renaudet, O. (2017) Heterovalent glycodendrimers as epitope carriers for antitumoral cancer vaccines, *Chem. Eur. J.* 10.1002/chem.201702708
2. Richard, E., Pifferi, C., Fiore, M., Samain, E., La Gouëllec, A., Fort, S., Renaudet O. and Priem, B. (2017) Chemobacterial synthesis of a sialyl-Tn cyclopeptide vaccine candidate, *ChemBioChem*, 18, 1730-1734.
3. Pifferi, C., Berthet N. and Renaudet, O. (2017) Cyclopeptide scaffolds in carbohydrate-based synthetic vaccines, *Biomater. Sci.*, 5, 953-965.
4. Pifferi, C., Daskhan, G. C., Fiore, M., Shiao, T. C., Roy R. and Renaudet, O. (2017) Aminooxylated carbohydrates: synthesis and applications, *Chem. Rev.*, 117, 9839-9873.
5. Henderson, A. S., Pifferi, C. and Galan, M. C. (2017) Synthesis of methyl 2-acetamido-3,4,6-tri-O-acetyl-2-deoxy- $\alpha$ - and  $\beta$ -D-glucopyranosides, *Carbohydrate Chemistry: Proven Synthetic Methods*, Volume 4, CRC press, ISBN 9781498726917.
6. Pifferi, C., Goyard, D., Gillon, E., Imberty A. and Renaudet, O. (2016) Synthesis of new series of mannosylated glycodendrimers and evaluation against BC2L-A lectin from *Burkholderia cenocepacia*, *ChemPlusChem*, 82, 390-398.
7. Daskhan, G. C., Pifferi C. and Renaudet, O. (2016) Synthesis of a new series of sialylated homo- and heterovalent glycoclusters by using orthogonal ligations, *ChemistryOpen*, 5, 477-484.
8. Ribeiro, J. P., Pau, W., Pifferi, C., Renaudet, O., Varrot, A., Mahal, L. K. and Imberty, A. (2016) Characterization of a high-affinity sialic acid-specific CBM40 from *Clostridium perfringens* and engineering of a divalent form, *Biochem. J.*, 473, 2109-2118.
9. Thomas, B., Pifferi, C., Daskhan, G. C., Fiore, M., Berthet N. and Renaudet, O. (2015) Divergent and convergent synthesis of GalNAc-conjugated dendrimers using dual orthogonal ligations, *Org. Biomol Chem.*, 13, 11529-11538.

## Posters and oral communications

1. [Poster] Journée scientifique du pôle chimie-biologie-santé, Grenoble, October 25<sup>th</sup> 2016 – Fully Synthetic Vaccine Prototypes bearing Tumor-Associated Carbohydrate Antigens – [Carlo Pifferi](#), Baptiste Thomas, David Goyard, Nathalie Berthet and Olivier Renaudet.
2. [Poster] XXVIII International Carbohydrate Symposium, New Orleans (U.S.A.), July 17<sup>th</sup>-21<sup>th</sup> 2016 – Fully Synthetic Vaccine Prototypes bearing Tumor-Associated Carbohydrate Antigens - [Carlo Pifferi](#), Baptiste Thomas, David Goyard, Nathalie Berthet and Olivier Renaudet.
3. [Oral Commun.] XV CSCC 2016, Pontignano (ITALY), June 19<sup>th</sup>-22<sup>th</sup> 2016 – Fully Synthetic Vaccine Prototypes bearing Tumor-Associated Carbohydrate Antigens – [Carlo Pifferi](#), Baptiste Thomas, David Goyard, Gour Chand Daskhan, Nathalie Berthet and Olivier Renaudet.
4. [Oral Commun.] Third Annual Meeting of the Doctoral School of Chemistry and Life Sciences 2016, Grenoble, June 16<sup>th</sup> 2016 – Fully Synthetic Vaccine Prototypes bearing Tumor-Associated Carbohydrate Antigens – [Carlo Pifferi](#), Baptiste Thomas, David Goyard, Gour Chand Daskhan, Nathalie Berthet and Olivier Renaudet.
5. [Oral Commun.] Journée Printemps-SCF Rhône-Alpes, Grenoble, June 9<sup>th</sup> 2016 – Fully Synthetic Vaccine Prototypes bearing Tumor-Associated Carbohydrate Antigens – [Carlo Pifferi](#), Baptiste Thomas, David Goyard, Gour Chand Daskhan, Nathalie Berthet and Olivier Renaudet.
6. [Oral Commun.] Third Chemical Ligation Meeting, Lille, May 26<sup>th</sup>-27<sup>th</sup> 2016 – Multi-click approaches for the synthesis of heteroglycoclusters – [Carlo Pifferi](#), Baptiste Thomas, David Goyard, Nathalie Berthet and Olivier Renaudet.
7. [Poster] 16<sup>th</sup> Tetrahedron Symposium, Berlin, June 16<sup>th</sup>-19<sup>th</sup> 2015 – Multi-click approaches for the synthesis of heteroglycoclusters – [Carlo Pifferi](#), Baptiste Thomas, David Goyard, Nathalie Berthet and Olivier Renaudet.

## **VIII.**

### **Bibliographic data**

- (1) Abbas, A. K., Lichtman, A. H., and Pillai, S. (2015) Cellular and Molecular Immunology. Elsevier.
- (2) Inman, F. P. (1972) Contemporary Topics in Immunochemistry. Springer.
- (3) Pomés, A., Chruszcz, M., Gustchina, A., Minor, W., Mueller, G. A., Pedersen, L. C., Wlodawer, A., and Chapman, M. D. (2017) 100 Years later: Celebrating the contributions of x-ray crystallography to allergy and clinical immunology. *J. Allergy Clin. Immunol.* *136*, 29–37.e10.
- (4) Lee, H.-C., Butler, M., and Wu, S.-C. (2012) Using recombinant DNA technology for the development of live-attenuated dengue vaccines. *Enzyme Microb. Technol.* *51*, 67–72.
- (5) Hein, W. R., and Griebel, P. J. (2003) A road less travelled: large animal models in immunological research. *Nat Rev Immunol* *3*, 79–84.
- (6) Iwasaki, A., and Medzhitov, R. (2010) Regulation of Adaptive Immunity by the Innate Immune System. *Science* *327*, 291 LP-295.
- (7) Kalos, M., and June, C. H. (2013) Adoptive T Cell Transfer for Cancer Immunotherapy in the Era of Synthetic Biology. *Immunity* *39*, 49–60.
- (8) Rosenberg, S. A., and Restifo, N. P. (2015) Adoptive cell transfer as personalized immunotherapy for human cancer. *Science* *348*, 62–68.
- (9) Schroeder Jr., H. W., and Cavacini, L. (2010) Structure and function of immunoglobulins. *J. Allergy Clin. Immunol.* *125*, S41–S52.
- (10) Nimmerjahn, F., and Ravetch, J. V. (2008) Fcγ receptors as regulators of immune responses. *Nat Rev Immunol* *8*, 34–47.
- (11) Barb, A. W., and Prestegard, J. H. (2011) NMR analysis demonstrates immunoglobulin G N-glycans are accessible and dynamic. *Nat Chem Biol* *7*, 147–153.
- (12) Feng, D., Shaikh, A. S., and Wang, F. (2016) Recent Advance in Tumor-associated Carbohydrate Antigens (TACAs)-based Antitumor Vaccines. *ACS Chem. Biol.* *11*, 850–863.
- (13) Nimmerjahn, F. (2005) Divergent Immunoglobulin G Subclass Activity Through Selective Fc Receptor Binding. *Science* *310*, 1510–1512.
- (14) Boes, M. (2000) Role of natural and immune IgM antibodies in immune responses. *Mol. Immunol.* *37*, 1141–1149.
- (15) Muramatsu, M., Kinoshita, K., Fagarasan, S., Yamada, S., Shinkai, Y., and Honjo, T. (2000) Class Switch Recombination and Hypermutation Require Activation-Induced Cytidine Deaminase (AID), a Potential RNA Editing Enzyme. *Cell* *102*, 553–563.
- (16) Doria-Rose, N. A., and Joyce, M. G. (2015) Strategies to guide the antibody affinity maturation process. *Curr. Opin. Virol.* *11*, 137–147.
- (17) Rickert, R. C. (2005) Regulation of B lymphocyte activation by complement C3 and the B cell coreceptor complex. *Curr. Opin. Immunol.* *17*, 237–243.
- (18) Freeman, S. A., Jaumouillé, V., Choi, K., Hsu, B. E., Wong, H. S., Abraham, L., Graves, M. L., Coombs, D., Roskelley, C. D., Das, R., Grinstein, S., and Gold, M. R. (2015) Toll-like receptor ligands sensitize B-cell receptor signalling by reducing actin-dependent spatial confinement of the receptor. *Nat. Commun.* *6*, 6168.
- (19) Groscurth, P., and Filgueira, L. (1998) Killing Mechanisms of Cytotoxic T Lymphocytes. *Physiology* *13*, 17–21.
- (20) Bendelac, A., Savage, P. B., and Teyton, L. (2007) The Biology of NKT Cells. *Annu. Rev. Immunol.* *25*, 297–336.
- (21) Godfrey, D. I., Stankovic, S., and Baxter, A. G. (2010) Raising the NKT cell family. *Nat Immunol* *11*, 197–206.
- (22) Cohn, M., Av Mitchison, N., Paul, W. E., Silverstein, A. M., Talmage, D. W., and Weigert, M. (2007) Reflections on the clonal-selection theory. *Nat Rev Immunol* *7*, 823–830.
- (23) Kurts, C., Robinson, B. W. S., and Knolle, P. A. (2010) Cross-priming in health and disease. *Nat. Publ. Gr.* *10*, 403–414.
- (24) Boland, C. R., and Ricciardiello, L. (1999) How many mutations does it take to make a tumor? *Proc. Natl. Acad. Sci. U. S. A.* *96*, 14675–14677.
- (25) Stumbles, P. A., Himbeck, R., Frelinger, J. A., Collins, E. J., Lake, R. A., and Robinson, B. W. S. (2004) Cutting Edge: Tumor-Specific CTL Are Constitutively Cross-Armed in Draining Lymph

- Nodes and Transiently Disseminate to Mediate Tumor Regression following Systemic CD40 Activation. *J. Immunol.* 173, 5923–5928.
- (26) Nelson, D. J., Mukherjee, S., Bundell, C., Fisher, S., van Hagen, D., and Robinson, B. (2001) Tumor Progression Despite Efficient Tumor Antigen Cross-Presentation and Effective “Arming” of Tumor Antigen-Specific CTL. *J. Immunol.* 166, 5557–5566.
- (27) Couzin-Frankel, J. (2013) Cancer Immunotherapy. *Science* 342, 1432–1433.
- (28) Coley, W. B. (1893) The treatment of malignant tumours by repeated inoculations of erysipelas: with a report of ten original cases. *Am. J. Med. Sci.* 105, 487–511.
- (29) Nauts, H. C., Bogatko, F. H., and Fowler, G. A. (1953) A review of the influence of bacterial infection and of bacterial products (Coley’s toxins) on malignant tumors in man: A critical analysis of 30 inoperable cases treated by Coley’s mixed toxins, in which diagnosis was confirmed by microscopic examination. *Acta Med Scand Suppl.* 276, 1–103.
- (30) Adams, G. P., and Weiner, L. M. (2005) Monoclonal antibody therapy of cancer. *Nat Biotech* 23, 1147–1157.
- (31) Parslow, A., Parakh, S., Lee, F.-T., Gan, H., and Scott, A. (2016) Antibody–Drug Conjugates for Cancer Therapy. *Biomedicines* 4, 14.
- (32) Floros, T., and Tarhini, A. A. (2015) Anticancer Cytokines: Biology and Clinical Effects of Interferon- $\alpha$ 2, Interleukin (IL)-2, IL-15, IL-21, and IL-12. *Semin. Oncol.* 42, 539–548.
- (33) Wong, H. H., Lemoine, N. R., and Wang, Y. (2010) Oncolytic Viruses for Cancer Therapy: Overcoming the Obstacles. *Viruses* 2, 78–106.
- (34) Kantoff, W. P., Higano, S. C., Shore, D. N., Berger, R. E., Small, J. E., Penson, F. D., Redfern, H. C., Ferrari, C. A., Dreicer, R., Sims, B. R., Xu, Y., Frohlich, W. M., and Schellhammer, F. P. (2010) Sipuleucel-T Immunotherapy for Castration-Resistant Prostate Cancer. *N. Engl. J. Med.* 363, 411–422.
- (35) Finn, O. J. (2003) Cancer vaccines: between the idea and the reality. *Nat. Rev. Immunol.* 3, 630–641.
- (36) Mellman, I., Coukos, G., and Dranoff, G. (2011) Cancer immunotherapy comes of age. *Nature* 480, 480–489.
- (37) Kirkwood, J. M., Butterfield, L. H., Tarhini, A. A., Zarour, H., Kalinski, P., and Ferrone, S. (2012) Immunotherapy of cancer in 2012. *CA. Cancer J. Clin.* 62, 309–335.
- (38) Melero, I., Gaudernack, G., Gerritsen, W., Huber, C., Parmiani, G., Scholl, S., Thatcher, N., Wagstaff, J., Zielinski, C., Faulkner, I., and Mellstedt, H. (2014) Therapeutic vaccines for cancer: an overview of clinical trials. *Nat. Rev. Clin. Oncol.* 11, 509–524.
- (39) Guo, C., Manjili, M. H., Subjeck, J. R., Sarkar, D., Fisher, P. B., and Wang, X. Y. (2013) Therapeutic cancer vaccines. Past, present, and future. *Adv. Cancer Res.* 119, 421–475.
- (40) Stagg, J., Johnstone, R. W., and Smyth, M. J. (2007) From cancer immunosurveillance to cancer immunotherapy. *Immunol. Rev.* 220, 82–101.
- (41) Vinay, D. S., Ryan, E. P., Pawelec, G., Talib, W. H., Stagg, J., Elkord, E., Lichtor, T., Decker, W. K., Whelan, R. L., Kumara, H. M. C. S., Signori, E., Honoki, K., Georgakilas, A. G., Amin, A., Helferich, W. G., Boosani, C. S., Guha, G., Ciriolo, M. R., Chen, S., Mohammed, S. I., Azmi, A. S., Keith, W. N., Bilsland, A., Bhakta, D., Halicka, D., Fujii, H., Aquilano, K., Ashraf, S. S., Nowsheen, S., Yang, X., Choi, B. K., and Kwon, B. S. (2015) Immune evasion in cancer: Mechanistic basis and therapeutic strategies. *Semin. Cancer Biol.* 35, S185–S198.
- (42) Garrison, K., Hahn, T., Lee, W.-C., Ling, L. E., Weinberg, A. D., and Akporiaye, E. T. (2012) The small molecule TGF- $\beta$  signaling inhibitor SM16 synergizes with agonistic OX40 antibody to suppress established mammary tumors and reduce spontaneous metastasis. *Cancer Immunol. Immunother.* 61, 511–521.
- (43) Ashizawa, T., Miyata, H., Ishii, H., Oshita, C., Matsuno, K., Masuda, Y., Furuya, T., Okawara, T., Otsuka, M., Ogo, N., Asai, A., and Akiyama, Y. (2011) Antitumor activity of a novel small molecule STAT3 inhibitor against a human lymphoma cell line with high STAT3 activation. *Int. J. Oncol.* 38, 1245–1252.
- (44) Ueno, A., Cho, S., Cheng, L., Wang, J., Hou, S., Nakano, H., Santamaria, P., and Yang, Y. (2007)



- Transient Upregulation of Indoleamine 2,3-Dioxygenase in Dendritic Cells by Human Chorionic Gonadotropin Downregulates Autoimmune Diabetes. *Diabetes* 56, 1686–1693.
- (45) Morgan, R. A., Chinnasamy, N., Abate-Daga, D. D., Gros, A., Robbins, P. F., Zheng, Z., Feldman, S. A., Yang, J. C., Sherry, R. M., Phan, G. Q., Hughes, M. S., Kammula, U. S., Miller, A. D., Hessman, C. J., Stewart, A. A., Restifo, N. P., Quezado, M. M., Alimchandani, M., Rosenberg, A. Z., Nath, A., Wang, T., Bielekova, B., Wuest, S. C., Nirmala, A., McMahon, F. J., Wilde, S., Mosetter, B., Schendel, D. J., Laurencot, C. M., and Rosenberg, S. A. (2013) Cancer regression and neurologic toxicity following anti-MAGE-A3 TCR gene therapy. *J. Immunother.* 36, 133–151.
- (46) Takeda, K., Kojima, Y., Uno, T., Hayakawa, Y., Teng, M. W. L., Yoshizawa, H., Yagita, H., Gejyo, F., Okumura, K., and Smyth, M. J. (2010) Combination Therapy of Established Tumors by Antibodies Targeting Immune Activating and Suppressing Molecules. *J. Immunol.* 184, 5493–5501.
- (47) Devaud, C., John, L. B., Westwood, J. A., Darcy, P. K., and Kershaw, M. H. (2013) Immune modulation of the tumor microenvironment for enhancing cancer immunotherapy. *Oncoimmunology* 2, e25961.
- (48) Walker, L. S. K. (2017) PD-1 and CTLA-4: Two checkpoints, one pathway? *Sci. Immunol.* 2.
- (49) von Mehren, M., Arlen, P., Gulley, J., Rogatko, A., Cooper, H. S., Meropol, N. J., Alpaugh, R. K., Davey, M., McLaughlin, S., Beard, M. T., Tsang, K. Y., Schlom, J., and Weiner, L. M. (2001) The Influence of Granulocyte Macrophage Colony-Stimulating Factor and Prior Chemotherapy on the Immunological Response to a Vaccine (ALVAC-CEA B7.1) in Patients with Metastatic Carcinoma. *Clin. Cancer Res.* 7, 1181–1191.
- (50) Gulley, J. L., Madan, R. A., and Schlom, J. (2011) Impact of tumour volume on the potential efficacy of therapeutic vaccines. *Curr. Oncol.* 18, 150–157.
- (51) Finn, O. J., and Forni, G. (2002) Prophylactic cancer vaccines. *Curr. Opin. Immunol.* 14, 172–177.
- (52) Lollini, P.-L., and Forni, G. (2002) Antitumor vaccines: is it possible to prevent a tumor? *Cancer Immunol. Immunother.* 51, 409–416.
- (53) Finn, O. J. (2014) Vaccines for Cancer Prevention: A Practical and Feasible Approach to the Cancer Epidemic. *Cancer Immunol. Res.* 2, 708–713.
- (54) Madan, R. A., Gulley, J. L., Fojo, T., and Dahut, W. L. (2010) Therapeutic Cancer Vaccines in Prostate Cancer: The Paradox of Improved Survival Without Changes in Time to Progression. *Oncol.* 15, 969–975.
- (55) Hodi, F. S., O’Day, S. J., McDermott, D. F., Weber, R. W., Sosman, J. A., Haanen, J. B., Gonzalez, R., Robert, C., Schadendorf, D., Hassel, J. C., Akerley, W., van den Eertwegh, A. J. M., Lutzky, J., Lorigan, P., Vaubel, J. M., Linette, G. P., Hogg, D., Ottensmeier, C. H., Lebbé, C., Peschel, C., Quirt, I., Clark, J. I., Wolchok, J. D., Weber, J. S., Tian, J., Yellin, M. J., Nichol, G. M., Hoos, A., and Urba, W. J. (2010) Improved Survival with Ipilimumab in Patients with Metastatic Melanoma. *N. Engl. J. Med.* 363, 711–723.
- (56) Therasse, P., Eisenhauer, E. A., and Verweij, J. (2017) RECIST revisited: A review of validation studies on tumour assessment. *Eur. J. Cancer* 42, 1031–1039.
- (57) Ward, S., Casey, D., Labarthe, M.-C., Whelan, M., Dalgleish, A., Pandha, H., and Todryk, S. (2002) Immunotherapeutic potential of whole tumour cells. *Cancer Immunol. Immunother.* 51, 351–357.
- (58) Jaffee, E. M., Hruban, R. H., Biedrzycki, B., Laheru, D., Schepers, K., Sauter, P. R., Goemann, M., Coleman, J., Grochow, L., Donehower, R. C., Lillemoe, K. D., O’Reilly, S., Abrams, R. A., Pardoll, D. M., Cameron, J. L., and Yeo, C. J. (2001) Novel Allogeneic Granulocyte-Macrophage Colony-Stimulating Factor–Secreting Tumor Vaccine for Pancreatic Cancer: A Phase I Trial of Safety and Immune Activation. *J. Clin. Oncol.* 19, 145–156.
- (59) Dranoff, G. (2002) GM-CSF-based cancer vaccines. *Immunol. Rev.* 188, 147–54.
- (60) Ludewig, B., Ochsenbein, A. F., Odermatt, B., Paulin, D., Hengartner, H., and Zinkernagel, R. M. (2000) Immunotherapy with Dendritic Cells Directed against Tumor Antigens Shared with

- Normal Host Cells Results in Severe Autoimmune Disease. *J. Exp. Med.* 191, 795–804.
- (61) Dudley, M. E., Wunderlich, J. R., Robbins, P. F., Yang, J. C., Hwu, P., Schwartzentruber, D. J., Topalian, S. L., Sherry, R., Restifo, N. P., Hubicki, A. M., Robinson, M. R., Raffeld, M., Duray, P., Seipp, C. A., Rogers-Freezer, L., Morton, K. E., Mavroukakis, S. A., White, D. E., and Rosenberg, S. A. (2002) Cancer Regression and Autoimmunity in Patients After Clonal Repopulation with Antitumor Lymphocytes. *Science* 298, 850–854.
- (62) Soares, M. M., Mehta, V., and Finn, O. J. (2001) Three Different Vaccines Based on the 140-Amino Acid MUC1 Peptide with Seven Tandemly Repeated Tumor-Specific Epitopes Elicit Distinct Immune Effector Mechanisms in Wild-Type Versus MUC1-Transgenic Mice with Different Potential for Tumor Rejection. *J. Immunol.* 166, 6555–6563.
- (63) Scanlan, M. J., Gure, A. O., Jungbluth, A. A., Old, L. J., and Chen, Y.-T. (2002) Cancer/testis antigens: an expanding family of targets for cancer immunotherapy. *Immunol. Rev.* 188, 22–32.
- (64) Novellino, L., Castelli, C., and Parmiani, G. (2005) A listing of human tumor antigens recognized by T cells: March 2004 update. *Cancer Immunol. Immunother.* 54, 187–207.
- (65) Tang, C.-K., and Apostolopoulos, V. (2008) Strategies used for MUC1 immunotherapy: preclinical studies. *Expert Rev. Vaccines* 7, 951–962.
- (66) Disis, M. L., Gooley, T. A., Rinn, K., Davis, D., Piepkorn, M., Cheever, M. A., Knutson, K. L., and Schiffman, K. (2002) Generation of T-Cell Immunity to the HER-2/neu Protein After Active Immunization With HER-2/neu Peptide-Based Vaccines. *J. Clin. Oncol.* 20, 2624–2632.
- (67) Chomez, P., De Backer, O., Bertrand, M., De Plaen, E., Boon, T., and Lucas, S. (2001) An Overview of the MAGE Gene Family with the Identification of All Human Members of the Family. *Cancer Res.* 61, 5544–5551.
- (68) Ranieri, E., Kierstead, L. S., Zarour, H., Kirkwood, J. M., Lotze, M. T., Whiteside, T., and Storkus, W. J. (2000) Dendritic Cell/Peptide Cancer Vaccines: Clinical Responsiveness and Epitope Spreading. *Immunol. Invest.* 29, 121–125.
- (69) Butterfield, L. H., Ribas, A., Dissette, V. B., Amarnani, S. N., Vu, H. T., Oseguera, D., Wang, H.-J., Elashoff, R. M., McBride, W. H., Mukherji, B., Cochran, A. J., Glaspy, J. A., and Economou, J. S. (2003) Determinant Spreading Associated with Clinical Response in Dendritic Cell-based Immunotherapy for Malignant Melanoma. *Clin. Cancer Res.* 9, 998 LP-1008.
- (70) Hardwick, N., and Chain, B. (2011) Epitope spreading contributes to effective immunotherapy in metastatic melanoma patients. *Immunotherapy* 3, 731–733.
- (71) Nath, S., and Mukherjee, P. (2017) MUC1: a multifaceted oncoprotein with a key role in cancer progression. *Trends Mol. Med.* 20, 332–342.
- (72) Gendler, S. J. (2001) MUC1, The Renaissance Molecule. *J. Mammary Gland Biol. Neoplasia* 6, 339–353.
- (73) Chang, J.-F., Zhao, H.-L., Phillips, J., and Greenburg, G. (2000) The Epithelial Mucin, MUC1, Is Expressed on Resting T Lymphocytes and Can Function as a Negative Regulator of T Cell Activation. *Cell. Immunol.* 201, 83–88.
- (74) Hanisch, F.-G., and Müller, S. (2000) MUC1: the polymorphic appearance of a human mucin. *Glycobiology* 10, 439–449.
- (75) Lau, S. K., Weiss, L. M., and Chu, P. G. (2004) Differential Expression of MUC1, MUC2, and MUC5AC in Carcinomas of Various Sites An Immunohistochemical Study. *Am. J. Clin. Pathol.* 122, 61–69.
- (76) Nakamori, S., Ota, D. M., Cleary, K. R., Shirotani, K., and Irimura, T. (1994) MUC1 mucin expression as a marker of progression and metastasis of human colorectal carcinoma. *Gastroenterology* 106, 353–361.
- (77) Simms, Hughes, Limb, Price, and Bishop. (2001) MUC1 mucin as a tumour marker in bladder cancer. *BJU Int.* 84, 350–352.
- (78) Imai, K., Hayashi, T., Suwa, T., Makiguchi, Y., Itoh, F., Hinoda, Y., and Takahashi, T. (2001) MUC1 as a human tumor marker. *Int. Congr. Ser.* 1223, 125–133.
- (79) Ferguson, K. M. (2008) Structure-Based View of Epidermal Growth Factor Receptor Regulation.

- Annu. Rev. Biophys.* 37, 353–373.
- (80) Hollingsworth, M. A., and Swanson, B. J. (2004) Mucins in cancer: protection and control of the cell surface. *Nat Rev Cancer* 4, 45–60.
- (81) Kufe, D. W. (2009) Mucins in cancer: function, prognosis and therapy. *Nat Rev Cancer* 9, 874–885.
- (82) Nath, S., Daneshvar, K., Roy, L. D., Grover, P., Kidiyoor, A., Mosley, L., Sahraei, M., and Mukherjee, P. (2013) MUC1 induces drug resistance in pancreatic cancer cells via upregulation of multidrug resistance genes. *Oncogenesis* 2, e51.
- (83) Ahmad, R., Raina, D., Joshi, M. D., Kawano, T., Ren, J., Kharbanda, S., and Kufe, D. (2009) MUC1-C Oncoprotein Functions as a Direct Activator of the Nuclear Factor- $\kappa$ B p65 Transcription Factor. *Cancer Res.* 69, 7013 LP-7021.
- (84) Hattrup, C. L., and Gendler, S. J. (2006) MUC1 alters oncogenic events and transcription in human breast cancer cells. *Breast Cancer Res.* 8, R37.
- (85) Roy, L. D., Sahraei, M., Subramani, D. B., Besmer, D., Nath, S., Tinder, T. L., Bajaj, E., Shanmugam, K., Lee, Y. Y., Hwang, S. I. L., Gendler, S. J., and Mukherjee, P. (2011) MUC1 enhances invasiveness of pancreatic cancer cells by inducing epithelial to mesenchymal transition. *Oncogene* 30, 1449–1459.
- (86) Sahraei, M., Roy, L. D., Curry, J. M., Teresa, T. L., Nath, S., Besmer, D., Kidiyoor, A., Dalia, R., Gendler, S. J., and Mukherjee, P. (2012) MUC1 regulates PDGFA expression during pancreatic cancer progression. *Oncogene* 31, 4935–4945.
- (87) Cascio, S., Zhang, L., and Finn, O. J. (2011) MUC1 protein expression in tumor cells regulates transcription of proinflammatory cytokines by forming a complex with nuclear factor- $\kappa$ B p65 and binding to cytokine promoters: Importance of extracellular domain. *J. Biol. Chem.* 286, 42248–42256.
- (88) Zhang, S., Cordon-Cardo, C., Zhang, H. S., Reuter, V. E., Adluri, S., Hamilton, W. B., Lloyd, K. O., and Livingston, P. O. (1997) Selection of tumor antigens as targets for immune attack using immunohistochemistry: I. Focus on gangliosides. *Int J Cancer* 73, 42–49.
- (89) Zhang, S., Cordon-Cardo, C., Zhang, H. S., Reuter, V. E., Adluri, S., Hamilton, W. B., Lloyd, K. O., and Livingston, P. O. (1997) Selection of tumor antigens as targets for immune attack using immunohistochemistry: II. Blood group-related antigens. *Int J Cancer* 73, 50–56.
- (90) Gildersleeve, J. C., Wang, B., Achilefu, S., Tu, Z., and Xu, M. (2012) Glycan array analysis of the antigen repertoire targeted by tumor-binding antibodies. *Bioorg. Med. Chem. Lett.* 22, 6839–6843.
- (91) Livingston, P. O., Wong, G. Y., Adluri, S., Tao, Y., Padavan, M., Parente, R., Hanlon, C., Calves, M. J., Helling, F., and Ritter, G. (1994) Improved survival in stage III melanoma patients with GM2 antibodies: a randomized trial of adjuvant vaccination with GM2 ganglioside. *J. Clin. Oncol.* 12, 1036–1044.
- (92) Cipolla, L., Peri, F., and Airoidi, C. (2008) Glycoconjugates in cancer therapy. *Anticancer. Agents Med. Chem.* 8, 92–121.
- (93) Astronomo, R. D., and Burton, D. R. (2010) Carbohydrate vaccines: developing sweet solutions to sticky situations? *Nat. Rev. Drug Discov.* 9, 308–324.
- (94) Peri, F. (2013) Clustered carbohydrates in synthetic vaccines. *Chem. Soc. Rev.* 42, 4543–4556.
- (95) Wilson, R. M., and Danishefsky, S. J. (2013) A vision for vaccines built from fully synthetic tumor-associated antigens: From the laboratory to the clinic. *J. Am. Chem. Soc.* 135, 14462–14472.
- (96) Helling, F., Shang, A., Calves, M., Zhang, S., Ren, S., Yu, R. K., Oettgen, H. F., and Livingston, P. O. (1994) GD3 Vaccines for Melanoma: Superior Immunogenicity of Keyhole Limpet Hemocyanin Conjugate Vaccines. *Cancer Res.* 54, 197–203.
- (97) Plante, O. J., Palmacci, E. R., and Seeberger, P. H. (2001) Automated Solid-Phase Synthesis of Oligosaccharides. *Science* 291, 1523 LP-1527.
- (98) Seeberger, P. H. (2015) The Logic of Automated Glycan Assembly. *Acc. Chem. Res.* 48, 1450–1463.

- (99) Sears, P., and Wong, C.-H. (2001) Toward Automated Synthesis of Oligosaccharides and Glycoproteins. *Science* 291, 2344 LP-2350.
- (100) Huang, X., Huang, L., Wang, H., and Ye, X.-S. (2004) Iterative One-Pot Synthesis of Oligosaccharides. *Angew. Chemie Int. Ed.* 43, 5221–5224.
- (101) Danishefsky, S. J., and Bilodeau, M. T. (1996) Glycals in Organic Synthesis: The Evolution of Comprehensive Strategies for the Assembly of Oligosaccharides and Glycoconjugates of Biological Consequence. *Angew. Chemie Int. Ed. English* 35, 1380–1419.
- (102) Monsan, P., Remaud-Siméon, M., and André, I. (2010) Transglucosidases as efficient tools for oligosaccharide and glucoconjugate synthesis. *Curr. Opin. Microbiol.* 13, 293–300.
- (103) Gabius, H. J. (2009) The sugar code : fundamentals of glycosciences (Gabius, H. J., Ed.). WILEY-VCH.
- (104) Tarbell, J. M., and Cancel, L. M. (2016) The glycocalyx and its significance in human medicine. *J. Intern. Med.* 280, 97–113.
- (105) Gabius, H. J., and Roth, J. (2017) An introduction to the sugar code. *Histochem. Cell Biol.* 147, 111–117.
- (106) Genbacev, O. D., Prakobphol, A., Foulk, R. A., Krtolica, A. R., Ilic, D., Singer, M. S., Yang, Z.-Q., Kiessling, L. L., Rosen, S. D., and Fisher, S. J. (2003) Trophoblast L-Selectin-Mediated Adhesion at the Maternal-Fetal Interface. *Science* 299, 405–408.
- (107) Kwon, D. S., Gregorio, G., Bitton, N., Hendrickson, W. A., and Littman, D. R. (2002) DC-SIGN-Mediated Internalization of HIV Is Required for Trans-Enhancement of T Cell Infection. *Immunity* 16, 135–144.
- (108) Van Kooyk, Y., and Rabinovich, G. A. (2008) Protein-glycan interactions in the control of innate and adaptive immune responses. *Nat Immunol* 9, 593–601.
- (109) Hernandez, J. D., and Baum, L. G. (2002) Ah, sweet mystery of death! Galectins and control of cell fate. *Glycobiology* 12, 127–136.
- (110) Mammen, M., Choi, S.-K., and Whitesides, G. M. (1998) Polyvalent interactions in biological systems: implications for design and use of multivalent ligands and inhibitors. *Angew. Chemie, Int. Ed.* 37, 2755–2794.
- (111) Kiessling, L. L., and Grim, J. C. (2013) Glycopolymer probes of signal transduction. *Chem. Soc. Rev.* 42, 4476–4491.
- (112) Puffer, E. B., Pontrello, J. K., Hollenbeck, J. J., Kink, J. A., and Kiessling, L. L. (2007) Activating B Cell Signaling with Defined Multivalent Ligands. *ACS Chem. Biol.* 2, 252–262.
- (113) Lundquist, J. J., and Toone, E. J. (2002) The cluster glycoside effect. *Chem. Rev.* 102, 555–578.
- (114) Cecioni, S., Imberty, A., and Vidal, S. (2015) Glycomimetics versus Multivalent Glycoconjugates for the Design of High Affinity Lectin Ligands. *Chem. Rev.* 115, 525–561.
- (115) Mu, C., Despras, G., Lindhorst, T. K., Mu, C., and Mu, C. (2016) Organizing multivalency in carbohydrate recognition. *Chem. Soc. Rev.* 45, 3275–3302.
- (116) Treanor, B. (2012) B-cell receptor: From resting state to activate. *Immunology* 136, 21–27.
- (117) Tangye, S. G., Ferguson, A., Avery, D. T., Ma, C. S., and Hodgkin, P. D. (2002) Isotype Switching by Human B Cells Is Division-Associated and Regulated by Cytokines. *J. Immunol.* 169, 4298–4306.
- (118) Kurosaki, T., Kometani, K., and Ise, W. (2015) Memory B cells. *Nat. Rev. Immunol.* 15, 149–159.
- (119) Guo, Z., and Wang, Q. (2009) Recent development in carbohydrate-based cancer vaccines. *Curr. Opin. Chem. Biol.* 13, 608–617.
- (120) Heimburg-Molinaro, J., Lum, M., Vijay, G., Jain, M., Almogren, A., and Rittenhouse-Olson, K. (2011) Cancer vaccines and carbohydrate epitopes. *Vaccine* 29, 8802–8826.
- (121) Nativi, C., and Renaudet, O. (2014) Recent Progress in Antitumoral Synthetic Vaccines. *ACS Med. Chem. Lett.* 5, 1176–1178.
- (122) Eggermont, A. M. M. (2009) Therapeutic vaccines in solid tumours: Can they be harmful? *Eur. J. Cancer* 45, 2087–2090.
- (123) Liu, C.-C., and Ye, X.-S. (2012) Carbohydrate-based cancer vaccines: target cancer with sugar bullets. *Glycoconj. J.* 29, 259–271.

- (124) Buskas, T., Thompson, P., and Boons, G.-J. (2009) Immunotherapy for cancer: synthetic carbohydrate-based vaccines. *Chem. Commun.* 5335–5349.
- (125) Wilson, R. M., and Danishefsky, S. J. (2013) A Vision for Vaccines Built from Fully Synthetic Tumor-Associated Antigens: From the Laboratory to the Clinic. *J. Am. Chem. Soc.* *135*, 14462–14472.
- (126) Berti, F., and Adamo, R. (2013) Recent Mechanistic Insights on Glycoconjugate Vaccines and Future Perspectives. *ACS Chem. Biol.* *8*, 1653–1663.
- (127) Slovin, S. F., Keding, S. J., and Ragupathi, G. (2005) Carbohydrate vaccines as immunotherapy for cancer. *Immunol. Cell Biol.* *83*, 418–428.
- (128) Svennerholm, L. (1957) Quantitative estimation of sialic acids. *Biochim. Biophys. Acta* *24*, 604–611.
- (129) Livingston, P. O. (1995) Approaches to Augmenting the Immunogenicity of Melanoma Gangliosides: From Whole Melanoma Cells to Ganglioside-KLH Conjugate Vaccines. *Immunol. Rev.* *145*, 147–166.
- (130) Kawashima, I., Kotani, M., Ozawa, H., Suzuki, M., and Tai, T. (1994) Generation of monoclonal antibodies specific for ganglioside lactones: Evidence of the expression of lactone on human melanoma cells. *Int. J. Cancer* *58*, 263–268.
- (131) Ragupathi, G., Meyers, M., Adluri, S., Howard, L., Musselli, C., and Livingston, P. O. (2000) Induction of antibodies against GD3 ganglioside in melanoma patients by vaccination with GD3-lactone-KLH conjugate plus immunological adjuvant QS-21. *Int. J. Cancer* *85*, 659–666.
- (132) Bilodeau, M. T., Park, T. K., Hu, S., Randolph, J. T., Danishefsky, S. J., Livingston, P. O., and Zhang, S. (1995) Total Synthesis of a Human Breast Tumor Associated Antigen. *J. Am. Chem. Soc.* *117*, 7840–7841.
- (133) Danishefsky, S. J., Behar, V., Randolph, J. T., and Lloyd, K. O. (1995) Application of the Glycal Assembly Method to the Concise Synthesis of Neoglycoconjugates of Ley and Leb Blood Group Determinants and of H-Type I and H-Type II Oligosaccharides. *J. Am. Chem. Soc.* *117*, 5701–5711.
- (134) Kudryashov, V., Kim, H. M., Ragupathi, G., Danishefsky, S. J., Livingston, P. O., and Lloyd, K. O. (1998) Immunogenicity of synthetic conjugates of Lewisy oligosaccharide with proteins in mice: towards the design of anticancer vaccines. *Cancer Immunol. Immunother.* *45*, 281–286.
- (135) Glunz, P. W., Hintermann, S., Williams, L. J., Schwarz, J. B., Kuduk, S. D., Kudryashov, V., Lloyd, K. O., and Danishefsky, S. J. (2000) Design and Synthesis of Ley-Bearing Glycopeptides that Mimic Cell Surface Ley Mucin Glycoprotein Architecture. *J. Am. Chem. Soc.* *122*, 7273–7279.
- (136) Danishefsky, S. J., Gervay, J., Peterson, J. M., McDonald, F. E., Koseki, K., Griffith, D. A., Oriyama, T., and Marsden, S. P. (1995) Application of Glycals to the Synthesis of Oligosaccharides: Convergent Total Syntheses of the Lewis X Trisaccharide Sialyl Lewis X Antigenic Determinant and Higher Congeners. *J. Am. Chem. Soc.* *117*, 1940–1953.
- (137) Deshpande, P. P., Kim, H. M., Zatorski, A., Park, T.-K., Ragupathi, G., Livingston, P. O., Live, D., and Danishefsky, S. J. (1998) Strategy in Oligosaccharide Synthesis: An Application to a Concise Total Synthesis of the KH-1(adenocarcinoma) Antigen. *J. Am. Chem. Soc.* *120*, 1600–1614.
- (138) Zhang, S., Graeber, L. A., Helling, F., Ragupathi, G., Adluri, S., Lloyd, K. O., and Livingston, P. O. (1996) Augmenting the Immunogenicity of Synthetic MUC1 Peptide Vaccines in Mice. *Cancer Res.* *56*, 3315–3319.
- (139) Kuduk, S. D., Schwarz, J. B., Chen, X.-T., Glunz, P. W., Sames, D., Ragupathi, G., Livingston, P. O., and Danishefsky, S. J. (1998) Synthetic and Immunological Studies on Clustered Modes of Mucin-Related Tn and TF O-Linked Antigens: The Preparation of a Glycopeptide-Based Vaccine for Clinical Trials against Prostate Cancer. *J. Am. Chem. Soc.* *120*, 12474–12485.
- (140) Gamblin, D. P., Scanlan, E. M., and Davis, B. G. (2009) Glycoprotein Synthesis: An Update. *Chem. Rev.* *109*, 131–163.
- (141) Gilewski, T., Ragupathi, G., Bhuta, S., Williams, L. J., Musselli, C., Zhang, X.-F., Bencsath, K. P., Panageas, K. S., Chin, J., Hudis, C. A., Norton, L., Houghton, A. N., Livingston, P. O., and Danishefsky, S. J. (2001) Immunization of metastatic breast cancer patients with a fully

- synthetic globo H conjugate: A phase I trial. *Proc. Natl. Acad. Sci.* 98, 3270–3275.
- (142) Koniev, O., and Wagner, A. (2015) Developments and recent advancements in the field of endogenous amino acid selective bond forming reactions for bioconjugation. *Chem. Soc. Rev.* 44, 5495–5551.
- (143) Kunz, H., and Birnbach, S. (1986) Synthesis of O-Glycopeptides of the Tumor-Associated Tn- and T-Antigen Type and Their Binding to Bovine Serum Albumin. *Angew. Chemie Int. Ed. English* 25, 360–362.
- (144) Kunz, H. (2003) Synthetic glycopeptides for the development of tumour-selective vaccines. *J. Pept. Sci.* 9, 563–573.
- (145) Corzana, F., Busto, J. H., García de Luis, M., Jiménez-Barbero, J., Avenoza, A., and Peregrina, J. M. (2009) The Nature and Sequence of the Amino Acid Aglycone Strongly Modulates the Conformation and Dynamics Effects of Tn Antigen's Clusters. *Chem. – A Eur. J.* 15, 3863–3874.
- (146) Kaiser, A., Gaidzik, N., Westerlind, U., Kowalczyk, D., Hobel, A., Schmitt, E., and Kunz, H. (2009) A synthetic vaccine consisting of a tumor-associated sialyl-T NMUC1 tandem-repeat glycopeptide and tetanus toxoid: induction of a strong and highly selective immune response. *Angew. Chemie - Int. Ed.* 48, 7551–7555.
- (147) Mali, S. M., Ganesh Kumar, M., Katariya, M. M., and Gopi, H. N. (2014) HBTU mediated 1-hydroxybenzotriazole (HOBt) conjugate addition: synthesis and stereochemical analysis of  $\beta$ -benzotriazole N-oxide substituted  $\gamma$ -amino acids and hybrid peptides. *Org. Biomol. Chem.* 12, 8462–8472.
- (148) Keil, S., Claus, C., Dippold, W., and Kunz, H. (2001) Towards the development of antitumor vaccines: A synthetic conjugate of a tumor-associated MUC1 glycopeptide antigen and a tetanus toxin epitope. *Angew. Chemie - Int. Ed.* 40, 366–369.
- (149) Carpino, L. A., Ionescu, D., and El-Faham, A. (1996) Peptide Coupling in the Presence of Highly Hindered Tertiary Amines. *J. Org. Chem.* 61, 2460–2465.
- (150) Ian Storer, R., Aciro, C., and Jones, L. H. (2011) Squaramides: physical properties, synthesis and applications. *Chem. Soc. Rev.* 40, 2330–2346.
- (151) Dziadek, S., Kowalczyk, D., and Kunz, H. (2005) Synthetic Vaccines Consisting of Tumor-Associated MUC1 Glycopeptide Antigens and Bovine Serum Albumin. *Angew. Chemie Int. Ed.* 44, 7624–7630.
- (152) Kagan, E., Ragupathi, G., Yi, S. S., Reis, C. A., Gildersleeve, J., Kahne, D., Clausen, H., Danishefsky, S. J., and Livingston, P. O. (2005) Comparison of antigen constructs and carrier molecules for augmenting the immunogenicity of the monosaccharide epithelial cancer antigen Tn. *Cancer Immunol. Immunother.* 54, 424–430.
- (153) Rohrer, J. S., and Miller, H. I. (2003) Detecting O-linked oligosaccharides on glycoproteins. *Anal. Biochem.* 316, 131–134.
- (154) Kurosaka, A., Kitagawa, H., Fukui, S., Numata, Y., Nakada, H., Funakoshi, I., Kawasaki, T., Ogawa, T., Iijima, H., and Yamashina, I. (1988) A monoclonal antibody that recognizes a cluster of a disaccharide, NeuAc $\alpha$ 2 $\rightarrow$ 6GalNAc, in mucin-type glycoproteins. *J. Biol. Chem.* 263, 8724–8726.
- (155) Nakada, H., Inoue, M., Numata, Y., Tanaka, N., Funakoshi, I., Fukui, S., Mellors, A., and Yamashina, I. (1993) Epitopic structure of Tn glycoporphin A for an anti-Tn antibody (MLS 128). *Proc. Natl. Acad. Sci. U. S. A.* 90, 2495–2499.
- (156) Slovin, S. F., Ragupathi, G., Musselli, C., Fernandez, C., Diani, M., Verbel, D., Danishefsky, S., Livingston, P., and Scher, H. I. (2005) Thomsen-Friedenreich (TF) antigen as a target for prostate cancer vaccine: clinical trial results with TF cluster (c)-KLH plus QS21 conjugate vaccine in patients with biochemically relapsed prostate cancer. *Cancer Immunol. Immunother.* 54, 694–702.
- (157) Scher, H. I., Eisenberger, M., D'Amico, A. V., Halabi, S., Small, E. J., Morris, M., Kattan, M. W., Roach, M., Kantoff, P., Pienta, K. J., Carducci, M. A., Agus, D., Slovin, S. F., Heller, G., Kelly, W. K., Lange, P. H., Petrylak, D., Berg, W., Higano, C., Wilding, G., Moul, J. W., Partin, A. N., Logothetis, C., and Soule, H. R. (2004) Eligibility and Outcomes Reporting Guidelines for Clinical Trials for Patients in the State of a Rising Prostate-Specific Antigen: Recommendations From

- the Prostate-Specific Antigen Working Group. *J. Clin. Oncol.* **22**, 537–556.
- (158) Ragupathi, G., Cappello, S., Yi, S. S., Canter, D., Spassova, M., Bornmann, W. G., Danishefsky, S. J., and Livingston, P. O. (2002) Comparison of antibody titers after immunization with monovalent or tetravalent KLH conjugate vaccines. *Vaccine* **20**, 1030–1038.
- (159) Ragupathi, G., Koide, F., Sathyan, N., Kagan, E., Spassova, M., Bornmann, W., Gregor, P., Reis, C. A., Clausen, H., Danishefsky, S. J., and Livingston, P. O. (2003) A preclinical study comparing approaches for augmenting the immunogenicity of a heptavalent KLH-conjugate vaccine against epithelial cancers. *Cancer Immunol. Immunother.* **52**, 608–616.
- (160) Oyelaran, O., and Gildersleeve, J. C. (2010) Evaluation of human antibody responses to keyhole limpet hemocyanin on a carbohydrate microarray. *Proteomics - Clin. Appl.* **4**, 285–294.
- (161) Keding, S. J., and Danishefsky, S. J. (2004) Prospects for total synthesis: A vision for a totally synthetic vaccine targeting epithelial tumors. *Proc. Natl. Acad. Sci. United States Am.* **101**, 11937–11942.
- (162) Fernández-Tejada, A., Brailsford, J., Zhang, Q., Shieh, J.-H., Moore, M. A. S., and Danishefsky, S. J. (2015) Total Synthesis of Glycosylated Proteins - Protein Ligation and Total Synthesis I (Liu, L., Ed.), pp 1–26. Springer International Publishing, Cham.
- (163) Allen, J. R., Harris, C. R., and Danishefsky, S. J. (2001) Pursuit of Optimal Carbohydrate-Based Anticancer Vaccines: Preparation of a Multiantigenic Unimolecular Glycopeptide Containing the Tn, MBr1, and Lewisy Antigens. *J. Am. Chem. Soc.* **123**, 1890–1897.
- (164) Biswas, K., Coltart, D. M., and Danishefsky, S. J. (2002) Construction of carbohydrate-based antitumor vaccines: synthesis of glycosyl amino acids by olefin cross-metathesis. *Tetrahedron Lett.* **43**, 6107–6110.
- (165) Keding, S. J., Atsushi, E., Biswas, K., Zatorski, A., Coltart, D. M., and Danishefsky, S. J. (2003) Hydroxynorleucine as a glycosyl acceptor is an efficient means for introducing amino acid functionality into complex carbohydrates. *Tetrahedron Lett.* **44**, 3413–3416.
- (166) Ragupathi, G., Coltart, D. M., Williams, L. J., Koide, F., Kagan, E., Allen, J., Harris, C., Glunz, P. W., Livingston, P. O., and Danishefsky, S. J. (2002) On the power of chemical synthesis: Immunological evaluation of models for multiantigenic carbohydrate-based cancer vaccines. *Proc. Natl. Acad. Sci.* **99**, 13699–13704.
- (167) Ragupathi, G., Koide, F., Livingston, P. O., Cho, Y. S., Endo, A., Wan, Q., Spassova, M. K., Keding, S. J., Allen, J., Ouerfelli, O., Wilson, R. M., and Danishefsky, S. J. (2006) Preparation and Evaluation of Unimolecular Pentavalent and Hexavalent Antigenic Constructs Targeting Prostate and Breast Cancer: A Synthetic Route to Anticancer Vaccine Candidates. *J. Am. Chem. Soc.* **128**, 2715–2725.
- (168) Zhu, J., Wan, Q., Lee, D., Yang, G., Spassova, M. K., Ouerfelli, O., Ragupathi, G., Damani, P., Livingston, P. O., and Danishefsky, S. J. (2009) From Synthesis to Biologics: Preclinical Data on a Chemistry Derived Anticancer Vaccine. *J. Am. Chem. Soc.* **131**, 9298–9303.
- (169) Livingston, P. O., Natoli, E. J., Calves, M. J., Stockert, E., Oettgen, H. F., and Old, L. J. (1987) Vaccines containing purified GM2 ganglioside elicit GM2 antibodies in melanoma patients. *Proc. Natl. Acad. Sci.* **84**, 2911–2915.
- (170) Cho, Y. S., Wan, Q., and Danishefsky, S. J. (2005) Organic synthesis in pursuit of immunology: Large-scale synthesis of peracetylated GM2 glycosylamino acid for preparation of a multiantigenic prostate cancer vaccine. *Bioorg. Med. Chem.* **13**, 5259–5266.
- (171) Wan, Q., Shin Cho, Y., Lambert, T. H., and Danishefsky, S. J. (2005) Olefin Cross-Metathesis: A Powerful Tool for Constructing Vaccines Composed of Multimeric Antigens. *J. Carbohydr. Chem.* **24**, 425–440.
- (172) Gildersleeve, J. C., Oyelaran, O., Simpson, J. T., and Allred, B. (2008) Improved Procedure for Direct Coupling of Carbohydrates to Proteins via Reductive Amination. *Bioconjug. Chem.* **19**, 1485–1490.
- (173) Ragupathi, G., Rao Koganty, R., Qiu, D., Lloyd, K. O., and Livingston, P. O. (1998) A novel and efficient method for synthetic carbohydrate conjugate vaccine preparation: synthesis of sialyl Tn-KLH conjugate using a 4-(4-N-maleimidomethyl) cyclohexane-1-carboxyl hydrazide

- (MMCCH) linker arm. *Glycoconj. J.* *15*, 217–221.
- (174) Buskas, T., Li, Y., and Boons, G.-J. (2004) The Immunogenicity of the Tumor-Associated Antigen Lewisy May Be Suppressed by a Bifunctional Cross-Linker Required for Coupling to a Carrier Protein. *Chem. - A Eur. J.* *10*, 3517–3524.
- (175) Yoshitake, S., Yamada, Y., Ishikawa, E., and Masseyeff, R. (1979) Conjugation of Glucose Oxidase from *Aspergillus niger* and Rabbit Antibodies Using N-Hydroxysuccinimide Ester of N-(4-Carboxycyclohexylmethyl)-Maleimide. *Eur. J. Biochem.* *101*, 395–399.
- (176) Partis, M. D., Griffiths, D. G., Roberts, G. C., and Beechey, R. B. (1983) Cross-linking of protein by  $\omega$ -maleimido alkanoylN-hydroxysuccinimido esters. *J. Protein Chem.* *2*, 263–277.
- (177) Dagan, R., Poolman, J., and Siegrist, C. A. (2010) Glycoconjugate vaccines and immune interference: A review. *Vaccine* *28*, 5513–5523.
- (178) Herzenberg, L. A., Tokuhisa, T., and Herzenberg, L. A. (1980) Carrier-priming leads to hapten-specific suppression. *Nature* *285*, 664–667.
- (179) Roldão, A., Mellado, M. C. M., Castilho, L. R., Carrondo, M. J. T., and Alves, P. M. (2010) Virus-like particles in vaccine development. *Expert Rev. Vaccines* *9*, 1149–1176.
- (180) Jegerlehner, A., Storni, T., Lipowsky, G., Schmid, M., Pumpens, P., and Bachmann, M. F. (2002) Regulation of IgG antibody responses by epitope density and CD21-mediated costimulation. *Eur. J. Immunol.* *32*, 3305–3314.
- (181) Lin, T., Chen, Z., Usha, R., Stauffacher, C. V., Dai, J.-B., Schmidt, T., and Johnson, J. E. (1999) The Refined Crystal Structure of Cowpea Mosaic Virus at 2.8 Å Resolution. *Virology* *265*, 20–34.
- (182) Wang, Q., Kaltgrad, E., Lin, T., Johnson, J. E., and Finn, M. G. (2002) Natural Supramolecular Building Blocks. *Chem. Biol.* *9*, 805–811.
- (183) Blum, A. S., Soto, C. M., Wilson, C. D., Cole, J. D., Kim, M., Gnade, B., Chatterji, A., Ochoa, W. F., Lin, T., Johnson, J. E., and Ratna, B. R. (2004) Cowpea Mosaic Virus as a Scaffold for 3-D Patterning of Gold Nanoparticles. *Nano Lett.* *4*, 867–870.
- (184) Lin, T. (2006) Structural genesis of the chemical addressability in a viral nano-block. *J. Mater. Chem.* *16*, 3673–3681.
- (185) Miermont, A., Barnhill, H., Strable, E., Lu, X., Wall, K. A., Wang, Q., Finn, M. G., and Huang, X. (2008) Cowpea Mosaic Virus Capsid: A Promising Carrier for the Development of Carbohydrate Based Antitumor Vaccines. *Chem. - A Eur. J.* *14*, 4939–4947.
- (186) Kaltgrad, E., Sen Gupta, S., Punna, S., Huang, C.-Y., Chang, A., Wong, C.-H., Finn, M. G., and Blixt, O. (2007) Anti-Carbohydrate Antibodies Elicited by Polyvalent Display on a Viral Scaffold. *ChemBioChem* *8*, 1455–1462.
- (187) Cruz, L. J., Tacke, P. J., Rueda, F., Domingo, J. C., Albericio, F., and Figdor, C. G. (2012) Chapter eight – Targeting Nanoparticles to Dendritic Cells for Immunotherapy, in *Methods in Enzymology*, pp 143–163.
- (188) Fallarini, S., Paoletti, T., Battaglini, C. O., Ronchi, P., Lay, L., Bonomi, R., Jha, S., Mancin, F., Scrimin, P., and Lombardi, G. (2013) Factors affecting T cell responses induced by fully synthetic glyco-gold-nanoparticles. *Nanoscale* *5*, 390–400.
- (189) Park, Y.-M., Lee, S. J., Kim, Y. S., Lee, M. H., Cha, G. S., Jung, I. D., Kang, T. H., and Han, H. D. (2013) Nanoparticle-Based Vaccine Delivery for Cancer Immunotherapy. *Immune Netw* *13*, 177–183.
- (190) Almeida, J. P. M., Figueroa, E. R., and Drezek, R. A. (2014) Gold nanoparticle mediated cancer immunotherapy. *Nanomedicine Nanotechnology, Biol. Med.* *10*, 503–514.
- (191) Foged, C., Brodin, B., Frokjaer, S., and Sundblad, A. (2005) Particle size and surface charge affect particle uptake by human dendritic cells in an in vitro model. *Int. J. Pharm.* *298*, 315–322.
- (192) Parry, A. L., Clemson, N. A., Ellis, J., Bernhard, S. S. R., Davis, B. G., and Cameron, N. R. (2013) “Multicopy Multivalent” Glycopolymer-Stabilized Gold Nanoparticles as Potential Synthetic Cancer Vaccines. *J. Am. Chem. Soc.* *135*, 9362–9365.
- (193) Nishat, S., and Andreato, R. P. (2016) Entirely Carbohydrate-Based Vaccines: An Emerging Field for Specific and Selective Immune Responses. *Vaccines* .



- (194) Mazmanian, S. K., and Kasper, D. L. (2006) The love-hate relationship between bacterial polysaccharides and the host immune system. *Nat Rev Immunol* 6, 849–858.
- (195) Tzianabos, A. O., Onderdonk, A. B., Rosner, B., Cisneros, R. L., and Kasper, D. L. (1993) Structural features of polysaccharides that induce intra-abdominal abscesses. *Science* 262, 416–419.
- (196) Baumann, H., Tzianabos, A. O., Brisson, J. R., Kasper, D. L., and Jennings, H. J. (1992) Structural elucidation of two capsular polysaccharides from one strain of *Bacteroides fragilis* using high-resolution NMR spectroscopy. *Biochemistry* 31, 4081–4089.
- (197) Kalka-Moll, W. M., Tzianabos, A. O., Bryant, P. W., Niemeyer, M., Ploegh, H. L., and Kasper, D. L. (2002) Zwitterionic Polysaccharides Stimulate T Cells by MHC Class II-Dependent Interactions. *J. Immunol.* 169, 6149–6153.
- (198) De Silva, R. A., Wang, Q., Chidley, T., Appulage, D. K., and Andreatina, P. R. (2009) Immunological Response from an Entirely Carbohydrate Antigen: Design of Synthetic Vaccines Based on Tn-PS A1 Conjugates. *J. Am. Chem. Soc.* 131, 9622–9623.
- (199) Shi, M., Kleski, K. A., Trabbic, K. R., Bourgault, J.-P., and Andreatina, P. R. (2016) Sialyl-Tn Polysaccharide A1 as an Entirely Carbohydrate Immunogen: Synthesis and Immunological Evaluation. *J. Am. Chem. Soc.* 138, 14264–14272.
- (200) Kalka-Moll, W. M., Wang, Y., Comstock, L. E., Gonzalez, S. E., Tzianabos, A. O., and Kasper, D. L. (2001) Immunochemical and Biological Characterization of Three Capsular Polysaccharides from a Single *Bacteroides fragilis* Strain. *Infect. Immun.* 69, 2339–2344.
- (201) Dryhurst, G. (1970) Chapter 3 – Mechanism Of Periodate Oxidation, in *Periodate Oxidation of Diol and Other Functional Groups*, pp 24–54.
- (202) Mata-Haro, V., Cekic, C., Martin, M., Chilton, P. M., Casella, C. R., and Mitchell, T. C. (2007) The Vaccine Adjuvant Monophosphoryl Lipid A as a TRIF-Biased Agonist of TLR4. *Science* 316, 1628–1632.
- (203) Takayama, K., Qureshi, N., Raetz, C. R., Ribi, E., Peterson, J., Cantrell, J. L., Pearson, F. C., Wiggins, J., and Johnson, A. G. (1984) Influence of fine structure of lipid A on *Limulus* amoebocyte lysate clotting and toxic activities. *Infect. Immun.* 45, 350–355.
- (204) Miles, D., Roché, H., Martin, M., Perren, T. J., Cameron, D. A., Glaspy, J., Dodwell, D., Parker, J., Mayordomo, J., Tres, A., Murray, J. L., Ibrahim, N. K., and Group, the T. S. (2011) Phase III Multicenter Clinical Trial of the Sialyl-TN (STn)-Keyhole Limpet Hemocyanin (KLH) Vaccine for Metastatic Breast Cancer. *Oncol.* 16, 1092–1100.
- (205) Pifferi, C., Berthet, N., and Renaudet, O. (2017) Cyclopeptide scaffolds in carbohydrate-based synthetic vaccines. *Biomater. Sci.* 5, 953–965.
- (206) Hackenberger, C. P. R., and Schwarzer, D. (2008) Chemoselective Ligation and Modification Strategies for Peptides and Proteins. *Angew. Chemie Int. Ed.* 47, 10030–10074.
- (207) Tang, W., and Becker, M. L. (2014) “Click” reactions: a versatile toolbox for the synthesis of peptide-conjugates. *Chem. Soc. Rev.* 43, 7013–7039.
- (208) Bay, S., Lo-Man, R., Osinaga, E., Nakada, H., Leclerc, C., and Cantacuzene, D. (1997) Preparation of a multiple antigen glycopeptide (MAG) carrying the Tn antigen. A possible approach to a synthetic carbohydrate vaccine. *J. Pept. Res.* 49, 620–625.
- (209) Posnett, D. N., Mcgrath, H., and Tam, P. (1988) A Novel Method for Producing Anti-peptide Antibodies. *Biochemistry* 263, 1719–1725.
- (210) Leclerc, C., Deriaud, E., Mimic, V., and van der Werf, S. (1991) Identification of a T-cell epitope adjacent to neutralization antigenic site 1 of poliovirus type 1. *J. Virol.* 65, 711–718.
- (211) Paulsen, H., and Hölck, J.-P. (1982) Synthese der glycopeptide O-β-d-galactopyranosyl-(1→3)-O-(2-acetamido-2-desoxy-α-d-galactopyranosyl)-(1→3)-l-serin und -l-threonin. *Carbohydr. Res.* 109, 89–107.
- (212) Lo-Man, R., Bay, S., Vichier-Guerre, S., Dériaud, E., Cantacuzène, D., and Leclerc, C. (1999) A Fully Synthetic Immunogen Carrying a Carcinoma-associated Carbohydrate for Active Specific Immunotherapy<sup>1</sup>. *Cancer Res.* 59, 1520–1524.
- (213) Numata, Y., Nakada, H., Fukui, S., Kitagawa, H., Ozaki, K., Inoue, M., Kawasaki, T., Funakoshi, I., and Yamashina, I. (1990) A monoclonal antibody directed to Tn antigen. *Biochem. Biophys. Res.*

- Commun.* 170, 981–985.
- (214) Nakada, H., Inoue, M., Tanaka, N., Numata, Y., Kitagawa, H., Fukui, S., and Yamashina, I. (1991) Expression of the Tn antigen on T-lymphoid cell line Jurkat. *Biochem. Biophys. Res. Commun.* 179, 762–767.
- (215) Zhang, S., Walberg, L. A., Ogata, S., Itzkowitz, S. H., Koganty, R. R., Reddish, M., Gandhi, S. S., Longenecker, B. M., Lloyd, K. O., and Livingston, P. O. (1995) Immune Sera and Monoclonal Antibodies Define Two Configurations for the Sialyl Tn Tumor Antigen. *Cancer Res.* 55, 3364–3368.
- (216) Lo-Man, R., Vichier-Guerre, S., Bay, S., Dériaud, E., Cantacuzène, D., and Leclerc, C. (2001) Anti-Tumor Immunity Provided by a Synthetic Multiple Antigenic Glycopeptide Displaying a Tri-Tn Glycotope. *J. Immunol.* 166, 2849–2854.
- (217) Lo-Man, R., Vichier-Guerre, S., Perraut, R., Dériaud, E., Huteau, V., BenMohamed, L., Diop, O. M., Livingston, P. O., Bay, S., and Leclerc, C. (2004) A Fully Synthetic Therapeutic Vaccine Candidate Targeting Carcinoma-Associated Tn Carbohydrate Antigen Induces Tumor-Specific Antibodies in Nonhuman Primates. *Cancer Res.* 64, 4987–4994.
- (218) Laubreton, D., Bay, S., Sedlik, C., Artaud, C., Ganneau, C., Dériaud, E., Viel, S., Puaux, A.-L., Amigorena, S., Gérard, C., Lo-Man, R., and Leclerc, C. (2016) The fully synthetic MAG-Tn3 therapeutic vaccine containing the tetanus toxoid-derived TT830-844 universal epitope provides anti-tumor immunity. *Cancer Immunol. Immunother.* 65, 315–325.
- (219) Grigalevicius, S., Chierici, S., Renaudet, O., Lo-Man, R., Dériaud, E., Leclerc, C., and Dumy, P. (2005) Chemoselective assembly and immunological evaluation of multiepitopic glycoconjugates bearing clustered Tn antigen as synthetic anticancer vaccines. *Bioconjug. Chem.* 16, 1149–1159.
- (220) Mutter, M., Hersperger, R., Gubernator, K., and Müller, K. (1989) The construction of new proteins: V. A template-assembled synthetic protein (TASP) containing both a 4-helix bundle and  $\beta$ -barrel-like structure. *Proteins Struct. Funct. Genet.* 5, 13–21.
- (221) Dumy, P., Eggleston, I. M., Cervigni, S., Sila, U., Sun, X., and Mutter, M. (1995) A convenient synthesis of cyclic peptides as regioselectively addressable functionalized templates (RAFT). *Tetrahedron Lett.* 36, 1255–1258.
- (222) Mutter, M., Dumy, P., Garrouste, P., Lehmann, C., Mathieu, M., Peggion, C., Peluso, S., Razaname, A., and Tuchscherer, G. (1996) Template Assembled Synthetic Proteins(TASP) as Functional Mimetics of Proteins. *Angew. Chemie Int. Ed. English* 35, 1482–1485.
- (223) Peluso, S., Rückle, T., Lehmann, C., Mutter, M., Peggion, C., and Crisma, M. (2001) Crystal structure of a synthetic cyclodecapeptide for template-assembled synthetic protein design. *Chembiochem* 2, 432–437.
- (224) Boturyn, D., Coll, J.-L., Garanger, E., Favrot, M.-C., and Dumy, P. (2004) Template Assembled Cyclopeptides as Multimeric System for Integrin Targeting and Endocytosis. *J. Am. Chem. Soc.* 126, 5730–5739.
- (225) Karageorgis, A., Claron, M., Jugé, R., Aspord, C., Thoreau, F., Leloup, C., Kucharczak, J., Plumas, J., Henry, M., Hurbin, A., Verdié, P., Martinez, J., Subra, G., Dumy, P., Boturyn, D., Auouacheria, A., and Coll, J.-L. (2017) Systemic Delivery of Tumor-Targeted Bax-Derived Membrane-Active Peptides for the Treatment of Melanoma Tumors in a Humanized SCID Mouse Model. *Mol. Ther.* 25, 534–546.
- (226) Bonnat, L., Dejeu, J., Bonnet, H., Génaro, B., Jarjays, O., Thomas, F., Lavergne, T., and Defrancq, E. (2016) Templated Formation of Discrete RNA and DNA:RNA Hybrid G-Quadruplexes and Their Interactions with Targeting Ligands. *Chem. - A Eur. J.* 22, 3139–3147.
- (227) Bonnat, L., Bar, L., Génaro, B., Bonnet, H., Jarjays, O., Thomas, F., Dejeu, J., Defrancq, E., and Lavergne, T. (2017) Template-Mediated Stabilization of a DNA G-Quadruplex formed in the HIV-1 Promoter and Comparative Binding Studies. *Chem. - A Eur. J.* 23, 5602–5613.
- (228) Galan, M. C., Dumy, P., and Renaudet, O. (2013) Multivalent glyco(cyclo)peptides. *Chem. Soc. Rev.* 42, 4599–4612.
- (229) Rose, K. (1994) Facile synthesis of homogeneous artificial proteins. *J. Am. Chem. Soc.* 116, 30–

- 33.
- (230) Shao, J., and Tam, J. P. (1995) Unprotected Peptides as Building Blocks for the Synthesis of Peptide Dendrimers with Oxime, Hydrazone, and Thiazolidine Linkages. *J. Am. Chem. Soc.* **117**, 3893–3899.
- (231) Cervigni, S. E., Dumy, P., and Mutter, M. (1996) Synthesis of Glycopeptides and Lipopeptides by Chemoselective Ligation. *Angew. Chemie Int. Ed. English* **35**, 1230–1232.
- (232) Rodriguez, E. C., Winans, K. A., King, D. S., and Bertozzi, C. R. (1997) A Strategy for the Chemoselective Synthesis of O-Linked Glycopeptides with Native Sugar–Peptide Linkages. *J. Am. Chem. Soc.* **119**, 9905–9906.
- (233) Canne, L. E., Botti, P., Simon, R. J., Chen, Y., Dennis, E. A., and Kent, S. B. H. (1999) Chemical Protein Synthesis by Solid Phase Ligation of Unprotected Peptide Segments. *J. Am. Chem. Soc.* **121**, 8720–8727.
- (234) Forget, D., Boturyn, D., Defrancq, E., Lhomme, J., and Dumy, P. (2001) Highly efficient synthesis of peptide-oligonucleotide conjugates: Chemoselective oxime and thiazolidine formation. *Chem. - A Eur. J.* **7**, 3976–3984.
- (235) Chen, J., Zeng, W., Offord, R., and Rose, K. (2003) A Novel Method for the Rational Construction of Well-Defined Immunogens: The Use of Oximation To Conjugate Cholera Toxin B Subunit to a Peptide–Polyoxime Complex. *Bioconjug. Chem.* **14**, 614–618.
- (236) Neuner, P., Gallo, P., Orsatti, L., Fontana, L., and Monaci, P. (2003) An Efficient and Versatile Synthesis of BisPNA–Peptide Conjugates Based on Chemoselective Oxime Formation. *Bioconjug. Chem.* **14**, 276–281.
- (237) Katajisto, J., Virta, P., and Lönnberg, H. (2004) Solid-Phase Synthesis of Multiantennary Oligonucleotide Glycoconjugates Utilizing On-Support Oximation. *Bioconjug. Chem.* **15**, 890–896.
- (238) Pifferi, C., Daskhan, G. C., Fiore, M., Shiao, T. C., Roy, R., and Renaudet, O. (2017) Aminoxyated Carbohydrates: Synthesis and Applications. *Chem. Rev.* **117**, 9839–9873.
- (239) Kalia, J., and Raines, R. T. (2008) Hydrolytic Stability of Hydrazones and Oximes. *Angew. Chemie Int. Ed.* **47**, 7523–7526.
- (240) Bousquet, E., Spadaro, A., Pappalardo, M. S., Bernardini, R., Romeo, R., Panza, L., and Ronsisvalle, G. (2000) Synthesis and Immunostimulating Activity of A Thioglycolipopeptide Glycomimetic As A Potential Anticancer Vaccine Derived From Tn Antigen. *J. Carbohydr. Chem.* **19**, 527–541.
- (241) Cipolla, L., Rescigno, M., Leone, A., Peri, F., La Ferla, B., and Nicotra, F. (2002) Novel Tn antigen-containing neoglycopeptides: synthesis and evaluation as anti tumor vaccines. *Bioorg. Med. Chem.* **10**, 1639–1646.
- (242) Vichier-Guerre, S., Lo-Man, R., Huteau, V., Dériaud, E., Leclerc, C., and Bay, S. (2004) Synthesis and immunological evaluation of an antitumor neoglycopeptide vaccine bearing a novel homoserine Tn antigen. *Bioorg. Med. Chem. Lett.* **14**, 3567–3570.
- (243) Keding, S. J., Endo, A., and Danishefsky, S. J. (2003) Synthesis of non-natural glycosylamino acids containing tumor-associated carbohydrate antigens. *Tetrahedron* **59**, 7023–7031.
- (244) El-Mahdi, O., and Melnyk, O. (2013)  $\alpha$ -Oxo Aldehyde or Glyoxylyl Group Chemistry in Peptide Bioconjugation. *Bioconjug. Chem.* **24**, 735–765.
- (245) Madsen, C. B., Pedersen, A. E., and Wandall, H. H. (2013) Glycan-mediated modification of the immune response. *Oncoimmunology* **2**, e23659.
- (246) Murphy, K. M., Heimberger, A. B., and Loh, D. Y. (1990) Induction by antigen of intrathymic apoptosis of CD4+CD8+TCR $\alpha$  thymocytes in vivo. *Science* **250**, 1720–1723.
- (247) Deres, K., Schild, H., Wiesmuller, K.-H., Jung, G., and Rammensee, H.-G. (1989) In vivo priming of virus-specific cytotoxic T lymphocytes with synthetic lipopeptide vaccine. *Nature* **342**, 561–564.
- (248) Borges, E., Wiesmüller, K.-H., Jung, G., and Walden, P. (1994) Efficacy of synthetic vaccines in the induction of cytotoxic T lymphocytes comparison of the costimulating support provided by helper T cells and lipoamino acid. *J. Immunol. Methods* **173**, 253–263.

- (249) Buwitt-Beckmann, U., Heine, H., Wiesmüller, K.-H., Jung, G., Brock, R., Akira, S., and Ulmer, A. J. (2006) TLR1- and TLR6-independent Recognition of Bacterial Lipopeptides. *J. Biol. Chem.* **281**, 9049–9057.
- (250) Hennessy, E. J., Parker, A. E., and O’Neill, L. A. J. (2010) Targeting Toll-like receptors: emerging therapeutics? *Nat Rev Drug Discov* **9**, 293–307.
- (251) O’Neill, L. A. J., Golenbock, D., and Bowie, A. G. (2013) The history of Toll-like receptors - redefining innate immunity. *Nat Rev Immunol* **13**, 453–460.
- (252) Hamley, I. W. (2015) Lipopeptides: from self-assembly to bioactivity. *Chem. Commun.* **51**, 8574–8583.
- (253) Hamley, I. W., Kirkham, S., Dehsorkhi, A., Castelletto, V., Reza, M., and Ruokolainen, J. (2014) Toll-like receptor agonist lipopeptides self-assemble into distinct nanostructures. *Chem. Commun.* **50**, 15948–15951.
- (254) Kaiser, A., Gaidzik, N., Becker, T., Menge, C., Groh, K., Cai, H., Li, Y.-M., Gerlitzki, B., Schmitt, E., and Kunz, H. (2010) Fully Synthetic Vaccines Consisting of Tumor-Associated MUC1 Glycopeptides and a Lipopeptide Ligand of the Toll-like Receptor 2. *Angew. Chemie Int. Ed.* **49**, 3688–3692.
- (255) Akira, S., and Takeda, K. (2004) Toll-like receptor signalling. *Nat Rev Immunol* **4**, 499–511.
- (256) Ingale, S., Wolfert, M. A., Gaekwad, J., Buskas, T., and Boons, G.-J. (2007) Robust immune responses elicited by a fully synthetic three-component vaccine. *Nat Chem Biol* **3**, 663–667.
- (257) Wilkinson, B. L., Day, S., Malins, L. R., Apostolopoulos, V., and Payne, R. J. (2011) Self-Adjuvanting Multicomponent Cancer Vaccine Candidates Combining Per-Glycosylated MUC1 Glycopeptides and the Toll-like Receptor 2 Agonist Pam3CysSer. *Angew. Chemie Int. Ed.* **50**, 1635–1639.
- (258) Jung, J. P., Nagaraj, A. K., Fox, E. K., Rudra, J. S., Devgun, J. M., and Collier, J. H. (2009) Co-assembling peptides as defined matrices for endothelial cells. *Biomaterials* **30**, 2400–2410.
- (259) Rudra, J. S., Tian, Y. F., Jung, J. P., and Collier, J. H. (2010) A self-assembling peptide acting as an immune adjuvant. *Proc. Natl. Acad. Sci.* **107**, 622–627.
- (260) Mond, J. J., Lees, A., and Snapper, C. M. (1995) T Cell-Independent Antigens Type 2. *Annu. Rev. Immunol.* **13**, 655–692.
- (261) Spohn, R., Buwitt-Beckmann, U., Brock, R., Jung, G., Ulmer, A. J., and Wiesmüller, K.-H. (2004) Synthetic lipopeptide adjuvants and Toll-like receptor 2—structure–activity relationships. *Vaccine* **22**, 2494–2499.
- (262) Cato, D., Buskas, T., and Boons, G. (2005) Highly Efficient Stereospecific Preparation of Tn and TF Building Blocks Using Thioglycosyl Donors and the Ph2SO/Tf2O Promotor System. *J. Carbohydr. Chem.* **24**, 503–516.
- (263) Metzger, J. W., Wiesmüller, K.-H., and Jung, G. (1991) Synthesis of N $\alpha$ -Fmoc protected derivatives of S-(2,3-dihydroxypropyl)-cysteine and their application in peptide synthesis. *Int. J. Pept. Protein Res.* **38**, 545–554.
- (264) Ingale, S., Buskas, T., and Boons, G.-J. (2006) Synthesis of Glyco(lipo)peptides by Liposome-Mediated Native Chemical Ligation. *Org. Lett.* **8**, 5785–5788.
- (265) Kent, S. (2010) Origin of the chemical ligation concept for the total synthesis of enzymes (proteins). *Biopolymers* **94**, iv–ix.
- (266) Bondalapati, S., Jbara, M., and Brik, A. (2016) Expanding the chemical toolbox for the synthesis of large and uniquely modified proteins. *Nat Chem* **8**, 407–418.
- (267) Burke, H. M., McSweeney, L., and Scanlan, E. M. (2010) Exploring chemoselective S-to-N acyl transfer reactions in synthesis and chemical biology **8**, 15655.
- (268) Kersten, G. F. A., and Crommelin, D. J. A. (1995) Liposomes and ISCOMS as vaccine formulations. *Biochim. Biophys. Acta - Rev. Biomembr.* **1241**, 117–138.
- (269) Buskas, T., Ingale, S., and Boons, G.-J. (2005) Towards a Fully Synthetic Carbohydrate-Based Anticancer Vaccine: Synthesis and Immunological Evaluation of a Lipidated Glycopeptide Containing the Tumor-Associated Tn Antigen. *Angew. Chemie Int. Ed.* **44**, 5985–5988.
- (270) O’Garra, A. (1998) Cytokines induce the development of functionally heterogeneous T helper

- cell subsets. *Immunity* 8, 275–283.
- (271) Ivanova, E. A., and Orekhov, A. N. (2015) T Helper lymphocyte subsets and plasticity in autoimmunity and cancer: An overview. *Biomed Res. Int.* 2015.
- (272) Saeland, E., van Vliet, S. J., Bäckström, M., van den Berg, V. C. M., Geijtenbeek, T. B. H., Meijer, G. A., and van Kooyk, Y. (2007) The C-type lectin MGL expressed by dendritic cells detects glycan changes on MUC1 in colon carcinoma. *Cancer Immunol. Immunother.* 56, 1225–1236.
- (273) Renaudet, O., BenMohamed, L., Dasgupta, G., Bettahi, I., and Dumy, P. (2008) Towards a self-adjuvanting multivalent B and T cell epitope containing synthetic glycolipopeptide cancer vaccine. *ChemMedChem* 3, 737–741.
- (274) Bettahi, I., Dasgupta, G., Renaudet, O., Chentoufi, A. A., Zhang, X., Carpenter, D., Yoon, S., Dumy, P., and BenMohamed, L. (2009) Antitumor activity of a self-adjuvanting glycolipopeptide vaccine bearing B cell, CD4+ and CD8+ T cell epitopes. *Cancer Immunol. Immunother.* 58, 187–200.
- (275) Renaudet, O., Dasgupta, G., Bettahi, I., Shi, A., Nesburn, A. B., Dumy, P., and BenMohamed, L. (2010) Linear and branched glyco-lipopeptide vaccines follow distinct cross-presentation pathways and generate different magnitudes of antitumor immunity. *PLoS One* 5.
- (276) Saito, G., Swanson, J. A., and Lee, K.-D. (2003) Drug delivery strategy utilizing conjugation via reversible disulfide linkages: role and site of cellular reducing activities. *Adv. Drug Deliv. Rev.* 55, 199–215.
- (277) Otto, K. R. W. and S. (2005) Reversible Covalent Chemistry in Drug Delivery. *Curr. Drug Discov. Technol.*
- (278) Wang, J., Li, S., Luo, T., and Zhao, C. W. and J. (2012) Disulfide Linkage: A Potent Strategy in Tumor-Targeting Drug Discovery. *Curr. Med. Chem.*
- (279) Góngora-Benítez, M., Tulla-Puche, J., and Albericio, F. (2014) Multifaceted Roles of Disulfide Bonds. Peptides as Therapeutics. *Chem. Rev.* 114, 901–926.
- (280) Hällbrink, M., Florén, A., Elmquist, A., Pooga, M., Bartfai, T., and Langel, Ü. (2001) Cargo delivery kinetics of cell-penetrating peptides. *Biochim. Biophys. Acta - Biomembr.* 1515, 101–109.
- (281) Meldal, M., and Breddam, K. (1991) Anthranilamide and nitrotyrosine as a donor-acceptor pair in internally quenched fluorescent substrates for endopeptidases: Multicolumn peptide synthesis of enzyme substrates for subtilisin carlsberg and pepsin. *Anal. Biochem.* 195, 141–147.
- (282) Röttschke, O., Falk, K., Stevanovic, S., Jung, G., Walden, P., and Rammensee, H.-G. (1991) Exact prediction of a natural T cell epitope. *Eur. J. Immunol.* 21, 2891–2894.
- (283) Alexander, J., del Guercio, M.-F., Maewal, A., Qiao, L., Fikes, J., Chesnut, R. W., Paulson, J., Bundle, D. R., DeFrees, S., and Sette, A. (2000) Linear PADRE T Helper Epitope and Carbohydrate B Cell Epitope Conjugates Induce Specific High Titer IgG Antibody Responses. *J. Immunol.* 164, 1625 LP-1633.
- (284) Jackson, D. C., Lau, Y. F., Le, T., Suhrbier, A., Deliyannis, G., Cheers, C., Smith, C., Zeng, W., and Brown, L. E. (2004) A totally synthetic vaccine of generic structure that targets Toll-like receptor 2 on dendritic cells and promotes antibody or cytotoxic T cell responses. *Proc. Natl. Acad. Sci. United States Am.* 101, 15440–15445.
- (285) Huang, S., Rutkowsky, J. M., Snodgrass, R. G., Ono-Moore, K. D., Schneider, D. A., Newman, J. W., Adams, S. H., and Hwang, D. H. (2012) Saturated fatty acids activate TLR-mediated proinflammatory signaling pathways. *J. Lipid Res.* 53, 2002–2013.
- (286) Braun, V., Fischer, E., Hantke, K., Heller, K., and Rotering, H. (1985) Functional Aspects of Gram-Negative Cell Surfaces BT - Subcellular Biochemistry (Roodyn, D. B., Ed.), pp 103–180. Springer US, Boston, MA.
- (287) BenMohamed, L., Wechsler, S. L., and Nesburn, A. B. (2002) Lipopeptide vaccines—yesterday, today, and tomorrow. *Lancet Infect. Dis.* 2, 425–431.
- (288) Chu, R. S., Targoni, O. S., Krieg, A. M., Lehmann, P. V, and Harding, C. V. (1997) CpG Oligodeoxynucleotides Act as Adjuvants that Switch on T Helper 1 (Th1) Immunity. *J. Exp. Med.*

- 186, 1623–1631.
- (289) Ercolini, A. M., Machiels, J.-P. H., Chen, Y. C., Slansky, J. E., Giedlen, M., Reilly, R. T., and Jaffee, E. M. (2003) Identification and Characterization of the Immunodominant Rat HER-2/neu MHC Class I Epitope Presented by Spontaneous Mammary Tumors from HER-2/neu-Transgenic Mice. *J. Immunol.* *170*, 4273–4280.
- (290) Richichi, B., Thomas, B., Fiore, M., Bosco, R., Qureshi, H., Nativi, C., Renaudet, O., and BenMohamed, L. (2014) A Cancer Therapeutic Vaccine based on Clustered Tn-Antigen Mimetics Induces Strong Antibody-Mediated Protective Immunity. *Angew. Chemie Int. Ed.* *53*, 11917–11920.
- (291) Jiménez-Barbero, J., Dragoni, E., Venturi, C., Nannucci, F., Ardá, A., Fontanella, M., André, S., Cañada, F. J., Gabius, H.-J., and Nativi, C. (2009)  $\alpha$ -O-Linked Glycopeptide Mimetics: Synthesis, Conformation Analysis, and Interactions with Viscumin, a Galactoside-Binding Model Lectin. *Chem. - A Eur. J.* *15*, 10423–10431.
- (292) Alexander, J., Sidney, J., Southwood, S., Ruppert, J., Oseroff, C., Maewal, A., Snoke, K., Serra, H. M., Kubo, R. T., Sette, A., and Grey, H. M. (1994) Development of high potency universal DR-restricted helper epitopes by modification of high affinity DR-blocking peptides. *Immunity* *1*, 751–761.
- (293) Boons, G.-J. (2010) Liposomes modified by carbohydrate ligands can target B cells for the treatment of B-cell lymphomas. *Expert Rev. Vaccines* *9*, 1251–1256.
- (294) Sun, Z. Y., Chen, P. G., Liu, Y. F., Zhang, B. D., Wu, J. J., Chen, Y. X., Zhao, Y. F., and Li, Y. M. (2016) Multi-component self-assembled anti-tumor nano-vaccines based on MUC1 glycopeptides. *Chem. Commun.* *52*, 7572–7575.
- (295) Ott, G., and Van Nest, G. (2007) Development of Vaccine Adjuvants: A Historical Perspective, in *Vaccine Adjuvants and Delivery Systems*, pp 1–31. John Wiley & Sons, Inc.
- (296) White, J. L., and Schlageter, E. A. (1934) Diphtheria toxoid: Comparative immunizing value with and with-out alum, as indicated by the schick test. *J. Am. Med. Assoc.* *102*, 915.
- (297) Freund, J. (1947) Some Aspects of Active Immunization. *Annu. Rev. Microbiol.* *1*, 291–308.
- (298) McKinney, R. W., and Davenport, F. M. (1961) Studies on the Mechanism of Action of Emulsified Vaccines. *J. Immunol.* *86*, 91 LP-100.
- (299) Kennedy, R., and Celis, E. (2008) Multiple roles for CD4<sup>+</sup> T cells in anti-tumor immune responses. *Immunol. Rev.* *222*, 129–144.
- (300) de Jong, E. C., Smits, H. H., and Kapsenberg, M. L. (2005) Dendritic cell-mediated T cell polarization. *Springer Semin. Immunopathol.* *26*, 289–307.
- (301) Duthie, M. S., Windish, H. P., Fox, C. B., and Reed, S. G. (2011) Use of defined TLR ligands as adjuvants within human vaccines. *Immunol. Rev.* *239*, 178–196.
- (302) Seya, T., Shime, H., Takeda, Y., Tatematsu, M., Takashima, K., and Matsumoto, M. (2015) Adjuvant for vaccine immunotherapy of cancer - focusing on Toll-like receptor 2 and 3 agonists for safely enhancing antitumor immunity. *Cancer Sci.* *106*, 1659–1668.
- (303) Liu, W., Sohn, H. W., Tolar, P., and Pierce, S. K. (2010) It's All About Change: The Antigen-driven Initiation of B-Cell Receptor Signaling. *Cold Spring Harb. Perspect. Biol.* *2*.
- (304) Pierce, S. K., and Liu, W. (2010) The tipping points in the initiation of B cell signalling: how small changes make big differences. *Nat Rev Immunol* *10*, 767–777.
- (305) Tomalia, D. A. (2005, March 1) The dendritic state. *Mater. Today*. Elsevier.
- (306) Lee, C. C., MacKay, J. A., Frechet, J. M. J., and Szoka, F. C. (2005) Designing dendrimers for biological applications. *Nat Biotech* *23*, 1517–1526.
- (307) Menjoge, A. R., Kannan, R. M., and Tomalia, D. A. (2010, March 1) Dendrimer-based drug and imaging conjugates: design considerations for nanomedical applications. *Drug Discov. Today*. Elsevier Current Trends.
- (308) Mintzer, M. A., and Grinstaff, M. W. (2011) Biomedical applications of dendrimers: a tutorial. *Chem. Soc. Rev.* *40*, 173–190.
- (309) Khandare, J., Calderon, M., Dagia, N. M., and Haag, R. (2012) Multifunctional dendritic polymers in nanomedicine: opportunities and challenges. *Chem. Soc. Rev.* *41*, 2824–2848.

- (310) Mignani, S., El Kazzouli, S., Bousmina, M., and Majoral, J. P. (2013, October 15) Expand classical drug administration ways by emerging routes using dendrimer drug delivery systems: A concise overview. *Adv. Drug Deliv. Rev.* Elsevier.
- (311) Shiao, T. C., and Roy, R. (2012) Glycodendrimers as functional antigens and antitumor vaccines. *New J. Chem.* 36, 324–339.
- (312) Sharma, R., Naresh, K., Chabre, Y. M., Rej, R., Saadeh, N. K., and Roy, R. (2014) “Onion peel” dendrimers: a straightforward synthetic approach towards highly diversified architectures. *Polym. Chem.* 5, 4321–4331.
- (313) Chabre, Y. M., and Roy, R. (2013) Multivalent glycoconjugate syntheses and applications using aromatic scaffolds. *Chem. Soc. Rev.* 42, 4657–4708.
- (314) Gingras, M., Chabre, Y. M., Roy, M., and Roy, R. (2013) How do multivalent glycodendrimers benefit from sulfur chemistry? *Chem. Soc. Rev.* 42, 4823–4841.
- (315) König, B., Fricke, T., Wassmann, A., Krallmann-Wenzel, U., and Lindhorst, T. K. (1998)  $\alpha$ -Mannosyl clusters scaffolded on azamacrocycles: Synthesis and inhibitory properties in the adhesion of type 1 fimbriated *Escherichia coli* to Guinea pig erythrocytes. *Tetrahedron Lett.* 39, 2307–2310.
- (316) Mattarella, M., Berstis, L., Baldrige, K. K., and Siegel, J. S. (2014) Synthesis of Bioconjugated sym-Pentasubstituted Corannulenes: Experimental and Theoretical Investigations of Supramolecular Architectures. *Bioconjug. Chem.* 25, 115–128.
- (317) Butterfield, A. M., Gilomen, B., and Siegel, J. S. (2012) Kilogram-Scale Production of Corannulene. *Org. Process Res. Dev.* 16, 664–676.
- (318) Maraval, V., Caminade, A.-M., Majoral, J.-P., and Blais, J.-C. (2003) Dendrimer Design: How to Circumvent the Dilemma of a Reduction of Steps or an Increase of Function Multiplicity? *Angew. Chemie Int. Ed.* 42, 1822–1826.
- (319) Baldini, L., Casnati, A., Sansone, F., and Ungaro, R. (2007) Calixarene-based multivalent ligands. *Chem. Soc. Rev.* 36, 254–266.
- (320) Sansone, F., and Casnati, A. (2013) Multivalent glycolixarenes for recognition of biological macromolecules: glycolyx mimics capable of multitasking. *Chem. Soc. Rev.* 42, 4623–4639.
- (321) Kolb, H. C., Finn, M. G., and Sharpless, K. B. (2001) Click Chemistry: Diverse Chemical Function from a Few Good Reactions. *Angew. Chemie - Int. Ed.* 40, 2004–2021.
- (322) Hein, C. D., Liu, X.-M., and Wang, D. (2008) Click Chemistry, a Powerful Tool for Pharmaceutical Sciences. *Pharm. Res.* 25, 2216–2230.
- (323) Hang, H. C., and Bertozzi, C. R. (2001) Chemoselective Approaches to Glycoprotein Assembly. *Acc. Chem. Res.* 34, 727–736.
- (324) Koniev, O., and Wagner, A. (2015) Developments and recent advancements in the field of endogenous amino acid selective bond forming reactions for bioconjugation. *Chem. Soc. Rev.* 44, 5495–5551.
- (325) Baskin, J. M., Prescher, J. A., Laughlin, S. T., Agard, N. J., Chang, P. V., Miller, I. A., Lo, A., Codelli, J. A., and Bertozzi, C. R. (2007) Copper-free click chemistry for dynamic in vivo imaging. *Proc. Natl. Acad. Sci.* 104, 16793–16797.
- (326) Tornøe, C. W., Christensen, C., and Meldal, M. (2002) Peptidotriazoles on Solid Phase: [1,2,3]-Triazoles by Regiospecific Copper(I)-Catalyzed 1,3-Dipolar Cycloadditions of Terminal Alkynes to Azides. *J. Org. Chem.* 67, 3057–3064.
- (327) Rostovtsev, V. V., Green, L. G., Fokin, V. V., and Sharpless, K. B. (2002) A stepwise Huisgen cycloaddition process: Copper(I)-catalyzed regioselective “ligation” of azides and terminal alkynes. *Angew. Chemie - Int. Ed.* 41, 2596–2599.
- (328) Meldal, M., and Tornøe, C. W. (2008) Cu-Catalyzed Azide–Alkyne Cycloaddition. *Chem. Rev.* 108, 2952–3015.
- (329) Bock, V. D., Perciaccante, R., Jansen, T. P., Hiemstra, H., and van Maarseveen, J. H. (2006) Click Chemistry as a Route to Cyclic Tetrapeptide Analogues: Synthesis of cyclo-[Pro-Val- $\psi$ (triazole)-Pro-Tyr]. *Org. Lett.* 8, 919–922.
- (330) Sletten, E. M., and Bertozzi, C. R. (2011) From Mechanism to Mouse: A Tale of Two

- Bioorthogonal Reactions. *Acc. Chem. Res.* **44**, 666–676.
- (331) van Geel, R., Pruijn, G. J. M., van Delft, F. L., and Boelens, W. C. (2012) Preventing Thiol-Yne Addition Improves the Specificity of Strain-Promoted Azide–Alkyne Cycloaddition. *Bioconjug. Chem.* **23**, 392–398.
- (332) Ulrich, S., Boturyn, D., Marra, A., Renaudet, O., and Dumy, P. (2014) Oxime Ligation: A Chemoselective Click-Type Reaction for Accessing Multifunctional Biomolecular Constructs. *Chem. - A Eur. J.* **20**, 34–41.
- (333) Agten, S. M., Dawson, P. E., and Hackeng, T. M. (2016) Oxime conjugation in protein chemistry: from carbonyl incorporation to nucleophilic catalysis. *J. Pept. Sci.* **22**, 271–279.
- (334) Kalia, J., and Raines, R. T. (2008) Hydrolytic Stability of Hydrazones and Oximes. *Angew. Chemie Int. Ed.* **47**, 7523–7526.
- (335) Horiya, S., MacPherson, I. S., and Krauss, I. J. (2014) Recent strategies targeting HIV glycans in vaccine design. *Nat Chem Biol* **10**, 990–999.
- (336) Hartmann, M., Papavlassopoulos, H., Chandrasekaran, V., Grabosch, C., Beiroth, F., Lindhorst, T. K., and Röhl, C. (2012) Inhibition of bacterial adhesion to live human cells: Activity and cytotoxicity of synthetic mannosides. *FEBS Lett.* **586**, 1459–1465.
- (337) Mckenzie, V. A. and I. f. c. (2001) Role of the Mannose Receptor in the Immune Response. *Curr. Mol. Med.*
- (338) Teodorof, C., Divakar, S., Soontornniyomkij, B., Achim, C. L., Kaul, M., and Singh, K. K. (2014) Intracellular mannose binding lectin mediates subcellular trafficking of HIV-1 gp120 in neurons. *Neurobiol. Dis.* **69**, 54–64.
- (339) Rosano, G., Caille, A. M., Gallardo-Ríos, M., and Munuce, M. J. (2007) d-Mannose-binding sites are putative sperm determinants of human oocyte recognition and fertilization. *Reprod. Biomed. Online* **15**, 182–190.
- (340) Turner, M. . (2003) The role of mannose-binding lectin in health and disease. *Mol. Immunol.* **40**, 423–429.
- (341) Darton, T. C., Jack, D. L., Johnson, M., Borrow, R., Guiver, M., Kaczmarek, E. B., Turner, M. W., Klein, N. J., and Read, R. C. (2014) MBL2 deficiency is associated with higher genomic bacterial loads during meningococemia in young children. *Clin. Microbiol. Infect.* **20**, 1337–1342.
- (342) Scorza, M., Liguori, R., Elce, A., Salvatore, F., and Castaldo, G. (2015) Biological role of mannose binding lectin: From newborns to centenarians. *Clin. Chim. Acta* **451**, 78–81.
- (343) Keler, T., Ramakrishna, V., and Fanger, M. W. (2004) Mannose receptor-targeted vaccines. *Expert Opin. Biol. Ther.* **4**, 1953–1962.
- (344) Irache, J. M., Salman, H. H., Gamazo, C., and Espuelas, S. (2008) Mannose-targeted systems for the delivery of therapeutics. *Expert Opin. Drug Deliv.* **5**, 703–724.
- (345) Renaudet, O., and Dumy, P. (2003) Chemoselectively Template-Assembled Glycoconjugates as Mimics for Multivalent Presentation of Carbohydrates. *Org. Lett.* **5**, 243–246.
- (346) Foillard, S., Rasmussen, M. O., Razkin, J., Boturyn, D., and Dumy, P. (2008) 1-Ethoxyethylidene, a New Group for the Stepwise SPPS of Aminoxyacetic Acid Containing Peptides. *J. Org. Chem.* **73**, 983–991.
- (347) Lee, M. D., Dunne, T. S., Siegel, M. M., Chang, C. C., Morton, G. O., and Borders, D. B. (1987) Calicheamicins, a novel family of antitumor antibiotics. 1. Chemistry and partial structure of calicheamicin .gamma.1I. *J. Am. Chem. Soc.* **109**, 3464–3466.
- (348) Renaudet, O., and Dumy, P. (2006) On-bead synthesis and binding assay of chemoselectively template-assembled multivalent neoglycopeptides. *Org. Biomol. Chem.* **4**, 2628–2636.
- (349) Brown, S. P., and Spiess, H. W. (2001) Advanced Solid-State NMR Methods for the Elucidation of Structure and Dynamics of Molecular, Macromolecular, and Supramolecular Systems. *Chem. Rev.* **101**, 4125–4156.
- (350) Thomas, B., Berthet, N., Garcia, J., Dumy, P., and Renaudet, O. (2013) Expanding the scope of oxime ligation: facile synthesis of large cyclopeptide-based glycodendrimers. *Chem. Commun.* **49**, 10796–10798.
- (351) Bernardi, A., Jimenez-Barbero, J., Casnati, A., De Castro, C., Darbre, T., Fieschi, F., Finne, J.,



- Funken, H., Jaeger, K.-E., Lahmann, M., Lindhorst, T. K., Marradi, M., Messner, P., Molinaro, A., Murphy, P. V., Nativi, C., Oscarson, S., Penades, S., Peri, F., Pieters, R. J., Renaudet, O., Reymond, J.-L., Richichi, B., Rojo, J., Sansone, F., Schaffer, C., Turnbull, W. B., Velasco-Torrijos, T., Vidal, S., Vincent, S., Wennekes, T., Zuilhof, H., and Imberty, A. (2013) Multivalent glycoconjugates as anti-pathogenic agents. *Chem. Soc. Rev.* *42*, 4709–4727.
- (352) Kiessling, L. L., Gestwicki, J. E., and Strong, L. E. (2006) Synthetic Multivalent Ligands as Probes of Signal Transduction. *Angew. Chemie Int. Ed.* *45*, 2348–2368.
- (353) Daskhan, G. C., Berthet, N., Thomas, B., Fiore, M., and Renaudet, O. (2015) Multivalent glycocyclopeptides: toward nano-sized glycostructures. *Carbohydr. Res.* *405*, 13–22.
- (354) Fiore, M., Berthet, N., Marra, A., Gillon, E., Dumy, P., Dondoni, A., Imberty, A., and Renaudet, O. (2013) Tetravalent glycocyclopeptide with nanomolar affinity to wheat germ agglutinin. *Org. Biomol. Chem.* *11*, 7113–7122.
- (355) Berthet, N., Thomas, B., Bossu, I., Dufour, E., Gillon, E., Garcia, J., Spinelli, N., Imberty, A., Dumy, P., and Renaudet, O. (2013) High Affinity Glycodendrimers for the Lectin LecB from *Pseudomonas aeruginosa*. *Bioconjug. Chem.* *24*, 1598–1611.
- (356) Bossu, I., Sulc, M., Krenek, K., Dufour, E., Garcia, J., Berthet, N., Dumy, P., Kren, V., and Renaudet, O. (2011) Dendri-RAFTs: a second generation of cyclopeptide-based glycoclusters. *Org. Biomol. Chem.* *9*, 1948–1959.
- (357) Yeoh, K. K., Butters, T. D., Wilkinson, B. L., and Fairbanks, A. J. (2009) Probing replacement of pyrophosphate via click chemistry; synthesis of UDP-sugar analogues as potential glycosyl transferase inhibitors. *Carbohydr. Res.* *344*, 586–591.
- (358) Miller, N., Williams, G. M., and Brimble, M. A. (2009) Synthesis of Fish Antifreeze Neoglycopeptides Using Microwave-Assisted “Click Chemistry.” *Org. Lett.* *11*, 2409–2412.
- (359) Nagel, L., Budke, C., Erdmann, R. S., Dreyer, A., Wennemers, H., Koop, T., and Sewald, N. (2012) Influence of Sequential Modifications and Carbohydrate Variations in Synthetic AFGP Analogues on Conformation and Antifreeze Activity. *Chem. - A Eur. J.* *18*, 12783–12793.
- (360) Boullanger, P., Maunier, V., and Lafont, D. (2000) Syntheses of amphiphilic glycosylamides from glycosyl azides without transient reduction to glycosylamines. *Carbohydr. Res.* *324*, 97–106.
- (361) Byrne, C., McEwan, P. A., Emsley, J., Fischer, P. M., and Chan, W. C. (2011) End-stapled homo and hetero collagen triple helices: a click chemistry approach. *Chem. Commun.* *47*, 2589–2591.
- (362) Goddard-Borger, E. D., and Stick, R. V. (2007) An Efficient, Inexpensive, and Shelf-Stable Diazotransfer Reagent: Imidazole-1-sulfonyl Azide Hydrochloride. *Org. Lett.* *9*, 3797–3800.
- (363) Chan, T. R., Hilgraf, R., Sharpless, K. B., and Fokin, V. V. (2004) Polytriazoles as Copper(I)-Stabilizing Ligands in Catalysis. *Org. Lett.* *6*, 2853–2855.
- (364) Godula, K., and Bertozzi, C. R. (2012) Density Variant Glycan Microarray for Evaluating Cross-Linking of Mucin-like Glycoconjugates by Lectins. *J. Am. Chem. Soc.* *134*, 15732–15742.
- (365) Dam, T. K., and Brewer, C. F. (2010) Multivalent Lectin—Carbohydrate Interactions, pp 139–164.
- (366) Dam, T. K., and Brewer, C. F. (2010) Lectins as pattern recognition molecules: The effects of epitope density in innate immunity. *Glycobiology* *20*, 270–279.
- (367) Dam, T. K., Gerken, T. A., Cavada, B. S., Nascimento, K. S., Moura, T. R., and Brewer, C. F. (2007) Binding Studies of  $\alpha$ -GalNAc-specific Lectins to the  $\alpha$ -GalNAc (Tn-antigen) Form of Porcine Submaxillary Mucin and Its Smaller Fragments. *J. Biol. Chem.* *282*, 28256–28263.
- (368) Sletmoen, M., Dam, T. K., Gerken, T. A., Stokke, B. T., and Brewer, C. F. (2009) Single-Molecule Pair Studies of the Interactions of the  $\alpha$ -GalNAc (Tn-Antigen) Form of Porcine Submaxillary Mucin with Soybean Agglutinin. *Biopolymers* *91*, 719–728.
- (369) Dam, T. K., Gerken, T. A., and Brewer, C. F. (2009) Thermodynamics of Multivalent Carbohydrate–Lectin Cross-Linking Interactions: Importance of Entropy in the Bind and Jump Mechanism. *Biochemistry* *48*, 3822–3827.
- (370) Thomas, B., Pifferi, C., Daskhan, G. C., Fiore, M., Berthet, N., and Renaudet, O. (2015) Divergent and convergent synthesis of GalNAc-conjugated dendrimers using dual orthogonal ligations.

- Org. Biomol. Chem.* **13**, 11529–11538.
- (371) Singh, R. P., Vij, A., Kirchmeier, R. L., and Shreeve, J. M. (2000) A Novel Synthesis of Hexakis(trifluoromethyl)cyclotriphosphazene. Single-Crystal X-ray Structures of N<sub>3</sub>P<sub>3</sub>(CF<sub>3</sub>)<sub>6</sub> and N<sub>3</sub>P<sub>3</sub>F<sub>6</sub>. *Inorg. Chem.* **39**, 375–377.
- (372) Abbassi, L., Chabre, Y. M., Kottari, N., Arnold, A. A., Andre, S., Josserand, J., Gabius, H.-J., and Roy, R. (2015) Multifaceted glycodendrimers with programmable bioactivity through convergent, divergent, and accelerated approaches using polyfunctional cyclotriphosphazenes. *Polym. Chem.* **6**, 7666–7683.
- (373) Greenfield, N. J. (2007) Using circular dichroism spectra to estimate protein secondary structure. *Nat. Protoc.* **1**, 2876–2890.
- (374) Melnyk, J. E., Mohanan, V., Schaefer, A. K., Hou, C.-W., and Grimes, C. L. (2015) Peptidoglycan Modifications Tune the Stability and Function of the Innate Immune Receptor Nod2. *J. Am. Chem. Soc.* **137**, 6987–6990.
- (375) Percec, V., Leowanawat, P., Sun, H.-J., Kulikov, O., Nusbaum, C. D., Tran, T. M., Bertin, A., Wilson, D. A., Peterca, M., Zhang, S., Kamat, N. P., Vargo, K., Mook, D., Johnston, E. D., Hammer, D. A., Pochan, D. J., Chen, Y., Chabre, Y. M., Shiao, T. C., Bergeron-Brelek, M., André, S., Roy, R., Gabius, H.-J., and Heiney, P. A. (2013) Modular Synthesis of Amphiphilic Janus Glycodendrimers and Their Self-Assembly into Glycodendrimersomes and Other Complex Architectures with Bioactivity to Biomedically Relevant Lectins. *J. Am. Chem. Soc.* **135**, 9055–9077.
- (376) Dowlut, M., Hall, D. G., and Hindsgaul, O. (2005) Investigation of Nonspecific Effects of Different Dyes in the Screening of Labeled Carbohydrates against Immobilized Proteins. *J. Org. Chem.* **70**, 9809–9813.
- (377) Hardouin, J., Cremer, A. G., and Delmas, A. F. (2011, July 30) Investigation of in-source decay of oxime-linked peptide by matrix-assisted laser desorption/ionization time-of-flight mass spectrometry. *Rapid Commun. Mass Spectrom.* John Wiley & Sons, Ltd.
- (378) Govan, J. R., and Deretic, V. (1996) Microbial pathogenesis in cystic fibrosis: mucoid *Pseudomonas aeruginosa* and *Burkholderia cepacia*. *Microbiol. Rev.* **60**, 539–574.
- (379) Aaron, S. D., Ferris, W., Henry, D. A., Speert, D. P., and MacDonald, N. E. (2000) Multiple Combination Bactericidal Antibiotic Testing for Patients with Cystic Fibrosis Infected with *Burkholderia cepacia*. *Am. J. Respir. Crit. Care Med.* **161**, 1206–1212.
- (380) Boukerb, A. M., Rousset, A., Galanos, N., Méar, J.-B., Thépaut, M., Grandjean, T., Gillon, E., Cecioni, S., Abderrahmen, C., Faure, K., Redelberger, D., Kipnis, E., Dessein, R., Havet, S., Darblade, B., Matthews, S. E., de Bentzmann, S., Guéry, B., Cournoyer, B., Imbert, A., and Vidal, S. (2014) Antiadhesive Properties of Glycoclusters against *Pseudomonas aeruginosa* Lung Infection. *J. Med. Chem.* **57**, 10275–10289.
- (381) Stach, M., Siriwardena, T. N., Köhler, T., van Delden, C., Darbre, T., and Reymond, J.-L. (2014) Combining Topology and Sequence Design for the Discovery of Potent Antimicrobial Peptide Dendrimers against Multidrug-Resistant *Pseudomonas aeruginosa*. *Angew. Chemie* **126**, 13041–13045.
- (382) Diggle, S. P., Stacey, R. E., Dodd, C., Camara, M., Williams, P., and Winzer, K. (2006) The galactophilic lectin, LecA, contributes to biofilm development in *Pseudomonas aeruginosa*. *Environ. Microbiol.* **8**, 1095–1104.
- (383) Ligeour, C., Vidal, O., Dupin, L., Casoni, F., Gillon, E., Meyer, A., Vidal, S., Vergoten, G., Lacroix, J.-M., Souteyrand, E., Imbert, A., Vasseur, J.-J., Chevolut, Y., and Morvan, F. (2015) Mannose-centered aromatic galactoclusters inhibit the biofilm formation of *Pseudomonas aeruginosa*. *Org. Biomol. Chem.* **13**, 8433–8444.
- (384) Tielker, D., Hacker, S., Loris, R., Strathmann, M., Wingender, J., Wilhelm, S., Rosenau, F., and Jaeger, K. E. (2005) *Pseudomonas aeruginosa* lectin LecB is located in the outer membrane and is involved in biofilm formation. *Microbiology* **151**, 1313–1323.
- (385) Lameignere, E., Malinová, L., Sláviková, M., Duchaud, E., Mitchell, E. P., Varrot, A., Šedo, O., Imbert, A., and Wimmerová, M. (2008) Structural basis for mannose recognition by a lectin

- from opportunistic bacteria & Burkholderia cenocepacia; *Biochem. J.* **411**, 307 LP-318.
- (386) Marchetti, R., Malinowska, L., Lameignère, E., Adamova, L., de Castro, C., Cioci, G., Stanetty, C., Kosma, P., Molinaro, A., Wimmerova, M., Imberty, A., and Silipo, A. (2012) Burkholderia cenocepacia lectin A binding to heptoses from the bacterial lipopolysaccharide. *Glycobiology* **22**, 1387–1398.
- (387) Lameignere, E., Shiao, T. C., Roy, R., Wimmerova, M., Dubreuil, F., Varrot, A., and Imberty, A. (2010) Structural basis of the affinity for oligomannosides and analogs displayed by BC2L-A, a Burkholderia cenocepacia soluble lectin. *Glycobiology* **20**, 87–98.
- (388) Beshr, G., Sommer, R., Hauck, D., Siebert, D. C. B., Hofmann, A., Imberty, A., and Titz, A. (2016) Development of a competitive binding assay for the Burkholderia cenocepacia lectin BC2L-A and structure activity relationship of natural and synthetic inhibitors. *Medchemcomm* **7**, 519–530.
- (389) Caumes, C., Gillon, E., Legeret, B., Taillefumier, C., Imberty, A., and Faure, S. (2015) Multivalent thioglycopeptoids via photoclick chemistry: potent affinities towards LecA and BC2L-A lectins. *Chem. Commun.* **51**, 12301–12304.
- (390) Reynolds, M., Marradi, M., Imberty, A., Penadés, S., and Pérez, S. (2013) Influence of ligand presentation density on the molecular recognition of mannose-functionalised glyconanoparticles by bacterial lectin BC2L-A. *Glycoconj. J.* **30**, 747–757.
- (391) Pifferi, C., Goyard, D., Gillon, E., Imberty, A., and Renaudet, O. (2017) Synthesis of Mannosylated Glycodendrimers and Evaluation against BC2L-A Lectin from *Burkholderia Cenocepacia*. *Chempluschem* **82**, 390–398.
- (392) Reynolds, M., and Pérez, S. (2011) Thermodynamics and chemical characterization of protein–carbohydrate interactions: The multivalency issue. *Comptes Rendus Chim.* **14**, 74–95.
- (393) Marchetti, R., Perez, S., Arda, A., Imberty, A., Jimenez-Barbero, J., Silipo, A., and Molinaro, A. (2016) “Rules of Engagement” of Protein-Glycoconjugate Interactions: A Molecular View Achievable by using NMR Spectroscopy and Molecular Modeling. *ChemistryOpen* **5**, 274–296.
- (394) Wittmann, V. (2013) Structural investigation of multivalent carbohydrate–protein interactions using synthetic biomolecules. *Curr. Opin. Chem. Biol.* **17**, 982–989.
- (395) Bennett, N. R., Zwick, D. B., Courtney, A. H., and Kiessling, L. L. (2015) Multivalent Antigens for Promoting B and T Cell Activation. *ACS Chem. Biol.* **10**, 1817–1824.
- (396) Gómez-García, M., Benito, J. M., Rodríguez-Lucena, D., Yu, J.-X., Chmurski, K., Ortiz Mellet, C., Gutiérrez Gallego, R., Maestre, A., Defaye, J., and García Fernández, J. M. (2005) Probing Secondary Carbohydrate–Protein Interactions with Highly Dense Cyclodextrin-Centered Heteroglycoclusters: The Heterocluster Effect. *J. Am. Chem. Soc.* **127**, 7970–7971.
- (397) Ortega-Muñoz, M., Perez-Balderas, F., Morales-Sanfrutos, J., Hernandez-Mateo, F., Isac-García, J., and Santoyo-Gonzalez, F. (2009) Click Multivalent Heterogeneous Neoglycoconjugates - Modular Synthesis and Evaluation of Their Binding Affinities. *European J. Org. Chem.* **2009**, 2454–2473.
- (398) Jimenez Blanco, J. L., Ortiz Mellet, C., and Garcia Fernandez, J. M. (2013) Multivalency in heterogeneous glycoenvironments: hetero-glycoclusters, -glycopolymers and -glycoassemblies. *Chem. Soc. Rev.* **42**, 4518–4531.
- (399) García-Moreno, M. I., Ortega-Caballero, F., Rísquez-Cuadro, R., Ortiz Mellet, C., and García Fernández, J. M. (2017) The Impact of Heteromultivalency in Lectin Recognition and Glycosidase Inhibition: An Integrated Mechanistic Study. *Chem. – A Eur. J.* n/a--n/a.
- (400) Ortiz Mellet, C., Nierengarten, J.-F., and Garcia Fernandez, J. M. (2017) Multivalency as an action principle in multimodal lectin recognition and glycosidase inhibition: a paradigm shift driven by carbon-based glyconanomaterials. *J. Mater. Chem. B* **5**, 6428–6436.
- (401) Horan, N., Yan, L., Isobe, H., Whitesides, G. M., and Kahne, D. (1999) Nonstatistical binding of a protein to clustered carbohydrates. *Proc. Natl. Acad. Sci. U. S. A.* **96**, 11782–6.
- (402) Ponader, D., Maffre, P., Aretz, J., Pussak, D., Ninnemann, N. M., Schmidt, S., Seeberger, P. H., Rademacher, C., Nienhaus, G. U., and Hartmann, L. (2014) Carbohydrate-Lectin Recognition of

- Sequence-Defined Heteromultivalent Glycooligomers. *J. Am. Chem. Soc.* **136**, 2008–2016.
- (403) Patel, A., and Lindhorst, T. K. (2002) Synthesis of “Mixed Type” Oligosaccharide Mimetics Based on a Carbohydrate Scaffold. *European J. Org. Chem.* **2002**, 79–86.
- (404) Katajisto, J., Karskela, T., Heinonen, P., and Lönnberg, H. (2002) An Orthogonally Protected  $\alpha,\alpha$ -Bis(aminomethyl)- $\beta$ -alanine Building Block for the Construction of Glycoconjugates on a Solid Support. *J. Org. Chem.* **67**, 7995–8001.
- (405) Ramström, O., Lohmann, S., Bunyapaiboonsri, T., and Lehn, J.-M. (2004) Dynamic Combinatorial Carbohydrate Libraries: Probing the Binding Site of the Concanavalin A Lectin. *Chem. - A Eur. J.* **10**, 1711–1715.
- (406) Wolfenden, M. L., and Cloninger, M. J. (2005) Mannose/Glucose-Functionalized Dendrimers To Investigate the Predictable Tunability of Multivalent Interactions. *J. Am. Chem. Soc.* **127**, 12168–12169.
- (407) Wolfenden, M. L., and Cloninger, M. J. (2006) Carbohydrate-Functionalized Dendrimers To Investigate the Predictable Tunability of Multivalent Interactions. *Bioconjug. Chem.* **17**, 958–966.
- (408) Ladmiral, V., Mantovani, G., Clarkson, G. J., Cauet, S., Irwin, J. L., and Haddleton, D. M. (2006) Synthesis of Neoglycopolymers by a Combination of “Click Chemistry” and Living Radical Polymerization. *J. Am. Chem. Soc.* **128**, 4823–4830.
- (409) Deguise, I., Lagnoux, D., and Roy, R. (2007) Synthesis of glycodendrimers containing both fucoside and galactoside residues and their binding properties to Pa-IL and PA-III lectins from *Pseudomonas aeruginosa*. *New J. Chem.* **31**, 1321–1331.
- (410) Thomas, B., Fiore, M., Bossu, I., Dumy, P., and Renaudet, O. (2012) Synthesis of heteroglycoclusters by using orthogonal chemoselective ligations. *Beilstein J. Org. Chem.* (Lindhorst, T. K., Ed.) **8**, 421–427.
- (411) Fiore, M., Daskhan, G. C., Thomas, B., and Renaudet, O. (2014) Orthogonal dual thiol–chloroacetyl and thiol–ene couplings for the sequential one-pot assembly of heteroglycoclusters. *Beilstein J. Org. Chem.* **10**, 1557–1563.
- (412) Thomas, B., Fiore, M., Daskhan, G. C., Spinelli, N., and Renaudet, O. (2015) A multi-ligation strategy for the synthesis of heterofunctionalized glycosylated scaffolds. *Chem. Commun.* **51**, 5436–5439.
- (413) Daskhan, G. C., Pifferi, C., and Renaudet, O. (2016) Synthesis of a New Series of Sialylated Homo- and Heterovalent Glycoclusters by using Orthogonal Ligations. *ChemistryOpen* **5**, 477–484.
- (414) Yu, H., and Chen, X. (2006) Aldolase-Catalyzed Synthesis of  $\beta$ -d-Galp-(1 $\rightarrow$ 9)-d-KDN: A Novel Acceptor for Sialyltransferases. *Org. Lett.* **8**, 2393–2396.
- (415) Pifferi, C., Thomas, B., Goyard, D., Berthet, N., and Renaudet, O. (2017) Heterovalent glycodendrimers as epitope carriers for antitumoral synthetic vaccines. *Chem. - A Eur. J.*
- (416) McFarland, B. J., Sant, A. J., Lybrand, T. P., and Beeson, C. (1999) Ovalbumin(323–339) Peptide Binds to the Major Histocompatibility Complex Class II I-Ad Protein Using Two Functionally Distinct Registers. *Biochemistry* **38**, 16663–16670.
- (417) Porgador, A., Yewdell, J. W., Deng, Y., Bennink, J. R., and Germain, R. N. (1997) Localization, Quantitation, and In Situ Detection of Specific Peptide-MHC Class I Complexes Using a Monoclonal Antibody. *Immunity* **6**, 715–726.
- (418) Mazal, D., Lo-Man, R., Bay, S., Pritsch, O., Dériaud, E., Ganneau, C., Medeiros, A., Ubillos, L., Obal, G., Berois, N., Bollati-Fogolin, M., Leclerc, C., and Osinaga, E. (2013) Monoclonal antibodies toward different Tn-amino acid backbones display distinct recognition patterns on human cancer cells. Implications for effective immuno-targeting of cancer. *Cancer Immunol. Immunother.* **62**, 1107–1122.
- (419) Roy, R., Baek, M.-G., and Rittenhouse-Olson, K. (2001) Synthesis of N,N'-bis(Acrylamido)acetic Acid-Based T-Antigen Glycodendrimers and Their Mouse Monoclonal IgG Antibody Binding Properties. *J. Am. Chem. Soc.* **123**, 1809–1816.
- (420) Tessier, M. B., Grant, O. C., Heimbürg-Molinaro, J., Smith, D., Jadey, S., Gulick, A. M., Glushka,

- J., Deutscher, S. L., Rittenhouse-Olson, K., and Woods, R. J. (2013) Computational Screening of the Human TF-Glycome Provides a Structural Definition for the Specificity of Anti-Tumor Antibody JAA-F11. *PLoS One* (Sem, D. S., Ed.) 8, e54874.
- (421) Wu, Z., Guo, X., and Guo, Z. (2010) Chemoenzymatic synthesis of glycosylphosphatidylinositol-anchored glycopeptides. *Chem. Commun.* 46, 5773–5774.
- (422) Chamoto, K., Wakita, D., Narita, Y., Zhang, Y., Noguchi, D., Ohnishi, H., Iguchi, T., Sakai, T., Ikeda, H., and Nishimura, T. (2006) An Essential Role of Antigen-Presenting Cell/T-Helper Type 1 Cell-Cell Interactions in Draining Lymph Node during Complete Eradication of Class II–Negative Tumor Tissue by T-Helper Type 1 Cell Therapy. *Cancer Res.* 66, 1809–1817.
- (423) Albericio, F., Andreu, D., Giralt, E., Navalpotro, C., Pedrosa, E., Ponsati, B., and Rue-Gayo, M. (1989) Use of the Npys thiol protection in solid phase peptide synthesis Application to direct peptide-protein conjugation through cysteine residues. *Int. J. Pept. Protein Res.* 34, 124–128.
- (424) Mezö, G., Mihala, N., Andreu, D., and Hudecz, F. (2000) Conjugation of epitope peptides with SH group to branched chain polymeric polypeptides via Cys(Npys). *Bioconjug. Chem.* 11, 484–491.
- (425) Huwiler, K. G., Mosher, D. F., and Vestling, M. M. (2003) Optimizing the MALDI-TOF-MS Observation of Peptides Containing Disulfide Bonds. *J. Biomol. Tech.* 14, 289–297.
- (426) Galibert, M., Dumy, P., and Boturyn, D. (2009) One-Pot Approach to Well-Defined Biomolecular Assemblies by Orthogonal Chemoselective Ligations. *Angew. Chemie Int. Ed.* 48, 2576–2579.
- (427) Giustarini, D., Dalle-Donne, I., Colombo, R., Milzani, A., and Rossi, R. (2008) Is ascorbate able to reduce disulfide bridges? A cautionary note. *Nitric Oxide - Biol. Chem.* 19, 252–258.
- (428) Eissler, S., Kley, M., Bächle, D., Loidl, G., Meier, T., and Samson, D. (2017) Substitution determination of Fmoc-substituted resins at different wavelengths. *J. Pept. Sci.* 23, 757–762.
- (429) Hancock, W. S., and Battersby, J. E. (1976) A new micro-test for the detection of incomplete coupling reactions in solid-phase peptide synthesis using 2,4,6-trinitrobenzene-sulphonic acid. *Anal. Biochem.* 71, 260–264.

## Résumé : Conception et synthèse de glycoconjugués multivalents pour l'immunothérapie anticancéreuse

Le cancer est l'une des principales causes de mort dans le pays développés ; bien que les opérations chirurgicales, la radiothérapie et la chimiothérapie représentent aujourd'hui les principales options de traitement des patients souffrants de tumeurs malignes, leurs effets secondaires sévères ont ouvert la voie au développement de l'immunothérapie antitumorale. À part l'immunothérapie passive, qui est basée sur les anticorps ou tout autre composant du système immunitaire synthétisés en dehors du corps dont la potentielle menace de réactions immunes a été prouvée, nous avons concentré nos efforts sur l'immunothérapie active, qui réside dans la stimulation du système immunitaire du patient pour éradiquer sélectivement les cellules malignes. L'identification d'antigènes carbohydrates associés aux tumeurs (TACAs), surexprimés à la surface des cellules cancéreuses, a permis le développement de vaccins spécifiques à ces antigènes. Il est connu depuis plus de 40 ans que la majorité des cancers chez l'homme sont caractérisés par une glycosylation aberrante. Les cellules tumorales peuvent surexprimer des versions tronquées d'oligosaccharides, une séquence terminale inhabituelle ou une augmentation de la sialylation des glycolipides et des glycoprotéines de surface. Un oligosaccharide d'une glycoprotéine tronqué peut rendre une partie de la chaîne principale du peptide, d'habitude caché par le sucre, plus accessible au système immunitaire. Parmi les différents TACAs, nous avons concentré notre attention sur les antigènes Tn et TF, qui peuvent être trouvés sur des glycoprotéines comme MUC-1, surexprimés sur plus de 90% des carcinomes du sein. Bien que la conception de ces immunomodulateurs repose toujours sur des règles empiriques, il est important de déclencher à la fois la réponse humorale et cellulaire, ainsi qu'un effet de mémoire. Ce défi peut être relevé en combinant, sur une seule molécule, l'antigène carbohydrate exprimés à la surface des tumeurs (épitope des cellules B), les peptides capables de stimuler les cellules CD4<sup>+</sup> et CD8<sup>+</sup> (épitopes des cellules T) et un adjuvant, pour recueillir tous les éléments du système immunitaire au niveau du site d'injection et renforcer l'absorption des antigènes. De précédentes études faites dans notre groupe de recherche ont publié pour la première fois la synthèse et l'évaluation immunologique d'un prototype de vaccin anticancéreux à quatre composant capable d'induire une réponse immunitaire de longue durée sur des modèles murins. Dans mon travail de thèse, nous avons voulu synthétiser des prototypes de vaccin anticancéreux basés sur les TACAs avec des propriétés immunologiques accrues. Notre stratégie de conception a été guidée par (i) l'importance d'une haute densité de carbohydrates pour promouvoir une capture d'antigène plus efficace et un traitement par les cellules présentatrices d'antigène, et (ii) l'expression hétérogène des TACAs au cours de la maladie et parmi différents patients. En respectant ces deux aspects, il sera possible de déclencher une réponse immunitaire plus forte et à plusieurs facettes.

---

### Abstract : Design and synthesis of multivalent glycoconjugates for anti-cancer immunotherapy

Cancer is one of the leading causes of death in developed countries; although surgical resection, direct irradiation and cytotoxic chemotherapy represent nowadays the main treatment options for patients suffering with malignancies, their severe side effects paved the way for the rise in popularity of antitumoral immunotherapy. Apart from passive immunotherapy, which is comprised of antibodies or other immune system components that are made outside of the body and has been shown to be associated to potentially life threatening immune reactions, we focused our efforts towards active immunotherapy, which purpose is stimulate the patient immune system to selectively eradicate malignant cells. The identification of tumor-associated carbohydrate antigens (TACAs) on the surface of cancer cells has allowed the development of antigen-specific vaccines. It has been known for over four decades that the majority of human cancers are characterized by aberrant glycosylation. Tumor cells may over-express truncated versions of oligosaccharides, unusual terminal oligosaccharide sequences, or increase sialylation of cell-surface glycolipids and O- and N-linked glycoproteins. A truncated oligosaccharide of a glycoprotein may render a part of the peptide backbone, which is normally shielded by the glycan, more accessible to the immune system. Among the assortment of TACAs we focussed our attention on Tn and TF antigens, which can be found in membrane-bound glycoproteins like MUC-1, over-expressed in more than 90% of breast carcinomas. Although the design of such immuno-modulators still relies on empiric rules, it is noteworthy important to trigger both humoral and cellular responses, and a memory effect. This challenge can be achieved by combining, within a single molecule, carbohydrate antigen expressed on the surface of tumors (B-cell epitope), peptides capable to stimulate both CD4<sup>+</sup> and CD8<sup>+</sup> T-cells (T-cell epitopes) and an adjuvant, to gather immune system elements in the injection site and boost the antigen uptake. Previous studies of our research group reported for the first time the synthesis and immunological evaluation of a four-component anticancer vaccine prototype capable of inducing a long-lasting immune response in mice models. In my PhD work we aimed to synthesize TACA-based anticancer vaccine prototypes with improved immunological properties. The principles which guided our design strategies rely on (i) the importance of a high density of carbohydrate epitopes to promote a more effective antigen capture and processing by antigen-presenting cells, and (ii) the evidence of heterogenic expression patterns of TACAs during the course of the disease and among different individuals. Addressing these two aspects would provide a stronger and multifaceted immune response.

**Key words:** tumor-associated carbohydrate antigens (TACAs), cancer immunotherapy, click chemistry, multivalent glycoconjugates.